

Directional Solidification of Steel Castings

BY

R. WLODAWER

*Sulzer Brothers Ltd.
Winterthur / Switzerland
(Central Department for Foundry Technique)*

TRANSLATED BY

L. D. HEWITT

ENGLISH TRANSLATION EDITED

BY

R. V. RILEY

Chesterfield, England

PERGAMON PRESS

OXFORD · LONDON · EDINBURGH · NEW YORK
TORONTO · PARIS · BRAUNSCHWEIG

Pergamon Press Ltd., Headington Hill Hall, Oxford
4 & 5 Fitzroy Square, London W.1

Pergamon Press (Scotland) Ltd., 2 & 3 Teviot Place, Edinburgh 1

Pergamon Press Inc., 44-01 21st Street, Long Island City, New York 11101

Pergamon of Canada, Ltd., 6 Adelaide Street East, Toronto, Ontario

Pergamon Press S.A.R.L., 24 rue des Écoles, Paris 5^e

Vieweg & Sohn GmbH, Burgplatz 1, Braunschweig

Copyright © 1966
Pergamon Press Ltd

First English edition 1966

Library of Congress Catalog Card No. 64-20641

A translation, with substantial additions and amendments by the author, of the original volume
Gelenkte Erstarrung von Stahlguß, Giesserei-Verlag G.m.b.H. / Düsseldorf

FOREWORD TO THE FIRST EDITION

IT IS of the utmost importance to be able to control reliably the solidification of steel castings and it is useless to employ the best qualities of steel if the resulting casting is not free from casting defects, such as shrinkage cavities and tears.

This book summarizes the results of a large number of investigations, mostly scientific in character, and develops them further from the practical aspect. It can serve in foundry operations as a basis for the directional solidification of steel castings. Diagrams, simple basic rules and formulae provide the practical man with the means by which calculations can be avoided or minimized. He can interpret the required data from graphs. The book is therefore particularly suitable for the foundry manager, foreman and technician; it will also be useful for the designer, in giving him an idea of the influence of the design of his casting on the technical possibilities of producing it in the foundry. The theoretician will be interested mainly in the derivations of the laws and formulae which are confined to separate sections and need not be studied in order to understand the practical sections. The commercial man can also obtain a general idea of the possibilities of steel casting design and the dangers to be avoided.

It is probably the first book of its kind, in which the problem of the directional solidification of steel castings has been treated comprehensively on a clear theoretical basis, accompanied by many practical examples.

A. HEUVERS

PREFACE TO THE ENGLISH EDITION

THE author thanks the English-speaking technical world for the friendly reception it has given to his book dealing with feeding techniques in steel casting practice.

The field of gating and feeding technology is at present in a state of rapid development. The modulus method due to Chvorinov⁽¹⁾ enables a deep, scientific insight to be obtained into the processes occurring during solidification, which, in combination with the latest results of research in many directions, such as the use of exothermic pads, has led to a revolution in feeding techniques.

Parts of the original manuscript (in German) of this book are already more than 15 years old. For this reason the English edition has been thoroughly revised and supplemented so as to bring it in line with the most recent developments.

As with all sciences, knowledge of this subject is never complete. However, the author hopes that he has been able to explain and illustrate the underlying theory in intelligible language, and to stimulate further development work.

Special acknowledgments are due to the publishers for the excellent translation and presentation of this book, and also to the firm of Sulzer Bros. Ltd. of Winterthur, Switzerland, for their kindness in supplying such a large number of illustrations.

R. WLODAWER

FROM THE INTRODUCTION TO THE FIRST EDITION

MANY excellent papers on feeding techniques have already been published; unfortunately most of them are scattered over many sources. For this reason well-established knowledge will be found here, as well as new information. For the sake of clarity this book will be based on the “classical” solidification theory of Chvorinov⁽¹⁾, who was the first to introduce the concept of “directional solidification”; in this he was at least twenty years before his time, and he anticipated a great deal of knowledge which today is often described as “new”—unfortunately in many instances without any acknowledgement to Chvorinov.

The author is particularly grateful to *Verein Deutscher Gießereifachleute* and to the *Wirtschaftsverband Gießereiindustrie* for their support in the publication of this book. With its publication it is hoped that a gap in the foundry industry will be filled. The author wishes success to all his readers in working through the book and putting its lessons into practice.

THE AUTHOR

Werth bei Stolberg
(Rheinland)

INTRODUCTION TO THE ENGLISH
EDITION

IMPORTANT FOR PRACTICE

*Please read first!***1.1. The Technical Side of This Book**

The quality demands made on castings have increased sharply in recent years and are becoming still more stringent. Foundries are faced by the need to produce high-grade castings, but nonetheless to produce them economically. To do this, experimental castings, especially for individual castings or small runs before mass production, are uneconomical.

Methods were therefore developed of analysing in a simple manner the physical processes occurring during the solidification of castings, and then applying the appropriate practical measures. These methods stem from Chvorinov⁽¹⁾ who was the first to answer the basic question: How long does it take for a casting, or a given part of a casting, to solidify?

This method enables the feeding conditions in the casting to be determined with more certainty; this in turn results in less scrap, fewer repairs to castings, a more punctual timetable and economies in liquid metal.

The method can be used, for example, to calculate external and internal chills, exothermic materials, cooling and insulating mould materials, etc. by the simplest method.

By the term "modulus" is meant the ratio:

$$\text{Modulus} = \frac{\text{volume}}{\text{cooling surface area}}$$

Many people fight shy of calculating volumes and areas, and consider the computation of the modulus to be time-consuming. This view has even led to the substitution of other—supposedly simpler—methods.

However, it will be shown in this book that the modulus technique, after further development, is simple in conception, requires no additional calculation in many cases, and can be interpreted from diagrams.

Even with apparently intricate castings the foundryman can always tackle the problem in terms of simple volumes and cooling surfaces so that the modulus method is a perfectly reliable guide.

In recent years, very vigorous development has taken place in the field of steel casting technology, a development which is still continuing, especially in the case of exothermic materials. For this reason a great deal of new material is included in the present edition. The author is indebted to several firms, particularly to Sulzer Bros. Ltd. of Winterthur, Switzerland, for releasing material

for the relevant illustrations. Numerous illustrations show very clearly the almost incredible possibilities existing in the field of steel casting production.

It is important to know, not only how castings can be made satisfactorily, but also the reason for poor results. A great deal of space therefore is devoted to the description of defects. It is true that many defects have nothing to do with "new methods" but have always occurred. Here also the numerous illustrations will simplify the text for reference purposes. The author thanks the publishers for their sympathetic consideration of his requests for illustrations.

1.2. The Psychological Side of This Book

Steel founding, as shown here, can be taught and learned. It is psychologically understandable that many practical men, some of whom have twenty, thirty or forty years experience behind them, treat new methods with distrust.

This attitude is completely unjustified. An old foundryman once confessed to the author "Since I got to know Chvorinov's method, many problems which I had been pondering over for years have suddenly become clear to me." Can any foundryman claim honestly that he is never confronted by problems which require reflection?

For this reason the book is written in easily comprehensible language, and has two facets: all sections which are of importance for the practical foundryman are headed IMPORTANT FOR PRACTICE. The theoretical foundations for these sections are kept separate. These theoretical sections are intended for the casting designer and for students; if the practical man does not read them, the book will still remain comprehensible. It is certainly not a "Sunday lecture", but must be worked through. With this in mind, the book has been provided with an unusually large number of practical examples, many of which have been worked out in detail.

The numerous aids which are to be found here should serve primarily as work preparation. "Work preparation" signifies *previous* consideration of what can happen *afterwards*. Scrap is usually found afterwards, and this is expensive. It is always cheaper to do some basic thinking beforehand, rather than cast scrap either once or even several times in succession.

Preparation takes time. "I haven't got the time to

spare" is a poor argument in view of the danger of casting scrap. *Who* takes this time, whether a separate department (in large concerns) or the foreman (in small foundries) is immaterial; it only matters that someone *does* take the time.

With all good wishes for your success in making use of the possibilities outlined in this book!

Winterthur, Switzerland

THE AUTHOR

September 1962

CHAPTER 2

THE INFLUENCE OF SHAPE AND DIMENSIONS ON THE TIME TAKEN FOR CASTINGS TO SOLIDIFY

2.1. Why Does a Casting Solidify? The Solidification Modulus

IMPORTANT FOR PRACTICE

If 10 kg (Fig. 1) of steel is cast, first as a sphere and

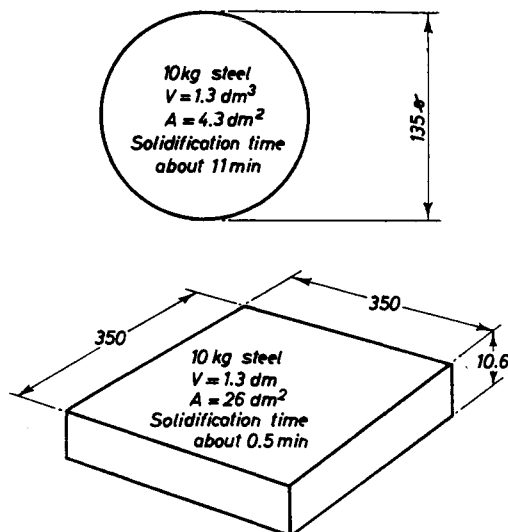


FIG. 1. Comparison of the solidification behaviour of a steel sphere and a plate of the same weight.

then as a thin plate, the plate will solidify much faster than the sphere. This is obviously because the heat contained in 10 kg ($\approx 1300 \text{ cm}^3$) is given off over a much larger surface area in the case of the plate, i.e. the larger the heat-emitting surface associated with a given volume, the faster the solidification. (A good example is the increased surface offered by the cooling fins on a motorcycle cylinder.) Chvorinov⁽¹⁾ was the first to introduce the ratio volume/surface area into the solidification calculation; we will name this ratio the "modulus".

A stepped wedge (Fig. 2) solidifies first at the thinnest step because its modulus is less than that of the next

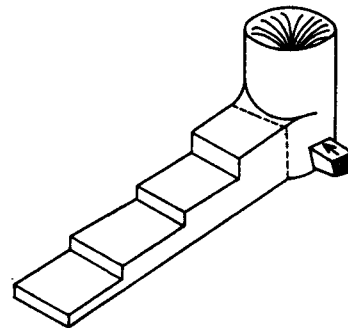


FIG. 2. Stepped wedge.

step 2. The thicker step 2 serves as a feeder for the thinner one and "nourishes" it. Step 2 is in turn fed by step 3, and so on, the last step being supplied with metal by the feeder head. Thus the feeder head supplies steel to the whole of the wedge by way of the individual steps, thereby providing metal to compensate for shrinkage cavities.

We have divided the stepped wedge into imaginary separate parts, and determined the appropriate solidification ratio—i.e. the modulus—of each step. The science of casting calculations is based on the subdivision of complex parts into simple basic components; the ratio modulus (M) = volume (V)/surface area (A) is then calculated for each component.

It must be borne in mind that this subdivision is only imaginary. The imaginary interface between two basic components is certainly not a cooling surface, so that it cannot enter in the calculation when determining the surface area.

Two bodies with the same modulus solidify in the same time. A cube as shown in Fig. 3 (length of side 3 cm, $V = (3)^3 = 27 \text{ cm}^3$, $A = 6 \times (3)^2 = 54 \text{ cm}^2$) has the modulus $M = \frac{V}{A} = \frac{27 \text{ cm}^3}{54 \text{ cm}^2} = \frac{1}{2} = 0.5 \text{ cm}$; in other words a volume of 1 cm^3 is associated with a surface area of 2 cm^2 , from which the heat content of 1 cm^3 of steel can be conducted away. This cube solidifies in the same

spare" is a poor argument in view of the danger of casting scrap. *Who* takes this time, whether a separate department (in large concerns) or the foreman (in small foundries) is immaterial; it only matters that someone *does* take the time.

With all good wishes for your success in making use of the possibilities outlined in this book!

Winterthur, Switzerland

THE AUTHOR

September 1962

CHAPTER 2

THE INFLUENCE OF SHAPE AND DIMENSIONS ON THE TIME TAKEN FOR CASTINGS TO SOLIDIFY

2.1. Why Does a Casting Solidify? The Solidification Modulus

IMPORTANT FOR PRACTICE

If 10 kg (Fig. 1) of steel is cast, first as a sphere and

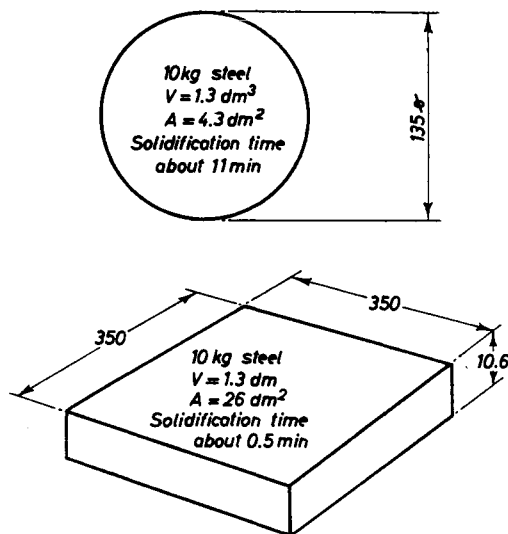


FIG. 1. Comparison of the solidification behaviour of a steel sphere and a plate of the same weight.

then as a thin plate, the plate will solidify much faster than the sphere. This is obviously because the heat contained in 10 kg ($\approx 1300 \text{ cm}^3$) is given off over a much larger surface area in the case of the plate, i.e. the larger the heat-emitting surface associated with a given volume, the faster the solidification. (A good example is the increased surface offered by the cooling fins on a motorcycle cylinder.) Chvorinov⁽¹⁾ was the first to introduce the ratio volume/surface area into the solidification calculation; we will name this ratio the "modulus".

A stepped wedge (Fig. 2) solidifies first at the thinnest step because its modulus is less than that of the next

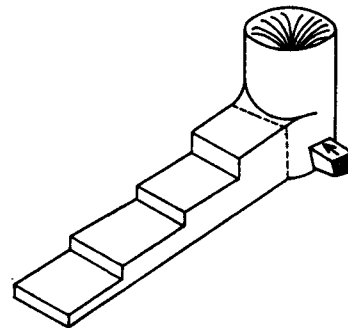


FIG. 2. Stepped wedge.

step 2. The thicker step 2 serves as a feeder for the thinner one and "nourishes" it. Step 2 is in turn fed by step 3, and so on, the last step being supplied with metal by the feeder head. Thus the feeder head supplies steel to the whole of the wedge by way of the individual steps, thereby providing metal to compensate for shrinkage cavities.

We have divided the stepped wedge into imaginary separate parts, and determined the appropriate solidification ratio—i.e. the modulus—of each step. The science of casting calculations is based on the subdivision of complex parts into simple basic components; the ratio modulus (M) = volume (V)/surface area (A) is then calculated for each component.

It must be borne in mind that this subdivision is only imaginary. The imaginary interface between two basic components is certainly not a cooling surface, so that it cannot enter in the calculation when determining the surface area.

Two bodies with the same modulus solidify in the same time. A cube as shown in Fig. 3 (length of side 3 cm, $V = (3)^3 = 27 \text{ cm}^3$, $A = 6 \times (3)^2 = 54 \text{ cm}^2$) has the modulus $M = \frac{V}{A} = \frac{27 \text{ cm}^3}{54 \text{ cm}^2} = \frac{1}{2} = 0.5 \text{ cm}$; in other words a volume of 1 cm^3 is associated with a surface area of 2 cm^2 , from which the heat content of 1 cm^3 of steel can be conducted away. This cube solidifies in the same

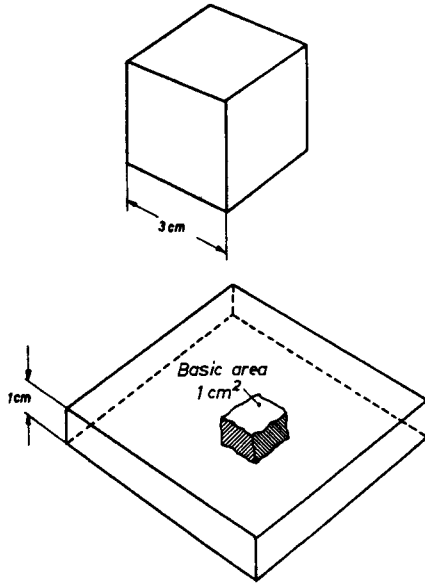


FIG. 3. A cube of 3 cm side and a plate of 1 cm in thickness have the same solidification modulus $M = 0.5$ cm.

time as any other body having the same ratio of volume to surface area.

Very simple reference bodies are provided by large plates, in which the progress of solidification can readily be determined. If we consider a cube cut out of a plate 1 cm thick (Fig. 3), the volume of the cube is 1 cm^3 and its (effective) radiating surface 2 cm^2 . The modulus of this cube is $M = \frac{1 \text{ cm}^3}{2 \text{ cm}^2} = 0.5 \text{ cm}$, so that it will solidify in the same time as the cube with a side of 3 cm. The plate can be considered to be made up of any given number of small cubes, each of which has the same modulus and therefore the same solidification time. Consequently the whole plate will have the same modulus as the cube, i.e. 0.5 cm. The edge of the plate will solidify more rapidly, but if the plate is considered to be very large, the influence of its edges can be neglected.

It is an advantage to carry out the modulus calculations in cm, or in dm for large pieces. Of course the volume and surface area can also be calculated in mm, but very large numbers are obtained, which can easily lead to errors.

The modulus $M = \frac{\text{cm}^3}{\text{cm}^2}$ represents a length, and can therefore be measured with a scale without any calculation, provided that the relationships are known. The plate of 1 cm thickness, mentioned above, has a modulus of 0.5 cm. The modulus of plates is consequently equal to half the plate thickness. The modulus of the cube with a length of 3 cm amounted to 0.5 cm. Hence the modulus of cubes with 6 cooling surfaces is equal to 1/6 of the length of the side. For other fundamental bodies similar simple relationships exist, which make separate calculation almost entirely unnecessary.

It should be pointed out that the modulus calculation can be carried out just as easily in any other unit of measurement, such as the inch.

2.2. The Solidification Time and Modulus of Large Plates

(The later sections intended for the practical man can still be followed if this section is omitted.)

Comprehensive experiments and calculations by Chvorinov⁽¹⁾ showed that the thickness X of the solidified layer after a time T obeys the following law:

$$X = k \sqrt{T} \tag{1}$$

where k is a constant dependent on the metal being cast and on the mould materials. According to the units of measurement selected, the expression for steel cast in sand or fireclay can be written:

$$\left. \begin{aligned} X_{(m)} &= 0.053 \sqrt{T_{(h)}} \\ X_{(cm)} &= 0.684 \sqrt{T_{(min)}} \\ X_{(cm)} &= 0.0885 \sqrt{T_{(sec)}} \\ X_{(mm)} &= 0.885 \sqrt{T_{(sec)}} \\ X_{(in.)} &= 0.273 \sqrt{T_{(min)}} \\ X_{(in.)} &= 0.0354 \sqrt{T_{(sec)}} \end{aligned} \right\} \tag{2}$$

Solidification of the plate is complete when the solidified layers meet in the centre (Fig. 4). The thickness of

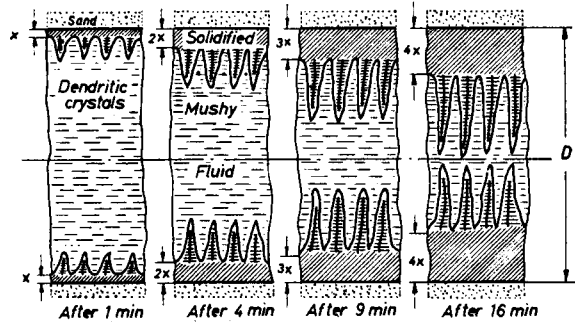


FIG. 4. Progressive growth of the solidified layer in cast steel plates.

Growth of the advancing solidified layer x on a cast steel plate of thickness D as a function of time T

$$x = k \sqrt{T} \quad (k = \text{constant})$$

each solidified layer is equal to half the plate thickness, or in other words the modulus of the plate. According to equation (1)

$$T = \left(\frac{x}{k}\right)^2 \tag{3}$$

If T is the time taken for the plate to solidify, then $X = M$, and

$$T = \left(\frac{X}{k}\right)^2 = \left(\frac{M}{k}\right)^2 = \frac{1}{k^2} \times M^2 = c \times M^2, \tag{4}$$

i.e. the time taken for a body to solidify is equal to the square of the modulus, multiplied by a constant c , which is determined by the mould and metal materials.

This second-order relationship is represented in the log-log diagram (Fig. 5) as a straight line of slope 1 : 2.

1. Plate 10 × 400 × 400 mm
2. Ribs 20 × 150 × 150 mm in plates 30 × 400 × 40 mm, at a distance of 50 mm from the gate
3. At a distance of 100 mm from the gate
4. Round bar, 50 mm diam., centre
5. Plate 30 × 400 × 400 mm
6. Plate 50 × 400 × 400 mm
7. Sphere 153 mm diam. (Briggs)
8. Plate 100 × 400 × 400 mm
9. Cylinder 150 mm diam. × 800 mm
10. Sphere 229 mm diam. (Briggs)
11. Cylinder 200 mm diam. × 800 mm
12. Plate 100 × 800 × 800 mm
13. Cylinder 400 mm diam. × 800 mm
14. Plate 200 × 1500 × 1800 mm
15. Plate 200 × 1800 × 2400 mm
16. Plate 350 × 1800 × 2400 mm
17. Ring gate
18. Feeder for above
19. Bedplate, weight 65 tons

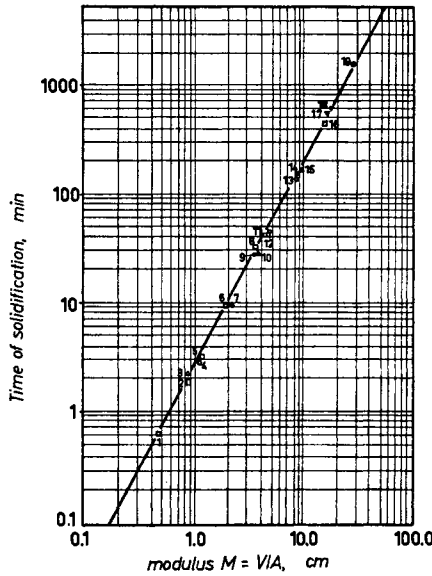


FIG. 5. Relationship of the solidification time of steel castings to the solidification modulus. After Chvorinov⁽¹⁾,

Chvorinov plotted in this diagram the measured solidification times of a large number of castings, so that there can be no doubt that this theory is correct.

Namur⁽⁴⁸⁾ maintained on the basis of a large number of calculations that curved bodies such as spheres solidify more rapidly than plates with an equal modulus. However, this does not apply to steel castings poured at any temperature; this has been demonstrated by the author, who has made numerous measurements under very carefully maintained, constant experimental conditions. This fact is also confirmed by a critical assessment of measurements reported in the literature. Independently of the shape of the steel casting (i.e. sphere, cube, plate, bar, etc.) it is true to say that *bodies with equal moduli solidify in the same time.*

2.3. The Influence of Mould Material and Casting Temperature

On the basis of theoretical calculations Chvorinov⁽¹⁾ had assumed the solidification rate of steel cast in permanent moulds to be four times that cast in sand moulds. He also referred to the cooling effect of other moulding materials, such as magnesite, and made use of them to produce controlled rates of solidification. The importance

of the heat conductance of the moulding material was thus recognized for the first time.

Mould materials with insulating properties act in the reverse direction, by delaying solidification. Even at high casting temperatures the time of solidification will obviously be prolonged. The influence exerted by these materials can be calculated, and this aspect will be treated in detail in Chapter 10.

2.4. The Practical Significance of Simplified Modulus Calculations

IMPORTANT FOR PRACTICE

It has already been mentioned that the modulus represents a length, and can be measured directly in simple basic components, as shown in Table 1.

TABLE 1. SOLIDIFICATION MODULUS OF SIMPLE GEOMETRICAL SHAPES

	<p>Discs of $a < 5d$ Plates of $a < 5d$ imaginary cube removed: $V = 1 \text{ cm}^2 \times d$; $A = 2 \text{ cm}^2$; $M = \frac{V}{A} = \frac{d}{2}$ (cm)</p> <p>As the plate can be considered to be composed of any desired number of such cubes, the plate modulus is $M = \frac{d}{2}$</p>																
	<p>Long bars. Section removed (in imagination) $V = a \times b \times 1 \text{ cm}$; $A = 2(a + b) \times 1 \text{ cm}$; $M = \frac{V}{A} = \frac{(a \cdot b)}{2(a + b)}$. The bar can be considered to be made up of any desired number of such pieces, so that its modulus is the same</p>																
	<table border="1"> <thead> <tr> <th></th> <th>Cube</th> <th>Cylinder</th> <th>Sphere</th> </tr> </thead> <tbody> <tr> <td>V</td> <td>a^3</td> <td>$\frac{a^3 \pi}{4}$</td> <td>$\frac{a^3 \pi}{6}$</td> </tr> <tr> <td>A</td> <td>$6 a^2$</td> <td>$a^2 \frac{\pi}{2} + a^2 \pi$</td> <td>$a^2 \pi$</td> </tr> <tr> <td>$M$</td> <td>$V/A = a/6$</td> <td>$V/A = a/6$</td> <td>$V/A = a/6$</td> </tr> </tbody> </table> <p>The modulus of these three bodies is the same i.e. $M = a/6$</p>		Cube	Cylinder	Sphere	V	a^3	$\frac{a^3 \pi}{4}$	$\frac{a^3 \pi}{6}$	A	$6 a^2$	$a^2 \frac{\pi}{2} + a^2 \pi$	$a^2 \pi$	M	$V/A = a/6$	$V/A = a/6$	$V/A = a/6$
	Cube	Cylinder	Sphere														
V	a^3	$\frac{a^3 \pi}{4}$	$\frac{a^3 \pi}{6}$														
A	$6 a^2$	$a^2 \frac{\pi}{2} + a^2 \pi$	$a^2 \pi$														
M	$V/A = a/6$	$V/A = a/6$	$V/A = a/6$														
	<p>$M = \frac{r \cdot b}{2(r + b)}$ (see also Table 2)</p>																
	<p>$M = \frac{a \cdot b}{2(a + b)}$ (see also Fig. 8)</p>																

It is interesting to note that the moduli for the cube and its inscribed sphere or cylinder are the same, i.e. $a/6$, where a is the length of side or the diameter. This signifies that each of these bodies takes the same time to solidify. It can be imagined that the corners of a cube solidify quickly, leaving a spherical, liquid body.

Many castings, as in Fig. 6, are made up of bars, which

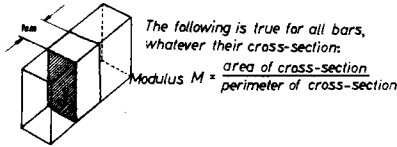
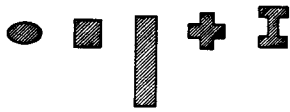
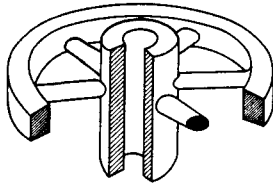


FIG. 6. Very many castings are made up of bars, in which the end cooling surfaces are absent.

either form a closed ring or else have no cooling surfaces at the ends, as they merge into parts of the casting having heavier walls. (Rings, etc. are "semi-infinite" bodies, because although their thickness can be measured, they have neither beginning nor end.) A section of any given size (for example 1 cm long) taken in imagination from this bar, having sides of length a and b , has a volume $V = a \times b \times 1$, and a cooling surface $A = 2 \times 1 \times (a + b)$ (the imaginary surfaces of separation are not included in the calculation) and its modulus is

$$M = \frac{V}{A} = \frac{a b}{2(a + b)} \tag{5}$$

hence $M = \frac{\text{cross-sectional area}}{\text{perimeter of the cross-section}}$

Simple determinations of an area and perimeter are thus substituted for wearisome calculations of volume and surface area. This principle is valid for bars of any given cross-section (cf. equation 41).

The moduli of bars of rectangular section can be read off from Fig. 7 without any calculation at all. The modulus curves are parallel in this log-log diagram.

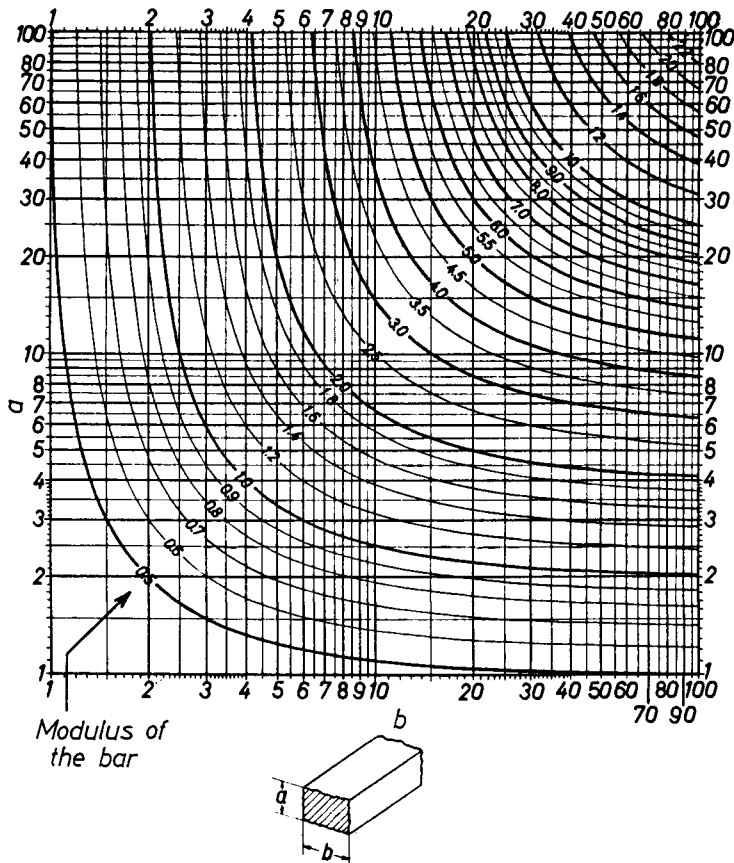


FIG. 7. Determination of the modulus of bars.
 The dimensions of a and b can be given in any required units (cm, in., etc.)

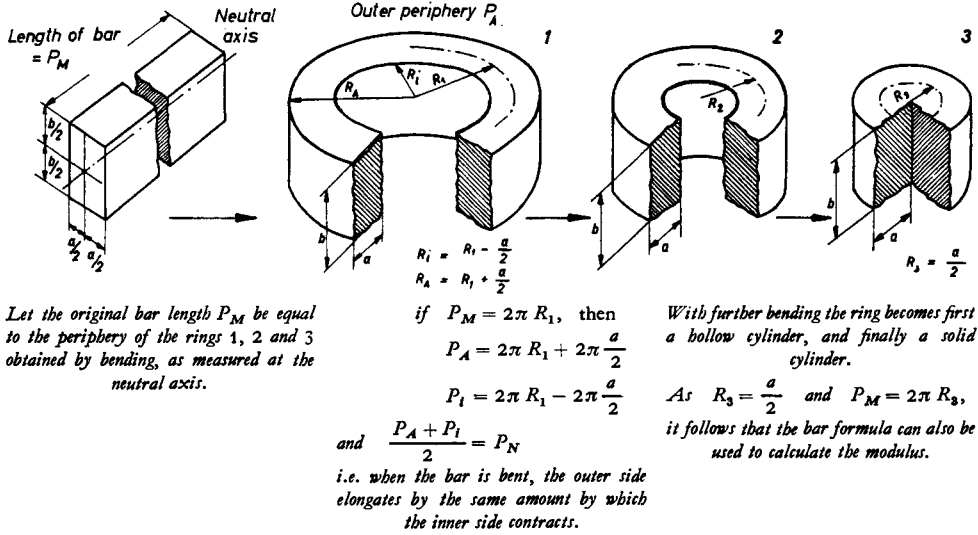


FIG. 8. If an initially straight bar is bent, no change takes place either in the volume or surface area. Consequently the modulus of the bar also remains unaltered.

If a bar is bent round the neutral axis, as in Fig. 8, the total surface area remains unchanged, because the outer curved side increases by the same amount that the inner surface contracts. Rings of all types can thus be determined by the use of equation (5) or Fig. 7.

With further bending the hollow cylinder finally closes up to form a solid cylinder. The bar formula of Fig. 7 can still be applied; this can be seen from Table 2, where the modulus is calculated, first by the bar formula and then by working out in full the ratio volume/surface area.

TABLE 2. CALCULATION OF THE MODULUS OF A SOLID CYLINDER FROM

1. The surface volume/area ratio and
2. The bar formula (equation 5)

1	<p>Volume $V = r^2 \pi b$</p> <p>Surface area $A = 2r^2 \pi + 2r \pi b = 2r \pi (r + b)$</p> <p>Modulus $M = \frac{V}{A} = \frac{r^2 \pi b}{2r \pi (r + b)} = \frac{r \cdot b}{2(r + b)}$</p>
2	<p>Calculation according to equation (5)</p> <p>$M = \frac{a \cdot b}{2(a + b)}$; corresponding to the symbols on the cylinder:</p> <p>$M = \frac{r \cdot b}{2(r + b)}$</p>

Both types of calculation give the same result, but it is simpler to determine the modulus by means of equation (5).

We have still not exhausted the uses to which Fig. 7 can be put. As cubes, parallelepipeds, etc. have the same moduli as the inscribed cylinders, angular bodies can also be considered as cylinders of equal modulus, in accordance with Fig. 9, and their modulus determined. Even when a circle can only be inscribed approximately, this is still true to a fair degree of accuracy.

Many finite bodies with cooling faces can be determined by the bar formula, or can be read off on Fig. 7 without calculation; these two diagrams represent an important aid to the practical man in calculating the modulus, and, as will be shown later, the feeding or riser system.

Bosses with an adjacent wheel disc (Fig. 10) can be conceived as bent bars with a non-cooling surface of width c .

The corresponding formulae are derived in the table incorporated in the diagram. The mean boss diameter D is n times the thickness of the cross-section a . The modulus is therefore, for $D = n \times a$:

$$M = \frac{V}{A} = \frac{a b}{2(a + b) - c \times \frac{n + 1}{n}} \quad (6)$$

From diameters of $D \approx 3$ to $4a$ onwards the boss becomes a ring, and the modulus approximates to:

$$M \approx \frac{a b}{2(a + b) - c} \quad (7)$$

At a diameter $D = \infty$ the ring becomes a bar, and equation (7) then applies accurately.

With bosses which are not bored or with a small hole, $D = a$, i.e. $n = 1$, and equation (6) becomes:

$$M = \frac{a b}{2(a + b - c)} \quad (8)$$

The validity of this equation was verified in Fig. 10 by comparing the result of the calculation using the

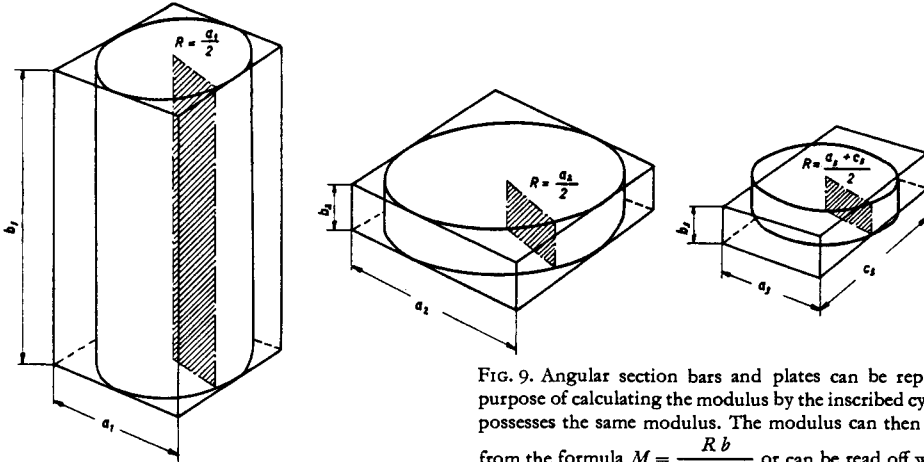


FIG. 9. Angular section bars and plates can be replaced for the purpose of calculating the modulus by the inscribed cylinder, which possesses the same modulus. The modulus can then be calculated from the formula $M = \frac{R b}{2(R + b)}$ or can be read off without calculation from the diagram.

With plates or bars which are not exactly tetragonal, the average of the sides a and c can be taken as the diameter of the circle.

of the heat during the solidification of the steel, and their solidification behaviour is similar to that of the steel casting itself.

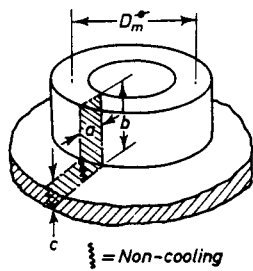
It can be calculated on the basis of the heat balance at a steel temperature of about 1600°C (in accordance with Chapter 7.4) that this is the case for tubular bodies when the ratio of the outside diameter to that of the core is equal to 3.74, or in other words the core diameter must be about 27 per cent of the outside diameter. This value can be less for rings and discs.

If the bore is less than this amount, the tubular body must be calculated as if it were a solid when determining its modulus. Due to the danger of steel penetration and fusion, the core must then consist of a highly refractory mould material or be omitted altogether.

2.5. Further Simplification of the Modulus Calculation by the Use of "Simulation" Bodies—Calculation of Junctions

IMPORTANT FOR PRACTICE

If the beater cross casting (Fig. 11) is resolved into

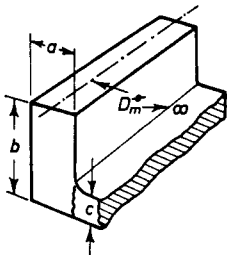


General case: ring casting ending in a wall section c . D_m^∞ is expressed as n times a , i.e. $D_m^\infty = n \cdot a$

$$V = D_m^\infty \cdot a \cdot b \cdot \pi = a^2 b n \pi$$

$$A = 2a^2 \pi n + a \pi (n+1)(b-c) + a \pi (n-1)b = a \pi (2an + 2bn - cn - c)$$

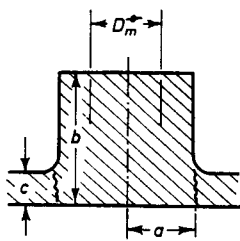
$$M = V/A = \frac{a b n}{2an + 2bn - cn - c} = \frac{a \cdot b}{2(a+b) - c} \cdot \frac{n+1}{n} \quad (6)$$



Limiting case 1: $D_m^\infty \rightarrow \infty$; the ring becomes a bar.

$$\frac{n+1}{n} = \frac{\infty+1}{\infty} \rightarrow 1$$

$$M \rightarrow \frac{a \cdot b}{2(a+b) - c} \quad (7)$$



Limiting case 2: $D_m^\infty \rightarrow a$; the ring becomes a solid cylinder.

$$D_m^\infty = a = n \cdot a; n = 1$$

$$\frac{n+1}{n} = 2$$

$$M = \frac{a \cdot b}{2(a+b) - 2c} = \frac{a \cdot b}{2(a+b-c)} \quad (8)$$

Note carefully the different positions of the brackets in equations 7 and 8.

FIG. 10. Calculation of the moduli of bosses, lugs, etc., ending in a wheel disc or housing wall.

ratio volume/surface area. This equation is used frequently in lugs, discs, etc. as well as bosses. **The different positions of the brackets in equations (7) and (8) will be noted.**

In the case of massive ring-shaped bodies with a small bore, the core can contain such a high proportion of the superheat of the steel that the core has reached a temperature of 1450 to 1480°C by the time the steel begins to solidify, i.e. the parts of the core heated up in this way are unable to take up the corresponding part

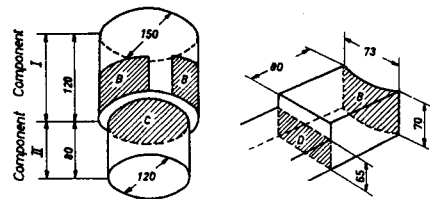
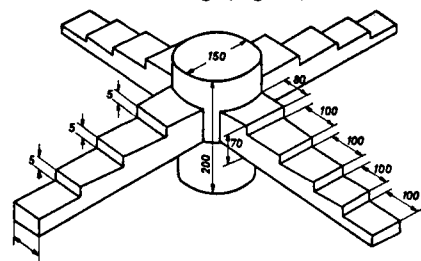


FIG. 11. Worked example of the determination of the modulus of a beater cross casting made from wear-resisting steel. (See also the attached table.)

Auxiliary Table to Fig. 11

Modulus calculations for the separate basic components of the beater cross casting. The calculation is begun at the end of the thinnest step and is continued in the direction of the boss.

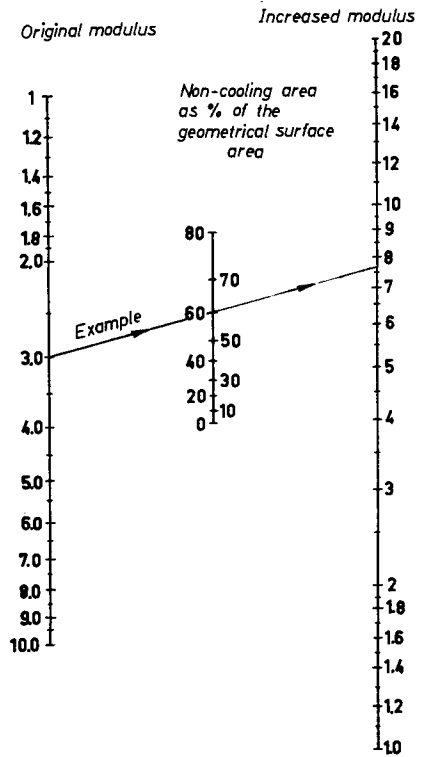
Component	Volume (cm ³)	Surface area (cm ²)	Modulus (cm)
VII	$V = 7.3 \cdot 10 \cdot 5.0$ = 365	$A = 2 \cdot 7.3 \cdot 10$ $+ 2 \cdot 5 \cdot 10$ $+ 7.3 \cdot 5$ 282	$M = \frac{365}{282}$ = 1.29
VI	$V = 7.3 \cdot 10 \cdot 5.5$ = 401	$A = 2 \cdot 7.3 \cdot 10$ $+ 2 \cdot 5.5 \cdot 10$ $+ 0.5 \cdot 7.3$ 260	$M = \frac{401}{260}$ = 1.54
V	$V = 7.3 \cdot 10 \cdot 6.0$ = 438	$A = 2 \cdot 7.3 \cdot 10$ $+ 2 \cdot 6 \cdot 10$ $+ 0.5 \cdot 7.3$ 270	$M = \frac{438}{270}$ = 1.57
IV	$V = 7.3 \cdot 10 \cdot 6.5$ = 475	$A = 2 \cdot 7.3 \cdot 10$ $+ 2 \cdot 6.5 \cdot 10$ $+ 0.5 \cdot 7.3$ 280	$M = \frac{475}{280}$ = 1.70
III	$V = 7.3 \cdot 8 \cdot 7$ = 410	$A = 2 \cdot 7.3 \cdot 8$ $+ 2 \cdot 7 \cdot 8$ $+ 0.5 \cdot 7.3$ 233	$M = \frac{410}{233}$ = 1.75
II	Based on the mean cylinder 130 mm \varnothing , 200 mm h	$A = 13^2 \cdot \pi \cdot 2$ 4	$M = \frac{2650}{881}$
I	$V = 13^2 \cdot 20 \cdot \frac{\pi}{4}$ = 2650	$+ 13^2 \cdot \pi \cdot 2$ $- 4 \cdot \text{Surface } B = 4 \cdot 7.3 \cdot 6$ 833	$M = \frac{881}{3}$ = 3.0

The branch components III to VII were calculated accurately in this instance, but bar formula (5) would be adequate in practice, for example for component V; $M \approx \frac{7.3 \cdot 6}{2 \times (7.3 + 6)} = 1.65$ cm

basic components, the "boundary surfaces" cannot enter into the calculation, as they are only imaginary. Nonetheless, the diagram of Fig. 7 can still be utilized in such cases, when the actual cooling surface is now only a fraction of the original geometrical surface, i.e. the modulus increases. The nomogram in Fig. 12 shows these changes of modulus. After some practice the proportion of "non-cooling surface" can be estimated (with the help at first of the table in Fig. 12).

As angular bodies and the round figures inscribed in them have the same modulus, they represent mutual "simulation" bodies, and either can be used for the calculation if any advantage is thereby obtained in computation. For example, the complicated bearing component of the housing shown in Fig. 13 can be circumscribed by a simple parallelepiped as a simulation. The size of this figure can easily be determined either from the drawing or, better still, from the pattern. The modulus is read off directly from the diagram of Fig. 7 and corrected from Fig. 12, as the parallelepiped adjoins other

FIG. 12. Increase in the modulus with reduction in the cooling surface area.



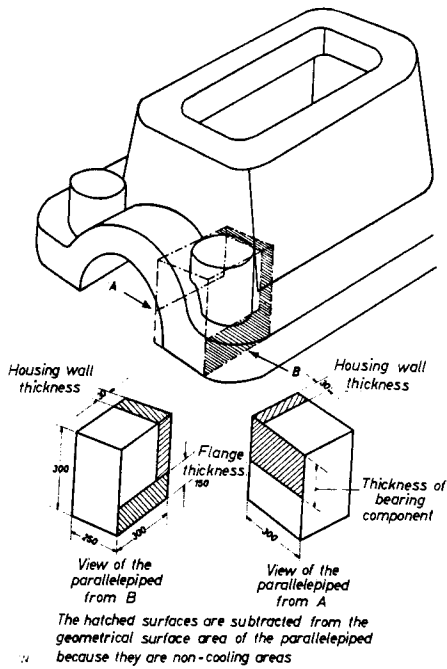
Sketch	Ratio of edges	Total surface area	Surface A ~%	Surface B ~%
	1 x 1 x 1/2		25	12.5
	1 x 1 x 1		17	—
	1 x 1 x 2		10	20
	1 x 1 x 3	100 *	7	22
	1 x 1 x 5		5	23

Auxiliary Table to Fig. 12. Estimation of the non-cooling surfaces of parallelepipeds or parallelepiped-shaped simulation bodies.

cross-sections. Even if the somewhat more complicated calculation of volume/surface area is preferred to Fig. 7 in such cases, the determination of the modulus of a parallelepiped is very simple.

The method of using simplified equivalent shapes is a technique of the greatest practical importance, and

FIG. 13. Determination of the modulus of the bearing component of a housing by circumscribing a simple parallelepiped round the complicated surface shape. (For further examples of the calculation of simulation bodies see Figs. 125, 126 and 127.)



enables numerous problems to be solved without the costly process of "trial and error" (i.e. without the production of foundry scrap), such as:

Is a casing wall heavy enough to feed a heavier section without forming a shrinkage cavity?

Is it necessary to place a feeder on a thicker section, or is this enlargement of section only apparent?

How thick must the dividing wall of a valve be made to feed the valve seating satisfactorily?

The method is an aid to the designer as well as the foundryman (see, for example, Figs. 125, 126a, 126b (page 61) and 127 (page 68)).

Irregular circular cross-sections can be replaced approximately by a rectangle, as in Fig. 14, and then determined from Fig. 7. It is only necessary to determine the adjacent cross-sections separately when they vary too greatly from one another.

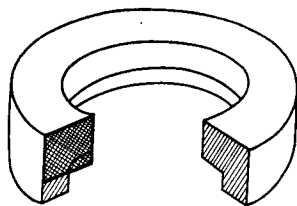


FIG. 14. Provided that a cross-section is not too irregular, a rectangle or quadrilateral can be drawn in, and its modulus read off directly from Fig. 7.

A circle is first inscribed at the intersections (which occur very frequently), as shown in Fig. 15. In crossed plates this circle gives the thickness of an equivalent plate with the same time of solidification as the intersection. The radius of the circle is therefore the required modulus. With crossed bars the inscribed cylinder determines the equivalent bar with the same modulus, which can be read off from Fig. 7. This method is not theoretically accurate, but is sufficiently so for practical purposes.

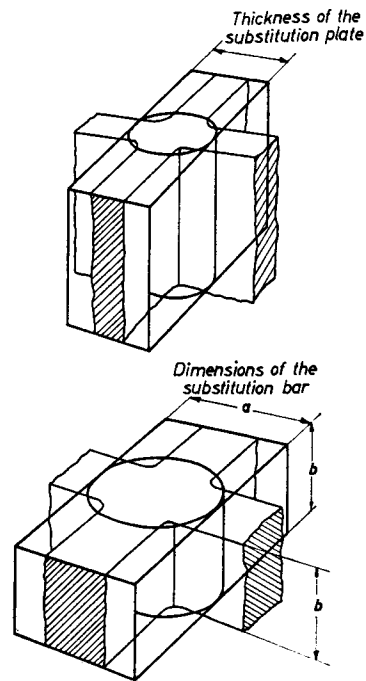


FIG. 15. Determination of the modulus of junctions, using simulations.

(a) Two intersecting plates: The circle inscribed in the junction gives the thickness of a substitution plate having approximately the same modulus as the junction.

$$\text{radius of circle} = \text{modulus}$$

(b) Two intersecting bars: The circle inscribed in the junction gives the dimensions of a substitution bar having approximately the same modulus

$$\text{as the junction } M = \frac{a b}{2(a + b)}$$

(can also be read off directly from Fig. 7 (circle)).

The accumulation of heat in fillets increases with rising casting temperature. It is sufficient in practice to make an estimate of this influence. The procedure is basically as follows.

Draw the intersection on a scale of 1:1. Estimate the sand fillet effect, based on the casting temperature. When this has been done, and only then, draw the inscribed circle which determines the modulus.

In most cases, however, it is sufficient to draw a fillet radius of $r \approx w/3$, and place the inscribed circle on this radius. Examples are shown in Figs. 16, 17 and 18.

FIG. 16. Determination of the junction modulus of a cover casting.

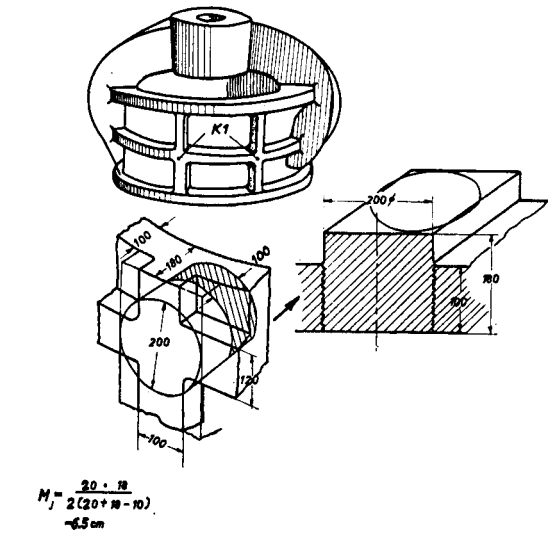
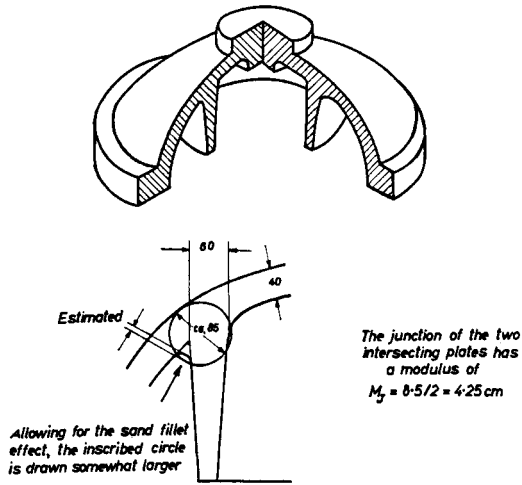


FIG. 17. Determination of the junction modulus of the strengthening web of a breaker shell casting.

The junction consists of the intersection of two bars with a plate. It has approximately the same modulus as a substitution bar with a section $200 \times 180 \text{ mm}$, but has two non-cooling faces (the interfaces at plate 100).

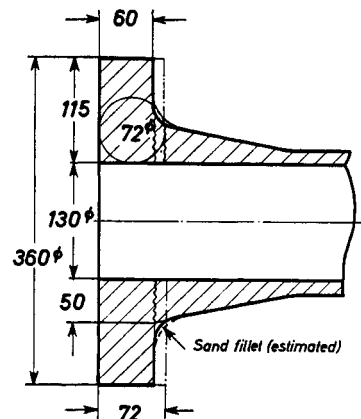


FIG. 18. Determination of the junction modulus of a flange.

The junction has approximately the same modulus as a substitution bar 72×115 , with a non-cooling face 50.

$$M_j = \frac{7.2 \times 11.5}{2(7.2 + 11.5) - 5} = \frac{82.8}{32.4} = 2.55 \text{ cm}$$

FIG. 19. Increase of solidification times in junctions.

Increase of solidification time in the junction, compared with a plate of wall thickness w .

Ratio d/w .

Note that the inscribed circle in this diagram is tangential to the geometrical corners, and no allowance is made for the heated sand fillets.

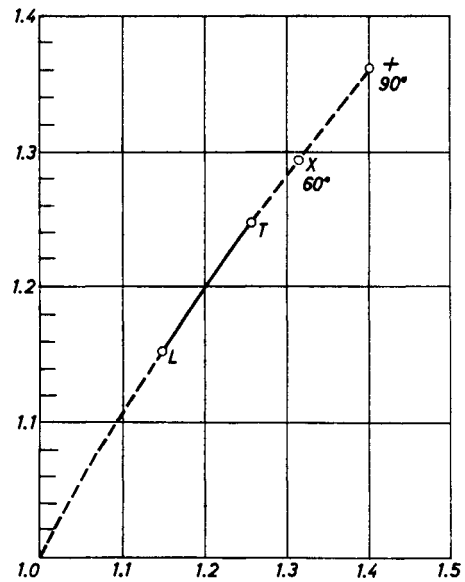
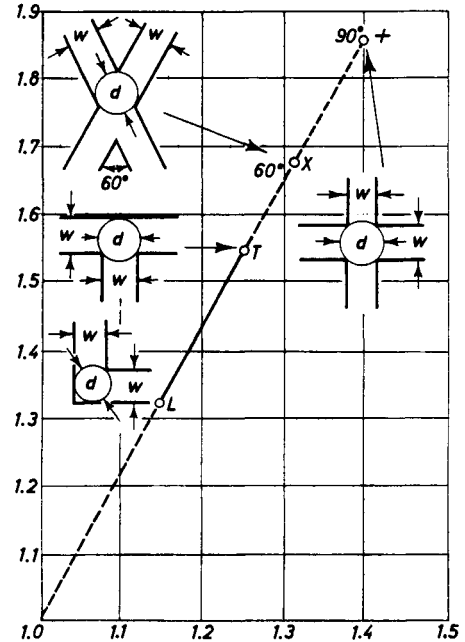


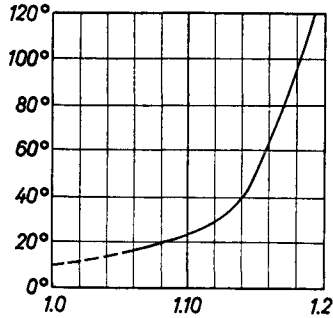
FIG. 20. Increase of modulus at junctions.

Increase of modulus at the junction, compared with the modulus of a plate of wall thickness w .

Ratio d/w .

FIG. 21. Increase in the modulus of an L-junction compared with the modulus of a flat plate of equal thickness.

Superheat above the liquidus °C.
Enlargement factor of the junction compared with a flat plate.



The results of solidification measurements at intersections † are reproduced in Fig. 19, which is valid for steel containing ~0.35% C. Figure 20 is derived from this diagram; it gives the corresponding modulus values for the intersections. It must be noted in both these diagrams that the geometrical corners are tangential to the inscribed circle, so that no allowance was made for the heating effect in the sand fillet. However, this effect can be significant, and this is discussed in more detail in Chapter 10.

2.6 Practical Examples of Modulus Calculations
IMPORTANT FOR PRACTICE

As the whole range of casting and feeder calculation is based on the determination of the modulus, the reader should attempt to work out some modulus calculations himself, using Figs. 22 to 34. The solutions obtained should be compared only when the results are all available. As soon as a certain amount of practice has been

† Brandt, F. A. and H. F. Bishop: Solidification at corner and core positions. *Trans. American Foundryman's Society*, 1953, 451-456.

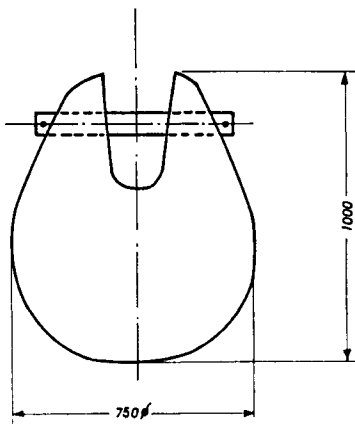


FIG. 22. Tup.

The tup corresponds to a sphere, as a close approximation

$$M_{\text{sphere}} = \frac{D}{6}, \text{ so } M = \frac{75}{6} = 12.5 \text{ cm.}$$

obtained in carrying out the processes of breaking down the casting into simple basic components, and simplifying the work as far as possible by constructing equivalent bodies or sections, it will be found that the modulus calculation itself will have become very simple.

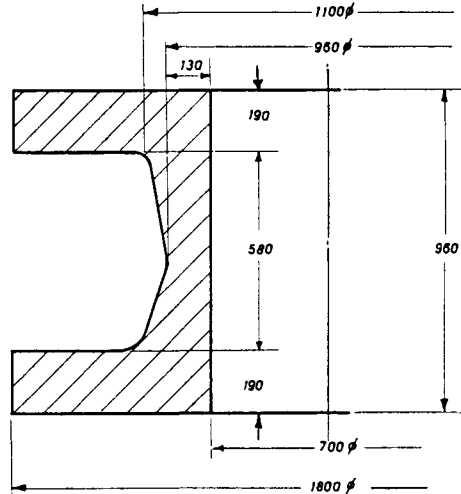


FIG. 23. Double flange.

Draw the junction 1 : 1 and inscribe a circle of about 240 mm diameter. Calculate the flange as a substitution bar 240 × 550 mm with a non-cooling surface of about 220 mm.

$$M = \frac{55 \times 24}{2(55 + 24) - 22} = 9.65 \text{ cm.}$$

Calculation of the central portion: trapezoidal bars; the boundary surfaces at the flange and in the centre are non-cooling surfaces.

$$\text{surface area} = \frac{22 + 13}{2} \times 29 = 508 \text{ cm}^2$$

$$\text{periphery} \approx 29 + 30 = 59 \text{ cm}$$

$$M = \frac{508}{59} = 8.62$$

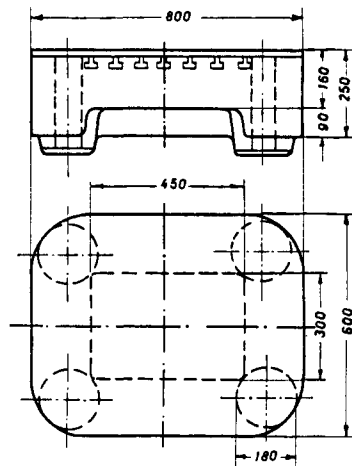


FIG. 24. Press plate (measurements include machining allowances). Rapid calculation (approximate): Imagine the plate to be square, 700 × 700 mm, with a mean thickness of 180 mm (estimated). Calculate as in Fig. 7 for a simulation cylinder R = 35; H = 18; M = 6.1 cm. Accurate calculation (the T-slots with an obviously smaller modulus and the radiusing were not taken into account).

$$\text{Volume } V = (80 \times 60 \times 25) - (45 \times 30 \times 90) = 107\,800 \text{ cm}^3$$

$$\text{Surface area } A = (2 \times 8 \times 60) + 2(80 + 60) \times 25 + 2 \times 9(45 + 30) = 9600 + 7000 + 1350 = 17,950 \text{ cm}^2$$

$$M = V/A = 6.0 \text{ cm.}$$

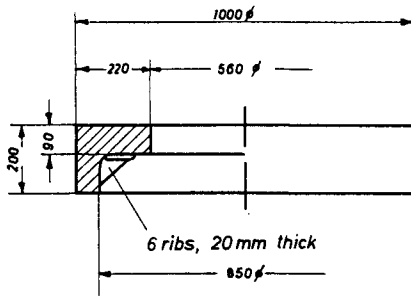


FIG. 25. Gear rim (the dimensions include machining allowances.)

Rapid calculation: extend the section to a bar 345 mm wide and with an average height of ~83 mm, $M = 3.6$ cm from Fig. 7.

Accurate calculation: determine the modulus of the heaviest section, allowing for the non-cooling surface:

$$M = \frac{22.9}{2(22 + 9) - 7.5} = \frac{198}{54.5} = 3.63 \text{ cm.}$$

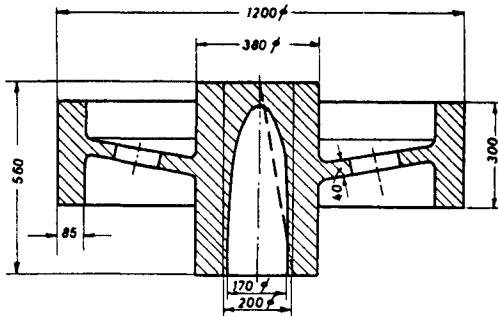


FIG. 26. Gear blank.

Draw the intersection disc/rim = 1:1, and inscribe a circle ~100 mm diam. The simulation bar of the rim has the dimensions 10 × 30, and $M = 3.8$ cm from Fig. 7. The hub cylinder is generated from a rotating

trapezoidal surface (broken line) $M = \frac{\text{area}}{\text{periphery}} \frac{\text{area}}{\text{trapez}} = \frac{19 + 9}{2} \times 56 = 784 \text{ cm}^2$;

periphery = 56 + 18 + ~56 + 9 = 141 cm.

$M = 5.56$ cm.

The wheel disc is a plate, with a modulus $M = \frac{d}{2} = \frac{4.0}{2} = 2$ cm.

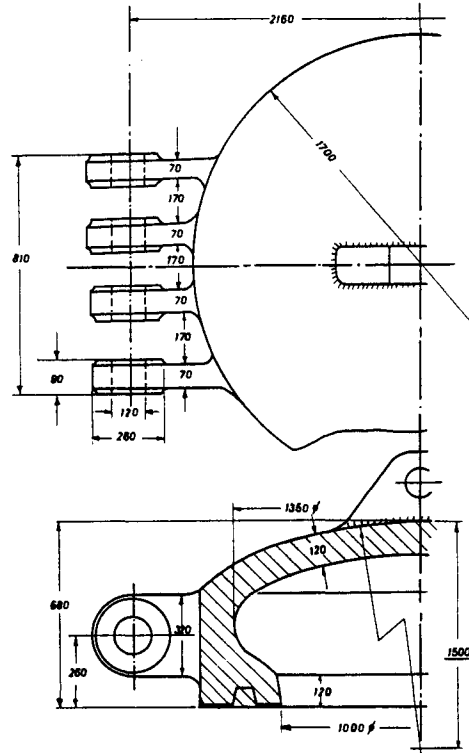


FIG. 27. Autoclave cover.

Bottom: curved plate, $M = \frac{d}{2} = \frac{12}{2} = 6$ cm. — Flange: bar with trapezoidal section 26 × 35, non-cooling surface ~12.0.

$A = \frac{35 + 2.5}{2} \times 26 = 618 \text{ cm}^2$; $P = 26 + 35 + 12 + \sim 23 = 96$ cm

$M = A/P = 6.4$ cm. — Hinge: bar 7 × 32, from Fig. 7

$M = 3$ cm. — Lugs on the hinges: bar 7 × 9, from Fig. 7
 $M = 2.0$ cm.

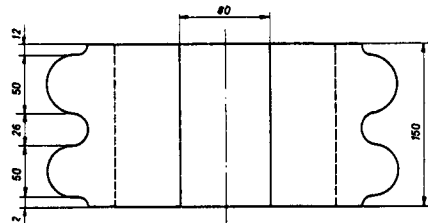
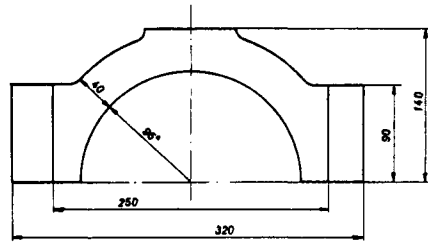


FIG. 28. Bearing cap.

Middle section (extends as far as the re-entrant corners). Bar 4.0 × 15.0 cm²; from Fig. 7 $M = 1.6$ cm. Corner section: simulation figure parallelepiped 6 × 9 × 15, interface with the middle section is subtracted as a non-cooling surface; $V = 810 \text{ cm}^3$; $A = 498 \text{ cm}^2$; $M = V/A = 1.62$ cm. Hint: In these and similar castings the modulus of corner sections, reinforcement ribs, lugs, etc. is frequently less than the modulus of the wall, in spite of first impressions to the contrary. This can be explained by the cooling of the corner section from three sides.

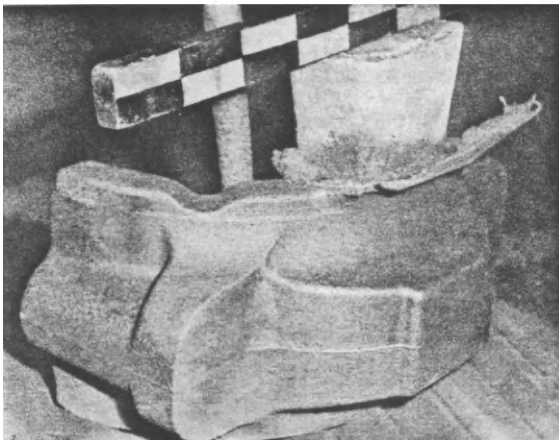
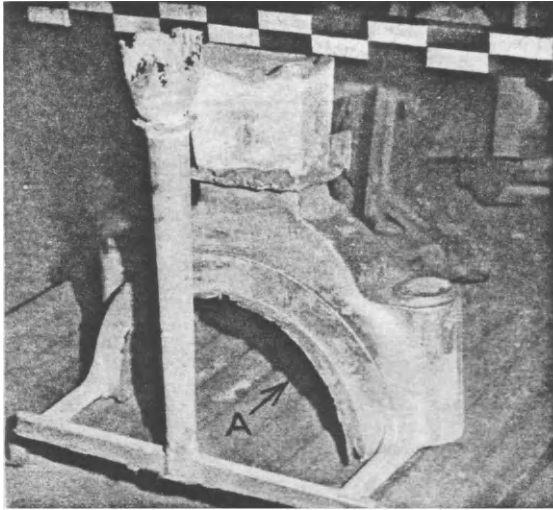


FIG. 28a. Practical example of a bearing cap as in Fig. 28. The modulus calculation has shown that the massive parts can be fed through the rectangular cross-section at *A*. If the modulus of the massive parts is somewhat too large for this to be done, this method can still be employed. (See Figs. 28b and c.)
(Courtesy Sulzer Bros.)

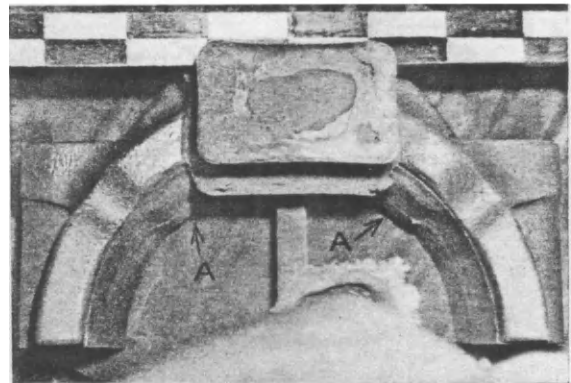
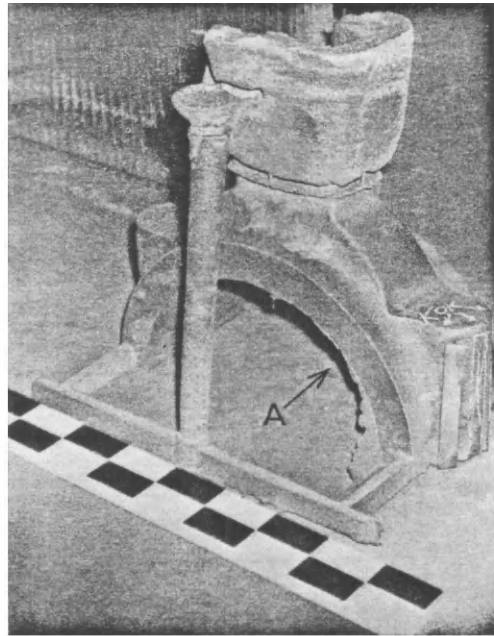


FIG. 28b. If the modulus of the massive parts is a little too large to feed it through the rectangular section, this section can be increased slightly by a shoulder at *A*.

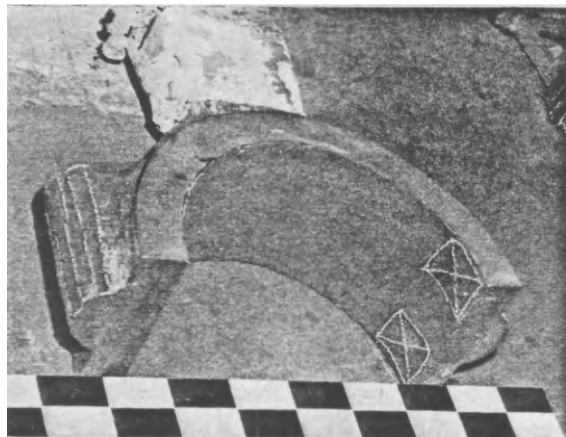
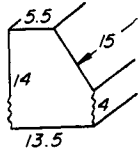


FIG. 28c. If the modulus of the massive parts is too large, they can be cooled by chills, so that the rectangular cross-section at *A* will be adequate for feeding.

FIG. 29. Bearing block.

Draw the block 1:1 and inscribe a trapezoidal simulation body in one half. Determine volume and surface area, allowing for non-cooling surfaces;



$$V = 2000 \text{ cm}^3; A = 911 \text{ cm}^2; M = V/A = 2.2 \text{ cm.}$$

Second alternative: Inscribe in the half section a circle of about 120 diam. The simulation cylinder so obtained, 120 diam. \times 150 high, has approximately the same modulus as the centre of mass; for $R = 6$, $H = 15$, Fig. 7 gives a modulus $M = 2.2$ cm. The fixing lug is a parallelepiped $7 \times 4.5 \times 15$ cm. Interface with the trapezium is a non-cooling surface.

$$V = 472 \text{ cm}^3; A = 330 \text{ cm}^2; M = 1.43 \text{ cm.}$$

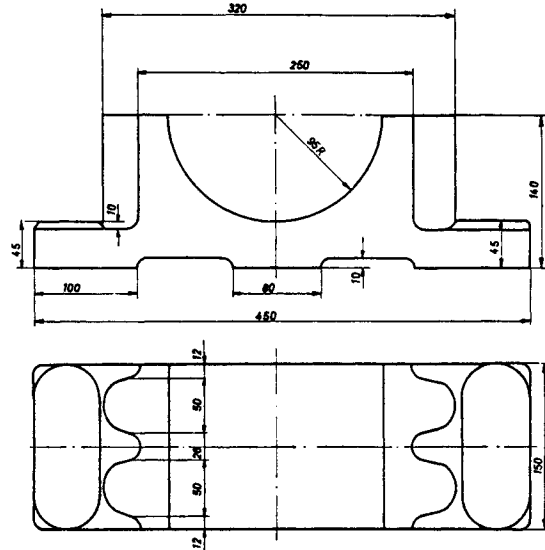
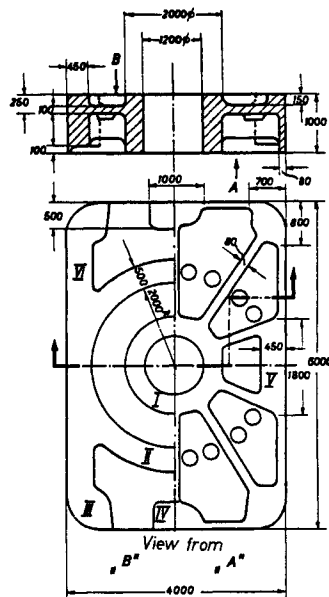
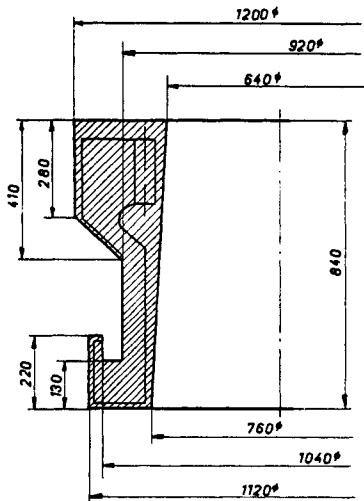


FIG. 30. Flange coupling.

Trapezoidal upper portion: $A = \frac{41 + 28}{2} \times 28 = 960 \text{ cm}^2$; $P = 28 + 41 + 28 + \sim 13\sqrt{2} = 115.4$ cm. Interface with the middle portion is a non-cooling surface. $M = A/P = 8.31$ cm. Middle portion: plate about 130 thick; $M = d/2 = 6.5$ cm. Lower portion: inscribe a circle, allowing for the sand fillet (estimated). Circle diameter ≈ 18 cm. The simulation bar (18×14.5 cm) has a non-cooling surface with the middle section, $A = 261 \text{ cm}^2$, $P = 18 + 14.5 + 14.5 + 10 = 57$ cm. $M = A/P = 4.58$ cm. Sufficient allowance is made for the small rim.

FIG. 31. Base plate.

Zone subdivision I to VI.

I. Bar 40×100 cm. Fig. 7, $M = 20$ cm.

II. Circular ring seat, interfaces with the plate are non-cooling surfaces;

$$M = \frac{25 \times 50}{2(25 + 50 - 10)} = 9.6 \text{ cm.}$$

III. Lug. Simulation body: parallelepiped $70 \times 80 \times 90$; $V = 504,000 \text{ cm}^3$, $A_{\text{tot}} = 2(70 \times 80 + 70 \times 90 + 80 \times 90) = 38,200 \text{ cm}^2$. Non-cooling surfaces: outer walls + ribs = $90 \times 8 \times 3$ and plate = $(70 + 80) \times 10$, total 3660 cm^2 . $A = 38,200 - 3660 = 34,540 \text{ cm}^2$. $M = V/A = 14.5$ cm.

IV. Lug. Simulation body: parallelepiped $100 \times 50 \times 90$ cm. Rapid determination as a cylinder 95 diam. ($R = 47.5$), $H = 50$ cm. $M = 12.5$ cm from Fig. 7.

V. Strengthening rib: Bar $45 \times 90 \times 180$. $V = 738,000 \text{ cm}^3$. $A_{\text{tot}} = 2(45 \times 90 + 45 \times 180 + 90 \times 180) = 62,700 \text{ cm}^2$. Non-cooling surfaces: outer walls + ribs: $8 \times 90 \times 4 = 2880 \text{ cm}^2$. Plate: $(45 + 180) \times 10 = 2250$. $A = A_{\text{tot}} - \text{non-cooling surfaces} = 57,570 \text{ cm}^2$. $M = V/A = 12.8$ cm.

VI. Seat. Bar 25×45 ; non-cooling surfaces at outer wall and plate.

$$M = \frac{25 \times 45}{2(25 + 45) - 8 - 10} = 9.25 \text{ cm.}$$

FIG. 32. Gate valve housing.

Zone subdivision:

Circular flange: bar 10×21 cm, 9 cm^2 non-cooling surface; draw the intersection, inscribed circle 13 cm diam.; simulation bar 13×21 cm.

$$M = \frac{13 \times 21}{2(13 + 21) - 9} = 4.65 \text{ cm.}$$

Oval flange: intersection circle 10 cm diam.; non-cooling surface 5 cm^2 ; simulation bar 10×14 cm. $M = \frac{10 \times 14}{2(10 + 14) - 5} = 3.25 \text{ cm.}$

Valve body: plate 5 cm thick; $M = d/2 = 2.5 \text{ cm.}$

Intersection valve body/seating: inscribed circle 7 cm diam. Represent by two crossed plates, simulation plate 7 cm thick, $M = d/2 = 3.5 \text{ cm.}$

Intersection valve body/external ribs: inscribed circle about 5.5 cm , $M = d/2 = 2.75 \text{ cm.}$

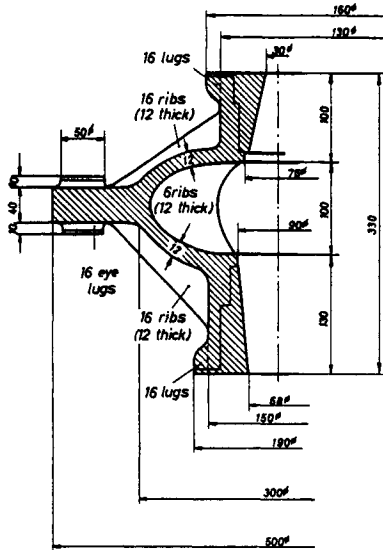
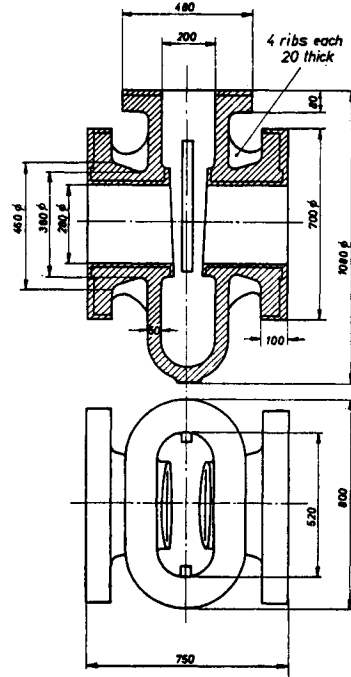


FIG. 33. Auto hub.

Zone subdivision:

Neck, upper: trapezium $A = \frac{2.7 + 5}{2} \times 10 = 37.5 \text{ cm}^2$; $P = 5 + 2.7 + 8.8 + \sim 11 = 27.5 \text{ cm}$; $M = A/P = 1.37 \text{ cm}$. Allowance for non-cooling surfaces of the 16 ribs and lugs, estimated at $\sim 10\%$, $M = 1.5 \text{ cm}$.

Neck, lower: trapezium $A = \frac{4.1 + 3}{2} \times 13 = 46.1 \text{ cm}^2$, $P = 4.1 + 3 + 11.8 + \sim 13 = 31.9 \text{ cm}$; $M = A/P = 1.45 \text{ cm} + 10\%$ for lugs and ribs, $M \approx 1.6 \text{ cm}$.

Grease box: plate, 1.2 cm thick; $M = d/2 = 0.6 \text{ cm}$.

Intersections: grease box/inner ribs: inscribed circle 1.8 cm diam.; $M = 0.9 \text{ cm}$.

Intersections: grease box/outer ribs: inscribed circle 2.4 cm diam.; $M = 1.2 \text{ cm}$.

Disc: bar $4 \times 11 \text{ cm}$, non-cooling surface inner:

$$M = \frac{11.4}{2(11 + 4) - 4} = 1.7 \text{ cm.}$$

Eye lugs on disc: cylinder 5.0 cm diam. $\times 6 \text{ cm}$ H; non-cooling surface:

$$4 \text{ cm wide strips; } M = \frac{2.5 \times 6}{2(2.5 + 6 - 4)} = 1.67 \text{ cm.}$$

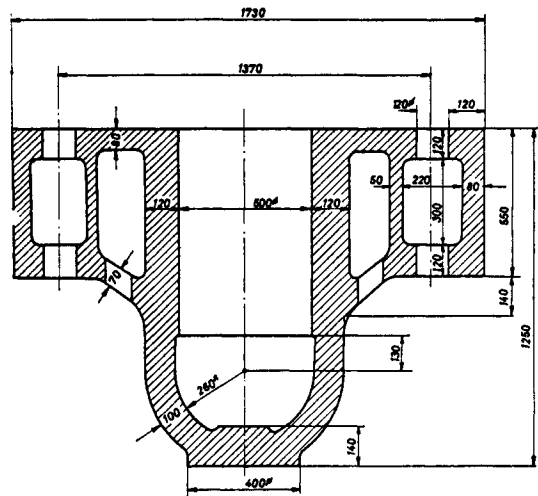


FIG. 34. Press cylinder.

Zone subdivision:

Cylinder base: disc 40 cm diam.; side cooling surfaces absent, as adjacent to cap; plate, $M = d/2 = 7 \text{ cm}$.

Cap: plate, 10 cm thick; $M = d/2 = 5 \text{ cm}$.

Cylinder body: plate 12 cm thick; $M = d/2 = 6 \text{ cm}$.

Upper plate: 8 cm thick; $M = d/2 = 4 \text{ cm}$.

Periphery of small drill holes 120 diam. ; outer wall: plate 8 cm thick; $M = 4 \text{ cm}$.

Intersection: cylinder/sloping wall: inscribed circle, 18 cm diam.; two crossed plates, $M = d/2 = 9 \text{ cm}$.

THE THERMAL GRADIENT
IN THE CASTING

3.1. What Is a Thermal Gradient ?

IMPORTANT FOR PRACTICE

The stepped wedge already mentioned (Fig. 2) solidifies at the thinnest position first. The metal in the thicker sections is still liquid at this time, and is therefore hotter and solidifies later. This is due to the difference in the amount of heat to be dissipated, and hence to the different moduli. Because the temperature falls towards the solidified extremity, a temperature gradient exists; a temperature gradient therefore develops when solidification progressively moves towards the riser.

According to Pellini⁽³⁾, the temperature gradient in a plate must amount to at least 0.5°C/cm length of the casting, for a sound casting to be obtained; i.e. at this gradient each cm of the solidifying casting can still be fed from the part of the casting which is 0.5°C hotter (Fig. 35).

To obtain a temperature gradient it is sometimes (but not always) sufficient to pour through the feeder head

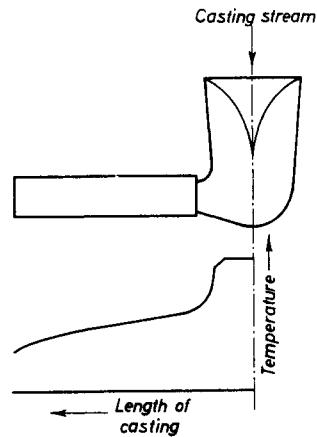


FIG. 36. Temperature pattern immediately after casting in a plate which was top poured through the feeder.

(Fig. 36) so that the coldest metal is found at the extremity of the casting, and the hottest in the feeder.

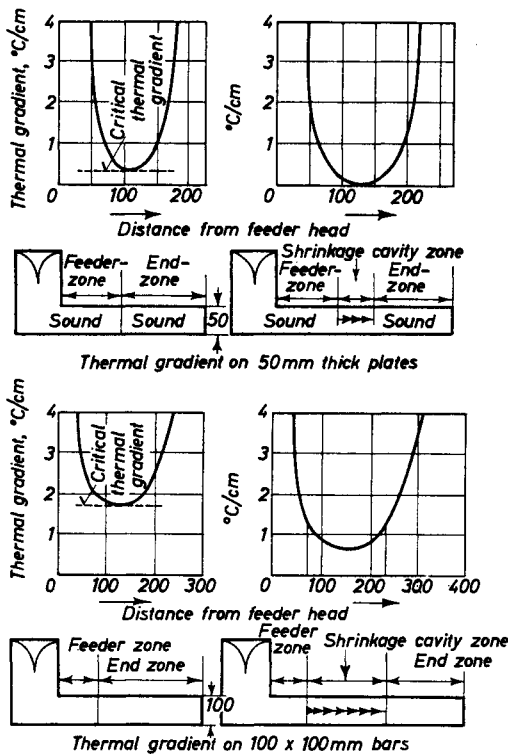


FIG. 35. Thermal gradients on plates and bars, after Pellini⁽³⁾.

3.2. Thermal Gradient and Difference in Modulus

IMPORTANT FOR PRACTICE

In order for a cross-section to remain liquid longer than a neighbouring one, it must contain more heat. A section with a longer solidifying time also has a larger modulus. Experiments have shown that the modulus must be larger by a factor of about 1.1 for the section to be able to feed a thinner adjoining section. Feeder heads also form such metal-supplying sections. The feeder head modulus must be at least 1.2 times larger than that of the casting (Fig. 37).

$$M_1 = 1.1 \cdot M_0$$

$$M_2 = 1.1 \cdot M_1$$

$$M_3 = 1.2 \cdot M_2$$

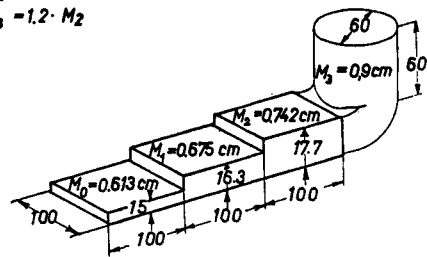


FIG. 37. For satisfactory feeding the modulus of each cross-section, both within the casting and at the transition to the feeder head, must be 1.1 to 1.2 times that of the preceding modulus.

The principle that the feeder should solidify last is well known, but often too tightly and too generously dimensioned feeders are found together in one and the same foundry. The latter are usually based on the bad habit of designating all blowholes, even slag blowholes and pinholes, as shrinkage cavities, and, due to lack of knowledge of the correct method of determining riser dimensions, attacking the problem from the feeder side. The true cause—metallurgical variations in the steel—was ignored in this way, but the economic efficiency of the foundry operation is certainly jeopardized by over-large feeders.

3.3. Effect of the Thermal Gradient on Solidification and Feeding Range

IMPORTANT FOR PRACTICE

Metals solidify as crystals; in many metals the “fir tree” (dendritic) crystals grow from outside inwards. Figure 38 shows the growth of a dendrite. The more

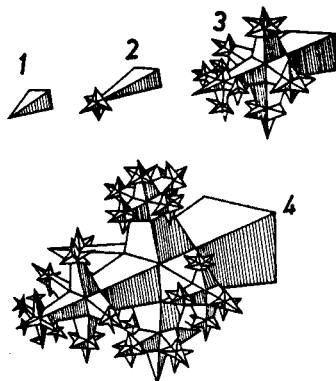


FIG. 38. Steps in the growth of a dendrite.

time there is available for crystal growth, the better the development of these starlike ramifications. Figures 39a–b show dendrites from a shrinkage cavity, while Fig. 40 illustrates a section with closely entangled crystals. In the



a



b

FIG. 39. Dendrites from a shrinkage cavity. (a) from a “cupola scaffold”; (b) from a horizontal “runout” (see also Fig. 72).

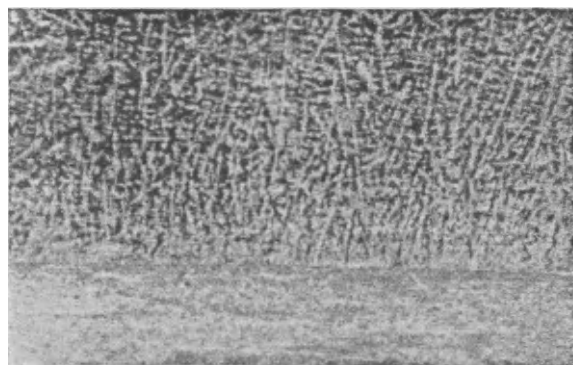


FIG. 40. Section of dendrites.

spaces between these crystals are found the solidified remains of the liquid metal which was present just before solidification, and which is enriched in constituents remaining liquid at still lower temperatures.

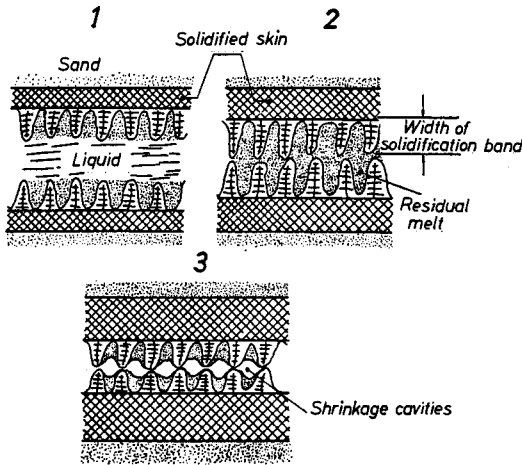


FIG. 41. Solidification of a plate in 3 phases.

Phase 1: The dendrites grow into the still liquid interior. Feeding of the interspaces possible.

Phase 2: The dendrite peaks are in contact. Flow of metal restricted.

Phase 3: Formation of more or less extensive cavities, due to the constriction of the feed channels by the dendrites.

According to Fig. 41 the solidification of a plate takes place in three phases: first, a solid edge zone is formed with a broad liquid region between the advancing crystal fronts; the liquid steel flows freely and always remains in contact with the dendrites, thus filling up the space which would otherwise be left as the solidified metal contracts. Secondly, the crystal peaks constrict the flow of metal and finally come into contact. Eventually the

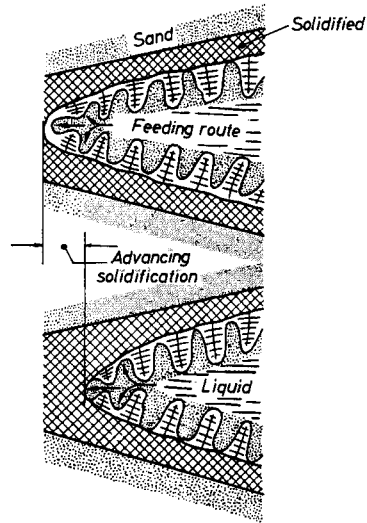


FIG. 43. Advancing solidification of a keel block.

Due to the wedge-shaped pattern of the solidification front, the liquid steel can reach even to the interstices of the enveloping crystallites, and fill up the cavities which are forming there.

flow of molten steel is cut off and more or less extensive shrinkage cavities are formed (Fig. 42).

Wedge castings as in Fig. 43 do not exhibit parallel solidification fronts, so that feeding of the intercrystalline spaces is possible even with advancing solidification. A thermal gradient also produces a similar wedge-shaped solidification front. A plate as shown in Fig. 44 solidifies at the edges first, where the crystals grow more



FIG. 42. Radiograph of the centre line cavity of a plate.

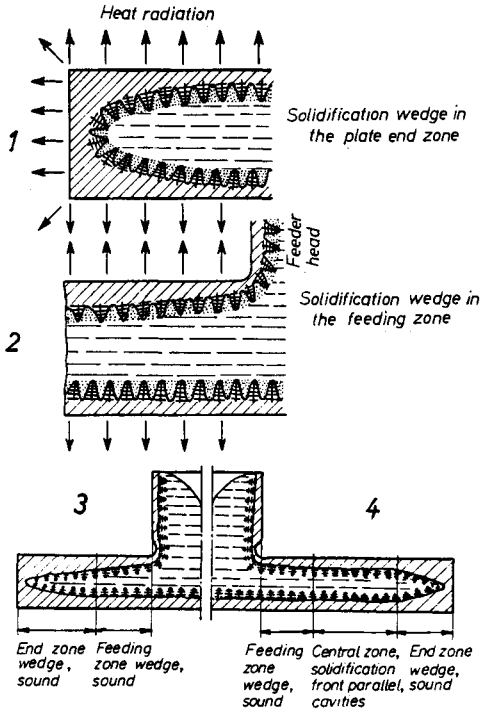


FIG. 44.

1. End section of the plate. Heat radiation from three sides, with the formation of a solidification wedge.
2. Feeder section of the plate. Diminished growth rate of the dendrites near the feeder due to its heating effect, hence a solidification wedge is formed.
3. End and feeder zones are continuous, giving a sound plate.
4. End and feeder zones are not continuous; cavities are formed in the central zone with a parallel solidification front.

rapidly than in the centre of the plate, due to cooling from both sides. The solidification fronts therefore taper towards the centre because the temperature gradient, i.e. the end zones of plates at which this wedge angle is sufficiently obtuse, will always solidify without cavities.

A thermal gradient is also formed near to the feeder head, as the feeder acts as a heat reservoir, which allows the adjacent zone of the casting to remain liquid for a longer period. For this reason the crystals in this zone solidify more slowly than in the centre of the plate, the solidification front is wedge-shaped and a sound casting produced. If the feeder and end zones are always in liquid/liquid contact the casting is sound; if these zones become separated (by solidified dendrites), cavities are unavoidable in the middle section, where the solidification fronts are parallel.

3.3.1. SOLIDIFICATION CHARACTERISTICS OF RECTANGULAR SECTION BARS

Cooling proceeds on four or five sides at the end of the bar (Fig. 45), i.e. the solidification wedge is at first very steep and short, so that the length which can be adequately fed to give a sound casting is also short. The thicker the plates or bars, the further the sides of the wedge can extend, and the longer the sound zones become (Fig. 46).

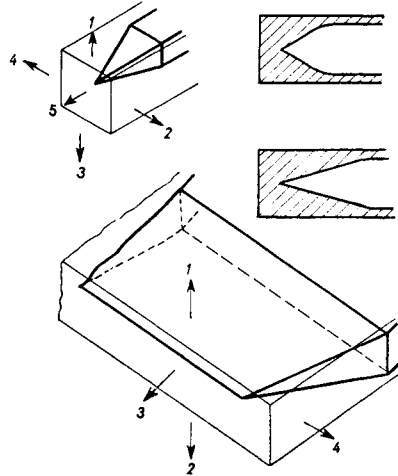


FIG. 45. Because of heat radiation from 5 sides in bars, the solidification wedges are steeper and shorter and the feeding ranges are less than with plates of equal thickness (diagrammatic).

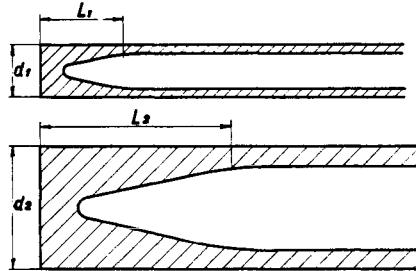


FIG. 46. The length of the sound solidification wedge increases with the depth of the cross-section (diagrammatic).

The transition from plate to bar is capable of infinite variations. Cech⁽⁴⁾ investigated the feeding ranges of unalloyed carbon steels (0.2–0.3 per cent C); the results are shown in Table 3 and Figs. 47, 48 and 49.

TABLE 3. FEEDING RANGES ON CAST STEEL PLATES AND SQUARE SECTION BARS

End zone	Feeding zone
EZ = 2.5 D	TZ = 2 D
$\left. \begin{aligned} &TZ + EZ \\ &= 6 \times \sqrt{D} \text{ (in.)} \\ &\text{or} \\ &= 9.5 \times \sqrt{D} \text{ (cm)} \\ &\text{or} \\ &= 30 \times \sqrt{D} \text{ (mm)} \end{aligned} \right\}$	
<p>A bar from a width ratio of 1 : 5 counts as a plate. The use of chills is explained in Chapter 8.</p>	

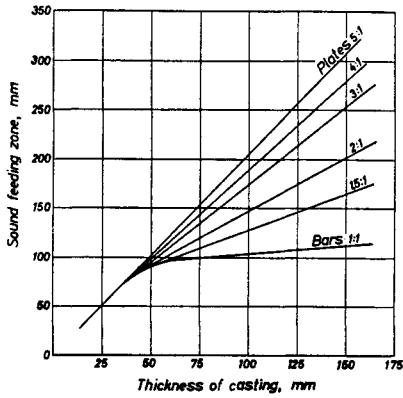


FIG. 47. Length of the sound feeder zone as a function of the dimensions of the casting.

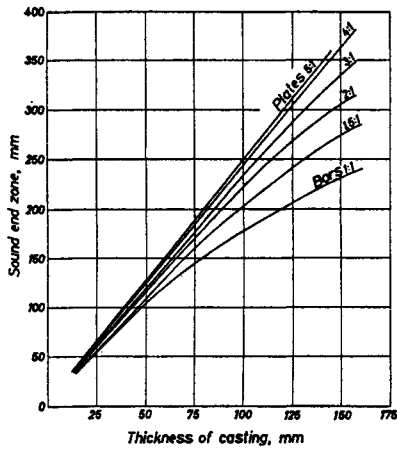


FIG. 48. Length of the sound end zone as a function of the dimensions of the casting.

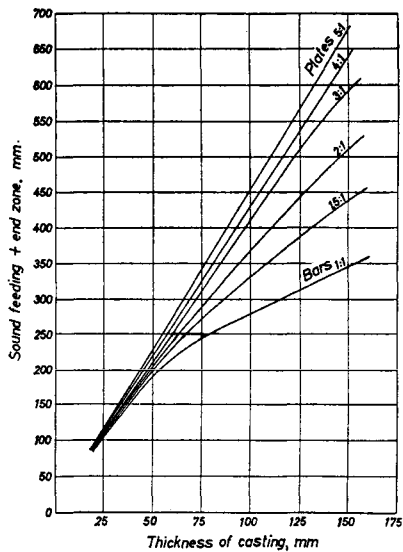


FIG. 49. Length of the sound feeder + end zone as a function of the dimensions of the casting.

By using highly exothermic antipiping materials the length of the sound feeder zone increases, because the thermal gradient is increased as a result of additional superheating in the feeder head (Fig. 50). This will be discussed more fully in Chapter 12.

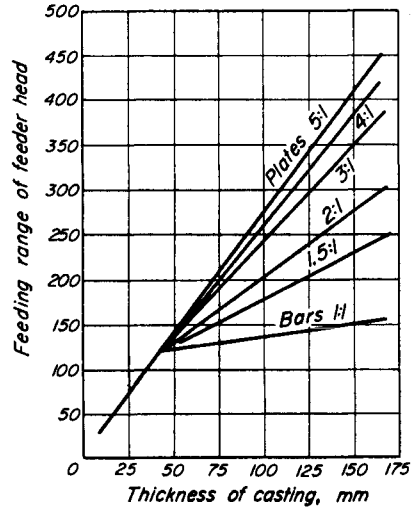


FIG. 50. Length of the sound feeder zone as a function of the dimensions of the casting when using exothermic feeders.

By placing chills in the faces of plates the end zone lengths can be increased by about 50 mm compared with Fig. 48. A similar increase of about 50 mm can be obtained by simulating end zones (by means of a chill placed between two feeding points—see Chapter 8 and Table 3).

The end zone lengths of bars are also increased by means of an end chill. The increase in this case is so slight, however, that it is better on safety grounds not to allow for it in the calculation.

The region of the casting which can be supplied by a single feeder head is known as the feeding area; it is only necessary to place a single feeder inside one feeding area. A second feeder would not only be wasteful (Fig. 51), but in some circumstances could even cause



FIG. 51. Waste of steel caused by using two feeders inside a single feeding area on the boss of a flange coupling. The flange feeder was incorrectly dimensioned, resulting in cavities (cf. Fig. 237).

damage. If one of the two feeders is only a little less than the other, it solidifies first and draws some metal from the larger one, which will then empty more completely, so that the shrinkage cavity can extend into the casting.

Feeding areas which are bounded by end zones are significantly larger than those without end zones (Fig. 52).

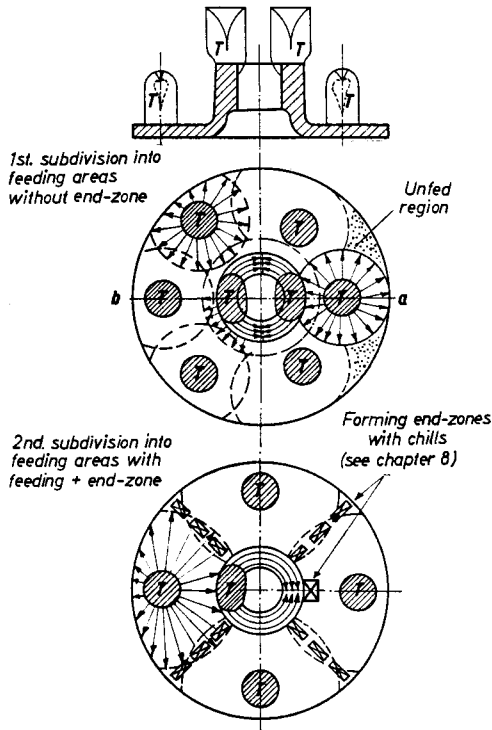


FIG. 52. Subdivision of a flange into feeding areas.

The casting in question, according to its shape, is divided into one or more feeding areas, and a feeder of suitable size placed in each area.

3.4. Factors Influencing the Feeding Range

Feeding becomes more satisfactory as the angle of the wedge between the solidification fronts increases. As the crystals themselves grow with a dendritic and therefore wedge-shaped structure, an angle is also formed between the crystals. The longer the crystals are (with the same base width) the smaller this angle becomes and the more difficult it is for the molten steel to reach the shrinkage cavities forming between the numerous crystallites (Fig. 53).

In the region of the growing crystals solid components (crystals) and liquid metal exist side by side. This zone is neither solid nor liquid, but is mushy, and is known as the "solidification band". The wider this band, the longer the crystals, and the more difficult feeding becomes. The width of the solidification band is influenced by the following circumstances⁽³⁾:

(1) The phase diagram of the metal indicates the interval during which solid and liquid metal exist together

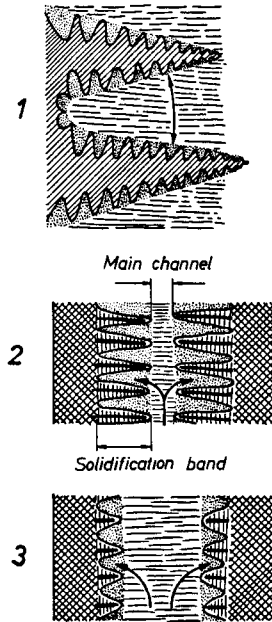


FIG. 53. Influence of the wedge angle between the crystals.

1. Wedge-shaped interstices are found between the dendrites. The larger this angle between the solidification fronts, the shorter the crystals and the more favourable the feeding conditions.
2. Freezing range small. Short crystals, large wedge angle between the crystals, feeding easy, even towards the end of solidification.
3. Freezing range large. Long crystals, small wedge angle between the crystals. Feeding difficult, especially towards the end of solidification, when the crystal peaks are almost in contact and only a small main channel is still present.

(the freezing range). The wider this interval, the longer the time available for the crystals to grow, and the more unfavourable the solidification pattern becomes (Fig. 54).

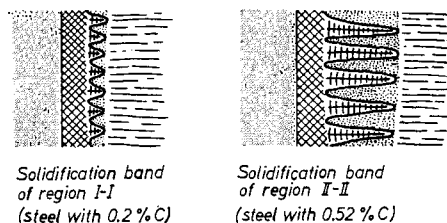
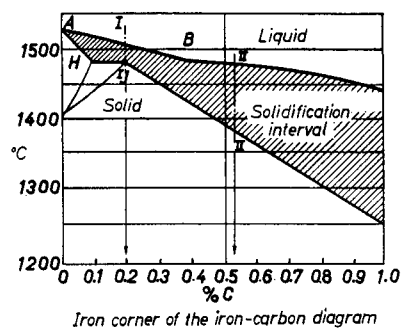


FIG. 54. Influence of the width of the freezing range on the width of the crystallite solidification band.

(2) The higher the solidification temperature, the more rapidly the temperature falls (hotter bodies radiate heat much more than cooler objects). With a high solidification temperature, therefore, the crystals have little time to increase in length, as the molten metal in the interstices will also solidify rapidly; the freezing range is small, and hence favourable to the production of sound castings (Fig. 55).

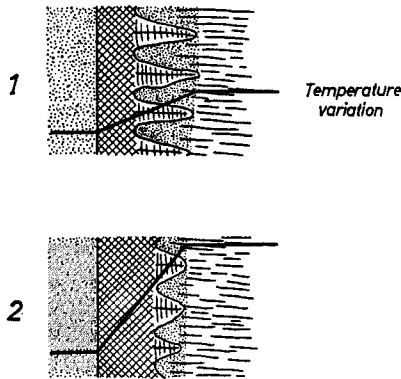


FIG. 55. Influence of the solidification temperature of the cast metal.

1. Solidification temperature low, temperature curve flat, thermal gradient small, crystals long, unfavourable feeding characteristics.
2. Solidification temperature high, rapid drop in temperature, large thermal gradient, crystals short, favourable feeding characteristics.

(3) The lower the thermal conductivity of the metal, the more the dendrites use up their store of heat during growth. With a low thermal conductivity heat is only slowly replenished from the residual melt, growth is hindered, the crystal length is short, and the freezing range is again short, and therefore favourable (Fig. 56).

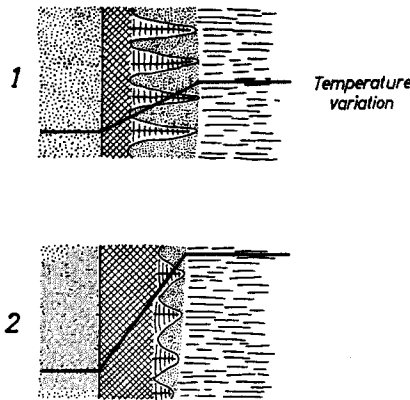


FIG. 56. Influence of thermal conductivity of the cast metal.

1. Thermal conductivity of the metal high; rapid supply of heat to the crystals; slow crystal growth, long crystals, unfavourable feeding characteristics.
2. Thermal conductivity of the metal low; slow conduction of heat to the crystals; rapid cooling of the crystals, rapid crystal growth, crystals short, feeding characteristics favourable.

(4) The more intensive the chilling (the heat absorption capacity and thermal conductivity) of the mould material, the more rapidly the heat will be withdrawn from the residual melt and the more rapidly will solidification proceed; the solidification band is again smaller and more favourable (Fig. 57).

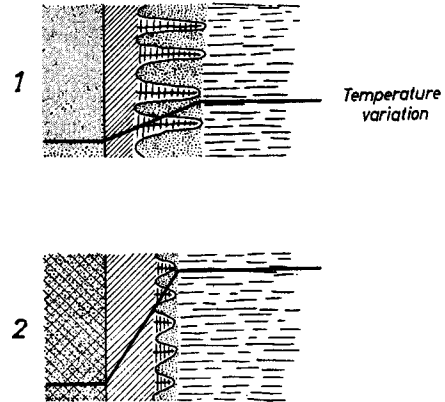


FIG. 57. Influence of the chilling action of the mould material.

1. Chilling action slight; temperature curve slight; very wide solidification band, unfavourable feeding characteristics.
2. Intense mould chilling action; steep temperature curve; solidification band narrow, favourable feeding conditions.

Points (1) to (3) are dependent on the metal and cannot be influenced by the foundryman. Improvements can be achieved only by selecting a more suitable mould material.

Every metal therefore exhibits a characteristic solidification pattern which can be influenced by the mould material, and also to some extent by the design of the casting, for example, a slowly solidifying sphere or a rapidly solidifying thin plate (Fig. 58).

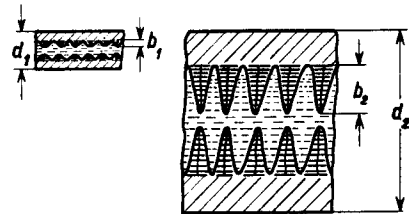


FIG. 58. Influence of wall thickness d .

The longer the time available for the dendrites to grow, the longer they will become, and the wider will be the solidification band (see also Fig. 4). Consequently very wide solidification bands exist in the interior of thick-walled castings, making satisfactory feeding difficult. Beyond a certain thickness the dendrites become so long that the interstices between the crystallites can no longer be fed to produce a sound casting (leading to unavoidable central segregation or microporosity in massive castings). The decreasing feeding ranges in thick-walled plates are also shown in Figs. 47 to 50.

DETERMINATION OF THE
CONNECTOR BETWEEN FEEDER
AND CASTING, HERE CALLED FEEDER NECK

(earlier known as the ingate, neck, shoulder, etc.)

4.1. Calculation of Transition Cross-sections between Feeder and Casting (without Allowing for the Effects of the Flow of Metal)

IMPORTANT FOR PRACTICE

Directional solidification must take place from the casting and across the ingate to the feeder, with an increase in modulus of about 10 per cent at each stage:

$$M_{\text{casting}} : M_{\text{neck}} : M_{\text{feeder}} = 1 : 1.1 : 1.2 \quad (9)$$

If this condition is satisfied then shrinkage cavities cannot occur near the feeder neck.

Unfortunately this rule is often broken (Fig. 59),

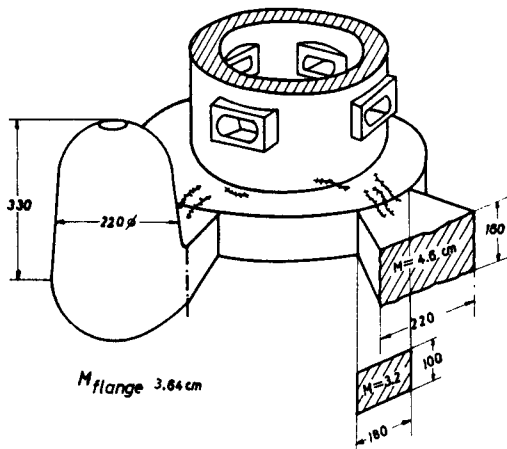


FIG. 59. Formation of cavities due to the constriction of the feeder neck towards the casting.

As the modulus of the neck at its narrowest point is only $M = 3.2$ cm, it freezes prematurely here, leading to shrinkage cavities in the flange.

leading in every case to premature solidification of the ingate, with the formation of shrinkage cavities.

The gate formula given by Namur⁽⁶⁾:

$$M_{\text{ingate}} = \frac{a \times b}{a + b} \geq M_F \quad (10)$$

supplies values which are too low; practical experience has shown that cavities are produced, and consequently the formula cannot be recommended.

Over-dimensioning of the neck can also lead to scrap due to the formation of secondary shrinkage cavities.

According to Fig. 60 every neck is a semi-infinite bar, because the end cooling surfaces are missing due to the adjoining feeder and casting. The modulus is therefore calculated by the bar formula or from Fig. 7. Because these parts often have very irregular shapes (Fig. 61), the greatest care must be taken to ensure that

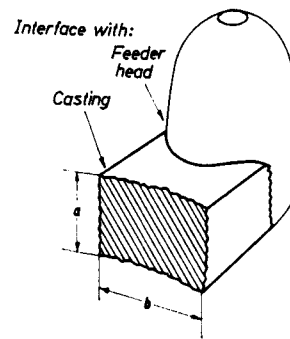


FIG. 60. Representation of the feeder neck as a semi-infinite bar.

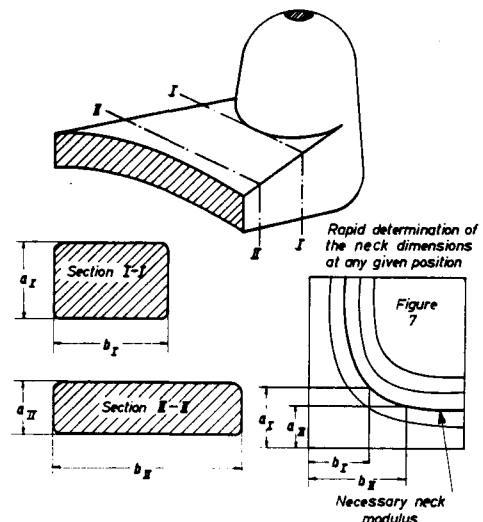


FIG. 61. Rapid determination of the dimensions of an irregularly shaped feeder neck, using Fig. 7.

the modulus remains the same throughout the neck. Figure 7 is an almost indispensable guide for this purpose.

The necessary modulus cannot be achieved solely by widening the gate, especially in plate-like castings; this fact is illustrated in Fig. 62. Only an enlargement in

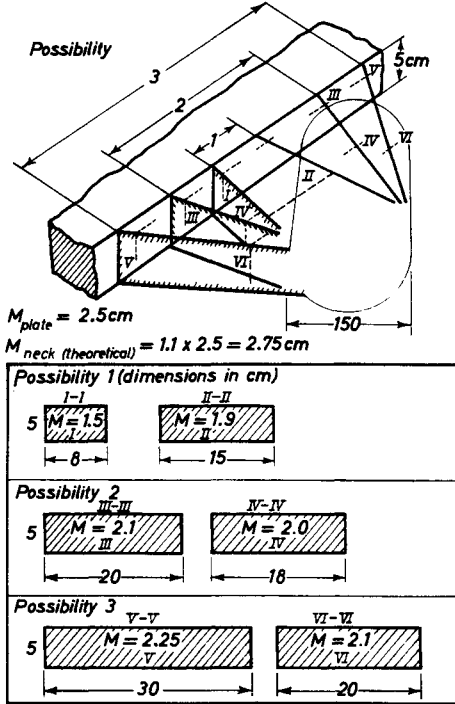


FIG. 62. The necessary modulus cannot be attained in plate-shaped castings merely by widening the neck.

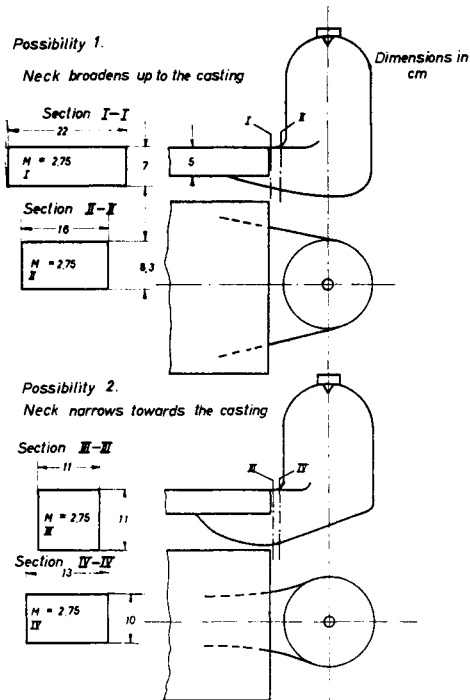


FIG. 63. Neck to a 50 mm thick plate; the modulus is correct due to enlargement in section.

cross-section, as in Fig. 63, can produce correct solidification; according to the size of the enlargement in cross-section the ingate can even contract towards the casting (Fig. 63, Example 2). These examples are not to be confused with the wedge-shaped pads to be described later.

Flanges, etc., often form junctions with a larger modulus. Obviously the ingate must be attached at these positions (Fig. 64, Example 2). Enlarged necks are absolutely necessary in this case.

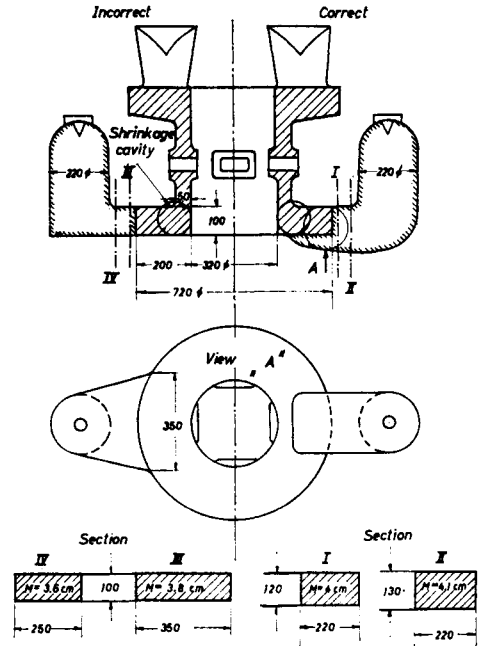


FIG. 64. Double flange with a correctly and incorrectly dimensioned neck.

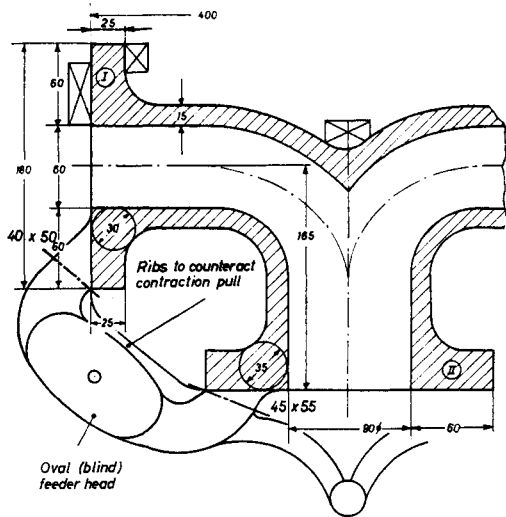


FIG. 65. Feeder neck of a distributor casting. Possibility 2: feeder more easily removable than in 1 (Fig. 66a).

Feeding each of two flanges by means of a single feeder head at the side. Alternatives 1 and 2 are encountered mainly in fittings with flanges closer together than those shown in this example.

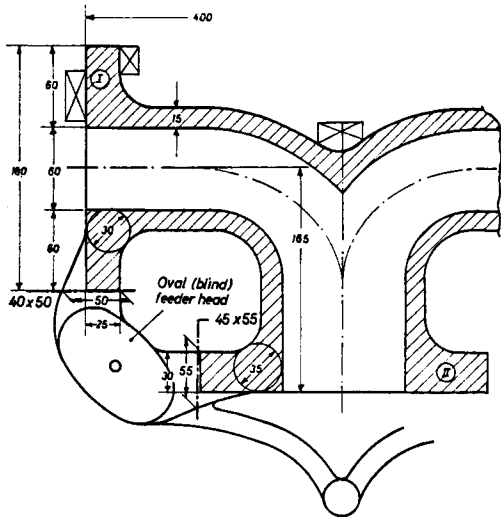
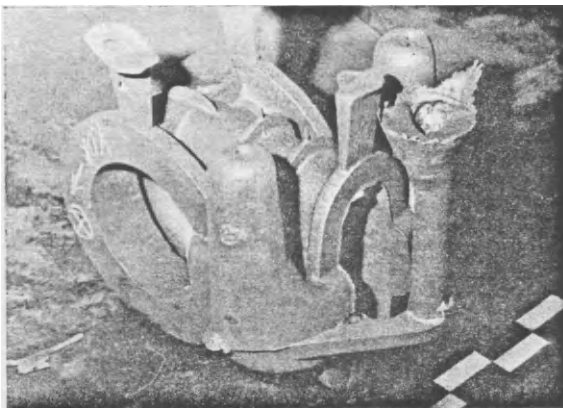


FIG. 66a. Feeder neck of a distributor casting. Alternative 1: feeding each of two flanges by a single feeder head.

Figs. 66b—d. Illustrative examples of necks for fittings.



(b) Valve housing (a feeder with an exothermic sleeve on the valve seating).



(c) Gate valve housing.



(d) Differential housing.

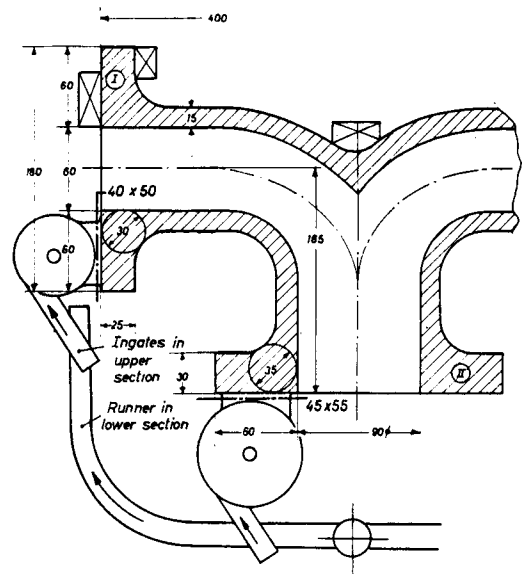


FIG. 67. Neck of a distributor casting. Alternative 3: separate, easily removable feeders.

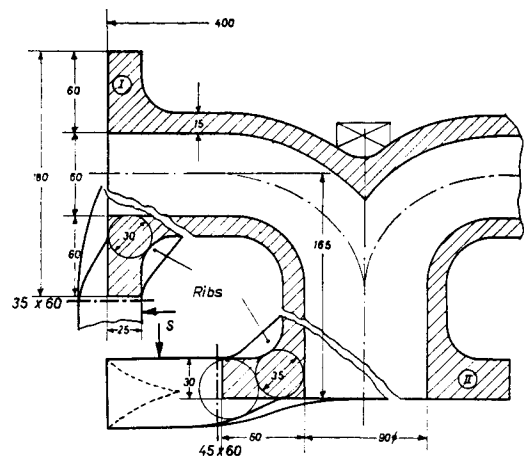


FIG. 68. Neck of a distributor casting. Alternative 4: feeding through open feeder heads.

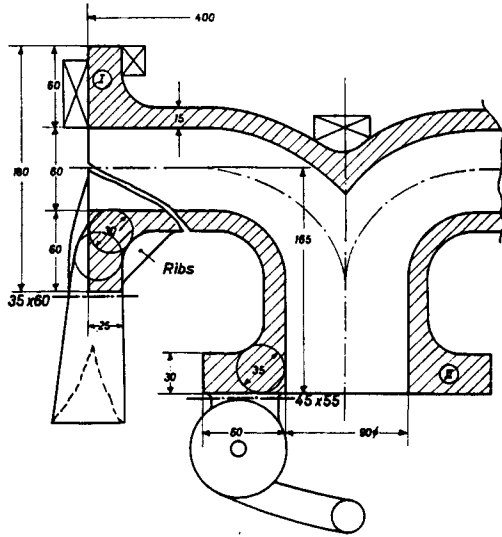


FIG. 69. Neck of a distributor casting. Alternative 5: simultaneous use of 3 and 4.

TABLE 4. DETERMINATION OF THE FEEDER NECKS OF A DISTRIBUTOR CASTING

Flange I $M_I = \frac{6 \times 2.5}{2(6 + 2.5) - 1.5} = 0.97 \text{ cm}$

Associated neck: $M_{GI} = M_I \times 1.1 = 1.07 \text{ cm}$

Flange II $M_{II} = \frac{6 \times 3}{2(6 + 3) - 1.5} = 1.1 \text{ cm}$

Associated neck: $M_{GII} = M_{II} \times 1.1 = 1.21 \text{ cm}$

Fig.	Flange I $M_{GI} = 1.07 \text{ cm}$	Flange II $M_{GII} = 1.21 \text{ cm}$
65	$a = 5 \text{ cm}$ $b = 4 \text{ cm}$ 	$a = 5.5 \text{ cm}$ $b = 4.5 \text{ cm}$
66	$a = 5 \text{ cm}$ $b = 4 \text{ cm}$ 	$a = 5.5 \text{ cm}$ $b = 4.5 \text{ cm}$
67	as Fig. 66	as Fig. 66
68	$a = 3.5 \text{ cm}$ $b = 6 \text{ cm}$ 	$a = 4.5 \text{ cm}$ $b = 6 \text{ cm}$

a is assumed on the basis of the junction circle
 b is then determined by using Fig. 7.

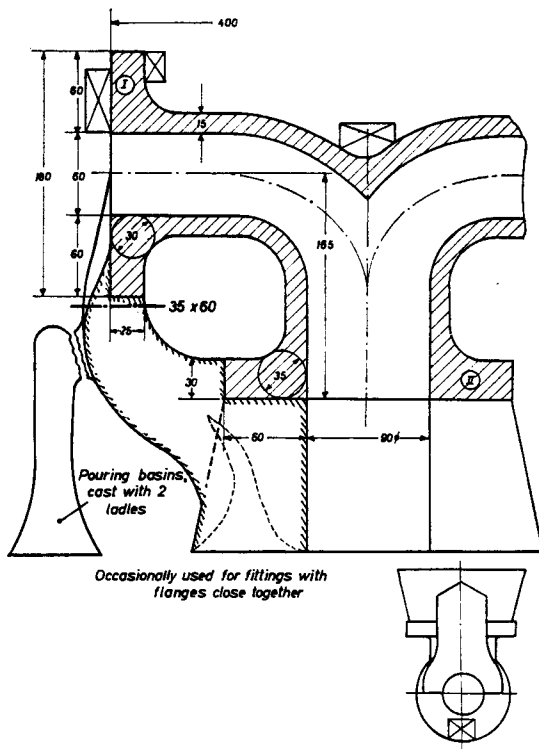


FIG. 70. Neck of a distributor casting. Alternative 6: moulded horizontally, bottom cast.

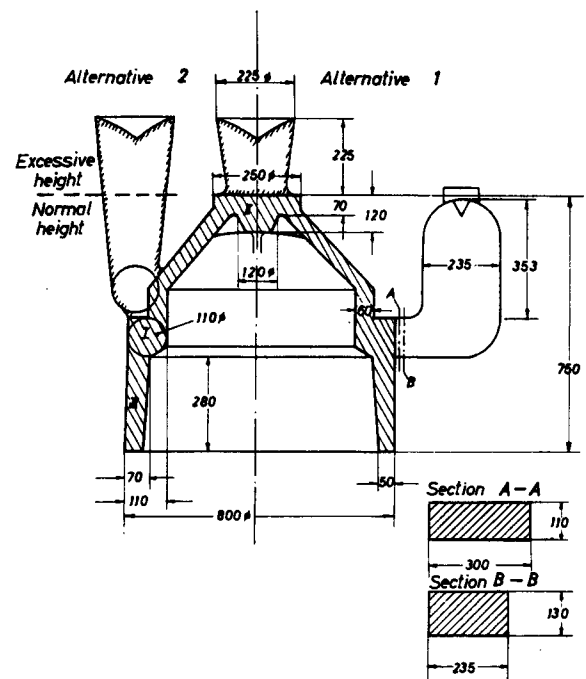
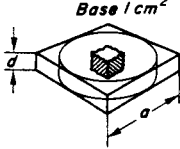
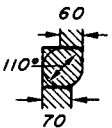

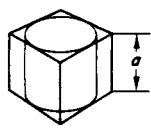
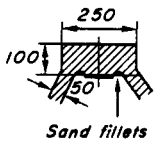


FIG. 71. Feeding possibilities of a cylinder. For method of calculation see Table 5.

TABLE 5. DETERMINATION OF THE FEEDER NECKS OF A CYLINDER, ACCORDING TO FIG. 71

	Modulus of the cross-section	Modulus of the neck	Feeder determination (see Chapter 5)
I	<p>Simulation body: Square section bar, with walls 60 and 70 mm, omitted as non-cooling surfaces</p>  <p style="text-align: center;"><i>Base 1 cm²</i></p> $M_I = \frac{11 \times 11}{2(11 + 11) - (6 + 7)} = 3.9 \text{ cm}$	<p>$M_{G1} = 1.1 \times M_I = 1.1 \times 3.9 = 4.3 \text{ cm}$ From Fig. 7</p> <p>(a) at the casting: (A-A) $a_1 = 11, b_1 = 30 \text{ cm}$ (a_1 is assumed)</p> <p>(b) at the feeder (B-B) $b_2 = \text{diam-feeder} = 23.5 \text{ cm}$ $a_2 = 13 \text{ cm}$</p>	<p>$M_{F1} = 1.2 \times M_I = 1.2 \times 3.9 = 4.7 \text{ cm}$</p> <p><i>Variant 1</i> <i>Variant 2</i> feeder diam. open feeder head $\approx 5 \times M_F = 235 \text{ mm}$</p> <p>$H = 1.5 \text{ diam.} = 353 \text{ mm}$</p> 
II	 <p>Sand fillets Allowing for the sand fillets a cylinder of 250 diam. \times 190 high is assumed. The wall 50 is omitted (non-cooling surface) According to equation (8):</p> $M_{II} = \frac{12.5 \times 10}{2(12.5 + 10 - 5)} = 3.55 \text{ cm}$	<p>Calculation of the ingate not necessary with an open feeder</p> 	<p>Open feeder: $M_F = 1.2 \cdot M_{II} = 4.25 \text{ cm}$</p> <p>from the feeder table for $H = 1.5 \text{ diam.}$ diam_F = 230 mm, $H_F = 345 \text{ mm}$</p>  <p style="text-align: center;"><i>Sand fillets</i></p>
III	<p>The cylinder sleeve is a curved plate of thickness $d = 70$ (at the thickest point) the modulus $M_{III} = \frac{d}{2} = 3.5 \text{ cm}$</p>		<p>Control of the modulus gradient: $M_I : M_{III} = 3.9 : 3.5 = 1.12$, i.e. section I can approach section II with sufficient safety</p>

Figures 65 to 70 show various examples in the design of ingates for pipe fittings; the necessary calculations are summarized in Table 4. When possible one feeder head should supply two flanges (to improve the metal yield). Chills are usually necessary for high-quality pipe fittings which are required to be tested radiographically (see Chapter 8). The cost of removing the feeder must also be taken into account when placing the neck; these costs vary according to the operation. A further example is illustrated in Fig. 71, with Table 5.

4.2. Calculation of Ingates, Allowing for the Heating Effects of Metal Flow

IMPORTANT FOR PRACTICE

Some of the superheat of the steel is lost to the mould walls while the metal is flowing, i.e. the walls absorb heat, thus reducing the directional cooling effect during solidification. The greater the superheat and the longer the period of flow through the section in question, the more pronounced this effect becomes. The safe utilization of this effect depends on the casting being satisfactorily supplied with metal by the feeder head. With one feeder head this is always true, but with three feeders special provisions must be made in the runner system.

According to Chvorinov⁽¹⁾:

$$T_f = 1.15 T_0 \tag{11}$$

where T_f is the time of solidification with, and T_0 without, metal flow. The equation is valid for superheats normally encountered in practice. In addition:

$$\frac{T_f}{T_0} = \frac{(M_f)^2}{(M_0)^2} = \frac{1.15 T_0}{T_0}; \text{ whence } M_f = 1.07 M_0 \tag{12}$$

This signifies that the modulus of cross-sections through which hot metal is flowing is increased only by 7 per cent by virtue of this flow of metal; for ingates of this type therefore the following relationship is valid:

$$M_{\text{casting}} : M_{\text{neck}} : M_{\text{feeder}} = 1 : (1.0-1.03) : 1.2 \tag{13}$$

in which the ratio 1.0 applies only to strongly superheated small parts (70-100°C superheat).

If the given examples of pipe fittings (Figs. 65-68) are re-calculated, the ingate dimensions are now reduced by 2-5 mm, i.e. by a far lesser amount than is frequently assumed. Very often obviously under-dimensioned necks are justified on the grounds of hot metal flow, scrap castings being produced time and time again from this cause. The shrinkage cavities are then falsely attributed in many cases to the provision of too small a feeder; this is then enlarged, the yield deteriorates, the defect is not eliminated and the feeding system as such is often abandoned.

FEEDER HEADS

5.1. General

IMPORTANT FOR PRACTICE

Chapter 5 is concerned with feeders in which highly exothermic antipiping material is not used, either in the form of sleeves or powder. Low-exothermic materials, which allow of no reduction in the size of the feeder, must be used with open feeder heads.

The mathematical basis for Chapter 5 is discussed in Section 5.6, so as not to interfere with the reading of the practical sections.

5.2. Action of Open Feeder Heads

IMPORTANT FOR PRACTICE

According to Fig. 72, a shrinkage cavity is formed

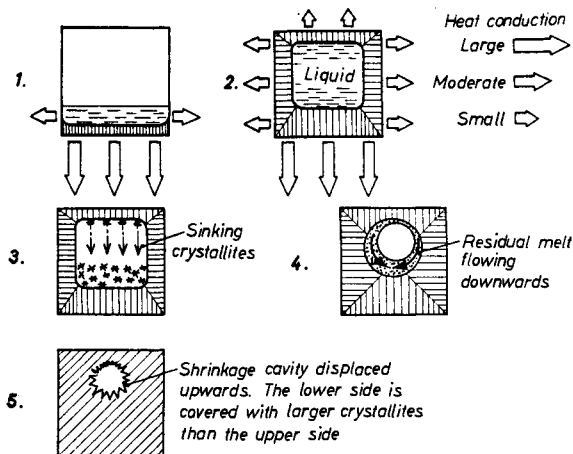


FIG. 72. Formation and position of the shrinkage cavity in a steel casting solidified without feeding.

1. During casting the lower parts of the mould are first flushed with steel; this gives up part of its heat to the walls, so that contraction and growth in thickness of the lower layers begin prematurely.
2. Even when the sand mould is completely filled, the bottom surfaces conduct heat best, due to improved contact with the steel, next in order follow the side walls, with the top surfaces conducting the least heat. Thus the solidified layers will be thickest at the bottom.
3. Crystals are formed everywhere in the melt and are deposited on nuclei, when the temperature has fallen sufficiently. In thick-walled castings considerable amounts of these floating crystals sink to the bottom, where they accumulate and increase the thickness of the bottom layer.
4. Immediately after the formation of a shrinkage cavity the residual melt flows downwards due to the action of gravity, and collects in the lower part as a sump.
5. The dendrites below grow more strongly than those above, because of improved feeding from this sump of metal.
6. After the supply of liquid steel to compensate for volume shrinkage ceases, a shrinkage cavity forms in the hot centre of the casting. For the reasons given, the position of the cavity is always displaced towards the top.

during solidification in a casting not supplied with a feeder, a considerable vacuum being generated. The pressure of the atmosphere drives the liquid metal from an attached feeder into this cavity, and the pressure energy is required to overcome the resistances to flow, which become very high towards the end of solidification and determine the feeding ranges.

A pressure column of liquid steel 1.45 m high with a specific gravity of 7 exerts a pressure of one atmosphere. The great majority of feeders have heights much less than this, and thus exert relatively little downward force. The expression "gravity feeder head" which is occasionally used is therefore misleading. Once the flow to the junction with the body of the casting is interrupted prematurely (because of incorrect dimensioning of the feeder neck or casting) then even 100 atm pressure could not force liquid metal through the solidified cross-section. It is therefore quite wrong to blame low feeder pressure for scrap which is actually caused by thermal effects. The usual language of the foundryman is inaccurate and misleading in this respect. Shrinkage cavities should refer to cavities which suck in liquid steel. In this way, false inferences based on incorrect terminology will be avoided, because the steel can no longer flow exactly as it would under the action of atmospheric pressure.

Premature freezing of the surface of the feeder head (Fig. 73) leads to the formation of secondary cavities

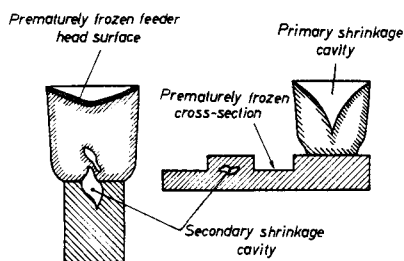


FIG. 73. Formation of secondary shrinkage cavities by premature freezing of the surface of the feeder head or of a section.

(because the liquid metal is cut off from the pressure of the atmosphere) which otherwise can penetrate deeply into the casting. The temperature gradient of the feeder must therefore increase towards the top. Methods of accomplishing this are shown in Fig. 74. The procedure using puncture cores, adopted by Pearson⁽⁶⁾ from the atmospheric feeder head, also merits consideration (Figs. 75, 76). It is remarkable that the atmospheric

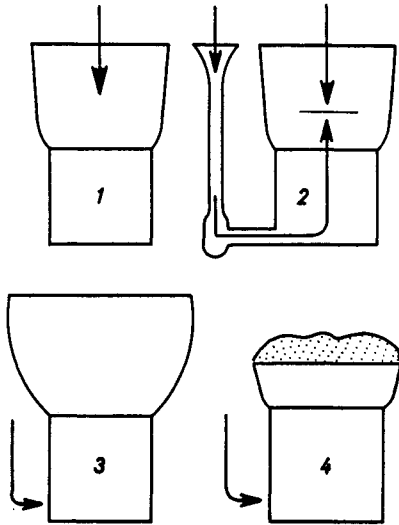


FIG. 74. Retarded solidification of the feeder by increasing the heat content by means of:

1. Top casting. The hottest steel is in the feeder.
2. Bottom casting, until the liquid level rises slightly above the lower edge of the feeder head, followed by top casting.
3. Very pronounced convex formation of the feeder head, whereby its volume and hence the proportion of heat contained in it are increased.
4. Use of highly exothermic agents in the form of antipiping compounds or exothermic sleeves.

A thermal gradient feeder → casting is generated by all these measures.

pressure acts via the core against gravity, even when the surface of the feeder has solidified (see also Fig. 79). Small feeders with a puncture core are more effective than larger feeders without one.

5.3. Mode of Action of Blind Feeder Heads

IMPORTANT FOR PRACTICE

The sphere has the smallest radiating surface area of any body of equal volume, and represents the ideal feeder shape as far as thermal conditions are concerned. From the point of view of moulding technology the production of spherical feeders is costly (Fig. 77). Shapes approximating to spheres are cheaper to mould (Fig. 78).

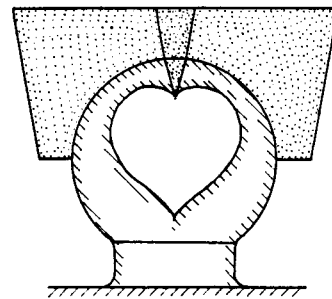
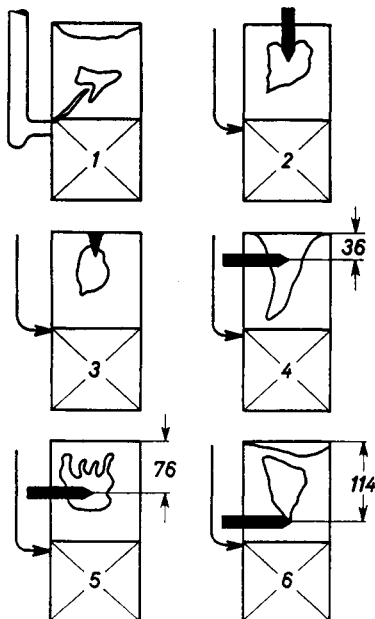


FIG. 77. Manufacture of spherical feeders by means of cores. This method of moulding is expensive, but is occasionally used with high-grade steels. The Cope core can also be manufactured from highly exothermic materials (see Chap. 12).



FIGS. 75/76. Penetration cores after Pearson⁽⁶⁾.

1. Without core. A shrinkage cavity is formed from the heated sand fillet to the runner.
2. With a pencil-shaped core made of oil sand or graphite. One way in which graphite acts is by lowering the melting point of the steel by carburization, so that the pressure of the atmosphere can be brought to bear on metal which remains liquid for a longer time.

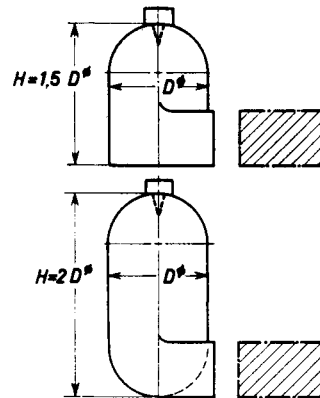
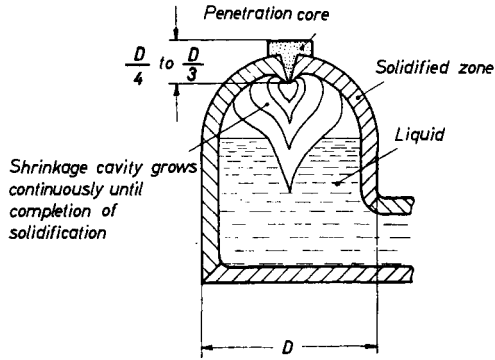


FIG. 78. Feeders (Williams risers) with simple and double spherical domes.

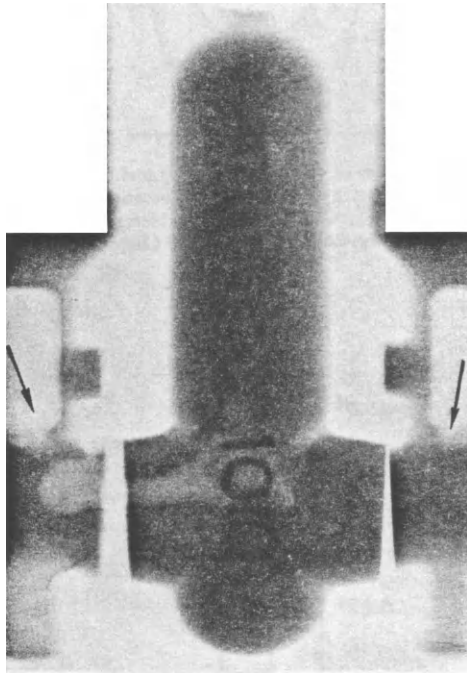
3. With a short, acute-angled pyramidal oil sand core.
- 4, 5, 6. Horizontal graphite pencil cores at various levels show that the atmospheric pressure can act against the force of gravity. The reliability of open feeder heads is increased by penetration cores of this type.

Using ordinary antipiping powders the radiation of heat from open and blind feeder heads is practically the same (the insulating effect of the sand in blind feeders is often overestimated).

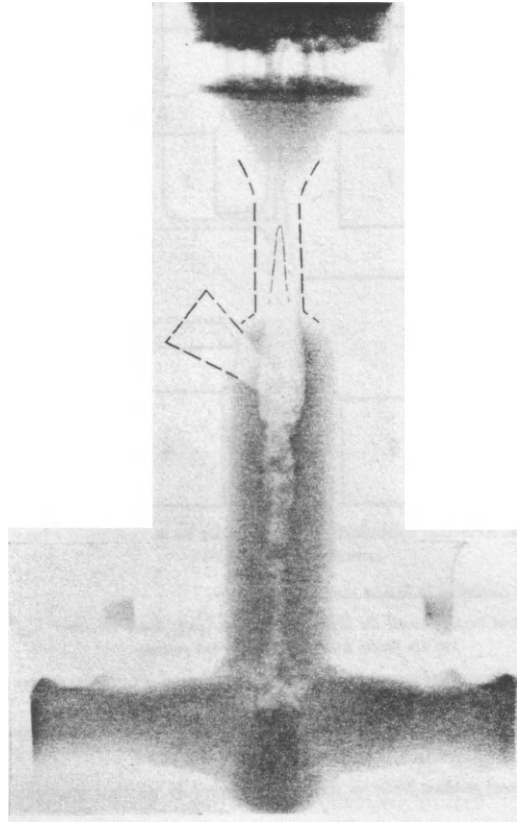
As a solidified skin forms round the feeder shortly after casting (Fig. 79), a way must be opened up from



a



b



c

Figs. 79a-c. Mode of operation of the pencil core (Williams penetration core) in a feeder.

Penetration core.

the atmosphere into the liquid interior by means of permeable cores. This also applies to "blind" feeder heads. Instead of the core a sharp sand fillet can also serve the same purpose; however, this is often unreliable, as it can break away due to insufficient sand strength or slovenly moulding; the fragments of sand can even enter the casting. Puncture cores should be permeable to gases, and acute-angled cores are to be preferred; because of the high heat concentration at the apex, the steel remains liquid for a long period (Fig. 80).

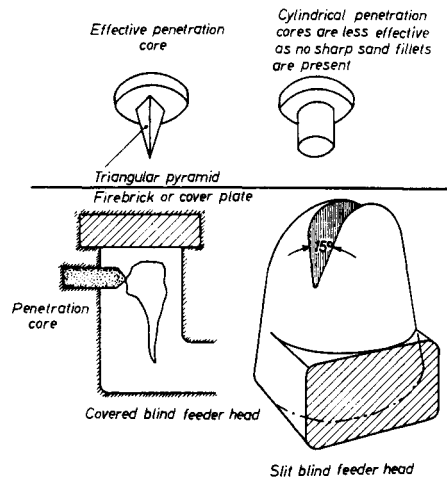


FIG. 80. Acute-angled and cylindrical pencil cores.

Should small feeder blocks (under 80 mm diameter) be used, the metal must not be too cold, otherwise they will not feed. The size of this appendage (Fig. 81) is less than required and the penetration core cannot reach hot metal and thus remains ineffectual, so that shrinkage cavities are inevitable.

Porosity is sometimes produced when using fluid feeders, the cause of which is usually wrongly interpreted. It may actually be due to incomplete filling (Figs. 82a-b). The caster is deceived by a spray of metal

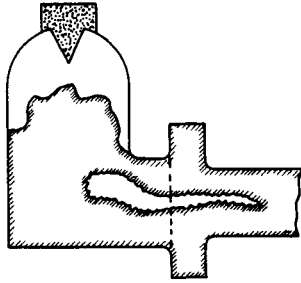


FIG. 81. Formation of cavity in a casting due to the metal not flowing out of the feeder head.

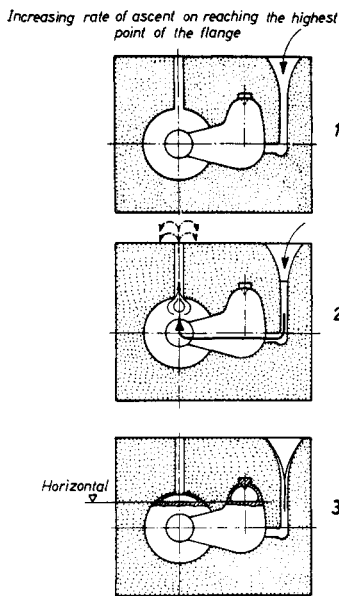


FIG. 82a. Formation of shrinkage cavities with horizontal bottoms under whistlers due to the spray effect (wrongly supposed to be air bubbles).

1. At a constant pouring rate the rate of rise of the steel in the mould increases with decreasing cross-section of the space being filled.
2. The rate of ascent in the highest part of the flange becomes so high that part of the steel is pushed upwards, rises in the whistlers and is ejected (the speed of the casting stream is transformed into pressure energy, exactly as in a spray). The resulting "fountain" gives the false impression that the mould is full, and pouring is interrupted.
3. Because too little metal was poured into the mould, the level of metal falls, producing a characteristic cavity under the thin skin of the casting, with a horizontal base. As spray effects can only occur with thin whistlers (very small cross-sections) these cavities are usually described falsely as blowholes caused by entrapped air.

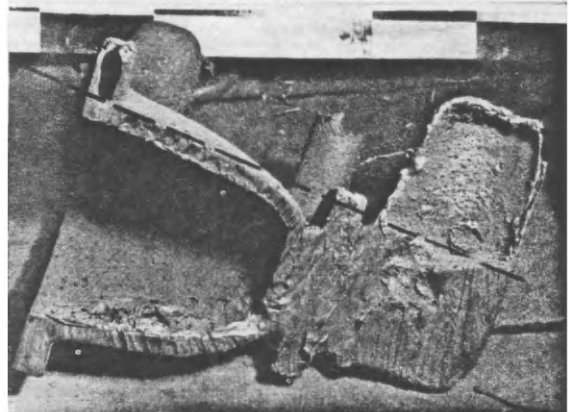


FIG. 82b. Cavities in flanges, bounded by a horizontal base, produced by incomplete filling, and erroneously termed "blow-holes".

into thinking that the mould is full, pouring is stopped prematurely, and shrinkage cavities are formed. No spraying effect is observed as long as the total cross-section of all the whistlers is larger than that of the downgate. This phenomenon has nothing to do with the ferrostatic pressure or with a suction effect exerted by the whistlers.



FIG. 83. Waste of steel due to overfilling the feeder.

The calculated casting yield using fluid feeders placed at the side is often less than when open feeders are placed on top, because of the extra weight of the ingate. As overfilling is impossible with blind feeders, however (Fig. 83), they are often more economical for that reason. This, and the feeding possibilities inherent in a low

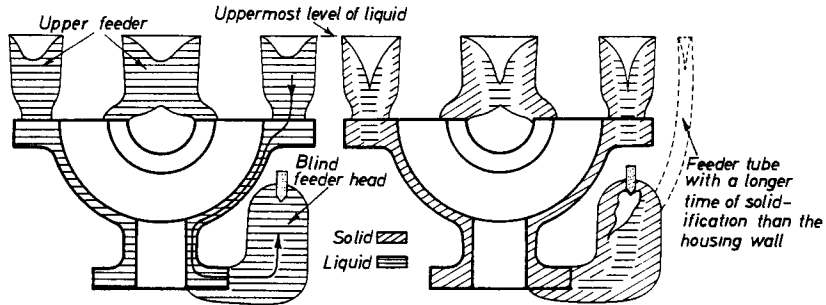


FIG. 84. Feeding conditions at the blind feeder of a turbine housing.

Phase 1. As long as liquid metal still connects the gravity feeder via the housing wall to the blind feeder, the upper feeders will supply metal to compensate for the shrinkage of all the metal below it, including the blind feeder. For this reason allowance must also be made for the blind feeder (to the extent of about 75% of its weight) when dimensioning the upper or top feeders.

Phase 2. The blind feeder acts independently only after the housing wall solidifies. Blind feeders can only operate in Phase 1 if an effective connecting tube exists between the feeder and the highest level of the liquid in the system.

centre of gravity, are the main advantages of the blind feeder.

It should be noted in the case of low-situated blind feeders that open feeders with a higher metal surface will help the low-positioned feeders to supply metal as long as a liquid connection remains between the upper and lower feeders (Fig. 84). Only after this connection has solidified does the blind feeder act independently. This means that about 66 to 75 per cent of the weight of the blind feeder must be added to the casting weight when calculating the size of this feeder, and only then must the uppermost, open feeders be determined.

The following basic rule applies to this type of casting: in calculating the feeders, always commence at the lowest point and proceed upwards.

5.4. Behaviour of the Feeder Head during Solidification

IMPORTANT FOR PRACTICE

Ideally, open topped feeder heads show a continuous shrinkage cavity in the form of a hollow cone, the generated surface of which is curved (Figs. 85a–b). The line of curvature is practically a parabola, and is theoretically a logarithmic curve (see also Figs. 341 and 342).

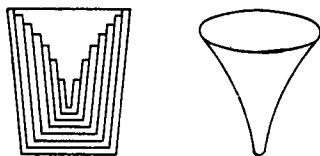


FIG. 85a. Formation of the conical type of shrinkage cavity due to the accumulation of solidified layers on the outer walls of the feeder head (after Schwietzke).

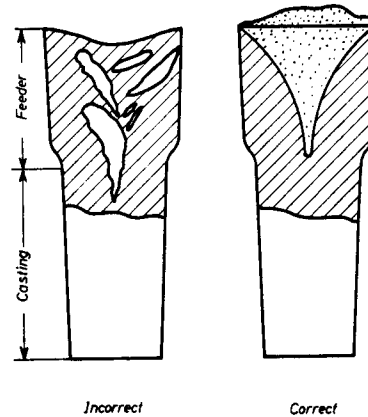


FIG. 85b. Unfavourable and favourable structure of the shrinkage cavity in the feeder head.

1. Formation of separate secondary cavities, separated by bridges of metal, due to unsuitable treatment of the feeder immediately after casting. These secondary cavities often extend far into the casting.
2. A coherent core is produced by spreading weakly exothermic antipiping compound on top of the feeder, or by immediate topping up with metal. In this way the metal in the feeder is utilized to better effect, and the casting is sound, using the same size of feeder.

The cavity is formed by evacuation of the feeder by the casting, resulting in a substantial reduction in the initial volume of the feeder. On the other hand, the heat radiating surface of the feeder is increased by the formation of the parabolic conical surface. If two cylinders of the same size are placed one above the other, as in Fig. 86, the modulus of the upper cylinder will decrease during solidification, due to a decrease in volume and an increase in surface area, i.e. it will solidify earlier than the casting (in this case the lower cylinder). The decrease in

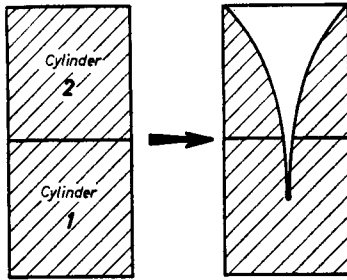


FIG. 86. Changes in two cylindrical castings of the same size during solidification.

At the moment of completion of pouring, both cylinders are the same size, and therefore possess the same modulus. During solidification metal is sucked out of the upper cylinder due to shrinkage, thereby reducing its volume and increasing its surface area. The modulus of the feeder cylinder thus decreases during solidification, with the result that such a feeder head will solidify earlier than the casting.

the modulus during solidification amounts to about 17 per cent of the original modulus. The modulus of the feeder at the beginning must therefore be about 1.2 times that of the casting, for the moduli of the feeder and casting to be equal after solidification is completed. This is the basis of the safety factor $f = 1.2$, which has been mentioned several times already (cf. Chapter 4, Sections 1 and 2 and Chapter 5, Section 6).

The expression "compensating factor" would be better, but the expression "safety factor" will be retained also, as it is in common use.

The shrinkage cone should not reach as far as the upper edge of the casting, but for safety the maximum permissible depth of the shrinkage cavity may be limited to $d = 0.8 H$ (where H = the height of the feeder). Parabolic shrinkage cones of this depth always occupy 14 per cent of the original feeder volume.

From this can also be calculated, from the contraction of the metal in question, the maximum volume or weight of casting that can be supplied from the feeder head. This volume should correspond to the capacity of the feeding range with economically designed feeders.

It is sometimes asserted in the literature that a feeder dimensioned to give the correct modulus will "automatically" contain enough liquid material to feed the casting. This is not always true by any means because of the 14 per cent limit due to a parabolic shrinkage cavity; the practical consequences will now be explained.

Massive bodies require less feeder metal than plate-shaped castings having the same modulus, in contradiction to the general opinion and to the "first impression."

Figure 87 and the attached table show that the shrinkage requirements of a plate can amount to several times those of a cube with the same modulus.

5.5. Shrinkage

By this is meant the reduction in volume of the metal in the liquid state up to the completion of solidification.

The reduction of volume in the solid state is known as contraction.

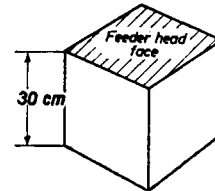
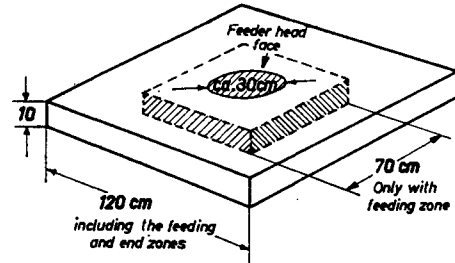


FIG. 87. Comparison of volumes and shrinkage requirements of a plate and a cube of the same modulus ($M = 5$ cm). Assumed shrinkage $S = 4.5\%$

	Volume, cm ³	Feeding requirements, cm ³
Plate without end zone	49,000	2200
Plate with end zone	144,000	6500
Cube	27,000	1220

The more intensive the shrinkage, the more rapidly the metal is drawn from the feeder and the more quickly the 14 per cent limit is reached. The temperature-dependent volume changes of the iron-carbon alloys were investigated by Benedicks, Ericsson, Ericson, Kothny and others^(7, 8); Fig. 88 shows the results. Figures 89 and 90 are derived from these results, Fig. 90 giving the

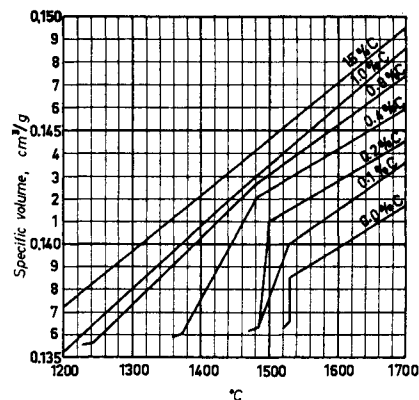


FIG. 88. Variations of specific volume with temperature of iron-carbon alloys (after Benedicks, Ericsson, Ericson and Kothny).

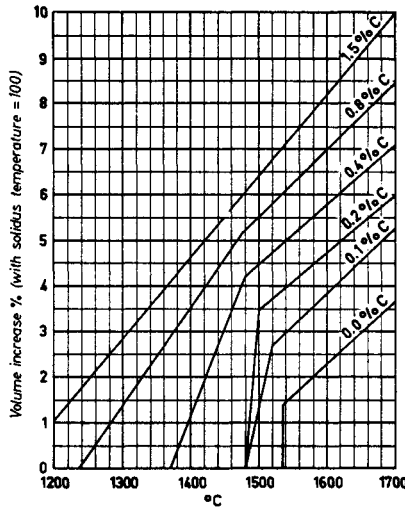


FIG. 89. Variations in the volume of iron-carbon alloys with temperature.

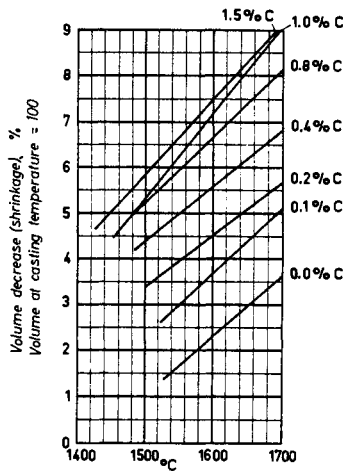


FIG. 90. Temperature dependence of the shrinkage of iron-carbon alloys.

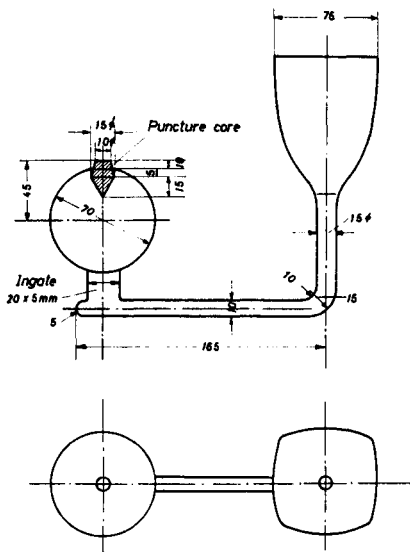
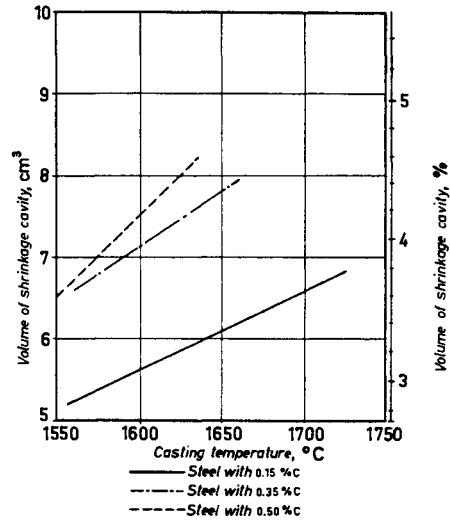


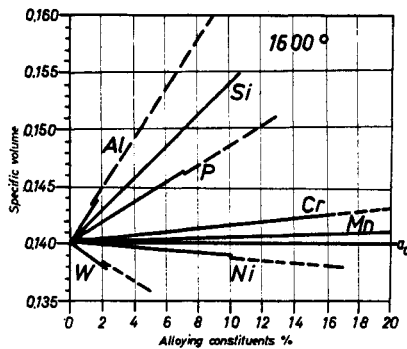
FIG. 91 a. Test piece for determining shrinkage volume (after Stein⁽⁹⁾).



According to Stein, these values are to be considered only as tendencies

FIG. 91 b. Influence of carbon content and casting temperature on the tendency of steels to form shrinkage cavities. The values were determined on a spherical sample (70 mm diam.), the cavity volumes being measured with low surface tension water (after Stein⁽⁹⁾).

shrinkage in per cent. The shrinkage of unalloyed steels is accordingly less than is normally assumed. Stein⁽⁹⁾ also made corresponding experiments (Figs. 91 a-b). The results in this case show trends only; nonetheless they agree fairly well in order of magnitude with the data published by the other authors. Due to the critical 14 per cent limit and to the small amount of shrinkage, small fluctuations are significant. For this reason the influence of other alloying elements was also investigated, unfortunately only at 1600°C (Fig. 92). However, if the



Calculation of shrinkage factor (values from table 6)

Specific volume

$$a_1 = a_0 + X_1 \times \tan \alpha$$

If the specific volume $a = 100\%$ at x , the shrinkage $S = (a_1 - a_0) / a_1$

$$S = \frac{100 \times X_1 \times \tan \alpha}{a_0 + X_1 \times \tan \alpha}$$

FIG. 92. Change in the specific volume of iron due to the presence of alloying elements at 1600°C.

same relationships are assumed to be approximately true for the entire temperature range, data of general validity can be derived for other temperatures (Table 6).

TABLE 6. CHANGE IN THE SHRINKAGE OF STEEL DUE TO ALLOYING ELEMENTS⁽⁷⁾

1. Change in shrinkage at 1600°C, after Benedicks, Ericsson *et al.*⁽⁷⁾.

Alloying element	Change in percentage shrinkage per 1% alloy content
Tungsten	- 0.53
Nickel	- 0.0354
Manganese	+ 0.0585
Chromium	+ 0.12
Silicon	+ 1.03
Aluminium	+ 1.70

2. Change in shrinkage at temperatures below 1600°C. Approximately linear relationships should be assumed between shrinkage factor and temperature, i.e. the above table is also valid at low temperatures. The shrinkage factors for carbon must be taken from Fig. 90.

3. Example: manganese steel, casting temp. about 1450°C.

Analyses		Shrinkage factor	× % Alloy content	Shrinkage %
Element	%			
C	1.5	from Fig. 90 →	—	+ 5
Mn	15	+ 0.0585	× 15	+ 0.88
Si	0.3	+ 1.03	× 0.3	+ 0.31
Cr	1.25	+ 0.12	× 1.25	+ 0.12
Sum				+ 6.31 → 6.5

4. Safety. As 2. is based on an assumption, the result should be rounded off to the nearest five-tenths, i.e. 6.31 → 6.5.

5.6. Calculations Giving the Shrinkage Cavity Characteristics of the Best Form of Feeder Head and the Compensating Factor

(Even if this section is omitted, the remaining sections on feeder calculation can be understood.)

Instead of taking the logarithmic curvature of the shrinkage cavity in the feeder head, a parabolic form can be assumed for practical purposes, corresponding to the equation:

$$y = \frac{x^2}{2p} \tag{14}$$

where p is the parameter. By rotating round the axis $a-a$ (Fig. 93) a parabolic cone is generated, having a depth

$$d = \frac{R^2}{2p} \tag{15}$$

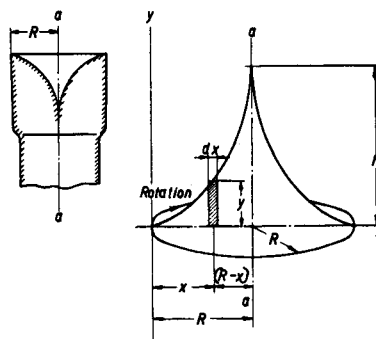


FIG. 93. Shrinkage cavity conceived as a parabolic core generated by rotation round the axis $a-a$.

R is also the radius of the feeder head. Volume and parameter can now be calculated. We have:

$$V_{sc} = 2\pi \int_0^R (R-x)y \, dx = 2\pi \int_0^R (R-x) \frac{x^2}{p} \, dx$$

$$= \frac{\pi}{p} \left(\frac{R^4}{3} - \frac{R^3}{3} \right) \text{ and} \tag{a}$$

$$V_{sc} = \frac{\pi R^4}{12p} \text{ or } p = \frac{\pi R^4}{12V_{sc}} \tag{16}$$

where V_{sc} is the volume of the parabolic shrinkage cone.

The surface area H of the cone is:

$$H = 2\pi \int_0^R (R-x) \sqrt{1+y^2} \, dx$$

$$y' = \frac{x}{p}; \quad y^2 = \frac{x^2}{p^2}$$

$$H = 2\pi R \int_0^R \sqrt{1 + \frac{x^2}{p^2}} \times dx - 2\pi \int_0^R x \sqrt{1 + \frac{x^2}{p^2}} \times dx$$

$$= \frac{2\pi R}{p} \int_0^R \sqrt{p^2 + x^2} \times dx - \frac{2\pi}{p} \int_0^R x \sqrt{p^2 + x^2} \times dx$$

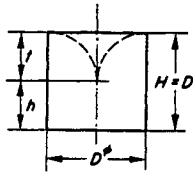
$$= 2\pi R \left[\frac{R}{2} \sqrt{p^2 + R^2} + \frac{p^2}{2} \ln(R + \sqrt{p^2 + R^2}) - \right.$$

$$\left. - \frac{p^2}{2} \ln p \right] - \frac{1}{3} [(p^2 + R^2)^{3/2} - p^3] - [(p^2)^{3/2} - p^3] \tag{17}$$

Instead of this unwieldy equation, individual curves can also be divided out into sections and determined planimetrically, or the arc lengths measured and the trapezoidal sections calculated.

Hence only the model cases for the radii $R = 10$ and $R = 14.2$ were calculated (cf. Table 7) and these were transposed to other radii in accordance with the law of geometrical similarity.

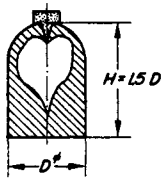
TABLE 7a.



Feeder values before commencement of shrinkage
 $V_F = 6280 \text{ cm}^3$
 Generated surface $A = D$;
 $H = 1280 \text{ cm}^2$;
 Cooling surface = 1594 cm^2
 Modulus = 3.95 cm

Depth of cavity t	cm	8	12	16	20
Vol. of cavity V_{sc}	cm^3	426	642	852	1070
Generated surface of the cavity cone H	cm^2	379	461	534	593
Steel volume in the feeder at the end of solidification VE	cm^3	5854	5638	5428	5210
Cooling surface on solidification = $A + H$	cm^2	1655	1730	1790	1880
Modulus on solidification = $\frac{VE}{A+H}$	cm	3.54	3.25	3.03	3.77
Data in fractions of the original values	Depth of cavity t_H	0.4	0.6	0.8	1.0
	Vol. of cavity V_{sc}/V_F	0.07	0.1	0.135	0.17
	Steel volume on solidification $VE/VF = \frac{V_F - V_{sc}}{V_F}$	0.93	0.9	0.865	0.83
	Modulus ME/V_F	0.895	0.82	0.77	0.70

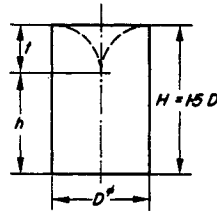
TABLE 7c.



Feeder values before commencement of shrinkage $V_F = 8340 \text{ cm}^3$
 Cooling surface = 1880 cm^2
 Modulus = 4.44 cm
 The depth of the shrinkage cavity can only be calculated approximately due to the spherical cap. The cavity measures at the most 17% of the initial volume, reducing to 14% if a safety limit is incorporated.

Vol. of cavity V_{sc}/V_T	0.02	0.05	0.10	0.13	0.17
Steel volume in the feeder at the end of solidification	0.98	0.95	0.90	0.87	0.83
Modulus at the end of solidification cm	4.35	4.21	4.00	3.86	3.70
Modulus in fractions of the initial modulus ME/M_F	0.98	0.95	0.90	0.87	0.835
Factor $f = \frac{M_F}{ME}$	1.04	1.05	1.11	1.15	1.2

TABLE 7b.

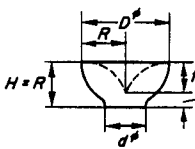


Feeder values before commencement of shrinkage
 $V_F = 9420 \text{ cm}^3$
 Generated surface $A = 1920 \text{ cm}^2$
 Cooling surface = 2234 cm^2
 Initial modulus = 4.21 cm

Depth of cavity t	cm	8	12	16	20	25	30
Vol. of cavity V_{sc}	cm^3	426	642	852	1070	1336	1606
Generated surface of the cavity cone H	cm^2	379	461	534	593	656	800
Steel volume in the feeder at the end of solidification VE	cm^3	8994	8778	8568	8350	8084	7814
Cooling surface on solidification = $A + H$	cm^2	2295	2370	2430	2520	2620	2700
Modulus on solidification = $\frac{VE}{A+H}$	cm	3.91	3.71	3.53	3.31	3.09	2.89
Data in fractions of the original values	Depth of cavity t_H	0.266	0.4	0.533	0.67	0.83	1.0
	Vol. of cavity V_{sc}/V_F	0.045	0.068	0.091	0.113	0.141	0.17
	Steel volume on solidification $VE/VF = \frac{V_F - V_{sc}}{V_F}$	0.955	0.932	0.909	0.887	0.859	0.83
	Modulus ME/M_F	0.93	0.88	0.84	0.785	0.735	0.685

The main part of the cavity volume lies near the base of the cone. An obvious step is to increase the size of this base and so reduce the depth d of the cavity for a given cavity volume. Not only cylindrical but also conical or hemispherical feeders, the exterior shape of which is adapted to the type of cavity, will be investigated.

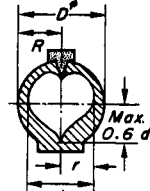
TABLE 7d.



Feeder values before commencement of shrinkage
 $V_F = 5980 \text{ cm}^3$
 Generated surface $A = 1153 \text{ cm}^2$
 Cooling surface = 1778 cm^2
 Modulus = 3.36 cm

Depth of cavity t	cm	5	7.5	10	14.2
Vol. of cavity V_{SC}	cm^3	528	794	1056	1500
Generated surface of the cavity cone H	cm^2	600	694	738	815
Steel volume in the feeder of solidification V_E	cm^3	5432	5186	4924	4480
Cooling surface on solidification = $A + H$	cm^2	1753	1847	1891	1968
Modulus on solidification $M_E = \frac{VE}{A+H}$	cm	3.11	2.81	2.61	2.28
Data in fractions of the original values	Depth of cavity t_H	0.35	0.53	0.70	0.1
	Vol. of cavity V_{SC}/V_F	0.088	0.133	0.18	0.25
	Steel volume on solidification $VE/V_F = \frac{V_F - V_{SC}}{V_F}$	0.912	0.867	0.82	0.75
	Modulus ME/M_F	0.93	0.86	0.78	0.68

TABLE 7c.



Assumptions $d \approx 0.67 D$
 $D = 1.49d$
 $R = 1.49r$

$$V_{\text{Parabola}} = \frac{r^4}{12p}$$

$$t = 0.6d = 1.2r = \frac{r^2}{2p} \quad p = \frac{r^2}{2t}$$

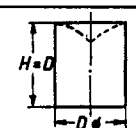
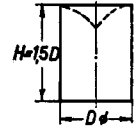
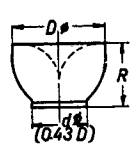
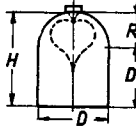
$$V_p = \frac{r^4}{12p} = \frac{r^4 \cdot 2 \cdot t}{12 \cdot r^2} = \frac{r^2 t}{6} = \frac{r^2 \cdot 1.2r}{6} = r^3 \cdot 0.2 = 0.626r^3$$

$$V_{\text{upper}} = 2.06r^3 \quad V_{\text{Q}} = \frac{2.06 + 0.626}{2.686}r^3$$

$$V_{\text{Solid sphere}} = 4.12R^3 = (1.49)^3 \cdot 4.12 \cdot r^3 = 13.6r^3$$

$$V_{\text{Q}} = 0.197 \cdot V_{\text{O}} \approx 0.2 \cdot V_{\text{O}} \text{ or } \sim 20\% \text{ of the solid sphere}$$

FIG. 94. Change in the characteristic values of various shapes of feeder using approximate and accurate methods of calculation.

Feeder shape	Characteristic values in relationship to the modulus of the feeder	
	accurate	approximate
	$V_F = 2R^3\pi = 99(M_F)^3$ $A_F = 5R^2\pi$ $M_F = 0.4R = 0.2D$ $R = 2.5M_F$ $R^3 = 15.8(M_F)^3$	$V_F = 2R^3\pi = 167(M_F)^3$ $A_F = 6R^2\pi$ $M_F = 0.1667D = \frac{D}{6} = \frac{R}{3}$ $R = 3.33M_F$ $R^3 = 37(M_F)^3$
	$V_F = 3R^3\pi = 122(M_F)^3$ $A_F = 7R^2\pi$ $M_F = 0.429R = 0.2145D$ $R = 2.33M_F$ $R^3 = 12.6(M_F)^3$	$V_F = 3R^3\pi = 179(M_F)^3$ $A_F = 8R^2\pi$ $M_F = 0.375R = 0.187D$ $R = 2.67M_F$ $R^3 = 19(M_F)^3$
Prematurely solidified corners	-	-
	$V_F = 2.09R^3 = 156(M_F)^3$ $M_F = 0.237R = 0.1185D$ $R = 4.21M_F; R^3 = 76(M_F)^3$ $r = 1.85M_F$ $M_{\text{neck}} = \frac{M_F}{1.1} = 0.5r = 0.91M_F$	$V_F = 2.09R^3 = 191(M_F)^3$ $A_F = 3R^2\pi$ $M_F = 0.222R$ $R = 4.5M_F$ $R^3 = 91(M_F)^3$ $r = 0.4R = 1.8M_F$
	$V_F = 8.34R^3 = 96(M_F)^3$ $A_F = 6R^2\pi$ $M_F = 0.444R = 0.222D$ $R = 2.25M_F$ $R^3 = 11.5(M_F)^3$	$V_F = 8.34R^3 = 156(M_F)^3$ $A_F = 7R^2\pi$ $M_F = 0.378R = 0.189D$ $R = 2.65M_F$ $R^3 = 18.7(M_F)^3$

It is an advantage for comparison purposes to give all feeder dimensions in connection with the modulus, which of course represents a length. The calculations must first of all be accurate, i.e. the feeder/casting interface, on which no cooling occurs, must not be included in the determination of the modulus. Figure 94 gives characteristic values for various forms of feeder, using both approximate and exact calculations, and shows the existence of differences.

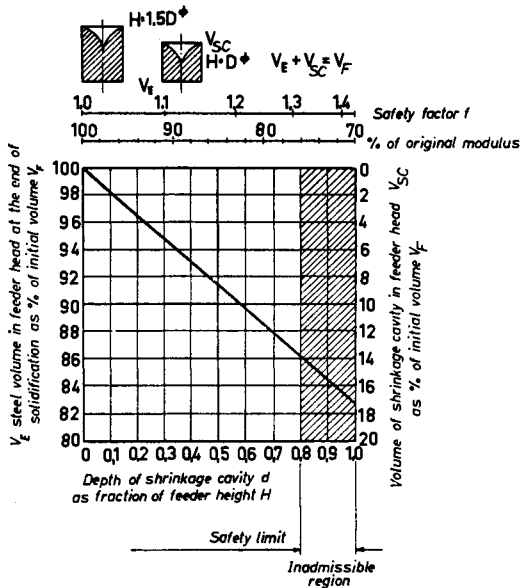


FIG. 95. Modulus and shrinkage cavity volume as a function of the depth of the cavity in the feeder. Applies to cylindrical feeders of the shapes $H = D$ and $H = 1.5D$.

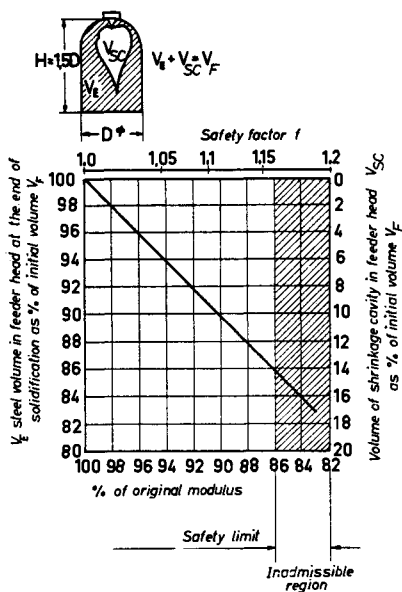


FIG. 96. Modulus and safety factor f as a function of the shrinkage cavity in blind feeder heads.

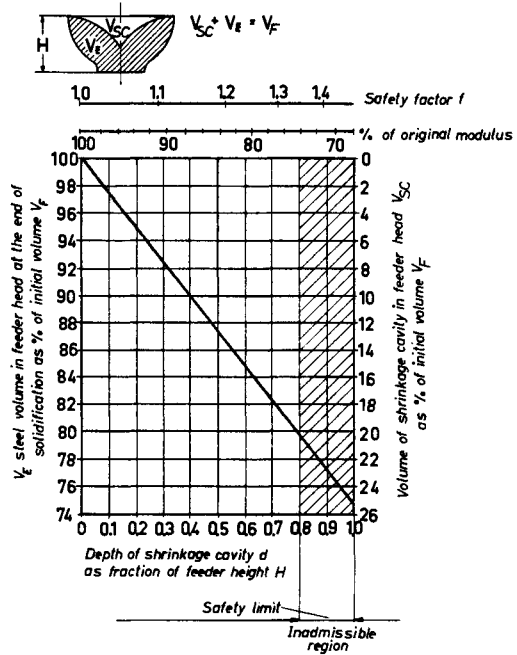


FIG. 97. Modulus and shrinkage cavity volume as a function of the depth of the cavity in the feeder. Applies to hemispherical feeder shapes.

These feeder types were calculated in Tables 7a-e as model cases, and the results converted to numbers having general validity. Figures 95-97 show the behaviour of the feeder when forming shrinkage cavities. The volume of the cavity increases in direct proportion to its depth, and the feeder modulus decreases linearly, which simplifies the subsequent calculations. The safety ("compensating") factor can be derived directly; it varies according to the depth of the cavity. The practical calculation may be based, not on the final modulus at the completion of solidification, but on the mean of the initial and final moduli. On true safety grounds, however, the requirement is laid down that the feeder modulus on the completion of solidification shall coincide with the modulus of the casting.

To the extent that the interface feeder/casting is not allowed for (always in the practical rapid calculation) so that it is included as a cooling surface in the calculation (approximate method), the result is a displacement of the factor f , the size of which is a function of the shape of the casting. Various factors are compared in Table 8.

In most castings this factor then lags by about 0.1, but becomes identical with massive parts. As, however, the degree of utilization of the feeder is low on massive parts, i.e. the depth of the shrinkage cavity is less and the 14 per cent limit is not reached as quickly, the factor is less in itself in such parts (cf. also Fig. 87). Consequently, the factor $f = 1.2$ can be used throughout in the approximate method. In the present section the accurate method of calculation will be used, so as to obtain exact values; but the approximate method will be employed for the remainder of the book.

TABLE 8. CHANGE IN THE EQUALIZATION FACTOR f WHEN THE APPROXIMATE CALCULATION IS COMPARED WITH THE ACCURATE ONE

	Calculation	
	accurate (allowing for feeder/casting interface)	approximate (no allowance made for feeder/casting interface)
Plate (with feeder zone only)	$f = 1.29$	$f = 1.23$
Bar 1 : 4, with feeder and end zone	$f = 1.33$	$f = 1.25$
Bar 1 : 1 with feeder and end zone	$f = 1.28$	$f = 1.19$
Cube	$f = 1.187$	$f = 1.187$

The f -values for approximate calculation are determined by back-calculation, i.e. the feeder dimensions are determined first by the accurate method, then the approximate modulus of the feeder determined in this way is calculated, and divided by the approximate casting modulus.

Nicolas⁽¹⁰⁾ introduced for the first time the feeder calculation using the factor $f = 1.2$ (but without the mathematical-physical basis that is given here) which enabled theoretically accurate (although practically unnecessary) calculations to be made. As the change in surface area of the feeder head is also taken into account, the method is more accurate than the calculating procedure given by Namur⁽⁶⁾ which only allowed for the changes in volume. As Namur's method is also complicated, the simpler method developed by Nicolas will be used for calculation.

Figure 98 shows the influence of the shrinkage S (in

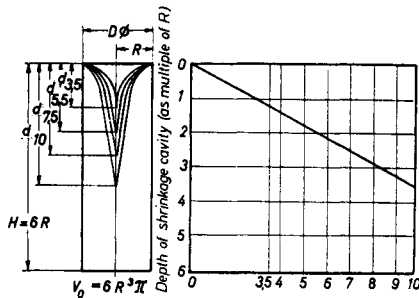


FIG. 98. Relationship: depth of shrinkage cavity-shrinkage in cylinder.

depth of cavity (as multiple of R)
shrinkage S , %
shrinkage cavity

$$V_{SC} = \frac{V_0 \cdot \text{shrinkage } \%}{100}$$

depth of cavity (calculated in this case without a safety allowance)

$$d = \frac{6V_{SC}}{R^2} = 36 \cdot R \cdot \frac{\text{shrinkage } \%}{100}$$

V_0 = initial volume of the whole block (before cavity begins to form)

d = depth of cavity

V_{SC} = volume of cavity

per cent) on the depth of the cavity d . We have:

$$V_{SC} = S/100 (V_{\text{casting}} + V_{\text{feeder}}) \text{ and}$$

$$V_{\text{casting}} = \frac{100 V_{SC} - S \cdot V_F}{S} \tag{18}$$

According to Figs. 95, 96 and 97 the following is true for cylindrical feeders:

$$V_{SC} = 0.14 V_F \tag{19}$$

and the max.

$$V_{\text{max}} = V_F \frac{14 - S}{S} \tag{20}$$

for hemispherical feeders:

$$V_{SC} = 0.20 V_F \text{ and} \tag{21}$$

$$V_{\text{max}} = V_F \frac{20 - S}{S} \tag{22}$$

Hence the feeder volume and the maximum volume of casting (V_{max}) which can be fed (**not to be confused with the feeding range!**) are related via the shrinkage S (Figs. 99a-b). In the feeder tables 9-19, therefore, the maximum volume which can be fed is entered for each feeder for different amounts of shrinkage.

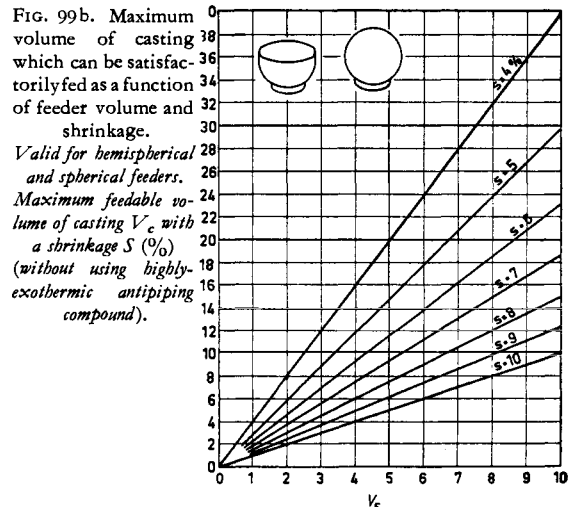
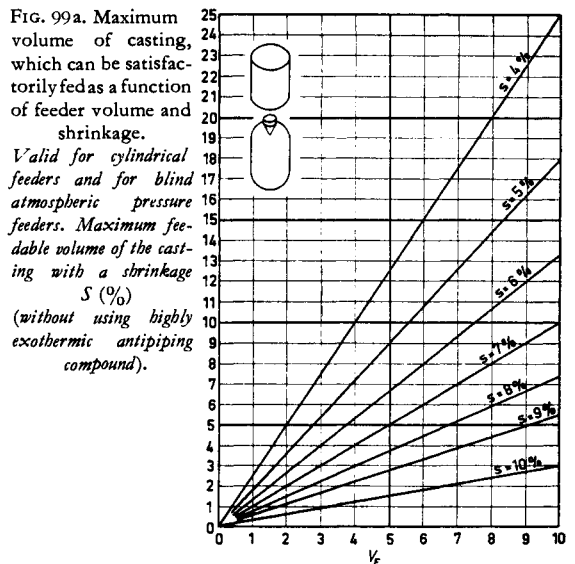
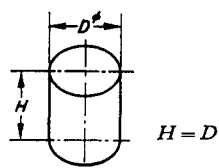
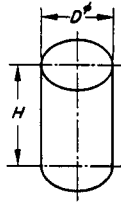


FIG. 99a. Maximum volume of casting, which can be satisfactorily fed as a function of feeder volume and shrinkage. Valid for cylindrical feeders and for blind atmospheric pressure feeders. Maximum feedable volume of the casting with a shrinkage S (%) (without using highly exothermic antipiping compound).

FIG. 99b. Maximum volume of casting which can be satisfactorily fed as a function of feeder volume and shrinkage. Valid for hemispherical and spherical feeders. Maximum feedable volume of casting V_c with a shrinkage S (%) (without using highly exothermic antipiping compound).

TABLE 9. CYLINDRICAL FEEDER HEAD $H = D$

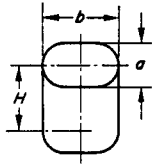
M_F cm	$D \varnothing$ H mm	V cm ³ litres	W kg m. tons	Max. feedable volume of casting V (wt W) for a shrinkage of:							
				4%		5%		6%		7%	
				V cm ³ , l.	W kg, t	V cm ³ , l.	W kg, t	V cm ³ , l.	W kg, t	V cm ³ , l.	W kg, t
0.5	30	22	0.15	55	0.43	40	0.32	30	0.24	22	0.17
0.6	36	37	0.26	93	0.73	67	0.53	50	0.39	37	0.29
0.7	42	57	0.39	143	1.12	104	0.82	77	0.60	57	0.45
0.8	48	86	0.59	215	1.68	155	1.20	116	0.91	86	0.67
0.9	54	123	0.84	318	2.50	220	1.82	165	1.30	123	0.96
1.0	60	169	1.15	422	3.30	305	2.40	228	1.80	169	1.31
1.1	66	225	1.55	562	4.40	405	3.17	304	2.37	225	1.75
1.2	72	290	1.97	725	5.70	525	4.10	392	3.85	290	2.26
1.3	78	370	2.52	925	7.20	670	5.25	500	3.90	370	2.90
1.4	84	460	3.12	1.2	9.40	830	6.50	625	4.90	460	3.60
1.5	90	570	3.88	1.4	10.9	1.0	7.80	770	6.00	570	4.45
1.6	96	690	4.70	1.7	13.3	1.3	10.2	940	7.30	690	5.40
1.7	102	820	5.60	2.1	16.4	1.5	11.7	1.1	8.60	820	6.40
1.8	108	980	6.70	2.5	19.5	1.8	14.0	1.3	10.2	980	7.75
1.9	114	1.2	8.20	3.0	23.5	2.2	17.2	1.6	12.5	1.2	9.35
2.0	120	1.4	9.50	3.5	27.4	2.5	19.5	1.9	14.8	1.4	10.9
2.2	132	1.9	13.0	4.8	37.5	3.4	26.5	2.6	20.3	1.9	14.8
2.4	144	2.3	15.5	5.8	45.2	4.1	32.0	3.1	24.2	2.3	18.0
2.6	156	3.1	21.0	7.8	61.0	5.6	43.6	4.2	32.8	3.1	24.2
2.8	168	3.7	25.1	9.3	72.5	6.7	52.2	5.0	39.0	3.7	28.9
3.0	180	4.5	30.5	11	86.0	8.1	63.5	6.1	47.6	4.5	35.2
3.2	192	5.5	37.5	14	109	9.9	77.5	7.5	58.5	5.5	43.0
3.4	204	6.6	45.0	17	133	12	93.5	9.0	70.5	6.6	51.5
3.6	216	7.8	53.0	20	156	14	109	11	86.0	7.8	61.0
3.8	228	9.3	64.0	23	180	17	133	13	101	9.3	72.5
4.0	240	11	75.0	28	218	20	156	15	117	11	86.0
4.25	256	13	88.0	33	256	22	172	18	141	13	101
4.50	270	15	102	38	298	27	210	20	156	15	117
4.75	285	18	123	45	352	33	256	24	187	18	141
5.00	300	21	143	53	415	38	296	29	226	21	164
5.25	315	25	170	63	491	45	352	34	265	25	195
5.50	330	28	190	70	548	51	400	38	296	28	218
5.75	345	32	218	80	625	58	452	43	336	32	250
6.0	360	37	252	93	725	67	523	50	390	37	290
6.25	375	41	278	104	810	74	580	56	436	41	320
6.50	390	46	312	115	900	83	650	63	490	46	360
6.75	405	52	352	130	1.0	94	735	70	545	52	405
7.0	420	58	395	145	1.1	105	825	80	625	58	452
7.25	435	64	435	160	1.2	115	900	86	670	64	500
7.50	450	71	482	180	1.4	130	1.0	96	750	71	555
7.75	465	78	530	198	1.5	140	1.1	105	820	78	610
8.0	480	87	592	220	1.7	157	1.2	118	920	87	680
8.25	495	95	650	240	1.9	172	1.3	130	1.0	95	740
8.50	510	104	710	260	2.0	190	1.5	140	1.1	104	810
8.75	525	113	765	282	2.2	205	1.6	154	1.2	113	880
9.0	540	123	840	310	2.4	222	1.7	165	1.3	123	960
9.25	555	131	890	330	2.6	235	1.8	177	1.4	131	1.0
9.50	570	144	980	360	2.8	260	2.0	195	1.5	144	1.1
9.75	585	155	1.1	385	3.0	280	2.2	210	1.6	155	1.2
10.0	600	169	1.2	422	3.3	305	2.4	228	1.8	169	1.3
10.5	630	195	1.3	490	3.8	350	2.7	262	2.1	195	1.5
11	660	224	1.5	560	4.4	405	3.2	304	2.4	224	1.7
11.5	690	256	1.8	640	5.0	460	3.6	350	2.7	256	2.0
12	720	290	2.0	730	5.7	525	4.1	392	3.1	290	2.3
12.5	750	328	2.3	820	6.4	595	4.7	440	3.4	328	2.6
13	780	370	2.5	930	7.3	665	5.2	500	3.9	370	2.9
13.5	810	415	2.8	1040	8.1	750	5.9	560	4.4	415	3.2
14	840	460	3.2	1150	9.0	825	6.5	625	4.9	460	3.6
14.5	870	515	3.5	1300	10.0	930	7.3	700	5.5	515	4.0
15	900	570	3.9	1430	11.1	1030	8.0	770	6.0	570	4.5
16	960	690	4.7	1730	13.5	1250	9.7	930	7.3	690	5.4
17	1020	830	5.7	2100	16.4	1500	11.7	1120	8.7	830	6.5
18	1080	980	6.7	2450	19.0	1800	14.0	1330	10.4	980	7.7
19	1140	1150	7.8	2860	22.5	2070	16.2	1550	2.0	1150	9.0
20	1200	1350	9.2	3400	26.5	2430	19.0	1830	14.3	1350	10.5



$H = 1.5 D$

TABLE 10. CYLINDRICAL FEEDER HEAD $H = 1.5 D \varnothing$

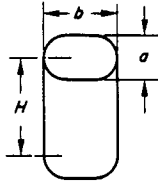
M_F	$D \varnothing$	H	V	W	Max. feedable volume of casting V (wt W) for a shrinkage of:							
					4%		5%		6%		7%	
					V	W	V	W	V	W	V	W
cm	mm	mm	cm ³ litres	kg m. tons	cm ³ , l.	kg, t	cm ³ , l.	kg, t	cm ³ , l.	kg, t	cm ³ , l.	kg t
0.5	27	40	24	0.17	60	0.47	43	0.34	33	0.26	24	0.19
0.6	32	48	40	0.27	100	0.78	72	0.56	54	0.43	40	0.31
0.7	38	57	62	0.42	155	1.20	112	0.87	84	0.65	62	0.49
0.8	43	65	93	0.63	230	1.80	167	1.30	126	0.98	93	0.73
0.9	48	72	131	0.90	330	2.58	236	1.85	177	1.37	131	1.02
1.0	54	81	180	1.22	450	3.52	324	2.54	244	1.90	180	1.41
1.1	59	89	239	1.63	600	4.70	430	3.35	324	2.55	239	1.85
1.2	64	96	315	2.14	790	6.20	570	4.45	425	3.33	315	2.46
1.3	70	105	400	2.72	1.0	7.80	720	5.60	540	4.30	400	3.12
1.4	75	113	500	3.40	1.3	10.0	900	7.0	680	5.30	500	3.90
1.5	80	120	610	4.15	1.5	11.7	1.1	8.6	830	6.50	610	4.76
1.6	86	130	740	5.0	1.9	14.9	1.3	10.0	1.0	7.80	740	5.80
1.7	91	137	890	6.1	2.2	17.2	1.6	12.5	1.2	9.30	890	7.00
1.8	96	144	1.0	6.8	2.5	19.5	1.8	14.0	1.4	10.9	1.0	7.80
1.9	102	153	1.2	8.2	3.0	23.5	2.2	17.1	1.6	12.5	1.2	9.35
2.0	107	160	1.5	10	3.8	29.6	2.7	21.0	2.0	15.6	1.5	12.7
2.2	118	177	1.9	13	4.7	36.7	3.4	26.5	2.6	20.2	1.9	14.8
2.4	128	192	2.5	17	6.3	49.0	4.5	35.1	3.4	26.5	2.5	19.5
2.6	140	210	3.4	23	8.5	66.5	6.1	47.8	4.6	36.0	3.4	26.5
2.8	150	225	4.0	27	10	78.0	7.2	56.2	5.4	42.3	4.0	31.3
3.0	160	240	4.9	34	12	93.0	8.9	69.5	6.7	52.3	4.9	38.3
3.2	172	258	5.8	40	15	117	11	86.0	7.8	61.0	5.8	45.3
3.4	182	274	7.2	49	18	141	13	102	9.7	76.0	7.2	56.2
3.6	192	288	8.5	58	21	164	15	117	12	93	8.5	65.3
3.8	204	306	10	68	25	195	18	141	14	109	10	78.0
4.0	214	320	12	82	30	235	22	172	16	125	12	93.5
4.25	228	344	14	95	35	273	25	195	19	148	14	109
4.50	240	360	16	109	40	312	29	226	22	172	16	125
4.75	255	384	19	130	48	375	34	265	26	203	19	148
5.0	266	400	22	150	55	430	40	312	30	235	22	172
5.25	280	420	26	180	65	510	47	366	35	274	26	203
5.50	294	440	30	205	75	586	54	422	41	320	30	235
5.75	308	460	35	240	88	686	63	491	47	366	35	273
6.0	320	480	39	270	97	760	70	548	53	414	39	305
6.25	335	500	44	300	110	860	79	618	60	470	44	343
6.50	347	520	50	340	125	960	90	705	68	531	50	390
6.75	361	542	56	380	140	1.1	100	780	76	596	56	436
7.0	375	562	62	420	155	1.2	112	875	84	655	62	485
7.25	388	582	69	470	175	1.4	125	970	94	735	69	540
7.50	400	600	77	520	195	1.5	140	1.1	104	815	77	600
7.75	415	625	84	570	210	1.6	150	1.2	114	890	84	655
8.0	428	642	93	630	235	1.8	170	1.3	126	1.0	93	733
8.25	440	660	103	700	260	2.0	185	1.5	140	1.1	103	800
8.50	455	680	112	760	280	2.2	202	1.6	151	1.2	112	875
8.75	470	705	122	830	305	2.5	220	1.7	165	1.3	122	950
9.0	482	725	133	900	335	2.6	240	1.9	180	1.4	133	1.0
9.25	495	742	143	960	360	2.8	257	2.0	195	1.5	143	1.1
9.50	508	762	156	1.1	390	3.0	280	2.2	212	1.7	156	1.2
9.75	522	785	168	1.2	425	3.3	305	2.4	228	1.8	168	1.3
10.0	535	800	180	1.3	450	3.5	325	2.5	244	1.9	180	1.4
10.5	561	845	210	1.4	525	4.1	380	2.9	284	2.2	210	1.7
11	590	885	240	1.6	600	4.7	430	3.4	325	2.5	240	1.9
11.5	615	920	276	1.9	675	5.3	500	3.9	375	2.9	276	2.2
12	645	970	315	2.2	790	6.2	565	4.4	425	3.3	315	2.5
12.5	670	1000	352	2.4	880	6.9	635	5.0	480	3.8	352	2.8
13	700	1050	400	2.7	1000	7.8	720	5.6	540	4.2	400	3.1
13.5	725	1090	445	3.1	1120	8.7	800	6.3	600	4.7	445	3.5
14	750	1130	500	3.4	1250	9.7	900	7.1	680	5.3	500	3.9
14.5	775	1160	554	3.8	1400	11.0	1000	7.8	750	5.9	554	4.3
15	805	1210	610	4.2	1530	12.0	1100	8.6	825	6.5	610	4.8
16	860	1290	744	5.1	1870	14.6	1350	10.5	1000	7.8	744	5.8
17	910	1370	890	6.1	2250	17.5	1600	12.5	1200	9.3	890	7.0
18	965	1450	1060	7.2	2650	20.7	1900	14.8	1450	11.3	1060	8.3
19	1020	1530	1250	8.5	3150	24.6	2250	17.5	1700	13.3	1250	9.7
20	1070	1600	1400	9.5	3500	27.4	2510	18.6	1900	14.8	1400	10.9



$$b = 1.5a \quad H = \frac{a + b}{2} = 1.25a$$

TABLE 11. OVAL FEEDER HEAD

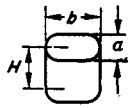
M_F	a	b	H	V	W	Max. feedable volume of casting V (wt W) for a shrinkage of:							
						4%		5%		6%		7%	
						V	W	V	W	V	W	V	W
cm	mm	mm	mm	cm ³ litres	kg m. tons	cm ³ , l.	kg, t	cm ³ , l.	kg, t	cm ³ , l.	kg, t	cm ³ , l.	kg, t
0.5	24	36	30	24	0.16	60	0.47	43	0.34	33	0.26	24	0.19
0.6	29	44	37	40	0.27	100	0.78	72	0.56	54	0.42	40	0.31
0.7	34	51	43	62	0.42	155	1.20	112	0.88	84	0.65	62	0.48
0.8	39	59	49	93	0.63	235	1.83	167	1.30	125	0.97	93	0.72
0.9	44	66	55	132	0.90	330	2.58	232	1.80	178	1.40	132	1.03
1.0	49	74	61	182	1.25	455	3.55	326	2.55	245	1.90	182	1.42
1.1	54	81	67	240	1.63	600	4.70	430	3.35	325	2.54	240	1.87
1.2	59	88	73	315	2.15	790	6.15	565	4.40	425	3.30	315	2.45
1.3	63	95	79	400	2.72	1.0	7.80	720	5.60	540	4.20	400	3.14
1.4	68	102	85	500	3.40	1.3	10.0	900	7.00	680	5.30	500	3.90
1.5	73	110	91	610	4.45	1.5	11.7	1.1	8.60	825	6.50	610	4.75
1.6	78	117	97	740	5.00	1.9	15.0	1.3	10	1.0	7.80	740	5.80
1.7	83	125	103	890	6.00	2.2	17.0	1.6	13	1.2	9.30	890	7.00
1.8	88	132	109	1.0	6.80	2.5	19.5	1.8	14	1.4	11	1.0	7.80
1.9	92	138	115	1.2	8.20	3.0	23.4	2.2	17	1.6	13	1.2	9.40
2.0	97	145	121	1.5	10.0	3.7	29.0	2.7	21	2.0	16	1.5	12
2.2	107	160	133	1.9	13.0	4.8	37.5	3.4	27	2.6	20	1.9	15
2.4	116	174	145	2.5	17.0	6.3	49.0	4.5	35	3.4	27	2.5	20
2.6	126	189	157	3.4	23.0	8.5	66.0	6.1	48	4.6	36	3.4	26
2.8	135	203	169	4.0	27.0	10	78.0	7.2	56	5.4	42	4.0	32
3.0	147	220	181	4.9	33.0	12	94.0	8.8	68	6.6	52	4.9	38
3.2	155	233	193	5.9	40.0	15	117	11	86	8.0	63	5.9	46
3.4	165	248	205	7.2	49.0	18	140	13	100	9.8	77	7.2	56
3.6	175	263	218	8.5	58.0	21	164	15	118	12	94	8.5	66
3.8	185	277	230	10	68.0	25	195	18	140	14	109	10	78
4.0	195	293	242	12	82.0	30	233	22	170	16	125	12	94
4.25	206	310	256	14	95.0	35	274	25	195	19	148	14	110
4.50	218	326	272	16	109	40	312	29	230	22	171	16	125
4.75	230	345	286	19	130	48	375	34	265	26	203	19	150
5.0	242	362	302	22	150	55	430	40	314	30	234	22	170
5.25	253	380	316	26	177	66	512	47	366	35	272	26	200
5.50	266	400	332	30	204	75	586	54	420	41	320	30	230
5.75	276	415	347	35	238	88	685	63	490	48	375	35	270
6.0	280	420	362	39	265	98	765	70	545	53	414	39	300
6.25	303	455	376	44	300	110	860	79	615	60	468	44	340
6.5	315	472	394	50	340	125	970	90	700	68	530	50	390
6.75	326	490	408	56	380	140	1.1	100	780	76	590	56	440
7.0	340	510	424	62	420	155	1.2	112	880	84	655	62	480
7.25	351	530	438	69	470	173	1.4	125	970	93	725	69	540
7.50	363	545	452	77	525	192	1.5	138	1.1	104	810	77	600
7.75	376	565	468	84	570	210	1.6	150	1.2	113	880	84	660
8.0	388	582	484	93	630	235	1.8	167	1.3	126	980	93	730
8.25	400	600	500	103	700	260	2.0	185	1.4	140	1.1	103	800
8.5	414	620	513	112	760	280	2.2	202	1.6	152	1.2	112	875
8.75	425	638	528	122	830	305	2.4	220	1.7	165	1.3	122	950
9.0	436	656	545	133	900	335	2.6	240	1.9	180	1.4	133	1.0
9.25	448	670	560	143	970	360	2.8	257	2.0	193	1.5	143	1.1
9.50	460	690	575	156	1.1	390	3.0	280	2.2	210	1.6	156	1.2
9.75	472	710	590	168	1.2	425	3.3	302	2.4	226	1.8	168	1.3
10.0	485	730	605	182	1.3	456	3.6	326	2.5	245	1.9	182	1.4
10.5	510	765	635	210	1.4	526	4.1	378	3.0	284	2.2	210	1.6
11	535	800	665	240	1.6	600	4.7	430	3.3	325	2.6	240	1.9
11.5	558	835	695	276	1.9	695	5.4	500	3.9	375	3.0	276	2.1
12	582	872	725	315	2.2	790	6.2	568	4.4	425	3.3	315	2.5
12.5	608	910	755	352	2.4	890	7.0	635	5.0	465	3.6	352	2.8
13	630	945	785	400	2.7	1000	7.8	740	5.8	540	4.2	400	3.1
13.5	656	982	815	445	3.0	1020	8.0	800	6.3	600	4.7	445	3.5
14	680	1020	845	500	3.4	1250	9.8	900	7.0	675	5.3	500	3.9
14.5	705	1040	875	555	3.8	1400	11.0	1000	7.8	750	5.9	555	4.3
15	730	1090	905	610	4.2	1530	12.0	1090	8.5	830	6.5	610	4.8
16	775	1160	975	745	5.1	1850	14.5	1350	10.5	1000	7.8	745	5.8
17	825	1240	1030	890	6.1	2210	17.5	1600	12.5	1200	9.4	890	7.0
18	875	1310	1090	1060	7.1	2660	21.0	1900	14.8	1430	11.2	1060	8.3
19	925	1390	1150	1250	8.5	3140	24.6	2240	17.5	1680	13.2	1250	9.8
20	970	1460	1210	1450	10	3650	28.5	2600	20.2	1950	15.3	1450	11.3



$$b = 1.5a \quad H = \frac{1.5 \times (a + b)}{2} \approx 1.9a$$

TABLE 12. OVAL FEEDER HEAD

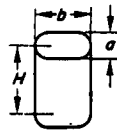
M_F	a	b	H	V	W	Max. feedable volume of casting V (wt W) for a shrinkage of:							
						4%		5%		6%		7%	
						V	W	V	W	V	W	V	W
cm	mm	mm	mm	cm ³ litres	kg m. tons	cm ³ , l.	kg, t	cm ³ , l.	kg, t	cm ³ , l.	kg, t	cm ³ , l.	kg, t
0.5	22	33	40	25	0.17	63	0.49	42	0.33	34	0.27	25	0.20
0.6	26	39	48	42	0.29	105	0.83	72	0.57	57	0.45	42	0.33
0.7	30	45	56	64	0.43	160	1.25	105	0.83	87	0.68	64	0.53
0.8	35	53	64	96	0.65	240	1.87	163	1.28	130	1.00	96	0.75
0.9	39	59	73	134	0.91	335	2.55	228	1.80	180	1.40	134	1.05
1.0	43	65	81	189	1.28	475	3.72	320	2.50	255	2.00	189	1.48
1.1	47	71	89	250	1.70	625	4.90	425	3.32	348	2.70	250	1.95
1.2	52	78	97	326	2.22	820	6.40	555	4.35	440	3.45	326	2.55
1.3	56	84	105	415	2.82	1.0	7.80	710	5.55	560	4.40	415	3.25
1.4	60	90	113	516	3.50	1.3	10.2	875	6.85	700	5.50	516	4.05
1.5	65	98	121	640	4.35	1.6	12.5	1.1	8.60	870	6.80	640	5.00
1.6	69	104	129	775	5.25	1.9	15.0	1.3	10.2	1.1	8.60	775	6.10
1.7	73	109	137	930	6.30	2.3	18.0	1.6	12.5	1.3	10.2	930	7.30
1.8	78	117	145	1.1	7.50	2.8	21.8	1.9	14.8	1.5	11.7	1.1	8.60
1.9	82	123	153	1.3	8.80	3.2	25.0	2.2	17.2	1.8	14.1	1.3	10.2
2.0	86	129	161	1.5	10.2	3.8	30.0	2.6	20.3	2.0	15.7	1.5	11.7
2.2	95	143	177	2.0	13.6	5.0	39.0	3.4	26.6	2.7	21.2	2.0	15.7
2.4	103	154	193	2.6	17.7	6.5	51.0	4.4	34.3	3.5	27.3	2.6	20.4
2.6	112	168	210	3.5	23.8	8.8	69.0	6.0	47.0	4.7	36.8	3.5	27.4
2.8	120	180	226	4.2	28.6	10	78.0	7.1	55.5	5.7	44.6	4.2	32.8
3.0	129	194	242	5.1	34.8	13	102	8.7	68.8	6.9	54.0	5.1	40.0
3.2	137	205	258	6.2	42.2	15	127	10	78.0	8.4	66.0	6.2	48.5
3.4	146	219	274	7.4	50.0	19	148	12	94.0	10	78.0	7.4	58.0
3.6	155	234	290	8.8	60.0	22	172	15	117	12	94.0	8.8	69.0
3.8	163	244	306	10	68.0	25	195	18	141	14	110	10	78.0
4.0	171	256	324	12	82.0	30	235	22	172	16	125	12	94.0
4.25	182	272	344	15	102	38	296	27	211	20	157	15	117
4.50	193	290	364	17	115	43	336	31	242	23	180	17	133
4.75	204	305	384	20	136	50	390	36	282	27	211	20	157
5.0	214	320	404	24	163	60	470	43	337	32	250	24	188
5.25	225	337	424	27	184	68	530	49	383	37	290	27	211
5.50	236	353	444	32	218	80	625	58	452	43	336	32	250
5.75	246	370	464	36	245	90	705	65	508	49	383	36	281
6.0	256	385	484	41	280	104	815	74	580	55	430	41	320
6.25	266	400	504	46	313	115	900	83	650	62	485	46	360
6.5	279	418	524	52	352	130	1.0	93	730	70	548	52	406
6.75	290	435	544	58	395	145	1.1	105	820	79	610	58	452
7.0	300	450	564	65	442	163	1.3	117	920	88	690	65	508
7.25	310	465	584	72	490	180	1.4	130	1.0	97	760	72	562
7.50	321	482	604	80	545	200	1.6	145	1.1	108	850	80	625
7.75	333	500	624	88	600	220	1.7	160	1.3	119	930	88	690
8.0	343	515	644	97	660	242	1.9	175	1.4	131	1.0	97	760
8.25	354	530	664	107	730	270	2.1	195	1.5	145	1.1	107	840
8.5	365	548	684	116	790	290	2.3	208	1.6	155	1.2	116	910
8.75	375	562	704	127	860	318	2.5	227	1.8	172	1.4	127	1.0
9.0	386	580	724	138	940	348	2.7	248	1.9	187	1.5	138	1.1
9.25	398	600	744	149	1.0	375	2.9	270	2.1	200	1.6	149	1.2
9.50	408	612	764	162	1.1	405	3.2	290	2.3	220	1.7	162	1.3
9.75	419	630	784	174	1.2	435	3.4	312	2.5	235	1.8	174	1.4
10.0	430	645	804	189	1.3	475	3.7	340	2.7	255	2.0	189	1.5
10.5	450	675	844	220	1.5	550	4.3	400	3.1	298	2.3	220	1.7
11	475	712	884	252	1.7	630	4.9	450	3.5	340	2.7	252	2.0
11.5	494	739	924	286	2.0	720	5.6	512	4.0	390	3.0	286	2.2
12	515	771	964	325	2.2	810	6.3	585	4.6	440	3.4	325	2.5
12.5	535	800	1010	368	2.5	920	7.2	660	5.2	498	3.9	368	2.9
13	558	836	1050	416	2.9	1050	8.3	750	5.9	562	4.4	416	3.3
13.5	580	870	1090	458	3.1	1150	9.0	830	6.5	620	4.9	458	3.6
14	600	900	1130	515	3.5	1300	10.2	930	7.3	700	5.5	515	4.0
14.5	625	938	1170	575	3.9	1450	11.3	1050	8.3	775	6.1	575	4.5
15	645	965	1210	640	4.4	1600	12.5	1150	9.0	860	6.7	640	5.0
16	686	1030	1290	775	5.3	1950	15.3	1400	11.0	1050	8.3	775	6.1
17	730	1090	1370	925	6.3	2300	18.0	1650	12.9	1250	9.7	925	7.3
18	775	1160	1450	1100	7.5	2750	21.5	2000	15.5	1490	11.6	1100	8.6
19	815	1220	1530	1300	8.8	3250	25.5	2340	18.3	1750	13.7	1300	10.0
20	860	1290	1610	1510	10.3	3760	29.6	2710	21.2	2040	16.0	1510	12.0



$$b = 2a \quad H = \frac{a + b}{2} = 1.5a$$

TABLE 13. OVAL FEEDER HEAD

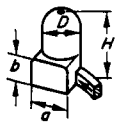
M_F	a	b	H	V	W	Max. feedable volume of casting V (wt W) for a shrinkage of:							
						4%		5%		6%		7%	
						V	W	V	W	V	W	V	W
cm	mm	mm	mm	cm ³ litres	kg m. tons	cm ³ , l.	kg, t	cm ³ , l.	kg, t	cm ³ , l.	kg, t	cm ³ , l.	kg, t
0.5	21	42	32	25	0.17	63	0.80	45	0.35	34	0.26	25	0.20
0.6	26	52	38	49	0.34	125	0.97	88	0.69	66	0.51	49	0.38
0.7	30	60	45	72	0.49	180	1.40	130	1.00	96	0.76	72	0.56
0.8	34	68	51	105	0.72	262	2.05	190	1.50	142	1.12	105	0.83
0.9	38	76	57	147	1.0	370	2.90	265	2.06	197	1.55	147	1.15
1.0	43	86	63	212	1.45	530	4.14	380	3.00	285	2.22	212	1.65
1.1	47	94	70	276	1.87	690	5.40	500	3.90	372	2.90	276	2.16
1.2	51	102	76	354	2.40	880	6.90	635	5.00	475	3.70	354	2.75
1.3	53	106	82	396	2.70	990	7.70	710	5.55	535	4.16	396	3.10
1.4	59	118	88	550	3.75	1.4	11.0	1.0	7.80	740	5.75	550	4.30
1.5	64	128	95	705	4.80	1.9	15.0	1.3	10.1	950	7.40	705	5.50
1.6	68	136	102	840	5.70	2.1	17.0	1.5	11.7	1.1	8.60	840	6.55
1.7	72	144	107	1.0	6.80	2.5	20.0	1.8	11.4	1.4	11.0	1.0	7.80
1.8	76	152	114	1.2	8.20	3.0	23.5	2.2	17.1	1.6	12.5	1.2	9.40
1.9	80	160	120	1.4	9.50	3.5	27.5	2.5	19.5	1.9	15.0	1.4	11.0
2.0	85	170	127	1.7	11.5	4.3	33.5	3.1	24.1	2.3	18.0	1.7	13.0
2.2	93	186	139	2.1	14.3	5.3	41.0	3.8	30.0	2.8	22.0	2.1	16.5
2.4	102	204	152	2.8	19.0	7.0	55.0	5.1	40.0	3.8	30.0	2.8	22.0
2.6	110	220	165	3.5	23.8	8.8	69.0	6.3	49.0	4.7	37.0	3.5	27.4
2.8	118	236	177	4.4	30.0	11	86.0	7.9	62.0	5.9	46.0	4.4	34.4
3.0	127	254	190	5.3	36.0	13	100	9.5	74.0	7.2	56.0	5.3	41.4
3.2	135	270	204	6.5	44.0	16	125	12	94.0	8.8	69.0	6.5	51.0
3.4	143	286	215	7.6	52.0	19	150	14	110	10	78.0	7.6	59.0
3.6	152	304	226	9.3	63.0	23	180	17	133	12	94.0	9.3	73.0
3.8	160	320	240	11	75.0	28	220	20	156	15	117	11	86.0
4.0	169	338	252	13	88.0	33	258	23	180	17	133	13	100
4.25	180	360	268	16	110	40	312	29	226	22	171	16	125
4.50	190	380	285	18	123	45	350	33	266	24	187	18	140
4.75	200	400	300	21	143	53	414	38	296	28	219	21	165
5.0	212	424	316	25	170	63	490	45	352	34	265	25	195
5.25	222	444	331	29	197	73	570	52	405	39	305	29	226
5.50	232	464	348	33	225	83	650	60	470	45	352	33	256
5.75	242	484	364	38	258	95	740	68	530	51	400	38	296
6.0	253	506	380	43	292	107	830	77	600	58	455	43	336
6.25	264	528	395	49	334	123	960	88	685	66	515	49	382
6.5	274	548	411	55	375	137	1.1	100	780	74	580	55	430
6.75	284	568	426	61	415	152	1.2	110	860	82	640	61	475
7.0	295	590	442	68	462	170	1.3	123	960	92	715	68	530
7.25	306	612	456	76	518	190	1.5	137	1.1	102	800	76	592
7.50	316	632	474	84	570	210	1.6	151	1.2	114	900	84	655
7.75	326	652	490	92	625	230	1.8	165	1.3	125	1.0	92	715
8.0	337	674	505	102	700	255	2.0	185	1.5	137	1.1	102	800
8.25	348	696	522	112	760	280	2.2	200	1.6	150	1.2	112	875
8.5	358	716	536	123	840	310	2.4	220	1.7	165	1.3	123	960
8.75	370	740	555	137	930	342	2.7	250	2.0	183	1.5	137	1.1
9.0	380	760	570	147	1.0	365	2.9	265	2.1	200	1.6	147	1.2
9.25	390	780	585	157	1.1	390	3.0	285	2.2	210	1.7	157	1.3
9.50	400	800	600	170	1.2	425	3.3	305	2.4	228	1.8	170	1.4
9.75	410	820	618	184	1.3	460	3.6	330	2.6	250	2.0	184	1.5
10.0	420	840	632	197	1.4	490	3.8	355	2.8	265	2.1	197	1.6
10.5	444	888	662	232	1.6	580	4.5	420	3.3	310	2.4	232	1.8
11	464	928	695	267	1.8	670	5.2	480	3.8	360	2.8	267	2.1
11.5	484	968	725	300	2.0	750	5.9	540	4.2	404	3.2	300	2.4
12	505	1010	760	343	2.3	860	6.7	620	4.8	465	3.6	343	2.7
12.5	528	1056	790	394	2.7	980	7.6	710	5.6	530	4.1	394	3.1
13	550	1100	820	440	3.0	1100	8.6	790	6.2	590	4.6	440	3.4
13.5	570	1140	850	493	3.4	1240	9.7	890	6.9	670	5.2	493	3.9
14	580	1160	885	520	3.5	1300	10.0	940	7.4	700	5.5	520	4.1
14.5	612	1224	915	610	4.2	1530	12.0	1100	8.6	820	6.4	610	4.8
15	632	1264	950	670	4.6	1670	13.0	1200	9.4	900	7.0	670	5.2
16	675	1350	1010	820	5.6	2050	16.0	1480	11.5	1100	8.6	820	6.4
17	718	1436	1070	985	6.7	2460	19.2	1800	14.1	1300	10.0	985	7.7
18	760	1520	1140	1170	8.0	2920	22.8	2100	16.4	1570	12.3	1170	9.1
19	800	1600	1200	1370	9.3	3410	26.6	2450	19.0	1850	14.5	1370	10.7
20	840	1680	1270	1570	10.7	3920	30.5	2820	22.0	2100	16.5	1570	12.3



$$b = 2a \quad H = \frac{1.5 \times (a + b)}{2} = 2.25a$$

TABLE 14. OVAL FEEDER HEAD

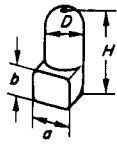
M_F	a	b	H	V	W	Max. feedable volume of casting V (wt W) for a shrinkage of:							
						4%		5%		6%		7%	
						V	W	V	W	V	W	V	W
cm	mm	mm	mm	cm ³ litres	kg m. tons	cm ³ , l.	kg, t	cm ³ , l.	kg, t	cm ³ , l.	kg, t	cm ³ , l.	kg, t
0.5	19	38	42	28	0.19	70	0.55	53	0.41	38	0.30	28	0.22
0.6	23	46	51	49	0.34	105	0.82	93	0.72	66	0.51	49	0.38
0.7	26	52	59	71	0.49	180	1.40	105	0.82	96	0.75	71	0.55
0.8	30	60	68	108	0.75	258	2.00	205	1.60	146	1.14	108	0.84
0.9	34	68	76	157	1.05	380	3.00	300	3.35	212	1.65	157	1.23
1.0	38	76	85	220	1.50	550	4.30	420	3.28	296	2.31	220	1.71
1.1	42	84	93	300	2.05	750	5.85	570	4.45	405	3.15	300	2.34
1.2	45	90	100	370	2.52	930	7.30	710	5.55	500	3.90	370	2.88
1.3	49	98	110	472	3.22	1.2	9.40	900	7.00	640	5.00	472	3.70
1.4	53	106	118	600	4.10	1.5	11.7	1.2	9.45	810	6.30	600	4.68
1.5	57	114	127	750	5.10	1.9	14.8	1.4	11.9	1.0	7.80	750	5.85
1.6	60	120	135	870	5.90	2.2	17.1	1.7	13.3	1.2	9.35	870	6.78
1.7	64	128	143	1.1	7.50	2.8	21.8	2.1	16.5	1.5	11.7	1.1	8.60
1.8	67	134	152	1.2	8.20	3.0	23.5	2.3	18.0	1.6	12.5	1.2	9.35
1.9	71	142	160	1.4	9.50	3.5	27.4	2.7	21.0	1.9	14.8	1.4	10.9
2.0	75	150	169	1.7	11.6	4.3	33.5	3.2	25.0	2.3	18.0	1.7	13.3
2.2	83	186	185	2.3	15.7	5.8	45.0	4.4	34.2	3.1	24.1	2.3	18.0
2.4	90	190	203	3.0	20.4	7.5	58.5	5.7	44.5	4.1	32.0	3.0	23.4
2.6	97	194	220	3.7	25.2	9.3	72.5	7.1	55.5	5.0	39.0	3.7	29.0
2.8	105	210	236	4.7	32.0	12	93.5	9.0	70.0	6.4	50.0	4.7	36.6
3.0	113	226	252	5.8	39.5	15	117	11	85.5	7.8	60.9	5.8	45.1
3.2	120	240	270	7.0	47.8	18	140	13	103	9.5	74.0	7.0	54.5
3.4	127	254	286	8.2	55.8	20	156	16	125	11	85.8	8.2	64.0
3.6	135	270	304	10	68.0	25	195	19	148	13	101	10	78.0
3.8	143	286	320	12	82.0	30	235	23	180	16	125	12	93.5
4.0	150	300	337	14	96.0	35	274	27	210	19	148	14	109
4.25	160	320	356	16	109	40	312	31	241	22	171	16	125
4.50	169	338	380	19	129	48	374	36	280	26	203	19	148
4.75	178	356	400	23	157	58	452	44	342	31	241	23	179
5.0	187	374	422	27	184	68	530	52	405	37	289	27	210
5.25	197	394	444	31	211	78	608	59	460	42	328	31	241
5.50	206	412	464	35	239	88	685	67	522	47	366	35	272
5.75	216	432	484	41	280	103	800	78	608	55	430	41	320
6.0	225	450	508	46	314	115	900	88	685	62	482	46	358
6.25	234	468	528	52	354	130	1.0	100	780	70	545	52	405
6.5	243	486	548	58	395	145	1.1	110	860	78	608	58	451
6.75	254	508	570	62	422	155	1.2	120	935	84	655	62	482
7.0	261	522	590	71	485	178	1.4	135	1.1	97	755	71	555
7.25	271	542	610	80	545	200	1.6	152	1.2	108	840	80	625
7.50	280	560	632	88	600	220	1.7	167	1.3	118	920	88	685
7.75	290	580	652	98	668	245	1.9	187	1.5	132	1.0	98	760
8.0	300	600	675	110	750	275	2.1	208	1.6	148	1.2	110	860
8.25	309	618	695	119	810	300	2.3	226	1.8	160	1.3	119	930
8.5	318	636	718	129	880	322	2.5	245	1.9	172	1.4	129	1.0
8.75	328	656	740	141	960	351	2.8	266	2.1	190	1.5	141	1.1
9.0	338	676	760	156	1.1	390	3.0	296	2.3	210	1.6	156	1.2
9.25	346	692	780	166	1.2	415	3.2	315	2.5	224	1.8	166	1.3
9.50	356	712	800	181	1.3	452	3.5	345	2.7	245	1.9	181	1.4
9.75	365	730	822	196	1.4	490	3.8	371	2.9	264	2.1	196	1.5
10.0	375	750	842	212	1.5	530	4.1	402	3.2	285	2.2	212	1.7
10.5	393	786	888	245	1.7	615	4.8	465	3.6	330	2.6	245	1.9
11	413	826	928	285	2.0	715	5.6	541	4.2	385	3.0	285	2.2
11.5	430	860	970	320	2.2	800	6.3	608	4.7	432	3.4	320	2.5
12	450	900	1010	365	2.5	910	7.1	690	5.4	492	3.9	365	2.8
12.5	468	936	1050	414	2.8	1040	8.1	790	6.2	560	4.4	414	3.2
13	486	972	1100	462	3.2	1160	9.1	880	6.9	625	4.9	462	3.6
13.5	506	1012	1140	524	3.6	1320	10.3	1000	7.8	710	5.6	524	4.1
14	525	1050	1180	580	4.0	1450	11.3	1100	8.6	780	6.1	580	4.5
14.5	545	1090	1230	650	4.4	1630	12.7	1230	9.6	880	6.9	650	5.1
15	565	1130	1270	720	4.9	1800	14.0	1370	10.7	970	7.6	720	5.6
16	600	1200	1350	860	5.9	2150	16.7	1670	13.0	1160	9.0	860	6.7
17	636	1272	1430	1025	7.0	2560	20.6	1950	15.2	1380	10.8	1025	8.0
18	673	1346	1522	1220	8.3	3050	23.7	2320	18.0	1630	12.7	1220	9.5
19	712	1424	1600	1440	9.8	3600	28.0	2740	21.4	1940	15.1	1440	11.2
20	750	1500	1690	1680	11.5	4200	32.2	3200	25.0	2260	17.6	1680	13.1



$H = 1.5D$ $a = D$ $b = 0.53a$

TABLE 15. BLIND FEEDER HEAD WITH PENETRATION CORE

M_F cm	$D\phi = a$ mm	b mm	H mm	V cm ³ litres	W kg m. tons	Max. feedable volume of casting V (wt W) for a shrinkage of:							
						4%		5%		6%		7%	
						V cm ³ , l.	W kg, t	V cm ³ , l.	W kg, t	V cm ³ , l.	W kg, t	V cm ³ , l.	W kg, t
0.5	27	15	41	20	0.14	50	0.39	36	0.28	27	0.21	20	0.16
0.6	32	17	48	35	0.24	88	0.69	63	0.49	48	0.38	35	0.27
0.7	37	20	56	53	0.36	129	1.00	95	0.74	72	0.56	53	0.42
0.8	43	23	65	79	0.54	200	1.55	142	1.11	107	0.83	79	0.62
0.9	48	26	72	105	0.71	255	2.00	190	1.48	143	1.12	105	0.82
1.0	53	28	80	156	1.06	390	3.05	280	2.18	210	1.64	156	1.22
1.1	59	32	89	207	1.40	520	4.05	372	2.90	280	2.19	207	1.62
1.2	64	34	96	270	1.83	675	5.25	486	3.80	365	2.85	270	2.10
1.3	69	37	104	342	2.32	850	6.62	612	4.80	460	3.58	342	2.67
1.4	75	40	113	424	2.88	1.1	8.60	760	5.95	570	4.45	424	3.30
1.5	80	43	120	525	3.55	1.3	10.0	940	7.30	710	5.55	525	4.10
1.6	85	45	128	640	4.40	1.6	12.5	1.2	9.30	865	6.75	640	5.00
1.7	90	48	135	765	5.20	1.9	14.8	1.4	10.9	1.0	7.80	775	6.10
1.8	96	51	145	910	6.18	2.3	18.0	1.6	12.5	1.2	9.30	910	7.10
1.9	100	53	150	1.1	7.45	2.8	21.9	2.0	15.6	1.5	11.7	1.1	8.55
2.0	106	56	160	1.3	8.80	3.3	25.8	2.3	18.0	1.8	14.0	1.3	10.0
2.2	117	62	185	1.7	11.5	4.3	33.5	3.1	24.1	2.3	17.9	1.7	13.3
2.4	127	68	190	2.2	15.0	5.5	42.9	4.0	31.2	3.0	23.4	2.2	17.1
2.6	138	74	208	2.9	19.7	7.3	57.0	5.2	40.5	3.9	30.4	2.9	22.6
2.8	150	80	225	3.4	23.0	8.5	66.2	6.1	47.6	4.6	35.8	3.4	26.5
3.0	160	85	240	4.2	28.5	11	85.6	7.6	59.2	5.7	44.5	4.2	32.8
3.2	170	90	255	5.1	34.7	13	101	9.2	71.8	6.0	53.9	5.1	39.8
3.4	180	96	270	6.2	42.0	15	117	11	85.6	8.4	65.5	6.2	48.2
3.6	190	100	285	7.3	49.5	18	140	13	101	9.9	77.0	7.3	57.0
3.8	200	106	300	8.6	58.5	22	171	16	125	12	93.0	8.6	67.0
4.0	212	113	320	10	68.0	25	195	18	140	14	109	10	78.0
4.25	225	120	348	12	81.5	30	234	22	171	16	125	12	94.0
4.5	240	127	360	14	95.0	35	272	25	195	19	148	14	109
4.75	252	134	380	17	115	43	335	30	234	23	179	17	133
5.0	265	140	400	20	135	50	390	36	280	27	210	20	156
5.25	276	147	415	23	155	58	450	42	326	31	240	23	179
5.5	292	155	440	26	177	65	510	47	366	35	272	26	203
5.75	305	162	456	30	204	75	585	54	420	41	320	30	234
6.0	318	168	480	34	230	85	662	61	475	46	358	34	265
6.25	331	176	500	38	258	95	740	68	530	51	398	38	296
6.5	345	183	520	43	291	107	840	78	610	58	450	43	335
6.75	356	190	535	48	326	120	930	86	670	65	505	48	375
7.0	371	197	560	53	360	132	1.0	96	750	72	560	53	405
7.25	385	204	580	59	400	147	1.1	106	830	80	625	59	460
7.5	398	212	600	66	448	167	1.3	120	930	90	700	66	515
7.75	410	217	618	73	495	182	1.4	132	1.0	99	770	73	570
8.0	425	226	640	80	542	200	1.6	145	1.1	108	840	80	625
8.25	436	232	656	88	600	220	1.8	158	1.2	120	930	88	685
8.5	450	239	675	96	650	240	1.9	173	1.4	130	1.0	96	750
8.75	465	247	700	105	710	262	2.1	190	1.5	142	1.1	105	810
9.0	477	253	715	114	775	285	2.2	205	1.6	154	1.2	114	890
9.25	490	260	735	123	840	307	2.4	220	1.7	165	1.3	123	960
9.5	505	266	760	135	920	335	2.6	242	1.9	183	1.4	135	1.0
9.75	517	272	780	145	980	362	2.8	260	2.0	195	1.5	145	1.1
10.0	530	282	800	155	1.0	390	3.1	280	2.2	210	1.6	155	1.2
10.5	555	292	830	181	1.2	450	3.5	325	2.5	245	1.9	181	1.4
11	585	310	880	207	1.4	520	4.1	370	2.9	280	2.2	207	1.6
11.5	610	324	915	236	1.6	590	4.6	426	3.3	320	2.5	236	1.8
12	635	338	955	270	1.8	675	5.3	486	3.8	365	2.8	270	2.1
12.5	665	353	1000	304	2.1	760	5.9	545	4.3	410	3.2	304	2.4
13	690	366	1040	342	2.4	860	6.7	615	4.8	462	3.6	342	2.7
13.5	730	388	1100	385	2.6	960	7.5	695	5.3	520	4.1	385	3.0
14	750	398	1130	425	2.9	1060	8.3	765	6.0	575	4.5	425	3.3
14.5	770	408	1150	475	3.3	1190	9.3	855	6.7	640	5.0	475	3.7
15	800	425	1200	525	3.6	1320	10.3	950	7.4	710	5.5	525	4.1
16	850	450	1280	640	4.4	1600	12.5	1150	9.0	865	6.7	640	5.0
17	900	476	1350	765	5.2	1920	15.0	1370	10.7	1040	8.1	765	6.0
18	960	510	1450	910	6.2	2280	17.8	1630	12.7	1230	9.6	910	7.1
19	1000	530	1500	1070	7.3	2660	20.6	1920	15.0	1450	11.3	1070	8.4
20	1060	565	1590	1250	8.5	3120	24.3	2250	17.5	1700	13.3	1250	9.6



$H = 2D$ $a = D$ $b = 0.615a$

TABLE 16. BLIND FEEDER HEAD WITH PENETRATION CORE

M_F	$D \varnothing = a$	b	H	V	W	Max. feedable volume of casting V' (wt W') for a shrinkage of:							
						4%		5%		6%		7%	
						V'	W'	V'	W'	V'	W'	V'	W'
cm	mm	mm	mm	cm ³ litres	kg m. tons	cm ³ , l.	kg, t	cm ³ , l.	kg, t	cm ³ , l.	kg, t	cm ³ , l.	kg, t
0.5	24	15	48	19	0.13	48	0.37	35	0.27	26	0.20	19	0.15
0.6	29	18	58	32	0.22	80	0.63	58	0.45	43	0.34	32	0.25
0.7	34	21	68	49	0.33	123	0.96	88	0.69	66	0.52	49	0.38
0.8	38	24	76	73	0.50	183	1.43	131	1.03	98	0.77	73	0.57
0.9	43	27	86	105	0.71	255	2.00	190	1.48	142	1.10	105	0.82
1.0	48	30	96	143	0.97	360	2.81	256	2.00	193	1.50	143	1.10
1.1	53	33	106	190	1.29	475	3.71	343	2.70	256	2.00	190	1.48
1.2	58	36	116	250	1.70	630	4.92	450	3.52	338	2.65	250	1.95
1.3	63	39	126	315	2.16	790	6.18	565	4.40	425	3.30	315	2.45
1.4	67	42	134	395	2.68	990	7.75	710	5.55	533	4.20	395	3.10
1.5	72	45	144	485	3.30	1.2	9.40	870	6.80	655	5.10	485	3.80
1.6	77	48	154	589	4.00	1.5	11.7	1.1	8.60	800	6.25	589	4.60
1.7	81	50	162	700	4.75	1.8	14.0	1.3	10.0	950	7.40	700	5.48
1.8	86	54	172	840	5.70	2.1	16.4	1.5	11.7	1.1	8.60	840	6.55
1.9	91	57	182	980	6.65	2.5	19.5	1.8	14.1	1.3	10.0	980	7.65
2.0	96	60	192	1.2	8.15	3.0	23.5	2.2	17.2	1.6	12.5	1.2	9.40
2.2	106	66	212	1.5	10.2	3.8	29.8	2.7	21.0	2.0	15.6	1.5	11.7
2.4	115	71	230	2.0	13.6	5.0	39.0	3.6	28.1	2.7	21.0	2.0	15.6
2.6	125	78	250	2.7	18.3	6.8	53.0	4.9	38.2	3.6	28.0	2.7	21.0
2.8	134	83	268	3.2	21.7	8.0	62.5	5.8	45.2	4.3	33.5	3.2	25.0
3.0	144	90	288	3.9	26.5	9.8	76.5	7.0	54.8	5.3	41.5	3.9	30.5
3.2	153	95	306	4.7	31.9	12	93.0	8.5	66.5	6.4	50.0	4.7	36.8
3.4	163	102	326	5.7	38.8	14	109	10	78.0	7.7	60.0	5.7	44.5
3.6	172	106	344	6.7	45.5	17	133	12	93.5	9.0	70.0	6.7	52.5
3.8	182	113	364	7.9	53.7	20	156	14	109	11	86.0	7.9	61.5
4.0	192	120	384	9.2	62.5	23	180	16	125	12	93.5	9.2	72.0
4.25	203	126	406	11	74.5	28	218	20	156	15	117	11	86.0
4.50	215	133	430	13	88.5	33	258	22	172	17	133	13	102
4.75	226	140	452	15	102	38	296	27	210	20	156	15	117
5.0	239	147	478	18	122	45	352	32	250	24	187	18	141
5.25	250	155	500	21	143	53	413	38	296	28	218	21	164
5.50	262	162	524	22	149	55	430	40	312	30	233	22	172
5.75	275	170	550	27	183	68	530	49	382	36	281	27	210
6.0	286	177	572	31	210	78	610	56	436	42	328	31	241
6.25	300	185	600	35	238	88	690	63	492	47	368	35	273
6.5	310	192	620	40	272	100	780	72	561	54	422	40	312
6.75	322	200	644	44	298	110	860	79	618	60	468	44	344
7.0	334	205	668	49	332	125	970	88	688	66	515	49	382
7.25	345	214	690	55	374	138	1.1	100	780	74	578	55	430
7.50	358	222	716	61	415	153	1.2	110	860	83	650	61	477
7.75	370	228	740	67	455	167	1.3	120	935	91	710	67	522
8.0	381	236	762	73	495	183	1.4	131	1.0	98	765	73	570
8.25	394	243	788	81	510	201	1.6	146	1.1	110	860	81	632
8.5	405	250	810	88	600	220	1.7	158	1.2	120	935	88	688
8.75	415	256	830	96	650	240	1.9	173	1.4	130	1.0	96	750
9.0	429	263	858	106	720	265	2.1	190	1.5	145	1.1	106	830
9.25	440	272	880	114	775	285	2.2	205	1.6	154	1.2	114	890
9.50	453	280	906	124	845	310	2.4	224	1.8	167	1.3	124	970
9.75	465	288	930	133	900	333	2.6	240	1.9	180	1.4	133	1.0
10.0	486	300	972	143	970	358	2.8	256	2.0	193	1.5	143	1.1
10.5	500	310	1000	156	1.1	390	3.0	280	2.2	210	1.6	156	1.2
11	525	325	1050	190	1.3	475	3.7	342	2.7	258	2.0	190	1.5
11.5	550	340	1100	216	1.5	540	4.2	390	3.0	290	2.2	216	1.7
12	575	355	1150	248	1.7	620	4.8	450	3.5	335	2.6	248	1.9
12.5	600	372	1200	280	1.9	700	5.5	505	4.0	378	2.9	280	2.2
13	620	384	1240	316	2.2	790	6.2	570	4.5	428	3.3	316	2.5
13.5	645	400	1290	352	2.4	880	6.9	635	5.0	475	3.7	352	2.8
14	670	415	1340	390	2.7	980	7.7	700	5.5	525	4.1	390	3.0
14.5	690	428	1390	436	3.0	1040	8.1	785	6.1	590	4.6	436	3.4
15	715	445	1430	482	3.3	1210	9.5	870	6.8	650	5.1	482	3.8
16	765	470	1530	590	4.0	1480	11.5	1060	8.3	800	6.3	590	4.6
17	810	500	1620	700	4.8	1750	13.7	1260	9.8	945	7.4	700	5.5
18	860	535	1720	840	5.7	2100	16.4	1510	11.8	1130	8.8	840	6.6
19	910	565	1820	980	6.7	2450	19.1	1760	13.7	1330	10.3	980	7.7
20	960	595	1920	1150	7.8	2860	22.3	2060	16.0	1550	12.0	1150	9.0

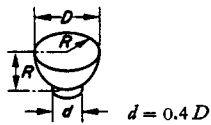


TABLE 17. HEMISPHERICAL FEEDER HEAD

M_F	$D\phi$	$d\phi$	R	V	W	Max. feedable volume of casting V (wt W) for a shrinkage of:							
						4%		5%		6%		7%	
						V	W	V	W	V	W	V	W
cm	mm	mm	mm	cm ³ litres	kg m. tons	cm ³ , l.	kg, t	cm ³ , l.	kg, t	cm ³ , l.	kg, t	cm ³ , l.	kg, t
0.5	45	18	23	26	0.18	104	0.85	78	0.61	60	0.47	49	0.38
0.6	55	22	28	43	0.3	173	1.35	129	1.0	100	0.78	81	0.63
0.7	64	26	32	67	0.5	270	2.10	200	1.55	154	1.20	127	1.00
0.8	73	29	37	100	0.7	400	3.10	300	2.35	230	1.80	189	1.47
0.9	82	33	41	177	1.2	710	5.60	530	4.15	410	3.20	330	2.60
1.0	91	37	46	196	1.3	780	6.10	590	4.60	450	3.50	370	2.90
1.1	100	40	50	260	1.8	1.1	8.60	780	6.10	600	4.70	490	3.83
1.2	109	44	55	340	2.3	1.4	11	1.0	7.80	780	6.10	640	5.00
1.3	119	48	60	431	3.0	1.7	13	1.3	10.0	1.0	7.80	810	6.30
1.4	128	51	64	535	3.6	2.1	17	1.6	12.5	1.2	9.40	1.0	7.80
1.5	137	55	69	660	4.5	2.7	21	2.0	15.5	1.5	11.5	1.2	9.40
1.6	146	58	73	805	5.5	3.2	25	2.4	18.7	1.9	15.0	1.5	11.7
1.7	155	62	78	960	6.5	3.8	30	2.9	22.6	2.2	17.0	1.8	14.0
1.8	164	66	82	1.1	7.5	4.4	35	3.3	25.6	2.5	19.5	2.1	16.5
1.9	173	69	87	1.4	9.5	5.6	44	4.2	32.8	3.2	25.0	2.6	20.0
2.0	182	73	91	1.6	11	6.4	50	4.8	36.5	3.7	29.0	3.0	24.0
2.2	200	80	100	2.1	15	8.4	66	6.3	49.0	4.8	37.5	4.0	31.0
2.4	219	88	110	2.7	19	11	86	8.1	63.0	6.2	48.5	5.1	40.0
2.6	236	95	118	3.7	25	15	117	11	86.0	8.5	66.5	7.0	55.0
2.8	255	102	128	4.3	30	17	133	13	100	10	78.0	8.1	63.0
3.0	274	109	137	5.3	36	21	164	16	125	12	94.0	10	78.0
3.2	291	116	146	6.4	43	25	195	19	150	15	117	12	94.0
3.4	310	124	155	7.8	53	31	241	23	180	18	140	15	117
3.6	326	131	163	9.2	63	37	290	28	220	21	164	17	133
3.8	346	138	173	11	75	44	344	33	260	25	195	21	164
4.0	365	145	183	13	88	52	405	39	300	30	235	25	195
4.25	387	155	194	15	100	60	470	45	350	35	273	28	218
4.50	410	164	205	18	123	72	560	54	420	42	330	34	265
4.75	431	173	216	21	143	84	660	63	490	48	375	40	312
5.0	455	182	228	24	163	96	750	72	560	55	430	45	350
5.25	480	190	240	29	197	116	910	87	680	67	520	55	430
5.50	500	200	250	32	218	128	1.0	96	750	74	575	60	468
5.75	525	210	263	37	255	148	1.2	111	860	85	665	70	545
6.0	545	216	273	43	292	172	1.4	129	1.0	99	775	81	630
6.25	570	227	285	48	328	194	1.5	144	1.1	110	860	90	700
6.5	591	236	296	54	368	216	1.7	162	1.3	124	970	102	800
6.75	615	245	308	60	408	240	1.9	180	1.4	138	1.1	113	870
7.0	638	252	319	68	462	272	2.1	204	1.6	156	1.2	128	1.0
7.25	660	262	330	77	525	310	2.4	231	1.8	177	1.4	145	1.1
7.50	683	273	342	83	562	330	2.6	250	1.9	190	1.5	157	1.2
7.75	705	280	353	91	630	365	2.9	272	2.1	210	1.7	172	1.4
8.0	730	290	365	100	680	400	3.1	300	2.4	230	1.8	188	1.5
8.25	750	300	375	110	750	440	3.4	330	2.6	252	2.0	208	1.6
8.5	775	308	388	120	815	480	3.7	360	2.8	276	2.1	226	1.8
8.75	800	316	400	132	900	530	4.1	400	3.1	304	2.4	250	2.0
9.0	820	326	410	145	1.0	570	4.5	435	3.4	333	2.6	275	2.2
9.25	840	335	420	155	1.1	620	4.8	465	3.6	357	2.8	295	2.3
9.50	865	345	433	168	1.2	660	5.2	505	4.0	386	3.0	318	2.5
9.75	890	355	445	182	1.3	730	5.7	545	4.3	420	3.3	344	2.7
10.0	910	363	455	196	1.4	770	6.0	585	4.6	450	3.5	370	2.9
10.5	950	380	475	224	1.5	940	7.3	670	5.2	515	4.0	420	3.3
11	1000	400	500	260	1.8	1040	8.1	780	6.1	600	4.7	490	3.8
11.5	1050	416	525	300	2.0	1200	9.4	900	7.0	690	5.4	565	4.4
12	1090	435	545	340	2.3	1360	10.6	1020	8.1	780	6.1	640	5.0
12.5	1140	452	570	380	2.6	1520	12.0	1140	8.9	870	6.8	720	5.6
13	1190	472	595	431	3.0	1730	13.5	1300	10.0	1000	7.8	810	6.3
13.5	1230	490	615	480	3.3	1920	15.0	1440	11.3	1100	8.6	910	7.1
14	1280	514	640	540	3.7	2160	17.0	1620	12.6	1240	9.6	1020	8.0
14.5	1320	525	660	600	4.1	2400	18.7	1800	14.0	1380	10.7	1130	8.8
15	1370	545	685	660	4.5	2650	20.6	1980	15.5	1520	12.8	1250	9.8
16	1460	580	730	800	5.5	3200	25.0	2400	18.7	1840	14.5	1510	11.8
17	1550	615	775	960	6.6	3850	30.0	2900	22.6	2200	17.0	1800	14.0
18	1640	655	820	1150	7.8	4600	36.0	3450	27.0	2650	21.0	2160	17.0
19	1730	690	865	1350	9.2	5400	42.0	4050	31.0	3100	24.0	2550	20.0
20	1820	725	910	1570	10.7	6300	49.0	4700	36.6	3600	28.0	2950	23.0

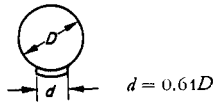
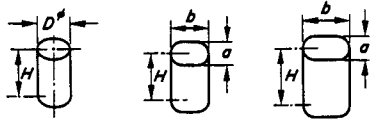


TABLE 18. SPHERICAL FEEDER HEAD

M_F cm	$D\varnothing$ mm	$d\varnothing$ mm	V cm ³ litres	W kg m. tons	Max. feedable volume of casting V (wt W) for a shrinkage of:							
					4%		5%		6%		7%	
					V cm ³ , l.	W kg, t	V cm ³ , l.	W kg, t	V cm ³ , l.	W kg, t	V cm ³ , l.	W kg, t
0.5	30	19	15	0.1	60	0.47	45	0.35	35	0.27	28	0.22
0.6	36	22	25	0.17	100	0.78	75	0.59	58	0.45	47	0.37
0.7	42	26	39	0.27	155	1.20	117	0.91	90	0.70	74	0.58
0.8	48	29	59	0.40	236	1.85	177	1.38	137	1.07	112	0.88
0.9	54	33	84	0.57	336	2.60	252	2.00	195	1.50	160	1.25
1.0	60	37	115	0.78	460	3.60	345	2.70	265	2.07	216	1.70
1.1	66	40	153	1.05	615	4.80	460	3.60	352	2.75	290	2.26
1.2	72	44	200	1.36	800	6.25	600	4.70	460	3.60	380	2.96
1.3	78	48	252	1.72	1.0	7.80	760	5.90	580	4.50	480	3.75
1.4	82	51	315	2.14	1.3	10.0	945	7.40	725	5.75	600	4.68
1.5	90	55	386	2.62	1.5	11.7	1.2	9.30	890	6.90	730	5.70
1.6	96	58	470	3.20	1.9	14.8	1.4	10.8	1.1	8.60	890	6.95
1.7	102	62	562	3.85	2.3	18.0	1.7	13.3	1.3	10.0	1.1	8.60
1.8	108	66	670	4.55	2.7	21.0	2.0	15.6	1.5	11.7	1.3	10.1
1.9	114	69	785	5.35	3.1	24.2	2.4	18.7	1.8	14.0	1.5	11.7
2.0	120	73	920	6.25	3.7	28.8	2.7	21.0	2.1	16.4	1.8	14.0
2.2	132	80	1.2	8.20	4.8	37.5	3.6	28.0	2.8	21.8	2.3	18.0
2.4	144	88	1.6	10.6	6.4	50.0	4.8	37.5	3.7	28.9	3.0	23.4
2.6	154	95	2.1	14.3	8.4	65.5	6.3	49.0	4.8	37.5	4.0	31.3
2.8	168	102	2.5	17.0	10	78.0	7.5	58.5	5.7	44.5	4.8	37.5
3.0	180	109	3.1	21.0	12	94.0	9.3	72.5	7.2	56.0	5.9	46.0
3.2	192	116	3.8	26.0	15	117	11	86.0	8.7	68.0	7.3	57.0
3.4	204	124	4.5	30.5	18	140	14	109	10	78.0	8.5	66.5
3.6	216	131	5.4	37.0	22	171	16	125	12	94.5	10	78.0
3.8	226	138	6.3	43.0	25	195	19	148	15	117	12	93.5
4.0	240	145	7.4	50.0	30	234	22	172	17	133	14	109
4.25	255	155	8.8	60.0	35	272	27	210	20	156	17	133
4.50	270	164	11	75.0	44	342	33	258	25	195	21	164
4.75	285	173	12	82.0	48	375	36	280	28	219	23	180
5.0	300	182	14	95.0	56	436	42	328	32	250	26	203
5.25	315	190	17	116	68	530	51	400	39	304	32	250
5.50	330	200	19	129	76	592	57	445	44	342	36	280
5.75	345	210	22	150	88	685	66	515	51	396	42	328
6.0	360	216	25	170	100	780	75	585	57	445	47	366
6.25	375	227	28	190	112	875	84	655	65	508	53	413
6.5	390	236	32	218	128	1.0	96	750	74	575	61	476
6.75	405	245	35	238	140	1.1	105	820	81	630	67	522
7.0	420	252	40	272	160	1.2	120	935	92	715	76	592
7.25	435	262	43	292	172	1.3	130	1.0	98	765	82	640
7.5	450	273	48	330	192	1.5	144	1.1	110	860	91	710
7.75	465	280	53	360	212	1.7	160	1.2	122	950	100	780
8.0	480	290	59	400	236	1.8	177	1.4	136	1.1	112	875
8.25	495	300	65	440	260	2.0	195	1.5	150	1.2	123	960
8.5	510	308	71	480	285	2.2	212	1.7	163	1.3	135	1.1
8.75	525	316	77	520	310	2.4	230	1.8	175	1.4	147	1.2
9.0	540	326	84	570	336	2.6	252	2.0	193	1.5	160	1.3
9.25	555	335	91	620	365	2.9	272	2.1	210	1.6	173	1.4
9.5	570	345	98	670	392	3.1	298	2.3	226	1.8	187	1.5
9.75	585	355	107	730	430	3.4	320	2.5	245	1.9	205	1.6
10.0	600	363	115	780	460	3.6	345	2.7	266	2.1	220	1.7
10.5	630	380	133	900	530	4.1	400	3.1	310	2.4	252	2.0
11	660	400	153	1.1	615	4.8	460	3.6	350	2.7	290	2.3
11.5	690	416	175	1.2	700	5.5	525	4.1	400	3.1	330	2.6
12	720	435	200	1.4	800	6.3	600	4.7	460	3.6	380	2.9
12.5	750	452	225	1.5	900	7.0	675	5.3	520	4.1	428	3.3
13	780	472	252	1.7	1000	7.8	752	5.9	580	4.5	480	3.7
13.5	810	490	285	1.9	1140	8.9	855	6.7	655	5.1	540	4.2
14	840	514	314	2.2	1260	9.8	940	7.3	720	5.6	600	4.7
14.5	870	525	350	2.4	1400	11.0	1050	8.2	810	6.3	665	5.2
15	900	545	390	2.8	1560	12.2	1170	9.1	900	7.0	740	5.8
16	960	580	470	3.2	1880	14.6	1410	11.0	1080	8.4	890	7.0
17	1020	615	560	3.8	2240	17.5	1680	13.1	1300	11.1	1060	8.5
18	1080	655	670	4.6	2680	21.0	2000	15.6	1540	12.0	1270	9.9
19	1140	690	790	5.4	3160	24.6	2380	18.6	1810	14.1	1500	11.7
20	1200	725	920	6.3	3700	28.8	2760	21.6	2120	16.5	1750	13.7



$$\begin{aligned}
 H &= 1.5D & b &= 1.5a & b &= 2a \\
 H &= 1.5 \frac{(a+b)}{2} & H &= \frac{1.5(a+b)}{2} & H &= \frac{1.5(a+b)}{2} \\
 &\approx 1.9a & & & & = 2.25a
 \end{aligned}$$

TABLE 19. ROUND AND OVAL FEEDER HEADS IN A CLEARLY VISIBLE LAYOUT

a; D∅ cm	b cm	H cm	M _F cm	V cm ³ litres	W kg m. tons	Max. feedable volume of casting V (wt W) for a shrinkage of:							
						4%		5%		6%		7%	
						V cm ³ , l.	W kg, t	V cm ³ , l.	W kg, t	V cm ³ , l.	W kg, t	V cm ³ , l.	W kg, t
3	∅	4.5	0.55	32	0.22	80	0.63	60	0.47	43	0.34	32	0.25
3	4.5	7	0.7	64	0.44	160	1.25	105	0.83	87	0.68	64	0.50
3	6	8	0.8	108	0.74	258	2.00	205	1.60	146	1.14	108	0.85
4	∅	6	0.75	82	0.56	200	1.55	130	1.00	105	0.83	82	0.64
4	6	7.5	0.9	140	0.96	345	2.70	235	1.83	195	1.52	140	1.09
4	8	9	1.1	300	2.05	750	5.85	570	4.45	400	3.12	300	2.35
5	—	7.5	0.95	165	1.12	400	3.12	290	2.26	200	1.56	160	1.25
5	7.5	9.5	1.2	320	2.18	800	6.25	550	4.30	430	3.36	320	2.50
5	10	11	1.3	480	3.26	1.2	9.30	950	7.40	650	5.11	480	3.75
6	∅	9	1.1	245	1.67	600	4.68	450	3.52	330	2.58	250	1.95
6	9	11	1.4	516	3.50	1.3	10.0	875	6.85	700	5.46	516	4.00
6	12	13.5	1.6	870	5.90	2.2	17.2	1.7	10.4	1.2	9.30	870	0.80
7	∅	10.5	1.3	400	2.72	1.0	7.80	720	5.60	540	4.20	400	3.12
7	10.5	13	1.6	780	5.30	1.9	10.5	1.3	10.0	1.1	8.60	780	6.10
7	14	16	1.9	1.4	9.50	3.5	27.4	2.7	21.0	1.9	10.5	1.4	10.9
8	∅	12	1.5	610	4.15	1.5	11.7	1.1	8.6	830	6.5	610	4.80
8	12	15	1.9	1.3	8.80	3.2	25.0	2.2	17.2	1.8	14.0	1.3	10.0
8	16	18	2.2	2.3	10.6	5.8	45.2	4.4	34.2	3.1	2.42	2.3	18.0
9	∅	13.5	1.7	890	6.10	2.2	17.2	1.6	12.5	1.2	9.30	890	7.00
9	13.5	17	2.1	1.9	13.0	4.9	38.2	3.3	25.8	2.6	20.3	1.9	14.8
9	18	20	2.4	3.0	20.4	7.5	58.6	5.7	44.5	4.1	32.0	3.0	23.4
10	∅	15	1.9	1.2	8.20	3.0	23.4	2.2	17.2	1.6	12.5	1.2	9.30
10	15	19	2.4	2.6	10.8	6.5	51.0	4.4	34.5	3.5	27.4	2.6	20.2
10	20	23	2.7	4.2	28.5	11.0	86.0	8.0	62.5	6.0	46.8	4.0	31.2
11	∅	16.5	2.0	1.6	10.9	4.0	31.2	3.0	23.4	2.3	18.0	1.7	13.3
11	16.5	21	2.6	3.5	23.8	8.8	68.8	6.0	46.8	4.7	36.6	3.5	27.2
11	22	25	3.0	5.8	39.5	15	117	11	86.0	7.8	61.0	5.8	45.2
12	∅	18	2.2	2.0	13.6	4.8	37.5	3.5	27.4	2.7	21.0	1.9	14.8
12	18	23	2.8	4.2	28.6	10	78.0	7.1	55.5	5.7	44.5	4.2	32.8
12	24	27	3.2	7.0	47.5	18	140	13	100	9.5	74.0	7.0	54.5
13	∅	19.5	2.4	2.5	17.0	6.3	49.2	4.5	35.2	3.4	26.5	2.5	19.5
13	19.5	24	3.0	5.1	34.8	13	100	8.7	68.0	6.9	54.0	5.1	40.0
13	26	29	3.5	9.5	64.8	23	180	17	133	12	94.0	9	70.0
15	∅	22.5	2.8	4.0	27.2	10	78	7.2	56.5	5.4	42.2	4.0	31.2
15	22.5	28	3.4	7.5	51.0	20	155	13	100	11	86.0	8.0	62.5
15	30	34	4.0	14	95.0	35	273	27	210	19	148	14	109
17	∅	25.5	3.2	5.8	39.5	15	117	11	86.0	7.8	61.0	5.8	45.2
17	25.5	32	4.0	12	82.0	30	235	22	172	16	125	12	94.0
17	34	38	4.5	19	129	48	375	36	280	26	202	19	148
20	∅	20	3.7	9.5	65.0	24	187	17	133	13	100	10	78.0
20	30	38	4.8	20	136	50	390	36	282	27	210	20	155
20	40	45	5.5	35	238	88	685	67	525	47	366	35	27.4
23	∅	34.5	4.3	14	95.0	35	274	25	195	19	148	14	109
23	34.5	43	5.4	30	204	76	595	56	438	41	320	30	235
23	46	52	6.2	50	340	125	970	96	750	67	523	50	390
25	∅	37.5	4.7	18	122	47	368	33	258	25	195	18	141
25	37.5	40	5.8	38	266	95	740	68	530	52	406	38	296
25	50	56	6.7	60	408	154	1.2	118	920	83	650	60	470
30	∅	45	5.6	34	232	86	670	62	485	46	360	34	265
30	45	56	7.0	65	442	163	1.3	117	910	88	690	65	510
30	60	68	8.0	110	750	275	2.1	208	1.6	148	1.2	110	860
35	∅	52.5	6.5	50	340	125	970	90	705	68	530	50	390
35	52.5	66	8.2	105	720	265	2.1	193	1.5	143	1.1	105	830
35	70	79	9.3	170	1.2	420	3.3	318	2.5	228	1.8	170	1.3
40	∅	60	7.5	77	520	195	1.5	140	1.1	104	810	77	600
40	60	75	9.3	149	1.0	375	2.9	270	2.1	200	1.6	149	1.2
40	80	90	10.5	250	1.7	620	4.9	470	3.7	340	2.7	250	2.0
45	∅	57.5	8.4	108	800	270	2.1	195	1.5	145	1.2	108	850
45	67.5	85	10.5	220	1.5	550	4.3	400	3.1	298	2.3	220	1.7
45	90	100	12	365	2.5	910	7.1	690	5.4	492	3.9	365	2.8
50	∅	75	9.4	150	1.0	375	2.9	270	2.1	205	1.6	151	1.2
50	75	94	11.6	295	2.0	730	5.7	520	4.1	400	3.1	390	3.0
50	100	110	13.5	510	3.5	1300	10.0	980	7.7	700	5.5	520	4.1
55	∅	82.5	10.3	205	1.4	520	4.1	370	2.9	278	2.2	205	1.6
55	82.5	105	12.8	408	2.8	1000	7.8	700	5.5	540	4.2	400	3.1
55	110	125	14.6	680	4.7	1700	13.3	1300	10.0	920	7.2	690	5.4

The amount to be fed is a function of the shape of the casting as well as the shrinkage. The characteristic values of the casting must therefore be linked with those of the feeder. We obtain from Fig. 94 for the case of a cylindrical feeder with height $H = \text{diam. } D$ the relationship:

$$V_F = 99(M_F)^3 \tag{23}$$

the value $q = 99$ being the shape-and-modulus-dependent characteristic.

Furthermore $M_F = f \times M_{\text{casting}}$, f being the compensating factor. Thus the maximum volume of casting which can be fed from a cylindrical feeder having $H = D$ can be calculated from equations 20 and 22.

$$\begin{aligned} V_C &\leq \frac{100 V_{sc} - S \cdot V_F}{S} = V_F = \left(\frac{14 - S}{S} \right) \\ &= 99(M_C)^3 \cdot f^3 \cdot \frac{14 - S}{S} \end{aligned} \tag{24}$$

For a cylindrical feeder with $H = 1.5 D$:

$$V_C \leq 122(M_C)^3 \cdot f^3 \cdot \frac{14 - S}{S} \tag{25 a}$$

For hemispherical feeders:

$$V_C = 156(M_C)^3 \cdot f^3 \cdot \frac{20 - S}{S} \tag{25 b}$$

But as the feeder calculation must be commenced from the casting, and not from the feeder, the factor f , with reference to the feeding conditions of cylindrical feeder heads having $H = D$, is given by:

$$\begin{aligned} f &= \sqrt[3]{\frac{V_C}{99(M_C)^3} \cdot \frac{S}{14 - S}} = \sqrt[3]{\frac{S}{99(14 - S)}} \times \\ &\times \sqrt[3]{\frac{V_C}{M_C}} = \frac{K}{M_C} - \sqrt[3]{V_C} \end{aligned} \tag{26}$$

In this expression K is a constant which is dependent only on the type of feeder and the metal shrinkage. For unalloyed steel castings ($S \approx 5$ per cent) the following values of K are obtained:

Cylindrical feeders $H = D \varnothing \quad K = 0.178$

Cylindrical feeders $H = 1.5 D \varnothing \quad K = 0.164$

Hemispherical feeders $\quad \quad \quad K = 0.158$

The feeding characteristics of the simple basic components into which the casting is divided are known. For each of these components the relationship:

$$V = q \cdot (M)^3 \tag{27}$$

is also valid, q being a constant which is entirely dependent on the shape of the component.

Table 20 gives the q values of various basic shapes, the size relationships of which were determined on the following assumptions:

(1) The region under the riser is sound in every case. The riser diameter amounts to $10 \times M_{\text{casting}}$, including a feeder neck.

(2) The basic component only comprises the sound region, in the sense of Figs. 47, 48 and 49 (after R. Cech). When the sound end zone is included in the calculation, the volume of the basic shape is increased, and so is its q value compared with the feeder zone itself.

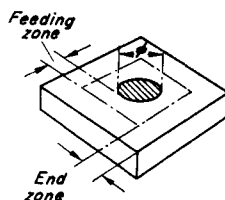
TABLE 20. RELATIONSHIP BETWEEN THE VOLUME AND MODULUS OF SIMPLE GEOMETRICAL BODIES (q-VALUES)

The modulus is a length, which is connected with a linear dimension of the body in question (for example the side of a cube). The volume of the body is a function of the 3rd power of this length (example cube).

$$M = \frac{a}{6}, \quad V = a^3.$$

We can also write $M = \frac{a}{6}$ and

$a = 6M$. Hence $V = a^3 = 216 \cdot M^3$. The number 216 is therefore the q -value of the cube. The feeding surface, that is the non-cooling surface, must not be included in the accurate determination of the modulus. In the approximate calculation the feeding surface is neglected. The uniform assumption is made that the feeder (with shoulders) has a diameter of $10 \times M_C$.



Basic shapes of unalloyed steel (with bodies made from other metals the sound feeding range and hence the dimensions are different)		Shape dependent constant q with	
		accurate calculation	approximate calculation
Plate	with end zone	1340	1560
	without end zone	432	646
Disc	with end zone	1000	1230
	without end zone	303	508
Bar 5 : 1	with end zone	690	900
	without end zone	354	560
Bar 4 : 1	with end zone	565	775
	without end zone	282	475
Bar 3 : 1	with end zone	480	675
	without end zone	230	410
Bar 2 : 1	with end zone	430	582
	without end zone	200	333
Bar 1 : 1	with end zone	395	500
	without end zone	170	285
Parallelepiped 1 : 1 : 2		182	250
Cube 1 : 1 : 1		125	216
Cylinder $H = D \varnothing$		142	197
Cylinder $H = 2D \varnothing$		167	98

Figures 100a-g enable the correct shape of feeder to be selected immediately as a function of the q value of the basic shape and of the relevant shrinkage S .

For metals having feeding ranges differing from those of steel, Table 20 must be re-calculated, and the q values will change (for smaller feeding ranges they become less, and vice versa). However, Fig. 99 is valid for all metals, except for grey, malleable and nodular graphite cast iron.

FIGS. 100a-g. Optimum feeder design or necessary compensation factor as a function of the shrinkage of the steel and of the weight and modulus of the casting.

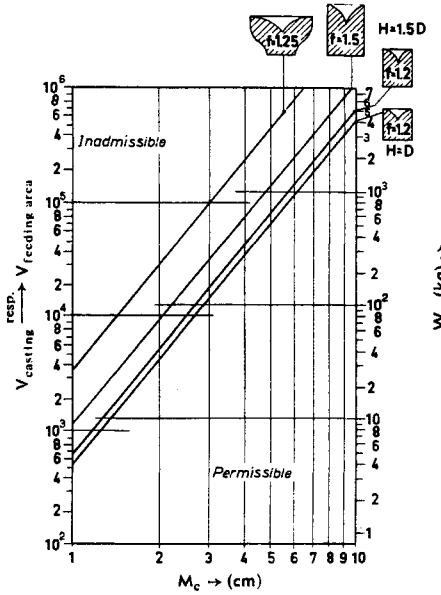


FIG. 100a. Modulus of the casting at the point of application of the feeder head, cm

Volume of the casting (feeding area), cm^3
 Weight of the casting (feeding area), kg
 Shrinkage 4%

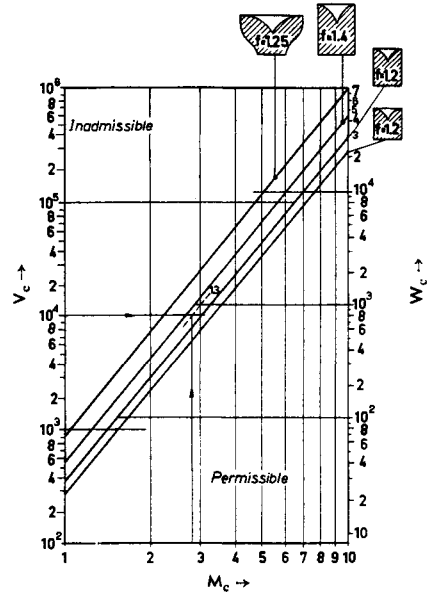


FIG. 100c. Modulus of the casting at the point of application of the feeder head, cm

Volume of the casting (feeding area), cm^3
 Weight of the casting (feeding area), kg
 Shrinkage 6%

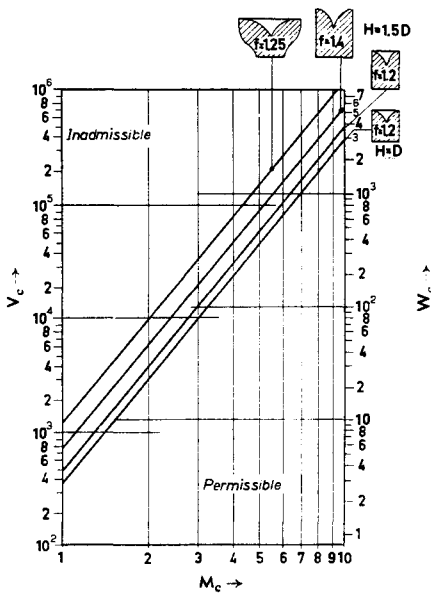


FIG. 100b. Modulus of the casting at the point of application of the feeder head, cm

Volume of the casting (feeding area), cm^3
 Weight of the casting (feeding area), kg
 Shrinkage 5%

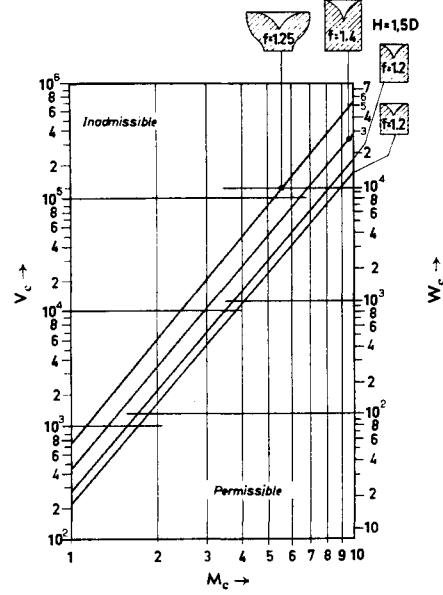


FIG. 100d. Modulus of the casting at the point of application of the feeder head, cm

Volume of the casting (feeding area), cm^3
 Weight of the casting (feeding area), kg
 Shrinkage 7%

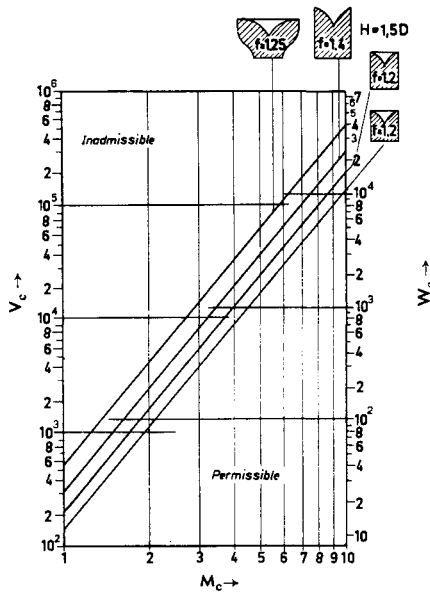


FIG. 100c. Modulus of the casting at the point of application of the feeder head, cm

Volume of the casting (feeding area), cm^3
 Weight of the casting (feeding area), kg
 Shrinkage 8%

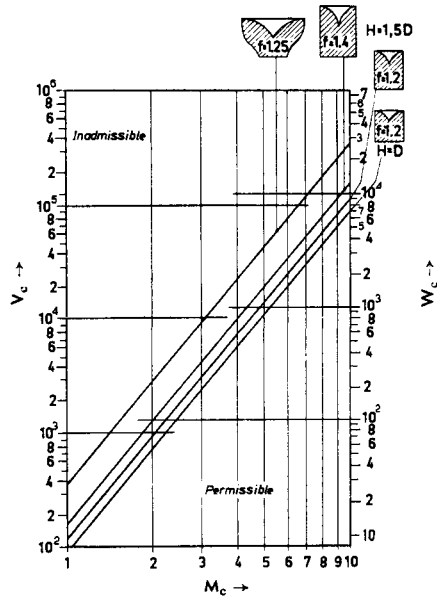


FIG. 100g. Modulus of the casting at the point of application of the feeder head, cm

Volume of the casting (feeding area), cm^3
 Weight of the casting (feeding area), kg
 Shrinkage 10%

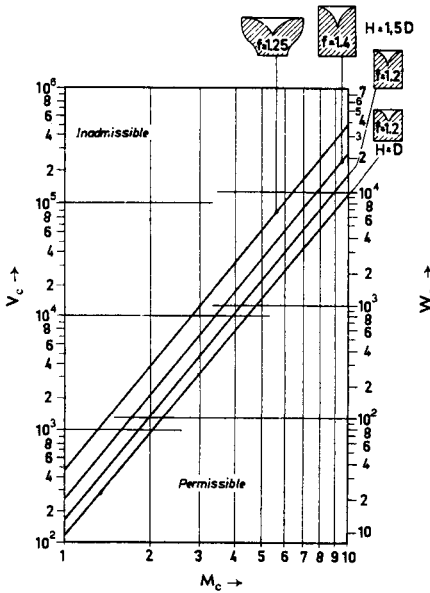


FIG. 100f. Modulus of the casting at the point of application of the feeder head, cm

Volume of the casting (feeding area), cm^3
 Weight of the casting (feeding area), kg
 Shrinkage 9%

When further cross-sections are fed by the basic body (stepped wedges, machine housing walls, etc.), their volume must also be taken into account, and Figs. 100a-g are applicable. The volume data are valid for all metals, again excepting grey, malleable and nodular graphite cast iron; but the weights apply only to steel.

A rapid determination of the suitable feeder types for different basic shapes which is easy to follow is provided by Fig. 101a. This shows immediately that basic shapes with end zones already have such large shrinkage requirements that larger feeder types must be selected than those which would be necessary purely on the basis of the appropriate moduli. Figures 101b-c are photographs of feeders of this kind.

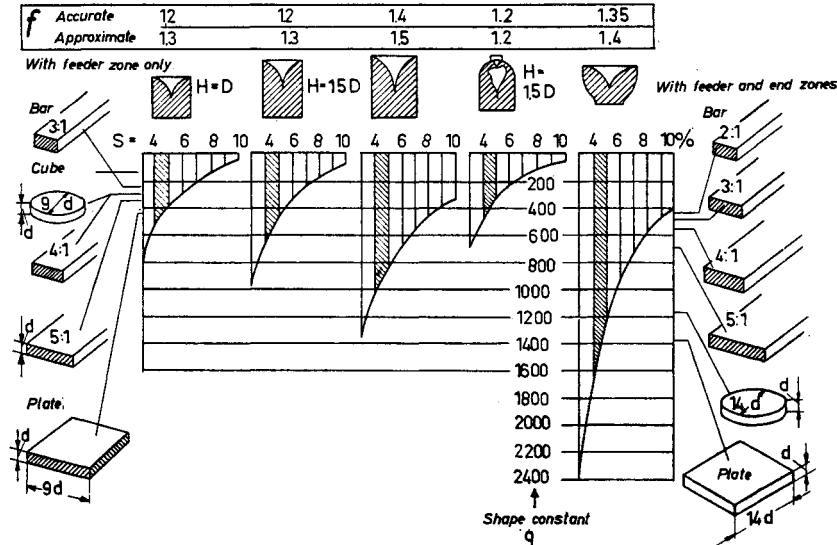
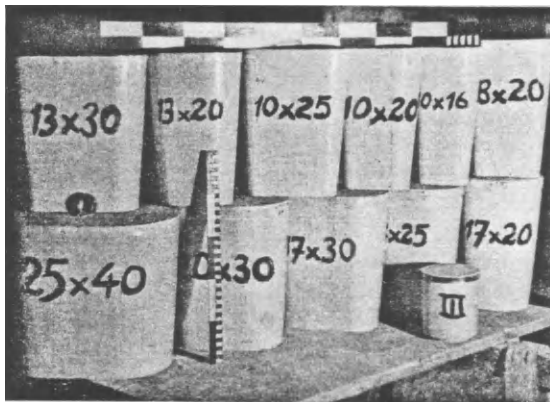


FIG. 101 a. Rapid determination of suitable feeder types for various basic shapes.



FIGS. 101 b and c. Various standard feeders (see Tables 9-19) for selecting from the point of view of moulding technology.



OF GREAT PRACTICAL IMPORTANCE

Even parts of the casting which are unsound are to some extent supplied with metal by the feeders. A plate of thickness d shows a sound feeder zone of $2d$, but the more distant portions also obtain some metal from the feeder. The supply of steel from this source is interrupted only in the last phase of solidification, and centre-line shrinkage cavities are then formed. The amount of steel required to fill up this residual cavity is very small as a rule, so that the volume and weight of the unsound parts of the casting must also be fully allowed for when dimensioning the feeder. This case occurs very often; it is only necessary to consider the "bulges" on fittings of all kinds, the housing walls of pumps, turbine blades, etc., which cannot be manufactured without centre line shrinkage cavities without troublesome modifications in design; these are in any case unimportant, except for certain steam-raising units.

Considerations arising from the parabolic shape of the cavity make some simplifications necessary for the sake of reliability. The very unfavourable structure of the shrinkage cavity can be almost completely eliminated by using highly exothermic materials. These materials are reliable in operation, and can be recommended for this reason, even if the saving resulting from a higher yield is lost again due to the cost of the powder. Exothermic compounds will be studied in detail in Chapter 12.

5.7. Influence of the Structure of the Shrinkage Cavity on the Maximum Yield

(If this section is omitted, the remaining sections on feeder calculations can still be understood.)

Only the overall yield will be treated here. The casting, together with machining allowances, which must also be supplied from the feeder, can be considered to be part of the casting. However, no allowance is made for the

runner and downgate system. Nonetheless, the overall yield can furnish valuable information, because the proportion machined can be determined accurately from the monthly returns of turnings, etc. The proportions of runners can be calculated for constantly recurring castings, classified into types, and weighed or estimated.

By yield is understood the proportion of the weight of the casting, expressed as a percentage of the liquid metal which must be used to obtain the casting. The calculation can also be based on the cold furnace charge, but the basis of calculation must be made clear before operating comparisons are made.

The feeder proportion F (per cent) is given by:

$$F(\%) = \frac{V_E \cdot 100}{V_{\text{casting}}} \quad (28)$$

where V_E represents the volume of metal in the feeder after solidification is complete.

Metal volume and the shrinkage cavity are connected by the relationship:

$$V_F = V_E + V_{SC} \quad (29)$$

where V_{SC} is known ($V_{SC \text{ max}} = 0.14 V_F$ for cylindrical feeders and $0.20 V_F$ for hemispherical feeders). Hence for cylindrical feeders (Fig. 102) we have:

$$F(\%) > \frac{86 S}{14 - S} \quad (30)$$

and for hemispherical feeders:

$$F(\%) > \frac{80 S}{20 - S} \quad (31)$$

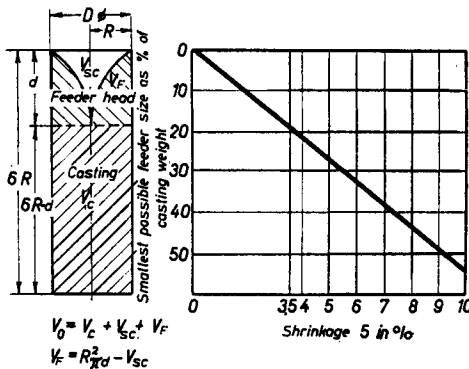


FIG. 102. Relationship: shrinkage-feeder proportion in cylinders.

It follows that hemispherical feeders are only superior to the cylindrical types when the feeder utilization is $V_{SC} = 0.14-0.20 V_F$, i.e. the hemispherical feeder is heavier and more uneconomical than the cylindrical feeder, a situation which changes only when the utilization exceeds 14%.

The total yield of liquid steel is

$$Y(\%) = \frac{W_{\text{casting}} \cdot 100}{W_{(\text{casting} + \text{total circulating scrap})}} \quad (32)$$

where W represents the weight in question.

The total yield of solid steel is

$$Y S(\%) = \frac{W_{(\text{casting} + \text{mach. allowance})} \cdot 100}{W_{(\text{casting} + \text{mach. allowance} + \text{feeder})}} \quad (33)$$

from this and from equation (28) we obtain:

$$Y S(\%) = \frac{100 \times 100}{(100 + F\%)} \quad (34a)$$

For a cylindrical feeder with maximum utilization this becomes from equations (34a) and (30):

$$Y S = \frac{10,000(14 - S)}{1400 - 14 S} \quad (34b)$$

$14 S$ is small compared with 1400. If the value $S = 6$ is substituted, fluctuations of $\pm 2\%$ will hardly be noticeable, and we then have:

$$Y S(\%) = \frac{10,000(14 - S)}{1290} = 7.75(14 - S) \quad (35)$$

and for hemispherical feeders:

$$Y S(\%) = 7.75(20 - S) \quad (36)$$

If the cold charge is taken as the starting point, then, assuming a melting loss of about 8 per cent, the constant 7.75 becomes 7.14.

As cylindrical feeder heads are more common than the hemispherical type, $(15 - S)$ can be inserted as a good average value. Figure 103 gives the relationship

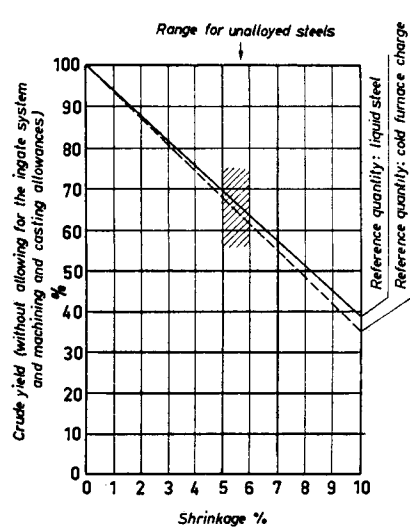


FIG. 103. Overall yield as a function of shrinkage. (When using highly-exothermic antipiping compounds the overall yield is higher than shown here.)

of the total solid yield to the shrinkage S . With maximum utilization of the feeder, then an actual yield of 50-55 per cent is obtained with 10-15 per cent for the gating system and machining allowances (rough estimate). As long as the actual yield of a foundry lies in this region, highly-exothermic antipiping materials can at best produce a further increase. The main advantage of the use of directional solidification consists in increased dependability and the production of quality castings. If the

average yield is much below the above value, then direct advantages are also possible by savings in circulating scrap.

5.8. Feeder Head Calculations

IMPORTANT FOR PRACTICE

Corresponding to the sequence adopted in this book, the feeder calculation will proceed as follows:

1. Breakdown of the casting into basic shapes and feeding areas.
2. Determination of the modulus of each feeding area.
3. Calculation of the feeder necks, so that no risk of premature freezing exists.
4. Assessment of the behaviour of the feeder during solidification.

Discussions in the literature are confined almost entirely to circular section feeders; but these cannot serve all needs in practice. Elongated castings of all kinds (for example, wheel rims) require oval feeders (see also Chapter 6, Section 1, and Fig. 127). The data for the calculation of various shapes of feeder are given in Fig. 104, on which Tables 9–19 are based.

The feeders are graded according to the modulus principle. Obviously there is no need to stock all the feeders; the ones suitable for each operation will be selected. Particularly while directional solidification is being introduced, a large selection of feeder types need not be stocked; the feeders must therefore be classified

on the basis of “unsatisfactory” and “satisfactory”. The author’s experience has shown that simple and easily recognizable figures which help to reduce errors are to be preferred. A degree of accuracy too meticulous to maintain in normal working conditions in the foundry, would be unjustified. A “psychological” table of this kind, which the author has used for years, is reproduced as Table 19.

If the modulus of the casting has been determined (for example, with the help of Fig. 7), this is multiplied by $f \approx 1.2$ to give the desired feeder modulus; the most suitable form of feeder head is then selected from Tables 9–19. In the case of massive castings (i.e. massive cylinders, cubes or parallepipeds) this completes the process of calculating the feeder. With platelike castings, however (such as machine housing walls and flanges), and in the feeding of adjacent cross-sections, control of the feeding volume of the feeder head on the basis of the proportion of the weight or volume of the casting is to be preferred. With small and medium castings it is quite sufficient to make an estimate based on the total weight, which is always known and can be roughly subdivided according to the type of feeding area.

As in many cases only the feeder modulus is of interest, there is no need to make a preliminary calculation of the modulus of the casting. For this reason Fig. 7 was redrawn in such a way that the appropriate feeder modulus is supplied directly; even the feeder dimensions could be plotted, but these were omitted for the sake of clarity (Figs. 105 a–d).

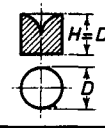
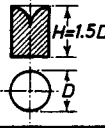
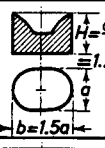
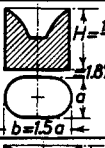
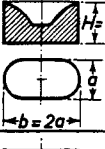
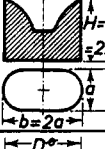
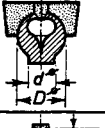
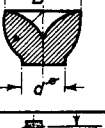
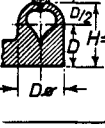
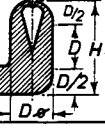
Feeder type	Characteristic values	Feeder type	Characteristic values
	$V = 0.785 D^3$ $= 1.69 M^3$ $M = 0.1667 D$ $D = 6M = H$		$V = 1.18 D^3$ $= 179 M^3$ $M = 0.187 D$ $D = 5.35 M$ $H = 8.02 M$
	$V = 1.605 a^3$ $= 181.5 M^3$ $M = 0.207 a$ $a = 4.84 M$ $b = 7.25 M$ $H = 6.05 M$		$V = 2.4 a^3$ $= 189 M^3$ $M = 0.233 M$ $a = 4.29 M$ $b = 6.43 M$ $H = 8.03 M$
	$V = 2.67 a^3$ $= 200 M^3$ $M = 0.237 a$ $a = 4.22 M$ $b = 8.45 M$ $H = 6.32 M$		$V = 4.01 a^3$ $= 211 M^3$ $M = 0.267 a$ $a = 3.75 M$ $b = 7.5 M$ $H = 8.42 M$
	$V = 0.533 D^3$ $= 115 M^3$ $M = 0.1667 D$ $D = 6M$ $d = 0.61 D$ $= 3.66 M$		$V = 0.261 D^3$ $= 196 M^3$ $M = 0.11 D$ $D = 9.1 M$ $d = 0.4 D$ $= 3.64 M$
	$V = 1.04 D^3$ $= 156 M^3$ $M = 0.189$ $D = 5.3 M$ $H = 7.94 M$		$V = 1.318 D^3$ $= 143 M^3$ $M = 0.21 D$ $D = 4.76 M$ $H = 9.52 M$

FIG. 104. The most important types of feeder head and their characteristic values.

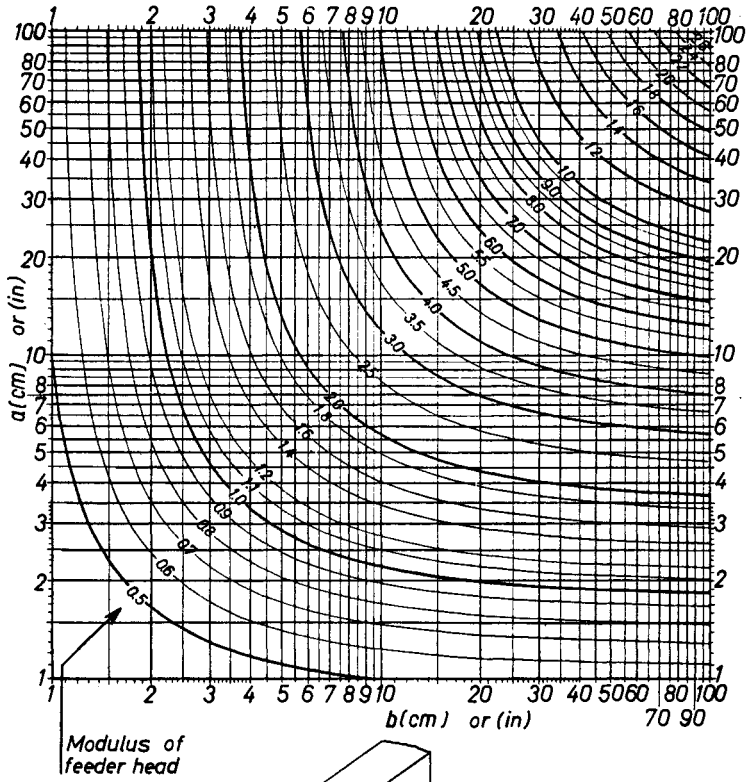


FIG. 105a. Feeder calculation of bars. $f = 1.1$

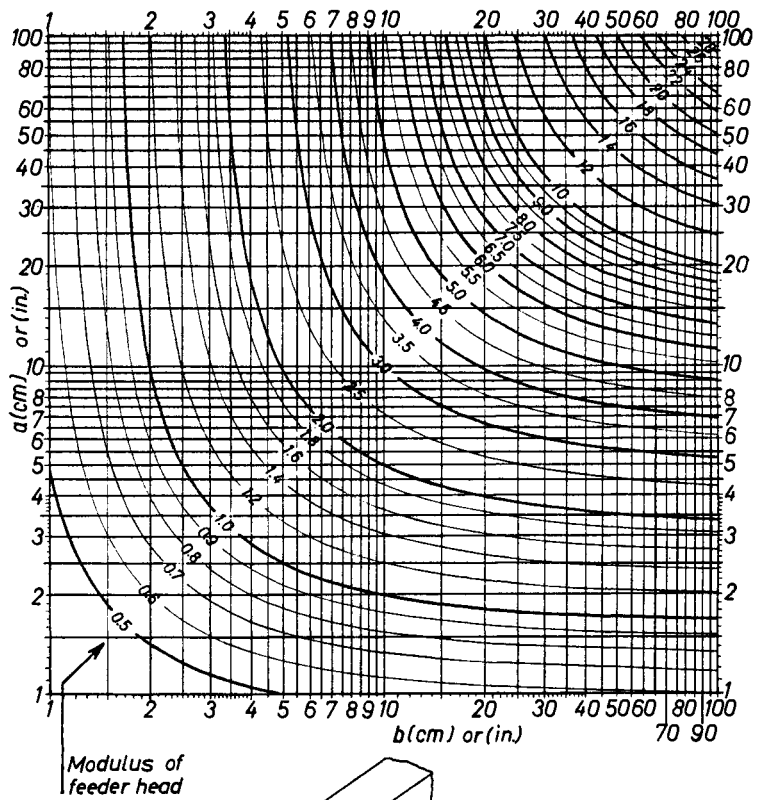


FIG. 105b. Feeder calculation of bars. $f = 1.2$

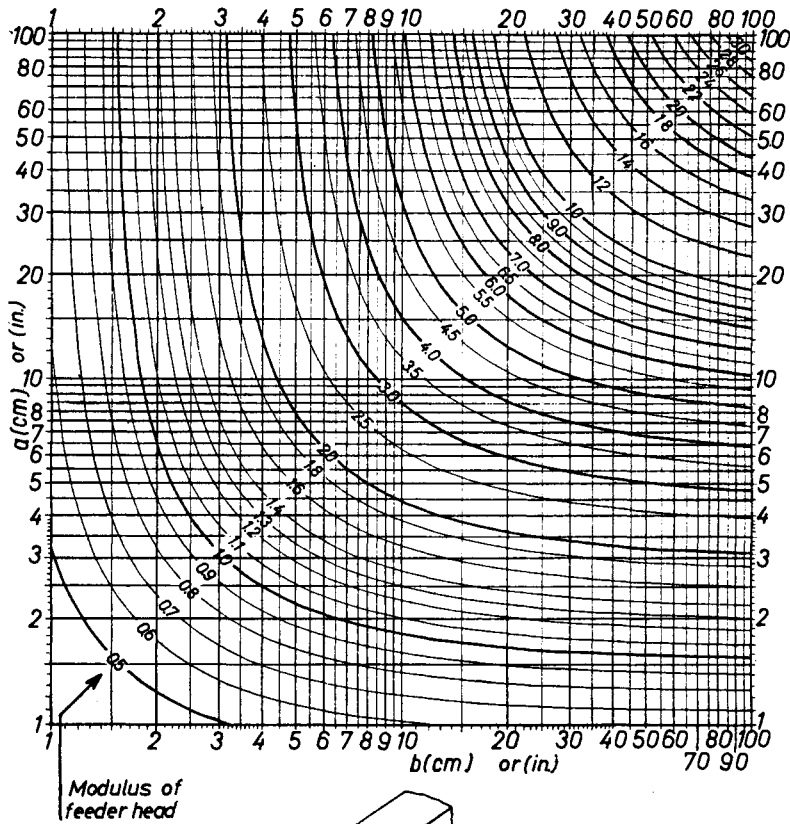


FIG. 105c. Feeder calculation of bars. $f = 1.3$

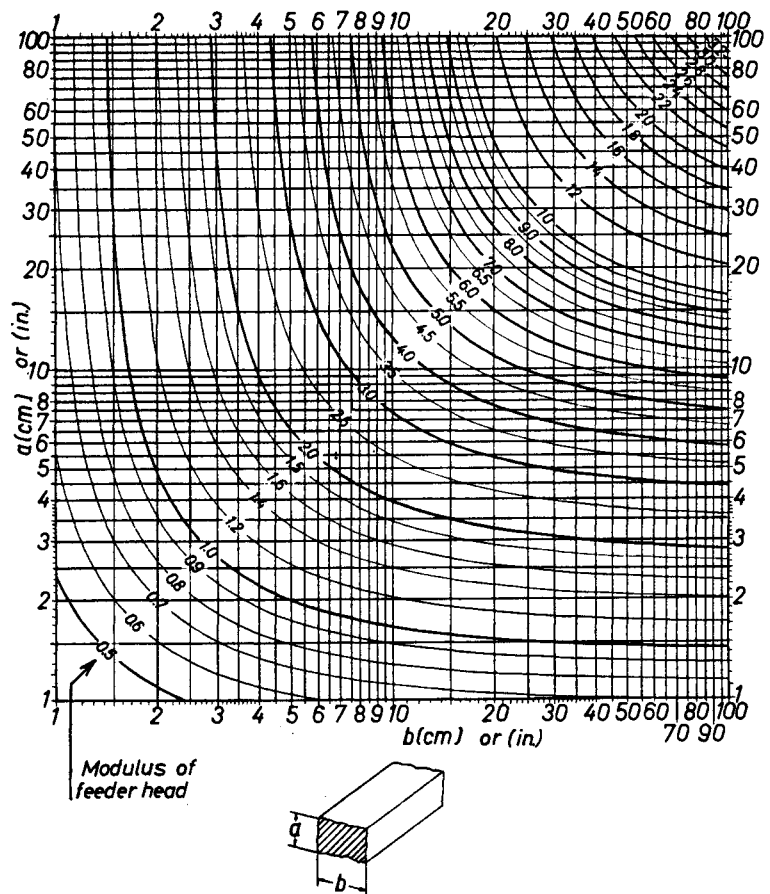


FIG. 105d. Feeder calculation of bars. $f = 1.4$

The following hints will be useful in helping the reader to construct these diagrams for himself.

The curves are parallel when drawn on log-log paper. One of the curves is plotted pointwise by means of the formula $M = a b / 2(a + b)$. The curve is symmetrical round the 45° axis. This curve is drawn on stiff card, cut out, and the point of transit of the 45° axis of symmetry marked out; this gives a curved rule which can be used as a drawing aid either for Fig. 7 or Fig. 105. The following relationships apply for the 45° axis:

$M = \frac{a}{4}$ for Fig. 7, and $M_F = \frac{a}{4} \times f$ for Fig. 105. It is only necessary to mark one point of the individual modulus on the axis, and to apply the curved rule at this point.

When selecting open gravity feeder heads, it must be borne in mind that, due to resistance to contraction after solidification, the feeder is often pulled off centre, and the casting is also distorted as a result (Figs. 106-108). If machine allowances are too small, or have not been

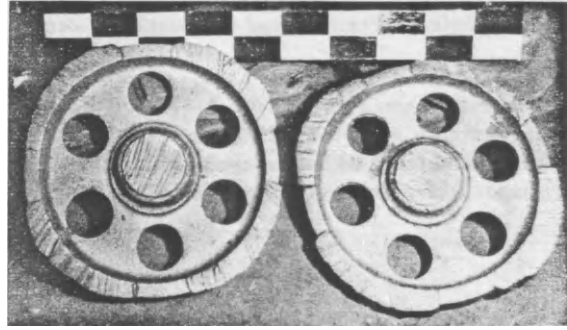


FIG. 107. Due to the resistance to contraction offered by the feeder head, the wheel rim was distorted to an angular shape.

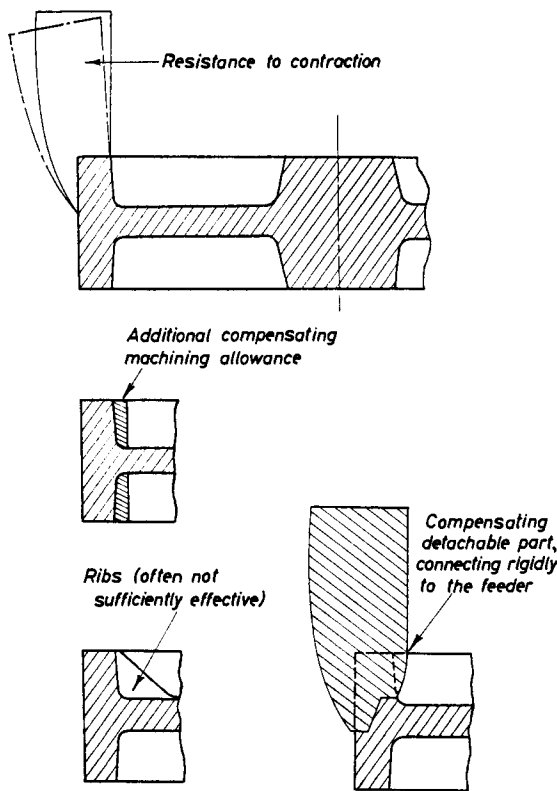


FIG. 106. Distortion on wheel rims and its compensation.

made at all, castings often become scrap; this danger must not be underestimated.

Corrective measures (more generous machining allowances, ribs, compensating additions, risers instead of gravity feeders) are illustrated in the diagrams.

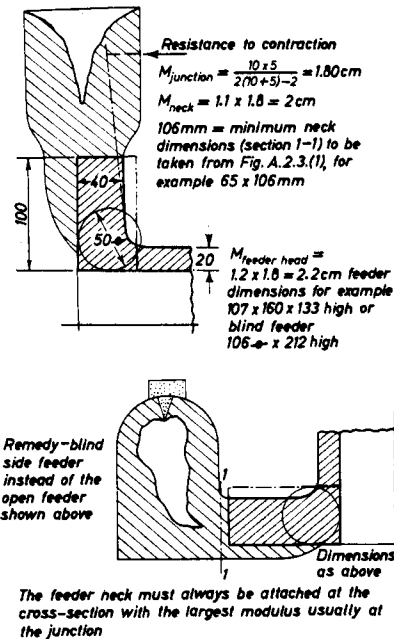


FIG. 108. Slope of the feeder head on valve flanges.

With larger castings only, there is a possibility that the feeder can be "released" shortly after casting by removing the moulding sand in the direction of tension, so that the feeder can yield to the forces of contraction without distortion.

5.9. Examples of Feeder Head Calculation

IMPORTANT FOR PRACTICE

The reader should try to solve for himself the following examples given in Figs. 109–126.

Some of the examples include castings from Chapter 2, the moduli of which were calculated in that chapter.

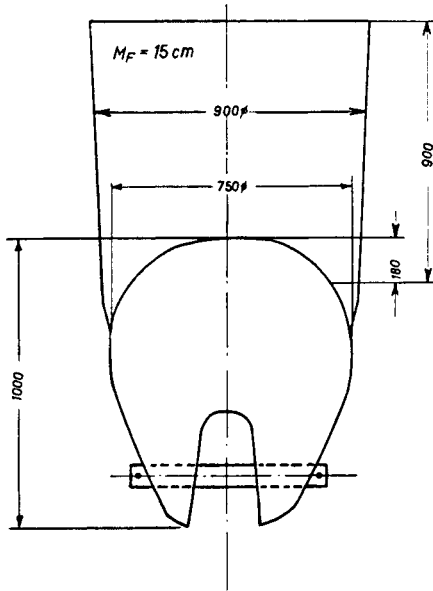
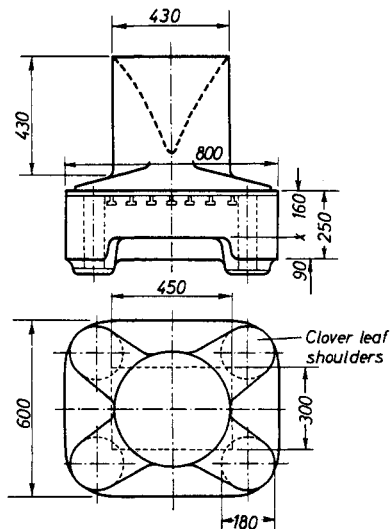


FIG. 109. Because of the possibility of shallow shrinkage cavities in massive bodies the feeder was cast lower by about 18 mm.

For further possibilities see:

Fig. 368a (with exothermic feeder)

Fig. 333 (with exothermic feeder and internal chill)



$M_C = 6 \text{ cm}; M_F = 1.2 \times 6 = 7.2 \text{ cm}$

FIG. 110. Press plate.

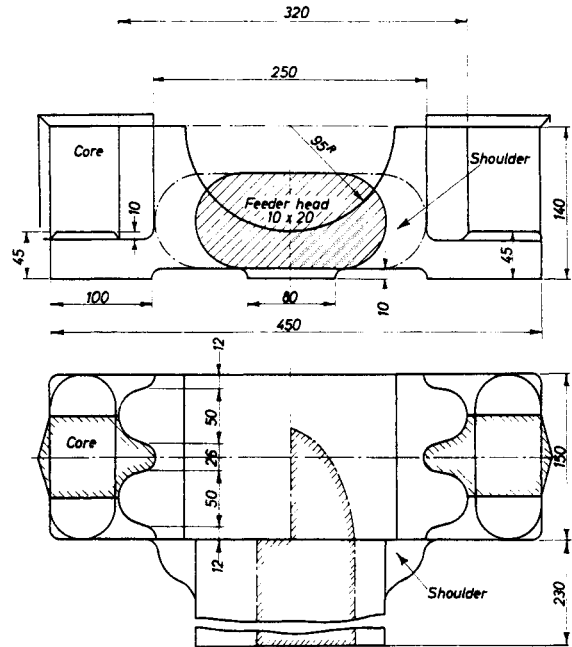


FIG. 111a. Bearing block. 1st alternative: moulded on the flat, gravity feeder with shoulder.

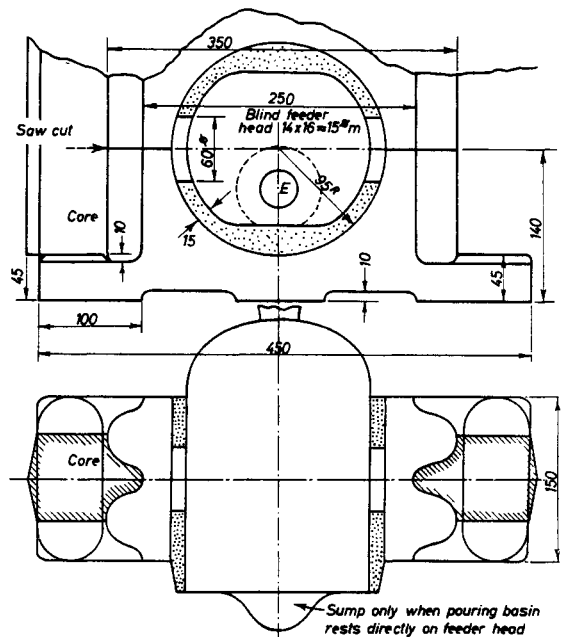


FIG. 111b. Bearing block. 2nd alternative: each of two bearing blocks moulded together on the flat, fed with tubular internal feeder (cf. Chap. 7).

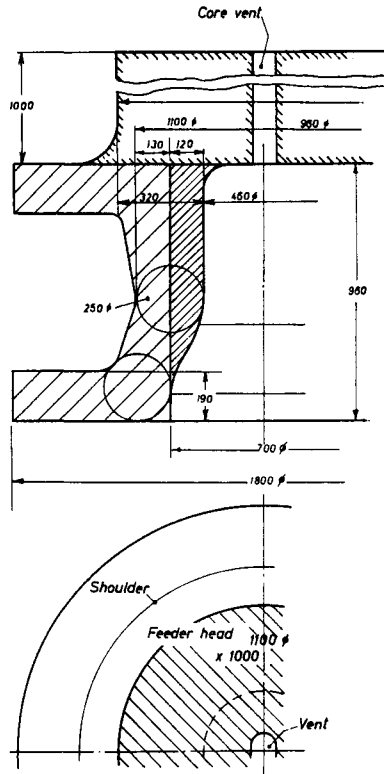


FIG. 112a. Double flange. 1st alternative: lower flange with Heuvers circles up to the feeder.

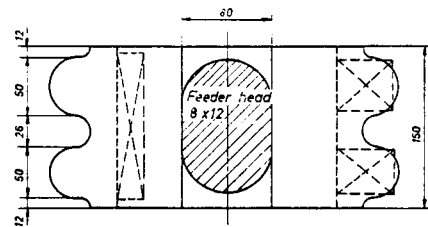
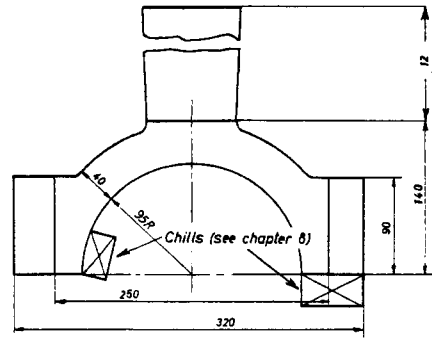


FIG. 113a. Bearing cap. 1st alternative: with gravity feeder and chills.

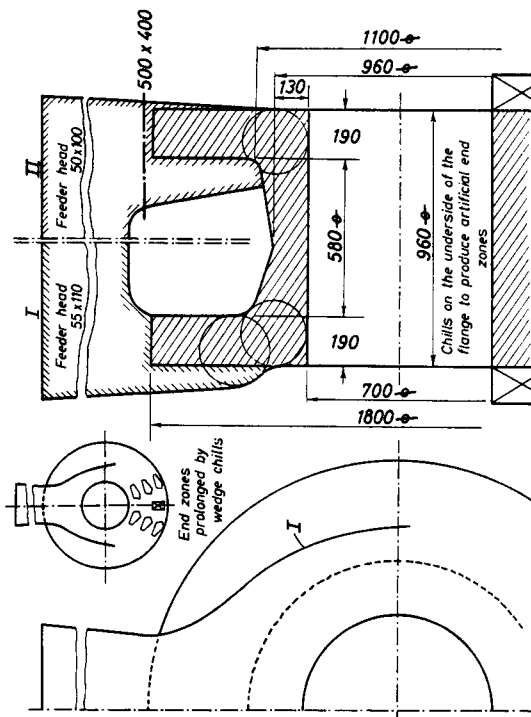


FIG. 112b. Double flange. 2nd alternative: feeding by only one gravity feeder, moulding on the flat.

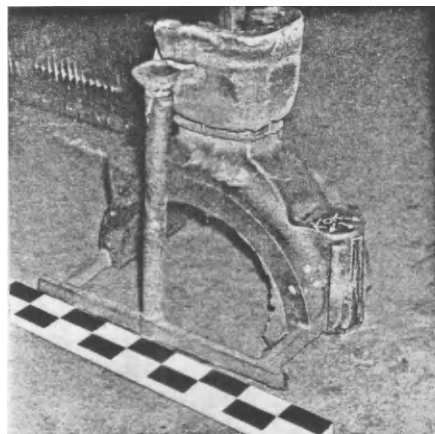


FIG. 113b. The massive eye lugs are cooled with chills. (This casting is not identical with that shown in Fig. 126b.)
(Courtesy SULZER Bros.)

FIG. 117a. Flange coupling. 1st alternative (top):

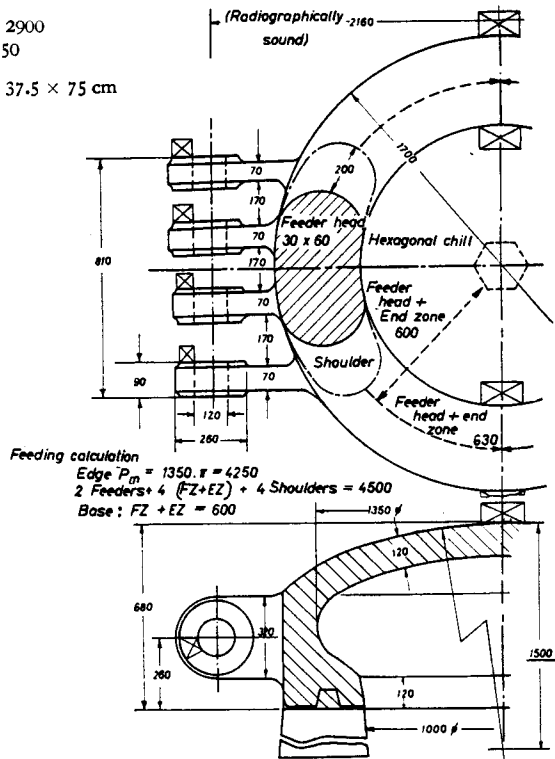
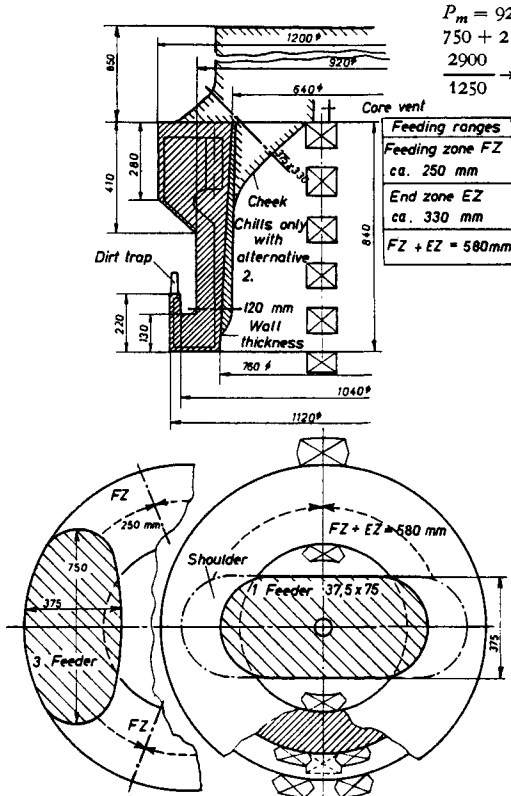


FIG. 118. Base plate. Alternative 1: with open-top feeders. Alternative 2: with exothermic sleeved feeders.

FIG. 117b. Flange coupling. 2nd alternative (below): $P_m = 2900$; $275 + 2(FZ + EZ) = 1535 \text{ mm}$, i.e. 1 feeder, using end-zone chills.

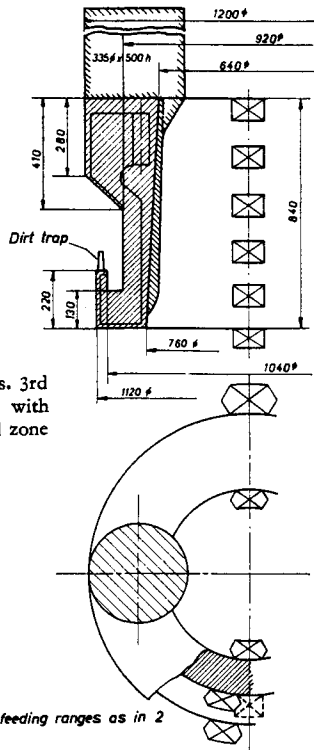


FIG. 117c. Flange couplings. 3rd alternative: use of feeders with exothermic sleeves and end zone chills.

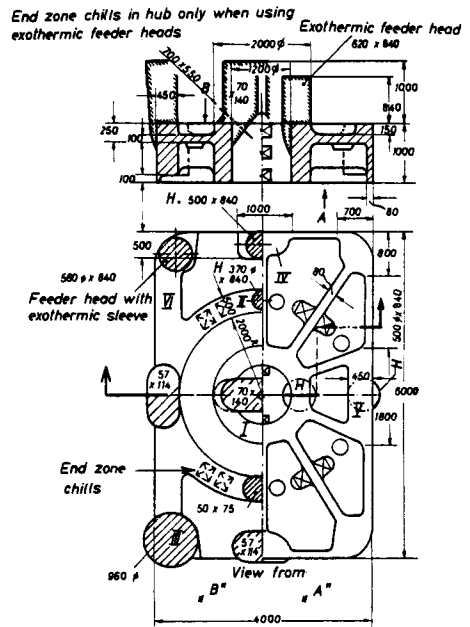


FIG. 119a. Autoclave cover. 1st alternative: 4 feeders on the flange, 1 blind feeder, centre of base.

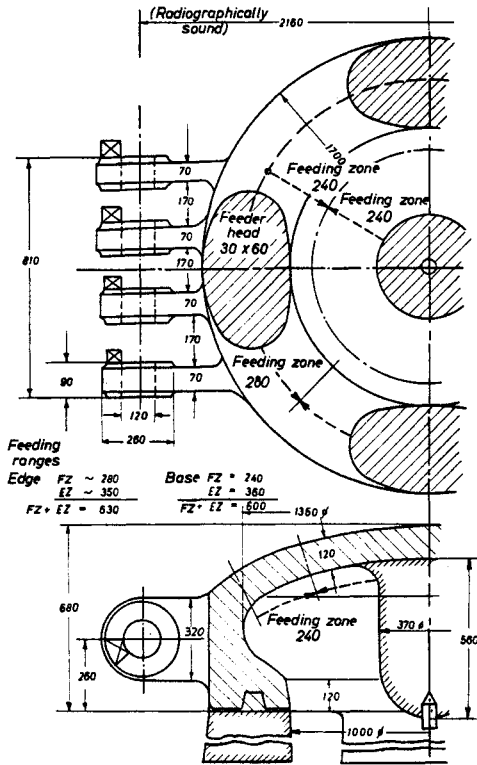


FIG. 119b. Autoclave cover. 2nd alternative: 2 feeders on the flange, through artificial end zones by means of chills at the flange and the centre of the base.

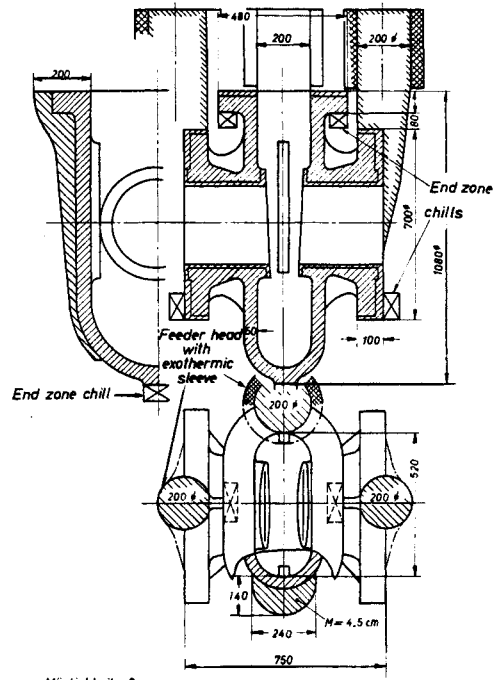
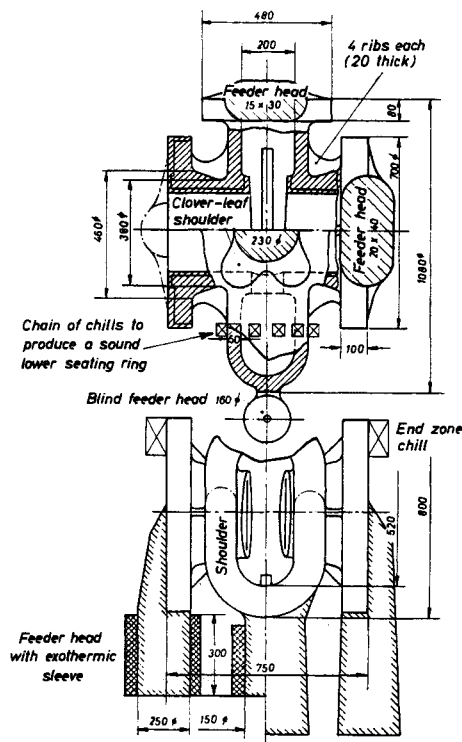


FIG. 120c. Gate valve body. 3rd alternative: pouring on end with padding added to the runner. Radiographically sound (highest grade) casting for most stringent requirements.



FIGS. 120a and b. Gate valve body. Possibility 1: open gravity feeder. Possibility 2: heated feeder.

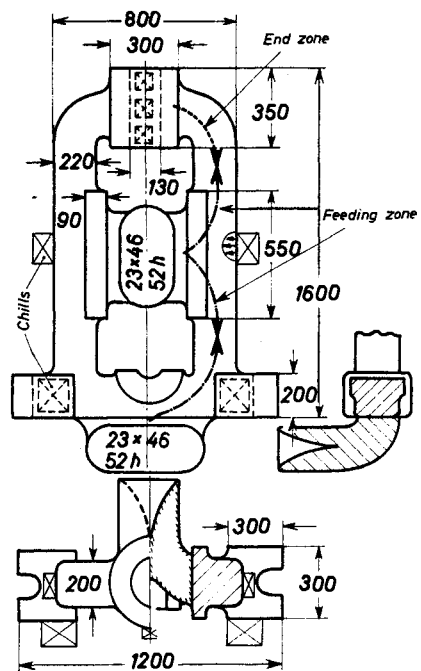


FIG. 121. Press standard housing.

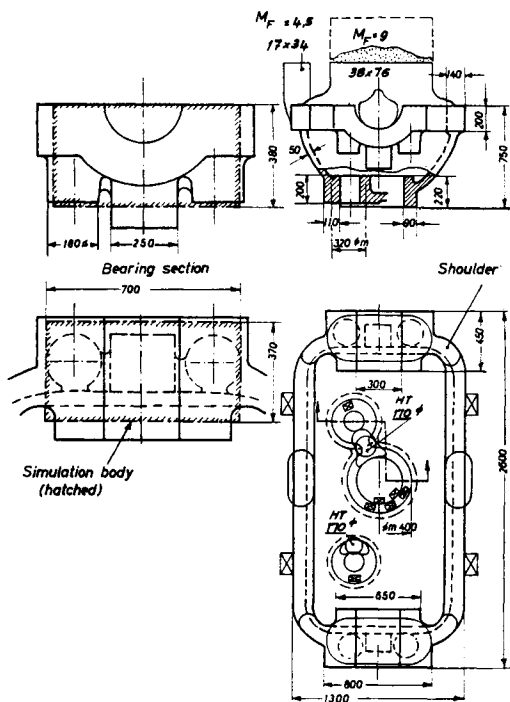


FIG. 122. Housing.

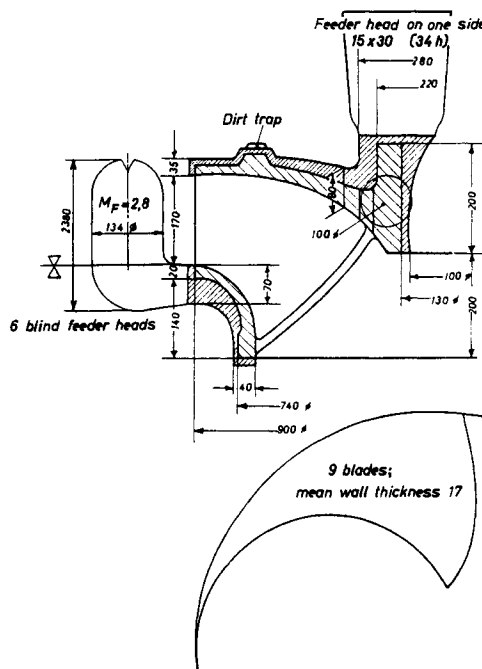


FIG. 123a. Turbine wheel. 1st alternative.

Bearing section:

Simulation body $37 \times 38 \times 70 \approx 37.5 \times 37.5 \times 70$

From Fig. 7:

$M_c = 7.5$; $M_F = 1.2 \cdot 7.5 = 9$ cm; $F = 38 \times 76 \times 75$ h

(height is reduced by exothermic materials) each feeder head feeds both halves of the bearing section.

Flange:

14×20 ; $M_F = 4.5$ cm; $F = 17 \times 34 \times 38$ h

Feeding ranges of the flange; feeder + end zone range = 420 mm. By placing a chill on the flange a considerable extension (i.e. increased safety) of the feeding range is achieved.

Double connecting piece:

11×20 ; $M_F = 4.2$; selected: covered exothermic feeder $170 \varnothing$ (Table 50)

Feeding ranges with feeder + end zone:

large connecting pieces	range =	220 mm
both sides		440 mm
+ shoulder width		300 mm
sum		740 mm
mean periphery		1240 mm
difference		500 mm

(this was spanned with elongated artificial end zones (see Fig. 252, Chapter 8).

Small connecting piece

feeding range	range =	370 mm
both sides		740 mm
shoulder width		260 mm
total		1000 mm

mean periphery 1000 mm. It is sufficient to place one end zone chill (Chapter 8).

Individual connecting pieces as before.

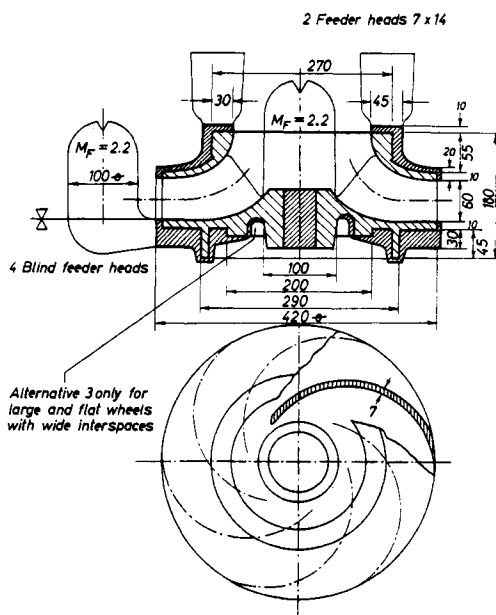


FIG. 123b. Turbine wheel. 2nd and 3rd alternatives.

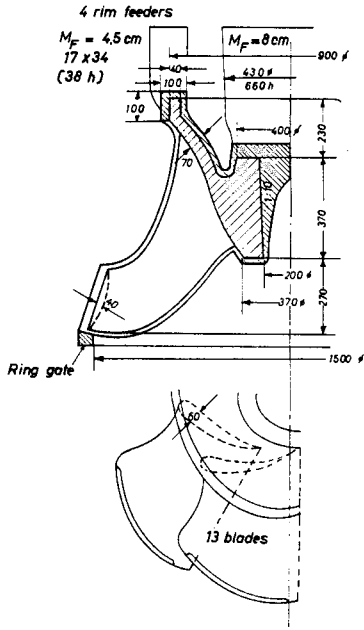


FIG. 123c. Francis turbine wheel.

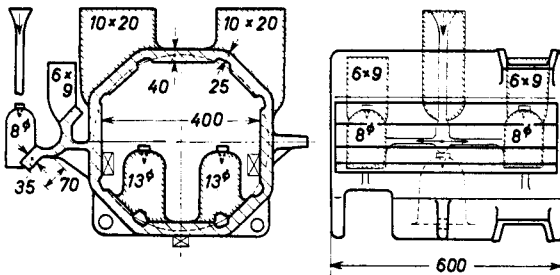


FIG. 124. Motor housing.

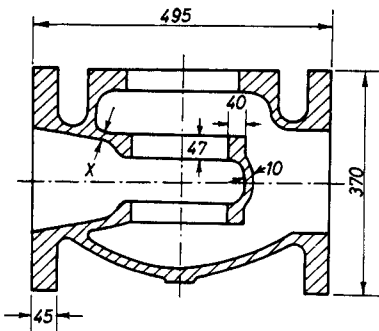


FIG. 125. Drawing of an unmachined valve casting.

The valve seating cannot be fed by a directly attached feeder head, but only through the housing wall "x".

What must the minimum thickness of "x" be, to guarantee a sound seating?

The seating represents a bar casting with a non-cooling surface (see also Fig. 73). Its modulus is

$$M = \frac{4 \times 4.7}{2(4 + 4.7) - 1.0} = \frac{18.8}{17.4} = 1.15 \text{ cm}$$

The modulus of the wall (= plate) x must be larger by 10%, i.e.

$$1.1 \times 1.15 = 1.27 \text{ cm. As } M_{\text{plate}} = \frac{x}{2}, \text{ therefore}$$

$$x = 2M = 2 \times 1.27 = 25.4 \text{ mm.}$$

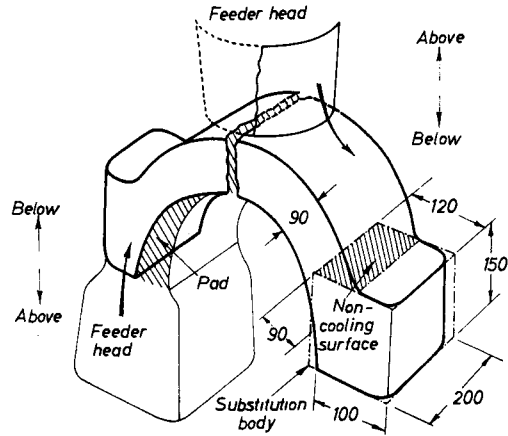


FIG. 126a. Bearing cover.

1. By the conventional method (left side of the diagram) a feeder head is placed on each end of the cover and the section circled out. The pads (and their removal) are expensive.

2. When it is possible to feed the ends satisfactorily through the central feeder head, the casting can be fed through one head only, without pads (right side of the diagram).

Draw a substitution body (see also Fig. 13) and calculate:

$$\text{volume} = 12.0 \times 15.0 \times 20.0 = 3600 \text{ cm}^3.$$

$$\text{Surface area} = 2(12 \times 15 + 12 \times 20 + 15 \times 20) - \text{non-cooling surface } 9 \times 20, = 1440 - 180 = 1260 \text{ cm}^2$$

$$M_{\text{end section}} = V/A = 3600/1260 = 2.85 \text{ cm.}$$

The modulus of the central section (= bar 9 x 20 cm) =

$$M_{\text{centre}} = 9 \times 20/2(9 + 20) = 3.10 \text{ cm.}$$

This is 10% larger than the modulus of the end section. Hence it is possible to use the much cheaper method 2.



FIG. 126b. A practical example of the use of the method of Fig. 126a.

(Courtesy Sulzer Bros.)

Note: This casting resembles, but is not identical with, the casting shown in Fig. 113b. The cross-section II of Fig. 113b is a little smaller than the corresponding cross-section shown here, so that in this case it is necessary to use chills.

I. Exothermic feeder head.

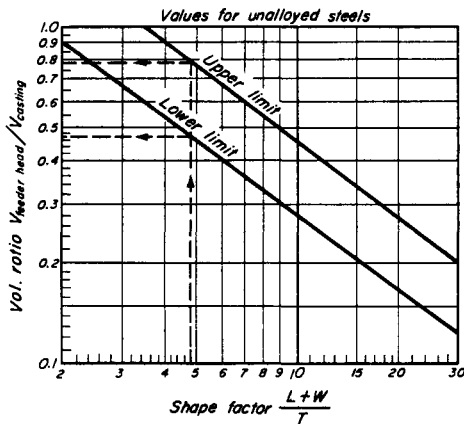
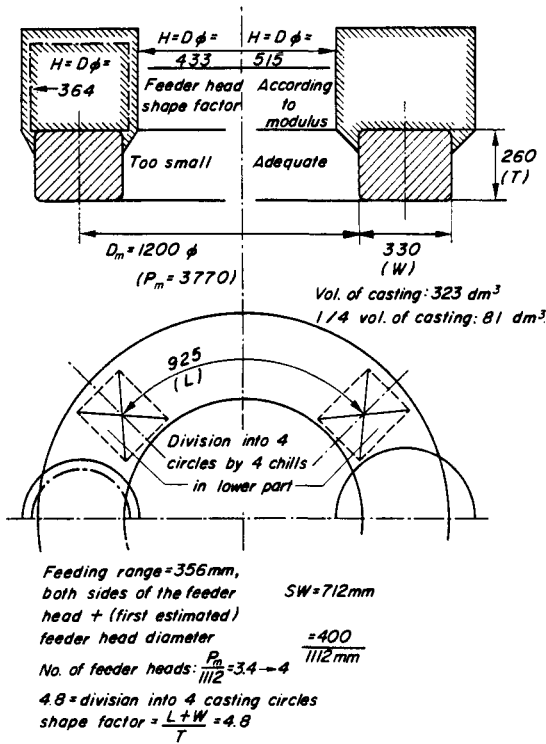
II. This section is rectangular, with a modulus about 10% larger than that of section III.

III. The modulus of this part of the casting is smaller than that of cross-section II.

5.10. Other Methods of Calculating Feeder Heads

This section need not be read to be able to understand the remainder.

TABLE 21. CALCULATION USING THE SHAPE FACTOR METHOD



	$V_{\text{feeder head}} / V_{\text{casting}}$	$V_{\text{feeder head}}$	Feeder head $H=D\phi$ mm	Determination by the modulus method
Lower limit	0.47	$81 \cdot 0.47 = 38 \text{ dm}^3$	364	According to Fig. 105: $M_F = 8.5$ to 8.6 $H=D\phi = 515 \text{ mm}$
Upper limit	0.79	$81 \cdot 0.79 = 64 \text{ dm}^3$	433	

Both values too small hence unsafe

TABLE 22. COMPARISON OF THE MODULUS AND SHAPE FACTOR METHODS

	Modulus method	Shape factor method
Plates	Determination of modulus unnecessary. Determination of feeder: direct reading from Fig. 105 or Tables 9-19	Calculate shape factor from: length + breadth/thickness; feeder detn.: calculate the plate volume; determine feeder volume from a diagram 1; determine the feeder dimensions from a diagram 2; correct the values in the light of experience in the case of very thin or very thick plates
Infinite bar, parallelepiped hollow and solid cylinders and similar bodies	Determination of modulus unnecessary. Determination of feeder: direct reading from Fig. 105 or Tables 9-19	Calculate shape factor from: length + breadth/thickness; feeder detn.: calculate the bar volume; determine the feeder volume from a diagram 1; determine the feeder dimensions from a diagram 2; correct the values in the light of experience with very thin or very thick bars
Compound bodies	Determination of modulus by the formula: $M = \frac{ab}{2(a+b)-c}$ $M_F = M \times 1.2$ Read off the suitable feeder directly from Tables 9-19	Calculate the shape factor from: length + breadth/thickness; calculate the volumes X and Y; calculate the wall thickness ratio a/c; determine the percentage of the volume of X which must be added when calculating the total volume (from a diagram 3); add the proportion so found to volume Y; determine the feeder volume from a diagram 1; determine the feeder dimensions from a diagram 2; correct the values in the light of experience for very thin or very thick bodies

The possibilities offered by the "classical" method of Chvorinov⁽¹⁾ were frequently not realized, and in order to avoid what were (falsely) assumed to be complicated calculations, the concept of the modulus was replaced by that of the "shape factor" by Caine⁽¹¹⁾ and Bishop and Johnson⁽¹²⁾. The calculated feeder values agree approximately in both methods, but obviously false results are obtained with the shape factor method when this is applied to very massive or very thin-walled bodies (Table 21), which has made the introduction of correction factors necessary. This has already been pointed out by Stein⁽¹³⁾. A mathematical relationship between shape factor and modulus exists only for geometrically similar bodies, a fact which accounts for the incorrect results already mentioned.

Table 22 gives a comparison of both calculating operations, and verifies that the shape factor method is more wearisome than the methods of calculation shown here.

The "classical" method satisfies the need of the practical man and gives a clear picture, even in difficult cases (volume/effective cooling surface) and this leads in general to reliable operation of the method in practice. The shape factor method, on the other hand, must involve extensive additions and corrections, even with the simplest of shapes, the need for which is in no way self-evident.

The calculation of internal and external chills, and of exothermic and insulating materials, as well as breaker cores and heating pads, is also more feasible by the "classical" method. Consequently the author decided to simplify the Chvorinov method, without abandoning the modulus principle, but leaving the shape factor method alone.

CHAPTER 6

INCREASING THE THERMAL GRADIENT IN THE CASTING BY PADDING AND BY THE UTILIZATION OF NATURAL END ZONES

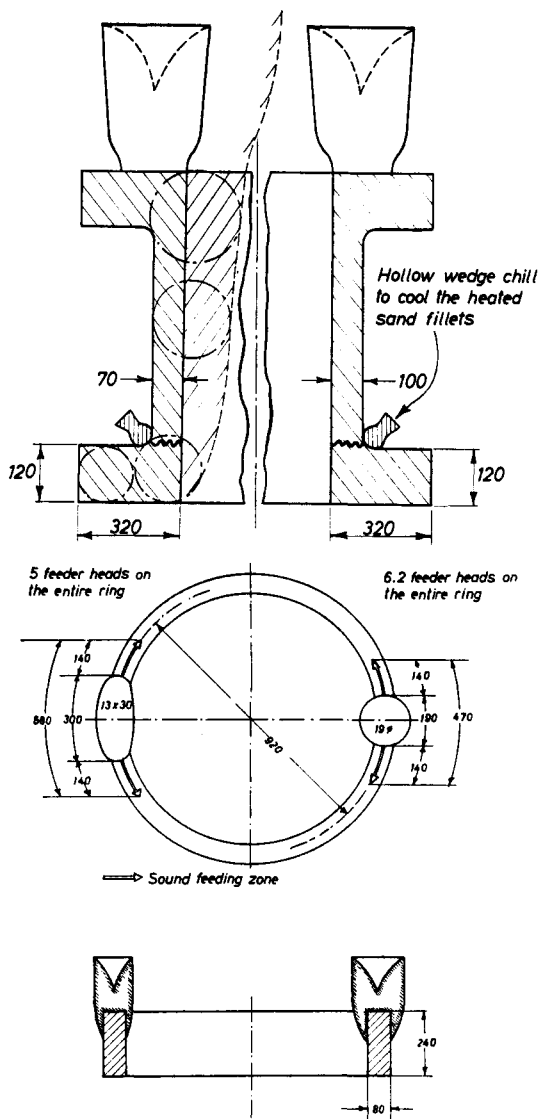


FIG. 127. Wheel rim. Oval feeder heads are better than round ones for long castings, because the sound region supplied by each feeder (zone under the feeder itself and the dependent feeder zone) is lengthened, so that the number of feeders required is less.

6.1. Utilization of Natural End Zones and Shape of the Feeder. General

IMPORTANT FOR PRACTICE

Given direct dimensioning of the feeder heads, the casting under the feeder will always be sound. With elongated castings such as the wheel rim in Fig. 127, oval feeders are to be preferred to round ones, because, although they are not substantially heavier, they extend the feeding influence.

As shown in Figs. 128 and 129, the natural end zones are often not utilized. Here also consideration of the problem can lead to a saving in feeder material.

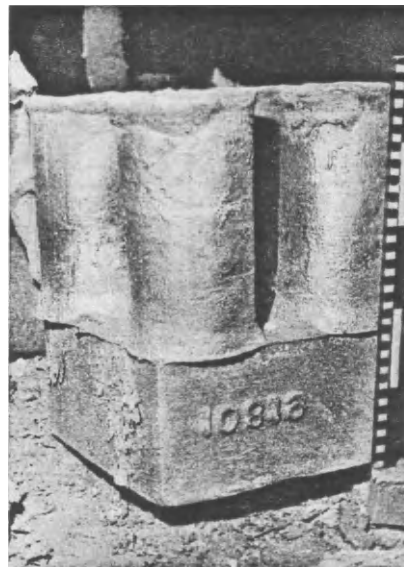


FIG. 128. Non-utilization of natural end zones on a box casting. One central feeder would have been sufficient. In addition, the feeders were unnecessarily tall.

The "classical" method satisfies the need of the practical man and gives a clear picture, even in difficult cases (volume/effective cooling surface) and this leads in general to reliable operation of the method in practice. The shape factor method, on the other hand, must involve extensive additions and corrections, even with the simplest of shapes, the need for which is in no way self-evident.

The calculation of internal and external chills, and of exothermic and insulating materials, as well as breaker cores and heating pads, is also more feasible by the "classical" method. Consequently the author decided to simplify the Chvorinov method, without abandoning the modulus principle, but leaving the shape factor method alone.

CHAPTER 6

INCREASING THE THERMAL GRADIENT IN THE CASTING BY PADDING AND BY THE UTILIZATION OF NATURAL END ZONES

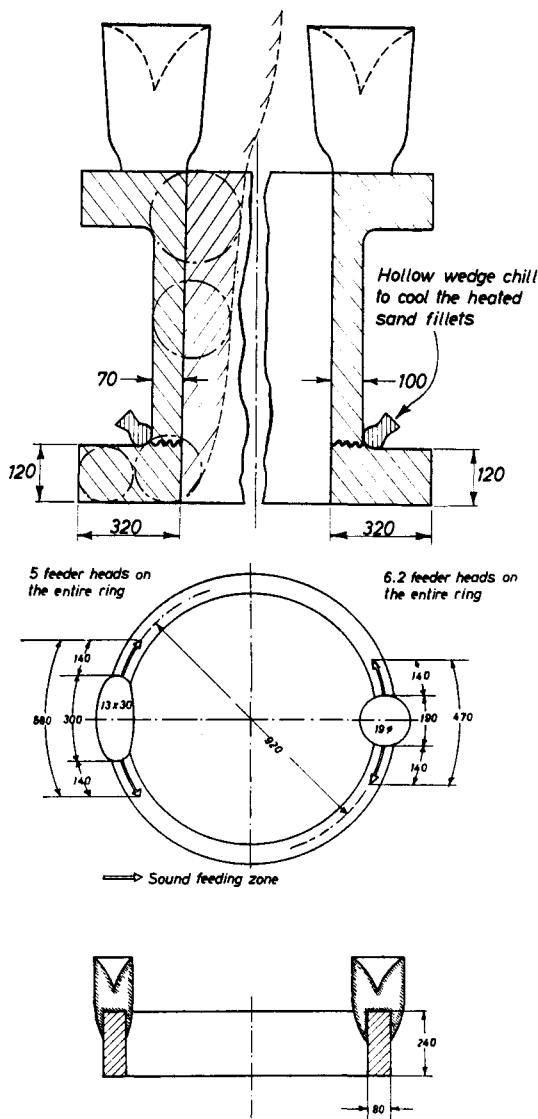


FIG. 127. Wheel rim. Oval feeder heads are better than round ones for long castings, because the sound region supplied by each feeder (zone under the feeder itself and the dependent feeder zone) is lengthened, so that the number of feeders required is less.

6.1. Utilization of Natural End Zones and Shape of the Feeder. General

IMPORTANT FOR PRACTICE

Given direct dimensioning of the feeder heads, the casting under the feeder will always be sound. With elongated castings such as the wheel rim in Fig. 127, oval feeders are to be preferred to round ones, because, although they are not substantially heavier, they extend the feeding influence.

As shown in Figs. 128 and 129, the natural end zones are often not utilized. Here also consideration of the problem can lead to a saving in feeder material.

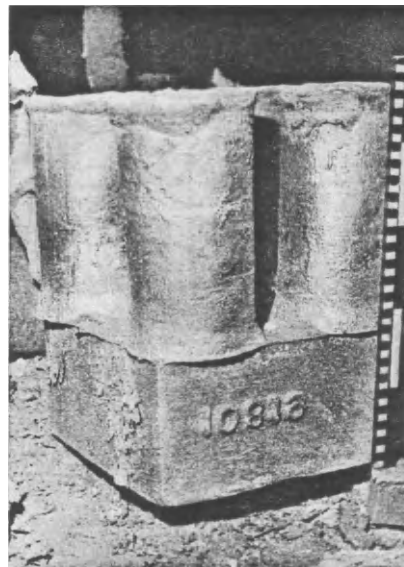


FIG. 128. Non-utilization of natural end zones on a box casting. One central feeder would have been sufficient. In addition, the feeders were unnecessarily tall.

FIG. 129. Non-utilization (top) and the proper utilization (bottom) of the natural end zones of a casting.

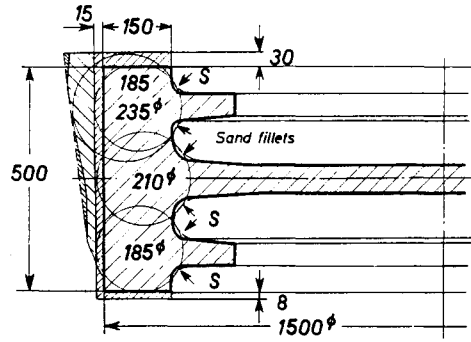
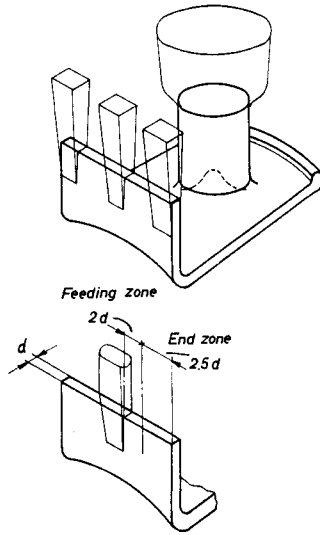


FIG. 131. Padding a gear wheel rim.

The work is accomplished in stages as follows:

1. Draw the rim to the scale 1 : 1 and draw in the machining allowance and the dirt trap.
2. Reinforce the fillet by the amount of the expected sand fillet effect.
3. Circle the intersection so obtained (the circles are tangential to the sand fillets).
4. Take the circles from the bottom upwards. First 185 diam. to the central intersection, 210 diam. from there with a further 210 diam. A new intersection 235 diam. occurs at the top circle 185 diam. due to padding the wall; this is to be carried up to the feeder head.
5. The curve so obtained can be replaced approximately by the straight line which has been drawn.
6. Further padding (as in Fig. 138) is not required here, because of the heavy wall (≈ 200 mm).

6.2. Use of the Heuvers⁽¹⁴⁾ Circle Method for Castings

IMPORTANT FOR PRACTICE

Some use was made of this method in the previous chapter. It implies that the modulus of a cross-section must increase continuously in the direction of the feeder, if freezing is to be prevented. Heuvers was the first to point out the practical method of inscribing a series of circles (spheres, when viewed three-dimensionally) the diameters of which increased in the direction of the

feeder head. A model of the casting is first sketched out as far as possible to the scale of 1 : 1, and the machining and contraction allowances drawn in. Then the circles can be inscribed. Examples are shown in Figs. 130-136.

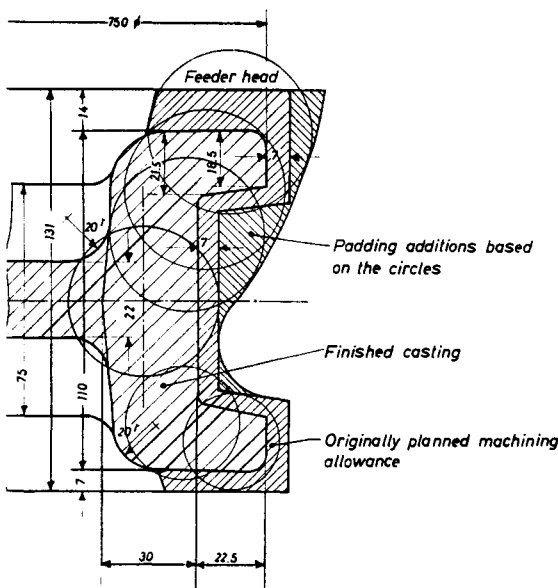


FIG. 130. Marking out a turbine wheel rim in Heuvers circles.

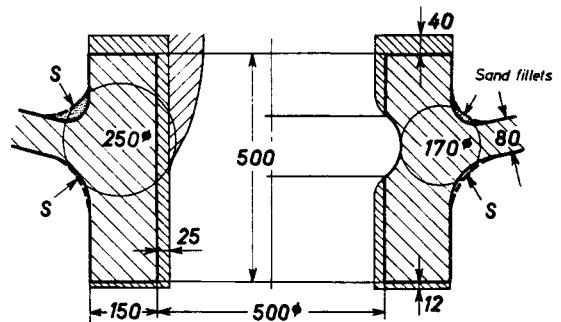


FIG. 132. Padding a wheel hub.

Proceed according to the following scheme:

1. Draw the hub to the scale 1 : 1 and draw the necessary machining allowances and dirt trap.
2. Estimate the sand fillet effect and draw this also. Circle the points of intersection.
3. Left half of drawing: better solution than the one on the left; discuss with the designer whether a recess as shown is permissible. If so, the hub becomes a body with a uniform wall thickness of 170 to 175 mm, and the hub feeder can be made considerably smaller.

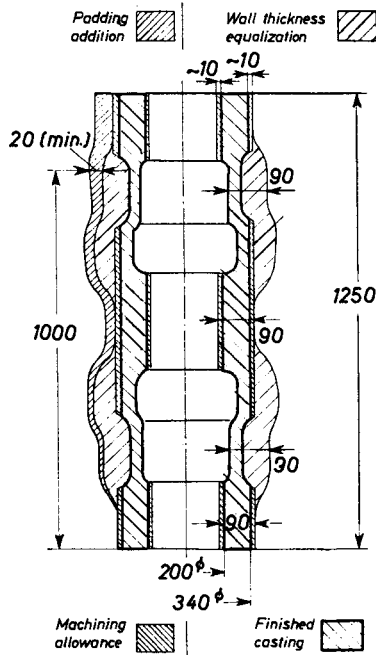


FIG. 133. Padding a hollow shaft.

Proceed in three stages:

1. Draw the casting to a scale of 1 : 1 and outline the machining allowances.
2. Equalize the wall thickness from the bottom upwards (right half of the drawing). In our case a shaped tubular body with $w = 90$ mm is obtained. It is also possible that varying minimum wall thicknesses will occur (for instance 120 mm at the centre of the shaft). The tube would then be continued from this point at 120 mm.
3. Pad the tube, with an equalized wall thickness, on the lines of Fig. 137 and 138 (left side of the drawing).

FIG. 135. Padding a flanged fitting.

Work to the following scheme:

1. Draw the flange to the scale 1 : 1 and add the machining allowances.
2. Estimate the sand fillet effect and circle the intersection (here 70 diam.).
3. Bring the flange (in imagination) to the thickness of the intersection = 70 mm. In this way a body of uniform wall thickness is produced.
4. Insert the centre-line of the flange, and divide it by radial lines into sections of 50 mm around the bend (100 mm in larger castings).
5. On the points so obtained insert the padding allowance in accordance with Fig. 138. In this instance 10 mm is to be added (difference $70 - 60 = 10$ mm, see point 3).
6. Correction of padding allowance: Fig. 138 applies to plates. Bars and rods have much smaller feeding ranges, and must therefore be given heavier padding additions. The correction factor is found from Table 24.
7. In most cases the pad curve so obtained can be replaced approximately by a straight line; it is sufficient to determine the starting and finishing points.
8. Pads of this kind produce radiographically sound castings, so that they are only to be used in the way described when highly-stressed (and suitably priced) castings subject to strict inspection (100% radiographic testing) are to be made.

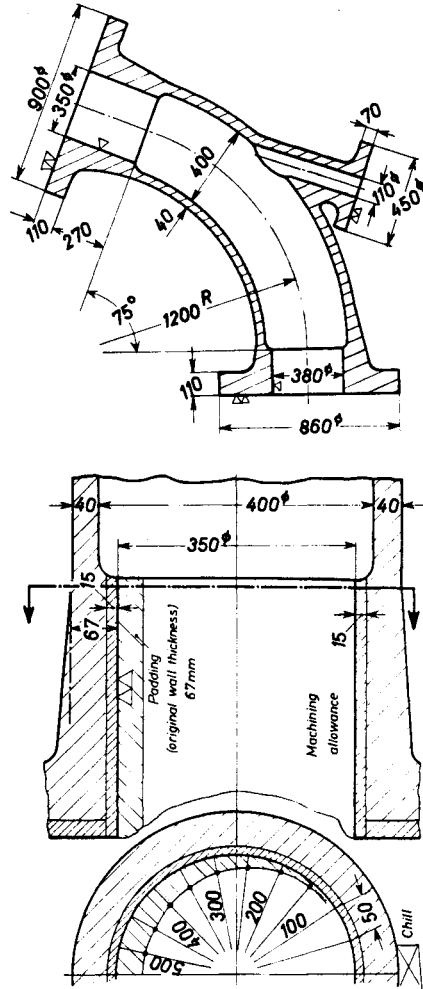
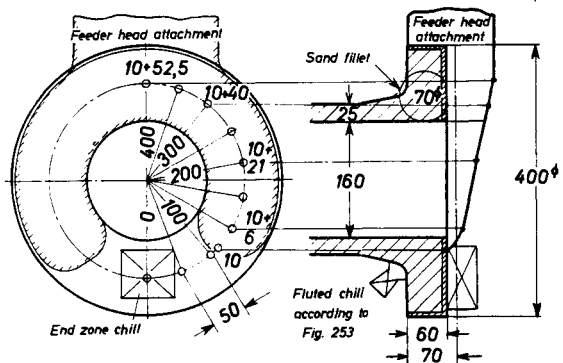


FIG. 134. Padding an elbow.

Work to the following scheme:

1. Draw the sections to be padded to the scale 1 : 1 and draw the necessary machining allowances.
2. Draw radial lines at an interval of 50 mm (around the bend), or 100 mm with larger castings. Plot the pads at each point from Fig. 138. The initial wall thickness is taken as the wall thickness at the weakest point; in the flange 900 diam $w_{min} = 67$ mm.
3. Use the same method with the other machined flanges.



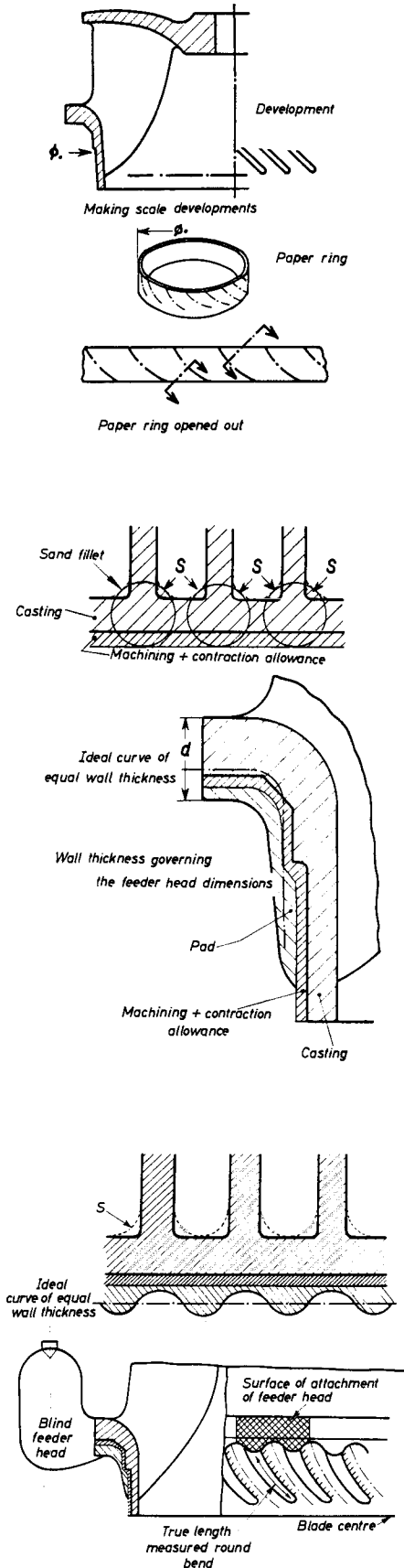


FIG. 136. Padding a Francis turbine wheel. Drawing partly schematic.

The drawing was made partly schematic in order to emphasize the essential points. Such turbine wheels are among the most difficult castings to make, and cannot be produced free from shrinkage cavities unless strict attention is paid to the many junctions and positions where heat will accumulate, especially at the lower flange.

The following procedure is adopted:

1. Make a reduced scale development of the lower flange, preferably by means of a paper ring on which the pattern of the blade can be drawn accurately, and which is then opened out.
2. Draw sections to the scale 1 : 1 at at least three levels, adding the necessary machining allowances and a safety margin to allow for irregular contraction.
3. Estimate the sand fillet and circle three of the blade junctions. Especially at the lower positions, where the blades lie very obliquely and therefore close together, the sand fillet effect is very pronounced and the circle becomes correspondingly large.
4. Establish the ideal curve of equal wall thickness for the three different levels of cross-section, and insert it in the cross-section. This curve—especially in the upper parts of the flange—can in some circumstances lie under the machining allowance. Whether this is to be left or corrected can only be assessed later.
5. Pad the ideal plate so obtained in accordance with Fig. 138. Here the true length (running obliquely towards the blades and measured around the bend) is to be inserted as the wall height.
6. Corrections. The padding calculated according to Fig. 138 applies to top poured castings and unalloyed steel. If bottom pouring is used partly or entirely, the natural thermal gradient of the plates is impaired and must be compensated by increased padding additions (multiply the values from Fig. 138 by 1.25). In the case of highly alloyed steels the values from Fig. 138 must also be multiplied by 1.25 (this is an approximate value only—accurate data can only be obtained for individual cases by casting trial plates from the steel in question). Example:
 (A) If alloy steel is to be top poured, it is only necessary to multiply by 1.25.
 (B) If the alloy steel is to be bottom poured, multiply by $1.25 \times 1.25 = 1.55$.
 (C) If unalloyed or low alloy steel is bottom poured, it is only necessary to multiply by 1.25.
7. If the intersection circles are much larger than the wall of the flange, it is recommended unreservedly that the padding should be built up in accordance with the basic rule of equal wall thickness (cheeks between the blades, a wavelike profile in section). These cheeks can be moulded by means of detachable parts on the pattern. When strickling the flange the shape of the blade must be accurately delineated by a joint strickle board. In setting the cores attention must be paid to the corresponding positions of the padding to the blades.
8. The maximum wall thickness of the wedge so obtained is decisive for the dimensioning of the feeder head:

$$\left(M_{\text{casting}} = \frac{W}{2}; M_F 1.2 \times M_{\text{casting}} \right)$$
- In most cases blind feeders with a large diameter are obtained. The ingate is calculated carefully using the modulus formula, in order to prevent premature freezing or alternatively an additional accumulation of heat.
9. If the wheel, together with the flange, is top poured (Fig. 123) the intersection must still be circled in a similar way.
10. The moulding method described is expensive in itself, but the end result is a satisfactorily sound casting, with low dressing costs and a small risk of scrap.

The problem of the amount by which the diameters of the circles should increase could only be solved “intuitively” at first for unalloyed steels, on the basis of the work by Brinson and Dumas⁽¹⁶⁾ and Stein⁽¹⁸⁾ (Figs. 137 and 138). No values have so far been published for alloy steels.

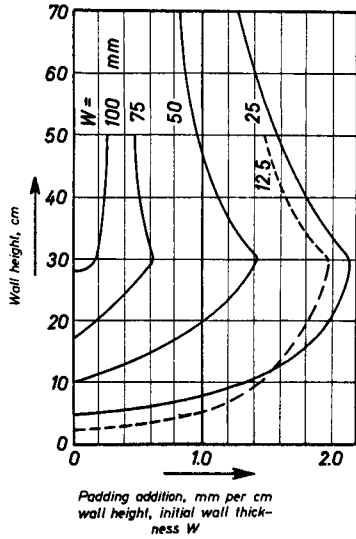


FIG. 137. Padding additions after Brinson-Dumas⁽¹⁵⁾

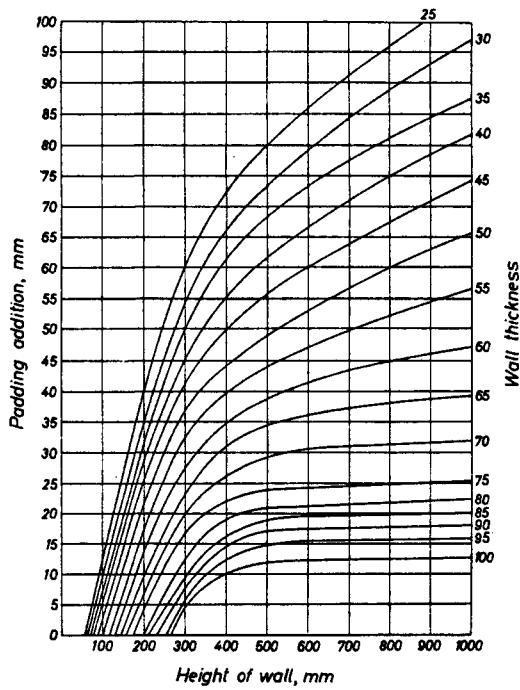


FIG. 138a. Necessary padding additions for steel castings with different wall thicknesses and wall heights⁽¹⁶⁾.

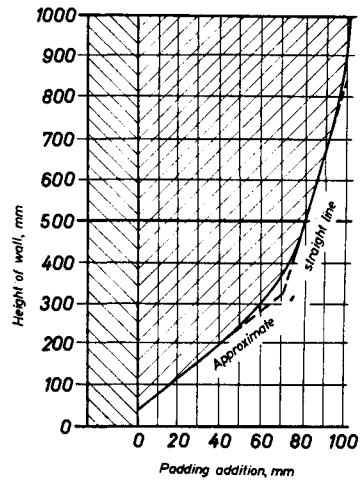


FIG. 138b. Padding a 25 mm thick plate of unalloyed cast steel.

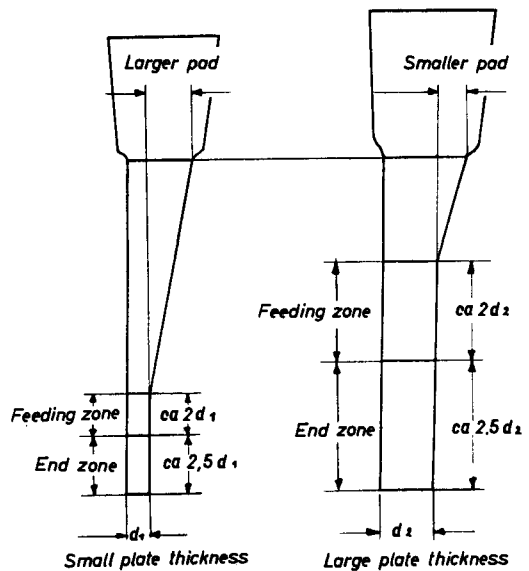


FIG. 139. Effect of plate thickness on the size and point of attachment of the pad.

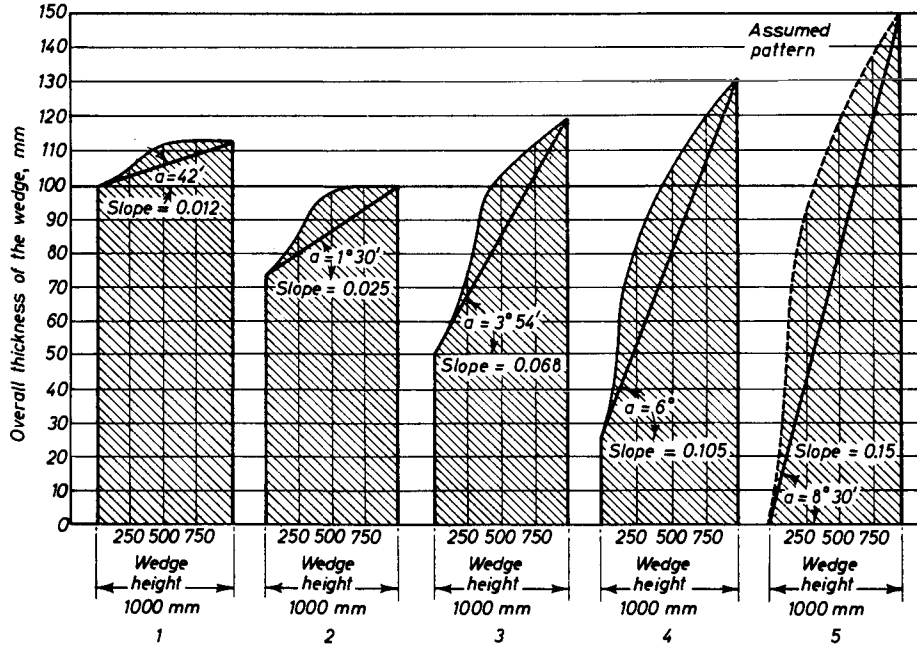


FIG. 140. Different padding additions, wedge angles and wedge slopes as a function of initial wall thickness and wedge height. Scale representation.

Padding requirements are dependent upon the cross-sectional area of the casting wall. For a given depth of casting wall, thin walls required heavier padding than thicker ones (Fig. 139). Finally, we will consider the end zone or the point at which the feeder zone ends. The thicker the plate the longer the end zone, and as the parallel feeder zone provides no padding, this can tend towards zero with thick plates.

According to Fig. 140, the angle of the pad is also a function of the wall height; the straight-line boundary of the pad is therefore really an approximation to a curved profile. When using feeding pads (see Section 6.2.2.), the curvature must be maintained.

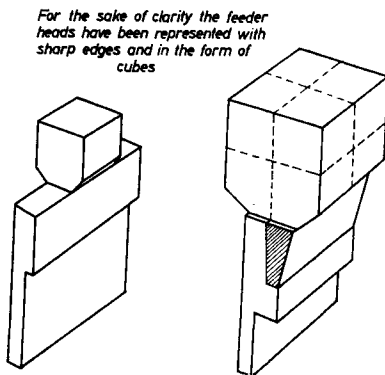


FIG. 141. If the wall thickness is doubled by padding, the volume of the feeder head is increased eight times!

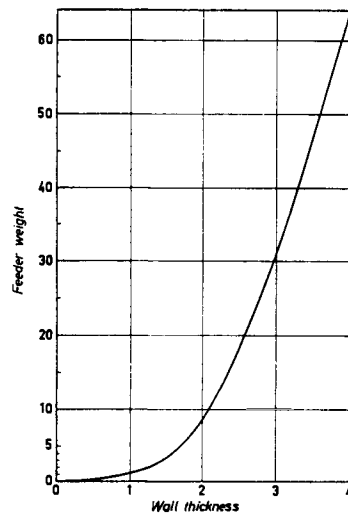


FIG. 142. The feeder weight increases as the cube of the wall thickness.

Pads can be looked upon as corrections to incorrectly designed castings, and they have to be removed again by expensive dressing operations. They also require considerable amounts of steel. By thickening the cross-section one increases the modulus, and therefore the size of the feeder, which increases as the cube of the plate thickness (Figs. 141 and 142). The expensive padding of whole regions of the casting cannot always be avoided

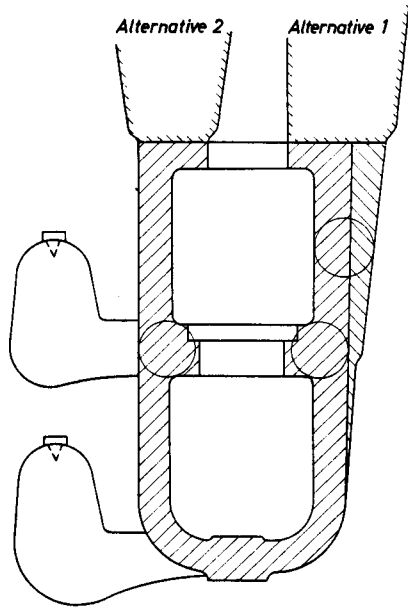


FIG. 143. In order to avoid padding as shown in the first alternative, additional feeders can occasionally be added. The placing of the feeders is usually expensive, and difficult from the point of view of moulding technique.

(Fig. 143), so further methods of ensuring the soundness of the mass in lower sections of the casting have been developed.

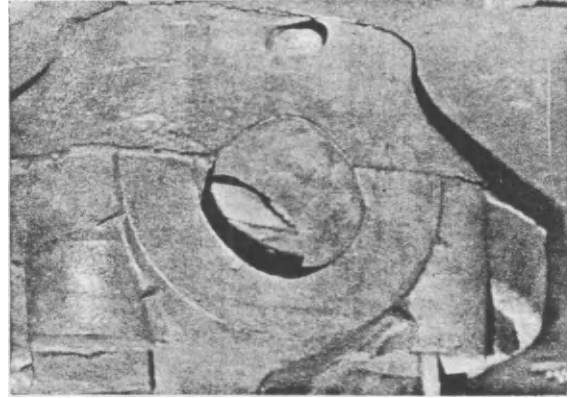
6.2.1. USE OF THE CIRCLE METHOD FOR EXTENDING FEEDER ZONES. FEEDING OF BARS AND BOSSES

The feeding zone of the head can be extended and the number of feeders reduced by padding as shown in Fig. 144. The maximum permissible length of such a pad may be determined as a modulus:

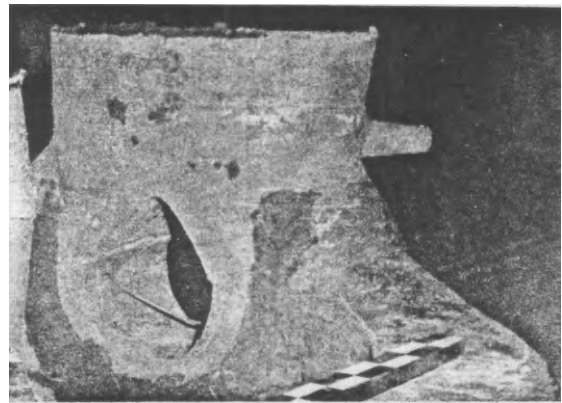
Plate thickness 50 mm, modulus 2.5 cm, feeder head modulus $2.5 \times 1.2 = 3$ cm. This modulus must not be exceeded at the point of attachment of the feeder, even by pads, otherwise a larger feeder would be necessary. Padding forms a special form of ingate (for calculation, see Chapter 4), so that the pad modulus must lie between that of the casting and feeder. According to Fig. 145, the modulus of the feeder will be attained with a length of pad (= wedge length) which corresponds to:

- 2.8 times the plate thickness
- or 5.6 times the plate modulus
- or 4.7 times (5 times) the feeder modulus.

FIG. 144c. Shoulders connect the centres of mass of a pump housing. The shoulders also act as an additional, easily removable dirt trap.



a



b

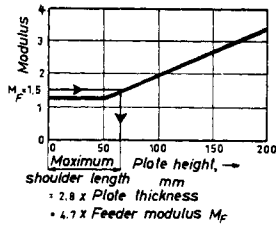
FIGS. 144a and b. With shoulders over the bearing section of a housing a single feeder head is sufficient. In Fig. 144a the feeder is covered with exothermic material. Note the "roof-shaped" structure of the core under the feeder.

(Courtesy Sulzer Bros.)



Model case of a 25 mm plate

Plate height	Addition mm	Modulus cm ²
to 50	0	1.25
75	6	1.55
100	12.5	1.9
150	28	2.6
200	40	3.3



Model case of a 50 mm plate

Plate height	Addition mm	Modulus cm ²
to 100	0	2.5
150	12	3.1
200	26	3.8
250	30	4.0
300	37	4.4

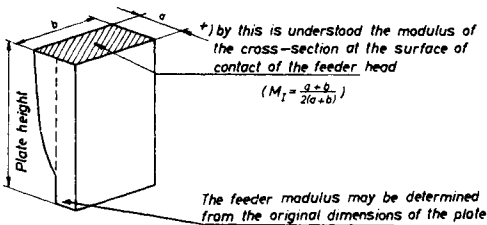
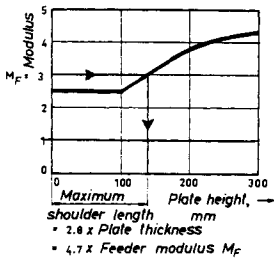


FIG. 145. Determination of the most suitable shoulder feed conditions, based on the pad curves after Stein.

These ratios also apply approximately to plates more than 50 mm thick. A maximum pad length is therefore associated with the modulus of each feeder. All pad dimensions may therefore be referred to the feeder modulus (Fig. 146). To simplify the calculation use stand-

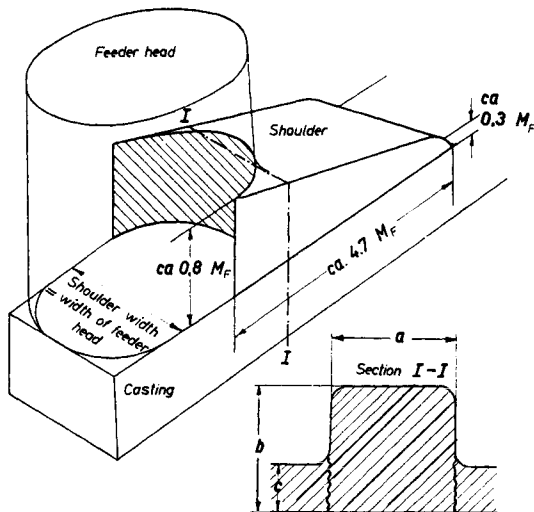


FIG. 146. Development and dimensions of the shoulder modulus as a function of the feeder modulus M_F .

In case of doubt: calculations of the shoulder modulus according to the method used for determining the ingate modulus, i.e. $M_I = \frac{a \cdot b}{2(a+b-c)} = M_F$ is sufficient in most cases to dimension the shoulder from the above data.

ard tables. When padding is to be employed frequently, loose wooden patterns are useful.

The pad must be designed in conformity with the modulus curve (see later), i.e. it must not run out at a shallow angle as in Fig. 147, but must be sharply defined. Examples are given in Figs. 148 and 149.

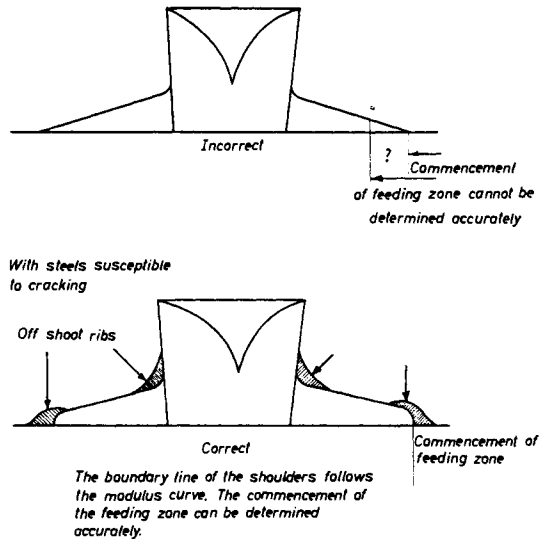


FIG. 147. Development of the end piece of the shoulder.

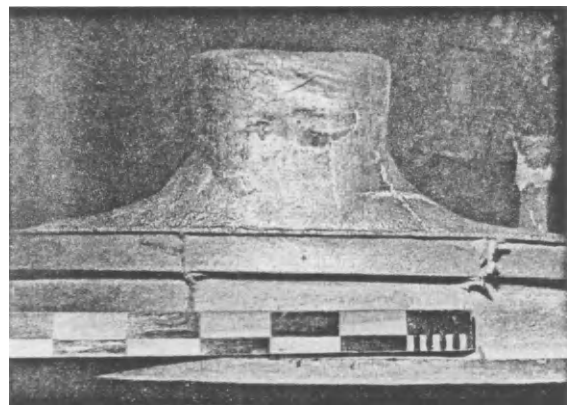


FIG. 148. Incorrect runout of the shoulder.



FIG. 149. Correct runout of the shoulder.

Figs. 150–152. Alternative methods of feeding bosses.

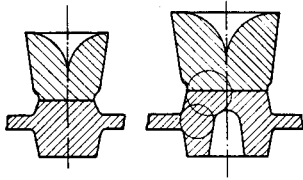


FIG. 150. Cylindrical feeder head on bosses, with or without small core.

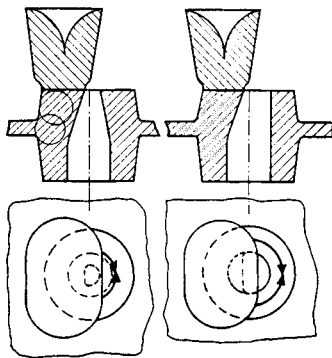


FIG. 151a. "Half feeder" with pointed core.

FIG. 151b. "Half feeder" with check on one side of the core.

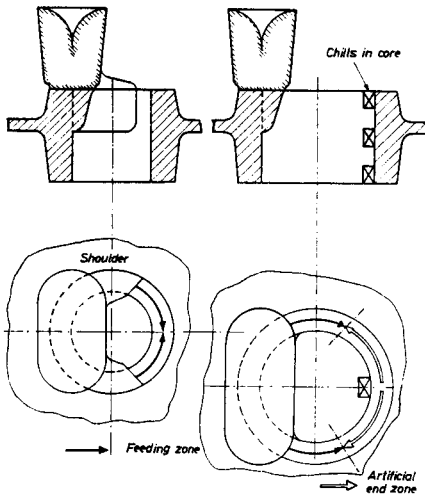


FIG. 152a. The feeding range of the feeder head can be enlarged by increasing the boss diameter.

FIG. 152b. With still larger boss diameters, or if further economies in the shoulder intersections are desired, one or more chills on the opposite side from the feeder head can be of assistance. For further details see Chapter 8.

Pads are also used to feed bosses. Figures 150–152 indicate various possibilities. In many cases "half heads" are used. It is sufficient for the junction of the feeder with the casting to make the point of intersection at a position having a cheek only on one side; when the boss is increased further, the feeding range of the one-sided "economy feeder" can be extended by means of padding or chills (see Chapter 8).

The economic limits of "full" and "half" feeder heads are indicated in Fig. 153 by means of the simple case of

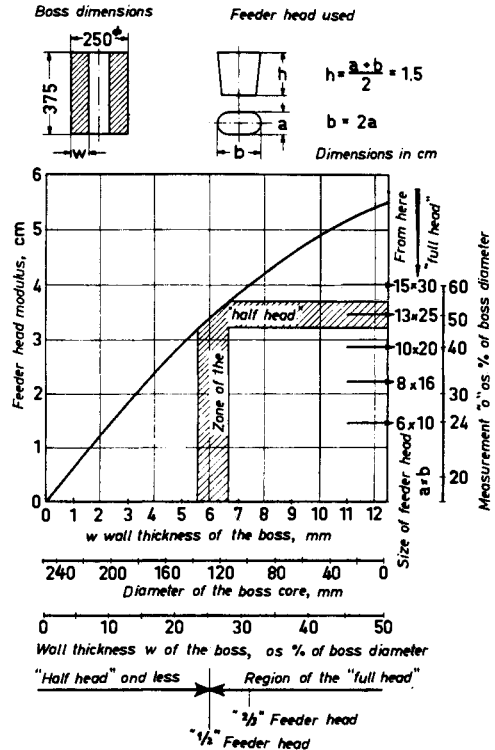
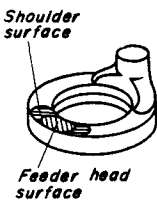
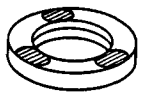


FIG. 153. Limits of applications of "full" and "half" boss feeder heads.

a boss having increasing wall thickness w . As soon as the core diameter reaches 40–50 per cent of the boss diameter, "half" heads can be adopted. A separate feeder calculation is then no longer necessary, as it would not produce a significantly more accurate result.

A casting with padding should not in the long run require more fettling than a similar casting without padding. It must not be forgotten in this connection that where there is no padding to remove there are probably some additional feeders. Limiting cases for the utilization of "padding systems" are often encountered and these should be decided only with the help of objective time studies. Even when burning off the feeders manually, the overall times are somewhat less with padded castings (Table 23); with mechanical flame cutting the padding method is often preferred in the fettling shop.

TABLE 23. INVESTIGATION OF THE ECONOMIC EFFICIENCY OF THE SHOULDER METHOD, CARRIED OUT IN THE DRESSING SHOP ON THE BASIS OF TIME STUDIES. THE CASTINGS WERE BURNT OFF UNDER EXACTLY THE SAME CONDITIONS

Gear rim blank with 2 risers (with shoulders)		
Time, min		
	Casting brought up by crane, setting up burner	1.60
	Burning 1st riser	3.70
	Setting up 2nd riser	0.15
	Burning 2nd riser	3.70
	2nd riser, correcting burned section	1.38
	Setting up ingate	0.28
	Burning ingate	1.60
	Casting removed by crane	0.93
	Risers and runners removed by crane	1.75
	Total	15.09 min
	Oxygen consumption (weighed)	3.6 kg
	Gear rim blank with 3 risers (without shoulders)	
	Time, min	
		Casting brought up by crane, setting up burner
Burning 1st riser		3.55
Setting up 2nd riser		0.20
Burning 2nd riser		3.20
Setting up 3rd riser		0.22
Burning 3rd riser		3.28
3rd riser, correcting burned section		0.58
Setting up ingate		0.38
Burning ingate		1.32
Casting removed by crane		0.95
Risers and runners removed by crane		2.05
Total		17.60 min
Oxygen consumption (weighed)		4.9 kg

section in question. Ingate calculation is recommended (cf. Fig. 146).

If the individual points of intersection are too far apart, a further hot junction is formed below the feeder due to the padding wedge; this can be eliminated by exothermic powders on the feeder head or placing chills underneath (Fig. 155). However, there is an economic limit to these methods.

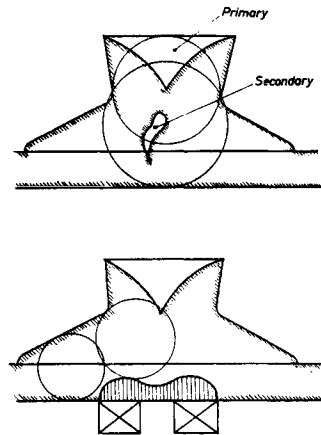


FIG. 155. With shoulders which are too steep secondary shrinkage cavities can form due to an increase in the cross-section fed. The widening of this cross-section can be prevented by placing chills underneath.

6.2.2. APPLICATION OF THE CIRCLE METHOD TO JUNCTIONS IN A COMPLEX CASTING

This method is illustrated in Fig. 154. The heaviest cross-section dictates the size of the feeder. Here the pad modulus must be 1.1 times the modulus of the cross-

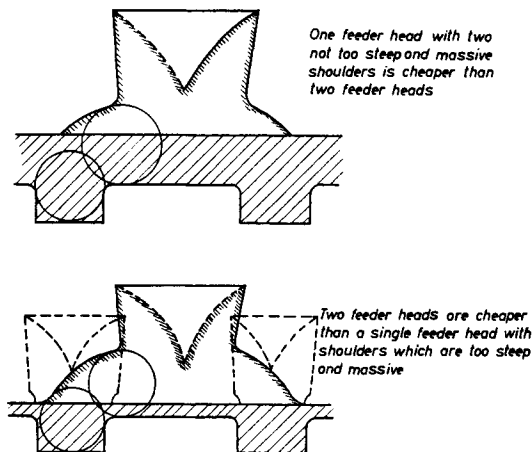


FIG. 154. Advantages and limitations of padding.

Examples are given in Figs. 156-162.

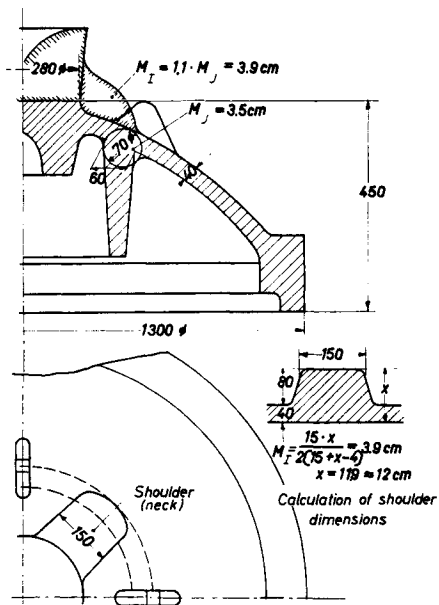
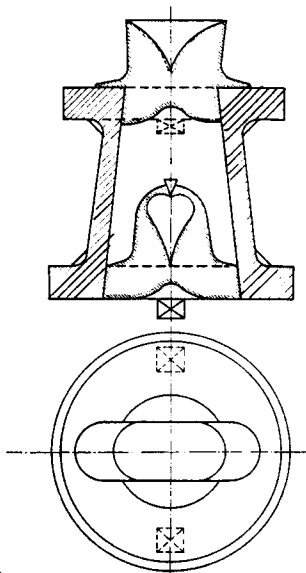
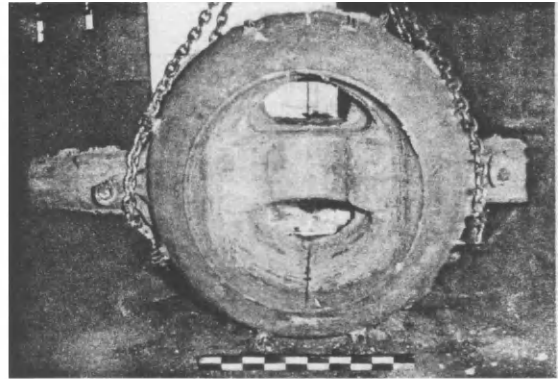


FIG. 156. Development of shoulder and calculation for a cover.

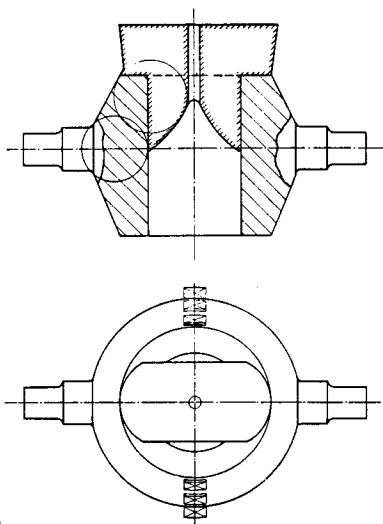
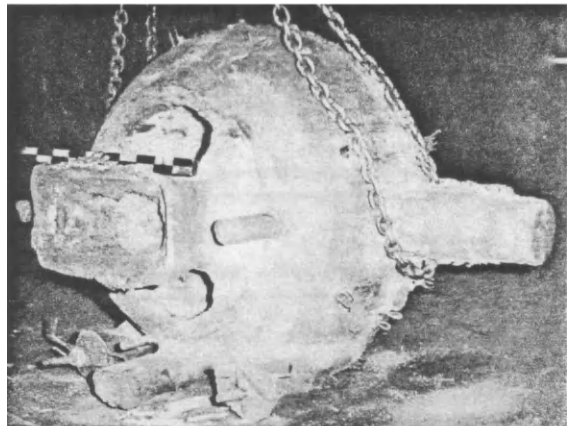


157a

FIG. 157a and b. Flanges and larger bosses can often be dealt with by a transversely positioned feeder head at two positions on opposite sides. Considerable amounts of circulating scrap in the foundry can be saved in this way, especially with larger castings. Artificial end zones are formed between the ingates by the use of chills (see Chapter 8).



157b



158a

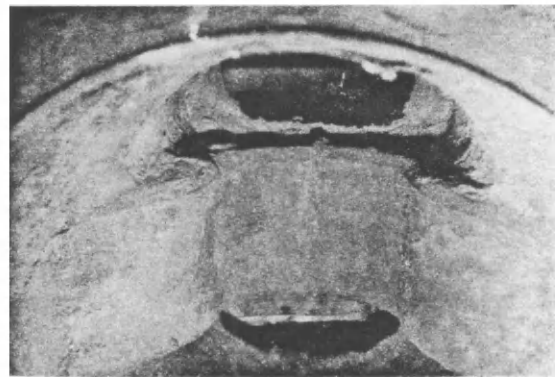


FIG. 158b. Plug of a globe valve, radiographically sound. The whole of the casting, even the two intersections of the journals, were fed from a single feeder head by means of padding.
(Courtesy Sulzer Bros.)

FIGS. 158a. Both journals fed from a single feeder. Artificial end zones formed with chills (see Chapter 8).



FIG. 159a. The rim section of a brake drum was fed through shoulders from the boss feeder head.

c



FIGS. 159b and c. Brake drums. b. With two rim and one boss feeder. c. Rim and boss fed by a single side feeder. An artificial end zone produced at the rim (see Chapter 8).

b

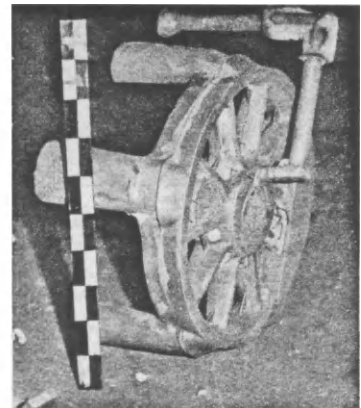
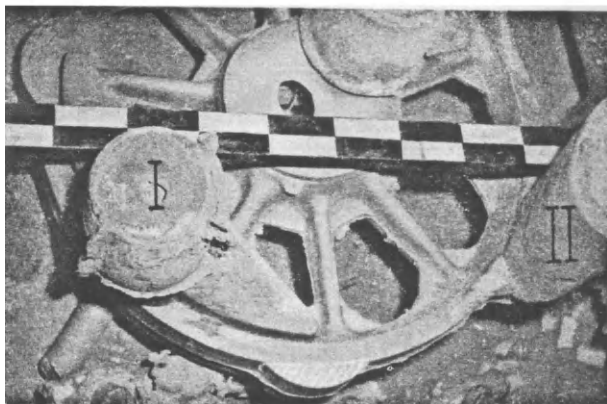


FIG. 160. Wheel centre of a narrow-gauge locomotive. Feeder head I feeds the counterweight, which in turn feeds the intersection of the adjacent spoke. Feeder head II is connected to each of two spoke intersections by means of shoulders.

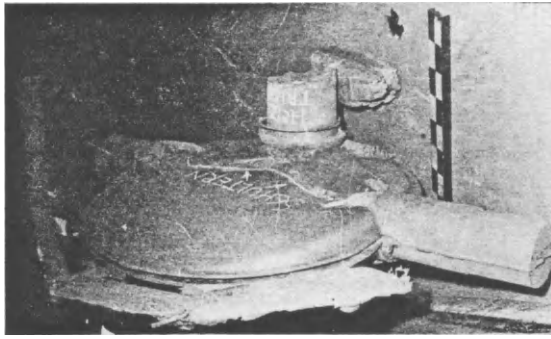


FIG. 161. Cover of rotary valve. By the use of the shoulders the central (exothermic) feeder head supplies not only the actual cover plate, but also the intersections of the two journals. The casting was radiographically sound.
(Courtesy Sulzer Bros.)

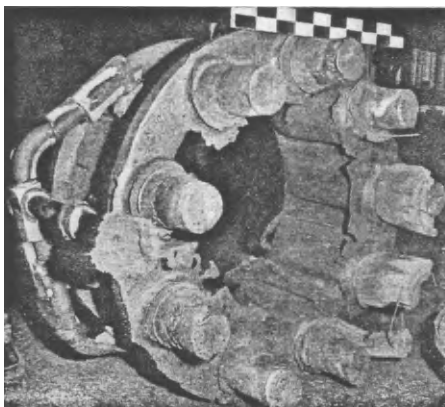
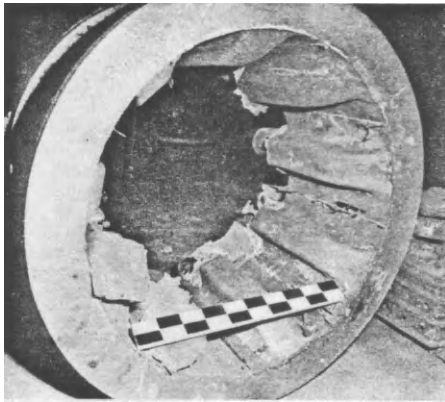


FIG. 162. Extension tube fed by feeder heads with exothermic sleeves. Lower flange fed by means of shoulders to give a sound casting.
(Courtesy Sulzer Bros.)

The padding method—whether it is used to extend the feeding range or to connect separated intersections—is on the whole one of the most important applications of the circle method, and occasionally makes possible a considerably increased yield.

6.3. Calculation of the Modulus Curve

(The other sections can still be understood if this part is omitted.)

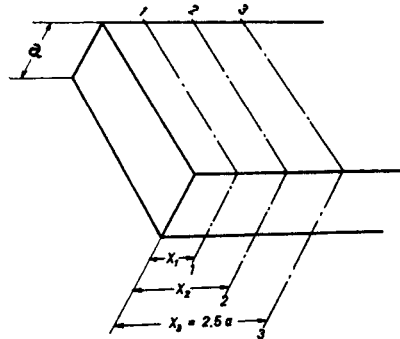


FIG. 163a. Breakdown of the end section of a plate into zones.

If the end section of a large plate is sectioned as shown in Fig. 163 a along x_1, x_2 , etc., the modulus of each slice so formed is:

$$M = \frac{ax}{a + 2x} \tag{36}$$

While the modulus of semi-infinite plates is equal to half the plate thickness, the plate end zone behaves as a semi-infinite stepped wedge with very small steps; this represents the “simulation body”.

For $x = 0; M = 0$
 $x = 2.5a; M = 0.416a$ (uncorrected)

Below an end zone length of $2.5a$, however, the cooling influence of the face is practically nil, so that below $x = 2.5a, M = 0.5a$ (corrected).

The difference was divided up uniformly (whether this is physically strictly correct remains open to question), and the equation of the modulus curve (Fig. 163 b) is written:

$$M = \frac{1.2ax}{a + 2x} \tag{37}$$

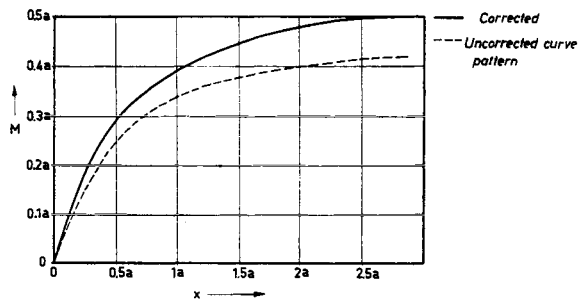


FIG. 163b. Path of the modulus curve in the end zone of parallel plates.

The angle of the advancing solidification fronts at a point $P(x)$ is given by the first derivative:

$$\tan \alpha = M^1 = \frac{a^2}{(a + 2x)^2} \quad (38)$$

for

$$x \rightarrow 0, \quad \tan \alpha \frac{a^2}{a^2} = 1, \quad \text{and} \quad \alpha = 45^\circ \quad (39)$$

for

$$x \rightarrow 2.5, \quad \tan \alpha 0.0278 \quad \text{and} \quad \alpha = 1^\circ 36' \quad (40)$$

Every transition between these two values can be imagined, so that we cannot speak of a constant "pad angle".

If the wedge pads according to Brinson and Dumas⁽¹⁵⁾ or Stein⁽¹⁶⁾ are drawn to scale for various wedge heights, similar curved boundaries are obtained, even although straight lines are a sufficiently good approximation in practice (cf. Fig. 140).

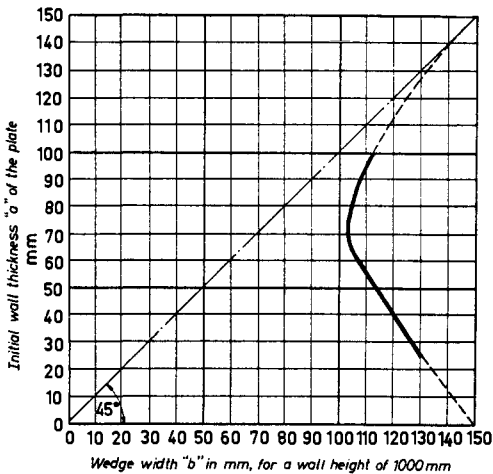
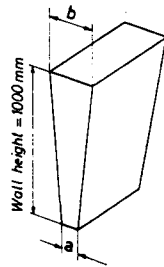


FIG. 164a. Initial and final wall thicknesses of wedges solidifying as sound castings at a wedge height of 1000 mm.

Figure 164a illustrates the influence of plate thickness. The wedge pad tends towards zero with increasing wall thickness, so that the upper branch of the curve tends towards the limit of a 45° straight line. The lower branch of the curve is practically a straight line, and can be extrapolated with a high degree of probability. With an initial wall thickness of zero (taper wedge) the wedge thickness is 150 mm ($\alpha = 8^\circ 30'$) at a height of 1000 mm. Here also the wedge will presumably be bounded by a curve; this also seems probable from the superimposed wedge pads drawn in Fig. 164b.

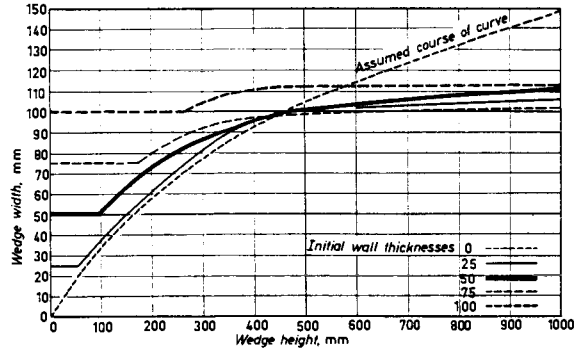


FIG. 164b. Wedge breadth and height on padded cast steel plate.

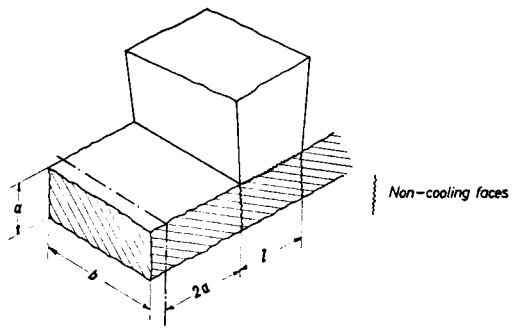


FIG. 165. Breakdown of the feeder zone of a plate into sections.

If similar considerations are applied to the feeder zone (Fig. 165), the following apply for semi-infinite plates for the section below the feeder:

$$\begin{aligned} \text{Volume } V &= a \cdot b \cdot 1 \\ \text{Cooling surface } A &= b \cdot 1 \\ \text{Modulus } M_3 &= V/A = a \end{aligned} \quad (41)$$

The modulus at the end of the feeder zone is $M = a/2$, hence the modulus also increases by $a/2$, and the slope of the modulus curve (assumed in the first place to be a straight line) is:

$$\frac{0.5 a}{2a} = 0.25, \quad \text{and} \quad \alpha = 13^\circ \quad (b)$$

As semi-infinite plates do not actually exist, M_3 is somewhat less than a ; α is also somewhat less, and is probably in the region of $\alpha = 12^\circ$, thus agreeing fairly well with the value for the end section.

Both values, especially that derived from practice for the end section, are about twice as high as the value of $\alpha = 6^\circ$ given by Namur⁽¹⁷⁾. Experiments have also shown that the Namur value is too small, and consequently important influencing factors do not appear to have been allowed for in his calculation.

Presumably the actual size of the pad, or the angle, is governed by hydraulic considerations, as laminar capillary flow exists between the crystal interstices, bringing the feed metal to the spot. The size of these interstices is influenced by the width of the solidification band.

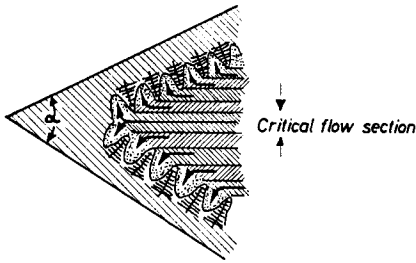


FIG. 166. Flow conditions during the solidification of a keel block. This diagram presumably represents the true conditions at the completion of solidification (in contrast to the views of a number of scientists).

The metal must flow between two crystal peaks, as shown in Fig. 166; this represents a constriction of the cross-sectional area of flow. The amount of liquid which penetrates is determined by the viscosity of the metal just below the liquidus temperature, but no suitable measurements exist, so that it is not possible at present to formulate a flow equation.

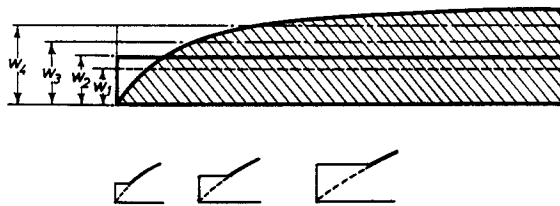
6.4. Further Development and Simplification in Practice of the Methods of Heuvers⁽¹⁴⁾ and Stein⁽¹⁶⁾

If the Stein curves are drawn to scale and superimposed, the surprisingly similar curve paths permit the construction of a characteristic curve (Fig. 164a) which is valid to a close approximation for all initial wall strengths of cast steel plates up to 100 mm.

The formula of the characteristic curve for plates is reproduced in Table 24. Bars, which according to Cech⁽⁴⁾ exhibit much less favourable, i.e. shorter, feeding ranges, must be padded with correspondingly steeper wedge angles. The padding curves, in accordance with the author's experience, are given in Table 24. It is possible to work safely to these values, but they can still be subject to slight corrections if very comprehensive, systematically classified works observations are available.

The characteristic curves can be used to make suitable curved scales or templates of plexiglass (Fig. 167), which simplify greatly both in work preparation and in pattern making the correct dimensioning of pads (Fig. 168) and even with curved sections they are easy to manipulate by rolling on (Fig. 169).

TABLE 24. ONE AND THE SAME STANDARD CURVE FORM CAN BE USED FOR VERY DIFFERENT INITIAL WALL THICKNESSES ψ . IT IS ONLY NECESSARY TO DISPLACE THE POINT OF APPLICATION



Approximate formula (inches)	Curve	Approximate formula (cm)	Applicable to
$d_{(in.)} = 1.072 \sqrt{b_{(in.)}}$	1	$d = 1.7 \sqrt{b_{(cm)}}$	unalloyed plates, and bars with a side ratio from 1 : 4
$d_{(in.)} = 1.351 \sqrt{b_{(in.)}}$	2	$d = 2.14 \sqrt{b_{(cm)}}$	unalloyed bars 1 : 3, high alloy plates and high alloy bars from 1 : 4 with top casting
$d_{(in.)} = 1.605 \sqrt{b_{(in.)}}$	3	$d = 2.54 \sqrt{b_{(cm)}}$	unalloyed bars 1 : 2, high alloy plates and high alloy bars from 1 : 4 with bottom casting
$d_{(in.)} = 1.742 \sqrt{b_{(in.)}}$	4	$d = 2.76 \sqrt{b_{(cm)}}$	unalloyed bars 1 : 1.5, high alloy bars 1 : 3 with bottom casting

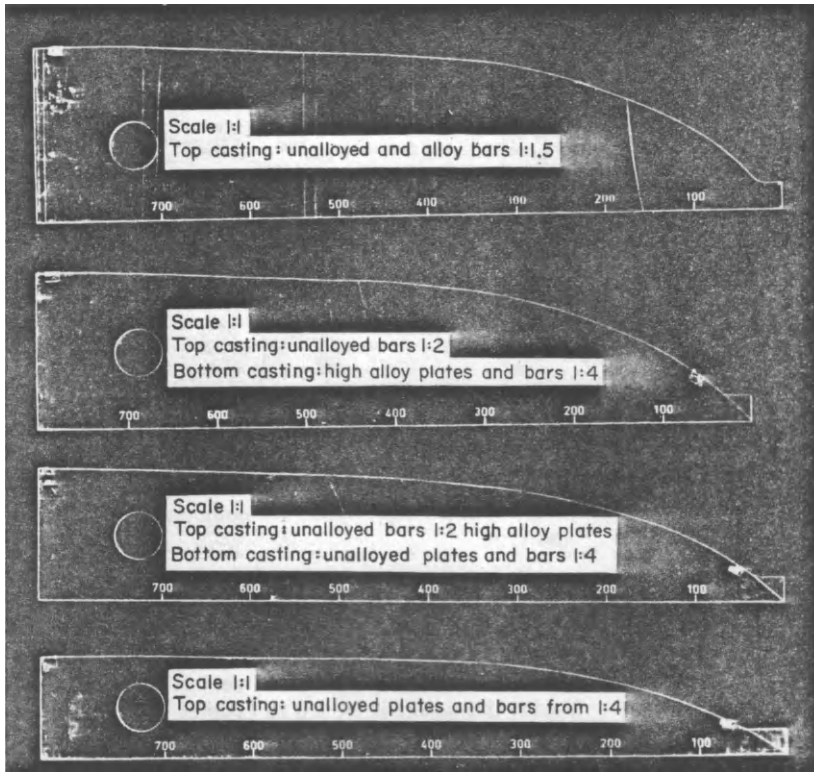


FIG. 167. Curved plexiglass scales for drawing pads (by courtesy of Sulzer Bros. Ltd., Winterthur, Switzerland).

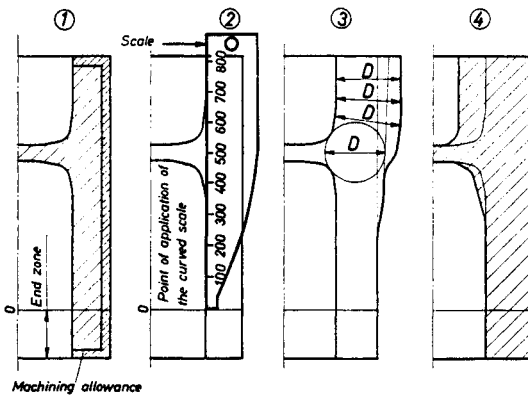


FIG. 168. Padding a wheel rim using a curved scale.

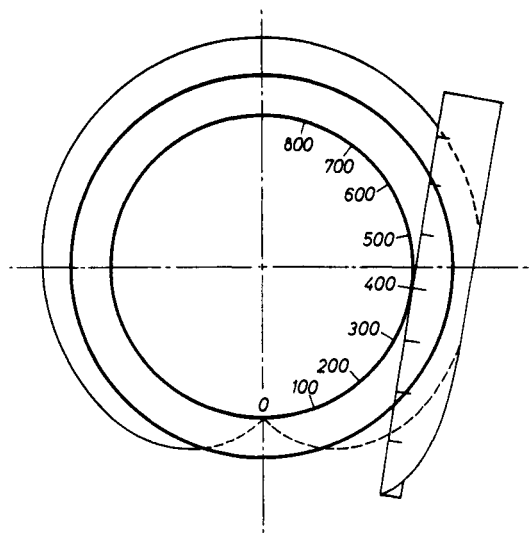


FIG. 169. Padding a tubular casting by rolling.

6.5. Casting Sound Tubes

The segregation zone in tubular castings is always displaced inwards, due to the smaller heat-conducting internal surface. The position of this segregation zone can be described mathematically according to several authors; of these the formula after Stein and Bohlen⁽⁴²⁾ gives good results both for light and heavy wall thicknesses (Fig. 170), i.e.:

$$x = d + W \frac{d}{D} \tag{42}$$

where

x is the diameter of the segregation zone
 d is the internal diameter of the tube,
 D its external diameter and W its wall thickness.

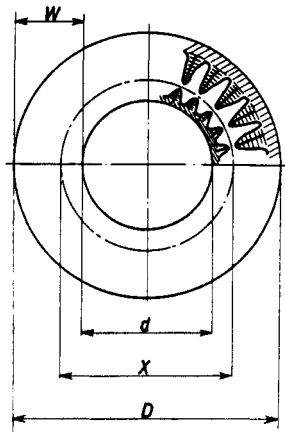


FIG. 170.

If the quantity n is substituted, such that

$$n = \frac{x}{d} \text{ or} \tag{43 a}$$

$$n = \frac{x}{D} \tag{43 b}$$

the following equations are obtained by transposing:

$$\log W = \log d + \log \left(\frac{n - 1}{3 - 2n} \right) \tag{44}$$

$$\text{and } \log W = \log \frac{D}{4} + \log (\sqrt{9 - 8n} - 1) \tag{45}$$

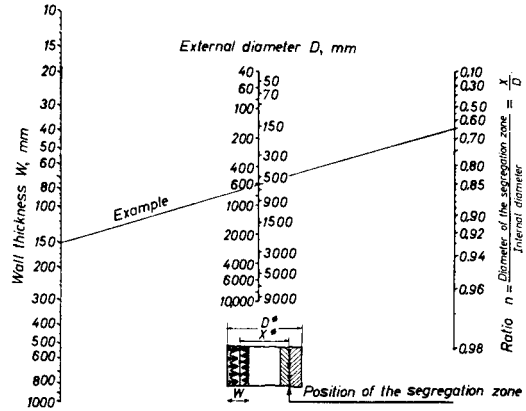
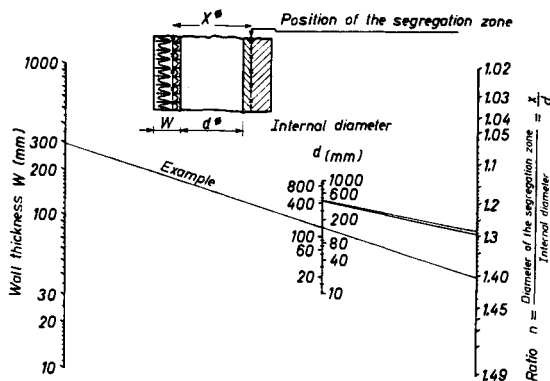


FIG. 172. Valid only when the outer mould and the core consist of the same moulding material (for example, quartz sand).

which can be represented as nomograms (Figs. 171 and 172).

These equations and nomograms are valid only when the outer mould and the core are made from the same moulding material. On the other hand if the outer mould is made, for example, of dry quartz sand and the core of zircon sand, the segregation zone is displaced as a result; this aspect is treated in Chapter 10, Section 4.

The practical importance of these nomograms, which are very simple to use and require no mathematical knowledge, may be illustrated by the following examples:

EXAMPLE 1

The axle journal for an electric locomotive, as in Fig. 173, is to be made radiographically sound. Adjacent

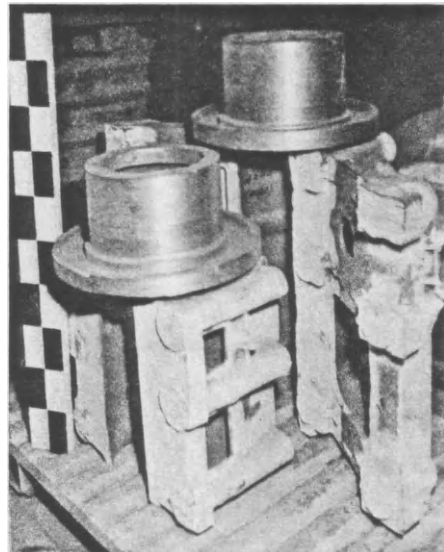


FIG. 173. Axle journal for electric locomotive. (Courtesy Sulzer Bros.)

FIG. 171. Valid only when the outer mould and the core consist of the same mould material (for example quartz sand).

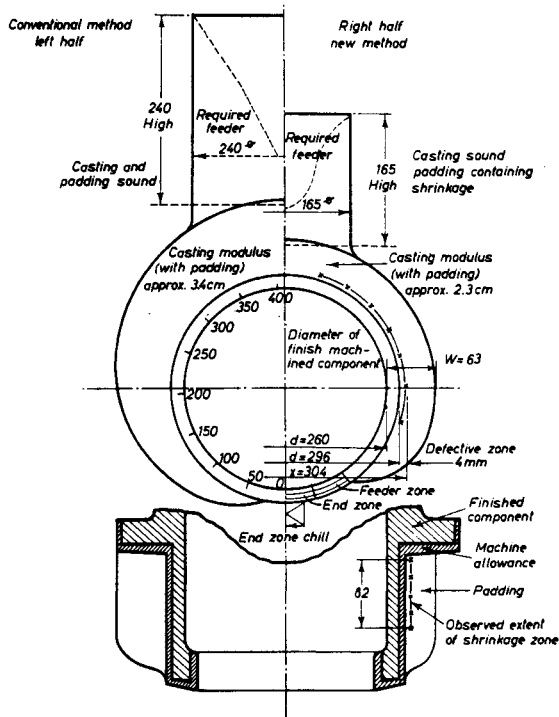


FIG. 174. Drawing of the most important cross-sections of the axle journal of an electric locomotive.

to this, according to Fig. 174 (left half) the tubular section is to be padded in accordance with the Stein curves or the curved scale. Both the actual casting and the padding would then solidify without shrinkage cavities. However, it is not necessary for the metal in the padding to be sound. According to the right half of Fig. 174 the internal diameter of the tube is $d = 296$ mm, i.e. the diameter of the casting ready for delivery, and which must be free from porosity. This is enclosed by a defective zone which is estimated to be at a distance of about 8 mm from the segregation centre X , so that the segregation zone $x \approx 304$ mm.

The ratio $x/d = 1.17$, giving a wall thickness of $w = 63$ mm from Fig. 172 (the control solution of equation (42) leads to the same result).

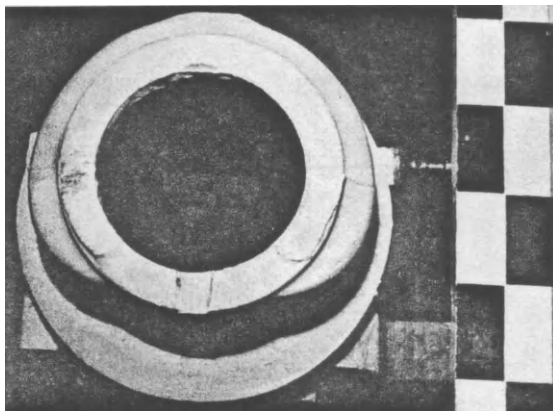


FIG. 175a

The observed zone of the centre-line shrinkage cavity in a tube produced in this way is limited by the cooling action of the end faces, and runs out into the feeder head at the top. The tube casting itself remains outside the segregation zone. The feeder head can similarly be kept much smaller by this method (Fig. 175).

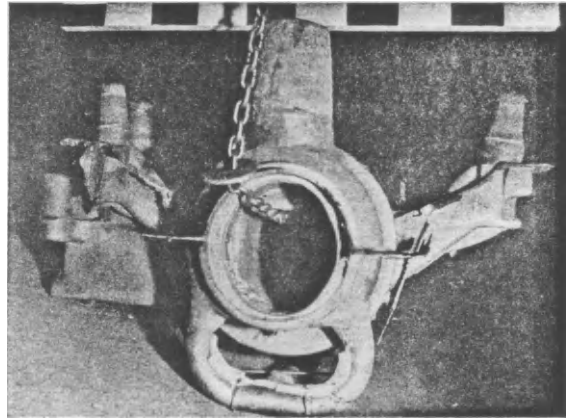


FIG. 175b

FIGS. 175a and b. Axle journal of an electric locomotive in the as-cast condition. Tubular component cast sound by means of special padding.

EXAMPLE 2

As shown in Fig. 176, all segregation zones formed by the usual inside padding are removed during final machining. Figure 177 shows the feeding relationships

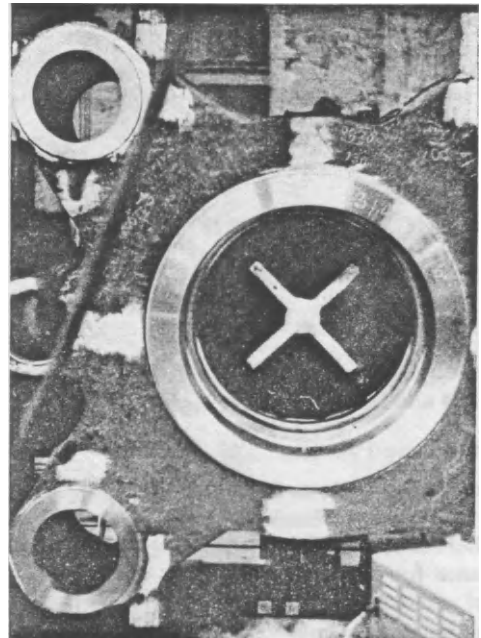


FIG. 176a

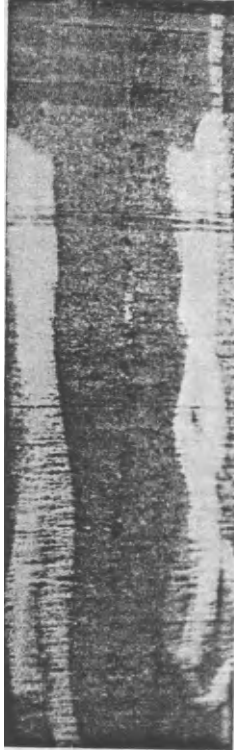


FIG. 176b



FIG. 176c

Figs. 176a-c. During the final machining of this press cylinder the segregation zone was cut.

corresponding to Fig. 174; only the nomogram of Fig. 171 (outside diameter as the initial dimension) was utilized.

With padding, irrespective of the method used, the position of the segregation zone can be displaced by hot material, i.e. by ingates, which can lead to foundry scrap or repair work, and this must be taken carefully into account.

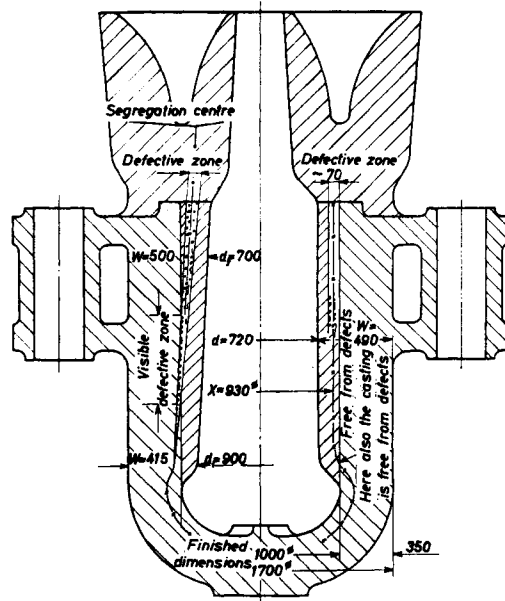


FIG. 177.

CHAPTER 7

INCREASING THE THERMAL GRADIENT BY MEANS OF MOULD HEATING PADS.

BREAKER CORES OR WASHBURN CORES

7.1. General Thermal Conditions Relating to Breaker Cores and Mould Heating Pads

IMPORTANT FOR PRACTICE

If the feeding neck, as in Fig. 178, is constricted by a thin wafer core (a breaker or Washburn core), the feeder head can be knocked off. The method has achieved importance for small castings and alloy steels, as the costs of removing feeder heads are high. Even with nickel-containing, ductile steels breaker cores are economic, although in this case the feeder cannot be knocked

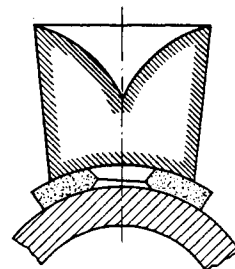


FIG. 178. Necked-down ingate, after Washburn^(18, 19).

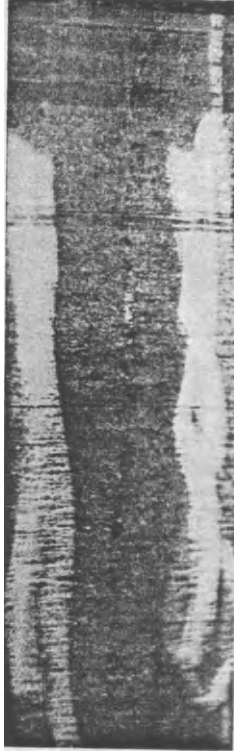


FIG. 176b



FIG. 176c

Figs. 176a-c. During the final machining of this press cylinder the segregation zone was cut.

corresponding to Fig. 174; only the nomogram of Fig. 171 (outside diameter as the initial dimension) was utilized.

With padding, irrespective of the method used, the position of the segregation zone can be displaced by hot material, i.e. by ingates, which can lead to foundry scrap or repair work, and this must be taken carefully into account.

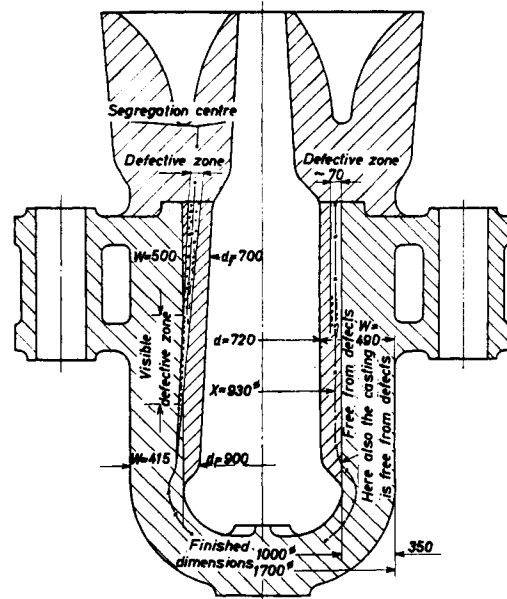


FIG. 177.

CHAPTER 7

INCREASING THE THERMAL GRADIENT BY MEANS OF MOULD HEATING PADS.

BREAKER CORES OR WASHBURN CORES

7.1. General Thermal Conditions Relating to Breaker Cores and Mould Heating Pads

IMPORTANT FOR PRACTICE

If the feeding neck, as in Fig. 178, is constricted by a thin wafer core (a breaker or Washburn core), the feeder head can be knocked off. The method has achieved importance for small castings and alloy steels, as the costs of removing feeder heads are high. Even with nickel-containing, ductile steels breaker cores are economic, although in this case the feeder cannot be knocked

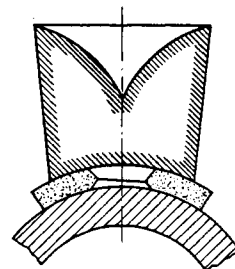
FIG. 178. Necked-down ingate, after Washburn^(18, 19).

TABLE 25 (a), PRINCIPAL DIMENSIONS OF BREAKER CORES

	M_F	M_C	T	$N\phi^*$	Breaker cores for side feeder heads**)		Dish-shaped breaker cores for round top feeder heads	
					a	b	$D\phi$	c
					mm	mm	mm	mm
Feeder head can be knocked off (with unalloyed steels)	1.0	0.84	4.2	19.5	53	30	65	12
	1.1	0.92	4.6	21.5	59	33	70	15
	1.2	1.00	5.1	23.5	64	36	75	16
	1.3	1.09	5.5	25.5	69	39	80	17
	1.4	1.17	5.9	27.5	75	42	85	18
	1.5	1.25	6.3	29	80	45	90	19
	1.6	1.34	6.7	31	85	48	100	20
	1.7	1.42	7.2	33	90	50	105	22
	1.8	1.51	7.6	35	96	54	110	23
	1.9	1.59	8.0	37	100	57	115	24
Feeder head cannot be knocked off but costs of removal are reduced	2.0	1.67	8.4	39	106	60	120	26
	2.2	1.84	9.2	43	117	66	135	28
	2.4	2.00	10	47	127	71	145	30
	2.6	2.20	11	51	138	78	155	33
	2.8	2.34	11.7	55	150	83	165	35
	3.0	2.50	12.6	59	160	90	175	38
	3.2	2.67	13.5	63	170	95	185	41
	3.4	2.84	14.5	66	180	102	195	44
	3.6	3.00	15	70	190	106	210	45
	3.8	3.17	16	74	200	113	220	48
4.0	3.34	17	78	212	120	230	51	
4.25	3.55	18	83	225	126	245	54	
4.5	3.75	19	88	240	133	260	57	
4.75	3.97	20	93	252	140	270	60	
5.0	4.18	21	97	265	147	285	63	

* The opening $N\phi$ can also be replaced by a rectangular shape with the same modulus (calculated from equation 5).
 ** The cores are suitable for both types of blind feeder head ($H = 1.5D$ and $H = 2D$).

off. The costs of removing the head (chiselling off, sawing, grinding or burning off) are less than with full ingates because of the constriction.

Breaker cores were invented by Washburn^(18,19) in USA, and have been in use for more than fifty years. Experience and trials extending over many years have established their dimensions very accurately. Even very slight deviations from these dimensions always lead to the production of scrap; the applicability of Washburn cores depends on a very strictly limited special set of thermal conditions.

According to Fig. 179, a metallic and a non-metallic

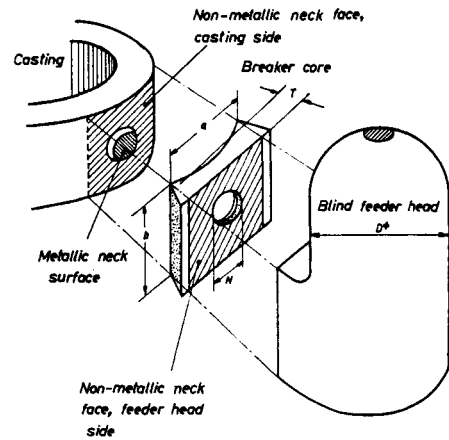


FIG. 179. Notation in the system casting—breaker core—blind feeder head.

TABLE 25 (b), WASHBURN CORES FOR FEEDER HEADS WHICH CAN BE KNOCKED OFF (UNALLOYED STEEL), SIMPLIFIED TO REDUCE STORAGE

M_F	M_C	a	b	d	$N\phi^*$	T	Radii of curvature of the standard breaker cores†)																
							a		e		f		b		k		m						
							∞	415 mm	330 mm	210 mm	170 mm	100 mm											
cm	cm	mm	mm	mm	mm	mm	from	to	from	to	from	to	from	to	from	to							
1.0	0.84	64	36	17	23.5	5.1	900	∞	—	—	400	900	—	—	280	400	180	280					
1.1	0.92						80	45	20	29	6.3	900	∞	—	—	400	900	—	—	280	400	180	280
1.2	1.00											96	54	24	35	7.6	900	∞	—	—	400	900	—
1.3	1.09	127	71	30	47	10	1300	∞	580	1300	—						—	360	580	280	360	—	—
1.4	1.17						2.2	1.84	2.2	1.84	2.2						1300	∞	580	1300	—	—	360
1.5	1.25	2.4	2.00	2.4	2.00	2.4						2.00	2.4	2.00	2.4	2.00	2.4	2.00	2.4	2.00	2.4	2.00	2.4

† The radii of curvature correspond to the radii of standard chills. In order to prevent confusion with chills in pattern data, standard breaker cores are denoted by lower case letters. f29, for example, denotes a core for curvatures from 400 to 900 ϕ , opening 29 mm.

connecting surface can be distinguished. The latter is only imaginary but allows the core dimensions to be calculated. The non-metallic neck must behave from the point of view of retarding solidification like hot steel, if the metallic neck is not to freeze. No cooling must therefore occur at the non-metallic neck, i.e. the core plate must attain a temperature of at least 1480°C, before the moment when the liquidus point of the metallic ingate is reached. The amount of heat required for this purpose must be obtained only from the superheat of the steel and not from its heat of fusion. If the latter were the case, the steel would begin to solidify, losing latent heat. This cannot be allowed to occur.

The non-metallic neck must be calculated in a similar way to the metal neck determination; this is best done by using Fig. 7. The values found from experience agree reasonably accurately with the requirement that the moduli must be stepped up in accordance with the ratios:

$$M_C : M_N : M_F = 1 : 1.1 : 1.2 \quad (c)$$

(M_C , M_N and M_F being the moduli of the casting, ingate and feeder head respectively). The factor relating the neck and feeder moduli varies in practice between 1.06 and 1.1.

Dimensions for breaker cores are given in Table 25; the dimensions of the blind feeders are contained in Table 19.

The following relationships were derived from the sizes which were tested in practice:

$$\text{Breaker core thickness } T_\phi \approx 0.093 D = 0.56 M_C \quad (46)$$

$$\text{Breaker core opening } N = 0.39 D = 2.34 M_C \quad (47)$$

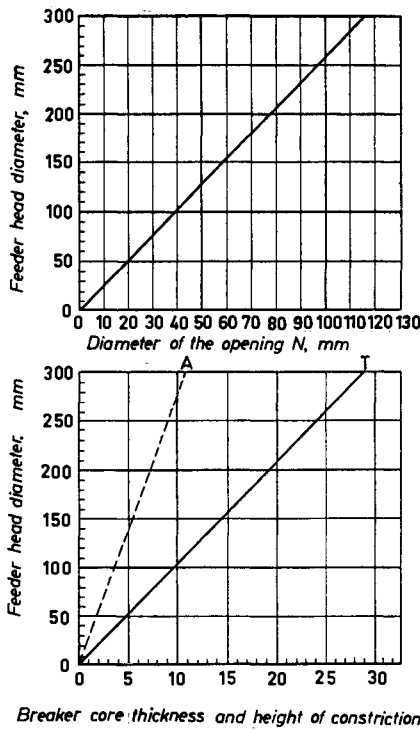


FIG. 180. Relationship: Feeder head diameter, breaker core opening, breaker core thickness and constriction height.

$$\text{Cross-section of metallic neck } \frac{N^2 \pi}{4} = 4.32 (M_C)^2 \quad (48)$$

$$\text{Modulus of metallic neck } M_{MN} = 0.59 M_C \quad (49)$$

in which D is the diameter of the blind feeder (Fig. 180).

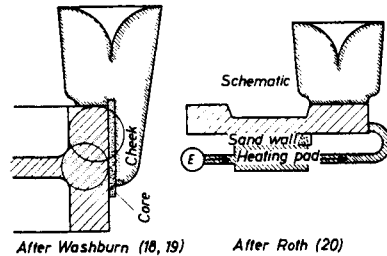


FIG. 181. Possible applications of padding and mould-heating pads separated from the casting.

According to Fig. 181 there is no fundamental difference between breaker cores and mould heating pads (introduced in Germany by Roth⁽²⁰⁾) which are also separated from the casting by a "non-metallic" hot steel surface.

7.2. Calculation of Washburn Cores and Mould Heating Pads on the Basis of the Thermal Conditions

(The applicability of breaker cores can still be understood by the practical foundryman even if this section is not read.)

Figure 182 shows the heat conducting relationships of a wafer core or a mould heating pad. As no solidifica-

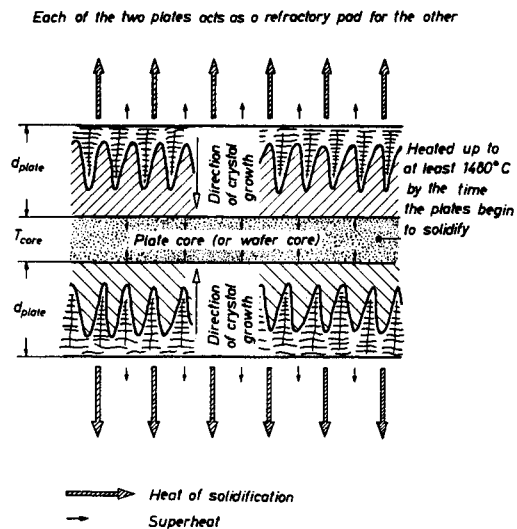


FIG. 182. Heat conducting conditions with correctly dimensioned plate core (or wafer core).

Only superheat is conducted to the plate core (or wafer core). When solidification commences the temperature of the plate core has already reached 1480°C, so that no heat of solidification can be taken up.

tion, and therefore no cooling, takes place at the wafer core, crystal growth takes place only from each side of the neck. In this way each of the two plates loses one of its two cooling surfaces, so that the plate volume remains unaltered. The modulus of a plate which cools only on one side is:

$$M_{(\text{with heating pad})} = V/\frac{1}{2}A = d \quad (50)$$

compared with that of a normal plate:

$$M_{(\text{without heating pad})} = V/A = d/2 \quad (d)$$

The plate modulus is thus doubled by the use of mould heating pads, and is equal to the plate thickness d . No further increase of modulus can be attained, because the effect of the pad is only to retard cooling, and not to provide additional heat. The wafer core is not in fact a donor of heat, but on the contrary takes superheat from the steel, so that it can never become hotter than the steel. The pattern of the temperature gradient on heating pads is shown in Fig. 183.

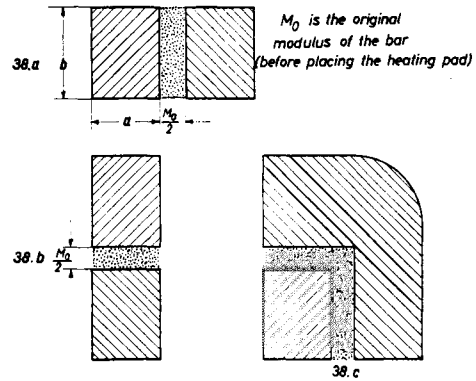


FIG. 184. Different methods of placing heating pads on bars.

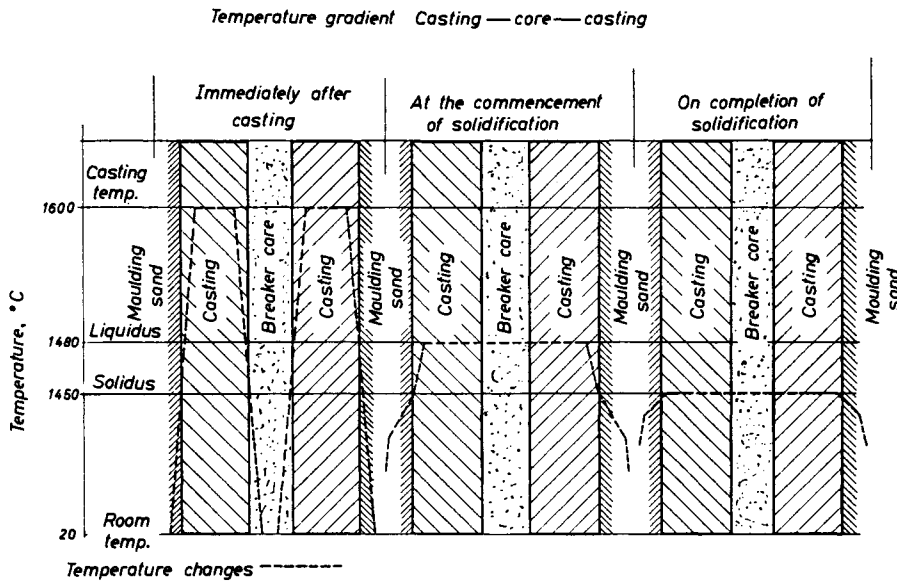


FIG. 183. Temperature gradient with correctly dimensioned heating pads.

The action of the heating pad ceases in every case when the crystal growth reaches the inner plate wall. Each of the plates of Fig. 182 acts as a heating pad for the other; crystal growth ends in both plates simultaneously. It follows that plate-like castings and the associated pads must be equal in thickness if it is desired to double the modulus.

No further increase in modulus is obtained by enlarging the pad beyond this minimum size; such an enlargement is therefore useless and uneconomical. Therein lies an essential difference compared with the metallic padding of cross-sections.

Bars have more cooling surfaces than plates, but the basic considerations are the same. Normally only one of the

cooling surfaces can be omitted (Fig. 184). The following formulae apply when the exothermic pad is placed on the surfaces a , b or $a + b$:

$$a \dots M = \frac{ab}{2(a+b) - a} \quad (51)$$

$$b \dots M = \frac{ab}{2(a+b) - b} \quad (52)$$

$$a + b \dots M = \frac{ab}{2(a+b) - a - b} = \frac{ab}{a+b} \quad (53)$$

The following is true according to Fig. 182 on the basis of the thermal conditions at a casting temperature

of 1600°C (superheat ≈ 120°C), an amount of superheat which is necessary and customary for small parts:

$$d \times 1 \text{ cm}^2 \times \gamma_{\text{steel}} \times C_{\text{steel}} \times 120 = T \times 1 \text{ cm}^2 \times \gamma_{\text{sand}} \times C_{\text{sand}} \times 1480 \quad (54)$$

Allowance has already been made for the fact that half the superheat from each of the two plates escapes unused, but the core is heated from two sides. The following values can be substituted:

	steel	sand
specific heat C	0.20	0.26
specific gravity γ	7.0	1.6
	for oil sand, rammed.	

Hence: $T_{\text{core}} = 0.275 d_{\text{plate}} \approx 0.25 d \quad (55)$

or: $T \approx 0.5 M_{\text{casting}} \quad (56)$

The superheat goes into equation (50) as a linear function, so that a simple relationship exists between superheat and casting thickness, in accordance with Fig. 185.

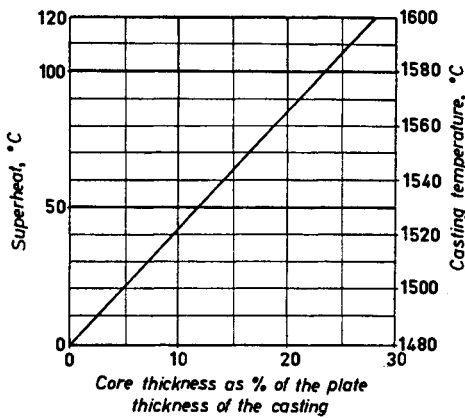


FIG. 185. Relationship: superheat-thickness of breaker core.

The correctness of the above formulae can be checked from dimensions which have proved satisfactory in practice. According to Fig. 180:

$$T \approx 0.093 D \quad (57)$$

[see also equation (46)].

The modulus of the blind feeder head $H = 1.5 D$ is:

$$M \approx 0.2 D \quad (58)$$

Thus the blind feeder solidifies in the same time as a plate of thickness d_1 .

$$d_1 = 2 M_F = 2 \times 0.2 D = 0.4 D \quad (59)$$

The relevant casting has the modulus:

$$M_C = \frac{M_F}{1.2} = \frac{0.2}{1.2} M_F \quad (e)$$

corresponding to a plate thickness:

$$d_2 = 2 M_C = \frac{2 \times 0.2}{1.2} D = 0.3 D \quad (60)$$

If the mean d_3 is used for the calculation:

$$d_3 = \frac{d_1 + d_2}{2} = 0.35 D, \quad (f)$$

then according to equation (57):

$$T = 0.093 D = 0.265 d_3 \quad (61)$$

which is in good agreement with equation (55). This proves at the same time the need for a casting temperature of 1580–1600°C for Washburn cores.

This heat balance is only approximate, however, because the core also loses heat from the end faces. This heat loss tends towards a limiting value which is always constant (as long as the superheat remains the same), as the thickness T , the dimensions of the non-metallic ingate a and b and hence the size of the end faces are all rigorously linked to the modulus. To compensate for the heat loss, which is similarly bound up with the modulus, a metallic ingate is required, the dimensions of which are again linked with the modulus; this is also expressed in the results obtained in practice.

7.2.1. CALCULATION OF INTERNAL FEEDERS

(The practical foundryman can still understand the use of internal feeders, even if this section is omitted.)

Internal feeders in tubular castings, as in Fig. 186, represent a special case of a heating core, as the whole of the superheat of the feeder flows into the central core. Heat is radiated only through the external surface of the tube, and the modulus of a tube with an external diameter D and wall thickness w is:

$$M \approx w \quad (62)$$

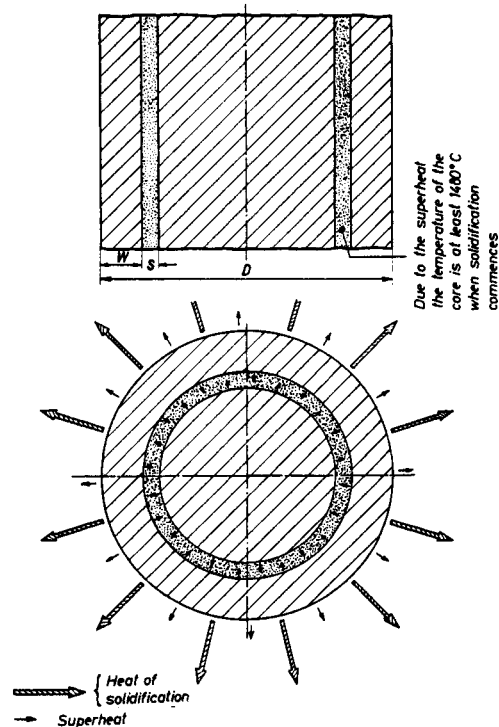


FIG. 186. Thermal conditions in internal feeders inside tubular castings.

because

$$M_F \geq 1.2 M_C \tag{g}$$

$$\geq 1.2 w$$

Due to the fact that the behaviour of the core is similar to that of hot steels the tube and feeder act as if they were a uniform steel mass with a modulus:

$$M_{tot} = M_F = \frac{D}{4} \geq 1.2 w, \text{ from which: } \tag{h}$$

$$D \geq 4.8 w \approx 5 w \tag{63}$$

Most tubular bodies where internal feeders are applicable fulfil this requirement.

It should be mentioned that, because of the danger of metal penetration at the core, internal feeders should only be used up to a diameter of about 150 mm.

The internal circumference of the tube is $\pi(D - 2w) = 3\pi w$, so that the total external and internal periphery of the tubular heating core is $2 \times 3 \times \pi \times w = 6\pi w$ (neglecting the small thickness of the sand layer s) and is therefore 1.2 times that of the external circumference of the tube ($\pi D = 5\pi w$); the surface areas of these tubes stand in a corresponding ratio. If we designate the total mass of steel (feeder + casting) by Q , and the mass of sand by S , then the sand mass will contain the following proportion of the superheat, corresponding to the surface ratios:

$$\% \text{ of superheat} = \frac{6\pi w \times 100}{6\pi w + 5\pi w} = 55\% \tag{64}$$

According to the thermal equilibrium existing at 120°C superheat:

$$Q \times \gamma_{\text{steel}} \times C_{\text{steel}} \times 120 \times 0.55 = S \times \gamma_{\text{sand}} \times C_{\text{sand}} \times 1480 = 615 S \tag{65}$$

$$Q = \frac{\pi D^2}{4} - S \tag{66}$$

$$S = (D - 2w - s) \pi s \tag{67}$$

$$w \approx D/5 \tag{i}$$

whence:

$$s = 0.073 D = 0.365 w \tag{68}$$

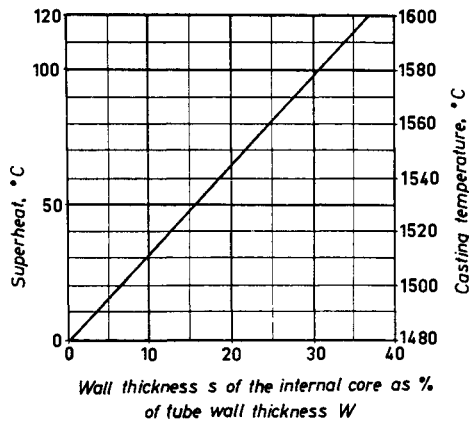


FIG. 187. Relationship: superheat, to core wall thickness/tube wall thickness in internal feeders.

Figure 187 gives the dependence on superheat. The feeder diameter is given by ≈ 45 per cent of the external diameter of the tube, or ≈ 2.25 times the wall thickness of the tube. The diameter of an external feeder head would be about 3 times the wall thickness; this external feeder would be about 1.8 times the weight of an equally effective internal feeder.

7.3. On the Practice of Washburn Cores, Heating Pads and Internal Feeders

IMPORTANT FOR PRACTICE

As Washburn cores are subjected to high stresses from the steel flowing through them, fine-grained quartz sand with 5–6 per cent of oil as binder is used as moulding material, with a drying temperature of 220–250°C. Well-burned cores must be able to scratch soft wood—a cheap, rapid method of testing. To prevent the penetration of gas into the casting due to the sand fillet effect of the core, with metal which is cast too hot, the gas permeability should be low. For this purpose 25–30 per cent of quartz powder should be mixed with the core sand. This is always necessary with hollow cores (tubular internal feeders). The oil addition must also be increased when necessary.

Breaker cores and heating pad parting cores should be standardized as far as possible, and can then be ordered as shaped fireclay pieces. (Cheap fireclay qualities are sufficient, provided they are dense and strong. All types of insulating fireclay are too weak.) The diameters of round bodies are collected into groups and designated by lower case letters. In addition, data on the relevant diameter of blind feeder head are required. For example, “f 100” signifies a breaker core which can be applied

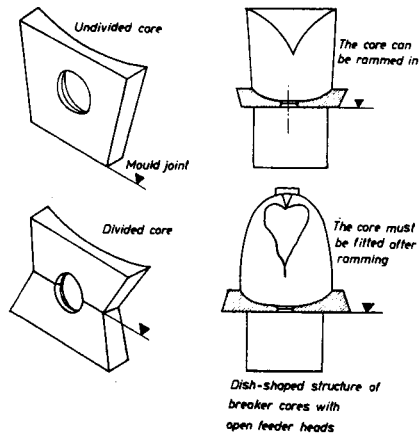
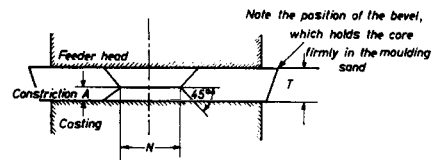


FIG. 188. Various designs of standardized breaker cores.

to all circular bodies of 580–740 mm diameter with a feeder head diameter of 100 mm.

$$(M_F = 2 \text{ cm; } M_C = \frac{M_F}{1.2} = 1.66 \text{ cm; } T = 9.5 \text{ mm;}$$

$$N \varnothing = 39 \text{ mm, etc.).} \quad (j)$$

Experience has shown that very little storekeeping is required, because only quite specific wall thicknesses, and, therefore, moduli occur in the diameter range in question.

Figure 188 shows various shapes of breaker core, according to the type and position of the ingate in the mould. With open-top feeder heads dish-shaped breaker cores are stiffer and hence are more solid. Breaker cores should as far as possible be rammed up with the mould, to prevent the formation of burrs which can hinder knocking-off (Fig. 189). If this is not feasible, the moulding sand must be pressed very carefully into the core prints.

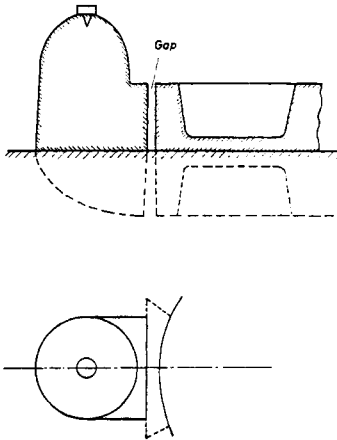


FIG. 189. A gap is left between pattern and feeder head for fitting the breaker core during moulding.

From the point of view of reliability, the metal should be poured through each breaker core gate, to conduct as much superheat as possible into the core. If this cannot be done, the cores can be made half of sand and half of a highly exothermic mouldable material, as shown in Fig. 190. The exothermic material must always lie on the feeder side of the mould.

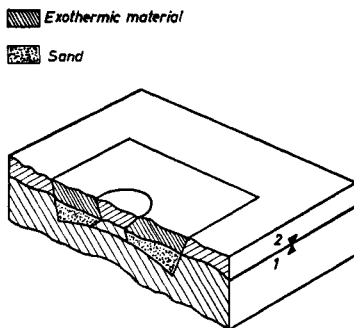


FIG. 190. Manufacture of breaker cores for cross-sections with no allowance for the effects of metal flow.

Manufacture of breaker cores with exothermic materials in two-part core boxes 1st part, ram solid with sand; strike off; set 2nd part on top and ram up with exothermic material.

In the case of mass-produced articles with complicated contours, which would be distorted by attaching a feeder head, breaker cores and heating pads are often the only economical method of gating. The manufacture of contoured core boxes is then unavoidable. Breaker cores increase the costs in the coremaking and moulding shops, but reduce the load on the fettling shop, decrease its costs and accelerate the fettling work considerably. With short delivery times and shortage of space and personnel in the dressing shop this last point is very important, even if the costs of the cores are as high as or even a little higher than the savings in fettling costs.

Figures 191–201 illustrate some applications of these cores.

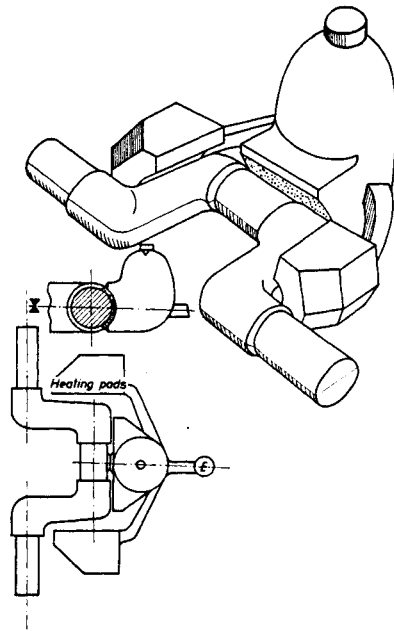


FIG. 191. Method of feeding small crankshafts with atmospheric feeder head and heating pads.

The dressing costs are very low by this method and the cast surface so pleasing (as it is not ground) that on the basis of this procedure alone the production of the crankshafts by drop forging could be discontinued.

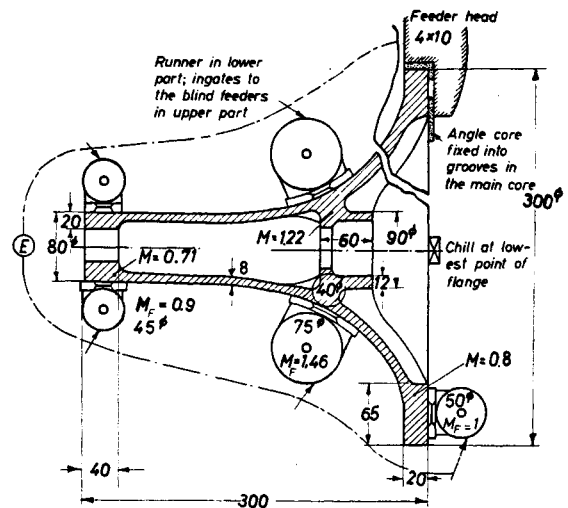


FIG. 192. Axle housing.

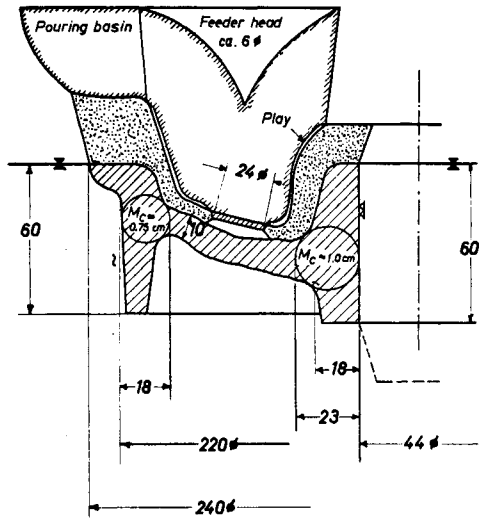


FIG. 193. Truck wheel with a knockoff head for the rim and hub.

The slight shrinkage gap between feeder head and shell core will be noted. The feeder head rests only on the knockoff stem, so that the thin shell core cannot be crushed even when under pressure in the moulding machine. By agreement with the customer the shape of the wheel disc was adjusted to suit the casting requirements. The knockoff stub remains undressed. A chill is situated in the hub core on the opposite side of the feeder.

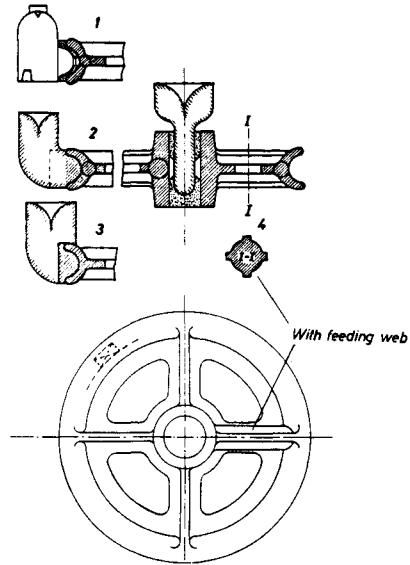


FIG. 195. Alternative methods of feeding rope pulleys.

In spite of their apparently simple appearance, rope pulley rims of all types and sizes are difficult to feed, and scrap is often produced unless very uneconomic methods of manufacture are selected. The following methods may be used:

1. Atmospheric feeder head with internal Washburn cores at each web junction. Chills in the core between the junctions. Not much dressing; reliable and cheap.
2. Peripheral core. 4 feeder heads at the 4 junctions (full-gated into the groove). Heavy dressing required!
3. Groove turned out of the solid material. 4 to 6 feeders at the periphery of the rim, which is now massive. Safe, but very expensive!
4. For small rope pulleys. An elegant solution by using 4 feeding webs to the junctions, with intermediate chills. Unfortunately the customer will not often agree to this method.

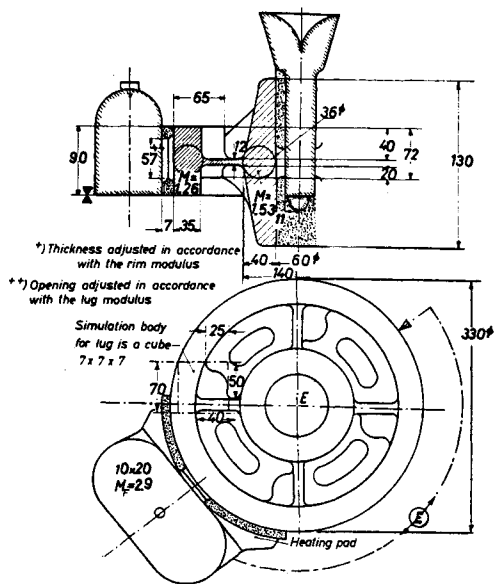


FIG. 194. Travelling crane wheel.

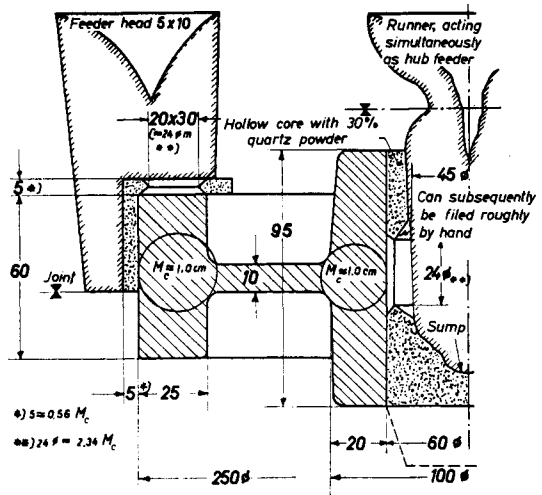


FIG. 196. Spur gear wheel with internal feeder at the hub, 3 rim feeders with Washburn cores and heating pads.

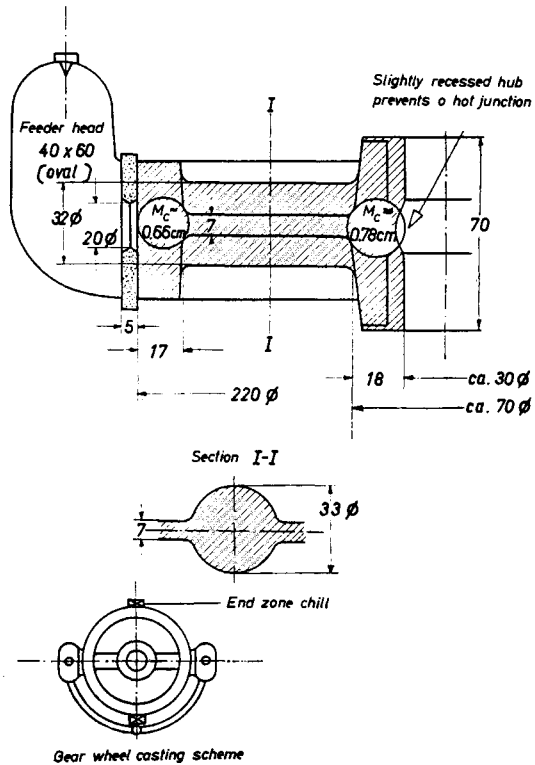
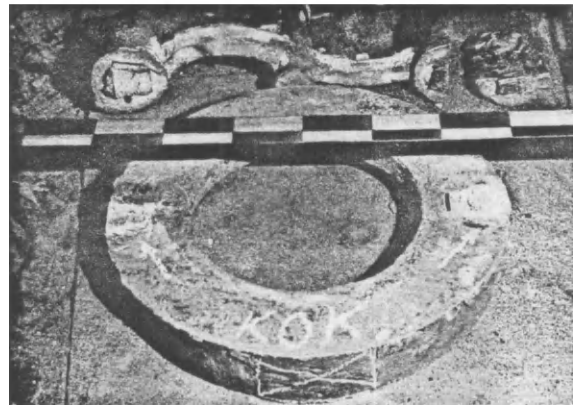
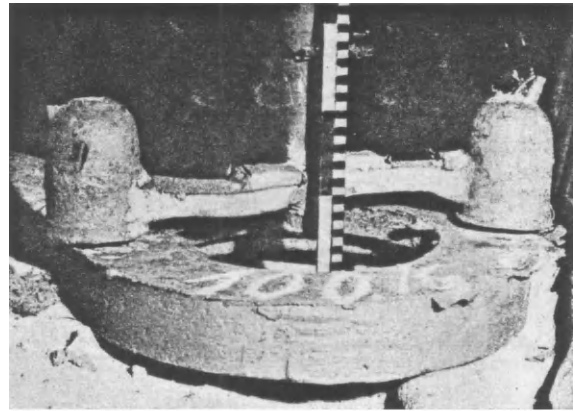
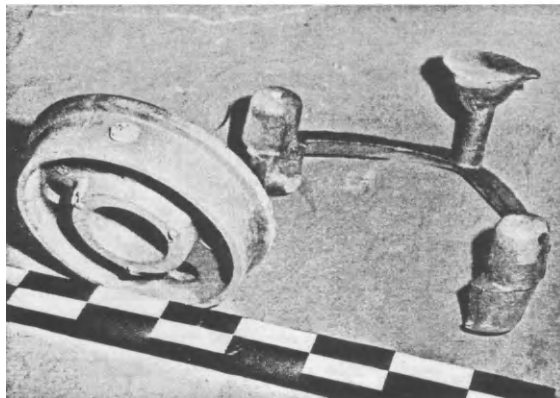


FIG. 197. Method of moulding wheels with feeding webs, Washburn cores and blind feeder heads.



FIGS. 200a and b. Gear wheel rim blank with atmospheric feeders which can be knocked off, and through which the metal was poured.



FIGS. 198, 199. Truck wheel with rim feeders which can be knocked off. The hub is fed from the rim by two ribs.

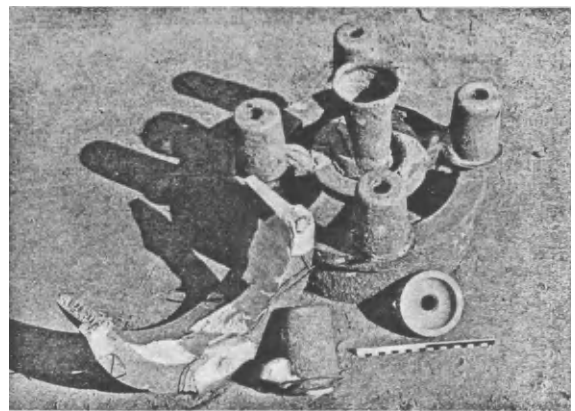


FIG. 201. Wear-resisting bushes of special steel. 4 atmospheric feeders which can be knocked off, and through which the metal was poured. Note the dish-shaped design of the breaker core.

7.4. The Heating of Thin Sections of Moulding Sand. Influence on the Size of the Feeder Head. The Minimum Lengths of Ingates Which Will Prevent Harmful Sand Fillet Effects

7.4.1. HARMFUL EFFECTS OF HOT SPOTS

IMPORTANT FOR PRACTICE

The previous sections 7.1–7.3 dealt with the utilization of hot spots for the directional control of solidification. We will now describe the harmful effects which can be produced together with suitable countermeasures which can be taken.

Penetration of gas into the casting is often observed on the corners of thin-walled core sections in massive castings (Fig. 202), at the sand fillets between the casting

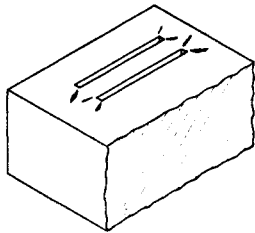


FIG. 202. Gas penetration at the edges of thin-walled core sections.

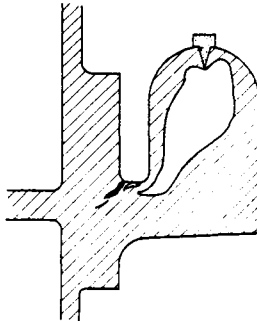


FIG. 203. Gas penetration between the casting and a blind feeder set in front.

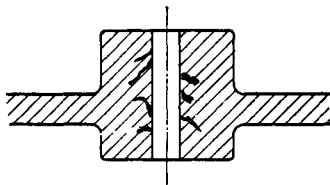
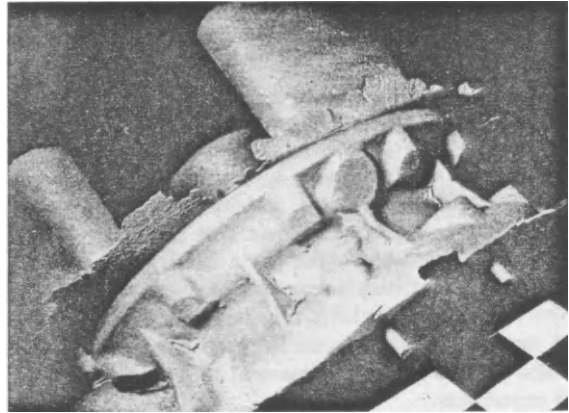


FIG. 204. Gas penetration on thin cores of thick-walled bosses.

and blind feeder in front of it (Fig. 203), and on thin cores in heavy-section bosses and tubes (Fig. 204).

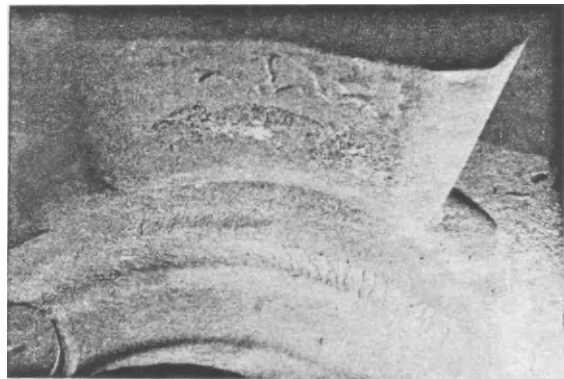
This “sand fillet effect” was described some time ago⁽⁴³⁾. There are at least two contributory causes; different views are held as to their relative importance. The author considers the following explanation⁽⁴⁴⁾ to be valid: cooling is retarded at re-entrant sand corners by the hot spot, i.e. the time of solidification is prolonged. The adjacent cross-sections will therefore freeze earlier, so that the supply of metal to the points where cooling has been retarded is stopped. This leads to the production of cavities at these positions, which form a vacuum into which the atmospheric pressure, together with the gases evolved on casting, can penetrate into these cavities and produce “worm holes” (Fig. 205). Defects of



a



b



c



d

FIGS. 205a–d. Hub and junction below the feeder head not systematically marked out with Heuvers circles; with the result that internal cavities are formed into which gases penetrate from the mould, leaving behind “wormholes”. Shrinkage cracks are also formed.

this kind on the surface of the casting are also found frequently with other cavities which are not caused by sand fillers.

An absolutely accurate theoretical calculation of the solidification time can only be made, if at all, with great difficulty and would be very time-consuming, because of the many factors involved; in particular, in the view of the author, problems of heat flow have not been satisfactorily solved. On the other hand solidification times can be calculated in a number of cases on the basis of very simple heat balance relationships between steel and moulding sand, without the use of higher mathematics, and with excellent agreement between calculation and experiment.

7.4.2. THE HEATING OF PLANE CORE PLATES BY THE SUPERHEAT OF THE LIQUID STEEL

In accordance with Fig. 206 a sand plate is preheated between steel walls by the superheat. The capacity for taking up the heat of solidification of the steel (later given up again) is thereby diminished, i.e. the effective cooling surface is reduced.

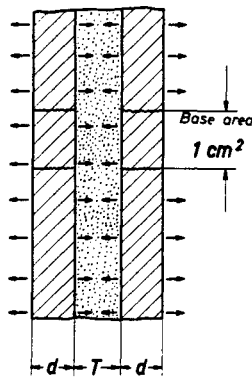


FIG. 206. Heating up a sand plate between two steel walls.

An imaginary parallelepiped element with a base area of 1 cm² can be taken from a plane steel wall. Its superheat S at a temperature (above the liquidus) of τ_s is given by:

$$S = \tau_s \times S_{\text{steel}} \times C_{\text{steel}} \times \gamma_{\text{steel}} \times d_{\text{cm}} \times 1 \text{ cm}^2 = \tau_s \times 0.2 \times 7.0 \times d_{\text{cm}} \quad (69)$$

where C is the specific heat and γ the specific gravity.

In the first place $S/2$ is drawn off to the outer and core side of the wall. Thus the core plate receives $S/2$ from each of the two steel walls, equal to the total superheat S . As a result the core temperature increases to:

$$\text{core } (^{\circ}\text{C}) = \frac{S \text{ (cal)}}{C_{\text{sand}} \times \gamma_{\text{sand}} \times T_{(\text{cm})}} = \frac{\tau_s \times d_{(\text{cm})} \times 1.4}{0.26 \times 1.6 \times T_{(\text{cm})}} \quad (70)$$

in which the mean value of 0.26 for the specific heat of sand in the temperature range in question has been selected as a simplifying assumption.

If the ratio $n = \frac{\text{core thickness}}{\text{steel thickness}} = \frac{T}{d} \quad (71)$

is substituted, we obtain:

$$\tau_{\text{core}} = \frac{\tau_s \times d \times 1.4}{n \times d \times 0.416} = \frac{\tau_s \times 3.37}{n} \quad (72)$$

This equation is represented in Fig. 207.

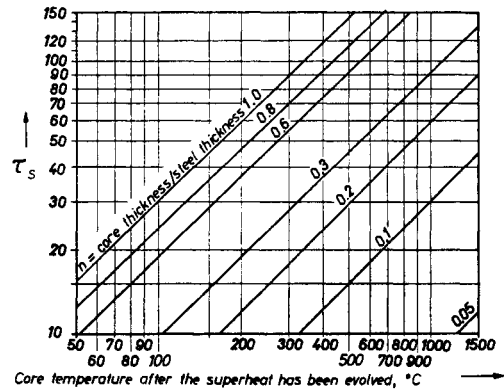


FIG. 207. Temperatures of flat core plates after the superheat has been evolved.

The temperature of the preheated core plate is now increased still further by the liberated heat of solidification L (≈ 64 cal/g) until steel and core have reached the same temperature. The following assumption must be made for the calculation:

The heat of solidification is given up uniformly during the solidification interval

$$\tau_{\text{liquidus}} - \tau_{\text{solidus}} \text{ (1510 - 1480 = 30}^{\circ}\text{C for average unalloyed steels)}$$

so that the amount of heat:

$$f = L/30 = 64/30 = 2.13 \text{ cal/g } ^{\circ}\text{C} \quad (73)$$

is given up for each 1°C fall in temperature.

Practical results indicate that these assumptions are probably of the correct order of magnitude.

Figure 208 illustrates diagrammatically the heat trans-

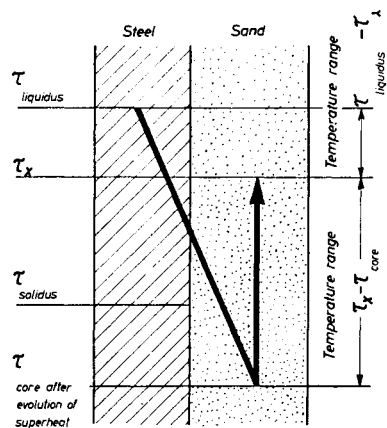


FIG. 208. Scheme of heat transfer and of the temperature relationships in the system steel-sand.

fer from steel to sand, in which the temperature of the core plate is raised to a maximum τ_x , after which it absorbs no further heat. For each parallelepiped element (1 cm² base) the following relationship holds true:

$$\begin{aligned} &(\tau_{\text{liquidus}} - \tau_x) \times f \times \gamma_{\text{steel}} \times d \\ &= (\tau_x - \tau_{\text{core}}) \times C_{\text{sand}} \times \gamma_{\text{sand}} \times T \end{aligned} \quad (74)$$

From this and from equation (4):

$$x = \frac{22500 + 1.4 \times \tau_s}{0.416 n + 14.9} \quad (75)$$

This equation is represented in Fig. 209, from which an average increase of 12°C in the core temperature is to be expected with an increase of 100°C in the superheat (above the liquidus point).

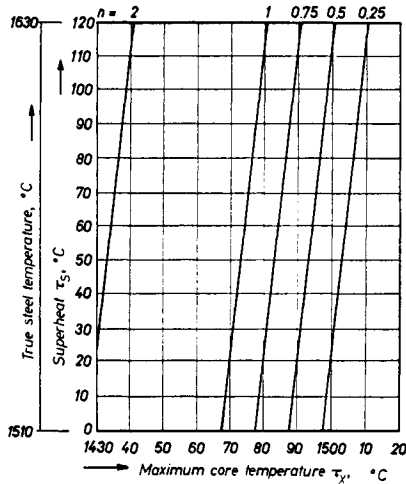


FIG. 209. Relationship: maximum core temperature/steel superheat.

7.4.3. THE DECREASE IN THE COOLING SURFACE AREAS OF CORE PLATES AS A RESULT OF HEATING

On attaining the maximum temperature τ_x , i.e. when the transfer of heat to the core sand has been completed, the following proportion of the heat of solidification (A%) has been absorbed by the core plate:

$$A\% = \frac{\tau_{\text{liquidus}} - \tau_x \times 100}{30 (\text{°C})} \quad (76)$$

The heat is derived proportionately from the surface of the casting (Chvorinov modulus principle, $M = V_{(\text{cm}^3)} / A_{(\text{cm}^2)}$).

This proportion of absorbed heat corresponds to the effective proportion of the cooling surface of the core. Equation (76) is represented in Figs. 210 and 211, in which the slight curvature was replaced by a simple straight line approximation.

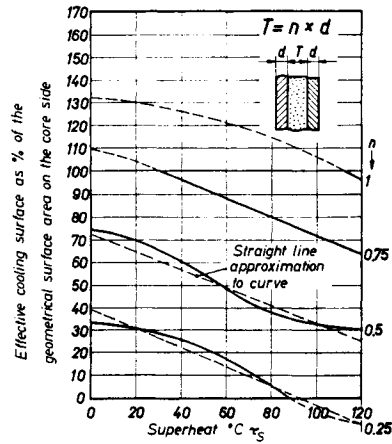


FIG. 210. Relationships superheat/reduction of the cooling core surface with flat plate cores.

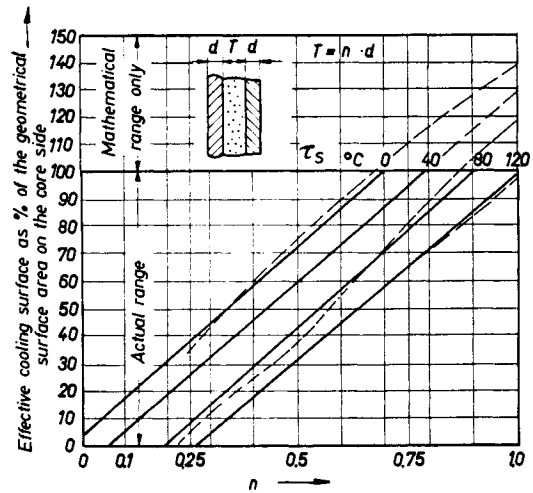


FIG. 211. Reduction of the cooling surface of the core with increasing wall thickness. in flat core plates.

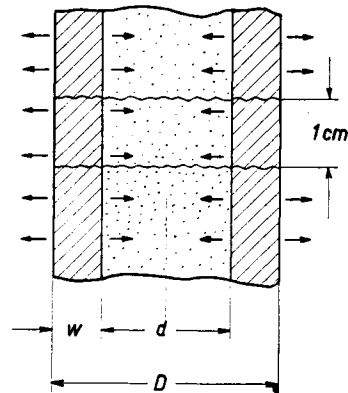


FIG. 212. Heating up a sand core in a steel tubular casting.

7.4.4. CALCULATION OF THE COOLING ACTION OF CORES IN LONG TUBULAR BODIES

This was determined by a method similar to that used in the previous sections. From a tubular element 1 cm in length (Fig. 212) the superheat:

$$S = \frac{\pi}{4} (D^2 - d^2) \times \gamma_{\text{steel}} \times C_{\text{steel}} \times \tau_s$$

$$= \tau_s \times 1.4 \times \frac{\pi}{4} (D^2 - d^2) \tag{77}$$

is given off; of this the amount escaping to the core, corresponding to the proportion of the internal surface area of the tube, is

$$S_i = \frac{\tau_s \times 1.4 \times \pi/4 \times (D^2 - d^2)}{(D + d)} \tag{78}$$

the temperature of the core being thereby heated to

$$\tau_{\text{core}} = \frac{S_i}{C_{\text{sand}} \times \gamma_{\text{sand}} \times d^2 \pi/4}$$

$$= \frac{\tau_s \times 3.37 (D - d)}{d} \tag{79}$$

This initial temperature τ_{core} is increased to τ_x by the heat of solidification which is now liberated:

$$(\tau_{\text{liquidus}} - \tau_x) \times f \times \gamma_{\text{steel}} \times \pi/4 (D - d) \times d$$

$$= (\tau_x - \tau_{\text{core}}) \times C_{\text{sand}} \times \gamma_{\text{sand}} \times d^2 \pi/4 \tag{80}$$

If $n = d/D$ is substituted, then:

$$\tau_x = \frac{(D - d) (22500 + \tau_s \times 1.4)}{0.416 d + 14.9 (D - d)} \tag{81}$$

$$= \frac{(1 - n) (22500 + \tau_s \times 1.4)}{14.9 - 14.484 n} \tag{82}$$

The proportion of the effective cooling surface of the core is determined from equation (76), in which the above value of τ_x is substituted (Fig. 213).

It may be mentioned here that these equations are valid only for tubular castings; they do not apply to

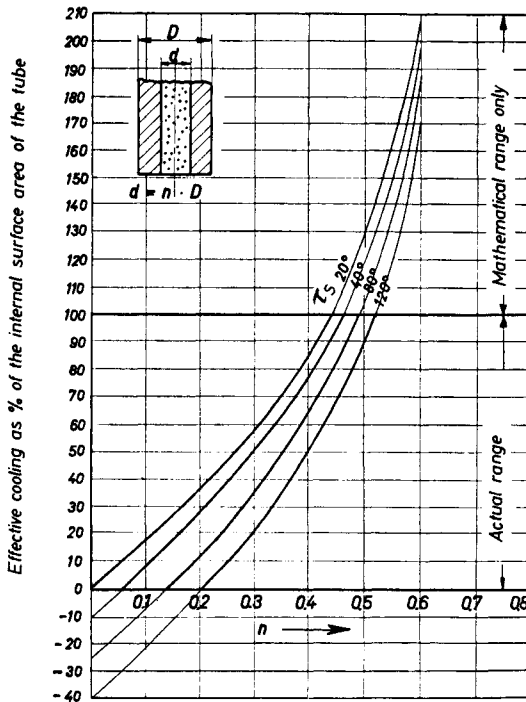


FIG. 213. Effective cooling surface of cores and steel tubes.

rings and discs having end faces with relatively large areas.

7.4.5. CALCULATION OF THE COOLING ACTION OF CORES IN SHORT TUBULAR BODIES (DISCS AND RINGS)

The treatment given here refers to rings with the dimensional ratios $H = D/4$, $H = D/2$, $H = D$ and $H = 2D$, but intermediate values can easily be interpolated. The proportion of the core surface is reduced in accordance with Fig. 213, corresponding to the two end cooling surfaces. Figure 214 shows the course of

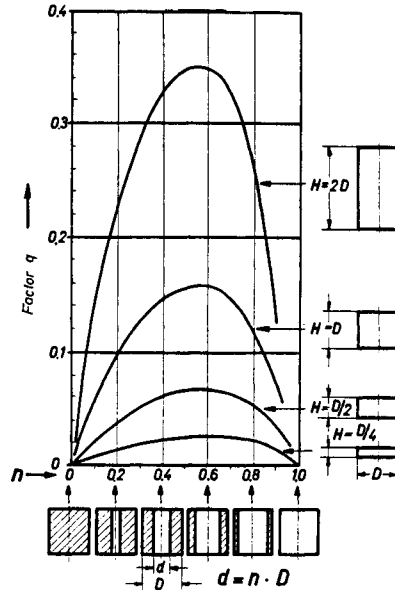


FIG. 214. Geometrical proportion A of the core surface area to the volume of the cylinder.

these proportion curves for various size ratios, in which the curves exhibit a typical maximum between $n = 0.5$ to 0.6 , which exerts a strong influence on the further values derived.

The internal surface proportion S_i of the superheat is transmitted to the core, from which the core temperature with a complete transfer of superheat is calculated as follows:

$$\tau_{\text{core}} = \frac{S_i}{C_{\text{sand}} \times \gamma_{\text{sand}} \times (d^2 \pi/4) \times H}$$

$$= \frac{\tau_s \times C_{\text{steel}} \times \gamma_{\text{steel}} \times D^3 \times 2}{0.416 \times d^2/4 \times H}$$

$$= \frac{D}{H} \frac{1.4 \times 2}{0.319 \times H^2} \tag{83}$$

The preheated core section is now heated further to a temperature of τ_x by the proportion of the heat of solidification which is absorbed, any further heat being transferred to the core when the temperatures of core and steel become equal.

Similarly to equations (80), (81) and (82), we obtain:

$$x = \frac{22500 \times 2 + \tau_{\text{core}} \times 0.416 \times V_{\text{core}}}{0.416 \times V_{\text{core}} + 14.9 \times 2} \tag{84}$$

According to equation (76), when τ_x is known the percentage effective cooling surface of the core can be determined immediately. The results are represented in Figs. 215, 216, 217 and 218.

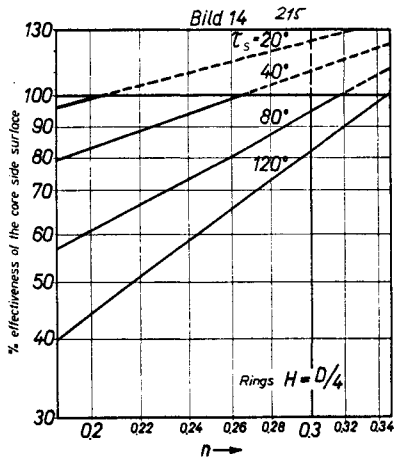


FIG. 215. Effective cooling surface of cores in flat steel rings.

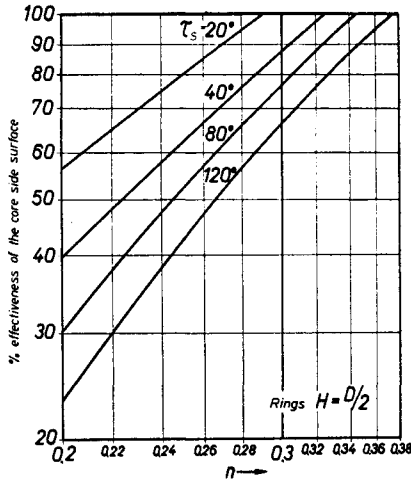


FIG. 216. Effective cooling surface of cores in steel rings.

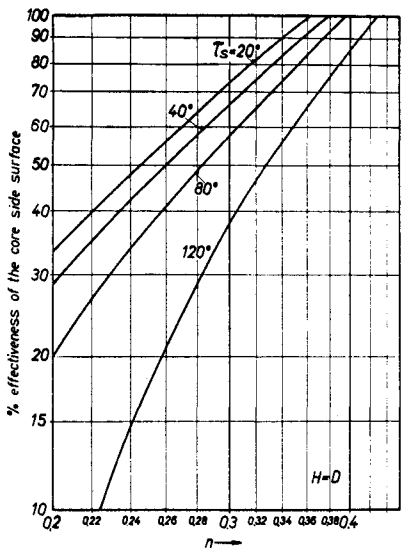


FIG. 217. Effective cooling surface of cores in hollow steel cylinders, $H = D$

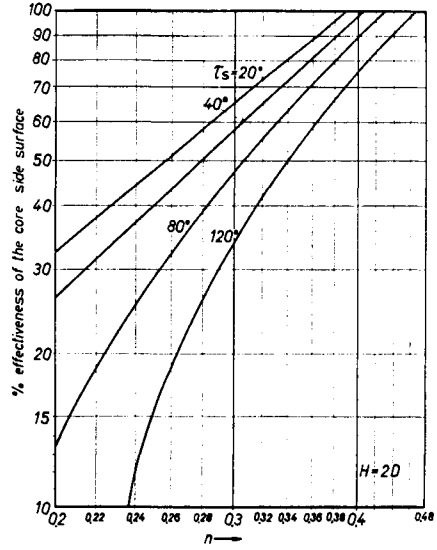


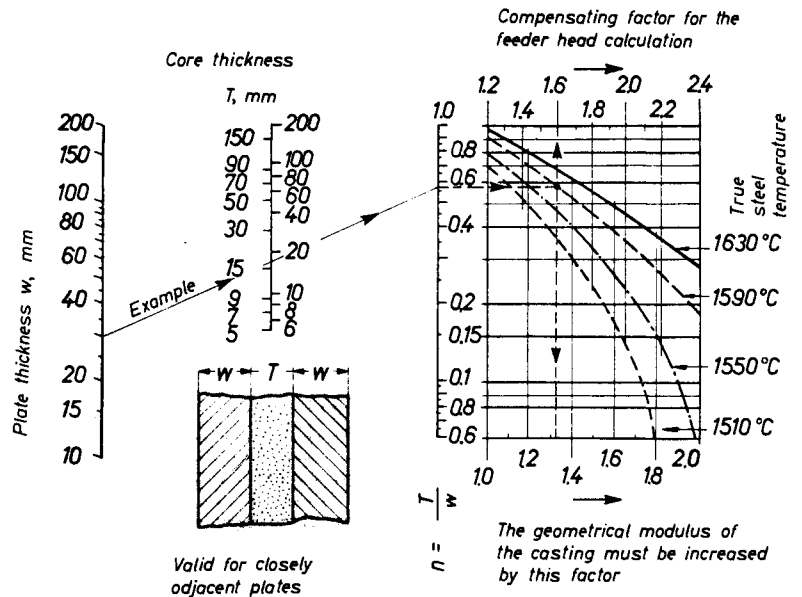
FIG. 218. Effective cooling surface of cores in hollow steel.

7.4.6. RETARDATION OF THE SOLIDIFICATION PERIOD BY HEATING

The reduction of the cooling surface areas by heating from the hot metal was determined in the previous sections. Such a reduction of cooling area has the effect of increasing the modulus.

Figure 219 represents the corresponding increase in modulus of closely adjacent cast steel plates, Fig. 220

FIG. 219. Increase in the modulus of closely adjacent cast steel plates.



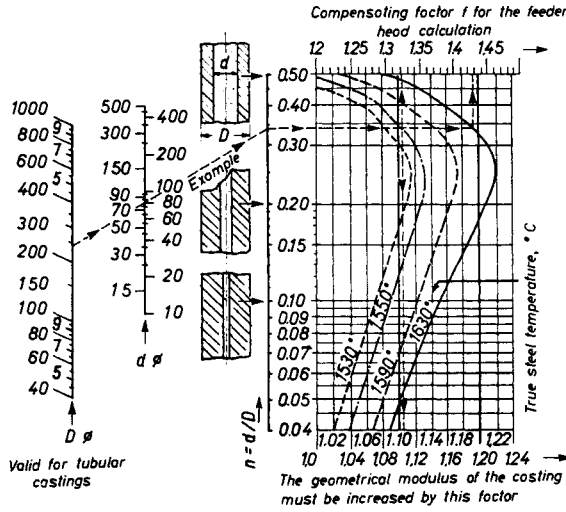


FIG. 220. Increase in the modulus of cast steel tubes with small internal diameters.

FIG. 221. Increase in the modulus of flat steel rings $H = D/4$ with a small internal diameter.

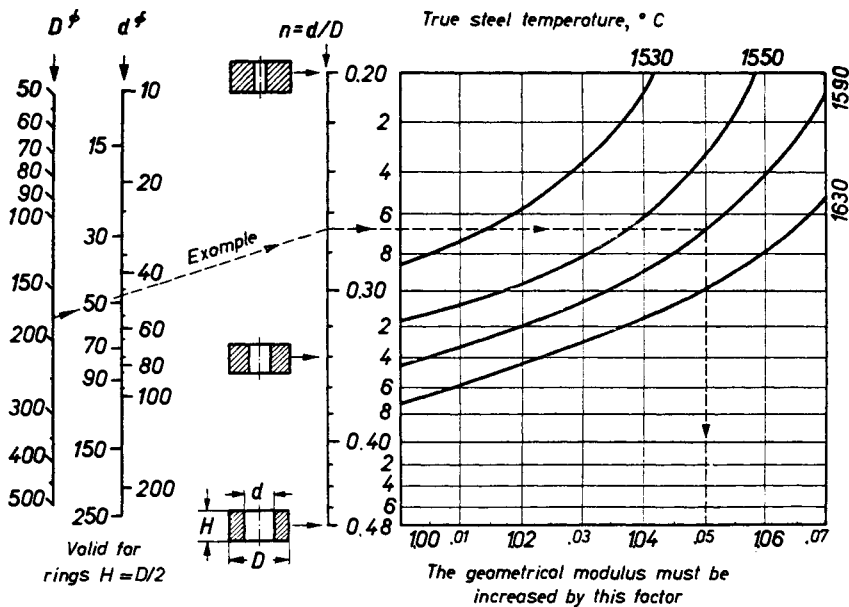
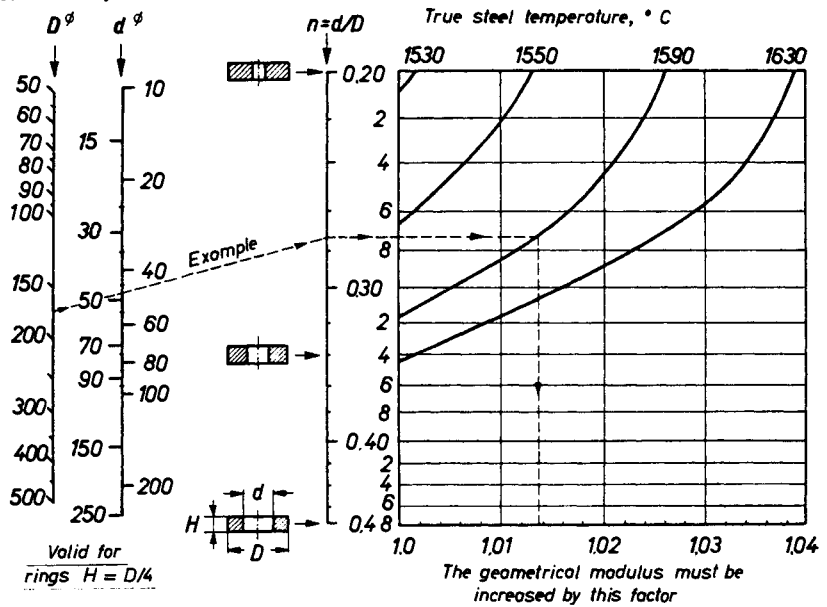


FIG. 222. Increase in the modulus of flat steel rings $H = D/2$ with a small internal diameter.

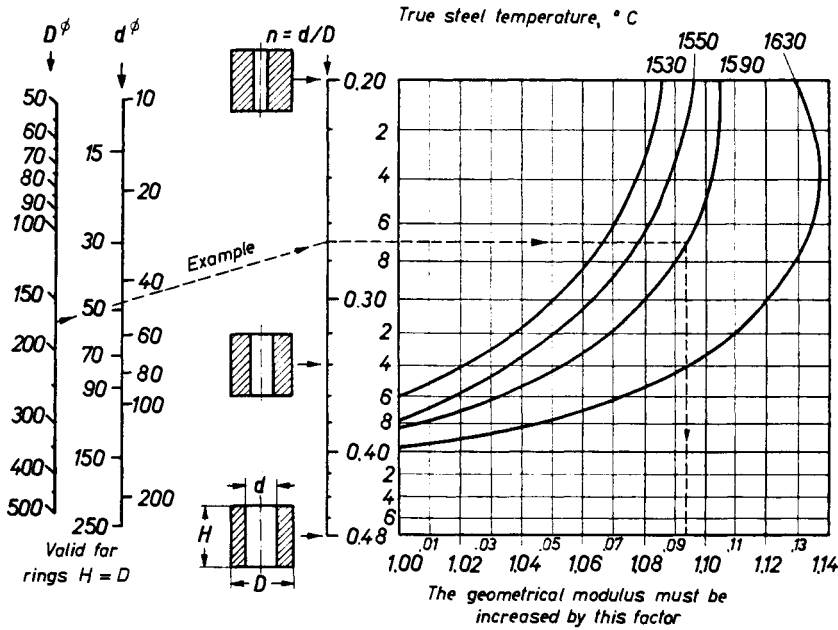


FIG. 223. Increase in the modulus of hollow cast steel cylinders, $H = D$, with a small internal diameter.

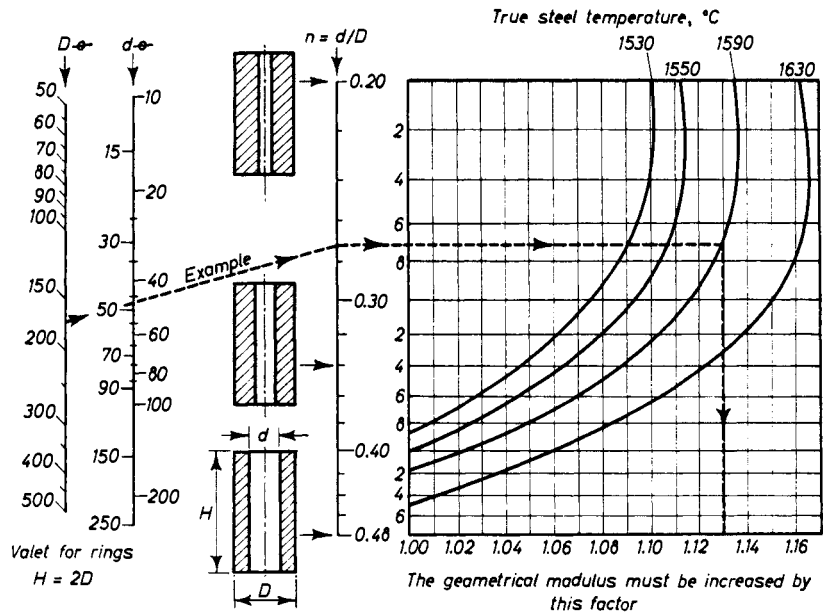


Fig. 224. Increase in the modulus of hollow cast steel cylinders. $H = 2/D$.

the increase of modulus in tubes with a small core diameter, and Figs. 221–224 the modulus increase in the case of rings. In order to make the diagrams easier to follow for the practical foundryman, the size ratios of tubes and rings are shown to scale in several positions.

7.4.7. CHECKING THE CALCULATIONS FOR TUBULAR CASTINGS BY MEASURING THE SOLIDIFICATION TIME

Based on the modulus increase in tubular castings (see Fig. 220) the solidification time of these tubes was determined from equation (84) for different amounts of

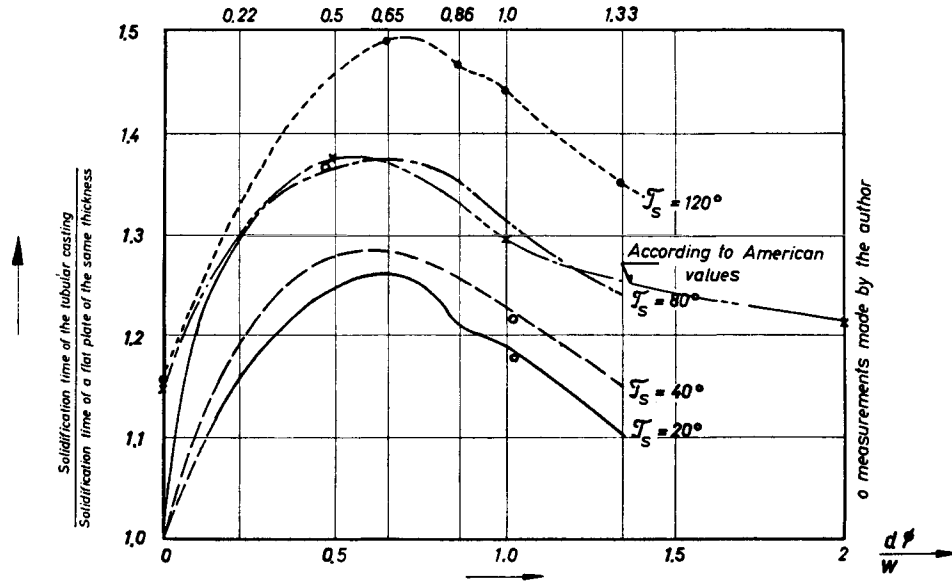


FIG. 225. Comparison of the calculated and actual solidification times in cast steel tubes.

superheat and various ratios of internal diameter to tube thickness. The results are represented in Fig. 225.

It is logical and was known long ago that the heating effect increases as the casting temperature of the steel becomes higher. The size of this effect can be seen clearly in Fig. 225. A solid cylinder with radius r (as a limiting case) shows no theoretical increase in solidification time and very little increase in practice, compared with a plate of wall thickness $w = r$. With a ratio of $d \varnothing / r \approx 0.65$ the increase in solidification time is a maximum. However, the larger the core diameter and the

thinner the surrounding iron wall, the more plate-like the tube wall becomes and the smaller the accumulation of heat: the solidification time again becomes shorter.

American measurements⁽⁴⁴⁾ gave a curve at about 60 to 75°C superheat which agrees very well, except for the zero point. Our own random sample measurements were also in excellent agreement with the calculated values, and have been plotted in Fig. 225. The experimental layout used for these measurements is shown in Fig. 226.

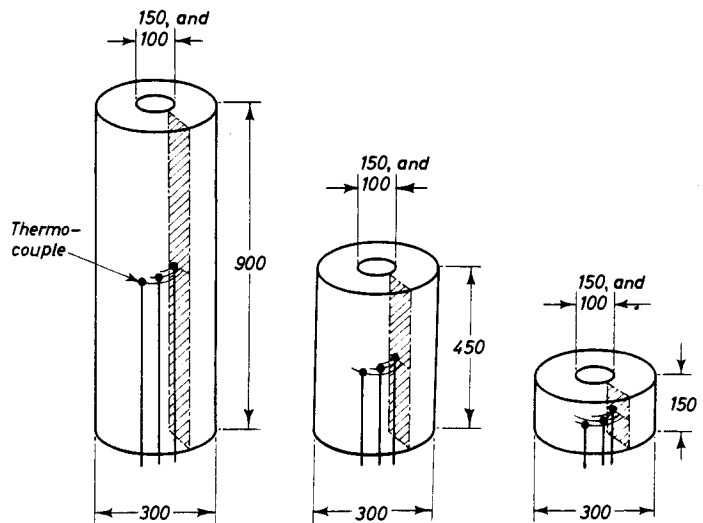


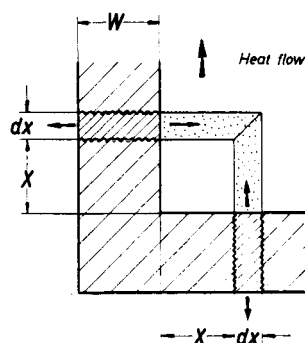
FIG. 226. Measurement of the solidification time of hollow cylinders. Arrangement of the thermocouple.

This measure of agreement makes it probable that the original assumptions on which the calculations were based were correct.

7.4.8. RETENTION OF HEAT IN JUNCTIONS

While the flow of heat from the region of stored heat can be neglected in closely adjacent plates and tubes, it must be taken into account in junctions. Only L-junctions can be calculated with reasonable accuracy from the stored heat alone, after making certain assumptions based on a heat flow model, while this method gives solidification times for T and + junctions which are too long.

In Fig. 227 a heat flow model is assumed for L-junctions with a wall thickness w , in which the direction of



$$\begin{aligned} \chi_1 &= n_1 \cdot W \\ \chi_2 &= n_2 \cdot W \dots \dots \end{aligned}$$

FIG. 227. Heat flow model of an L-junction.

flow is vertical to the walls. At a distance x the amount of heat contained in a plate element $w \cdot dx$ is opposite to the inside of a sand element in the form of a strip (here also termed the core) $x \cdot dx$.

The inside portion of the superheat ($S_i = S/2$) will first be conducted to the sand, as a result of which the sand element will be heated to a temperature $\tau_{core\ x}$; the core will then take up the heat of solidification until the temperatures are equalized.

If we substitute $x = n_x \times w$, the heat balance is expressed by:

$$\begin{aligned} S/2 &= w \times dx \times \gamma_{steel} \times C_{steel} \times S \\ &= \tau_{core\ x} \times C_{sand} \times \gamma_{sand} \times n_x \times w \times dx \end{aligned}$$

from which:

$$\tau_{core\ x} = 1.685 \times \tau_s \times 1/n_x \quad (85)$$

On absorbing the heat of solidification:

$$\begin{aligned} (\tau_x - \tau_{core}) \times C_{sand} \times \gamma_{sand} \times n_x \times w \times dx \\ = (\tau_{liquidus} - \tau_x) \times f_{steel} \times \gamma_{steel} \times w \times n_x \times 1/2 \end{aligned}$$

from which:

$$\tau_x = \frac{11250 + 0.416 \times 1.67 \times \tau_s}{7.45 + 0.416 \times n_x} \quad (86)$$

The value of τ_x determined in this way gives in equation (76) the proportion of heat of solidification ab-

sorbed, which is equal to the effective cooling portion of the core surface. These proportions, which are a function of the superheat and of the distance x (or $n_x \times w$) give parallel straight lines in Fig. 228, having a slope of $\tan \alpha = 2.71$.

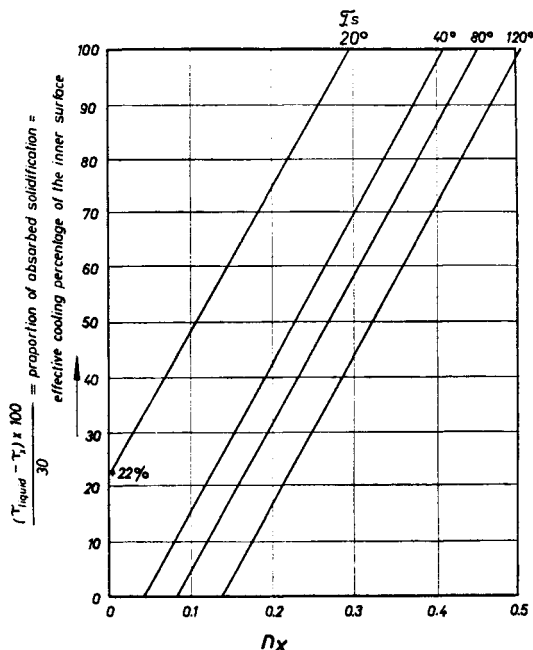


FIG. 228. Cooling effectiveness of the inner side of L-junctions at a distance n_x .

This diagram shows immediately at what distance x (or n_x) the cooling action is once more equal to 100 per cent i.e. the distance at which the heat storage region ends. At $\tau_s = 40^\circ\text{C}$ this region lies within $n_x = 0.42$ (with a wall thickness of 100 mm, for example, this would correspond to a distance of 42 mm from the inside edge of the junction). By simple trigonometrical calculation of the boundary lines it is possible to determine the mean effective surface area within the heat storage zone; the results are reproduced in Fig. 229.

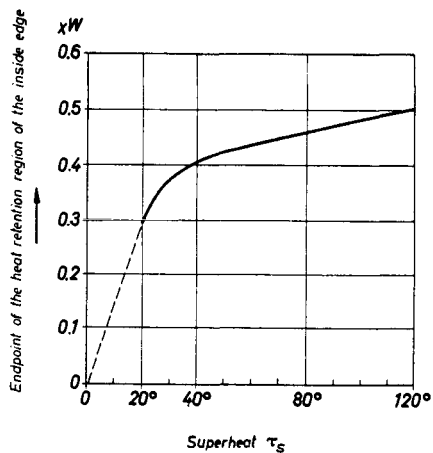


FIG. 229a. Limit of the region of heat retention in L-junctions.

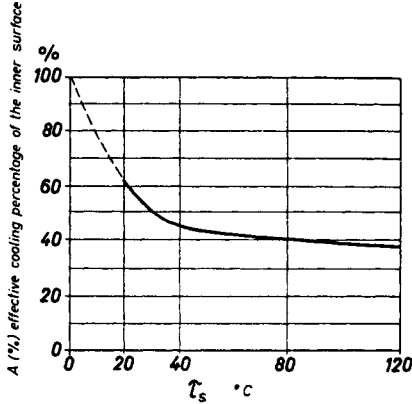
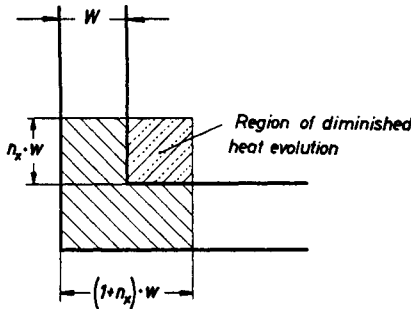


FIG. 229b. Mean cooling efficiency of the inner surface of L-junctions in the overall heat retention region.



F_{junction} in the heat retention region

$$F_K = (1 + n_x) \cdot W^2 + n_x \cdot W^2$$

Extent of heat evolution in the heat retention region

$$U_K = 2 \cdot (1 + n_x) \cdot W + 2 \cdot n_x \cdot W \cdot A$$

A—proportion of the effective inner cooling surface

FIG. 230. Geometry of the L-junction.

Figure 230 shows the geometry of L-junctions and the inside (geometrical) proportion of the surface area to the total volume. The thermally effective junction is limited to the heat retaining zone, as conditions similar to those obtained with a flat plate prevail outside this region.

The inside (geometrical) surface area of the junction must be reduced by the effective cooling factor A from Fig. 228, so that the corrected modulus becomes:

$$M_{L\text{-junctions}} = w \frac{1 + 2n_x}{2[1 + (1 + A) \times n_x]} \quad (87)$$

Figure 21 (page 11) shows these moduli for various casting temperatures; this diagram also provides the data required for the feeder calculation.

According to the fundamental Chvorinov equation (4), the solidification times T of two bodies 1 and 2 are

related by:

$$\left(\frac{T_1}{T_2}\right) = \left(\frac{M_1}{M_2}\right)^2 = f \quad (88)$$

where f is the prolongation factor of the solidification time.

The modulus of body 2, which in this case is a flat plate of thickness w , is

$$M_2 = w/2, \quad M_2^2 = w^2 \times 0.25$$

From this, and from Fig. 21 which gives the values of body 1 (of the junction), f (which is thus the increase in solidification time compared with that of a flat plate) is calculated, and is represented in Fig. 231. Experimentally

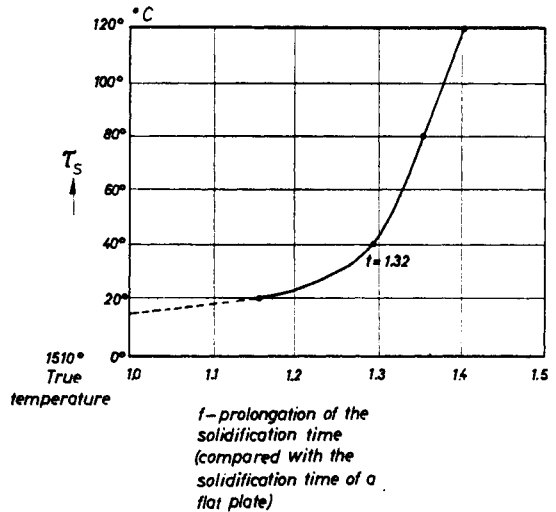


FIG. 231. Increase in the solidification time of L-junctions compared with flat plates of equal thickness.

determined points⁽⁴⁴⁾ were plotted in this diagram, and showed good agreement. The values from the calculated curve may be higher than the actual results; this can be attributed to the fact that the heat flow is not entirely negligible.

The cooling effect of the junction walls may also be of special importance, as these act as relatively thin cooling fins on the thick cross-section of the junction. The greater the difference in cross-section (or in modulus or in solidification time) the more marked the cooling effect becomes. This cooling action can only be calculated approximately at present, so that the accuracy obtainable is insufficient for the purpose, and heat retention calculations will not be given here for T and $+$ junctions. Measured values will be found in Figs. 19 and 20 (see page 10).

7.4.9. THE IMPORTANCE OF THE HEATING EFFECT IN FEEDER CALCULATIONS

(This section is of importance to the practical foundryman.)

The modulus and hence the solidification time of closely adjacent plates and of tubes is increased by the heating action or heat storage at the sand fillets; the

solidification time of the feeder head must also be correspondingly increased.

The empirical formula given by Nicolas⁽¹⁰⁾ for the modulus relationship is well known [see page 39]:

$$M_{\text{feeder}} \approx 1.2 \times M_{\text{casting}} \quad (89)$$

The starting point in determining the modulus is the geometry of the casting. This geometrical modulus can be physically increased by the heating effect, or—which gives the same result in the end—the compensating factor $f = 1.2$ of the above equation must be increased. Thus the simplicity of the geometrical modulus calculation is ensured even when allowance is made for the heating of the casting.

This compensating factor can be read off directly from Fig. 219 for closely adjacent plates, from Fig. 220 for tubes, and from Figs. 221–224 for rings. The simplicity of the method will be illustrated by two examples:

1. Let two plates ($w = 80$ mm) be separated by a thin core ($T = 40$ mm). The metal is to be cast as cool as possible, corresponding to about 1570°C in the ladle; allowing for a drop in temperature in the casting stream, this should give a temperature of 1550°C on entering the mould. It is required to determine the size of the feeder head.

Calculation of the geometrical plate modulus is very simple; it is $M = w/2$, so that $M = 8/2 = 4$ cm in this case.

The ratio $n = T/w = 40/80 = 0.5$ can be read off without calculation, similarly the compensating factor for the feeder head calculation, $f \approx 1.6$. The feeder modulus must therefore be $M_{\text{feeder}} = 1.6 \times M_{\text{casting}} = 1.6 \times 4 = 6.4$ cm.

In many cases the standardized feeder Tables 9–19 will be used; the following dimensions can then be read off without further calculation:

Round feeder head: $H = D \varnothing \approx 390$ mm

Round feeder head: $D \varnothing = 340$ mm;

$$H = 1.5 D \approx 520$$

Oval feeder head (elliptical section):

$$a = 315 \quad b = 472 \quad H = 394$$

$$a = 279 \quad b = 418 \quad H = 524$$

$$a = 274 \quad b = 548 \quad H = 411$$

$$a = 243 \quad b = 486 \quad H = 548$$

Blind feeder heads:

$$D \varnothing = 345 \quad H = 520$$

$$D \varnothing = 310 \quad H = 620$$

The large number of equally effective standard feeder heads which are possible shows clearly that this method is not rigid, but is very flexible in fulfilling practical requirements (most favourable placing of the feeder head, allowing for the box height and lateral position in the casting box).

2. A fireclay core is to be placed in a tubular body (high wheel hub $D \varnothing = 240$, $w = 80$, $d = 80$, height $H = 400$). The casting temperature, as before, is to be

1550°C in the mould. Because tubes are curved plates, the geometrical modulus can easily be established, $M = w/2$, or $M = 4$ cm in this case.

The compensating factor of 1.32 can be read off without further calculation from Fig. 218. The feeder modulus must therefore amount to $M_F = 1.32 \times 4 = 5.28$ cm. As in the first example, the feeder head dimensions can then be read off directly from the tables:

Round feeder head $H = D \varnothing = 315$ mm,

Wt. = 170 kg

Round feeder head $D \varnothing = 280$, $H = 420$ mm,

Wt. = 180 kg, etc.

Feeder heads calculated in this way combine maximum efficacy with maximum economic efficiency. Instead of these feeders exothermic feeder heads can be selected, the dimensions of which can also be read off directly.

EXAMPLE

The hub mentioned above, with $M_{\text{geometrical}} = 4$ cm, weighs 125 kg; to this must be added every part (≈ 40 kg) of the wheel disc which is fed from the hub, so that a total weight of 165 kg is to be fed.

The correction factor for the geometrical modulus can be read off directly from Fig. 220; it amounts to 1.10, so that the true modulus $M_{\text{feeder}} = 4 \times 1.1 = 4.4$ cm. From the diagrams for exothermic sleeve feeders an exothermic sleeve of the following dimensions can be derived without calculation: internal diameter = 170 mm, height = 240 mm, wall thickness = 35 mm.

Figures 219–224 show very clearly the strong influence of casting temperature. Taking the example mentioned above of the hub, a compensating factor of $f = 1.425$ is obtained at 1630°C , corresponding to a feeder modulus of $M_F = 1.425 \times 4 = 5.70$ cm, requiring one of the following round feeder heads:

Round feeder head $H = D \varnothing = 345$ mm,

Wt. = 218 kg

Round feeder head $D \varnothing = 308$, $H = 460$ mm,

Wt. = 240 kg

These feeder heads are larger and much heavier than before. Various cases of scrap due to the formation of shrinkage cavities with unnecessarily high superheat can now be explained. Understandably it is not unusual when this happens to go to the other uneconomic extreme and increase the feeders to far beyond the correct dimensions. Both errors can be avoided if the true casting temperatures are prescribed, at least approximately, and maintained.

7.4.10. APPROXIMATE HUB CALCULATIONS

IMPORTANT FOR PRACTICE

The results so far obtained and the examples given in the previous sections enable very accurate calculations to be made. These in turn enable the limits of validity for use in works practice to be laid down. It was mentioned on page 7 that if the core diameter d was less than ~ 0.27 – $0.3 D$, the hub modulus can be calculated

as for a solid cylinder. This also allows with safety for the effects of high casting temperatures. Moreover, hubs are normally massive bodies or sections of castings. The necessary compensating factor in the feeder calculation need only be $f \approx 1.1$, because of the solidification geometry. As, however, a factor of $f=1.2$ is always used in practice, this also constitutes a considerable additional measure of safety.

7.4.11. SPECIAL FEATURES OF THE HEATING EFFECT IN THE PLACING OF BLIND FEEDER HEADS

IMPORTANT FOR PRACTICE

As shown in Fig. 203, sand fillet effects, i.e. gas penetration, often occur at the ingates of blind feeders. The sand tongue between the feeder and the casting is geometrically not simple. However, it can be treated approximately at the critical (narrowest) positions as a flat sand plate, so that the feeder (ingate) can first be simulated by a plate having the same solidification period. The modulus of the feeder head ($M_{feeder} = 1.2 \times M_{casting}$) is known, and hence the thickness w of the simulation plate.

$$M_{plate} = w/2, \text{ from which:}$$

$$w = 2 M_{simulation\ plate} = 2 M_{feeder}$$

$$= 2 \times 1.2 \times M_{casting} = 2.4 M_{casting} \quad (90)$$

The length of the feeder ingate should be so selected that no undesired gas penetration occurs. The compensating factor should not therefore exceed 1.2 in any circumstances. Consequently the ratio $n = \text{sand thickness/plate thickness} = T/w$ can be read off directly from

Fig. 217 for various superheats. For example,

at 1550°C $n = T/w = 0.8$ and $T = 0.8 w$

at 1590°C $n = 0.9$ $T = 0.9 w$

and for the most usual superheat of about 100°C:

1630°C $n = 1.0$ $T = w$

Hence the most suitable feeder distance T is obtained from equation (90):

$$T = w = 2.4 \times M_{casting} \quad (91)$$

EXAMPLE

Plate-like casting 60 mm thick

$$M_{casting} = 6/2 = 3 \text{ cm}$$

Feeder distance $T = 2.4 \times 3 = 7.2$ cm at the narrowest point.

or:

The calculation of another casting has given a feeder modulus $M_F = 5$ cm. The feeder distance according to equation (90) should therefore be $T = 2 M_F = 10$ cm.

The opinion is often expressed that the feeder ingate could be made thinner because of the above-mentioned heating effect. The danger of this in practice must be pointed out forcibly, because the heating effect fluctuates very strongly with the amount of superheat. The steel temperature cannot be adjusted so accurately that the heating effect and hence the desired reduction in the ingate section can be kept constant. Only a negligibly small saving in steel can be achieved by such a reduction, which cannot in any way be set against the increased risk of scrap arising from shrinkage cavities.

CHAPTER 8

INCREASING THE THERMAL GRADIENT BY EXTERNAL COOLING (IRON CHILLS)

8.1. The Formation of Artificial End Zones by the Use of Chills

IMPORTANT FOR PRACTICE

Because of its cooling action solidification begins earlier at the surface of application of a chill than in the adjacent cross-section. The solidification front will therefore advance at this position, i.e. it will be "dished" (Fig. 232). The solidification wedge produced in this way is equivalent, according to Pellini⁽²¹⁾, to the solidification wedge of a natural end zone (see Chapter 3), so that an artificial end zone is formed by placing chills between two feeder heads (Fig. 233). As a rough guide it is true to say that each chill replaces a feeder. As, however, end zones are longer than feeder zones, the actual relationships are more favourable. The savings in feeder metal

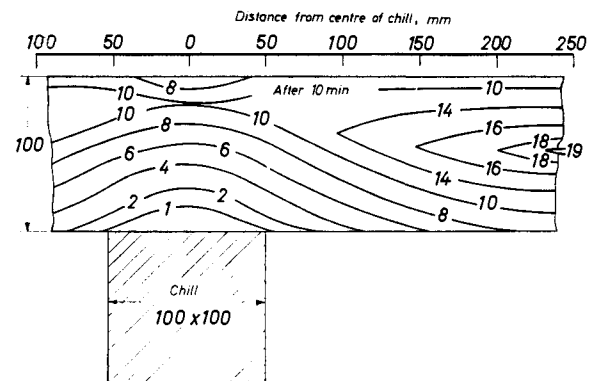


FIG. 232. Advance of the solidification front and its constriction near the chill⁽²¹⁾.

as for a solid cylinder. This also allows with safety for the effects of high casting temperatures. Moreover, hubs are normally massive bodies or sections of castings. The necessary compensating factor in the feeder calculation need only be $f \approx 1.1$, because of the solidification geometry. As, however, a factor of $f=1.2$ is always used in practice, this also constitutes a considerable additional measure of safety.

7.4.11. SPECIAL FEATURES OF THE HEATING EFFECT IN THE PLACING OF BLIND FEEDER HEADS

IMPORTANT FOR PRACTICE

As shown in Fig. 203, sand fillet effects, i.e. gas penetration, often occur at the ingates of blind feeders. The sand tongue between the feeder and the casting is geometrically not simple. However, it can be treated approximately at the critical (narrowest) positions as a flat sand plate, so that the feeder (ingate) can first be simulated by a plate having the same solidification period. The modulus of the feeder head ($M_{feeder} = 1.2 \times M_{casting}$) is known, and hence the thickness w of the simulation plate.

$$M_{plate} = w/2, \text{ from which:}$$

$$w = 2M_{simulation\ plate} = 2M_{feeder}$$

$$= 2 \times 1.2 \times M_{casting} = 2.4 M_{casting} \quad (90)$$

The length of the feeder ingate should be so selected that no undesired gas penetration occurs. The compensating factor should not therefore exceed 1.2 in any circumstances. Consequently the ratio $n = \text{sand thickness/plate thickness} = T/w$ can be read off directly from

Fig. 217 for various superheats. For example,

at 1550°C $n = T/w = 0.8$ and $T = 0.8 w$

at 1590°C $n = 0.9$ $T = 0.9 w$

and for the most usual superheat of about 100°C:

1630°C $n = 1.0$ $T = w$

Hence the most suitable feeder distance T is obtained from equation (90):

$$T = w = 2.4 \times M_{casting} \quad (91)$$

EXAMPLE

Plate-like casting 60 mm thick

$$M_{casting} = 6/2 = 3 \text{ cm}$$

Feeder distance $T = 2.4 \times 3 = 7.2$ cm at the narrowest point.

or:

The calculation of another casting has given a feeder modulus $M_F = 5$ cm. The feeder distance according to equation (90) should therefore be $T = 2 M_F = 10$ cm.

The opinion is often expressed that the feeder ingate could be made thinner because of the above-mentioned heating effect. The danger of this in practice must be pointed out forcibly, because the heating effect fluctuates very strongly with the amount of superheat. The steel temperature cannot be adjusted so accurately that the heating effect and hence the desired reduction in the ingate section can be kept constant. Only a negligibly small saving in steel can be achieved by such a reduction, which cannot in any way be set against the increased risk of scrap arising from shrinkage cavities.

CHAPTER 8

INCREASING THE THERMAL GRADIENT BY EXTERNAL COOLING (IRON CHILLS)

8.1. The Formation of Artificial End Zones by the Use of Chills

IMPORTANT FOR PRACTICE

Because of its cooling action solidification begins earlier at the surface of application of a chill than in the adjacent cross-section. The solidification front will therefore advance at this position, i.e. it will be "dished" (Fig. 232). The solidification wedge produced in this way is equivalent, according to Pellini⁽²¹⁾, to the solidification wedge of a natural end zone (see Chapter 3), so that an artificial end zone is formed by placing chills between two feeder heads (Fig. 233). As a rough guide it is true to say that each chill replaces a feeder. As, however, end zones are longer than feeder zones, the actual relationships are more favourable. The savings in feeder metal

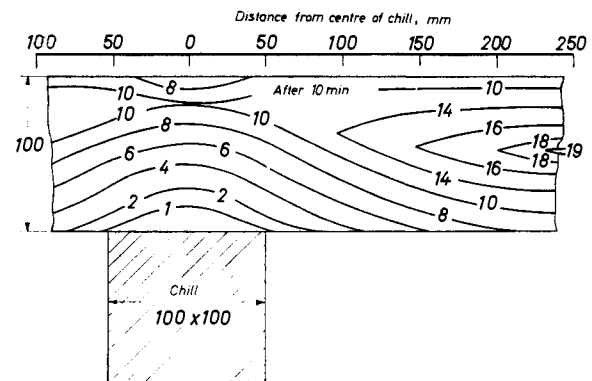


FIG. 232. Advance of the solidification front and its constriction near the chill⁽²¹⁾.

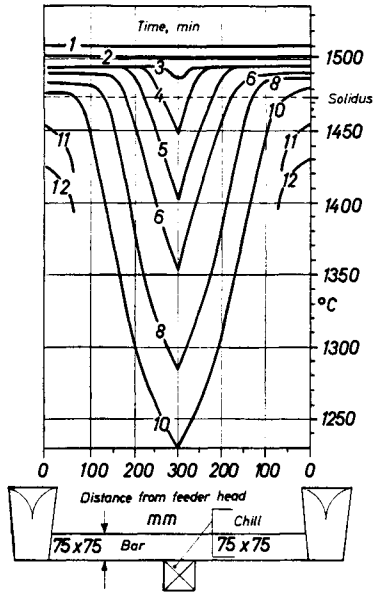


FIG. 233. Artificial end zone formed by placing a chill on a bar⁽²¹⁾.

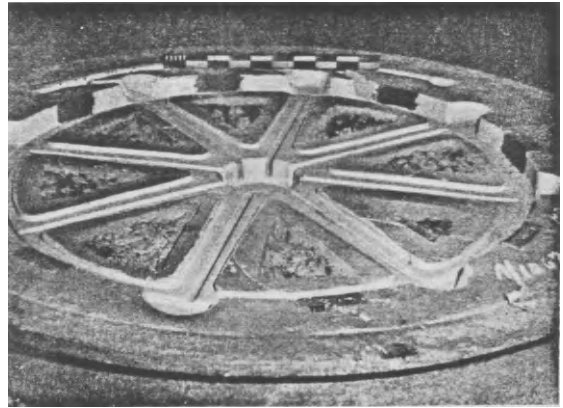


FIG. 235. Mould of a wheel with artificial end zones between the spokes.

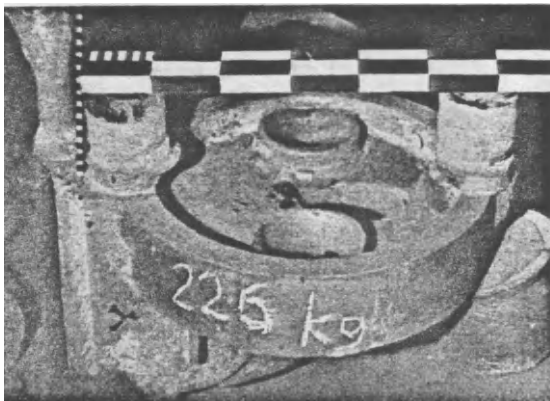
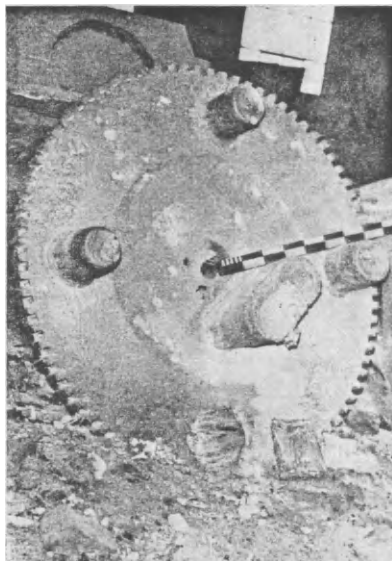
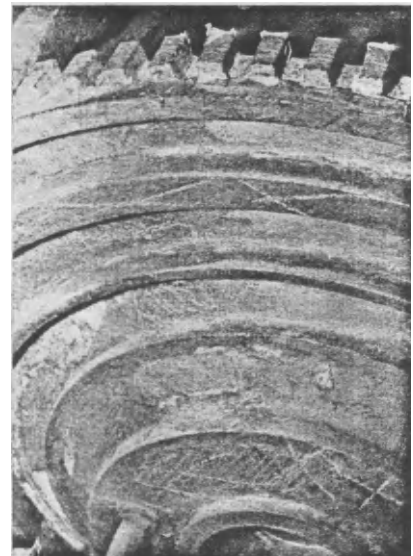


FIG. 234. Turntable with artificial end zones and exothermic feeder heads.



a



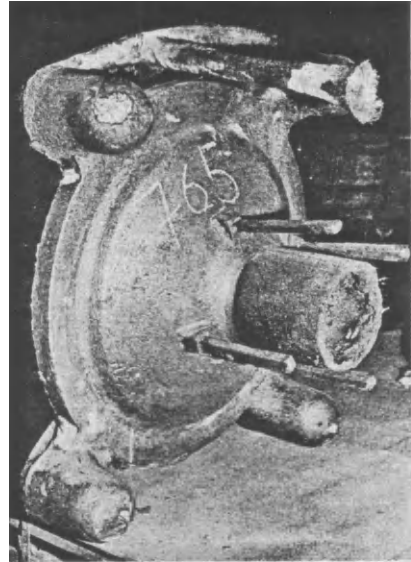
b

FIGS. 236a-c. Gear coupling disc with blind feeder heads and artificial end zones.

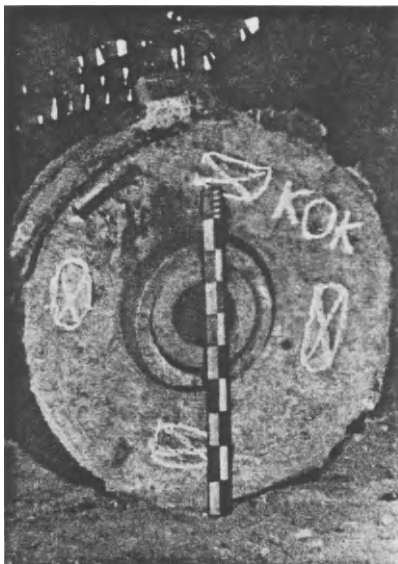
c



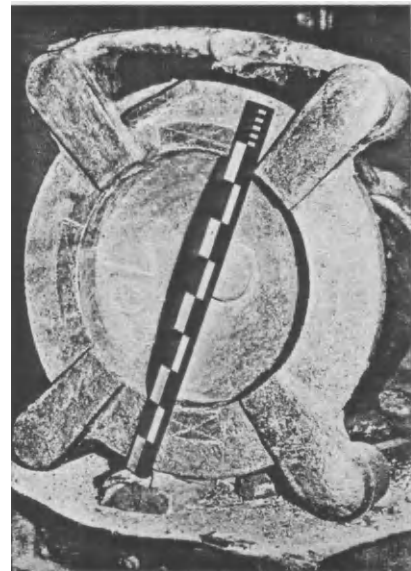
a



a



b



b

FIGS. 237a and b. Coupling boss with blind feeder heads and artificial end zones. Side boss feeder.

FIGS. 238a and b. Piston cover with atmospheric feeder heads and artificial end zones.

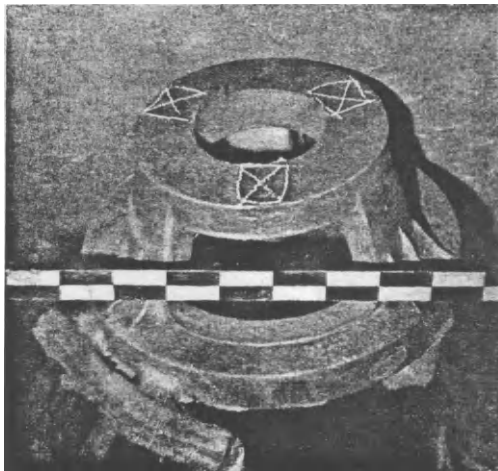


FIG. 238c

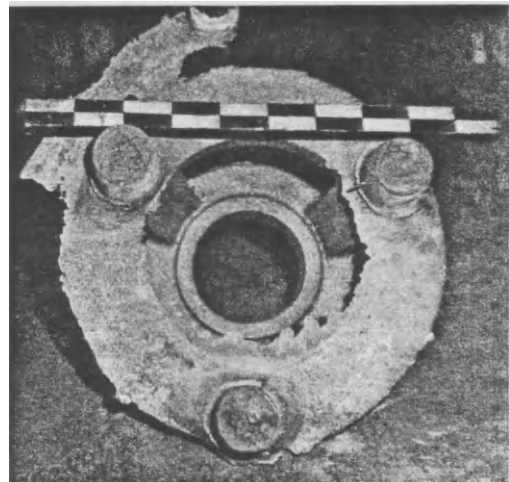
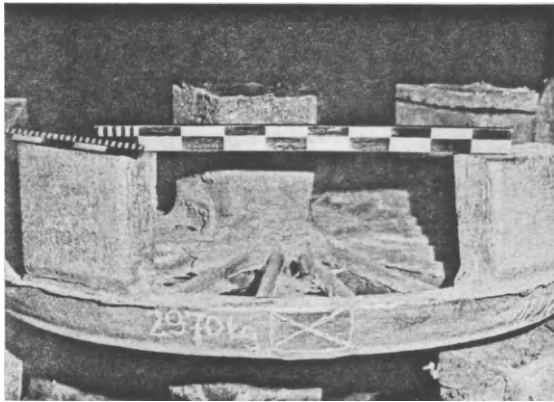


FIG. 238d



a



b



c

FIGS. 239a and b. Locomotive wheel centre. (a) without and (b) and (c) with artificial end zones. With this order alone the method used in (b) and (c) gave a saving of £ 2500 in melting costs.

are substantial. Examples are shown in Figs. 234–239.

Artificial end zones on plates, which are formed by placing a chill between two feeder heads, are longer by about 50 mm than the natural end zones according to Fig. 48 (page 20) because of the steeper thermal gradient. Consequently, the values derived from Fig. 48 are increased by about 50 mm, irrespective of the plate thickness. (To increase the chance of success the author refrains from making use of this addition in most cases. This does not imply any doubt that the above-mentioned addition of 50 mm is correct, but experience has shown that the moulder often does not place the chills exactly at the correct position, but displaces them somewhat to one side. It is always a good thing to have something in reserve in such cases.)

The elongation of the end zone by chills is also found in the case of bars, but it is very slight, and is again ignored on safety grounds.

According to Pellini⁽²²⁾ the thermal gradient and hence the feeding range can be increased still further in bronze castings by applying wedge chills (Figs. 240, 241 and 242). Long wedge chills are not employed with steel

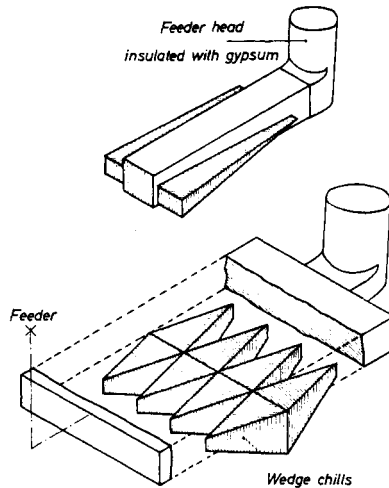


FIG. 240. Cooling cast gunmetal bars and plates with double-tapered wedge chills (after Pellini)⁽²²⁾.

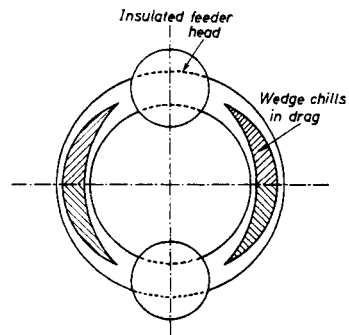


FIG. 241. Placing wedge chills on a cast gunmetal ring (after Pellini)⁽²²⁾.

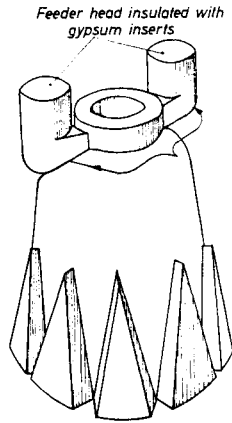


FIG. 242. Placing wedge chills on a cast gunmetal cylinder (after Pellini)⁽²²⁾.

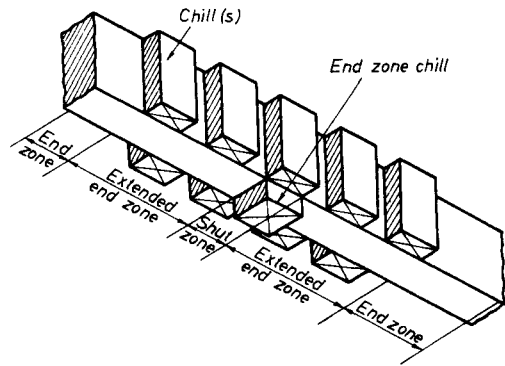


FIG. 244b. End zone prolonged in stages by placing chills on three sides of a bar.

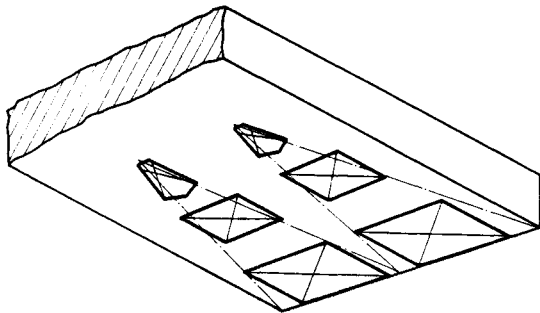


FIG. 243. Distribution of large wedge chill areas on steel castings.

castings, however, because of the risk of cracking, and the wedges must be subdivided as shown in Fig. 243.

The author used a similar method with success several years ago, in which the artificial end zones are lengthened in stages by applying chills to plates and bars on two or three sides (Figs. 244 and 245). Some surprising possibilities are illustrated in Figs. 246–251.

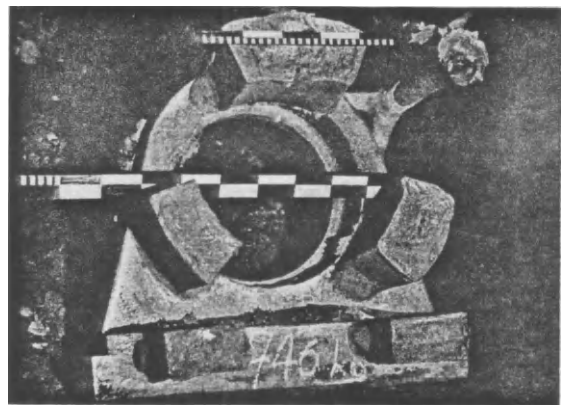


FIG. 245a. Original method of moulding a housing. Heavy penetration of steel into the core.

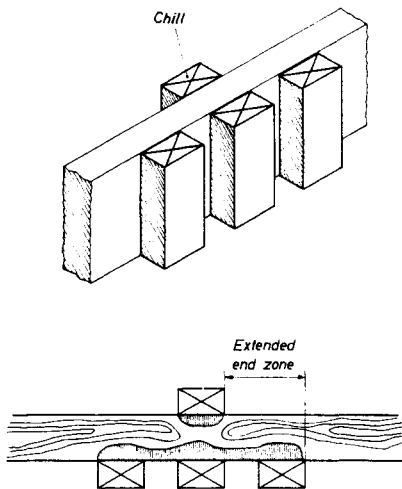


FIG. 244a. The artificial end zone can be extended by means of chills placed on two sides.

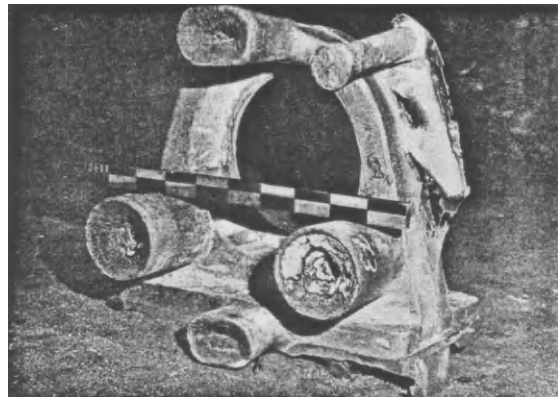
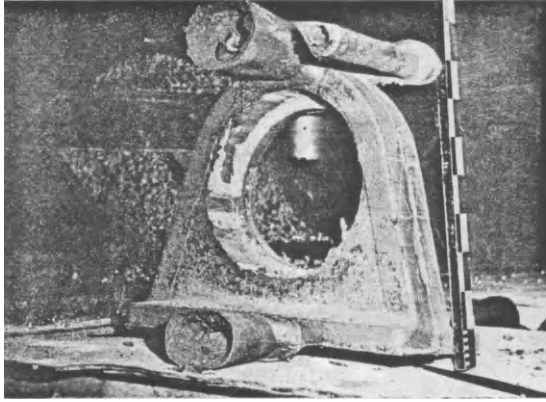


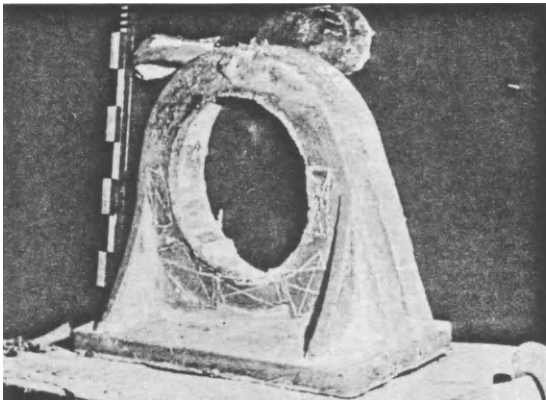
FIG. 245b. Improving the method of moulding by rounded feeder head and utilization of natural end zones on the flange.



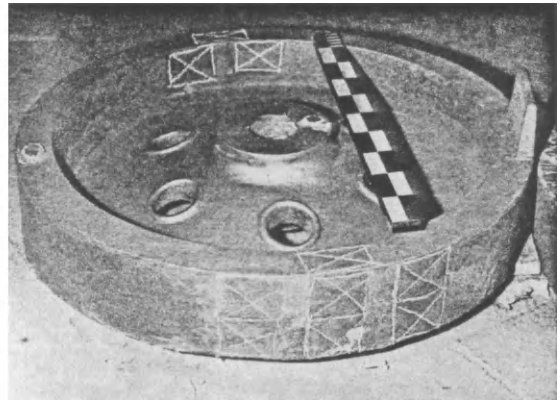
c



a



d



b

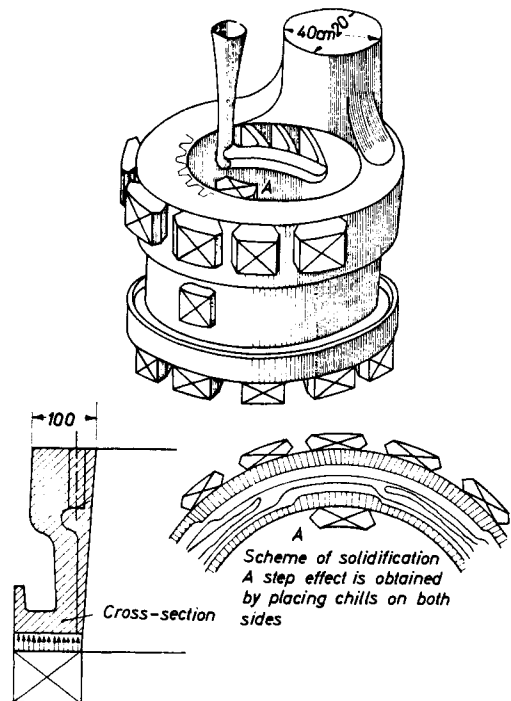
FIG. 245 c and d. Cooling the ring by means of extended end zones, thereby eliminating the hot spot in the core and the associated penetration of steel.

FIGS. 247 a and b. Gear blank with only two rim feeder heads with shoulders and with extended artificial end zones. Boss feeder on one side.



FIG. 246 a. Boss with internal gear, fed with only one feeder head and extended artificial end zones.

FIG. 246 b. Thick-walled coupling collar with internal gear, fed by only one feeder head.

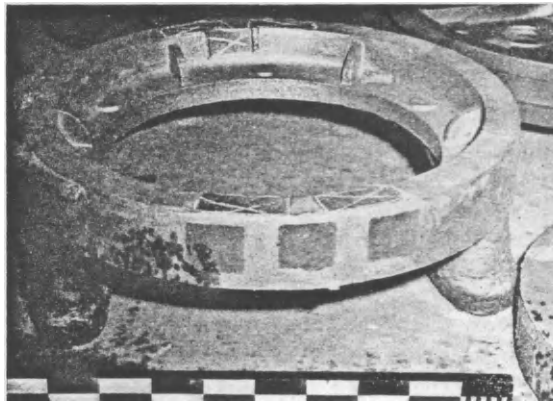




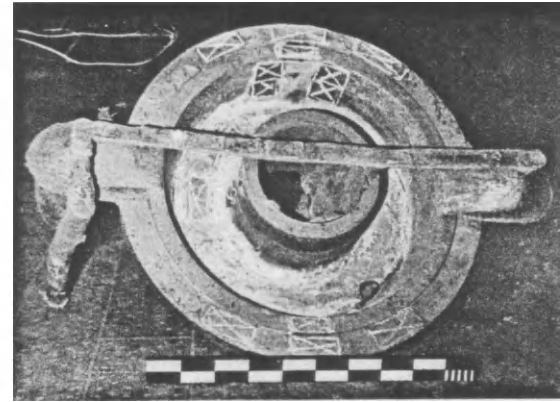
a



a



b



b

FIGS. 248a and b. Gear rim with two rim feeder heads. Effective range increased by shoulders. Extended artificial end zones.

FIGS. 250a and b. Brake drum. Atmospheric feeder head and artificially extended end zones at the flange. Boss feeder on one side and artificial end zone on the boss.

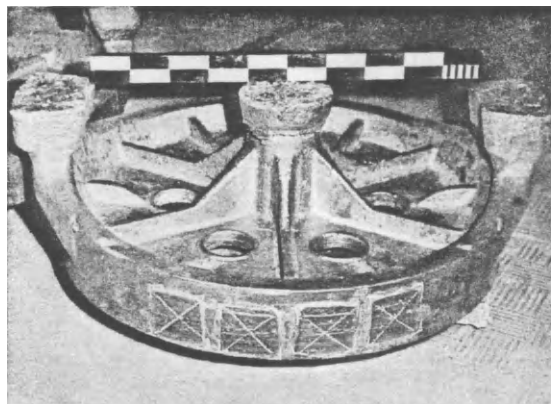


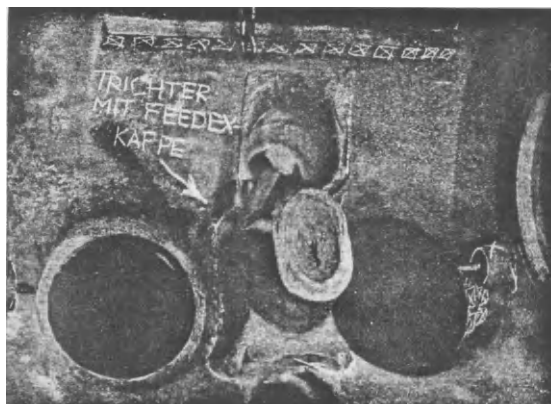
FIG. 249. Crane wheel with extended artificial end zones and feeder heads, the effective range of which was increased by shoulders.



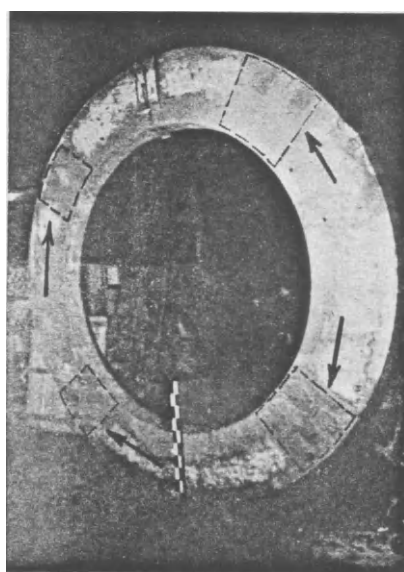
FIG. 251a



b



a



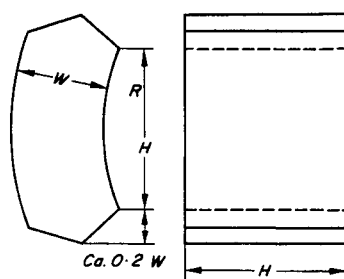
c



b

FIGS. 252a and b. End zones on turbine housing flanges extended by chills. Fed by central feeder head with exothermic cap. (By courtesy of Sulzer Bros. AG, Winterthur, Switzerland.)

FIGS. 251a-c. 12-t ring casting with extended end zones, ultrasonically sound. Fed by 4 exothermic feeder heads (see Chapter 12), yield 91%.



If round bodies are classified into groups according to diameter, and designated by *A, B, C*, etc., the chills can be standardized. *D 60*, for example, indicates a chill 60 mm thick, which can be applied from outside or inside or below, to all round castings with diameters ranging from 900–1300 mm (Fig. 252). The dimensions of the chills, based on practical experience, are given in Table 26.

TABLE 26. PRINCIPAL DATA OF STANDARD CHILLS

Mark	R	Applicable for diameters		W	H	Area ca. cm ²	Weight kg
		from	to				
A	∞	130	∞	60	130	166	9.75
B	800	680	1300	60	120	146	9.15
C	550	420	680	60	100	99.8	6.3
D	350	280	420	50	90	78.3	4.5
E	250	220	280	50	80	62	3.45
F	190	160	220	40	70	49	2
G	140	120	160	40	60	35	1.4
H	100	175	250	25	50	25	0.7
J	70	118	175	25	50	19	0.5
K	50	90	118	20	40	15	0.34
L	40	70	90	15	30	8	0.14

Example: Notation for a standard chill to be placed on a wheel rim of 970 mm diameter will be: *B 60*.

8.2. Measures Against Cracking Taken by the Use of Chills. Cooling of Junctions

IMPORTANT FOR PRACTICE

Hot tears in castings are produced at those positions which remain hot longer than adjacent cross-sections. While the cross-sections which have already solidified undergo a thermal contraction, the elongation and tensile strengths of the solid casting are still insufficient to withstand the stresses imposed upon them and hot tears are produced. By placing chills the cooling of such thick-walled positions is accelerated, and equalized with that of the thinner adjacent sections, thus reducing the risk of hot tears.

FIG. 253a. Some common standard chills.

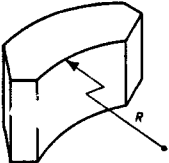
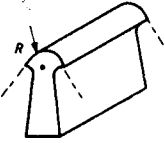
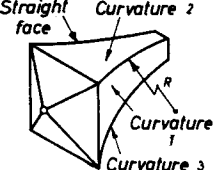
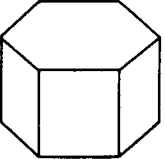
	<p>Chill with various contact radii according to Table 26.</p>
	<p>Fillet chills. This type has a larger heat-storage capacity than, for example, a circular chill, and so has less tendency to weld up, particularly with massive junctions.</p>
	<p>Wedge chills. By attaching wedge-shaped "cooling pads" the risk of cracks forming between the chills is lessened. Each of the four surfaces of contact has a different radius of curvature, making the chills universally applicable.</p>
	<p>Hexagonal chill for absorbing larger amounts of heat from massive castings.</p>



FIG. 253b. Common types of standard chill.

Hollow channels at junctions are especially dangerous in this respect, and the use of (standardized) chills as shown in Fig. 253 counteracts the hot spot caused by the sand fillet effect; by forming a solidified surface zone the danger of cracking can be minimized (Fig. 254). The formation of a shrinkage cavity in the hot centre of the junction cannot always be prevented in this way, but can usually be made more or less harmless.

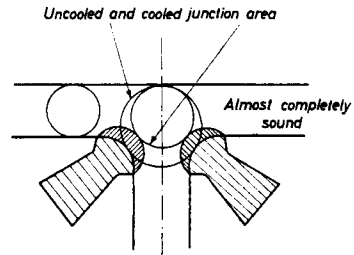


FIG. 254. By the use of fillet chills the uncooled junction circle should be reduced only to a diameter corresponding to that of the wall circle. The risk of cracking is reduced by eliminating the hot spot.

Figures 255–257 show arrangements of chills and cooling patterns at intersections with the aim of inhibiting the formation of shrinkage cavities. L- and T-junctions can be made satisfactorily sound; this can only be

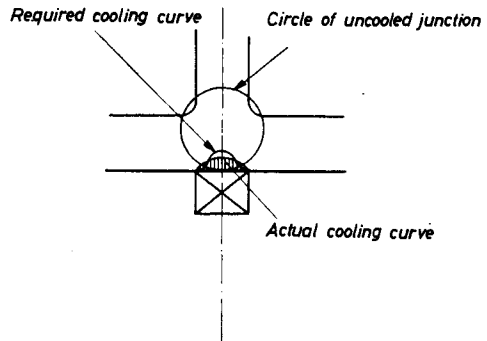


FIG. 255a. Cooling a T-junction by means of an end chill.

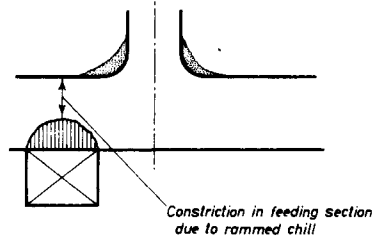


FIG. 255b. Casting sound junction and reducing risk of tears by using extended chills. Defects caused by external chills on junctions.

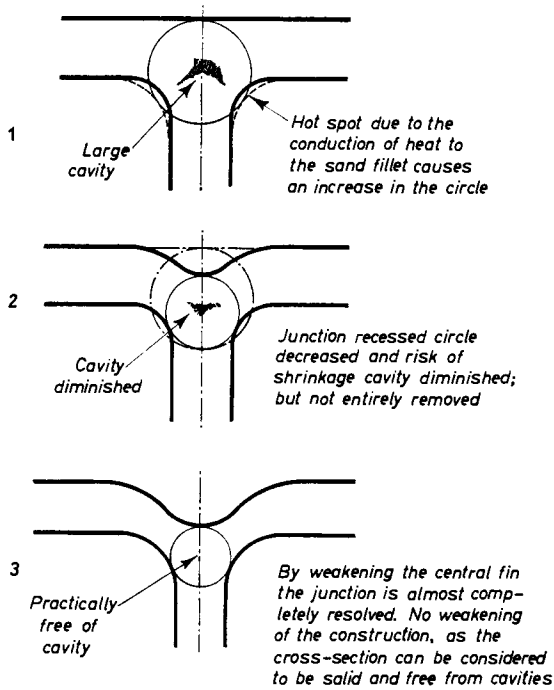


FIG. 255c. Resolving T-junctions

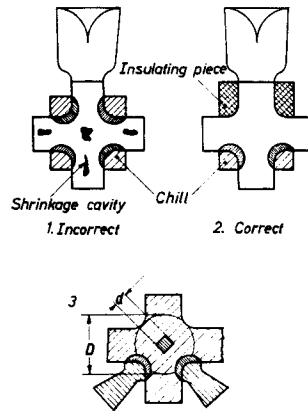


FIG. 256b. Making sound cross castings.

The residual cavity has no significant effect on strength. Cross + junction (3) usually found in association with wells. 2. Making reliably sound junction, after Krestschanovski⁽²³⁾. By calculating internal chills (Chapter 11) together with the use of (external) chills these sections can also be made satisfactorily sound.

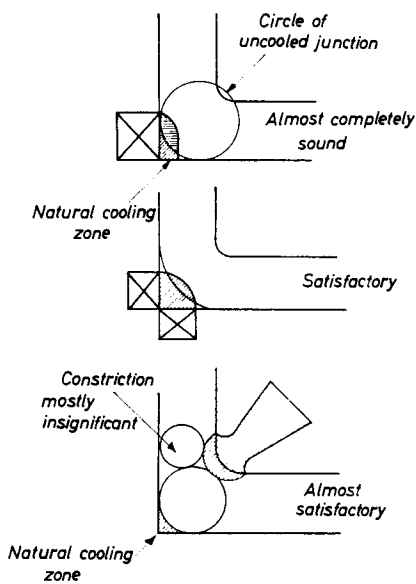
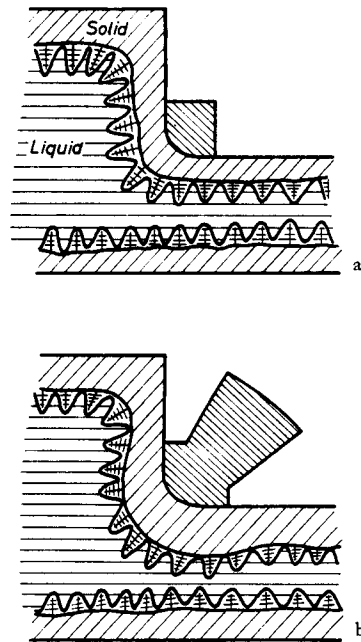


FIG. 256a. Alternative methods of cooling L-junctions by means of chills.



FIGS. 257a and b. Attaching fillet chills so as to reduce the risk of hot tears.

Fillet chill with a low heat-storage capacity. It can prevent the sand fillet effect to some extent, but frequently fuses on to the casting due to high thermal stresses.

Improved fillet chill with a high thermal capacity. Does not fuse on, constitutes a more intensively solidified zone than the adjacent section, and fundamentally improves the feeding conditions at the change of section.

Figs. 257c, d and e. Use of fillet chills.

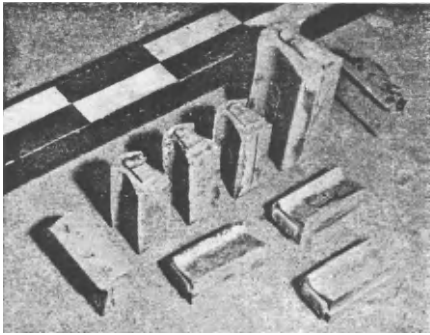


FIG. 257c. Various correctly designed fillet chills.



FIG. 257d
(Courtesy Sulzer Bros.)

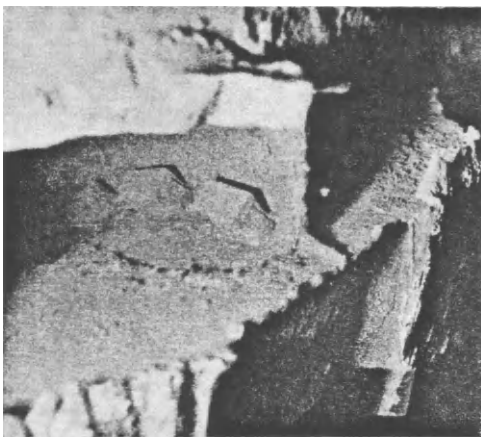


FIG. 257e

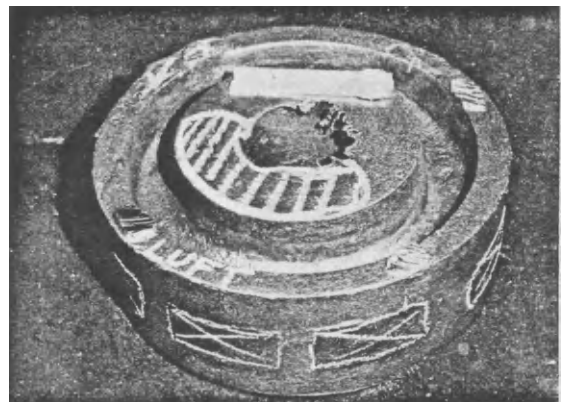
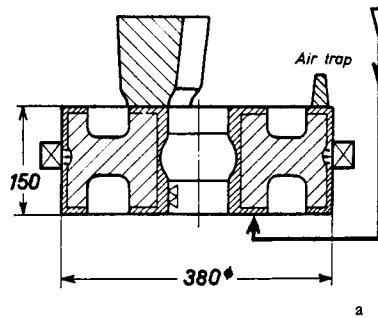
Figs. 257d and e. Use of fillet chills to produce sound joints. Flange/blade in turbine rotors.

achieved at + junctions by the use of insulating pieces⁽²³⁾ or internal chills. However, the residual cavity does not impair the strength of intersections cooled on four sides, because the cavity is formed in the neutral axis.

It is especially important with external chills at T-junctions that the chills are not rammed as in Fig. 255c, but must be placed at the correct position. The patterns must be accurately dimensioned, as junctions are usually formed by fitting cores later, so that the position of the junction cannot be seen from outside by the moulder. The dimensioned patterns are then marked out with an indelible colour (not with chalk!).

The method shown in Fig. 255c is safer, where junctions are resolved by retracted walls. If this is practicable in specific cases from the point of view of moulding technology, consultation with the engineer is recommended. Occasionally very unfavourable + junctions can be resolved to T-junctions, the T-junctions being made safe by the methods shown. Considerable increases in strength are possible by this technique.

The connection wheel rim-wheel disc also represents a junction. With a suitable disc thickness the feeder head to the rim can be omitted (Fig. 258) if the junction is cooled as shown.

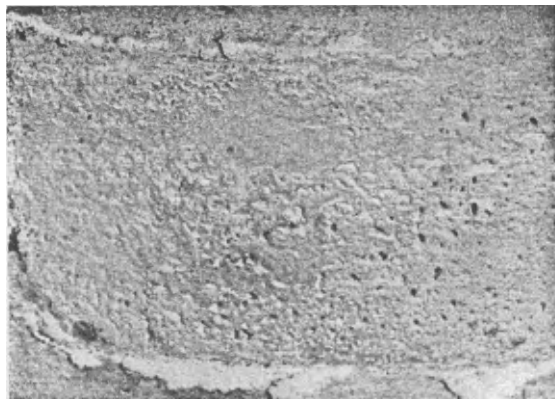


Figs. 258a and b. Junction wheel disc-wheel disc cooled by chills. The whole wheel is fed by a simple side feeder head.

8.3. Porosity at the Point of Attachment of Chills

8.3.1. POROSITY CAUSED BY CHILLS

If "worm holes" occur at the surface of contact (Fig. 259) and are driven deep into the casting as elongated blow holes, the cause can be porosity of the chill-



a



b

FIGS. 259a and b. A test was carried out by placing a shot blasted and a scaled chill on the same casting. The gases at the scaled chill led to the formation of wormholes on the surface of the casting. The pores were up to 40 mm deep

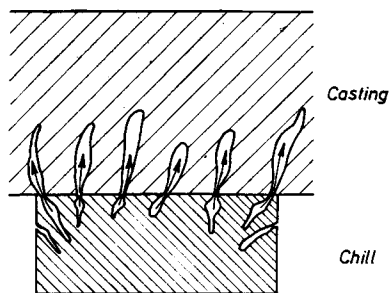
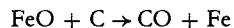
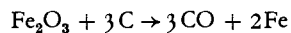


FIG. 260. The air in the pores of the chill expands in contact with the liquid steel and forms blowholes extending far into the casting.

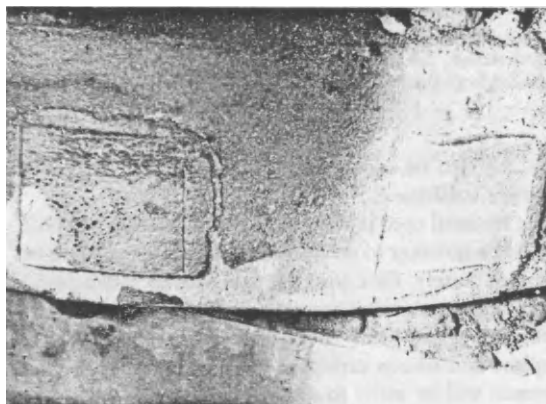
itself (Fig. 260). The air entrapped in the chill surface expands considerably in contact with the liquid steel and penetrates into the casting. Another very frequent cause of porosity is a residue of rust or scale on the surface of the chill, which reacts with the carbon in the steel according to:



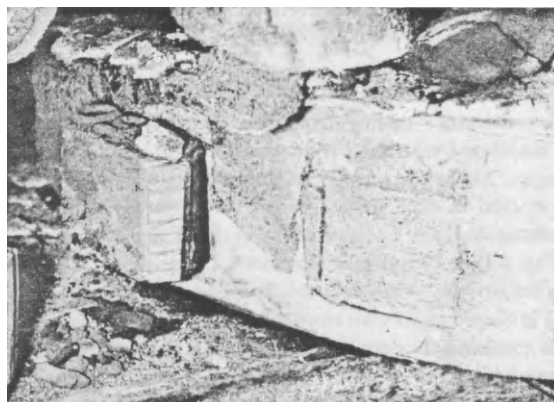
or



so that locally refined, low-carbon steel is formed. Because such steels are readily welded, the chills often become welded on at these positions (Fig. 261) which should always act as a warning signal.



a



b

FIGS. 261a and b. Welded-on chills often signify unsatisfactory cleaning of the chills, leading to porosity.

Because of the air gap which is formed, the chills become scaled to a greater or lesser extent each time they are used, and they must be sand blasted after each operation. Tumbling is not sufficient, as the scale is only polished without being removed. Large chills can be ground clean. The bright surface is then protected against further rusting by applying a coat of varnish (before ramming into the mould). Because they evolve gas, tar lacquers are not as satisfactory as aluminium bronze, such as is used for "silvering" furnace tubes, etc., and which is suspended in an alcoholic solution of resin in the proportion of 1 : 5 to 1 : 8.

As chills must not be made as low-grade, defective castings, they must be fed methodically. Figure 262 shows a chill layout forming a stepped wedge which can be fed by a single feeder head. Individual chills or a line of

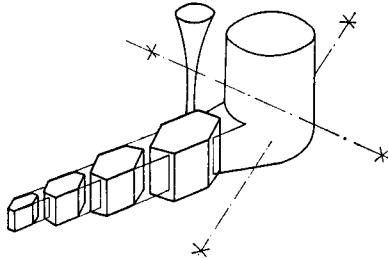


FIG. 262. Chills of different sizes can be cast together to form a stepped strand. Each strand represents a stepped wedge which can be fed from a single head. Several such strands can be attached to one feeder head.

chills can also be added to other castings, according to the space available.

The material used is steel, as high in carbon as possible so as to be resistant to wear; such steel chills can often be used indefinitely. Cast iron has not proved satisfactory, as oxidation penetrates into the interior along the graphite plates and leads to porosity after repeated use. Graphite and silicon carbide can also be used for chills; reference will be made to this later.

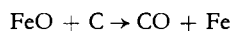
8.3.2. AIDS IN RECOGNIZING POROSITY ARISING FROM THE MOLTEN STEEL

IMPORTANT FOR PRACTICE

A satisfactory casting technique and first-class metal are associated with the production of good quality steel castings. Defects arising from steel quality are often not recognized as such, and a misdirected attempt is made to eliminate them by improved moulding techniques.

The author found that porosity in steel castings (except for cavities or micro-porosity associated with shrinkage) is caused mainly by oxygen⁽²⁴⁾, so that it disappears with a satisfactory deoxidation treatment (the addition of aluminium).

During solidification the residual liquid between the crystallites becomes enriched in ferrous oxide and carbon as a result of segregation processes. This residual liquid steel is displaced towards the interior during slow solidification, and equalization of composition with consequent dilution of the harmful impurities is possible. With rapid solidification segregation is accelerated, the residual liquid is trapped by the quickly growing dendrites and the equalization of composition by diffusion becomes more difficult. The reaction:



commences, and peripheral blowholes (pinholes) are formed at positions where solidification is rapid.

All such locations (edges, corners, thin plates, etc.), are particularly exposed to this danger with insufficiently deoxidized steel, because their rate of solidifica-

tion is $\sqrt{2} = 1.41$ times greater than at the remaining positions (Fig. 263).

The rate of solidification at chill surfaces is about twice the rate at a corresponding area of sand (Figs. 264 a-b),

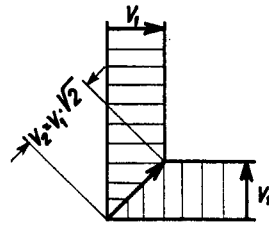


FIG. 263. More rapid growth of the solidified layers on the corners of a casting.



a



b

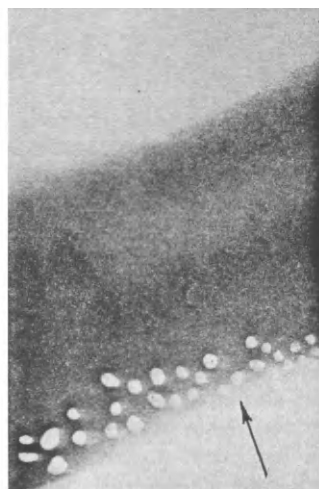
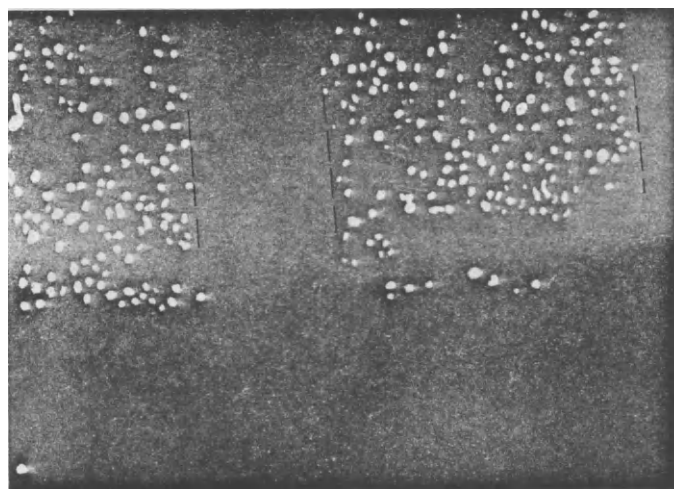
FIGS. 264 a and b. When the steel melting practice is unsatisfactory, porosity occurs preferentially at all positions with a higher solidification rate, such as fins, fillets, pattern numbers, etc.

so that sharply defined zones of porosity can also be formed at these positions (see the radiographs illustrated in Figs. 265 a-b).



FIG. 265 a. Sharply delineated zone of porosity under a ring chill. Porosity was also found on the same casting at thin sections with a high rate of solidification.

FIG. 265 b. Sharply delineated zones of porosity underneath the chills of a flange. The flange also showed porosity at the remaining parts of the edge where no chills were attached.



a

b

Careful examination of such castings almost always reveals porosity in other positions. Due to the thick chilled skin under the chill, blowholes are often found several mm below the surface, are not visible from the outside, and appear after machining in the form of silver-white blowholes (Fig. 266) similar to the subcutaneous blowholes found in rimmed steel ingots.

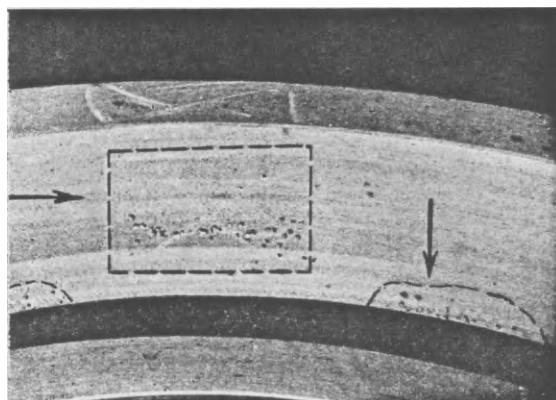


FIG. 266. Pore zone at the surface of attachment of the chill. Porosity can also be observed at all other positions (edges) which also have a high solidification rate.

In some cases the use of chills has led to modifications in melting practice and an improvement in steel quality.

Porosity of this kind is often attributed to hydrogen without further examination being made. Undoubtedly the steel can become charged with hydrogen as a result of faulty melting practice, such as an inadequate boil, the use of damp fluxes in the finishing period, prolonged holding after the boiling period under an inactive slag, frequent opening of the furnace door in the finishing period, etc. Even a damp ladle or stopper can cause hydrogen pickup, because residual water vapour is forced into the steel due to the low gas permeability of the ladle lining.

Hydrogen is taken up by the steel only to a very small extent from the actual mould. As a matter of interest, this small pickup of 2 to 3 ml $H_2/100$ g Fe is of the same order of magnitude whether the metal is cast in chills or in dry or green sand moulds, as shown by measurements reported in the literature^(45 46). (Only hydrogen absorbed between the casting stream and the mould should be taken into account in these measurements.) This small pickup of hydrogen from the mould materials was confirmed by indirect measurements⁽²⁴⁾ and by direct measurements by Heide⁽²⁵⁾ (see Fig. 267) in which a strong temperature dependence is clearly recognizable.

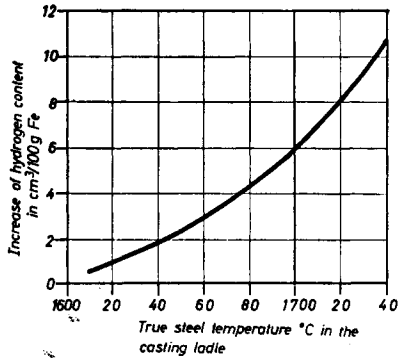


FIG. 267. Increase in the hydrogen content of a steel due to casting in bentonite-sand moulds. After Heide⁽²⁵⁾.

Pinholes cannot be produced experimentally from the increased water content of green sand moulds. In experiments of this kind a reference casting must always be cast at the same time from the same melt in a standard mould, in order to be able to recognize a defect caused by the steel, and not to attribute it erroneously to the experimental casting. With 8-9 per cent of water in the mould-sand gas holes begin to be formed, but these are not to be confused with pinholes.

Satisfactory melts (well deoxidized, and not charged with hydrogen) can also be cast into green sand moulds of low gas permeability (60 to 70 units measured on the GF apparatus on test pieces 50 mm \varnothing \times 50 mm *b*). With melts which were intentionally deoxidized incompletely, it was found that all the resulting castings were porous, but that porosity was more severe in experimental castings made from sands of lower gas permeability. Beyond a gas permeability of hundred units, however, no further difference could be observed. Hence a gas permeability of at least hundred units is to be recommended for facing sand and backing sand.

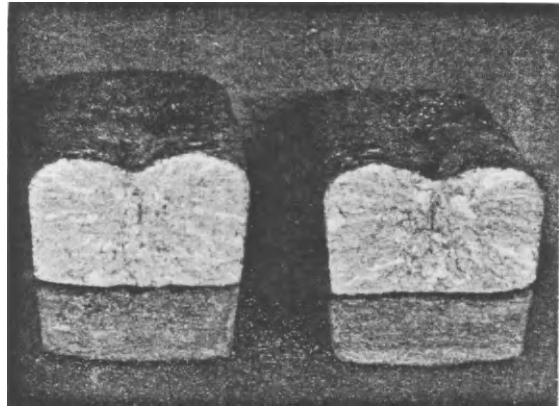
A very sensitive test for checking the susceptibility of the steel to porosity is shown in Fig. 268. The test piece is moulded at the furnace in green sand (dry core assembly moulds are unreliable) cast with a hand shank and fractured at the notch. Even with low concentrations



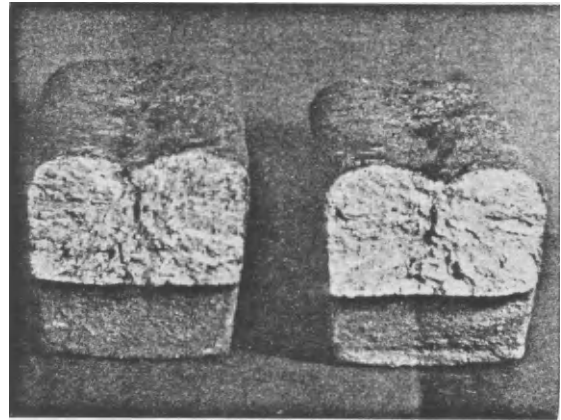
FIG. 268. Test piece for the rapid determination of the gas content of steel.

The sample is cast in a green sand mould (~5% H₂O), which is rammed immediately before casting. The mould must not in any circumstances be dried or manufactured from cores. Immediately after casting the test piece is quenched in water and broken with a powerful hammer blow.

of gas-generating impurities the fractured surface shows unmistakable porosity (Fig. 269a-c). This test can also be used to follow the enrichment of the steel in unwanted



a



b

FIGS. 269a and b. Appearance of the fractured surface with a steel sufficiently low in gas content.

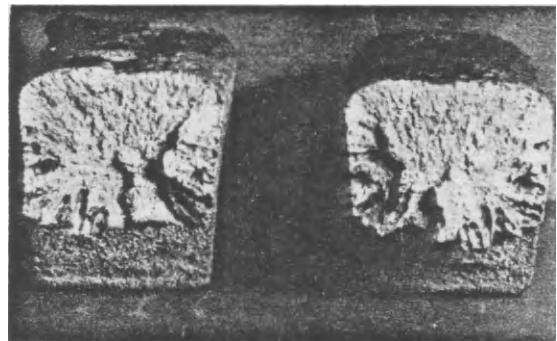


FIG. 269c. Appearance of the fractured surface of steel with high gas contents.

The test piece is fairly sensitive and indicates even low gas contents at a harmful level. However, the sample gives no indication of the origin of the gases, whether these are H₂, CO₂ or N₂, for example, or are of an organic nature (methane).

impurities during the melting and casting processes, i.e.

- 1st sample from the furnace, after final deoxidation. Time: immediately before tapping.
- 2nd sample from the ladle. Time: before casting.
- 3rd and 4th samples during casting, taken in the casting stream.

8.4. Tears at the Points of Attachment of Chills

8.4.1. CRACKS ATTRIBUTABLE TO THE CHILLS

IMPORTANT FOR PRACTICE

The metal solidifies first at the face of the chill, and also begins to contract there. The metal is still viscous at the sand surfaces, and is unable to withstand the contraction pull, with the result that tears are produced, according to Pellini⁽²¹⁾ (Figs. 270a-b).

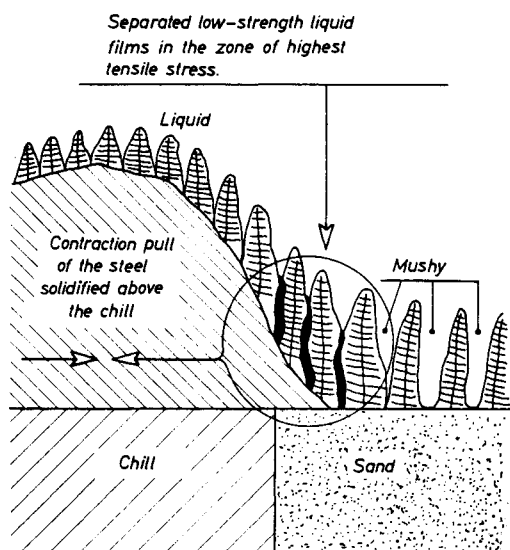


FIG. 270a. Formation of hot tears at the end of the chill due to the breakage under contraction of liquid films⁽²¹⁾.

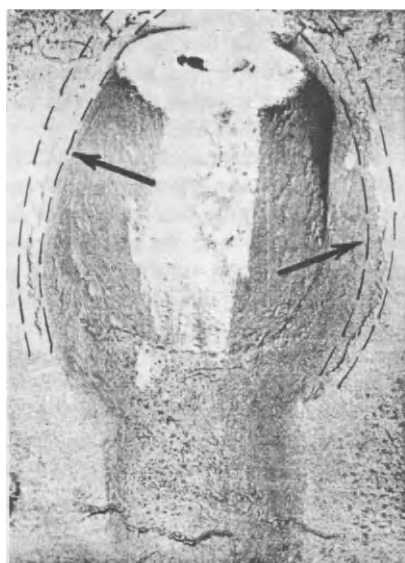


FIG. 270b. Lugs in housing wall, cast sand by the use of ring chills. Tears resulting from contraction pull.

The contraction of the surface area of a chill should not therefore exceed the (very small) thermal expansion of the sand surface, if cracks are to be avoided. By subdividing large chill surfaces into several small ones the contraction pull per chill surface area is diminished (Fig. 271). The length of the chill should be about three

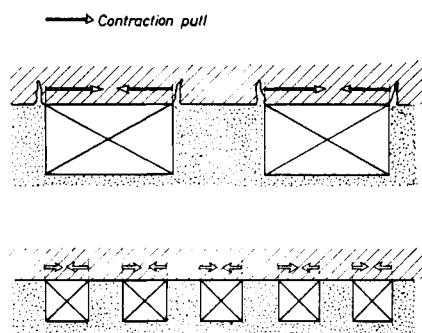


FIG. 271. By subdividing large chills into several smaller ones the contraction pull of the solidified steel layer at the surfaces of attachment of the chills can be diminished and the danger of cracking thereby reduced.

to four times that of the thickness of the wall to be cooled; the dimensions of the standard chills were adjusted with this in mind. The buffer of moulding material between the chills should be approximately equal in length to the chill, but in exceptional cases half the chill length is sufficient.

The thermal expansion of the metal at the buffer is improved when instead of the usual moulding sand (or fireclay) a material of higher thermal conductivity (magnesite, zircon, silicon carbide) is applied; this also has the effect of accelerating cooling (Fig. 272). The distance between the chills can then be reduced. For more details see Chapter 10.

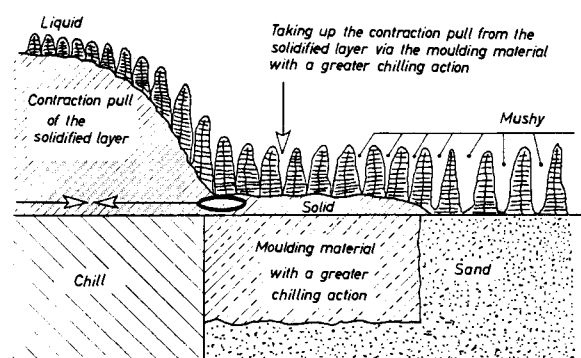


FIG. 272. Moulding materials with a greater chilling action reduce the risk of cracking at the ends of the chill.

The position of the chills on the casting must be such that the existing, substantial contraction stresses are not intensified. The contraction of ring castings requires a corresponding collapsibility of the internal core. This depends on the rapid burning-out of the organic constituents of the sand. Chills incorporated in this type of core first store up the heat, i.e. the sand burns incompletely in their vicinity and does not yield; this intensifies the contraction stresses and can lead to tears (Fig. 273).

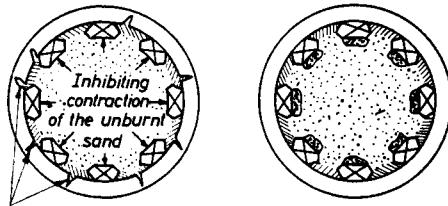


FIG. 273. Formation of hot tears due to chains of chills in the core. Remedy.

Hot tears at the chain of chills in the enclosed core due to inhibition of contraction.

Compensation of contraction inhibitions and prevention of cracking by placing flexible materials (for example tow or straw) behind the chills.

Individual chills in the core are harmless as a rule; chains of chills are better incorporated in the mould (Figs. 244, 245). If they cannot be avoided in the core, then straw rope, etc., must be placed behind the chills (Figs. 273, 274).

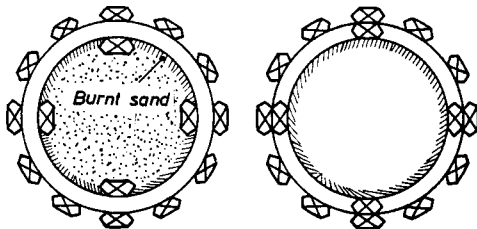


FIG. 274. Preventing the formation of hot tears by transferring the chain of chills to the outside or below.

Preventing the formation of hot tears by transferring the chain of chills to the outside. Individual chills in the core or ball are harmless as a rule.

Preventing the formation of hot tears by transferring the chain of chills to the outside or below.

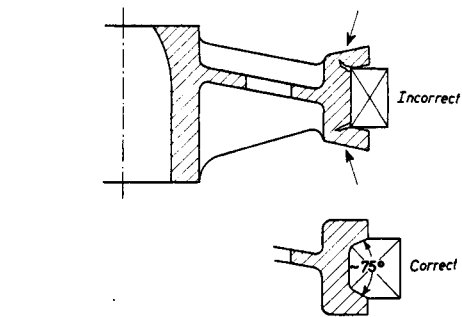


FIG. 276. Formation of hot tears on chills which are clamped between projections, ridges, etc.

If chills between projections cannot be avoided, suitable levels must be provided so that the chill can "creep" during contraction.

Chills should not be clamped in, either by unsatisfactory ramming (Fig. 275) or by projections (Fig. 276); otherwise tears are unavoidable. It is an advantage to ram in the chills rather than insert them subsequently.

8.4.2. CRACKS AT THE POINT OF ATTACHMENT OF THE CHILL, ATTRIBUTABLE TO THE STEEL. ADVICE ON THE CONTROL OF THE STEELMAKING PROCESS TO PREVENT SUCH CRACKS

IMPORTANT FOR PRACTICE

Because of the many impurities contained in it, especially sulphur, Bessemer steel is very susceptible to hot tears. However, even satisfactorily desulphurized heats from the electric arc furnace show at times a marked tendency to hot tears, without any recognizable cause related to the chemical composition.

According to Pellini's film theory, ferrous oxide and manganese oxide segregate at the grain boundaries of the crystallites, forming a low-strength layer at which the casting cracks even during solidification. The liquid deoxidation products also act in the same direction, if they had not time to separate in the ladle, or if they only form in the mould during casting. According to the author's experience, porosity and susceptibility to hot cracking are often found together, which also indicates unsatisfactory deoxidation of the steel.

Heats worked as follows were much less liable to produce hot tears: Pre-refine at a low temperature, and slag off (phosphorus elimination); final refining at as high a temperature as possible, with the minimum addition of ore or oxygen. At about 0.1–0.14% C the bath should not be boiled vigorously, and should not be refined below this level. Work up a white slag with carbon only, then pre-deoxidize by additions made in the following sequence: aluminium (immerse completely), silicon and manganese. Hold for as short a time as possible. Before tapping add silicon and manganese as required, and again immerse aluminium (1–1.2 kg Al/t). The casting

FIG. 275. Formation of burrs on chills as a result of slipshod ramming, with consequent hot tearing.

should contain 0.035–0.04% Al. By working the heat in this way the bath is not over-refined, a high proportion of the oxides is removed as CO, the remainder being transformed to a harmless form, and the aluminium content is adjusted to the value where hot or cold cracking is least likely and the tendency to porosity is reduced to a minimum.

Chains of chills can therefore be used successfully with steel of a satisfactory quality. With Bessemer steel the use of individual standard chills of normal width leads to cracking, but here also artificial end zones can be formed with steel chills with an approximately rectangular cross-section. The use of modern operating techniques in the moulding shop also involves examining the relationship of steelmaking factors to the tendency to crack formation.

8.5. Principles of Calculating External Chills

(Sections 8.5.1–8.5.8 need not necessarily be studied by the practical foundryman.)

8.5.1. GENERAL

The time taken for a casting to solidify should be reduced by the use of chills. Part of the superheat and the heat of fusion must therefore be taken up by the chills, and this absorption of heat must also take place during a certain time—up to the end of solidification. Both conditions must be fulfilled.

A study of Sections 8.5.2–8.5.7 is desirable for a better understanding of the subject, but it is not absolutely necessary. Section 8.5.8 summarizes the results, without going into the underlying principles in detail.

8.5.2. THE APPARENT REDUCTION IN VOLUME

A casting with the volume V_0 should show the same diminished solidification time as a casting with the smaller volume V_r . The amount of heat corresponding to the difference in weight $= (V_0 - V_r) \times \gamma \times (L + S)$ should be taken up by the applied chills. Hence the chills produce an apparent reduction of volume.

According to the heat balance:

$$W_{ch} = \frac{\text{amount of heat to be drawn off (kcal)}}{\text{amount of heat to be absorbed (kcal/kg)}} \quad (92)$$

or:

$$(V_0 - V_r) \gamma (L + S) = W_{ch} \times t_{ch} \times c \quad (93)$$

from which:

$$W_{ch} = (V_0 - V_r) \frac{\gamma(L + S)}{t_{ch} \times c} \quad (94)$$

In order to simplify the calculation we have:

$$\begin{aligned} V_0 - V_r &= \frac{V_0 - V_r}{1} \times \frac{A_0 \times V_0}{A_0 \times V_0} \\ &= V_0 \frac{A_0(V_0 - V_r)}{V_0 A_0} = V_0 \frac{V_0 - V_r}{A_0/M_0} \\ &= V_0 \frac{M_0 - M_r}{M_0} \end{aligned} \quad (95)$$

whence according to Nicolas⁽¹⁰⁾:

$$W_{ch} = \frac{\gamma(L + S)}{t_{ch} \times c} \times V_0 \frac{M_0 - M_r}{M_0} \quad (96)$$

At an average superheat temperature of 1550°C and an assumed chill temperature of $t_{ch} = 600^\circ\text{C}$ at the completion of solidification, we obtain with sufficient accuracy:

$$W_{ch} = 7.4 V_0 \frac{M_0 - M_r}{M_0} \quad (97)$$

The corresponding numerical values can be read off from Fig. 277.

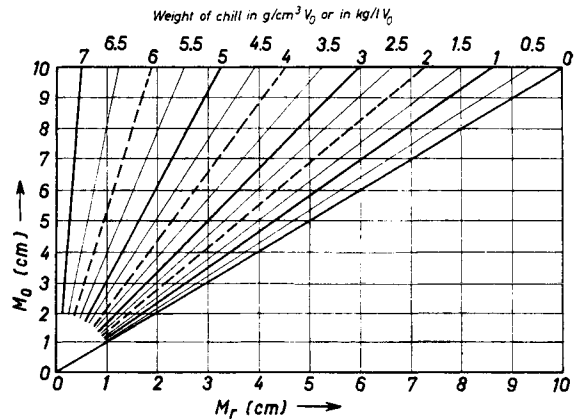


FIG. 277. Weight of chills as a function of M_0 and M_r .

8.5.3. THE APPARENT INCREASE OF SURFACE AREA

A casting with a volume V_0 and a surface area A_0 should have the same reduction in solidification time as a casting with the same volume V_0 and an increased surface area A_s . Hence the application of chills should produce an apparent increase in surface area to A_s due to the more rapid removal of heat compared with the sand mould.

Locke and Briggs⁽²⁾ cast a steel ball of 150 mm diameter in various moulding materials and determined the solidification times (cf. Fig. 305, Chapter 10, page 140). The times in steel or copper moulds were 4 min, and averaged 16 min in sand moulds.

According to Chvorinov⁽¹⁾ the solidification times are related as follows:

$$\frac{T_1}{T_2} = \frac{M_1^2}{M_2^2} \quad (98)$$

giving for our case:

$$\frac{T_1}{T_2} = \frac{4 \text{ (min)}}{16 \text{ (min)}} = \frac{(M_{chill})^2}{(M_{sand})^2} \quad (k)$$

from which:

$$M_{chill} = 1/2 M_{sand} \quad (99)$$

By casting in closed chills, therefore, the modulus M is reduced to half of the corresponding value for sand moulds.

As the ball had a diameter of 150 mm in both cases, the volume remained unaltered, and the apparent increase in surface area can be determined as

$$M_{chill} = \frac{V_0}{A_s} \quad \text{and} \quad M_{sand} = \frac{V_0}{A_0} \quad (l)$$

from which:

$$A_s = A_0 \sqrt{\frac{T_{\text{sand}}}{T_{\text{chill}}}} = 2A_0 \quad (100)$$

Casting of the ball in closed chill moulds therefore produces an apparent doubling of its surface area.

8.5.4. THE TRANSFER OF HEAT AT THE POINT OF APPLICATION OF THE CHILL

It is well-known that an air gap is formed between the shrinking casting and the chill which makes further transfer of heat more difficult. Continuous transfer of heat takes place only where the chill lies close against the casting.

The advance of the solidified wall was measured on ingots of Thomas steel⁽²⁸⁾; the results are shown in Fig. 278. Because of the formation of an air gap the

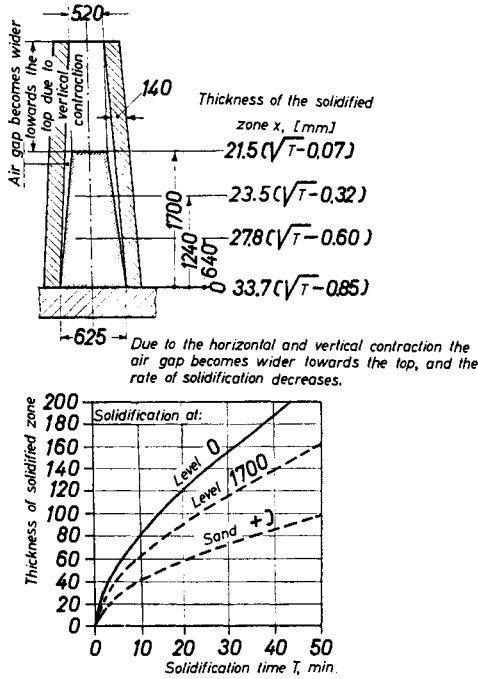


FIG. 278. Advance of solidifications in an ingot of Thomas steel, as a function of the thickness of the air gap between ingot and mould. (Values from *Stahl und Eisen*, 1955, pp. 724-727.)

† Reference values for sand after Krestschanowski⁽²³⁾.

solidified zone near the base of the ingot becomes much thicker in a given time than at the top.

Figure 278 also shows the advance of solidification x of the casting with good and with poor contact with the mould. The curves show good agreement with the results published by other authors^(1,23). It must be assumed that the value of x will fall still further with an increased air gap, and will approximate to the values for sand, especially when the chills are arranged in the upper section.

Pellini⁽²⁷⁾ also reported on the effect of the air gap between the casting and chill, and holds the view that the transfer of heat then takes place by radiation, as it does in a sand mould.

According to Fig. 279, therefore, the cast steel ball

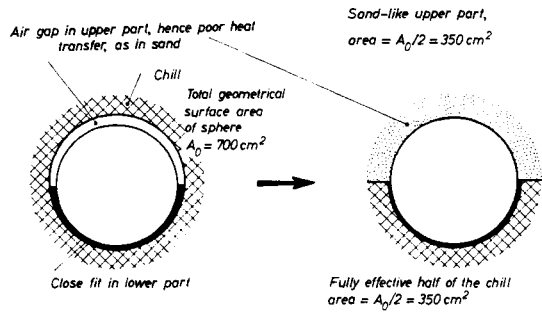


FIG. 279. Formation of air gap in the ball experiment, with a consequent unsatisfactory heat transfer in the upper part of the chill.

will lie in good contact with the lower half, while an air gap is formed at the upper half. The accelerated removal of heat to the chill mould is thus largely due to the contact in the lower part.

If it is assumed that the upper half of the ball behaves thermally like a sand mould, then the total surface area of the sphere becomes:

$$A_0 = (\text{surface area of the sand-like upper part}) + (\text{surface area of the effective half of the chill})$$

$$= A_{\text{sand}} + A_{\text{chill}}$$

$$\text{and } A_{\text{sand}} = A_{\text{chill}} = A_0/2 \quad (101)$$

If the factor of the apparent increase of the area of contact of the chill is designated by y , then

$$\begin{aligned} A_{\text{apparently increased}} &= A_s = A_{\text{sand}} + y A_{\text{chill}} \\ &= A_{\text{sand}} + y \times A_{\text{sand}} \\ &= \frac{A_0}{2} (1 + y) \end{aligned} \quad (102)$$

and from equation (100)

$$y = 2 \sqrt{\frac{T_{\text{sand}}}{T_{\text{chill}}}} - 1 \quad (103)$$

For steel in the chill

$$y = 3 \quad (104)$$

The surface area is apparently increased three-fold at chill contact surfaces without an air gap.

According to the thickness of the air gap produced, an infinitely large number of transitions exists between chill contact surfaces which are apparently doubled and trebled. Practice shows, however, that only two cases need be distinguished for a reliable calculation, namely with and without an air gap.

8.5.5. CHECKING THE PREVIOUS CHILL CALCULATIONS BY THE EXPERIMENTS REPORTED BY BRANDT, BISHOP AND PELLINI⁽³³⁾

The above-named authors cast slightly tapered ingots of various metals into sand and chill moulds. The solidification times or the progress of solidification were deter-

sand surfaces are also present in the moulds fitted with chills, namely:

1. The bottom surface of the ingot.
2. The surface of the feeder head (from the solidification point of view the feeder head forms part of the casting and must be included in the calculation of the volume and area).
3. The interface upper side of the riser/air which due to the strewn sand should be calculated approximately as a sand surface.

The dimensions of the sand and chill surfaces are as shown in the diagram.

The surface area is apparently increased y times at the surfaces of contact of the chills due to the cooling action. The apparent total surface area with chill moulded castings is therefore:

$$A_s = A_{\text{sand}} + y \times A_{\text{chill}} \quad (105)$$

The modulus of sand moulded castings $M_0 = V_0/A_0$; the modulus reduced by chills is:

$$M_r = \frac{V_0}{A_s} = \frac{V_0}{A_{\text{sand}} + y \times A_{\text{chill}}} \quad (106)$$

The solidification times T were measured; according to equation (98):

$$\frac{M_0}{M_r} = \sqrt{\frac{T_{\text{sand}}}{T_{\text{chill}}}} = \sqrt{\frac{T_0}{T_r}} \quad (107)$$

and from equations (105) and (106):

$$M_r = M_0 \sqrt{\frac{T_0}{T_r}} = \frac{V_0}{A_{\text{sand}} + y \times A_{\text{chill}}} \quad \text{and (m)}$$

$$y = \frac{(\sqrt{T_0/T_r} \times A_0) - A_{\text{sand}}}{A_{\text{chill}}} \quad (108)$$

In the present case:

$$y = \frac{(\sqrt{T_0/T_r} \times 6210) - 2710}{3500} \quad (n)$$

Table 26a gives y values for various grades of steel and shows that the mean value of $y = 3$ calculated in the previous section is correct.

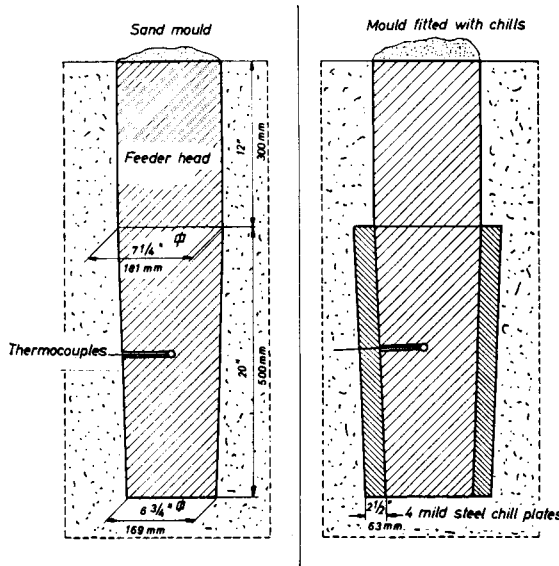


FIG. 280. Experimental layout, after Brandt, Bishop and Pellini⁽²⁸⁾.

Areas	
Total geometrical surface area of the square section ingot: $A_0 = 6210 \text{ cm}^2$	Area of the part of the ingot covered with sand: $F_{\text{sand}} = 2710 \text{ cm}^2$ Area of the part of the ingot covered by chills: $F_{\text{chill}} = 3500 \text{ cm}^2$

mined in the usual way by thermocouples; the experimental layout can be seen from Fig. 280.

Because of the ingot taper no air gap is formed at the surface of contact with the chill. As shown in Fig. 280,

TABLE 26a. y -VALUES FOR VARIOUS GRADES OF STEEL

Experimental results after Brandt, Bishop and Pellini ⁽²⁷⁾								Derived calculations		
Steel type	Analysis %					Solidification time in min in		$\sqrt{\frac{T_0}{T_r}}$	Apparent increase in the chill contact face by the factor y	
	C	Mn	Si	Cr	Ni	Sand moulds T_0	With attached chills T_r		Without air gap formation $y = \frac{\sqrt{\frac{T_0}{T_r}} \cdot 6210 - 2710}{3500}$	With air gap formation $y_L = \frac{y+1}{2}$
C-steel	0.63	0.81	0.66	—	—	48	9	2.3	3.3	2.15
12% Cr-steel	0.13	0.59	0.41	12.2	2.7	44	9.8	2.12	3.0	2.0
18-8-Cr-Ni-steel	0.2	—	—	16.9	9.1	45	9.7	2.15	3.05	2.02

According to Fig. 279 the apparent increase in area during the formation of the air gap at chill surfaces can also be calculated with the aid of existing experimental results.

The lower half of the sphere is apparently increased by y as a result of good contact between the chill mould and the casting. The upper half of the sphere behaves from the solidification point of view like a sand mould, due to the formation of an air gap.

If A_0 is the geometrical surface area of the sphere, the apparently increased total surface area due to chilling action is:

$$A_s = \frac{A_0}{2} + \frac{A_0}{2} \times y = A_0 \frac{1+y}{2} \quad (109)$$

The factor of apparent increase of surface area with chills with air gap formation is:

$$v_L = \frac{A_s}{A_0} = \frac{1+y}{2} \quad (110)$$

TABLE 27. CHILLING EFFECT ON THE CONTACT FACES OF CHILLS PLACED ON SIMPLE BASIC SHAPES, AS A FUNCTION OF THE POSITION OF THE CHILLS IN THE MOULD

Type	Sketch	Calculation	Type	Sketch	Calculation
Platelike castings		Without chill: $M_r \approx d/2$	Lugs, etc.		$M_r \max = \frac{D(a+d)}{4(D+d)}$ $a \approx \frac{0.95 D d}{1.05 D - 2d}$
		$M_r \max \approx M_0/2$ $\approx d/4$			Without chill $M_0 = \frac{A \cdot B}{2(A+B)}$
		$M_r \max \approx 2/3 M_0$ $\approx d/6$			$M_r \max = \frac{A \cdot B}{2(A+2B)}$
		$M_r \max \approx 1/3 M_0$ $\approx d/6$			$M_r \max = \frac{A \cdot B}{3A+2B}$
Lugs, etc.		Without chill $M_0 = \frac{D(a+d)}{2(D+2a)}$	Rod and bar-shaped castings		$M_r \max = \frac{A \cdot B}{2(2A+B)}$
		$M_r \max = \frac{D(a+d)}{4(D+a)}$ whence: $a \approx \frac{0.95 D d}{1.05 D - 2d}$			$M_r \max = \frac{A \cdot B}{3A+4B}$
		$M_r \max = \frac{D(a+d)}{3D+4a}$ $a \approx \frac{0.45 D d}{1.05 D - 2d}$			$M_r \max = \frac{A \cdot B}{4(A+B)}$

The values from Table 27 also show very good agreement with the results of the calculations in the previous section. As the experimental conditions according to Locke, Briggs and Ashbrook⁽²⁾ and according to Brandt, Bishop and Pellini⁽³³⁾ are completely different and independent of each other, but the calculations derived from them still provide concordant results, the equations derived here are correct within the limits of accuracy required in practice.

8.5.6. CALCULATION OF THE NECESSARY CHILL CONTACT SURFACES

According to the (schematic) Fig. 281 the actual total surface area of a casting consists of the sand area plus the chill area:

$$A_0 = A_{\text{sand}} + A_{\text{chill}} \quad (o)$$

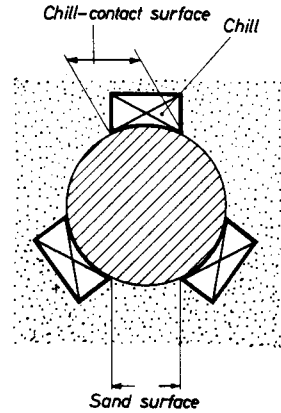


FIG. 281. Thermal conditions on a partially cooled cylinder (schematic).

Total geometrical surface area = A_0 . It is equal to (sum of all sand areas) + (sum of all chill areas) hence $A_0 = A_{\text{sand}} + A_{\text{chill}}$.

On closely-fitting chills the apparently increased surface area, according to equation (104), is:

$$A_s = A_{\text{sand}} + 3 A_{\text{chill}} = A_0 + 2 A_{\text{chill}} \quad (p)$$

$$A_{\text{chill}} = \frac{A_s - A_0}{2} \quad (q)$$

As $M_r = A_0/A_s$; $A_s = A_0/M_r$; $M_0 = V_0/A_0$;

$$A_0 = V_0/M_0, \quad (r)$$

therefore:

$$A_{\text{chill}} = \frac{V_0(M_0 - M_r)}{2 M_0 M_r} \quad (111)$$

without air gap

From the same considerations we obtain from equation (111) the surface of contact:

$$A_{\text{chill}} = \frac{V_0(M_0 - M_r)}{M_0 M_r} \quad (112)$$

with air gap

Shrunk-on chill surfaces (for example on the inside surfaces of rings) and on chills in the lower section are calculated by means of equation (111), while equation (112) is used for chill surfaces which have shrunk away. The nomograms of Figs. 282 and 283 are derived from these equations.

Chills in the top part are comparatively ineffective because of the size of the air gap; their use is associated with increased uncertainty, especially with medium and large castings. For this reason they have not been treated.

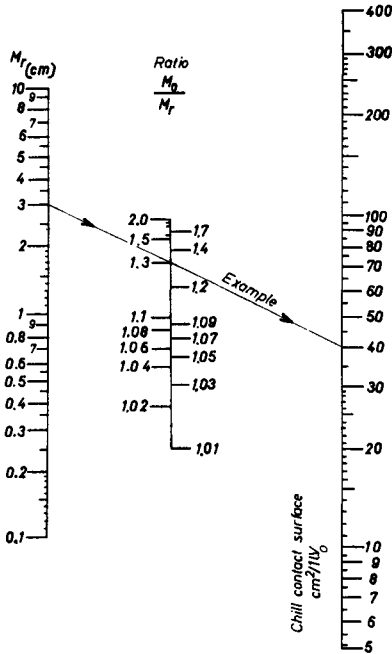


FIG. 282. Contact surfaces of chills without the formation of an air gap.

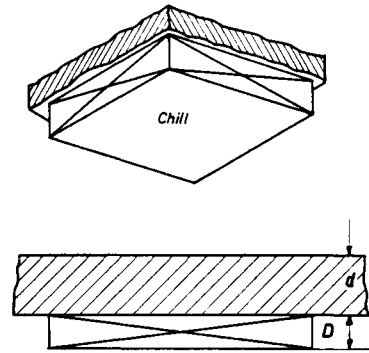


FIG. 284. Plate, partially cooled on the underside by a chill.

8.5.7. MAXIMUM COOLING ACTION ON SIMPLE BASIC SHAPES

If a plate (Fig. 284) with a surface area A_0 , volume $V_0 = \frac{A_0}{2} d$ and modulus $M_0 = \frac{V_0}{A_0} \approx \frac{d}{2}$ has attached to it a chill of the same size, then $A_{\text{chill}} = A_0/2$; it follows from equation (111) for chills in the lower section that:

$$M_r = \frac{M_0}{2} \quad (113)$$

Hence a maximum of half the cross-section can be cooled at the areas of contact of the chill. With chills placed at the side, in accordance with equation (112):

$$M_r = \frac{2M}{3} \quad (114)$$

It is frequently necessary to feed lugs, eyes, etc., on castings at positions where it is impossible or expensive to place a feeder head. Table 27 gives a survey of the attainable cooling effect on various parts of this kind, in relationship to the position in the mould.

Stein⁽²⁸⁾ determined experimentally the dimensions of chills for feeding eyes and lugs. The results are compared in Table 28 with the formulae given above, and show a wide measure of agreement. The results deviated in only one case; this was possibly caused by the slope of the mould during casting, with the consequent formation of an air gap.

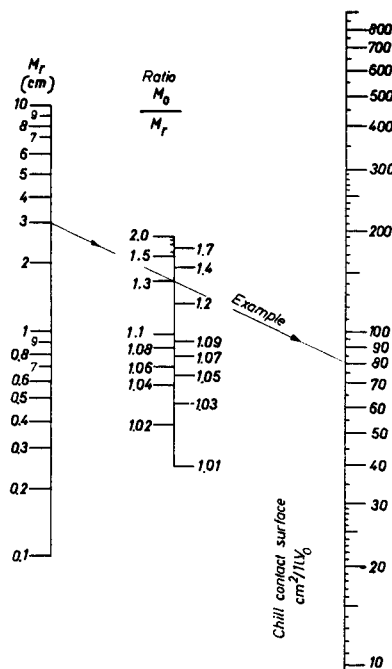
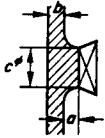


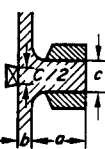


FIG. 283. Contact surfaces of chills with the formation of an air gap.

TABLE 28. COMPARISON OF THE EXPERIMENTAL RESULTS AFTER STEIN AND LINTING AND THOSE OBTAINED BY THE CHILL CALCULATIONS

Results according to:	
Experiment	Calculation
	$\text{Volume } V = \frac{9 b^2 \pi (a + b)}{4} \quad f = 1.2$ $\text{Actual surface} = 3 b \pi (1.5 b + a) \quad a = 0.56 b$ <hr/> $\text{Apparently increased surface} \quad f = 1.15$ $A_{\text{app}} = 3 b \pi (2.25 b + a) \quad a = 0.75 b$ <hr/> $\text{Reduced Modulus } M_r = \frac{V}{A_{\text{app}}} = \frac{3 b (a + b)}{9 b + 4 a}$ $M_r f = M_{\text{plate}} \text{ where } f \text{ is a safety factor. } M_{\text{plate}} = \frac{b}{2} \quad f = 1.1$ <hr/> $a = 0.92 b$
	$A_{\text{app}} = 3 b \pi (2.44 b + a) \quad f = 1.1$ $M_r = \frac{V}{A_{\text{app}}} = \frac{0.75 b (a + b)}{2.44 b + a} \quad a = 1.21 b$ <hr/> $f = 1.05$ $a = 1.45 b$
	$A_{\text{app}} = 3 b \pi (1.69 b + a) \quad f = 1.05$ $M_r = \frac{V}{A_{\text{app}}} = \frac{0.75 b (a + b)}{1.69 b + a} \quad a = 0.38 b$ <hr/> $\text{By slanting the plate slightly in the casting, formation of air gap is prevented, and:} \quad f = 1.05$ $M_r = \frac{0.75 b (a + b)}{1.87 b + a} \quad a = 0.53 b$
	$A_{\text{app}} = 23 b^2 \pi \text{ (for } a = 3 b) \quad f = 1.25$ $M_r = \frac{V}{A_{\text{app}}} = 0.392 b \quad a = 3 b$ $M_r f = M_{\text{plate}} = \frac{b}{2}$ <p>(when changing from $a = 3 b$ to $a = 10 b$ M_r does not alter significantly)</p>

8.5.8. CHILL DIMENSIONS

From equation (113)

$$\frac{M_0 - M_r}{M_0} = \frac{1}{2} \quad (v)$$

and
$$D = 0.46 d \quad (115)$$

which comes very close to the value given by Stein⁽²⁹⁾ with

$$D = 0.5 d \quad (116)$$

For platelike castings with a thickness d , a chill contact face (without air gap) of A_{ch} and a chill thickness D , we have:

$$V_{\text{plate}} = A_{\text{ch}} \times d = V_0 \quad (s)$$

$$V_{\text{chill}} = A_{\text{ch}} \times D; \quad (t)$$

$$\left. \begin{aligned} W_{\text{chill}} &= A_{\text{ch}} \times D = V_0 \times 7.4 \frac{M_0 - M_r}{M_0} \\ \text{from (equation) 97} \\ &= A_{\text{ch}} \times d \times 7.4 \frac{M_0 - M_r}{M_0} \end{aligned} \right\} (u)$$

and is a further confirmation of the heat transfer hypothesis.

Thickening the chill beyond this amount does not produce an intensified cooling effect. Nonetheless, it is an advantage from the point of view of moulding technology to keep the chill thickness, after Pellini, to

$$D = d \quad (117)$$

In practice the influence of an eventual superheat is compensated in this way, especially by steel flowing over it.

The condition of the thermal balance according to equation (92) will therefore be fulfilled in most cases, but not the necessary cooling effect in accordance with equations (111) and (112).

The available cooling surface A_{ch} is determined by the type of casting. In the ideal case the whole surface area of the part of the casting in question is available. Bearing in mind the risk of cracking, however, chills should not lie too close together, especially with large parts. According to the wall thickness, an interval between chills of up to the width of a chill may be necessary to take up the casting strain through the moulding sand buffer.

In such an unfavourable case, therefore, only half the surface area of the casting is available for attaching chills. The maximum cooling effect is therefore governed by the type of casting, and is calculated from equations (111) and (112):

$$\boxed{M_{r \text{ max}} = \frac{V_0 M_0}{2 A_{\text{ch}} M_0 - V_0} \text{ without air gap}} \quad (118)$$

and

$$\boxed{M_{r \text{ max}} = \frac{V_0 M_0}{A_{\text{ch}} M_0 + V_0} \text{ with air gap}} \quad (119)$$

8.5.9. SUMMARY

IMPORTANT FOR PRACTICE

Parts cast in chills solidify more quickly, and thus exhibit the same, shortened solidification time as another casting equal in weight but with a substantially larger surface area (hence a smaller modulus). Therefore, the surface area is apparently increased by attaching chills.

According to the position of the chills on the casting an air gap can be produced when contraction commences, or the contact casting/chill becomes more intimate (Fig. 285). In the case where an air gap is formed the apparent increase in surface area is double, and without an air gap three times, that of an equal sand surface.

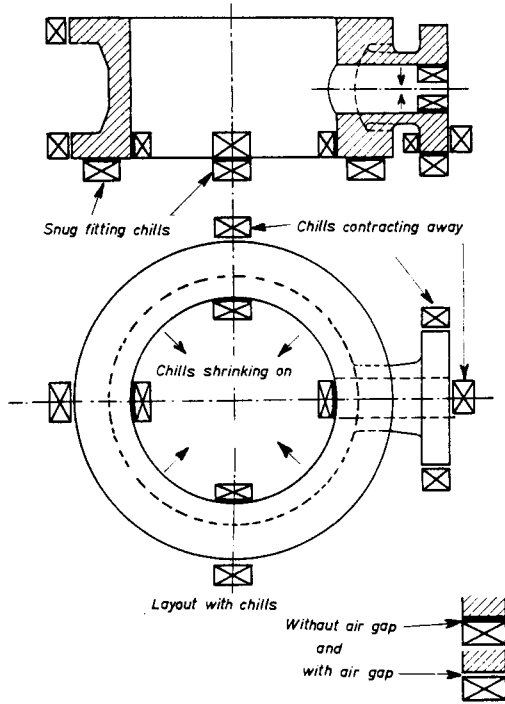


FIG. 285. Layout of chills, shown schematically. The layout diagram does not actually show all the chills indicated here.

Beyond a certain minimum size the cooling action of a chill cannot be further increased by thickening it. The beginner should be especially warned against attempting to produce a given cooling action by using too thick a chill.

The standard chills shown in Table 26 are so dimensioned that their cooling action is adequate for most purposes.

8.6. Operating Practice in Cooling Heavy Cross-sections by Means of Chills

IMPORTANT FOR PRACTICE

A heavy cross-section (for example the roll in Fig. 286) should be so strongly cooled by attaching chills that it can still be fed satisfactorily (hence with a safety factor of 1.1 to 1.2) by a smaller adjacent cross-section. Because of the danger of cracking, the whole of the cross-section cannot be covered with chills, and the following rule-of-thumb can be used:

Cooling by means of chills is possible only when the cross-section feeding liquid metal has a modulus which is at least sixty-six per cent of that of the cross-section to be cooled.

Table 29 gives the maximum cooling effect on simple basic shapes. The difference in modulus of the cross-sections can be ascertained very quickly, so that it can be decided without further calculation whether chills can be used for cooling. If cooling is insufficient, a slight padding of the cross-section supplying liquid metal

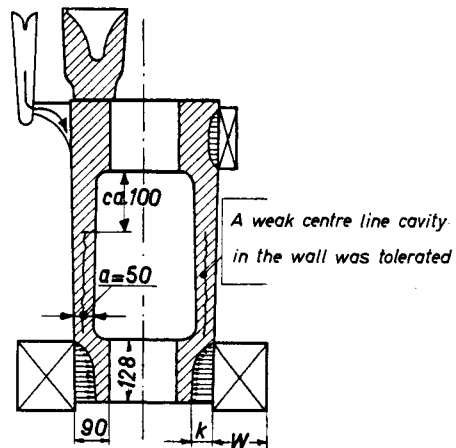


FIG. 286. Roll, the lower shoulder of which was cooled by chills. Side feeder head with artificial end zone at the upper shoulder.

can solve the problem, and the metal can be left on the casting.

Starting with the casting, the maximum chill contact surface and the initial modulus M_0 , the reduced modulus can be determined at once with the help of Figs. 282 and 283 (or equations 118 and 119). If chills with and without an air gap are attached to the same cross-section, the procedure is as follows: first determine the reduced modulus without air gap; this now becomes the initial modulus for determining the modulus associated with the formation of an air gap, and is therefore substituted in the second determination for M_0 .

Alternatively, the casting, the chill contact surfaces, the number of standard chills which can be attached (calculated from the dimensions of the casting: chill-interval-chill, etc.) are known; it is also known whether an air gap will be formed or not. The total cooled

TABLE 29. CALCULATIONS IN CONNECTION WITH FIG. 290

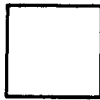
The joint can be imagined as the adjacent simulation body.
 $V = 28 \times 28 \times 30 = 23,520 \text{ cm}^3$
 $A_{\text{geom.}} = 4928 \text{ cm}^2$
 non-cooling faces = $2 \times 15 \times 30 = 900 \text{ cm}^2$
 \therefore effective cooling surface = $4928 - 900 = 4028 \text{ cm}^2$ and effective modulus of the uncooled body = $M_0 = V/A = 5.84 \text{ cm}$

The modulus of the adjacent cross-section 15×30 is only 5 cm. As the joint solidifies earlier, its modulus must be reduced from 5.84 to 4.5 cm.

Chill calculation

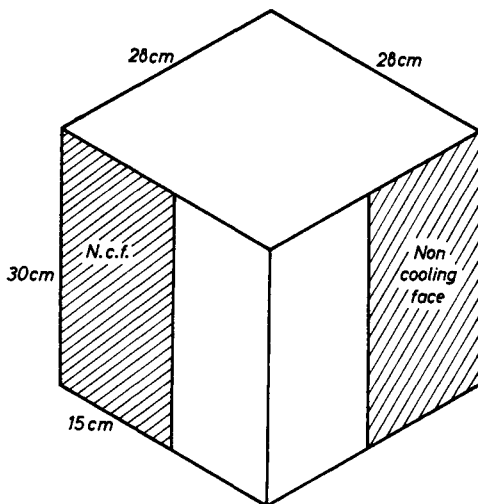


chill underneath $A = 3 \text{ dm}^2 = 300 \text{ cm}^2$ without air gap, hence $2 \times 300 = 600 \text{ cm}^2$ are to be added.



chill at the side, with air gap: $A_{\text{tot}} = 6.2 \text{ dm}^2$ hence $1 \times 620 = 620 \text{ cm}^2$ to be added.

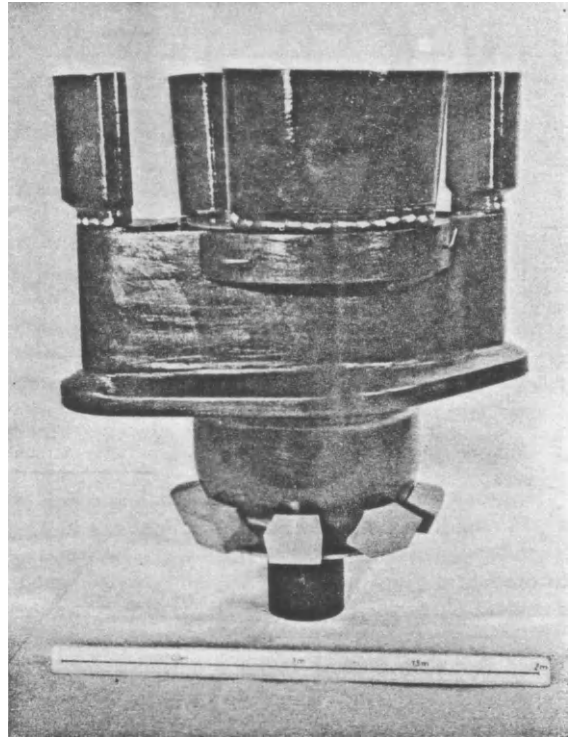
Apparent increase in surface area: $600 + 620 = 1220 \text{ cm}^2$
 Apparently increased area: $4028 + 1220 = 5248 \text{ cm}^2$
 i.e. reduced modulus = $V/A_{\text{app}} = 23,520/5248 = 4.5 \text{ cm}$



a

surface area on the casting by which the surface of the casting is apparently increased is also known. Cooling surfaces with an air gap are simply added to the geometrical area of the casting, while surfaces without an air gap are doubled and then added. Figure 286 was calculated by this method.

Roth⁽²⁹⁾ described the cooling of a heavy cylinder base. By means of the sketch and the incorporated scale it was possible subsequently to check his experimentally determined values with the formulae shown here; the results were almost completely in agreement (see Fig. 287 with its attached table).



b

FIGS. 287a and b. Cylinder base cooled with chills. After Roth⁽²⁹⁾

Auxiliary Table to Fig. 287.

Calculation of the chill parameters of a cooled cylinder base.

A. Calculation of the chill weight after Roth⁽²⁹⁾ and Nicolas⁽¹⁰⁾:

$V_{\text{base}} = 825 \text{ dm}^3$; $A_{\text{base}} = 523 \text{ dm}^2$; $M_{\text{base}} = V/A = 1.57 \text{ dm}$

M_{cylinder} (up to the machined part) = 1.25 dm.

In order that the cylinder wall shall be able to feed the base adequately

$M_{\text{base reduced}}$ should be equal to $M_{\text{cylinder}}/1.2$

whence $M_{\text{B. red.}} = 1.05$

weight of chills from equation 97

$$= W_{\text{ch}} = V_{\text{base}} \cdot \frac{M_{\text{B}} - M_{\text{B. red.}}}{M_{\text{B}}} \cdot \frac{\gamma L}{t \cdot c} = 1638 \text{ kg}$$

8 chills used with a total weight of $W_{\text{ch}} \approx 1700 \text{ kg}$.

B. Calculation of the necessary chill contact surface, after Wlodawer.

This refers to contact without an air gap (equation 111).

$$A_{\text{ch}} = \frac{V_{\text{base}} (M_{\text{B}} - M_{\text{B. red.}})}{2 \cdot M_{\text{B}} \cdot M_{\text{B. red.}}} = \frac{825 (1.57 - 1.05)}{2 \cdot 1.57 \cdot 1.05} = 130 \text{ dm}^2$$

The actual surface of contact was $3 \times 5 \text{ dm} = 15 \text{ dm}^2$ per chill, with a total of 8 chills giving $A_{\text{ch}} = 120 \text{ dm}^2$. This (subsequent) calculation therefore showed good agreement with the result of the practical test.

Two further examples drawn from the author's experience are shown in Figs. 288 and 289 with the appropriate auxiliary tables. The toggle in Fig. 289 was cooled in order to reduce the feeder head dimensions and increase the yield. An unusual feature of the calculation is that the simpler determination of surface area/periphery was selected instead of volume/surface area.

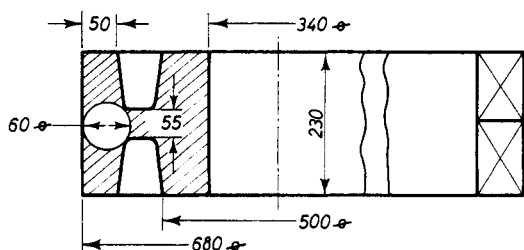


FIG. 288. Wheel casting. Rim cooled by chills and fed by the hub feeder head (on one side) through the wheel disc. Sand fillet effects were inhibited by the severe chilling.

Auxiliary Table to Fig. 288.

$$M_{disc} \approx 2.5 \text{ cm}; M_{rim} \approx 6/2 = 3 \text{ cm}; V_{rim} = 218,000 \text{ cm}^3$$

$$A_{rim} = 47,000 \text{ cm}^2$$

$$M_{rim \text{ reduced}} \text{ should be } \frac{M_{disc}}{1.1} = 2.3 \text{ cm.}$$

This refers to chills with an air gap.

According to equation (112) we have:

$$A_{ch} = \frac{V_0(M_0 - M_r)}{M_0 M_r} = \frac{218,000(3 - 2.3)}{3 \cdot 2.3} = 21,100 \text{ cm}^2,$$

i.e. about half of the rim surface (47,000 cm²) must be covered with chills. 22 standard chills C60 (Table 26) were applied. (Surface of each chill 100 cm²).

The value of A_{ch} can also be obtained from Fig. 283.

A very interesting example of the cooling of a press stand is illustrated in Fig. 290. The casting is highly stressed, and must be a hundred per cent ultrasonically sound. By means of the carefully calculated chill dimensions (see Table 29) three technical moulding requirements and problems were dealt with by one and the same procedure.

g*

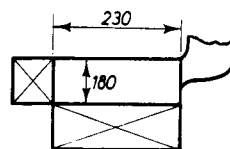


FIG. 289. Massive toggle, heavily chilled on economic grounds. Note the small feeder head.

Auxiliary Table

The toggle was inclined 10° during pouring, so that both chills would fit without an air gap. The calculation was carried out approximately using the cross-section-periphery ratio.

$$\text{Cross-sectional area } A_0 = 23 \times 18 = 414 \text{ cm}^2$$

$$\text{Periphery of cross-section } P_0 = 2(23 + 18) = 85 \text{ cm}$$

$$\text{Modulus } M_0 = A/P = 5 \text{ cm}$$

$$M_r \text{ should be equal to } 2.5 \text{ cm}$$

According to equation (111), we have:

$$P_{chill} = \frac{A_0(M_0 - M_r)}{2M_0 \cdot M_r} = \frac{414(5 - 2.5)}{2 \times 5 \cdot 2.5} = 41 \text{ cm,}$$

i.e. chills are to be attached on a length of 41 cm of the periphery, which was done in the manner shown. As the standard chills are dimensioned fully, calculation of the chill weight was omitted. A suitable feeder head was selected from Table 17 for the casting ($W_{casting} = 130 \text{ kg}$).

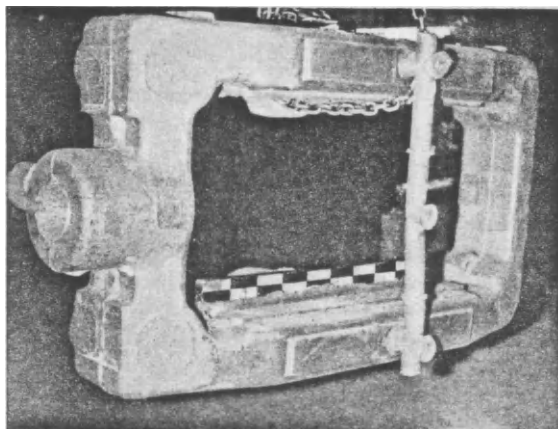
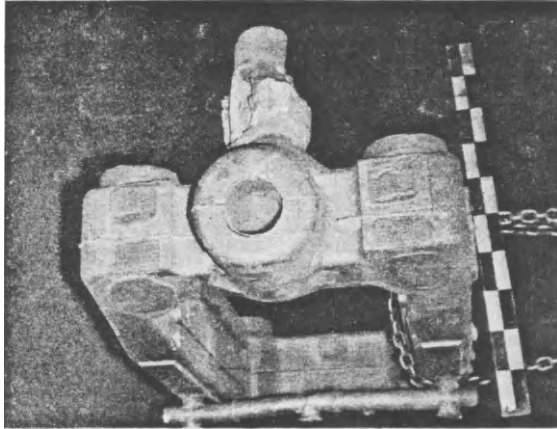
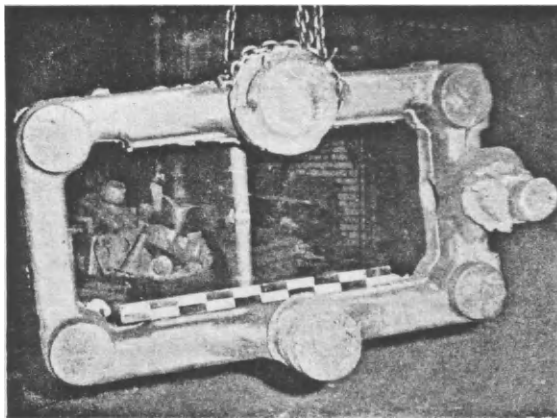


FIG. 290 (1)
(Courtesy Sulzer Bros.)



(2)



(3)

FIG. 290. Press housing.

The massive junctions at the four corners were chilled. This led to:

1. A greatly increased yield. (Without the chills a feeder head would have been necessary at each corner.)
2. Generation of artificial end zones at the four corners, thus extending the feeding range of the feeder head.
3. Reduced risk of hot tears. (There is a great danger of hot tears with feeder heads at each corner.)

For calculation see Table 29.

8.7. Shrinkage Cavity Due to the Incorrect Placing of Chills

If the interior of a massive casting exhibits shrinkage cavities in spite of cooling with chills, the directions which have been given regarding dimensioning of the chill contact surfaces, chill thickness and the minimum cross-section which can be fed satisfactorily cannot have been followed correctly. In this section only the constriction of the feeding section by the chills will be considered.

Chills were placed on a bush (Fig. 291 a) in order to cast the thicker parts sound and to feed the casting from a central feeder head. However, the chill marked 1 constricts the feeding section, so that it solidifies prematurely

with the formation of a shrinkage cavity. The defect is prevented if chill 1 is either omitted or displaced.

The base of a cylinder is to be cast sound by the use of chills (Fig. 291 b). Attaching a large bowl-shaped

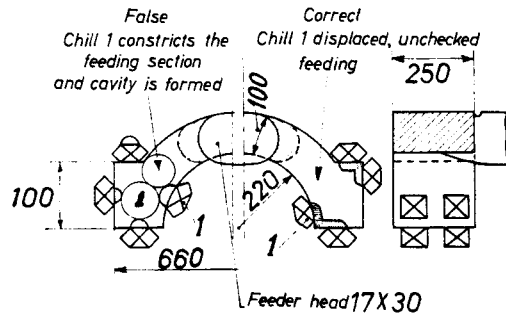


FIG. 291 a. Correct and incorrect position of the chills on a bearing box.

Feeder head calculations:
 From Fig. 7, $M = 3.7$ cm
 The appropriate feeder head modulus
 $M_F = 4.4$ cm
 selected: Oval feeder head 17×30 cm
 $W \approx 100$ kg

Without chilling the end sections a second feeder head of the same size (one on each end casting) would be required. The casting can be poured downhill (with the same feeder head and the same arrangement of chills).

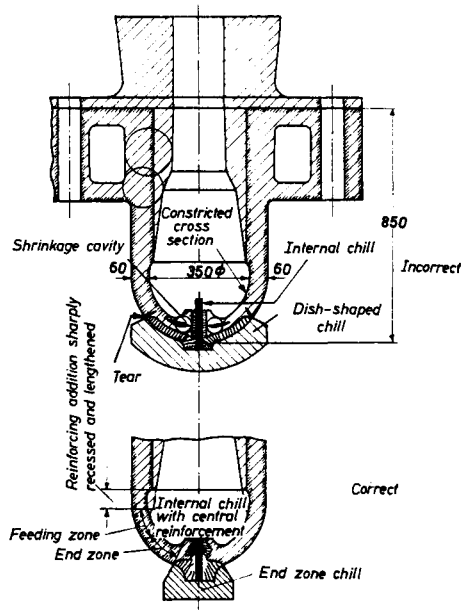


FIG. 291 b. Incorrect and correct chilling of a cylinder base.

Incorrect:

The dish chill constricts the feeding section. Shrinkage cavity formed in the constricted thermal centre. Tear produced due to the large size of the chill.

Correct:

The casting reinforcement was lengthened, thus improving the feeding of the base. The internal chill was provided with a central enlargement in the thermal centre of the casting. The chill was only placed round the lug, thus producing an end zone.

contour chill, in spite of additional cooling of the central portion by an internal chill, gave rise to severe shrinkage cavities from the constriction of the feeding section. This defect was eliminated by a suitable reduction in the size of the chill.

If the wall thickness of the chill mould is small in comparison with the casting cross-section — when casting an ingot, for example — then, according to Fig. 292⁽³⁰⁾

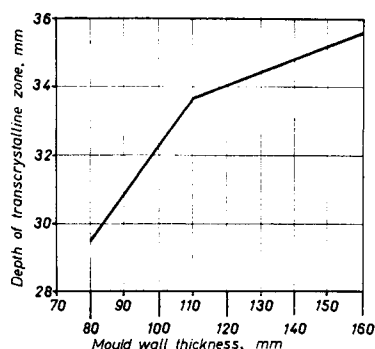


FIG. 292. Chill wall thickness and transcrystalline zone on ingots. After Bardenhauer⁽³⁰⁾.

the chilling effect is exerted to 3 or 4 times the thickness of the chill mould. This must not give the misleading impression that a plate can be cooled completely with a chill of three times the thickness (Fig. 293). We know

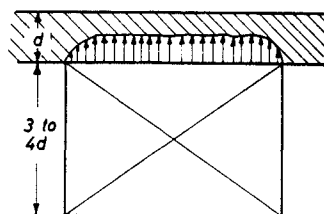


FIG. 293. Supposed cooling effect due to false interpretation of the Bardenhauer diagram.

Even with an overdimensioned chill (three to four times the plate thickness) a maximum of only half the plate can be cooled. The beginner often falls into the error of trying to cool a cross-section by means of over-thick chills.

that in the limiting case only half of the plate can be chilled, and that a thin chill is sufficient for this purpose (cf. Chapter 7). Stepwise cooling of a steel casting can only be achieved by stepwise placing of the chills, as in Fig. 294, when the heaviest chill has a thickness of half that of the plate. The remaining chills are then so thin that it is difficult to obtain reliable results with them in practice. Cooling from two sides — as in elongated end zones — is far more reliable, and is independent of the chill thickness.

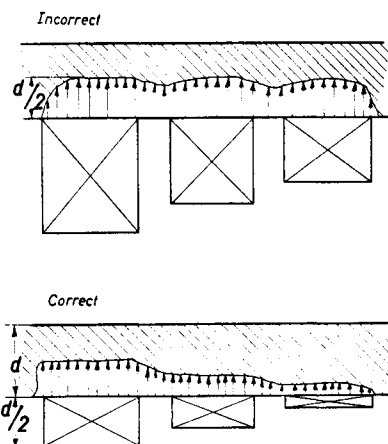


FIG. 294. Incorrect and correct stepped chilling of cross-sections.

Incorrect:

Chills larger than half the thickness of the plate are still unable to cool more than a thickness of $d/2$ at the surface of contact. Stepped chilling cannot be achieved by stepping-down chills of this type.

Correct:

The thicknesses of the heaviest chill should not exceed $d/2$; the remaining chills are to be kept correspondingly thinner.

The chill thickness is very small with this type of stepped chilling. The chills are often placed in an incorrect sequence. Stepped chilling achieved by placing chills on two or three sides is much more reliable.

(See Figs. 244 a and b.)

8.8. Use of Contoured Chills

Even standard chills follow the shape of the casting, and in this sense they are in fact contoured chills. By a systematic classification in DIN (German equivalent of British) standards of similar castings which recur frequently, contoured chills with a wide range of application can also be manufactured⁽³¹⁾.

EXAMPLES

The standards for crane bogie wheels are abstracted in Table 30, and the standard chill tables 31 and 32 are derived from it. Figures 295 and 296 show the wheels manufactured in accordance with these standards or their moulds.

The “historical” development of the moulding techniques for bogie wheels is shown in Fig. 297. In this case the use of chills not only increases the yield, but also lowers the machining costs.

In the sprocket wheel centre (Figs. 298 a–c), the expensive machining of the teeth was prevented, and 232 kg of steel were also saved.

Very massive parts of manganese steel can often be made only by the use of chills (Figs. 299, milling roll). Small crusher jaws of manganese steel can be moulded in synthetic bentonite sand, larger ones can with advantage be made in magnesite, zircon or olivine sands. If standard chills as in Table 33 are used, a cheaper quartz moulding sand can also be employed.

TABLE 30. SUMMARY OF STANDARDIZED CRANE BOGIE WHEELS

Section	Nominal diam. D mm	Width of rail mm		Width of tread mm	
		b_1	b_2	W_1	W_2
I	200	45	—	55	—
II	250	45	—	55	—
	300	45	—	55	—
III	400	45	50	55	60
	500	45	50	55	65
IV	600	55	65	65	75
	700	55	65	65	75
V	800	55	65	65	75
	900	55	65	65	75
VI	800	75	90	85	100
	900	75	90	85	100
	1000	75	90	85	100
	1200	75	90	85	100
VII	1200	120	—	130	—

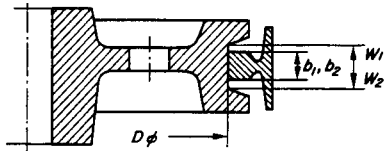


TABLE 31. CHILL PROFILES FOR STANDARDIZED CRANE BOGIE WHEELS

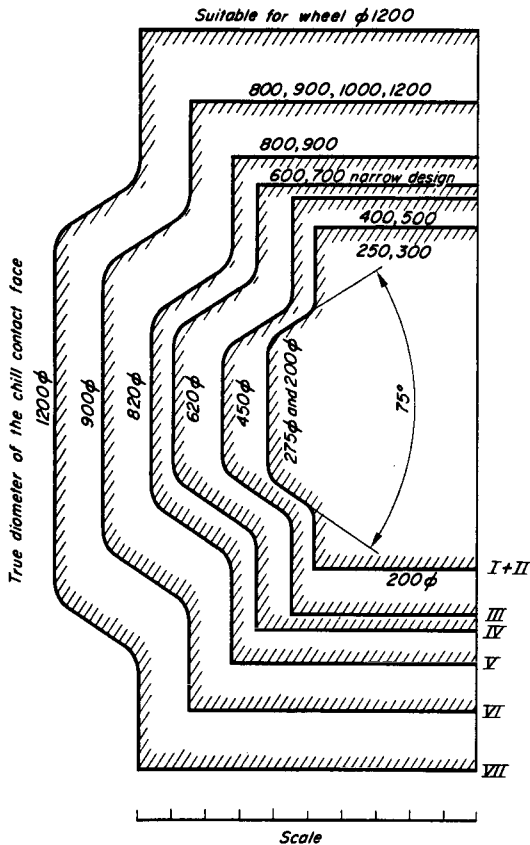


TABLE 32. SUITABLE WIDTHS OF STANDARD CHILLS FOR CRANE BOGIE WHEELS

A 3D perspective diagram of a curved chill. The chill is shown as a block with a curved top surface. The width of the chill is labeled B .

Section no.	Chill width W mm
I, II	70
III	100
IV	120
V, VI, VII	150

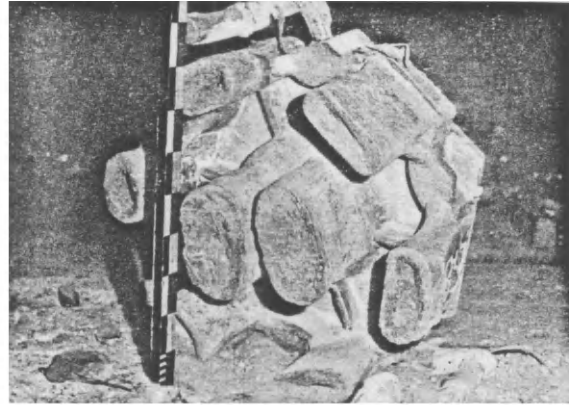
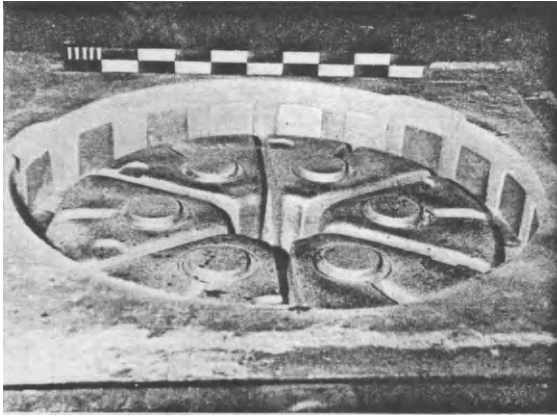


a



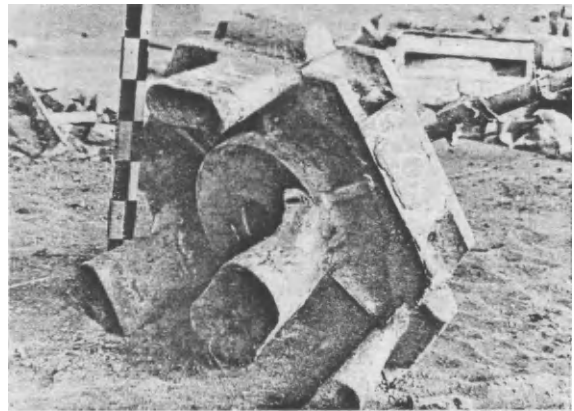
b

FIGS. 295a and b. Mould and casting of a crane pulley which was made with the use of contoured chills. A small feeder head is attached at the rim to feed the remaining cross-section.



a

FIG. 296. Mould of a crane pulley. Rim cooled with chills, and the remainder of the cross-section fed by small, flat feeder heads.



b

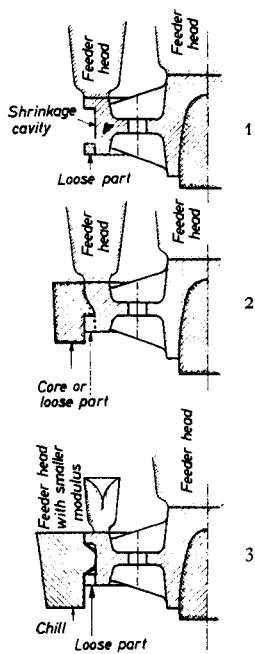
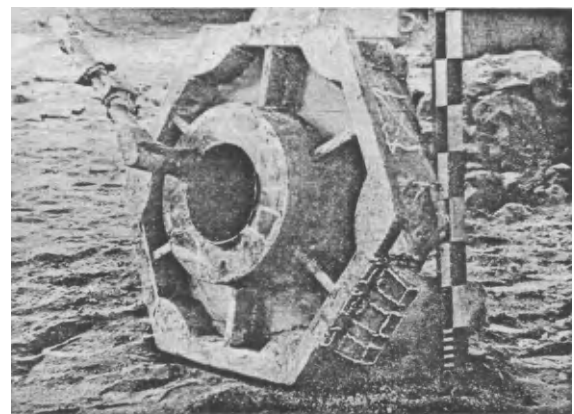


FIG. 297. Development of moulding technique for bogie wheels.

1. Original method of moulding with loose parts. Shrinkage cavity in the rim.
2. Later method of moulding after Heuvers, with external core or loose parts. Rim cavity-free, but high steel consumption and heavy machining costs.
3. New moulding method with external chills. If these chills are standardized, this method is cheaper than (2).



c

FIG. 298. Sprocket wheel centre.

Steel consumption:	(a) 857 kg
Steel saved:	(b) 660 kg
	197 kg

- (a) With rim feeder beads on each side; two boss feeder beads within a single feeding area.
- (b) and (c) One boss feeder head, three small rim feeder beads. Gear profile cooled by contoured chills. Not only is there a considerable saving in circulating material, but costly machinery of the gear profile is also saved.

TABLE 33. CHILL PROFILES FOR MANGANESE STEEL CRUSHER JAWS

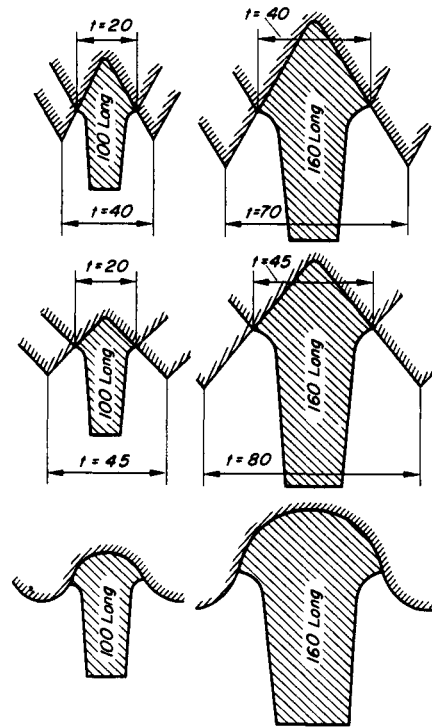
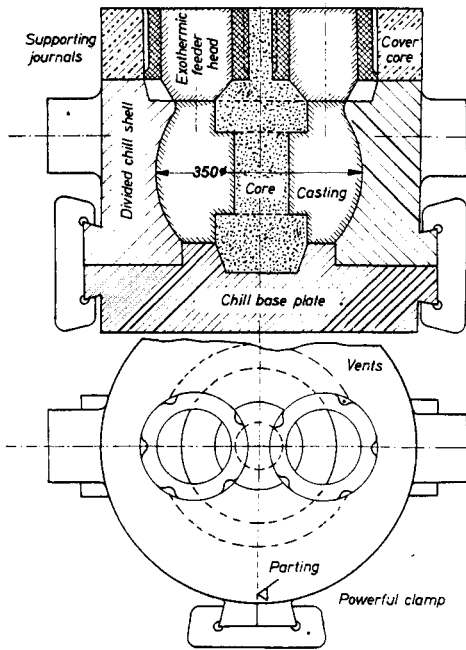


FIG. 299. Casting of a milling roll of 14% manganese steel in chills.

CHAPTER 9

INCREASING THE THERMAL GRADIENT BY MEANS OF COOLING FINNS

9.1. General Discussion of the Action of Cooling Fins

Cooling fins have been in use for some time, i.e. in air-cooled cylinders for motor cycles, etc.

A cooling fin represents a thin plate with a very short solidification time, which forms part of the casting (Fig. 300). It must be noted in this connection that a

measurable cooling effect is only obtained when

$$M_{\text{cooling fin}} \leq 0.25 M_{\text{casting}} \quad (120)$$

If the modulus of the cooling fin is higher than this value, the fin forms a junction which remains liquid even longer than the original casting. This undesired effect, acting in the opposite direction, has been established by the author by measurements of solidification times.

A sufficient distance must remain between the fins to prevent crumbling of the sand ridges and hot spots at the sand corners (sand fillet effect) which would tend to counteract the desired cooling effect. As shown by the scale drawing of Fig. 300 and by works trials, this distance should amount to about 4 d.

The smallest possible cooling fin thickness d, taking into account practical requirements, lies between 4 and 20 mm according to the casting.

There is no point in making fins too thin on heavy cross-sections cast in a steel which is not very fluid, as they will not run and will be ineffective.

The use of cooling fins offers the following main advantages compared with chills:

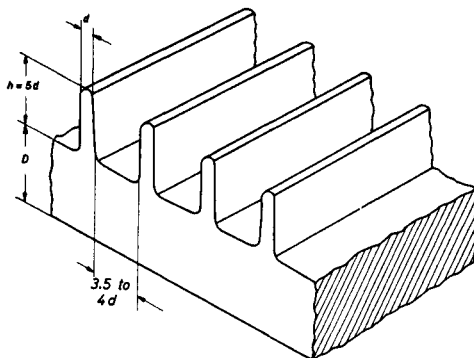


FIG. 300. Plate cooled on one side by pins.

TABLE 33. CHILL PROFILES FOR MANGANESE STEEL CRUSHER JAWS

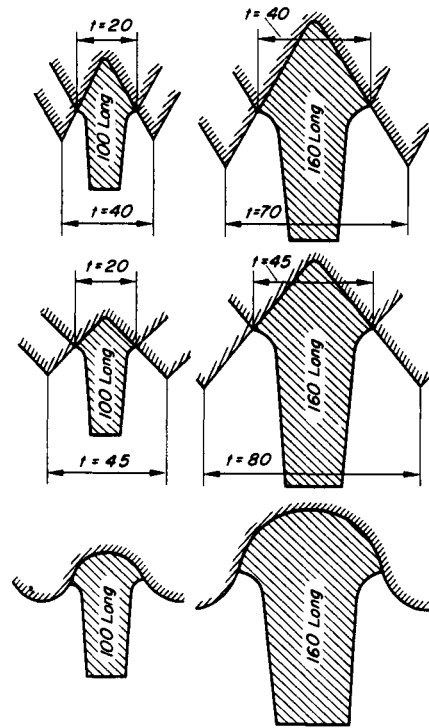
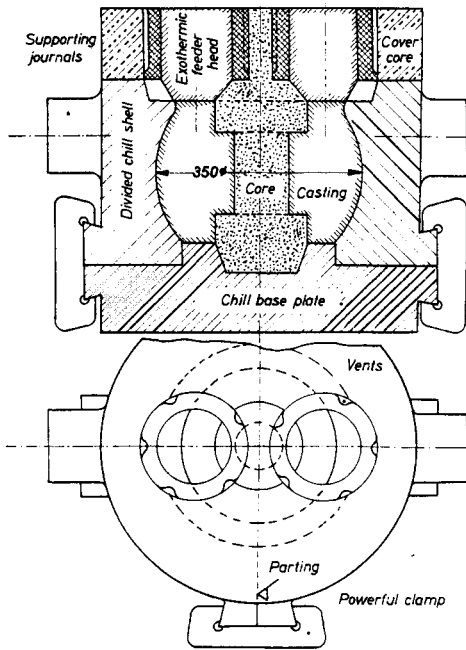


FIG. 299. Casting of a milling roll of 14% manganese steel in chills.

CHAPTER 9

INCREASING THE THERMAL GRADIENT BY MEANS OF COOLING FINNS

9.1. General Discussion of the Action of Cooling Fins

Cooling fins have been in use for some time, i.e. in air-cooled cylinders for motor cycles, etc.

A cooling fin represents a thin plate with a very short solidification time, which forms part of the casting (Fig. 300). It must be noted in this connection that a

measurable cooling effect is only obtained when

$$M_{\text{cooling fin}} \leq 0.25 M_{\text{casting}} \quad (120)$$

If the modulus of the cooling fin is higher than this value, the fin forms a junction which remains liquid even longer than the original casting. This undesired effect, acting in the opposite direction, has been established by the author by measurements of solidification times.

A sufficient distance must remain between the fins to prevent crumbling of the sand ridges and hot spots at the sand corners (sand fillet effect) which would tend to counteract the desired cooling effect. As shown by the scale drawing of Fig. 300 and by works trials, this distance should amount to about 4 d.

The smallest possible cooling fin thickness d, taking into account practical requirements, lies between 4 and 20 mm according to the casting.

There is no point in making fins too thin on heavy cross-sections cast in a steel which is not very fluid, as they will not run and will be ineffective.

The use of cooling fins offers the following main advantages compared with chills:

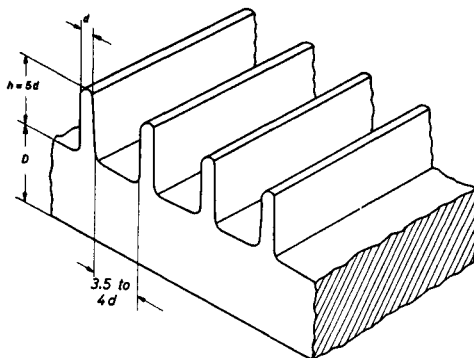


FIG. 300. Plate cooled on one side by pins.

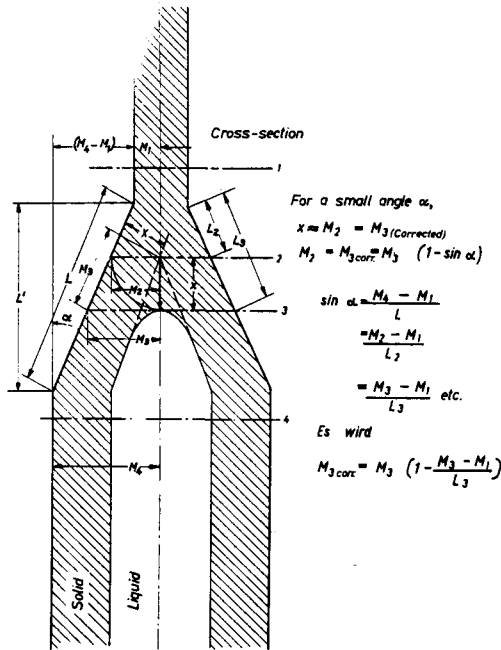


Fig. 301a. Solidification plane of a wedge plate with cooling fins. Solidification geometry after Chvorinov⁽¹⁾.

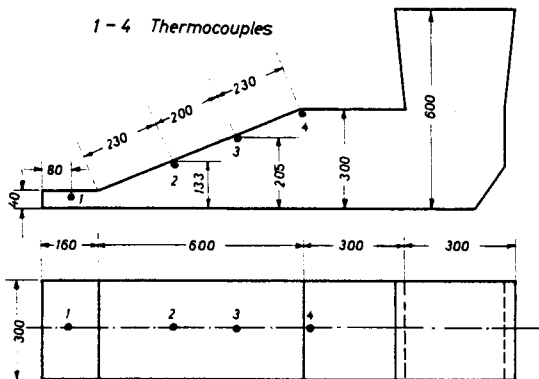


Fig. 301b. Cooling of a wedge plate by means of a fin attached to one front side. Calculation and measured results after Chvorinov⁽¹⁾.

1. They are not susceptible to stress cracks and porosity, even with poor-quality steels such as Bessemer steels.

2. Occasional combination of cooling and strengthening ribs.

On the other hand, cooling fins have the following disadvantages:

1. The fins often do not run satisfactorily, especially with cooler metal and when the fins do not lie in the direction of flow of the liquid steel, i.e. the casting process is less reliable.

2. If the finned patterns are not made of metal: often more difficult and costly to carve the fins by hand (in the sand mould).

3. Increased dressing costs.

4. Curvature of the casting with long fins, due to the contraction pull of the fins.

The necessary works inspection and care in operation are about the same whether chills or fins are used.

9.2. Effect on the Modulus of the Prior Solidification of Adjacent Cross-sections on Wedge Plates with Attached Fins. Determination of the Modulus on Wedge Plates

The following method of calculation for castings as in Fig. 301a is almost completely accurate and has already been given by Chvorinov⁽¹⁾:

The further advance of the solidification front from a cross-section 2 which has already solidified proceeds in the direction of the arrow. The progress of solidification X in the direction of the arrow, according to Section 2.2, is equal to the thickness of skin X at the cross-section 2, and is given by:

$$X = k \sqrt{T} \tag{1}$$

Because the modulus of a plate section is equal to half the thickness of the plate, the skin thickness in this case is:

$$X = M_2 \tag{121}$$

Part measured	1	2	3	4
Modulus M (cm)	$\frac{16 \cdot 30 \cdot 4}{2(16 \cdot 30 + 16 \cdot 4) + 30 \cdot 4}$ $M_1 = 1.58$	$\frac{13.3 \cdot 30}{2(13.3 + 30)}$ $M_2 = 4.66$	$\frac{20.5 \cdot 30}{2(20.5 + 30)}$ $M_3 = 6.10$	$\frac{30 \cdot 30}{2(30 + 30)}$ $M_4 = 7.50$
Corrected modulus M_{corr} (cm)	—	$M_2 \left(1 - \frac{M_2 - M_1}{23}\right)$ $M_{2K} = 4.05$	$M_3 \left(1 - \frac{M_3 - M_2K}{20}\right)$ $M_{3K} = 5.70$	$M_4 \left(1 - \frac{M_4 - M_3K}{23}\right)$ $M_{4K} = 6.93$
Solidification time in min, calculated for M	5.5	46	84	125
Solidification time in min, calculated for M_{corr}	—	38.4	67.3	102
Solidification time in min, measured	6	36	70	100

Because of the growth in the direction of the arrow, the solidification fronts of cross-section 3 are "forced back", i.e. curved, and seal up prematurely, so that section 3 solidifies in the same, shorter time T_2 as cross-section 2. The modulus of the cross-section is therefore less, and must be corrected:

$$T_3 = T_2; \quad M_3 \text{ (corrected)} = M_2 \quad (122)$$

If the wedge angle α of the plate is small, then approximately:

$$X = M_2 \approx M_3 \times (1 - \sin \alpha) = M_3 \text{ (corrected)} \quad (123)$$

$$\sin \alpha = \frac{M_4 - M_1}{L_4} = \frac{M_3 - M_1}{L_3} \quad (124)$$

from which
$$M_3 = M_3 \left(1 - \frac{M_3 - M_1}{L_3} \right) \quad (125)$$

corrected

M_1 being the modulus of the cooling fin.

Chvorinov himself has checked the accuracy of this equation on a wedge plate, according to Fig. 301b. About 20 years later Pellini⁽³²⁾ carried out the experiment illustrated in Fig. 302a. As the edges of a plate solidify first, a wedge-shaped plate remains, the slope of which in this case amounts in cross-section 2 to:

$$L \approx \frac{D}{2} \sqrt{2} = 3.75 \times 1.41 = 5.3 \text{ cm}$$

Hence the actual modulus can be calculated by the Chvorinov rule (equation 125). Figure 302b shows the modulus of the uncooled and fin-cooled plate on the basis of the actual solidification times measured by Pellini. These values agree almost completely with those calculated from equation (125).

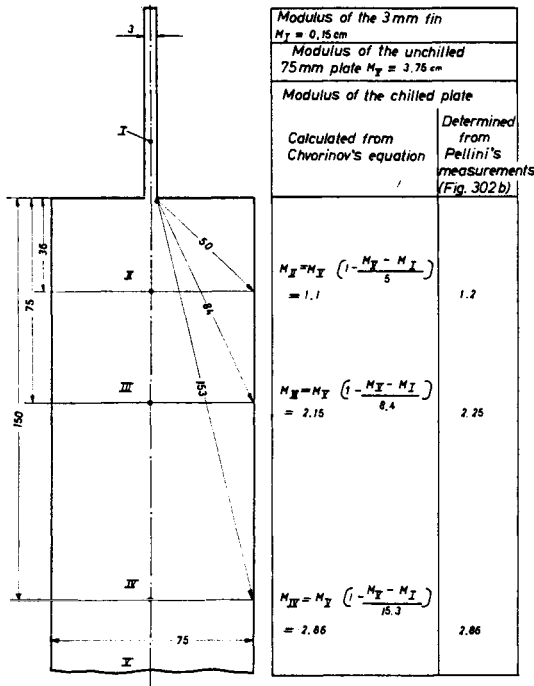


FIG. 302a. Checking the cooling calculation after Chvorinov⁽¹⁾ by Pellini's experimental results⁽³²⁾.

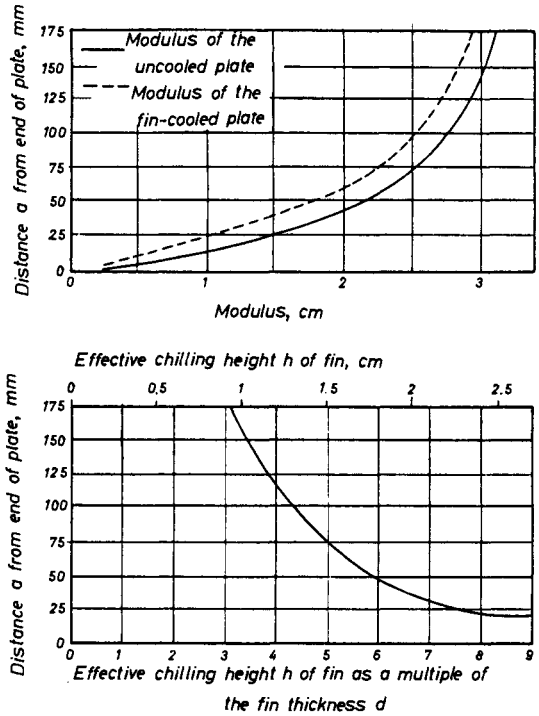


FIG. 302b. Chilling action of a 3 mm fin on a 75 mm thick plate.

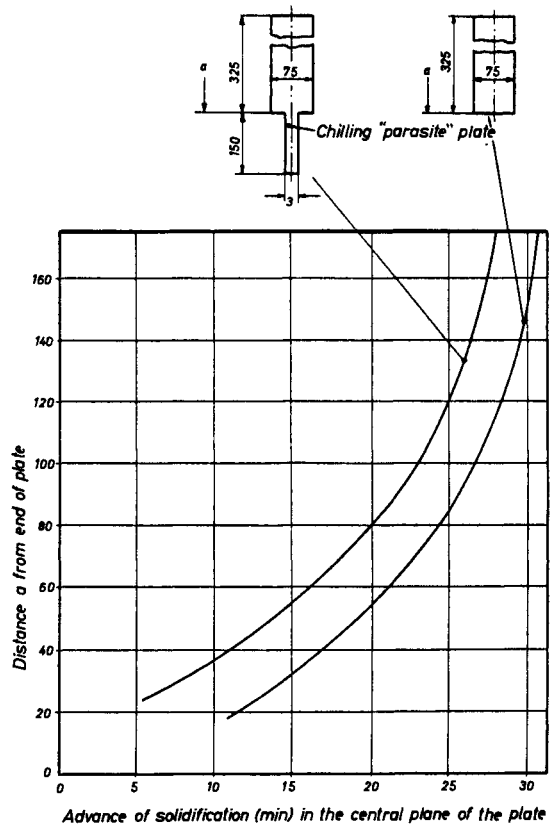


FIG. 302c. Accelerated advance of solidification on a plate due to the attachment of a cooling fin. After Pellini⁽³²⁾.

The very accurate equation (125) is only true for plates with cooling fins attached at the end face. Fins attached at the very long sides produce "chilled junctions" (Fig. 303) the solidification time of which is affected by several other influences (sand fillets, effect of the cooling

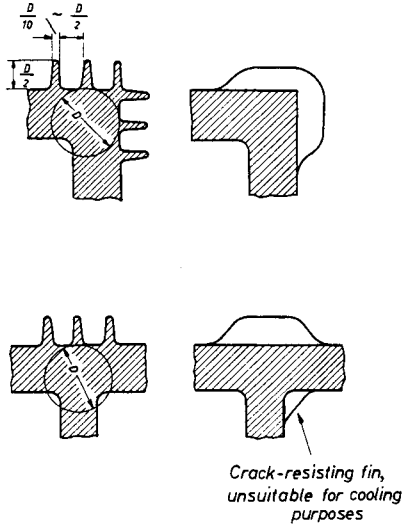


FIG. 303a. Longitudinal and transverse cooling fins at junctions.

fins, etc.). Appropriate methods of calculation are not available at present; suitable experiments should be devised.

Experiments have shown (Fig. 303) that end zones, even extended end zones, can also be produced by cooling fins as shown in Figs. 244 and 245. Here again, there is at present no simple method of calculation which is reliable in practice, so that suitable experiments are again indicated.

The modulus of a tapered wedge plate (with the cross-section of an elongated triangle) is also calculated by equation (125). It is:

$$M_1 = A \tag{w}$$

and on any given cross-section 2 at a distance (measured along the slant side) of L_2 from the apex:

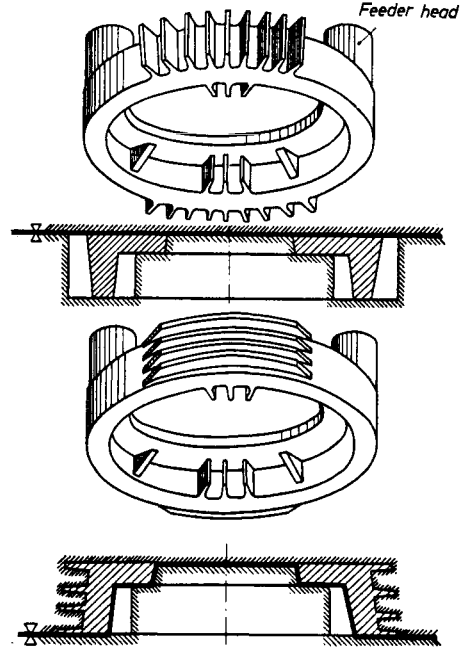


FIG. 303b. Generation of artificial and extended end zones by means of cooling fins on a gear rim. Joining requirements in longitudinal and transverse fins, cut by hand.

$$M_2 = \frac{d_2}{2} \tag{x}$$

where d is the plate thickness at the cross-section in question. Then:

$$M_2 = M_2 \left(1 - \frac{M_2 - M_1}{L_2} \right) = M_2 \left(1 - \frac{M_2}{L_2} \right) \tag{y}$$

Example: tapered wedge plate 100 cm long, wedge thickness at this length 10 cm. $M_2 = 5$ cm

$$M_2 = 0.95 M_2 \approx M_2 \tag{z}$$

i.e. with elongated wedge plates beyond a ratio of $\approx 1:5$ practically no reduction of the modulus occurs due to the action of the previously solidified peaks.

CHAPTER 10

INCREASING THE THERMAL GRADIENT BY MEANS OF MouldING MATERIALS WITH A CHILLING ACTION

10.1. Different Heat Removal Rates of Various Moulding Materials. Defects Arising from Their Use

In order to determine the cooling times in various moulding materials, Locke, Briggs and Ashbrook⁽²⁾ carried out fundamental and extremely important mea-

surements on steel spheres of 6 in. diam. According to Fig. 304, the spheres were cast in shells made of various moulding materials. The results are shown in Fig. 305 and the measurements were plotted by the author on a Chvorinov diagram (Fig. 306), enabling the solidification times to be read off directly as a function of the modulus.

The very accurate equation (125) is only true for plates with cooling fins attached at the end face. Fins attached at the very long sides produce "chilled junctions" (Fig. 303) the solidification time of which is affected by several other influences (sand fillets, effect of the cooling

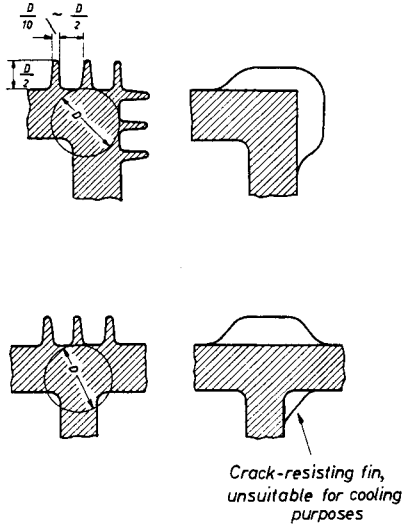


FIG. 303a. Longitudinal and transverse cooling fins at junctions.

fins, etc.). Appropriate methods of calculation are not available at present; suitable experiments should be devised.

Experiments have shown (Fig. 303) that end zones, even extended end zones, can also be produced by cooling fins as shown in Figs. 244 and 245. Here again, there is at present no simple method of calculation which is reliable in practice, so that suitable experiments are again indicated.

The modulus of a tapered wedge plate (with the cross-section of an elongated triangle) is also calculated by equation (125). It is:

$$M_1 = A \tag{w}$$

and on any given cross-section 2 at a distance (measured along the slant side) of L_2 from the apex:

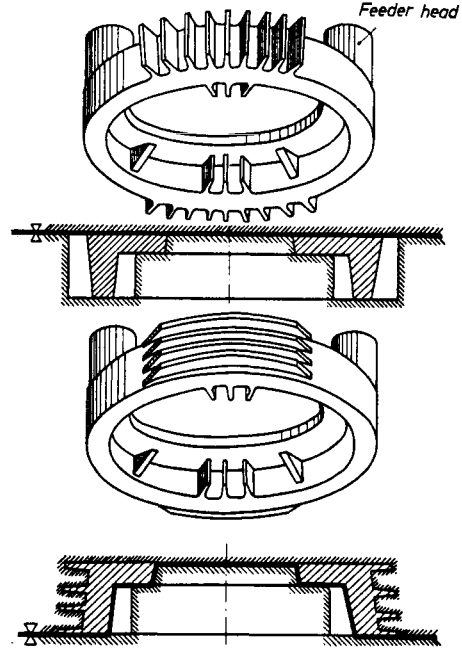


FIG. 303b. Generation of artificial and extended end zones by means of cooling fins on a gear rim. Joining requirements in longitudinal and transverse fins, cut by hand.

$$M_2 = \frac{d_2}{2} \tag{x}$$

where d is the plate thickness at the cross-section in question. Then:

$$M_2 = M_2 \left(1 - \frac{M_2 - M_1}{L_2} \right) = M_2 \left(1 - \frac{M_2}{L_2} \right) \tag{y}$$

Example: tapered wedge plate 100 cm long, wedge thickness at this length 10 cm. $M_2 = 5$ cm

$$M_2 = 0.95 M_2 \approx M_2 \tag{z}$$

i.e. with elongated wedge plates beyond a ratio of $\approx 1:5$ practically no reduction of the modulus occurs due to the action of the previously solidified peaks.

CHAPTER 10

INCREASING THE THERMAL GRADIENT BY MEANS OF MOULDING MATERIALS WITH A CHILLING ACTION

10.1. Different Heat Removal Rates of Various Moulding Materials. Defects Arising from Their Use

In order to determine the cooling times in various moulding materials, Locke, Briggs and Ashbrook⁽²⁾ carried out fundamental and extremely important mea-

surements on steel spheres of 6 in. diam. According to Fig. 304, the spheres were cast in shells made of various moulding materials. The results are shown in Fig. 305 and the measurements were plotted by the author on a Chvorinov diagram (Fig. 306), enabling the solidification times to be read off directly as a function of the modulus.

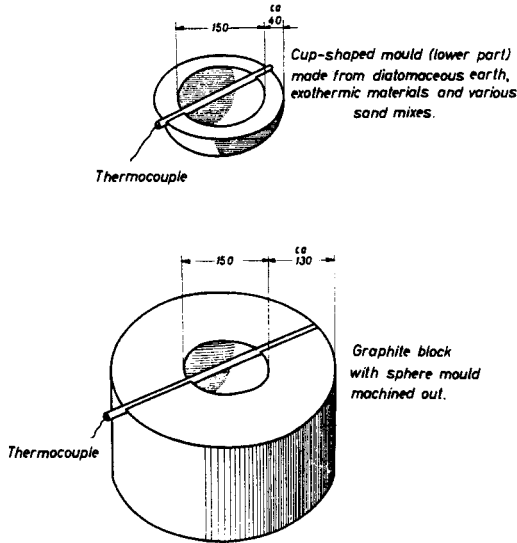


FIG. 304. Experimental layout, after Locke, Briggs and Ashbrook⁽²⁾.

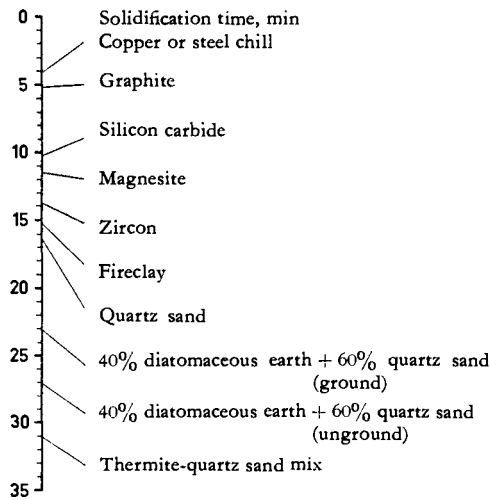


FIG. 305. Solidification times of a sphere of 150 mm diameter in various moulding materials (after Locke and Briggs).

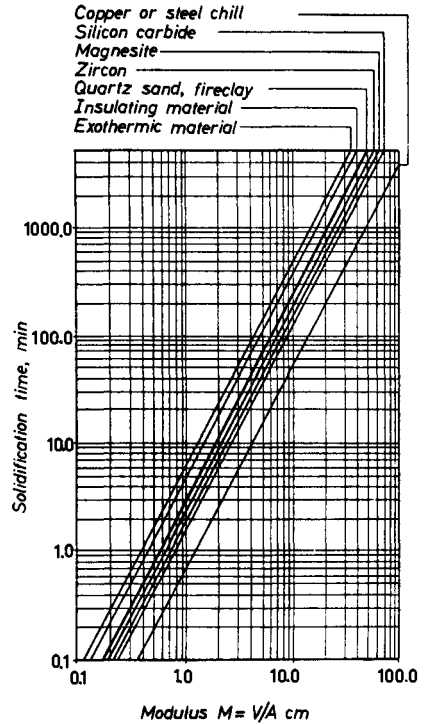


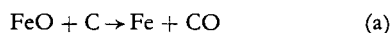
FIG. 306. Solidification times of cast steel parts as a function of the solidification modulus M and the moulding material.

A main field of application of high heat conductivity sands is the filling material between two chills (Fig. 272, sect. 8.4.1.) with the object of reducing the risk of hot tears by the rapid formation of a solid skin of steel. Compositions of these materials are given in Table 34. These sand mixes must not be adopted uncritically, but should be used only as a guide, to be adjusted by trial to the prevailing operating conditions. High-carbon chilling materials (for example, graphite, coke, silicon carbide) frequently cause a slight carbon pickup in the upper layers of the steel casting; this is usually not harmful, because of subsequent decarburization while annealing the casting.

TABLE 34. COMPOSITIONS OF HIGH THERMAL CONDUCTIVITY MATERIALS, AFTER LOCKE, BRIGGS AND ASHBROOK⁽²⁾, KRETSCHANOVSKI⁽²⁸⁾ AND FROM THE AUTHOR'S OWN EXPERIENCE

Data in parts by weight	Cooling materials								
	Copper pyrites	Steel grit	Cast iron turnings	Silicon carbide	Zircon	Magnesite	Forsterite	Chrome ore	Rutile
Base material	100	100	100	100	100	100	100	100	100
Sand (SiO ₂) Bentonite	5	2		4.5	1.25	3	2.5	2.4	1.25
Maize starch binder	2	0.5		0.5		2	0.5	1.0	0.5
Dextrine	1	1.0		1.5	0.1	2	1.25		
Waterglass			7						
Water	1	1.5		3	1.1	3	3	3	1.0
Remainder			Burn at minimum temp. of 700 °C	Watch for possible gas reactions with the steel!	These materials are roughly equivalent in their chilling action				
Remarks:	The data merely represent approximate values, to be checked previously in accordance with operating conditions								

If the carbon-containing materials are not dense (i.e. plates of graphite or silicon carbide) but are granular and therefore porous, the very fluid scale (FeO) which is always formed on solidification penetrates occasionally into the pores, and the following reactions take place:



and $3\text{Fe} + \text{C} \rightarrow \text{Fe}_3\text{C}$, or C dissolved in Fe.

The iron material permeated in this way can thus consist occasionally of graphitic grey cast iron, a phenomenon which can also be observed in starch-containing sands †.

Because the melting point of ferrous oxide is 1450°C and that of grey cast iron about 1280°C, penetration also occurs after the steel has solidified. Depending on the position on the casting (i.e. sand fillets, etc.), steel penetration which is difficult to dress out, or mixtures of FeO and grey iron in the form of a shell which breaks off easily can occur. The carbon monoxide produced often penetrates into the casting, with the formation of "wormholes" or porosity on the viscous surface of the casting. It is therefore recommended that mixtures of this type should be made as compact as possible, i.e. with a very high proportion of fines, which will reduce the volume of pores in the sand.

ro.2. Calculation of Moulding Materials with a Chilling Action

(It is desirable, but not absolutely necessary for the understanding of the use of such moulding materials, to study this section.)

The calculation is based on the principles discussed in Section 8.5, in particular on the apparent increase by a factor of y in the surface area of the casting, at the points of application of the chill or cooling sand (8.5.3.). The apparently increased surface A_s is calculated from equation 100, which is written, using the normal notation, as:

$$A_s = A_0 \sqrt{\frac{T_{\text{sand}}}{T_{\text{cooling material}}}} = A_0 \times y \quad (126)$$

which was used to plot Fig. 307.

According to Fig. 281, the true (geometrical) surface area of a casting is:

$$A_0 = A_{\text{sand}} + A_{\text{cooling material}} \quad (127)$$

The apparently increased total surface is then:

$$A_{\text{app.}} = A_{\text{sand}} + y \times A_{\text{cooling material}} \quad (128)$$

From equations 122 and 123 we obtain:

$$A_{\text{app.}} = A_0 + (y - 1) A_{\text{cooling material}}, \quad (129)$$

i.e. in the rapid calculation the known geometrical surface area A_0 is to be added to the cooling surface times $(y - 1)$. This factor is also given by Fig. 307.

† According to a personal communication from Prof. Dr.-Ing. K. Roesch, Remscheid.

The cooling surface of contact necessary to obtain the reduced modulus M_r is, according to equations (114) and (112):

$$A_{\text{cooling material}} = V_0 \frac{M_0 - M_r}{(y - 1) M_0 \times M_r} \quad (130)$$

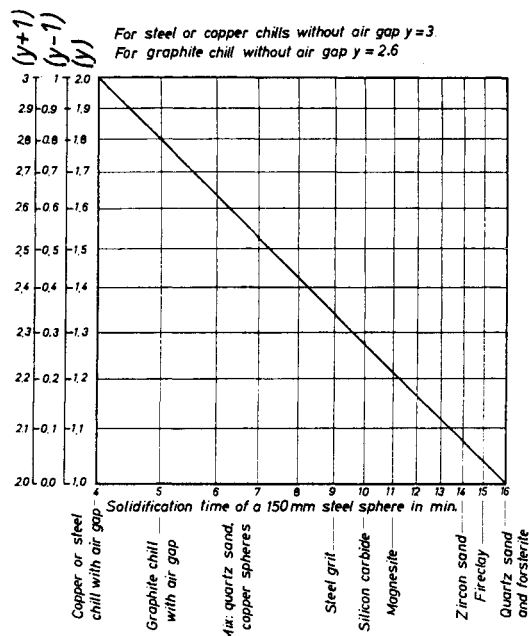


FIG. 307. Diagram for the determination of the apparent increase of chill areas using various heat-conducting materials.

From this the maximum chilling action can be calculated from Section 8.5.7, Fig. 284:

$$M_{r \text{ max}} = \frac{2 M_0}{y + 1} \quad (131)$$

In accordance with section 8.5.8 the thickness of the applied cooling material, cb is calculated from the heat balance (equation 96). In the usual notation this is given by:

$$W_{\text{ch}} = V_{\text{ch}} \times \gamma_{\text{ch}} = \frac{\gamma_{\text{metal}}(L + S)_{\text{metal}}}{t_{\text{ch}} \times C_{\text{ch}}} \times V_0 \frac{M_0 - M_r}{M_0} \quad (132)$$

According to equation (126):

$$\frac{M_0 - M_r}{M_0} = \frac{y - 1}{y + 1} \quad (133)$$

Hence at the surface of contact A_{ch} :

$$V_{\text{ch}} = A_{\text{ch}} \times D_{\text{ch}} \quad (134)$$

and the volume of a plate of thickness d over the point of contact

$$V_0 = A_{\text{ch}} \times d \quad (135)$$

and

$$D_{\text{cooling material}} = \frac{\gamma_{\text{metal}}(L + S)_{\text{metal}}}{y_{\text{ch}} \times t_{\text{ch}} \times c_{\text{ch}}} \times \frac{y - 1}{y + 1} \times d \quad (136)$$

This equation can only be used for cooling sands (on various foundations) when the temperature distribution in the chill packing material is known at the end of solidification, i.e. the mean temperature t_{ch} can be estab-

lished. On the other hand the necessary minimum thickness of chill materials of any degree of compactness with a uniform temperature distribution (for example chills of silicon carbide, light metal or graphite) can be determined immediately; this can also be done for cast metals other than steel. For example the necessary thickness of a graphite chill ($\gamma = 2.1, \gamma = 1.63, c_{ch} 0.36$) with cast steel, at a temperature of 500°C, amounts to:

$$D_{\text{graphite}} = d_{\text{casting}} \times \frac{7.8 \times 72}{2.1 \times 500 \times 0.36} \times \frac{0.63}{2.63} = 0.35 \times d_{\text{casting}}, \quad (137)$$

i.e. graphite chills can be somewhat thinner than corresponding iron chills. Table 35 gives some values for other cooling materials.

TABLE 35. DATA ON THE THICKNESS OF HIGH-CONDUCTIVITY PACKING FOR VARIOUS MATERIALS

Symbols:
 d_0 = wall thickness of the plate to be cooled
 γ = sp. gr. (g/cm³)
 c = sp. heat (cal/g)
 t_{ch} °C = temperature (at the completion of solidification of the plate)
 D = minimum thickness of the high-conductivity packing, according to equation 131, as a multiple of d_0

High thermal conductivity material	γ	γ	c	t_{ch}	$D_{min.}$	
Steel chill	with air gap	2	7.8	0.16	600	0.5
	without air gap	3				
Graphite Chill ⁽¹⁾	with air gap	1.8	2.1	0.36	500	0.36
	without air gap	2.6				
Steel grit ⁽²⁾		1.35		0.16	600	
Silicon carbide brick ⁽³⁾		1.27	2.4	0.23	500	2.42
Magnesite brick		1.22	2.8	0.25	600	1.32
Rammed zircon sand		1.08	3	0.24	35	1.0 ⁽⁴⁾

(¹) Calculated from equation (110).
 (²) c assumed to be the same as for steel.
 (³) Value uncertain, because the C content of the brick (which varies between 40 and 90%) was not given in the experiments.
 (⁴) Value determined experimentally after Stein⁽³⁴⁾, and calculated assuming $t_{ch} 35^\circ\text{C}$.

According to Chvorinov⁽¹⁾ the various cooling effects for each ceramic moulding material and each cast metal can be calculated as follows:

In general, according to section 2.2:

$$M = k \sqrt[3]{T} \quad (1a)$$

where k is a constant and T the solidification time.

Experiments have been carried out with the aim of deriving this constant theoretically from the physical values of sand and metal. Up to the present, it has not been possible to obtain a practical result which can be verified experimentally. The reason for this is that on the sand side an infinitely large number of intermediate

stages exist between the high metal/sand interface temperature on the one hand and room temperature on the other. Each of these intermediate stages possesses different thermal values. In addition the high temperature zones diffuse into the moulding sand, so that the thermal equilibria also change as a function of time.

On the metal side a metal/sand interface equal to the solidus temperature is assumed. This assumption is only approximately true, and the temperature distribution in the casting itself cannot be calculated accurately for the reasons outlined above.

For the purpose of this book, therefore, it would be pointless to give approximate calculations which are (1), very extensive and (2), give less satisfactory results than suitably devised experiments. For this reason the constants k given here were derived directly from experimental results.

10.3. Practical Application and Calculation of Moulding Materials Having a Chilling Action

IMPORTANT FOR PRACTICE

The modulus calculation will be carried out on the basis of Fig. 308 (flange) as an example. The cast steel flange will be fed without a feeder head from the thinner wall. Because of the risk of hot tears, chills can only be attached to the outer and lower sides, with a moulding material buffer equal to the width of the chill. The cooling action achieved in this way is not sufficient in itself, and instead of quartz sand a magnesite sand is placed between the chills.

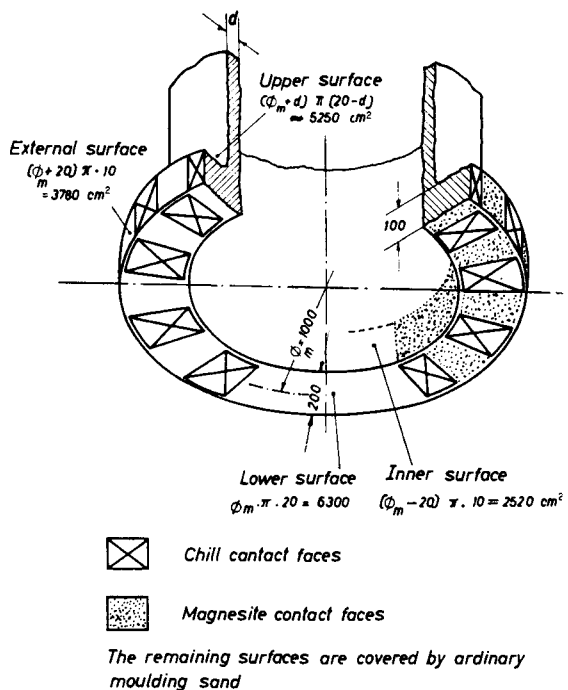


FIG. 308 Flange casting cooled.

(a) by chills.
 (b) by chills and magnesite.

The process of calculation can be seen from Table 36. First of all, values of volume/surface area are calculated by the "classical" method. This method was compared with the much simpler calculation using the ratio volume/periphery, which gives practically the same results.

Fundamentally, an apparent increase in the effective cooling area occurs when cooling materials are attached, and hence the modulus decreases. The apparently in-

creased surface area A_{app} , is obtained from equation (129): the surface of contact of the cooling material multiplied by the factor $(y - 1)$ is added to the geometrical surface A_0 . This factor can be obtained for various chilling materials from Fig. 307.

Two cases were calculated in Table 36, i.e. the use of chills with and without magnesite. Using magnesite the thickness of the wall "feeder" can be reduced only to a limited extent; ceramic chilling materials are much less effective cooling agents than metal chills.

These calculated results are confirmed by the experiments of Stein and co-workers⁽³⁴⁾, who attached steel and graphite chills and zircon sand packing to tubular castings. While steel and graphite behaved almost in the same way, and the cast tube quality was good, the zircon sand packing had only a slight effect and the quality of the casting was much inferior.

TABLE 36. PROCESS OF CALCULATION USED FOR FIG. 308

Chill material	$y - 1$
Steel chill with air gap	0.2
Steel chill without air gap	1.0
Magnesite	2.0

No.	Calculation using the	
	(a) vol./surface area ratio	(b) the bar formula
1	Geometrical surface area: outside $(\varnothing_m + 20) \times \pi \times 10 = 3780 \text{ cm}^2$	Geometrical periphery: 10 cm
2	below $\varnothing_m \times \pi \times 20 = 6300$	20
3	inside $(\varnothing_m - 20) \pi \times 10 = 2520$	10
4	above $(\varnothing_m + d) \times \pi \times (20 - d) = 5250$	16
5	$A_0 = \text{Sum} = 17,850 \text{ cm}^2$	$P_0 = 56 \text{ cm}$
6	Volume: $\varnothing_m \times 20 \times 10 = 63,000 \text{ cm}^3$	Area of face: $A_0 = 10 \times 20 = 200 \text{ cm}^2$
7	Modulus $M_0 = V_0/A_0 = 3.53 \text{ cm}$	$M_0 = A_0/P_0 = 3.55 \text{ cm}$
Chill calculation		
8	Face 1a half covered with chills with air gap $A_{1a} \times 0.5 \times (y - 1) = 1890 \text{ cm}^2$	Length 1b half covered with chills $L_{1b} \times 0.5 (y - 1) = 5 \text{ cm}$
9	Face 2b half covered with chills, without air gap $A_{2b} \times 0.5 \times (y - 1) = 6300 \text{ cm}^2$	Length 2b half covered with chills $L_{2b} \times 0.5 (y - 1) = 20 \text{ cm}$
10	Face 1a other half covered with magnesite $A_{1a} \times 0.5 \times (y - 1) = 378 \text{ cm}^2$	Length 1b other half covered with magnesite $L_{1b} \times 0.5 (y - 1) = 1 \text{ cm}$
11	Face 2a other half covered with magnesite $A_{2a} \times 0.5 (y - 1) = 630 \text{ cm}^2$	Length 2b other half covered with magnesite $L_{2b} \times 0.5 (y - 1) = 2 \text{ cm}$

No.	Calculation using the	
	(a) vol./surface area ratio	(b) the bar formula
12	Inner face 3a covered with magnesite $A_{3a} \times (y - 1) = 504 \text{ cm}^2$	Inner length 3b covered with magnesite $L_{3b} \times (y - 1) = 2 \text{ cm}$
Determination of apparently increased surface using chills without magnesite		
13	$A_{app} = \text{Sum of rows 5a, 8a, 9a gives apparently increased area } 26,040 \text{ cm}^2$	Sum of rows 5b, 8b, 9b gives $P_{app} = 81 \text{ cm}$
Reduced modulus using chills without magnesite		
14	$M_r = V_0/A_{app} = 63000/26040 = 2.42 \text{ cm}$	$M_r = A_0/P_{app} = 200/81 = 2.48 \text{ cm}$
Determination of the apparently reduced surface area using chills and magnesite		
15	$A_{app} = \text{Sum of rows 5a, 8a, 9a, 10a, 11a, 12a} = 27,552 \text{ cm}^2$	Sum of rows 5b, 8b, 9b, 10b, 11b, 12b $P_{app} = 86 \text{ cm}$
Reduced modulus using chills and magnesite		
16	$M_r = V_0/A_{app} = 63000/27552 = 2.28 \text{ cm}$	$M_r = A_0/P_{app} = 200/86 = 2.32 \text{ cm}$
Determination of min. thickness d of the housing wall necessary for feeding the flange. $d = 2M_r, 1.1$		
In case 14 (chill without magnesite)		
17	$d = 53 \text{ mm}$	54 mm
In case 16 (chill and magnesite)		
18	$d = 50 \text{ mm}$	51 mm

10.4. Manufacture of Extended Artificial End Zones by Means of Chilling Materials

IMPORTANT FOR PRACTICE

The layout and results of the experiments by Stein and co-workers⁽³⁴⁾ are shown in Fig. 309. In the absence

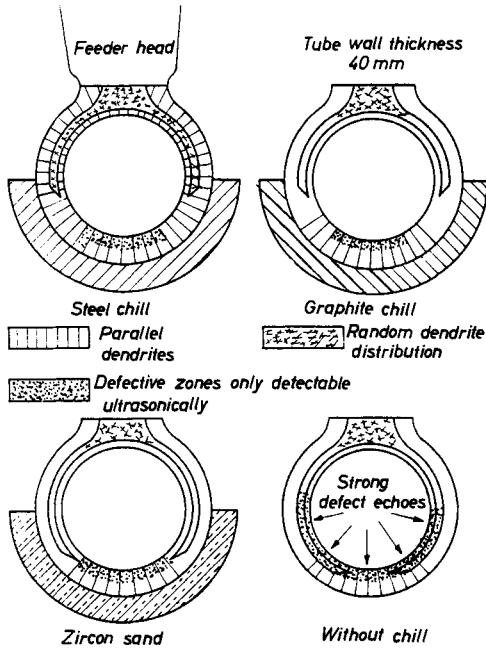


FIG. 309. Diagrammatic representation of the primary structure of steel tubes, cast in various heat-conducting materials.

of stepped chills as in Figs. 244 and 245, it is understandable that slight porosity must occur at the points indicated in the centre of the end zone. With stepwise cooling similar conditions to those found on parasite plates can be produced in which the thicker step feeds the thinner one.

In experiments by the author (cf. Fig. 310) the feeding range was stepped, and thus extended, by attaching

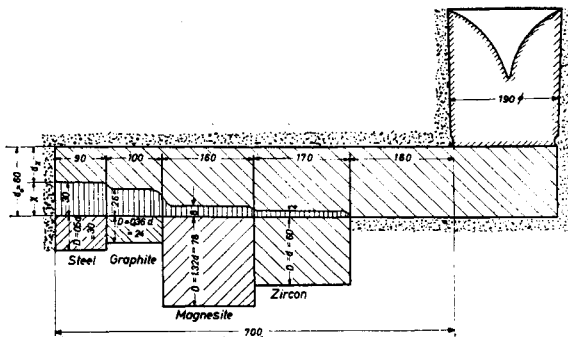


FIG. 310. Plate cooled in steps by attaching various heat-conducting materials.

various cooling materials. In practice the chilling sand packing can only be placed as cores of various thicknesses, because free ramming by hand is too inaccurate. In special cases the possibility of chill cores will be considered. Krestschanovski⁽²³⁾ also described the different chilling effects of various materials, without giving generally valid formulae.

The feeding range when using mould materials with a chilling action (and metal chills) is of importance. According to sect. 3.4 (Fig. 57), the dendrites are shortened on cooled surfaces, i.e. the solidification band becomes smaller. This corresponds to smaller flow resistances towards the end of solidification, that is the feeding range becomes greater.

The author observed an increase of fifty per cent in the lengths of the sound zones when using zircon moulding sand, compared with the values shown in Figs. 47 and 48. However, the amount of material observed is too small for generally valid conclusions to be drawn from the results, and the author recommends, on safety grounds, that the values of Figs. 47 and 48 should continue to be used until the results of large-scale trials are available.

10.5. Displacement of the Segregated Zone by the Use of Moulding Materials with a Chilling Action

It is clear with the more rapid growth of the dendrites at the cooling walls that the segregated zone will be displaced in the direction of the uncooled walls. The stronger the chilling action of the moulding material, the greater this displacement will be. By using chills of steel, copper or graphite (all of which are practically equivalent) this displacement is at a maximum. The amount of displacement attainable can be calculated from equations (105) and (128). Both these equations deal with the apparent increase in surface area caused by chill moulding materials.

EXAMPLE 1

According to Fig. 311, the position of the segregated zones is to be established when one side (b) is covered with chills (c) with magnesite brick (d) with zircon sand.

To calculate the segregated zone it is appropriate to use equation (42) after Stein⁽⁴²⁾. The distance X of the segregated zone from the uncooled surface is given by:

$$X = \frac{d}{2} \times \frac{A_{\text{sand}}}{y \times A_{\text{cooling material}}} \quad (138)$$

where y is the factor of the apparent surface increase, which amounts to $y \approx 3$ for chills without an air gap, and $y \approx 2$ for chills with an air gap, and which can be obtained for other cooling materials from Fig. 307. In this example, the upper part consists of quartz sand and the lower portion (without air gap) of the cooling material. The calculations are shown in the relevant tables.

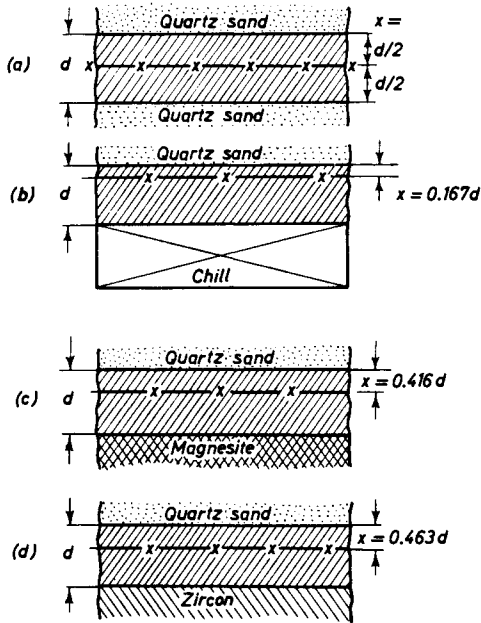


FIG. 311. Displacement of the segregating zone $\times - \times - \times$ by the use of heat-conducting mould materials.

(a) Top and bottom quartz sand. Segregated zone approximately in the centre.

(b) Top quartz sand, bottom chill without air gap, equation (105).

$$A_{app} = A_{sand} + y \cdot A_{chill}; y \approx 3 \text{ (chill without air gap)}$$

$$x_{chill} = \frac{d}{2} \cdot \frac{1}{3} = \frac{d}{6} = 0.167 d$$

(c) Top quartz sand, bottom magnesite. From Fig. 307:

$$J_{magnesite} \approx 1.2$$

$$x_{magnesite} = \frac{d}{2} \cdot \frac{A_{sand}}{y \cdot A_{magnesite}} = \frac{d}{2} \cdot \frac{1}{1.2} = 0.416 d$$

(d) Top quartz sand, bottom zircon sand. From Fig. 307:

$$J_{zircon} \approx 1.08$$

$$x_{zircon} = \frac{d}{2} \cdot \frac{A_{sand}}{y \cdot A_{zircon}} = \frac{d}{2} \cdot \frac{1}{1.08} = 0.463 d$$

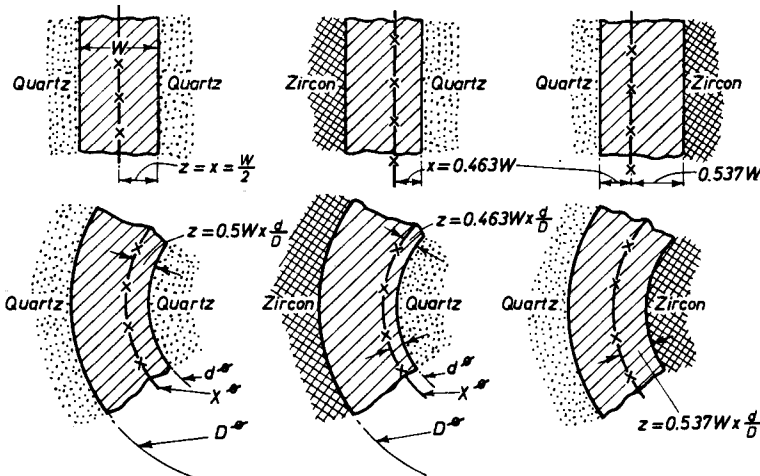


FIG. 313. Position of the segregated zone in tubular bodies using zircon sand.

EXAMPLE 2

The displacement of the segregated zones by various moulding and core sands is to be determined for a tubular casting.

First of all the equation (42) derived by Stein⁽⁴²⁾ will be used (Fig. 312) starting with flat plates. With such plates the segregated zone lies in the centre of the plates.

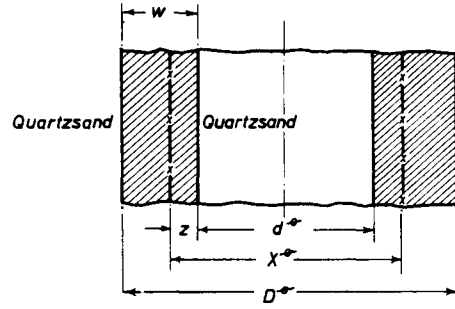


FIG. 312. Position of the segregated zone⁽⁴²⁾ in tubular castings. Derivation of Stein's equation⁽⁴²⁾.

With flat plates $x_{plate} = \frac{W}{2}$. When the plates are curved to form tubes, x is reduced by a factor equal to the ratio of the internal to the external diameter.

$$x_{tube} = \frac{W}{2} \cdot \frac{d}{D}$$

The diameter X of the segregated zone is

$$X = d + 2x_{tube} \tag{42a}$$

If mould and core are formed from the same sand, then:

$$X = d + 2 \cdot \frac{W}{2} \cdot \frac{d}{D} = d + W \cdot \frac{d}{D} \tag{42b}$$

By placing zircon sand on one side, as shown in Fig. 311 c, the segregated zone is displaced. With flat plates, we have

$$X = 0.463 d$$

where X is the distance of the segregate from the unchilled surface. This displaced zone is further displaced by curvature, according to Fig. 313.

TABLE 37. POSITION OF THE SEGREGATED ZONE IN TUBULAR CASTINGS

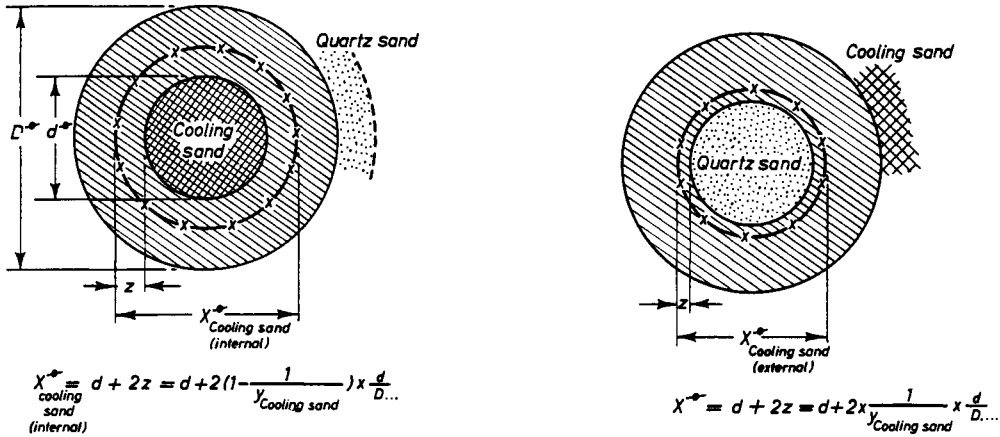


Table 37 names the corresponding factors for establishing the position of the segregates in tubular bodies in a generally valid form.

For tubes with small core diameters a further dis-

placement of the segregated zone by the action of heat takes place in the sense of Section 7.4. The calculation of this effect for cooling sands would go beyond the scope of the present work.

CHAPTER 11

INCREASING THE THERMAL GRADIENT BY THE USE OF INTERNAL CHILLS

11.1. General

IMPORTANT FOR PRACTICE

To the extent that the experience available is limited, the use of internal chills in steel castings is risky. The dimensions of internal chills for specific cases have been established by means of numerous experiments carried out by various authors. The author has attempted to derive generally applicable formulae from these special results, and has relied mainly on the very instructive investigations reported by Lanzendörfer^(34, 35), which have the same fundamental importance as the sphere experiments of Locke, Briggs and Ashbrook⁽²⁾. Satisfactory steel quality is also essential with internal chills. Figure 314a shows a chilled lug in which can be seen pinhole porosity in the rapidly solidified edges, similar to that illustrated in Figs. 224, 225 and 226. In the quenched zone of the internal chill the porosity is much more pronounced as a result of the very much higher rate of solidification.

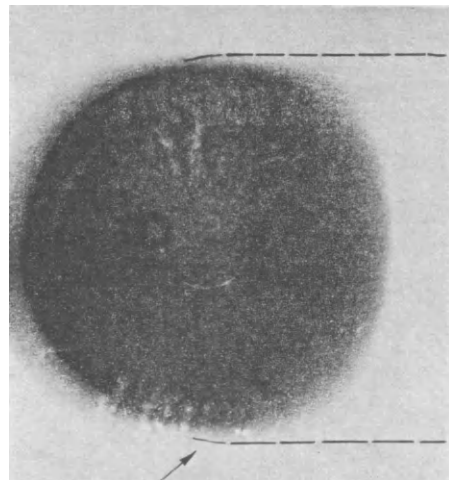


FIG. 314 a. Porosity at the internal chill of a lug. Note the porosity zone at the edge of the lug, which has no connection with the porosity zone of the internal chill.

TABLE 37. POSITION OF THE SEGREGATED ZONE IN TUBULAR CASTINGS

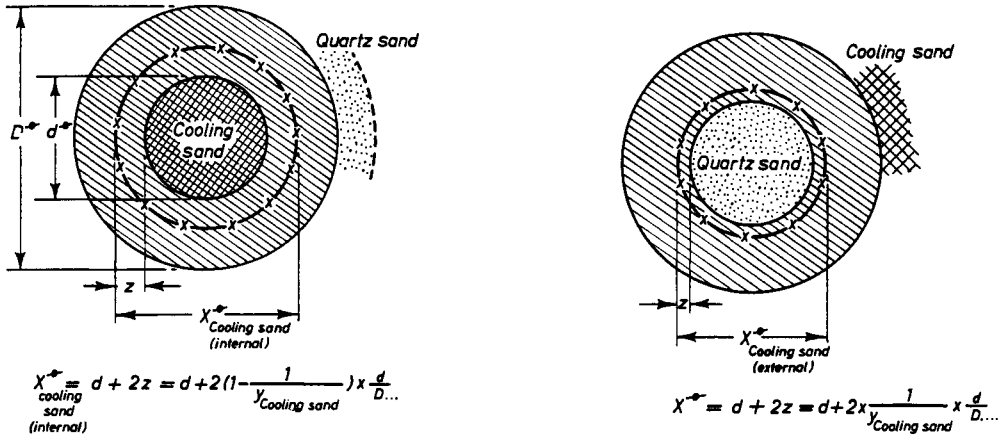


Table 37 names the corresponding factors for establishing the position of the segregates in tubular bodies in a generally valid form.

For tubes with small core diameters a further dis-

placement of the segregated zone by the action of heat takes place in the sense of Section 7.4. The calculation of this effect for cooling sands would go beyond the scope of the present work.

CHAPTER 11

INCREASING THE THERMAL GRADIENT BY THE USE OF INTERNAL CHILLS

11.1. General

IMPORTANT FOR PRACTICE

To the extent that the experience available is limited, the use of internal chills in steel castings is risky. The dimensions of internal chills for specific cases have been established by means of numerous experiments carried out by various authors. The author has attempted to derive generally applicable formulae from these special results, and has relied mainly on the very instructive investigations reported by Lanzendörfer^(34, 35), which have the same fundamental importance as the sphere experiments of Locke, Briggs and Ashbrook⁽²⁾. Satisfactory steel quality is also essential with internal chills. Figure 314a shows a chilled lug in which can be seen pinhole porosity in the rapidly solidified edges, similar to that illustrated in Figs. 224, 225 and 226. In the quenched zone of the internal chill the porosity is much more pronounced as a result of the very much higher rate of solidification.

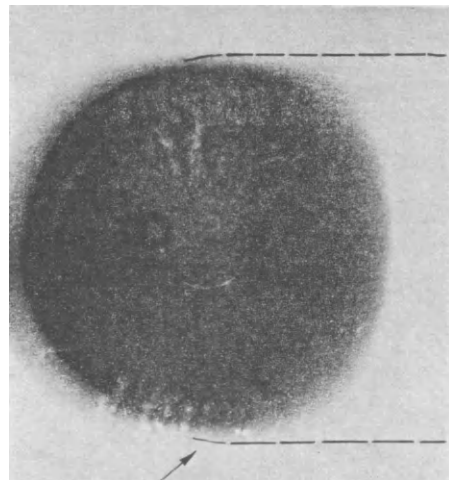


FIG. 314 a. Porosity at the internal chill of a lug. Note the porosity zone at the edge of the lug, which has no connection with the porosity zone of the internal chill.

It is also important for the chill material to be made of killed steel, free from gases, otherwise defects will occur such as those illustrated in Figs. 314b-c. (The same is also true for chaplets.)

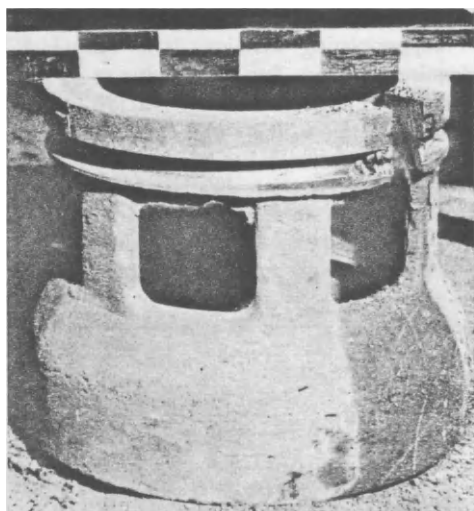
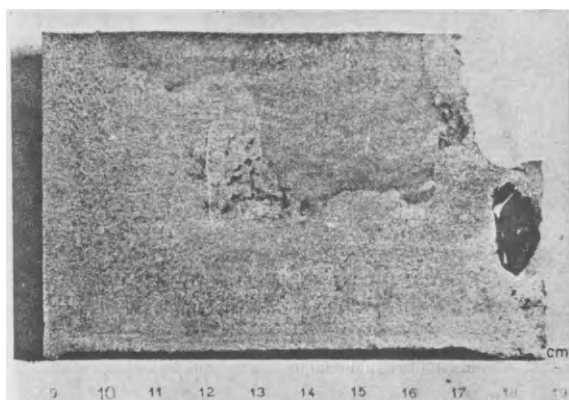
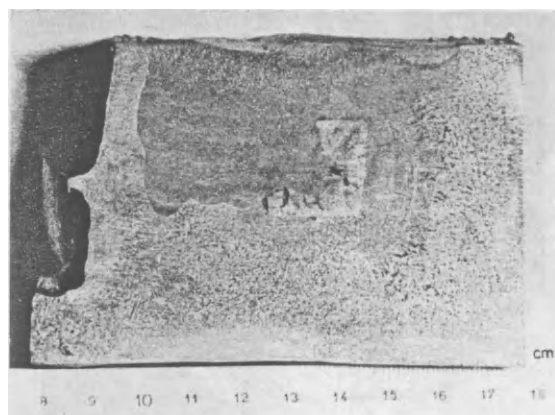


FIG. 314b. An internal chill was inserted in the lower flange of this casting, in order to economize in feeder metal. Large defective zones were found on ultrasonic and radiographic inspection. An attempt to save the casting by welding failed.



c (1)



c (2)

Mild steel is often used for internal chills, which weld on easily. This is correct practice but it must be remembered that mild steels are often supplied in rimmed qualities. In the author's experience low-carbon steels which have been deoxidized mainly with aluminium have proved satisfactory.

Internal chills represent internal surfaces in castings. Foreign bodies such as gases, slag and sand particles, separate preferentially on these surfaces. This precipitation is made more difficult when the internal chills stand vertically in the casting (Fig. 314d). In the hori-



FIG. 314d. Internal chills in the lugs of LKW. The chills stand vertically in the casting.

zontal position it will usually be found that such foreign bodies occur on the underside of the chill.

Internal chills are to a large extent harmless when they are subsequently removed by machining (drilling). In this case a safety margin can be left round the chill, so that the blowholes, etc., can be safely machined out.

The coating applied to internal chills is of importance. It is clear that rust, and oxidation of all kinds, must lead to a heavy evolution of gas. Condensed moisture (especially with green sand moulds) also leads to blowholes.

Tinning has been adopted as a means of preventing internal chills from rusting but the tinning process must be carried out satisfactorily. When this is not done, rust is often found underneath the tin coating.

The tin (Sn) forms a separating layer in the casting. In the most favourable case it is floated off by the steel flowing past it, and distributed through the metal. In the most unfavourable case an Fe-Sn layer with a lower strength is formed. With steels which are poured cold the tin finally hinders any bonding with the casting.

FIG. 314c. Section taken from the lower flange (314b) etched deeply with sulphuric acid. The following causes of the defects were established:

- (1) The material of the chill is not fused on. This defect would be prevented if calculations were carried out by means of the rules given later.
- (2) The chill material (rimmed steel) is also porous in itself. Presumably the gas-containing chill material has even given up gas to the casting.

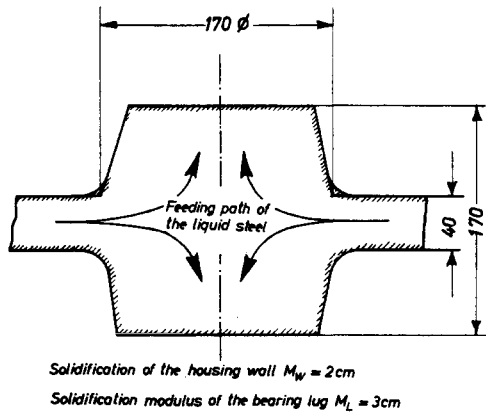


FIG. 315a. Bearing lug which is difficult to reach, and which is to be fed from the housing wall.

Low-grade chills are sometimes galvanized. The zinc (Zn) forms an extremely brittle Fe-Zn alloy with the iron, which greatly reduces the strength of the casting.

A copper (Cu) coating has proved fairly satisfactory with small internal chills (and chaplets). Fe-Cu alloys sometimes possess favourable properties. However, the correct copper-plating technique is an art which has been acquired by very few manufacturers of internal chills.

According to the author's experience, it is best to use a chill material which has been bright ground, or at least has a perfectly clean, sandblasted surface. Small chills must be kept in airtight containers which are stored in a dry environment. Each container must be provided with a strongly hygroscopic cartridge (of burnt lime for example).

Larger chills are ground to a bright metallic surface before use.

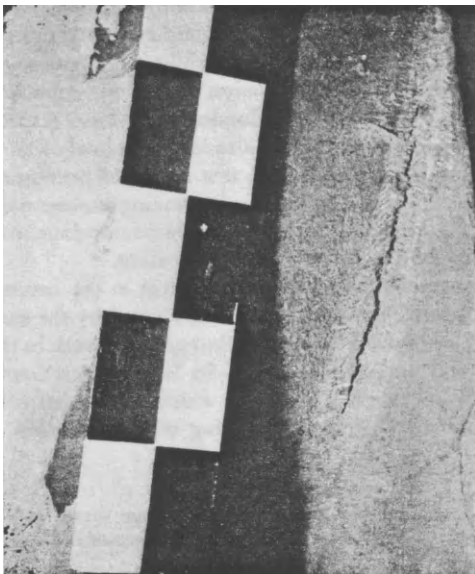
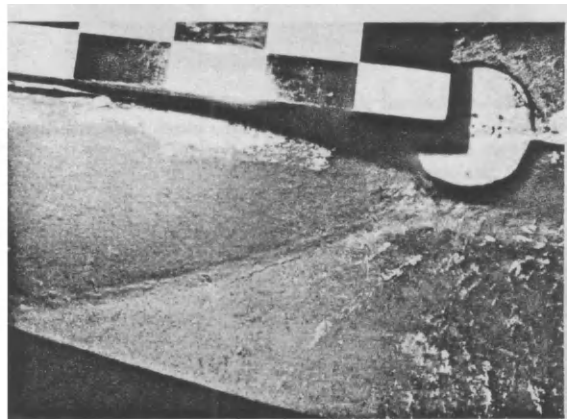
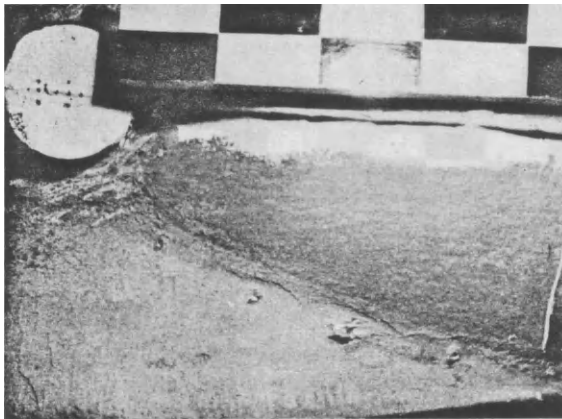
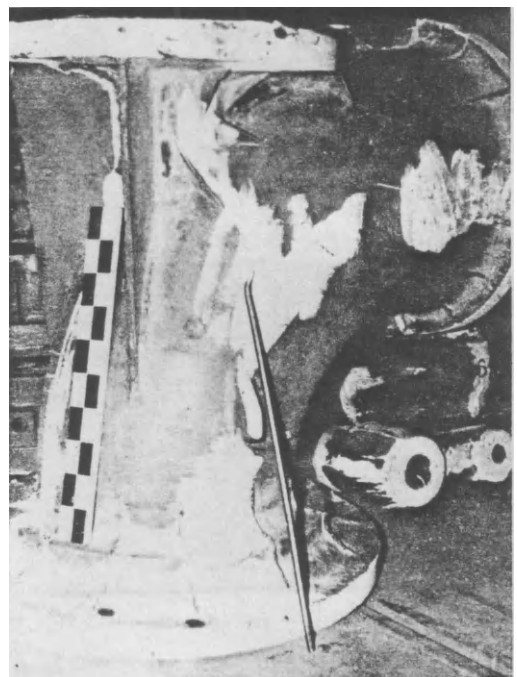


FIG. 315b. Inadequate and incorrectly dimensioned chill on the joints of housing wall and ribs. Shrinkage tears were formed subsequently.



The measures described may seem troublesome to many foundrymen, but the decisive question is whether low-grade commercial castings are to be made, or whether value is to be placed on quality.

In many cases the trend is in the direction of high-grade castings. Many castings which ten years ago were still accepted without hesitation are now rejected.

Similar basic considerations apply both to internal and external cores. It must not be forgotten, however, that in spite of accelerated solidification, the casting must still be fed. A chilled accumulation of material, such as the lug in Fig. 315 a, is fed from the housing wall. The thickness of the housing wall limits the chilling of the lug to a specific amount if it is to be cast sound.

It is often necessary to cool junctions of all types (for example, from housing wall to fin). Junctions represent a considerable increase in modulus, which can be calculated in accordance with sect. 2.5. This calculation must be based on the rules mentioned here.

In this case the junction must be fed by the thinner housing wall. The chill material must be so dimensioned that the junction solidifies earlier than the housing wall, which is not the case in housings as shown in Fig. 315 b. The so-called "fir tree configuration" was used in chilling fins; shrinkage cavities were produced in the junctions, which led to the formation of hot tears.

According to the author's experience it is safer:

1. When possible, to cast the fins separately and subsequently weld them on, making a good joint. The necessary welding work is less, and is more reliable than the repair welding shown in Fig. 315 b.

2. When this is impossible, to cast the junction sound by placing special fillet chills (cf. Figs. 253 a-c), or at least to keep the shrinkage cavity down to an amount where it will be harmless (Figs. 254-257). Internal chills should only be used as a last resort.

Unfortunately, this feeding range was not mentioned in most of the investigations which have so far been carried out. In many cases feeding took place through the pouring cup via the ingate to the casting. However, the important ingate dimensions are not mentioned in this case. A severely chilled test piece can nonetheless exhibit shrinkage cavities if adequate feeding of the residual cross-section is not ensured.

Sections 11.2-11.8 give the physico-mathematical principles; it is not absolutely necessary to study them in order to understand the summary for the practical man given in sect. 11.9.

11.2. The Heat Balance of Welded-in Chills

When internal chills are inserted in a body with a solidification modulus M_0 , and an associated solidification time T_0 , it should solidify in the same reduced time T_r as a simulated body with the smaller modulus M_r .

Modulus and solidification time are related according to Chvorinov⁽⁴⁾ by the equation:

$$T_{min} = M_{cm}^2 \times 2.1 \quad \text{or} \\ T_{sec} = M_{cm}^2 \times 126 \quad (141)$$

2.1 and 126 are constants which apply with sufficient accuracy for most bodies.

The housing wall (Fig. 315 a) has a modulus of 2 cm, while the lug has a modulus $M_0 = 3$ cm. In order to be certain that the lug will solidify sound, its modulus must be about 10 per cent less than that of the housing wall which feeds it. M_r is therefore 1.8 cm. From the equation the relevant solidification time T_r is $(1.8)^2 \times 126 = 408$ sec. Hence the internal chill must be welded to the casting within 408 sec.

The available time for welding is therefore dependent only on the reduced modulus M_r , and is not a function of the original modulus M_0 . The influence of steel temperature is still to be investigated.

Using an internal chill, a body with a volume V_0 should solidify in the same reduced time as a simulation body with a smaller volume V_r .

The volume of the inserted internal chill V_{ch} is first subtracted from V_0 , so that

$$V_0 - V_{ch} = V_a$$

and

$$V_a - V_r = \Delta V \quad (142)$$

In the transfer of the heat from the casting to the chill the laws of heat flow must be taken into account. The chill can only be welded after it has reached a temperature of about 1485°C. As heat transfer is possible only from the hotter to the cooler body, the temperature of the casting must not previously have fallen below 1485°C.

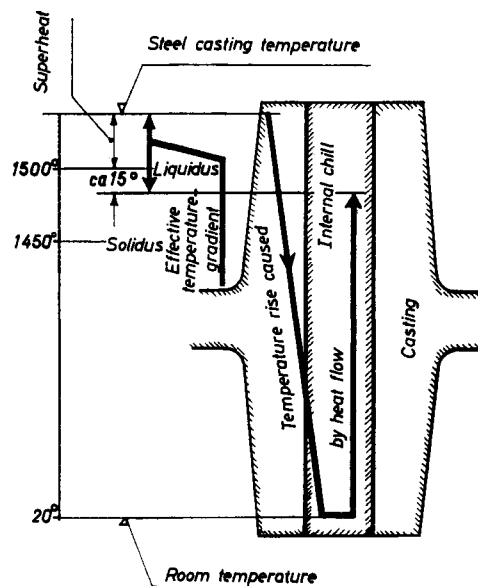


FIG. 316. Heat flow on fused-in chills.

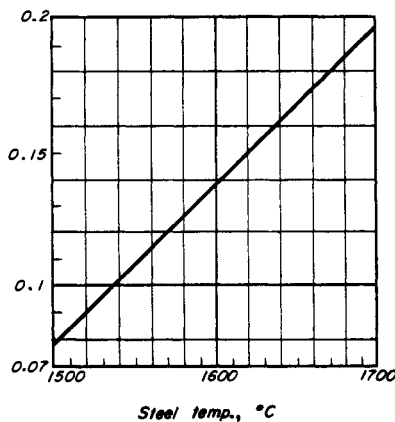
The amounts of heat liberated from the casting below this temperature can no longer be taken up by the chill to weld it into the casting. Figure 316 illustrates the heat flow in internal chills. It can be seen from this scheme that the maximum amounts of heat available for welding on an internal chill are as follows:

The superheat for the region above 1500°C plus about 1/3 of the latent heat of fusion or solidification, which is liberated between 1450–1500°C (the superheat is generally calculated from 1450°C in the equations formulated here). As no welding, or very little, occurs below 1500°C, the heat balance in this case is calculated for a temperature range beyond 1500°C.

The amounts of heat available for fusion are given in Table 38 for various superheats.

TABLE 38. DATA FOR CALCULATION OF WELDED-IN CHILL MATERIAL

Steel temp. °C	Amount of heat available for the chill welding-in cal/g			f
	1/3 L	S	Sum	
1500	21	—	21	0.0782
1550	21	10	31	0.1096
1620	21	24	45	0.1500
1700	21	40	61	0.1930



The amount of heat given off by the volume difference ΔV is:

$$\Delta V \times \gamma \times (1/3 L + S) = (V_0 - V_{ch} - V_r) \times \gamma \times (1/3 L + S) \quad (143)$$

This amount of heat must correspond to the quantity which can be taken up by the internal chill. The chill must first be heated to about 1450°C, after which it is partly melted on welding in, for which about half the latent heat of fusion of the material of the chill is required. The amount of heat taken up by the internal chill is thus:

$$V_{ch} \times \gamma \times (c \times 1450 + L/2) = (V_0 - V_{ch} - V_r) \times \gamma \times (c \times 16 \times 1450 + 64/2) = 264 V_{ch} \times \gamma \quad (144)$$

According to the condition—amount of heat given off = amount of heat taken up—we have:

$$V_{ch} \times \gamma \times 264 = (V_0 - V_{ch} - V_r) \times \gamma \times (1/3 L + S) \quad (c)$$

from which:

$$V_{ch} = \frac{(1/3 L + S)(V_0 - V_r)}{264 + (1/3 L + S)} = \frac{(1/3 L + S)}{264 + (1/3 L + S)} \times V_0 \times \frac{(M_0 - M_r)}{M_0} = f \times V_0 \times \frac{M_0 - M_r}{M_0} \quad (145)$$

in which the latent heat of fusion L , the superheat S and the number 264 are incorporated into a factor f . Table 38 gives some values of f .

From the above equation the necessary weight of the internal chill becomes:

$$W_{ch} = f \times \gamma \times V_0 \times \frac{M_0 - M_r}{M_0} \quad (146)$$

The calculation W_{ch} is facilitated by the nomogram of Fig. 317.

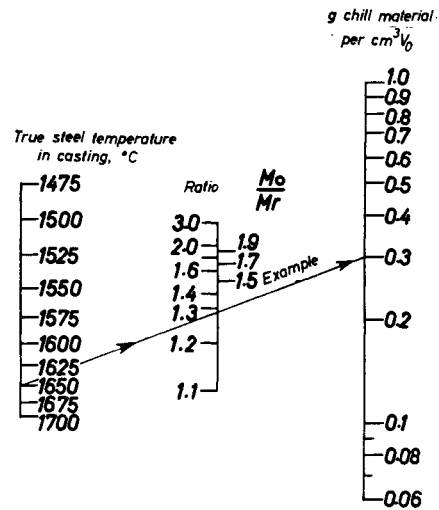


FIG. 317. Amount of fused-in chill material as a function of the modulus and temperature.

The example in Fig. 317 indicates that with a true steel temperature in the casting of 1650°C and a ratio $M_0/M_r = 1.28$, about 0.3 kg chill material can be inserted per dm^3 casting volume. In this case “casting volume” obviously denotes the volume of the part of the casting to be chilled. Table 39 also helps in obtaining the chill dimensions quickly.

EXAMPLE

The part of the casting to be chilled has a volume of $10 dm^3$ (the remaining relationships as given in the above data), so that $10 \times 0.3 = 3$ kg chill material are to be inserted. The following examples of chill dimensions are taken from Table 39:

cross-section length wt. of chill
 20 × 20 mm 1 m 3.14 kg
 or 10 × 10 mm 4 m 3.16 kg
 or 8 × 8 mm 6 m 3.0 kg
 etc.

The large number of possible shapes indicates that in addition to the heat balance other factors must be considered in determining the most suitable dimensions of the chill.

TABLE 39. WEIGHT IN kg/m OF SQUARE SECTION CHILLS WITH A LENGTH ACROSS THE SECTION OF d

d mm	No. of chills P										d mm	No. of chills P									
	1	2	3	4	5	6	7	8	9	10		1	2	3	4	5	6	7	8	9	10
1	7.9	16	24	32	40	48	56	63	71	79	30	7.07	14.1	21.2	28.4	35.4	42.5	49.5	56.6	63.6	70.7
1.5	18	36	54	72	90	108	126	144	162	180	32	8.04	16.1	24.1	32.2	40.2	48.2	56.3	64.3	72.3	80.4
2	32	64	96	128	160	192	224	256	288	320	34	9.08	18.2	27.3	36.4	45.5	54.6	63.7	72.8	81.9	90.8
3	71	142	213	284	355	426	497	568	639	710	36	10.2	20.4	30.6	40.8	51.0	61.2	71.4	81.6	91.8	102
4	125	250	375	500	625	750	875	1000	1125	1250	38	11.3	22.6	34.0	45.4	56.6	68.0	79.1	90.4	102	113
5	0.2	0.4	0.6	0.8	1.0	1.2	1.4	1.6	1.8	2.0	40	12.6	25.2	37.8	50.6	63.2	75.8	88.2	101	113	126
6	0.28	0.56	0.84	1.12	1.4	1.68	1.96	2.24	2.52	2.8	42	13.9	27.8	41.6	55.6	69.5	83.5	97.3	111	125	139
7	0.39	0.78	1.17	1.57	1.95	2.34	2.74	3.12	3.52	3.9	44	15.2	30.4	45.6	60.8	76.0	90.2	107	122	137	152
8	0.50	1.0	1.5	2.0	2.5	3.0	3.5	4.0	4.5	5.0	46	16.6	33.2	50.0	66.5	83.0	99.5	116	123	149	166
9	0.64	1.28	1.92	2.56	3.2	3.84	4.48	5.12	5.76	6.4	48	18.1	36.2	54.3	72.4	90.6	109	127	145	163	181
10	0.79	1.58	2.37	3.16	3.95	4.75	5.54	6.34	7.11	7.90	50	19.6	39.2	58.8	78.4	98.0	118	137	157	177	196
11	0.95	1.90	2.85	3.80	4.75	5.70	6.65	7.60	8.55	9.50	52	21.2	42.4	63.6	84.8	107	128	149	170	192	212
12	1.13	2.26	3.39	4.42	5.65	6.76	7.9	9.02	10.2	11.3	54	22.9	45.8	68.7	91.5	114	137	161	183	206	229
13	1.33	2.66	4.0	5.32	6.65	8.00	9.32	10.6	12.0	13.3	56	24.6	49.2	74.0	99.0	123	148	172	197	222	246
14	1.54	3.08	4.62	6.16	7.70	9.24	10.8	12.3	13.9	15.4	58	26.4	52.8	79.2	105	132	158	185	211	238	264
15	1.77	3.54	5.32	7.10	8.86	10.7	12.4	14.2	15.9	17.7	60	28.3	56.6	85.0	113	142	170	198	226	255	283
16	2.01	4.02	6.03	8.04	10.1	12.1	14.1	16.1	18.1	20.1	62	30.2	60.4	90.6	121	152	182	212	243	273	303
17	2.27	4.54	6.82	9.10	11.3	13.7	15.9	18.2	20.4	22.7	64	32.2	64.4	96.6	129	162	194	226	258	290	322
18	2.54	5.08	7.62	10.1	12.7	15.2	17.8	20.3	22.8	25.4	66	34.2	68.4	103	137	172	206	240	274	308	342
19	2.83	5.66	8.49	11.3	14.2	17.0	19.8	22.6	25.5	28.3	68	36.3	72.6	109	145	182	218	254	290	326	363
20	3.14	6.28	9.42	12.6	15.7	18.8	22.0	25.2	28.3	31.4	70	38.5	77.0	116	154	193	231	270	308	346	385
21	3.46	6.92	10.4	13.9	17.3	20.8	23.3	27.6	31.2	34.6	72	40.7	81.4	122	163	204	245	285	326	366	407
22	3.80	7.60	11.4	15.2	19.0	22.8	26.6	30.4	34.2	38.0	74	43.0	86.0	129	172	215	258	302	344	388	430
23	4.20	8.40	12.6	16.8	21.0	25.2	29.5	33.6	37.8	42.0	76	45.3	90.6	137	183	227	272	318	364	410	453
24	4.52	9.04	13.6	18.1	22.6	27.1	31.6	36.2	40.6	45.2	78	47.8	95.6	144	192	240	287	335	383	431	478
25	4.91	9.82	14.8	19.7	24.6	29.5	34.4	39.4	44.3	49.1	80	50.2	100	151	202	252	303	352	404	454	502
26	5.31	10.6	16.0	21.4	26.6	31.9	37.3	42.5	47.8	53.1	85	56.7	113	170	227	283	340	396	454	510	576
27	5.72	11.5	17.2	23.0	28.6	34.4	40.1	45.9	51.7	57.2	90	63.6	127	191	255	318	382	446	510	574	636
28	6.15	12.3	18.5	24.6	30.7	37.0	43.0	49.2	55.5	61.5	95	70.9	142	213	284	355	425	496	568	638	709
29	6.60	13.2	19.8	26.4	33.0	39.6	46.2	52.8	59.4	66.0	100	78.5	157	236	314	392	471	550	629	708	785

Example: A rod 1 m long, 22 × 22 mm weighs 3.80 kg
 8 rods each 1 m long, 22 × 22 mm weigh 30.4 kg
 1 rod 0.8 m long, 22 × 22 mm weighs 3.04 kg, etc.

11.3. The Transfer of Heat When Welding the Chill to the Casting

We will now determine the dimensions of the chill material which are necessary to weld the chill satisfactorily to the casting without melting the insert completely.

Lanzendörfer^(34, 35) carried out a number of immersion tests to determine the behaviour of cooling materials at steel-pouring temperatures and their melting-down times. Figure 318 shows that the cooling material behaves at first like a chill when it is immersed in a steel bath at a constant temperature, that is, relatively large amounts of steel solidify on to the cooling material. For example, on immersing a platelet 2 mm in thickness

in a steel bath at 1650°C, an amount of steel equal to 360 per cent of the weight of the platelet had solidified on to it after four seconds. This deposited steel melted again, and after seven seconds' immersion the cooling body had regained its original weight. Only then did the plate itself begin to melt, indicating that it had reached a temperature of about 1485°C. After a total immersion time of 10 seconds the platelet had gone completely into solution.

The author checked Lanzendörfer's data by means of extensive dip tests on chill sections of up to 60 × 60 mm. These chills were immersed in the steel bath of an induction furnace, which was regulated to a constant temperature. The basic pattern of the curve in Fig. 318 was confirmed, but it was found that the melting period

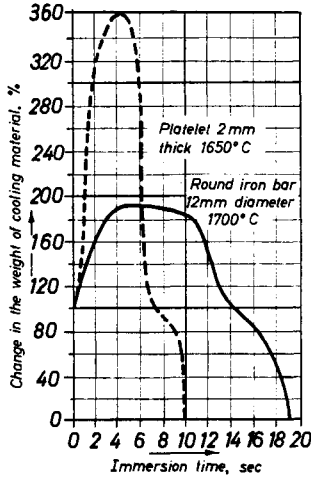


FIG. 318. Cooling effect and time to melting of a round bar 12 mm diam. and of a core platelet 2 mm thick. After Lanzendörfer.

was much shorter than that given in the data published by Lanzendörfer. Nonetheless the longer time was retained as a factor of safety for the calculation.

A similar result was obtained by Lanzendörfer in an immersion test with a round bar 12 mm in diameter. If the total time of immersion of this bar is taken as 100 per cent, it reaches a temperature of 1485°C after about 70 per cent of the immersion time has elapsed, only 30 per cent of the total time being required for the actual melting-down process.

Complete dissolution of the chill is not always necessary, however; it is sufficient for the outer layers to be melted. This process will have taken place after 75 per cent, or at the most 80 per cent, of the total period of immersion. This fusion time corresponds to the solidification time of the chilled casting, and is to be substituted in equation (141). In the example mentioned (Fig. 315) this time amounts to 408 seconds. Hence a chill must be selected with a total melting time of $(408 \times 100)/75 = 545$ seconds at the temperature in question.

Lanzendörfer carried out further experiments⁽³⁵⁾ to determine the melting-down times of various chill sections at given temperatures; the results are shown in Fig. 319.

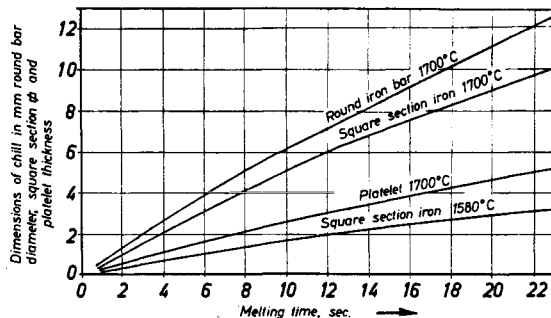


FIG. 319. Melting time of various chill sections as a function of temperature. After Lanzendörfer⁽³⁵⁾.

II.4. The Influence of Temperature on the Melt-down Time of Chill Sections

Figure 320 shows, in an evaluation of Lanzendörfer's experiments, the melt-down times of a three mm square section iron as a function of temperature. The values in the range 1580–1700°C were established experimentally, while those between 1450 and 1580°C were estimated. The resulting curve is a hyperbola; as no further melting of the chill occurs at 1450°C, the melting time at this temperature is infinitely long. Conversely, when superheating the steel much above 1700°C melting takes place after a very short time. It is very seldom that a superheat higher than 1700°C is obtained in practice, so that the melting time of a section at 1700°C can be taken as unity. Figure 320 also indicates to what extent the melting time is prolonged at temperatures below 1700°C. The prolongation factor is denoted by ρ .

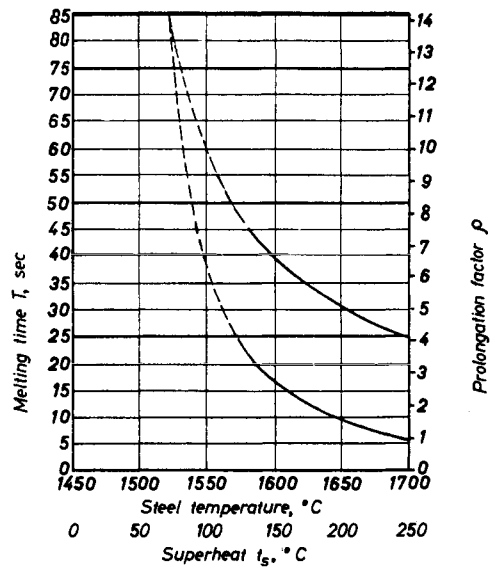


FIG. 320. Melting times of a 3 mm sq. iron bar as a function of the steel temperature.

These immersion trials were carried out in steel at an approximately constant temperature. During the solidification of castings, however, a drop in temperature will take place from the casting temperature to the solidification temperature. For this reason therefore the casting temperature and its corresponding factor ρ are not used in the calculation, but instead a much larger mean prolongation factor ρ_m is introduced, which corresponds to the temperature drop and is also plotted in Fig. 320 for the appropriate steel temperatures. ρ is calculated in Table 40.

Figure 320 shows the strong temperature dependence of the action of internal chills. It is necessary to introduce into the calculations the temperature of the steel where it comes into contact with the chill. In most cases this temperature will be less than the casting temperature at the ladle nozzle, since the steel becomes colder while

TABLE 40. LAWS OF FORMATION OF THE CURVES OF FIGS. 318 AND 320

1. Fig. 318.

Law of formation for the melting time of round iron bar at 1700°C.

- x or t = melting time in sec up to complete fusion
- d or y = diameter of bar in mm
- M = modulus of the casting already cooled, cm
- n = exponent of x

The curve corresponds to a parabola of the form $y = x^n$

Determination of n

$n =$		log
x_1	4	0.6021
y_1	2.6	0.4150
x_2	12	1.0792
y_2	7	0.8451

$$n = \frac{\log y_1 - \log y_2}{\log x_1 - \log x_2} = \frac{0.4301}{0.4771} = 0.9$$

Hence $d_{mm}^{\varnothing} = T_{(sec)}^{0.9}$

According to Chvorinov⁽¹⁾ the time of solidification of a body is $T_{sec} = 126 M^2$. Complete dissolution of the chill body is not necessary; only 75% of the melting time should be inserted. Solidification must be completed after this 75% has elapsed, i.e. this time is equal to the solidification time of the cooled body. Hence:

$$d^{\varnothing} = \frac{126}{0.75} \cdot M^2)^{0.9} = 168^{0.9} M^{1.8} = 100 M^{1.8}$$

2. Fig. 320.

Melting time curve of a 3 mm sq. bar

- x or s = superheat of the steel, beyond 1450°C
- y or z = melting time of the square bar, sec.
- g = a constant factor
- n = exponent of x

Determination of n with a hyperbolic form $y = \frac{q}{x^n} = q \cdot x^{-n}$:

		log
x_1	130°C	2.1139
y_1	22 sec	1.3424
x_2	250°C	2.3979
y_2	6 sec	0.7782

$$n = \frac{\log y_2 - \log y_1}{\log x_2 - \log x_1} = \frac{-0.5642}{+0.2840} = -1.985 \approx -2$$

Determination of q : $x_1 = 130^\circ\text{C}$; $x_1^{-2} = \frac{1}{16,900}$

$$y_1 = 22 \text{ sec} = 1 \cdot \frac{q}{16,900}$$

$$q = 16,900 \times 22 = 3.73 \times 10^5$$

Checks: $x_2 = 250^\circ\text{C}$; $x_2^{-2} = \frac{1}{62,500}$

$$y_2 = 6 \text{ sec} = \frac{q}{62,500}$$

$$q = 62,500 \times 6 = 3.73 \times 10^5$$

from which the formation formula gives:

$$T_{sec} = \frac{3.73 \times 10^5}{S^2}$$

The melting time equation was calculated for a constant steel temperature. As, however, there will be a temperature interval between the casting and solidification temperatures, the corresponding mean temperature t_m must be calculated.

$$t_m = \frac{\int_{S_1}^{S_2} t \times dS}{S_2 - S_1}; \quad \int_{S_1}^{S_2} t \times dS = \int_{S_1}^{S_2} \frac{3.73 \times 10^5}{(S)^2} dS$$

$$= -\frac{3.73 \times 10^5}{S} \Big|_{S_1}^{S_2} = -\frac{3.73 \times 10^5}{S_2} + \frac{3.73 \times 10^5}{S_1}$$

$$t_m = \frac{-\frac{3.73 \times 10^5}{S_2} + \frac{3.73 \times 10^5}{S_1}}{S_2 - S_1}$$

If a steel temperature of 1510°C ($S_1 = 60^\circ\text{C}$) is the lower limit below which welding-on is no longer possible, then the following examples can be calculated.

T in °C	S in °C	t_m	q_m	$\frac{1000}{S_2}$
1700	250	24	4	4
1650	200	30	5	5
1600	150	41.5	6.9	6.7
1550	100	62.4	10.3	10

Determination of the prolongation factor q :

This states by how much the melting time changes at lower casting temperatures compared with $t = 6$ sec at 1700°C (constant steel temperature). Hence:

$$q = \frac{t}{t_{1700}} = \frac{t}{6}, \text{ and the mean prolongation factor}$$

$$q_m = \frac{t_m}{t_{1700}} = \frac{t_m}{6}$$

Values of q_m are given in the above table. The law of formation for this curve is:

$$q_m = \frac{1000}{S}$$

flowing in the mould. In practice it is impossible satisfactorily to allow for all these different factors by calculation.

11.5. The Dimensions of Welded-in Chill Sections as a Function of Steel Temperature and the Desired Chilling Effect

According to Fig. 319 the diameter of round cross-sections can be determined as a function of time to complete melting, with a steel temperature of 1700°C, by means of the formula:

$$d \varnothing_{mm} = T_{sec}^{0.9} \quad (147)$$

If this value is substituted in the Chvorinov equation (141) we obtain:

$$d \varnothing = (126 \times M^2)^{0.9} \quad (d) \quad (148)$$

However, complete dissolution of the densener is not required. Adequate bonding is obtained after about 75%

of the meltdown time (Fig. 317). The above formula then becomes:

$$d \varnothing_{(mm)} = \left(\frac{126}{0.75} M^2 \right)^{0.9} = 100 M^{1.8} \quad (148)$$

This formula gives the maximum diameter of the chill as a function of the desired reduced modulus, at a constant steel temperature of 1700°C. Because of the cooling of the steel the melting or bonding time must be increased by the mean prolongation factor q_m . The law of formation of q_m can be seen from Fig. 318 or Table 40, and is represented by:

$$q_m = \frac{1000}{t S} \quad (e)$$

$$d \varnothing = \frac{100 \times M^{1.8}}{m}$$

and

$$d \varnothing_{(mm)} = S \times M^{1.8} \times 0.1 \quad (149)$$

TABLE 41. CALCULATED VALUES FOR $M_r^{1.8}$ AND $D^{1.8}$

$D; M_r$	$D^{1.8}; M_r^{1.8}$	$D; M_r$	$D^{1.8}; M_r^{1.8}$	$D; M_r$	$D^{1.8}; M_r^{1.8}$
1.1	1.2	3.4	9.0	7.5	37.7
1.2	1.4	3.6	10.0	8.0	42.2
1.3	1.6	3.8	11.1	8.5	47.5
1.4	1.8	4.0	12.2	9.0	52.5
1.5	2.1	4.2	13.2	9.5	57.5
1.6	2.3	4.4	14.4	10.0	63.1
1.7	2.6	4.6	15.7	10.5	66.1
1.8	2.9	4.8	16.9	11.0	77.0
1.9	3.2	5.0	18.1	11.5	81.7
2.0	3.5	5.2	19.6	12.0	87.3
2.2	4.1	5.4	20.8	12.5	94.0
2.4	4.9	5.6	22.2	13.0	102.0
2.6	5.6	5.8	23.6	13.5	110.0
2.8	6.4	6.0	24.5	14.0	115.0
3.0	7.2	6.5	29.1	14.5	124.0
3.2	8.1	7.0	33.2	15.0	132.0

Values rounded off, up or down

The diameter of the chill can therefore be determined directly as a function of the superheat and of the desired reduced modulus.

Table 41 gives values for $M_r^{1.8}$ and facilitates the calculation of the chill. In addition equation (149) is represented as a nomogram in Fig. 321.

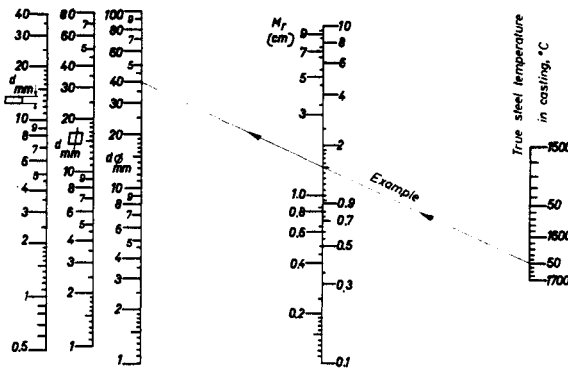


FIG. 321. Dimension d_{max} of fused-in chills.

Lanzendörfer also investigated the melting characteristics of square section bars and platelets, the melting times of which differ by a specific factor from those of round sections, and which are also plotted in Fig. 321. For example, a platelet 4.2 mm thick, an 8.1 mm square section bar and a round bar 10 mm in diameter will all melt in the same time, according to this diagram.

These equivalent melting times and the related chilling effects are allowed for in the nomograms. The section most suitable for practical requirements (i.e. in accordance with the spatial relationships of the casting) can be selected. However, the choice between several chill sections must not lead to the error of changing the weight of chill material. If, for example, a weight of 500 g was determined, then 500 g of platelet or of round bar material having suitable dimensions will be required.

11.6. The Use of Non-bonding Internal Chills

Non-bonding internal chills can be employed where they are either removed by subsequent machining (i.e. drilled out) or where the stresses to which the casting is subjected allow this to be done. Chaplets also represent non-bonding chills. If chills of this type are used, tears such as the one shown in Fig. 322 should not be formed, provided that the chill has reached a temperature of at least 1450°C at the completion of solidification, so that the chill and casting can then contract together.

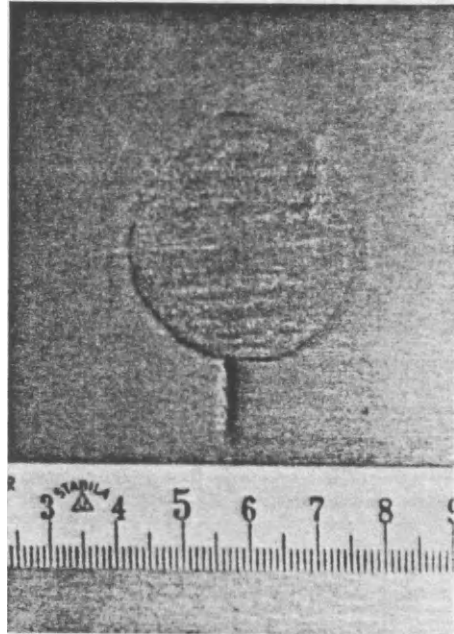


FIG. 322. Contraction crack at a cast-in chill.

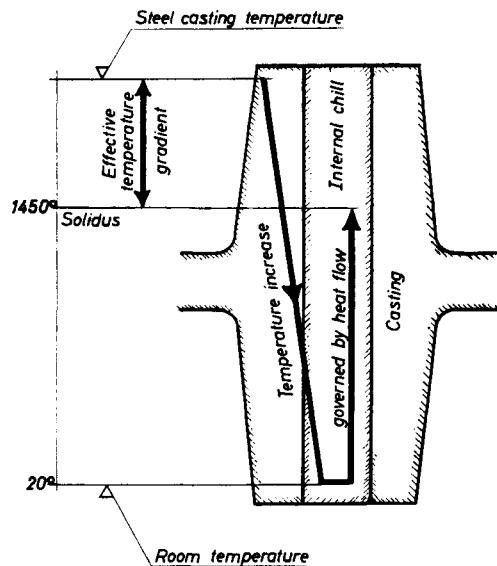


FIG. 323. Heat flow in cast-in chills which are non-bonding but are free from contraction cracks.

According to Fig. 323 a larger amount of heat is available for the chill than with welded-on chills, because of the steeper temperature gradient. As the basic considerations were similar, the heat balance was calculated as in equation (146). It is only necessary to note

TABLE 42. DATA FOR CALCULATING NON-WELDING CHILL MATERIAL

Steel temp. °C	Heat available for heating the chill cal/g			f_r
	L	S	Sum	
1500	64	—	64	0.246
1550	64	10	74	0.274
1620	64	24	88	0.310
1700	64	40	104	0.347

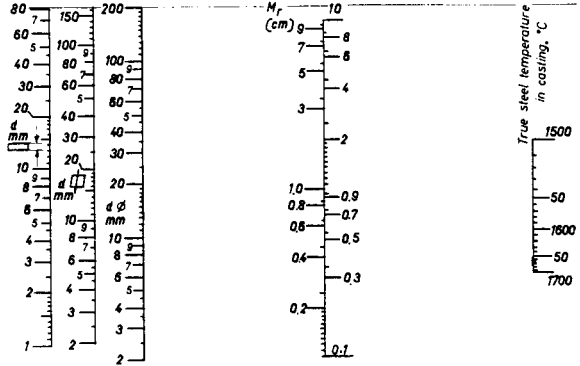
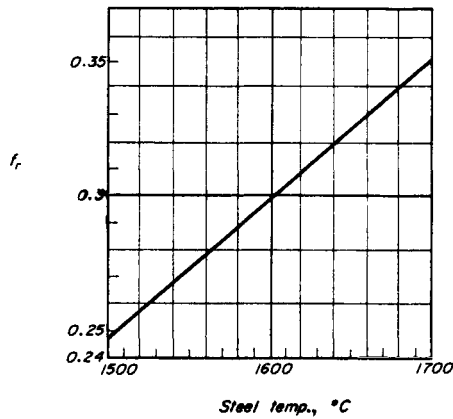


FIG. 324. Amount of cast-in chill material which is non-bonding and is cast free from cracks.

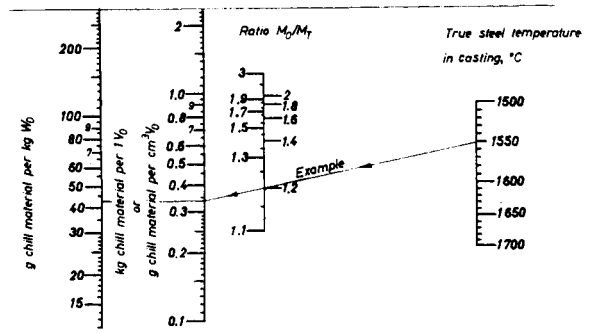


FIG. 325. Dimension d_{max} of non-bonding chills.

that the total latent heat of solidification of the liquid steel is available to heat the chill, and that the chill need no longer be partially melted. Hence the factor f of equation (145) will be changed to f_r . The equation for the weight of a non-bonding chill is as follows:

$$W_{ch} = f_r \times V_0 \times \frac{M_0 - M_r}{M_0} \quad (150)$$

The dimensions of the chill are determined from the same considerations as those discussed in Section 11.3.

In accordance with Fig. 318 solidified steel is first deposited on the densener. After about 50 per cent of the melting period has elapsed, the deposited steel begins to melt again, so that the chill has then reached a temperature of 1450°C. Hence only 50 per cent of the melting time needs to be introduced into the calculation, and we obtain:

$$d_{mm} \varnothing = S \times M_r^{1.8} \times 0.20 \quad (151)$$

This expression was used to construct the nomograms of Figs. 324 and 325. The diameter of a non-bonding chill can thus amount to twice that of the bonding type.

Safety considerations are discussed in section 11.9.2. Temperature fluctuations must always be allowed for.

11.7. Checking the Methods of Calculating Internal Chills

Lanzendörfer⁽³⁶⁾ investigated the behaviour of a square section chill with a side of 8 mm, which was cast in various specimen castings, particular attention being paid to the casting temperature. The results are reproduced in Table 43.

The samples were subsequently calculated on the basis of the formulae which have been developed here. Far-reaching agreement between the calculated chill sections and the actually inserted 8 mm square bars was achieved in the case of the samples described as "good". Those sections showing good agreement are specially emphasized. The method of calculation is illustrated by a numerical example.

Good agreement was also obtained with the results reported by other authors⁽³⁶⁾ as well as with those obtained by the author of the present work, as long as attention was given to the extremely important steel temperature.

TABLE 43. EXPERIMENTAL RESULTS GIVEN BY LANZENDÖRFER AND THEIR EVALUATION

Sample No.	Values after Lanzendörfer				Evaluation								
	Dimensions of the test block (all samples 80 mm high)	Casting temp. °C	Chill is % bonded	General findings	Data of the unchilled test block			Wt. (g)	$\frac{W_{ch}}{V_0} = \frac{32}{V_0} = \frac{g}{cm^3 V_0}$	Ratio $\frac{M_0}{M_r}$; values from nomogram (Fig. 317)	Modulus of chilled sample M_r (cm)	Length of edge d_{em} of a welded bar chill; values from nomogram (Fig. 321)	No. of sq. section chills with edge d to give total wt. of 32 g
					Surf. area A_0 (cm ²)	Vol. V_0 (cm ³)	Modulus $M_0 = \frac{A_0}{V_0}$ (cm)						
1	2	3	4	5	6	7	8	9	10	11	12	13	14
1	15 × 15	1700	0	Needle-sharp delineation	52.5	18	0.35	140	1.78	—	cannot be established with certainty	—	—
		1620	0										
		1550	0										
2	20 × 20	1700	25†	Needle-sharp delineation	72	32	0.45	250	1.0	3.0	0.15	under 1mm	—
		1620	25†										
		1550	25†										
3	25 × 25	1700	60†	Needle-sharp delineation	92.5	50	0.54	390	0.64	1.7	0.31	2.2	10
		1620	45†										
		1550	35†										
4	30 × 30	1700	80	Slight porosity	114	72	0.63	562	0.45	1.4	0.46	4.5	2.5
		1620	60										
		1550	50										
5	35 × 35	1700	90	Slight porosity	136.5	98	0.72	765	0.325	1.30	0.55	6.8	1.2
		1620	75										
		1550	60										
6	40 × 40	1700	95	Good	160	128	0.80	1000	0.25	1.20	0.67	9.0	0.65
		1620	80										
		1550	60										
7	50 × 50	1700	100	Cavity	210	200	0.95	1550	0.15	1.13	0.84	14.5	0.25
		1620	90										
		1550	80										
8	60 × 60	1700	100	Good, dissolution, cavity	264	288	1.08	2250	0.12	1.03	1.05	23	0.1
		1620	100										
		1550	100										

A chill 8 × 8 × 80 mm was cast into all samples $K_{ch} = 32$ g

Worked example:
Sample 6, 1700°C

1. Nomogram (Fig. 317)
Lay a (transparent) rule over 1700°C to $K_{ch} = 0.25$
Read off a modulus ratio $M_0/M_r = 1.2$, from which by calculation:

$$M_0/M_r = 0.8M_r = 1.2, \text{ and } M_r = 0.67 \text{ cm.}$$

2. Nomogram (Fig. 321)

Lay a (transparent) rule over 1700°C to $M_r = 0.67$ cm; read off at "square section chill" $d = 9$ mm

Good agreement with the actually selected chill section of 8 × 8 mm

† Only bonded by zinc alloy!

‡ Suitable spirals can also be inserted instead of numerous individual wire chills.

‡‡ The number 0.65 signifies that the chill should not extend over more than 65% of the length of the test block.

11.8. The Chilling Characteristics of Chaplets

11.8.1. GENERAL

IMPORTANT FOR PRACTICE

Chaplets represent—usually unwanted—chills, which impair the soundness of the casting, and give rise to tears, etc. The term “welded-in chaplets” involves all the requirements associated with “welded-in chills”. With high-grade castings, therefore, the chaplets must often be removed afterwards, by chiselling or drilling, and replaced by a satisfactory weld.

Chaplets should also stay in the correct position in the core, both during and after filling, so that they must also possess adequate resistance to compression and buckling at elevated temperatures. Chills (or chaplets) which fulfil the conditions of bonding or freedom from hot tears on solidification, are heated by the steel to temperatures exceeding 1400°C, where their strength drops to a much lower level. With the bonding type of chill in particular the hot strength tends towards zero. The greater the buoyancy and other displacing forces, which act in the core, the greater the strength of the chaplets must be, and the more impossible it becomes to fulfil the requirement of “bonding” or even “crack-free” solidification alone.

The following calculations only supply the dimensions of “bonding” or crack-free melting chaplets, without taking strength requirements into account; these must be estimated from the forces acting on the core. The results of the calculation must be considered as showing trends only.

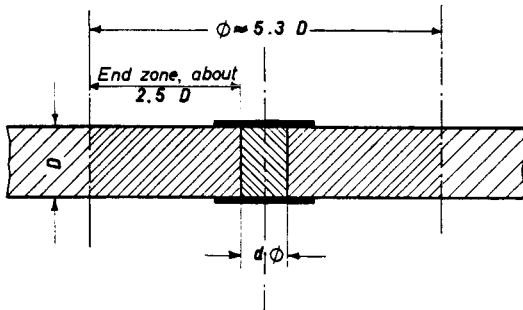


FIG. 326. Cooling relationships with single-web chaplets.

11.8.2. CHAPLETS WELDING INTO PLATES

According to Fig. 326, a chaplet generates a ring-shaped chilled zone of width 2.5 D (approximately, as the end zone lengths of Fig. 48 were determined on plates, but not on discs). According to an assumed, estimated value of $d = 0.3 D$:

$$V_0 = \frac{\varnothing^2 D \pi}{4} = 210 D^3 \tag{152}$$

From this, and from equations (145) and (149):

$$V_{ch} = \frac{d^2 \pi D}{4} = f \times 210 D^3 = \frac{M_0 - M_r}{M_0} \frac{D}{2} - \sqrt[1.8]{\frac{10 \times d_{(mm)}}{S}} \tag{f}$$

and:

$$f \times 210 D^2 - f \times 1510 \times \sqrt[1.8]{\frac{d_{(mm)}}{S}} - \frac{d_{(cm)}^2 \pi}{4} = 0 \tag{g}$$

as d is small compared with D , $\frac{d^2 \pi}{4}$ can be neglected and:

$$\left. \begin{aligned} d \varnothing_{mm} &= 2.86 \times 10^{-2} D_{cm}^{1.8} \times S \\ &= 4.54 \times 10^{-5} D_{mm}^{1.8} \times S \end{aligned} \right\} \tag{153}$$

Table 41 gives values of $D^{1.8}$. The nomogram (Fig. 327) was derived from equation (153).

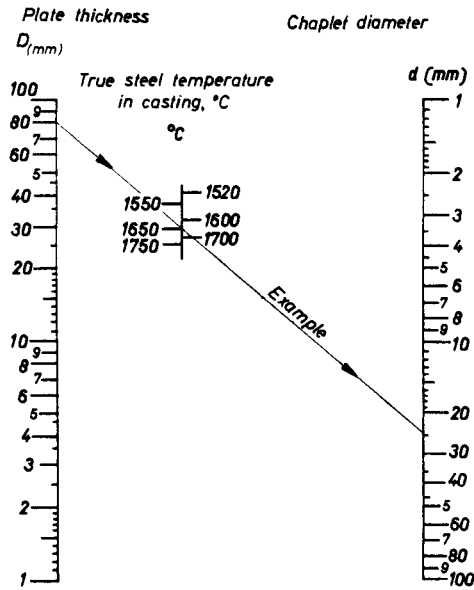


FIG. 327. Diameter of fused-in chaplets.

11.8.3. NON-BONDING, CRACK-FREE CHAPLETS

Based on the same considerations as the previous section, but starting from equation (151) we have:

$$\left. \begin{aligned} d \varnothing_{mm} &= 8.32 \times 10^{-2} \times D_{cm}^{1.8} \times S \\ &= 1.32 \times 10^{-4} \times D_{mm}^{1.8} \times S \end{aligned} \right\} \tag{154}$$

from which the nomogram of Fig. 328 was plotted.

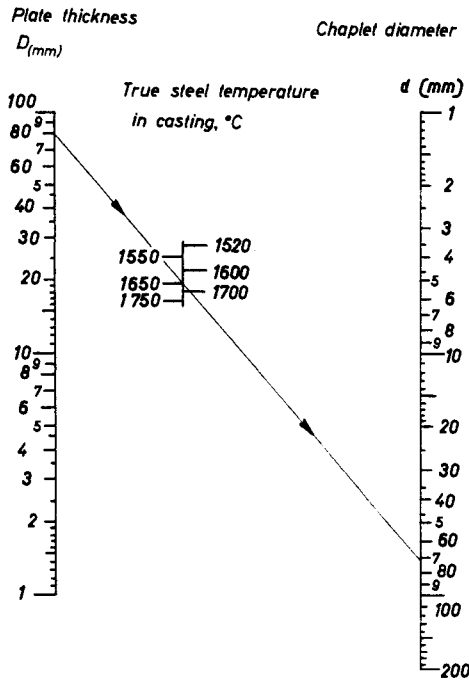


FIG. 328. Diameter of non-bonding chaplets, melting without producing cracks.

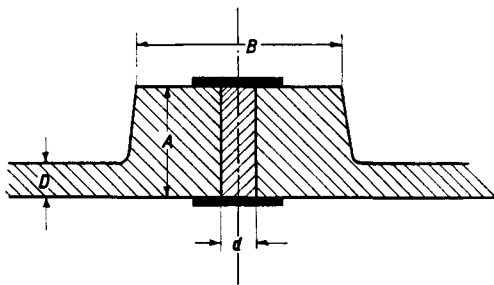


FIG. 329. Cooling relationships of chaplets on thin cast plates with a boss-shaped reinforcement.

11.8.4. LUGS AND BOSSES FOR IMPROVING THE WELDING OF CHAPLETS INTO THIN-WALLED PLATES

As shown in Fig. 329, thin-walled castings are often strengthened by a boss-shaped reinforcement at chaplets, so as to increase the modulus at these positions and thus improve the bonding, or at least ensure crack-free solidification.

The boss chilled by the chaplet must have the same (or a somewhat smaller) modulus as the thin surrounding wall of the casting to ensure that no shrinkage cavity is formed at the chaplet. The same conditions prevail as in the bearing lug of Fig. 315.

In order to simplify the calculation the following assumptions will be made:

1. Chaplet diameter $d^\varnothing =$ thickness of plate D
2. Height of the lug = half the lug diameter

Equation (145) then becomes:

$$V_{ch} = \frac{d^2 \pi}{4} A = A^3 \pi f \frac{M_0 - M_r}{M_0} \quad (155)$$

Because

$$M_r = 0.9 M_{plate} = 0.45 D \quad \text{and} \quad (h)$$

$$M_0 = \frac{A}{4} \quad (i)$$

therefore

$$\frac{M_0 - M_r}{M_0} = \frac{A - 1.8 D}{A} \quad (j)$$

from which, and from equation (155), the height of the lug, with $d = D$, is:

$$A = D \left(0.9 + \sqrt{0.81 + \frac{0.25}{f}} \right) \quad (156)$$

with a lug diameter $B \varnothing = 2 A$.

Figure 330 shows the relationship of the dimensions to the casting temperature.

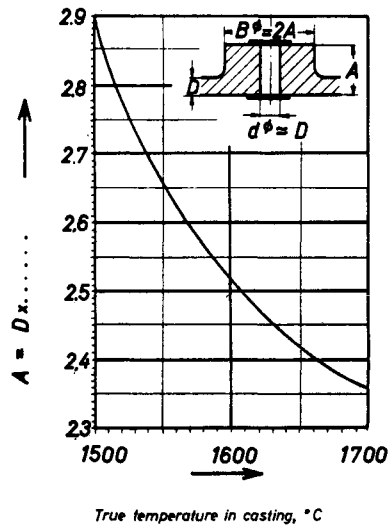


FIG. 330. Relationship of the desired lug dimensions to the steel temperature.

11.8.5. RELATIONSHIPS OF CHAPLETS. WELDING-IN WITHOUT CRACKS IN REINFORCING BOSSES

Basically the same considerations apply as before, so that equation (156) becomes:

$$A = D \left(0.9 + \sqrt{0.81 + \frac{0.25}{f_r}} \right) \quad (157)$$

and is also represented in Fig. 330 as a function of casting temperature. The fluctuations are much less than with chaplets which are welded in. The following good mean values can be expected:

$$\left. \begin{aligned} d^\varnothing &= D \\ A &= 2.2 D \\ B^\varnothing &= 4.4 D \end{aligned} \right\} \quad (158)$$

11.9. Examples of the Use of Internal Chills

IMPORTANT FOR PRACTICE

11.9.1. GENERAL EXAMPLES

In order to understand the following calculations the fundamental Section 11.1 should be read first.

Before a casting is cooled by an internal chill, the basic question should be asked—what purpose is to be achieved?

The bearing lug in Fig. 315, for example, must be so severely chilled that it can still be fed from the much thinner housing wall. In other words the lug must be made to solidify in a shorter time than the housing wall, by using an internal chill. This also means that the modulus of the lug must be less (by about ten per cent) than that of the housing wall. The above question is therefore answered as follows in this case: the modulus must be reduced to a specific amount at the position to be cooled by means of an internal chill.

EXAMPLE

The bearing lug (Fig. 315) has (unchilled) a modulus of 3 cm, while the modulus of the surrounding wall is 2 cm. Hence, for the lug to solidify sound, its modulus must be decreased from 3 cm to 2 cm—10 per cent = 1.8 cm.

To achieve this cooling action a certain weight of cooling material must be introduced. The hotter the cast steel, the greater this weight must be.

In general, internal chills are very strongly temperature-dependent. Even small fluctuations of steel temperature cause considerable deviations in chilling action. This fact will be considered again later, together with suitable safety precautions.

The nomogram of Fig. 317 gives the weight of cooling material. The amount of cooling material in non-welding chills can be read off from Fig. 324.

EXAMPLE

The bearing lug of Fig. 315 is cast at 1550°C (true steel temperature in the casting). The ratio $M_0/M_r = 3/1.8 = 1.67$. Place a rule from 1550°C over point 1.67 and read off a weight of 0.31 kg chill material per dm³ casting volume. The lug has a total volume of 4.580 dm³, hence $0.31 \times 4.580 = 1.42$ kg of chill material must be inserted.

Nothing has so far been said about the most suitable dimensions of the chill. This 1.42 kg can be inserted, for example, either as a thin wire or a thick rod. The dimensions must be selected so that the chill will weld in satisfactorily. We utilize Fig. 321 for welded-on chills, and Fig. 325 for non-welding chills.

EXAMPLE

The same lug Fig. 321: Place a rule over 1550°C and $M_r = 1.8$ cm and read off for round iron a diameter of $d = 29^\circ$. A corresponding square section of $d = 24 \times 24$ mm can also be chosen. How long must this 24×24 mm bar be made to provide a chill weight of 1.42 kg? Take from Table 39 at 24×24 mm a weight

of 4.52 kg/m. For 1.42 kg this gives a length of 0.32 m = 320 mm. The lug is 170 mm high, so that two bars 24×24 mm, 160 mm long, must be inserted.

11.9.2. INFLUENCE OF TEMPERATURE FLUCTUATIONS

First let us state the problem. The moulds, with the internal chills in position, are ready for casting but the steel supplied from the furnace is hotter (or colder) than was assumed when making the calculation. Obviously there is not time to take the moulds apart and insert new chills. What can be done about it?

This problem illustrates why failures are so frequent when internal chills are used. We will first determine the influence of temperature fluctuations on the lug in question.

EXAMPLE a

Casting temperature 1575°C, which is higher than originally planned.

Place a rule in Fig. 317 over 1575°C on the originally calculated weight of chill (which has been inserted in the mould)—i.e. 0.31 kg/dm³ V_0 . Read off the modulus ratio of $M_0/M_r = 1.50$. We know that $M_0 = 3$ cm, hence $M_r = 3/1.50 = 2$ cm. Therefore the lug now has the same modulus as the surrounding wall. If the steel temperature was somewhat higher, the modulus in the lug would be even larger than 2 cm, so that there is a risk of shrinkage cavities.

How is this danger to be avoided? Set the rule in Fig. 317 at a casting temperature about 25°C higher than originally assumed (in this case 1575°C). At a ratio of $M_0/M_r = 3/1.8 = 1.67$, this gives a chill weight of 0.36 kg/dm³. This corresponds in the lug to an internal chill weighing $4.58 \times 0.36 = 1.65$ kg.

EXAMPLE b

The casting temperature is lower by 25°C than originally assumed, i.e. 1525°C. However, a chill of 1.66 kg, corresponding to the higher temperature, has already been inserted. What is to be done?

By placing the rule in Fig. 317 over 1525°C and 0.36 kg/dm³ the modulus ratio is found to be $M_0/M_r = 2.2$. As $M_0 = 3$ cm, M_r becomes $3/2.2 = 1.36$ cm. The chill is thus much heavier than required. Will this impair the quality of the steel casting? No—it is only necessary to ensure that the chill welds on satisfactorily. In Fig. 321, place a rule from 1525°C over $M_r = 1.36$ cm, and read off a round section of $d = 14$ mm or a square section of $d = 12 \times 12$ mm. From Table 39 we derive a weight of 1.13 kg/m at 12×12 mm. For a chill weight of 1.65 kg this corresponds to a length of 1880 mm. The length of the lug is 170 mm; this means that 11 bars of 12×12 mm must be inserted. In some circumstances the chill can be introduced in the form of a spiral spring.

EXAMPLE c

It is difficult to introduce the required weight of 1.66 kg in the form of a 12×12 mm section. The question then arises: how thick can the bar be made if

welding-on is not required and only crack-free solidification is necessary? This is very often the case, for example, when the internal chill is later removed by drilling out.

Figure 325. Lay the rule from 1525°C over $M_r = 1.36$ cm and read off a round section of $d = 28$ mm \varnothing , or a square section of $d = 24 \times 24$ mm. The originally calculated chill section ($d = 24 \times 24$ at 1550°C) can thus be retained. In Table 39, 1.66 kg corresponds to a length of 370 mm, i.e. two bars must be inserted, which will project slightly beyond the outer surface of the lug.

These considerations may appear wearisome at first sight, but thanks to the nomograms almost no calculation is necessary. In any case the question must be asked, which is cheaper, to calculate ten times or to produce "scrapers"?

Finally the rules for allowing a safety margin for steel temperature fluctuations may be summarized as follows:

1. Assume a suitable steel temperature in the casting. This temperature must be increased by a certain amount to obtain the temperature in the casting ladle. This temperature will be aimed at by the furnace operators.

2. Allow for a temperature fluctuation of +25°C. Determine the required weight of chill from Fig. 317 (welding-on) or Fig. 324 (non-welding) corresponding to this increased casting temperature.

3. This weight of chill will therefore be inserted in the mould. Now assume a temperature fluctuation of -25°C. Calculate from Fig. 321 (or 324) the unnecessarily increased chill M_r , so obtained. Determine from Fig. 321 (or Fig. 325) the appropriate section thickness at the lower casting temperature. Determine from Table 39 the length of this section necessary to obtain the weight of chill calculated under (2).

In many cases it will be found that this type of chilling is not feasible (too much chill material, difficulties in inserting the material). Even this represents a success for the method of investigation. Or is it perhaps better to produce scrap by a useless and unnecessary trial?

11.9.3. FURTHER EXAMPLES OF THE USE OF INTERNAL CHILLS

When several chill bars are inserted, care must be taken to distribute them uniformly (Fig. 331) in order to prevent self-constriction of the cross-section, with the formation of shrinkage cavities.

Further examples of the practical application of internal chills are shown in Figs. 332-335, with the relevant tables.

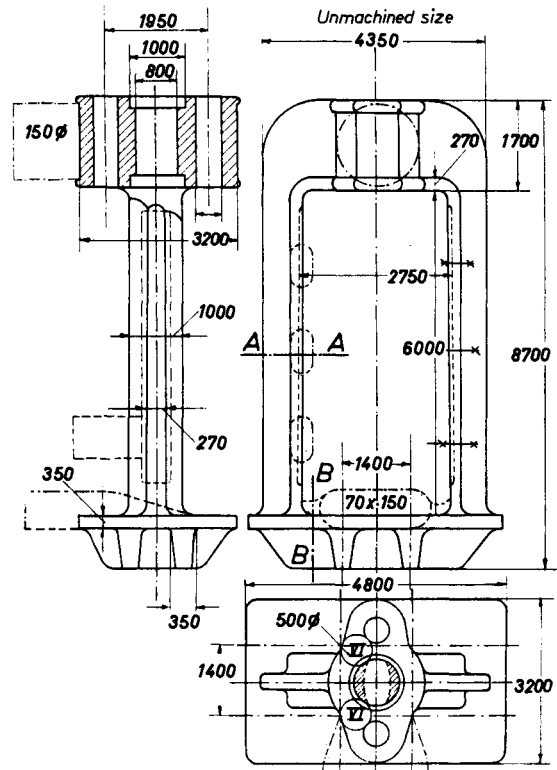
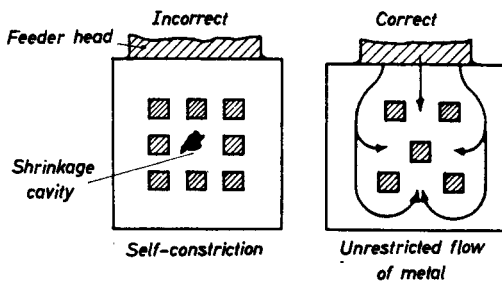


FIG. 332. Press housing.

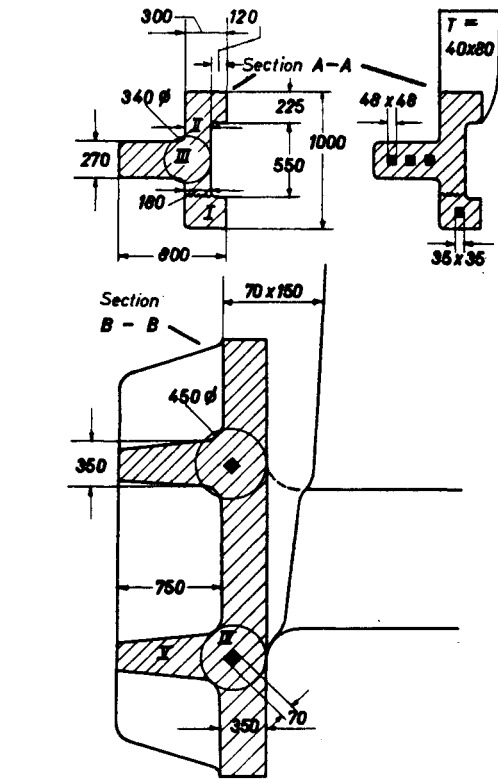


FIG. 331. Arrangement of several chills.

FIG. 332 (cont.)

I. (Section A-A)

$$M_I = \frac{30 \cdot 22.5}{2(30 + 22.5) - 18} = \frac{675}{87} = 7.8 \text{ cm}$$

II. Bar, ratio of sides 180 : 1000, larger than 1 : 5, so treat as a plate.

$$M_{II} = 18/2 = 9 \text{ cm}$$

III. Junction 340 \varnothing . Simulation bar 34 \times 68

$$M_{III} = \frac{34 \times 68}{2(34 + 68)} = \frac{2310}{204} = 11.3 \text{ cm}$$

The steel temperature should be 1590°C. Junction III should be so far cooled by a fused-in internal chill that it can be fed via cross-section II. The modulus should increase by a factor of 1.1, hence:

$$M_{III}(\text{reduced}) = \frac{M_{II}}{1.1} = \frac{9}{1.1} = 8.15 \text{ cm}$$

It need only be calculated according to the heat balance. The ratio $M_0/M_r = 11.3/8.15 = 1.39$. From Fig. 317 we obtain the value 0.26 kg chill material per 1 (dm³) chill volume. The chill volume per m length amounts to $2.7 \times 7.8 \times 10 = 210$ l, consequently $210 \times 0.26 = 54.8$ kg chill material per m length must be inserted. This is divided into three bar chills, so that the downward flow is not restricted. Fig. 321 shows that with $M_r = 8.15$ cm these bars will fuse in every case.

Hence each bar contains $54.8/3 = 18.3$ kg/m. From Table 39 for square section bar we find that the section measures 48 \times 48. This means that 50 \times 50 bar can be used to allow for grinding necessary to remove rust and scale.

To intensify the end zone effect a bar chill should also be inserted in part I. Volume per m length is $3 \times 2.25 \times 10 = 67$ l. The desired

$$\text{modulus reduction of } \frac{M_I}{M_{I_r}} = \frac{7.8}{6.8} = 1.15$$

From Fig. 317: 0.13 kg/l totalling $67 \times 0.13 = 8.7$ kg/m. From Table 39 we obtain 35 \times 35 bars, which are ground from 36 \times 36 bar. The feeder bead must correspond to a casting modulus of $M_{II} = 9$ cm, hence $M_r = 1.2 \times 9 = 10.8$ cm; from Table 13, for example, this gives dimensions of 400 \times 800 mm. (In fact the feeder can be kept smaller, if it is suitably back-filled.)

No weakening of the strut due to the chill is found, because the chill axis also runs in the direction of the lines of force.

The junction of the base plate can be partly fed with a 70 \times 150 feeder head. This feeder has too small a modulus, so must be back-filled. The junctions strut/base plate must be completely sound, so they are not chilled, but are fed by means of two shoulders from the central feeder head.

The ribs on the base plate are chilled, to the extent that they are not fed by the feeder head. The modulus of a rib (bar cross-section) is $M_{IV} = 17$ cm and must not be constricted by the junction chill. We have:

$$\frac{M_{IV}}{M_V} = \frac{22.5}{17} = 1.33$$

The weight of chill material, from Fig. 317, is equal to 0.25 kg/l. The function volume per m is $\frac{4.5^2}{4} \pi \times 10 = 160$ l, so that a bar of 160 \times 0.25 = 40 kg/m will be inserted (70 \times 70).

The head is fed only by a feeder head. The junction VI (500 \varnothing) in the lower half requires an oval drill hole, so far as external reinforcements which are difficult to remove are not incorporated. $M_{VI} = 25$ cm. $M_{F_{VI}} = 23$ cm. A round feeder head $H = D = 1500$ was set up, and this was back-filled.

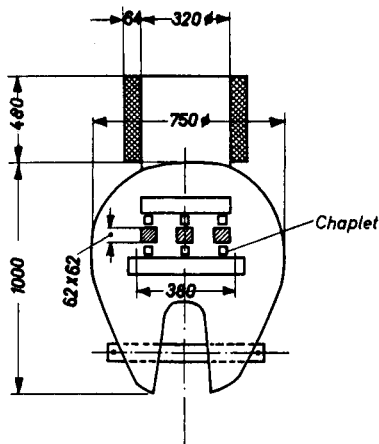


FIG. 333. Tup with internal chill.

Weight of the tup about 2900 kg (about 390 l) $M_0 = 12.5$ cm. An extensive but still reliable chilling effect should be aimed for by the use of a welded-in chill. Casting temperature 1550°C. Assumed modulus ratio $\frac{M_0}{M_r} = 1.5$, i.e. $M_r = 8.3$ cm. The quantity 0.27 kg/l is derived from Fig. 317, totalling $390 \times 0.27 = 105$ kg chill material. If a grid of 9 bars each about 380 mm long is inserted, so as to distribute the chilling effect as uniformly as possible, this will give a total length of 3.5 m, corresponding to $105/3.5 = 30$ kg/m. This corresponds to a 62 \times 62 section (Table 39). The grid is best made of bright-ground bars, to which chaplets are spot welded.

The exothermic feeder head is calculated in Chapter 12, Fig. 368 a.

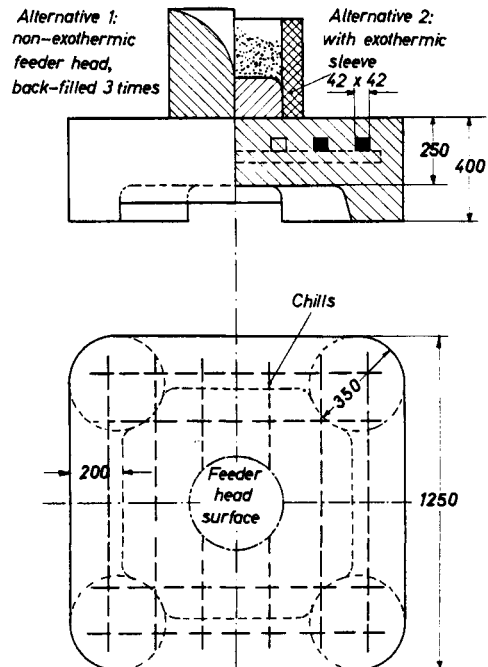


FIG. 334. Shield plate with internal chill.

Weight about 4.1 t (volume 525 l); modulus of the unchilled plate $M_0 = 9$ cm; casting temperature about 1590°C.

On economic grounds the feeder must be kept as small as possible, so extensive chilling is used. Question 1: How often can back-filling be carried out? This depends on operating conditions. In this case three times will be assumed.

FIG. 334 (cont.)

With triple back-filling the feeder head can be emptied three times beyond the 14% limit. Hence a head must be selected which will feed a weight of $4.1/3 = 1.37$ t with a shrinkage $S = 5\%$. For example from Table 9, $H = D \varnothing = 510$ mm, feeding capacity 1.5 t at $S = 5\%$,

$$M_F = 8.5 \text{ cm, weight } W_F = 710 \text{ kg.}$$

The feeder head $M_F = 8.5$ cm requires a casting modulus

$$M_C = \frac{M_F}{1.2} = \frac{8.5}{1.2} = 7.1 \text{ cm}$$

Back-filling prolongs the solidification time of the feeder head, i.e. increases its modulus. Although not assumed on safety grounds, it is quite possible, by continual back-filling, to keep the feeder head correspondingly liquid.

$$\text{The cooling ratio } \frac{M_0}{M_r} = \frac{9}{7.1} = 1.27$$

From Fig. 317: Lay a rule on 1590, +15°C safety allowance for super-

$$\text{heat, } = 1605^\circ\text{C, over } \frac{M_0}{M_r} = 1.27, \text{ and read off:}$$

0.29 kg chill material per l casting volume,
or 37 g chill material per kg casting weight.

Hence a total weight of $0.29 \text{ kg} \times 525 = 153 \text{ kg}$ of chill materials must be inserted.

The arrangement of cooling bars follows from the diagram. No chills should lie underneath the feeder head, so that access of hot material will not be restricted. The grid-like arrangement of bar chills has a total length of about 9 m. Table 39 gives a section of 47×47 mm at 153 kg and $p = 9$.

48×48 iron can be used, to allow for grinding off rust and scale. It must be checked whether welding-on of this chill will be ensured if the metal is cast cold. At the reduced temperature of $\approx 1570^\circ\text{C}$, $\frac{M_0}{M_r} = 1.45$ from Fig. 317, and $M_r = 9/1.45 = 6.2$ cm. We find from Fig. 321 that at 1570°C and with $M_r = 6.2$ cm, the 47×47 bars will weld on in every case.

2nd alternative:

Combination with exothermic materials. The calculation of exothermic materials is dealt with in Chapter 12, and will not be carried out in full at this point.

From Table 50 (feeder head with exothermic sleeve) we obtain for a feeding capacity of 4.1 t a feeder head of $320 \varnothing \times 480 H$, with a corresponding exothermic sleeve. The casting could have a modulus of 7.9 cm, so that it is about the same size as calculated under (1), and the same chill can be used. The actual weight of the head is 270 kg, and the yield would amount to:

$$\frac{4100 \times 100}{4370} = 93\%$$

This represents the maximum upper limit, which cannot be exceeded even theoretically.

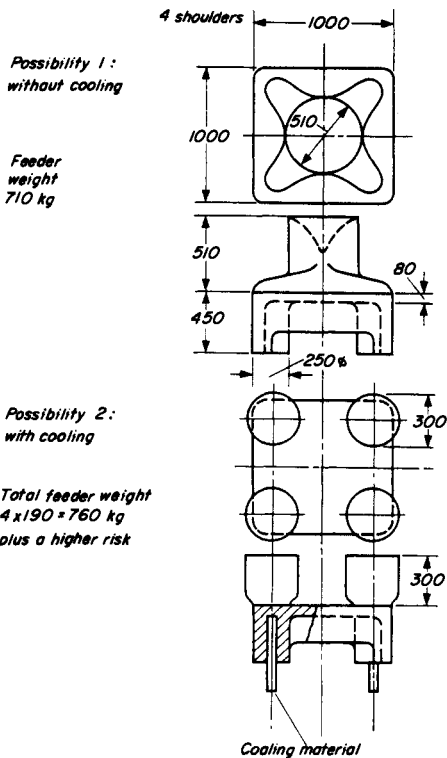


FIG. 335. Chilling the lug of a squeezer plate at various casting temperatures.

- (a) fused-in chills
- (b) non-bonded chills

In many cases an internal chill is not necessary; it increases the costs of production and increases the risk of scrap. The following example starts—intentionally—from internal chills and shows in the course of subsequent calculation that the chills are both expensive and unnecessary.

This squeezer plate of a disc-casting machine possesses four massive lugs. The modulus of the lugs in the uncooled condition is calculated as follows: Substitution body $4.5 \times 2.5 \times 2.5$ dm, volume = 28 dm^3 , geometrical surface area = 57.5 dm^2

Non-cooling surfaces to be subtracted:

on the plate 80 mm thick, $2 \times 2.5 \times 0.8 = 4 \text{ dm}^2$, and on the edge 40 mm thick, $2 \times 4.5 \times 0.4 = 3.6 \text{ dm}^2$, or 7.6 dm^2 altogether.

A cooling surface remains of $57.5 - 7.6 = 49.9 \text{ dm}^2$. The modulus is thus $V/A = 28/49.9 = 0.561 \text{ dm} = 5.61 \text{ cm}$. The modulus of the actual plate 80 mm thick is $d/2 = 4 \text{ cm}$.

The casting weighs about 1500 kg.

As the lugs solidify earlier than the plate, the lug modulus of $M_{\text{uncooled}} = 5.61 \text{ cm}$ is reduced to: $M_r = M_{\text{cooled}} = 4 \times 0.9 = 3.6 \text{ cm}$. Hence $M_0/M_r = 5.61/3.6 = 1.56$. The following weights of chill are obtained from Fig. 317, and the following maximum diameters for welded-in chills are derived from Fig. 321:

Casting temp. (in the casting) °C	Wt. of chill kg/dm³	Total wt. of chill for 1 lug/kg = 25 dm³	Max. diam. mm	Selected from Table 39 sq. section mm
1540	0.28	7	} 100 mm	44 × 44
1590	0.37	9.2		52 × 52
1635	0.42	10.5		56 × 56
1689	0.50	12.5		60 × 60

The following possibilities exist:

1. The whole casting (1500 kg weight) is supplied with a single central feeder head, for example a round feeder $H = D \varnothing$, with a steel shrinkage of 5% and $W = 1.5$ m tons. Table 9 gives $H = D \varnothing = 510$ mm. The modulus of this feeder head is $M_F = 8.5$ cm, which is thus substantially larger than the modulus of the uncooled lugs. However, the feeder head must have the above dimensions in order to supply the metal necessary for feeding 1500 kg. This raises the question: Why were the lugs chilled at all? Is it not much simpler to extend the range of action of the feeder head by means of four clover leaf shoulders to the lugs?

2. A feeder head is placed on each of the four lugs. Thus each feeder has to supply $1/4$ of the total weight of casting, i.e. $1500/4 = 375$ kg with metal. Read off from Table 9, for a shrinkage of 5% (for steels which are cast at a lower temperature) and a weight $W = 400$ kg, a feeder head $H = D = 330$ mm. This feeder head has a modulus of $M_F = 5.5$ cm.

Question:

If a feeder head $H = D = 405$ mm, $M_F = 6.75$ cm had been selected, this head would have fed the lugs without any chilling. Would this not be the safer way? Each internal chill involves an increased risk of scrap.

FIG. 335 (cont.)

3. Comparison of alternatives 1 and 2.

Alternative 1. The feeder head $H = D = 510$ mm weighs about 710 kg. There is no need to use chills with this feeder head.

Alternative 2. Each head $H = D = 330$ mm weighs about 190 kg. As four of these are used, the total weight is about 760 kg. Chills must be used with these feeder heads.

On comparing these alternatives, it is seen that method 1, with a single feeder head 510 ϕ and clover leaf shoulders is cheaper than method 2 with chills!

We thus arrive at the basic principle:

Internal chills always involve an increased risk of scrap (on the ground of possible steel temperature fluctuations alone).

Internal chills represent internal surfaces of the casting, on which foreign bodies such as gases, slag and sand particles are deposited preferentially. Even a careful calculation is powerless against this.

For this reason the attempt is first made to manage without internal chills when making high-grade castings; as we have shown, the chills are in many cases unnecessary. The internal chill remains as a last resort, when all other possibilities fail.

If internal chills are subsequently removed by machining, (drilling) with sufficient reliability the risk of scrap is much less.

CHAPTER 12

THE CALCULATION OF EXOTHERMIC FEEDER HEAD MATERIALS

12.1. General

IMPORTANT FOR PRACTICE

The use of feeder heads with exothermic sleeves is still based entirely on rule of thumb in many cases. However, experience is only gained by making mistakes, with the result that doubt is often cast on the efficiency of this type of feeder head. At one time, various authors examined the use of exothermic feeder heads for basic geometrical bodies, for example bars of all kinds. The work of Snelson⁽⁴⁷⁾ deserves special mention in this connection. A generally valid calculation for these feeder heads, which is applicable to any castings encountered in practice, has been reported by the author, and this will be summarized here, developed further, and supplemented to include exothermic sleeves of all kinds. The basis of the method of calculation is the determination of the modulus, which will be taken as known in this case.

In the exothermic feeder calculation the modulus method is basically superior to the shape factor method, because the behaviour of sleeves moulded by any method, with any given wall thickness and on any casting, can be determined very simply after making a few basic experiments. A great deal of experimental work would be required to apply the shape factor method to the same examples.

Almost unbelievable economies can sometimes be achieved with exothermic materials. The conditions for this success are

(1) Calculation is essential. The calculations are very easy and are greatly simplified by the use of diagrams, but they must be made. Whoever relies merely on "intuition" will sooner or later have to pay with reject castings, and scrap castings, as we know, are expensive; will the person responsible then be willing to admit, either to himself or others, that he has not made the necessary calculations?

(2) The quality of the exothermic materials must be of a uniform and high standard. The author will describe a few important methods of testing these materials.

The methods described here were bought dearly (i.e. at the expense of reject castings) by experience both in

Germany and in other countries. However, they have withstood their "trial by fire" during the past ten years.

12.2. Principles of Calculation of Exothermic Feeder Heads, with Reference to Exothermic Sleeves

12.2.1. WHAT DO EXOTHERMIC MATERIALS ACCOMPLISH, AND HOW DO WE TEST THEIR EFFICIENCY?

Exothermic materials consist of thermite-like mixes with a carrier material, which in simple cases consists of sand, but is more often a special fireclay (Fig. 336).

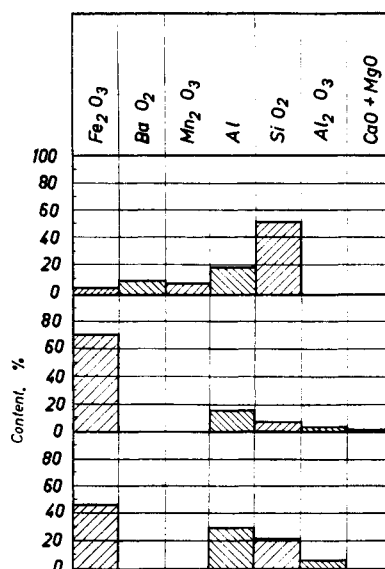


FIG. 336. Composition of various exothermic materials.

As will be shown later (Section 12.8) exothermic materials can be considered as self-heating insulating materials, i.e. their function is essentially that of heat insulation. Only with low melting point metals (grey cast iron, and light and heavy metals) does the temperature of the metal rise in the feeder, and this is often undesirable. With steel castings there is no rise in temperature—or at any rate very little—in the feeder head; this has been demon-

FIG. 335 (cont.)

3. Comparison of alternatives 1 and 2.

Alternative 1. The feeder head $H = D = 510$ mm weighs about 710 kg. There is no need to use chills with this feeder head.

Alternative 2. Each head $H = D = 330$ mm weighs about 190 kg. As four of these are used, the total weight is about 760 kg. Chills must be used with these feeder heads.

On comparing these alternatives, it is seen that method 1, with a single feeder head 510 \varnothing and clover leaf shoulders is cheaper than method 2 with chills!

We thus arrive at the basic principle:

Internal chills always involve an increased risk of scrap (on the ground of possible steel temperature fluctuations alone).

Internal chills represent internal surfaces of the casting, on which foreign bodies such as gases, slag and sand particles are deposited preferentially. Even a careful calculation is powerless against this.

For this reason the attempt is first made to manage without internal chills when making high-grade castings; as we have shown, the chills are in many cases unnecessary. The internal chill remains as a last resort, when all other possibilities fail.

If internal chills are subsequently removed by machining, (drilling) with sufficient reliability the risk of scrap is much less.

CHAPTER 12

THE CALCULATION OF EXOTHERMIC FEEDER HEAD MATERIALS

12.1. General

IMPORTANT FOR PRACTICE

The use of feeder heads with exothermic sleeves is still based entirely on rule of thumb in many cases. However, experience is only gained by making mistakes, with the result that doubt is often cast on the efficiency of this type of feeder head. At one time, various authors examined the use of exothermic feeder heads for basic geometrical bodies, for example bars of all kinds. The work of Snelson⁽⁴⁷⁾ deserves special mention in this connection. A generally valid calculation for these feeder heads, which is applicable to any castings encountered in practice, has been reported by the author, and this will be summarized here, developed further, and supplemented to include exothermic sleeves of all kinds. The basis of the method of calculation is the determination of the modulus, which will be taken as known in this case.

In the exothermic feeder calculation the modulus method is basically superior to the shape factor method, because the behaviour of sleeves moulded by any method, with any given wall thickness and on any casting, can be determined very simply after making a few basic experiments. A great deal of experimental work would be required to apply the shape factor method to the same examples.

Almost unbelievable economies can sometimes be achieved with exothermic materials. The conditions for this success are

(1) Calculation is essential. The calculations are very easy and are greatly simplified by the use of diagrams, but they must be made. Whoever relies merely on "intuition" will sooner or later have to pay with reject castings, and scrap castings, as we know, are expensive; will the person responsible then be willing to admit, either to himself or others, that he has not made the necessary calculations?

(2) The quality of the exothermic materials must be of a uniform and high standard. The author will describe a few important methods of testing these materials.

The methods described here were bought dearly (i.e. at the expense of reject castings) by experience both in

Germany and in other countries. However, they have withstood their "trial by fire" during the past ten years.

12.2. Principles of Calculation of Exothermic Feeder Heads, with Reference to Exothermic Sleeves

12.2.1. WHAT DO EXOTHERMIC MATERIALS ACCOMPLISH, AND HOW DO WE TEST THEIR EFFICIENCY?

Exothermic materials consist of thermite-like mixes with a carrier material, which in simple cases consists of sand, but is more often a special fireclay (Fig. 336).

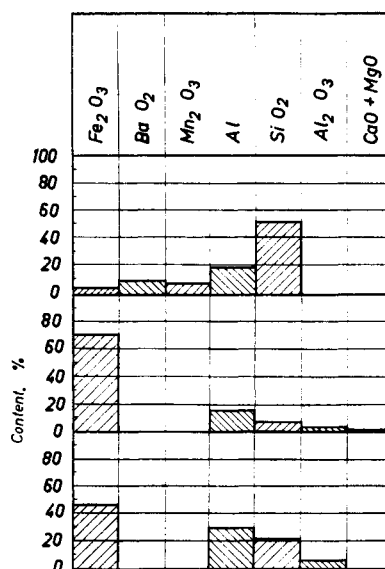


FIG. 336. Composition of various exothermic materials.

As will be shown later (Section 12.8) exothermic materials can be considered as self-heating insulating materials, i.e. their function is essentially that of heat insulation. Only with low melting point metals (grey cast iron, and light and heavy metals) does the temperature of the metal rise in the feeder, and this is often undesirable. With steel castings there is no rise in temperature—or at any rate very little—in the feeder head; this has been demon-

strated by several hundred measurements made by the author with many commercial exothermic materials.

Many methods have been developed for testing these materials. An obvious step is to obtain the calorific value directly by a theoretical calculation from the content of metallic aluminium, or in the bomb calorimeter. It has been found, however, that expensive exothermic materials with high aluminium contents are sometimes less satisfactory in practice than substances lower in aluminium. Other methods of measurement involve testing the rate of combustion and the temperature. The fact is that none of these methods can determine more than a proportion of the properties required in practice, and they often lead to false and dangerous conclusions. The author is aware from his own experience that, for example, changes in the rate of combustion can act in a way quite

different from the predicted effect, or, to quote another example, changes in the grain size of the aluminium powder can achieve the same effect as an increase in the aluminium content of the mix. In another case it was clearly established that the aluminium in an aluminothermic mix produced a cooling effect before ignition similar to that of a chill, which together with lower steel temperatures and small feeder head dimensions, caused a very rapid freezing of the steel in the feeder, which of course was far from being the purpose of using the material.

For these reasons the author improved the well-known sphere test developed by American investigators⁽²⁾; a sketch of the experimental layout is shown in Fig. 337. Photographs of the cast spheres are reproduced in Fig. 338.

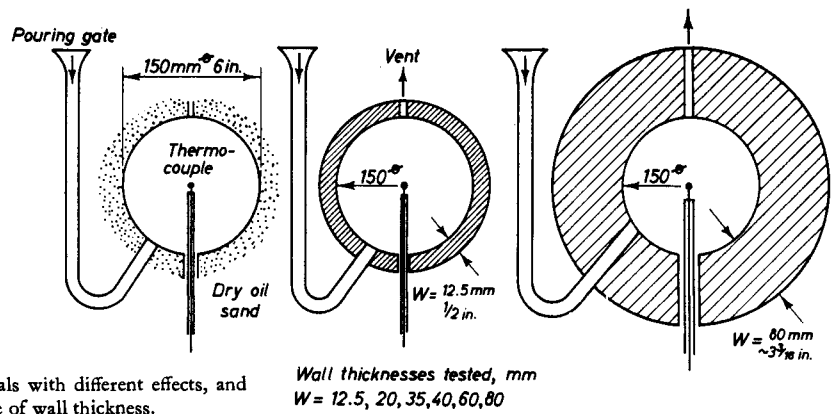


FIG. 337. Testing exothermic materials with different effects, and investigating the influence of wall thickness.

A reference sphere was cast at the same time in dry sand in each test with exothermic materials. The solidification times were measured in minutes. The relative solidification time was measured, i.e. how much longer the sphere in the exothermic material remained liquid than the sphere cast in sand. The time of solidification of the sand-cast sphere was made equal to unity.

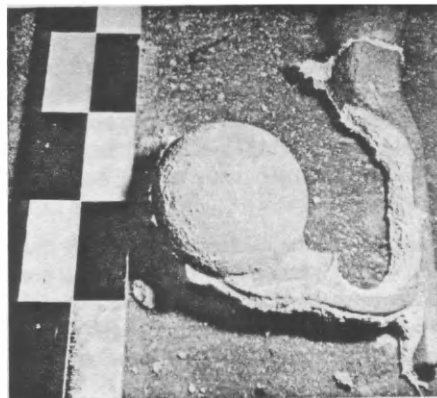
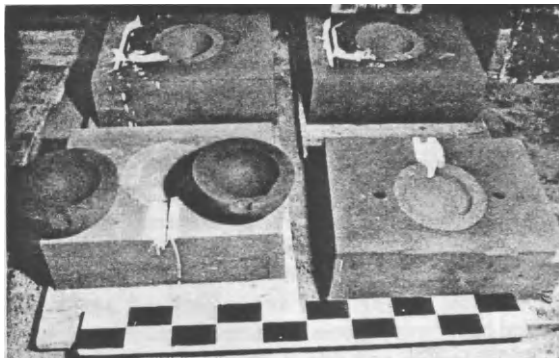
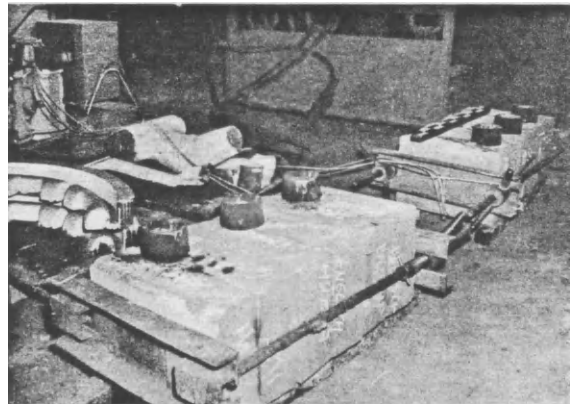


FIG. 338. Experimental layout for testing mouldable exothermic materials.

(Courtesy Sulzer Bros.)

Spheres are considered to represent the ideal test body for investigations, as the results can be transposed directly to practical conditions. The first experiments were made with spheres of 150 mm \varnothing , and these were later extended to spheres with diameters of 75 and 300 mm. In each test the sphere was first cast in dry oil sand and its solidification time plotted accurately on a recording instrument, using a thermocouple. Spheres of the same size were cast simultaneously in exothermic sleeves of various wall thicknesses or of different qualities, and the extension of the solidification time compared with that in sand was measured. The longer the sphere remains liquid, other conditions remaining unaltered, the more effective is the exothermic material. The sphere test provides a definite practical quality test. The influence of the casting temperature of the metal itself (particularly important in the case of grey cast iron) can also be evaluated by this method. Sphere tests can be used with any metal, and enable an accurate feeder head calculation to be made. The example of cast steel will be used for a detailed account of the method.

Figure 339a shows a typical solidification curve, and Fig. 339b the prolongation of the solidification of cast

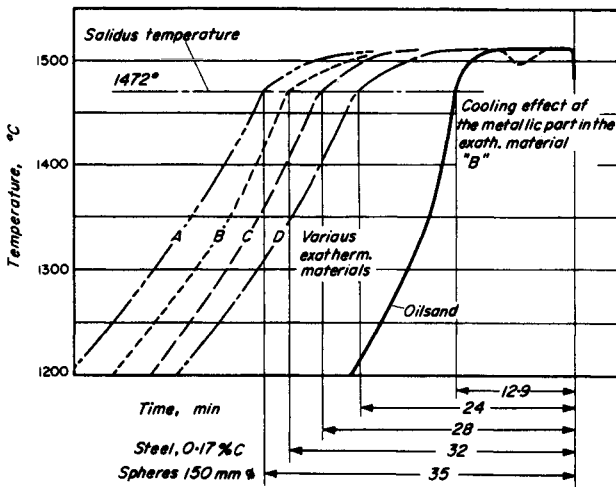


FIG. 339a. Typical cooling curves of one of the exothermic sphere tests.

steel spheres, using various exothermic materials *A*, *B*, *C* and *D*, and different thicknesses of exothermic sleeve. Material *C*, which corresponds most closely to the compositions normally used, forms the basis for further investigations. However, the composition must be modified for small and large spheres, for the same effect to be obtained (shown here for 150 mm \varnothing). The solidification time of a sphere cast in oil sand is given as unity for the purpose of comparison, so that the time of solidification is doubled using material *C* and a wall thickness of 35 mm. To facilitate subsequent calculations the wall thickness *d* was also given as a percentage of the modulus of the sphere. It should be remembered at this point that the modulus of a body has the dimension of a length (which can be expressed in cm, in., etc.) and therefore its use as a measure of the thickness of the exothermic sleeve is permissible.

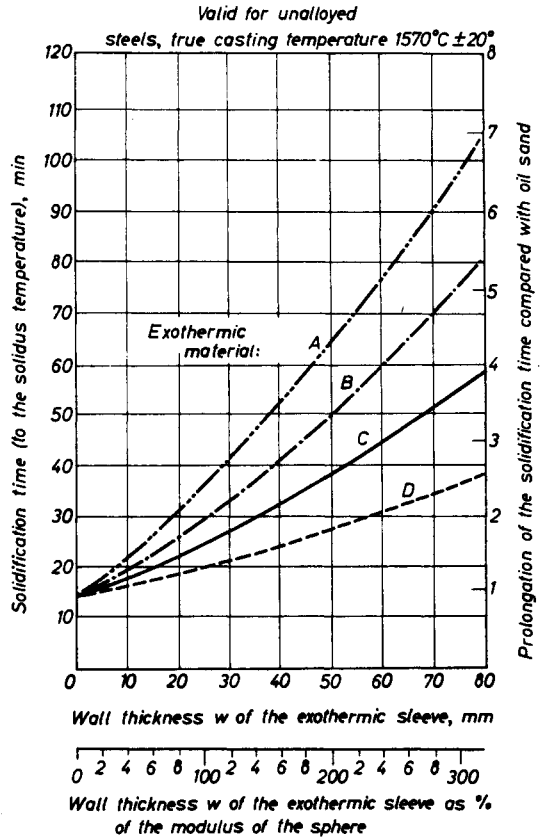


FIG. 339b. Solidification times of cast steel spheres 150 mm \varnothing , cast in exothermic sleeves of various wall thicknesses.

Figure 340 shows the increase in the modulus of the heated spheres compared with spheres cast in oil sand. This diagram is derived directly from Fig. 339; a second-

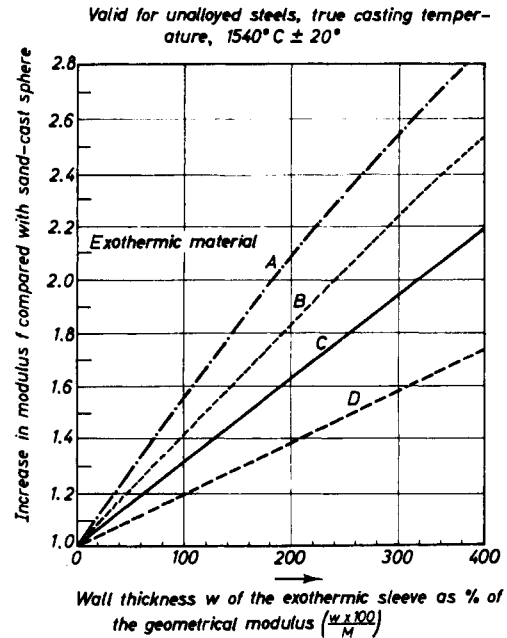


FIG. 340. Increase in the modulus of cast steel spheres 150 mm \varnothing due to casting in exothermic sleeves of various wall thicknesses.

order relationship is known to exist between solidification time and modulus.

EXAMPLE

The test sphere of 150 mm \varnothing has a modulus of 2.5 cm. At a wall thickness (w) of 35 mm of the exothermic sleeve the thickness amounts to 140 per cent of the modulus of the sphere. At this wall thickness the solidification time is doubled according to Fig. 339; the modulus is increased by $f = \sqrt{2} = 1.41$ compared with sand, which can be read off directly in Fig. 340.

It was shown in Section 2.4 (p. 5) that a cube, its inscribed sphere and its inscribed cylinder all possess the same modulus, and therefore solidify in the same time. (Slight deviations of the order of magnitude of a few per cent are completely without significance in practice.) The effect of the wall thickness in the sphere tests can therefore be transformed directly to the wall thicknesses of the heated feeder head, to the extent that exothermic feeder heads are cylindrical bodies. Control tests in practice have shown that this method is completely valid within the scope of the accuracy and safety required on the industrial scale.

It must be clearly emphasized once again that only a method using a test casting (such as the sphere described here) is suitable for the effective quality control of steel castings. Testing must be carried out with the same metal with which the exothermic material is to be used. Conclusions cannot be drawn from other metals, i.e. grey cast iron or copper alloys with reference to steel castings, according to the author's experience. The author carried out many analogous experiments with grey cast iron, light alloys and copper base metals, and established, for example, that marked deterioration in the quality of the exothermic material observed with cast steel was not observed when casting grey cast iron, and vice versa.

The sphere test has now been introduced at a number of works, and since then no rejects due to unrecognized fluctuations in quality have been obtained. Before introducing the test rejects were frequent, in spite of the use of other, supposedly satisfactory test methods.

It must be pointed out that only part of the necessary oxygen is combined chemically in the exothermic powder. All exothermic materials (with the exception of pure thermite) are characterized by subsequent combustion with atmospheric oxygen. The gas permeability (see Section 12.4.2.) and the ventilation (Section 12.4.3.) are therefore significant, as not only are gases drawn off by the action of the flue, but fresh air is also introduced. A poor supply of air leads to inadequate combustion, i.e. poor utilization of the fuel (in this case metallic aluminium). Aluminium makes the exothermic material expensive, and an inadequate supply of air represents inefficient operation.

12.2.2. THE DEVELOPMENT OF THE SHRINKAGE CAVITY IN UNHEATED AND EXOTHERMIC FEEDER HEADS. INFLUENCE OF THE CAVITY ON THE EFFECTIVENESS OF THE FEEDER HEAD

Figure 341 shows a large sectioned cast steel feeder head, with the well-known conical structure of the

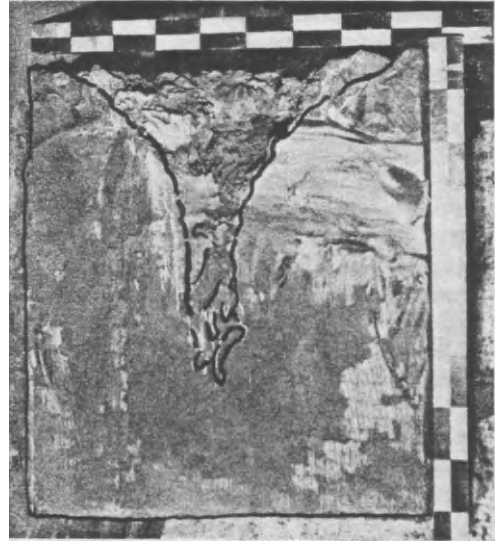


FIG. 341. Conical shape of shrinkage cavity in a cast steel cylindrical feeder head 900 \varnothing \times 900 H.

shrinkage cavity. The involute curve of the cone, due to the continuous advance of solidification, is theoretically a logarithmic curve. In practice the equation of a parabola is sufficiently accurate as an approximation formula, as Fig. 342 shows. Due to this unfavourable

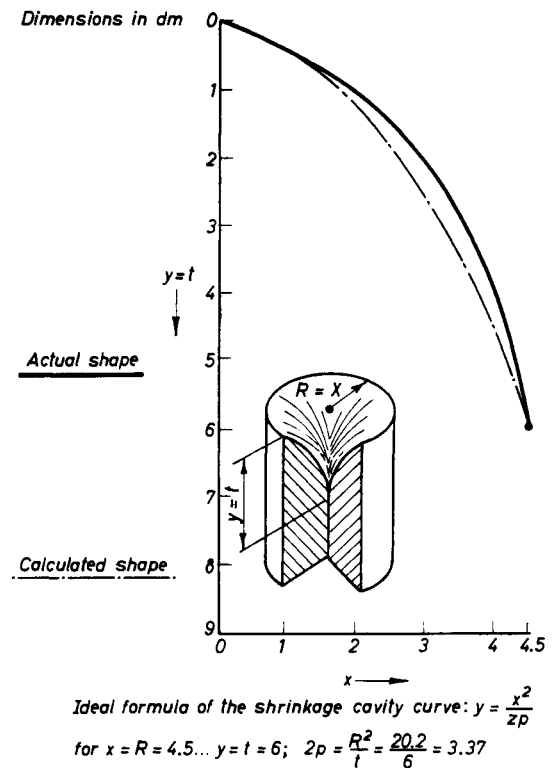


FIG. 342. Calculated and actual shape of the shrinkage cavity cone of the cylindrical feeder head illustrated in Fig. 341.

cavity shape, only about 14 per cent of the initial volume of the feeder head is contained in the shrinkage cavity in cylindrical feeders of all types, irrespective of the height/diameter ratio. It must not be forgotten that the feeder head itself undergoes a contraction in volume during solidification, i.e. the 14 per cent cavity serves not only to feed the casting, but also for the partial feeding of the residual metal of the feeder head itself. Only a fraction of the feeder head volume is thus actually utilized for feeding the casting. According to the conditions, 6 to a maximum of 10 per cent of the original volume of the feeder head can be assumed to be utilized in feeding the casting.

Figures 343 and 344, on the other hand, show an almost flat surface of liquid after sinking in the exothermic



FIG. 344 a. Horizontal sinking of the metal surface of an exothermic feeder head on a large squeezer plate (for a press).

(Courtesy Sulzer Bros.)



FIG. 343. Horizontal sinking of the metal surface in medium-size exothermic feeder heads.

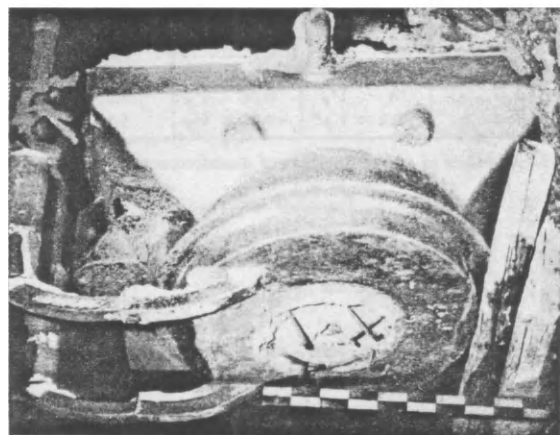


FIG. 344 b. Horizontal sinking of metal surface in a large exothermic feeder head, as a proof that the principles underlying the exothermic feeder head calculation are also valid for large castings.

feeder head. This requires an exothermic sleeve with a minimum wall thickness $w = 0.15 \times d_1$, where d_1 is the internal diameter of the sleeve.

In contrast to the acute-angled cone of non-exothermic feeder heads, the shrinkage cavity in this case forms a hollow cylinder, while the residual metal in the cavity represents a solid cylinder, if a small amount of porosity in this cylinder is disregarded. Even when strong suction conditions are present, the residual body should also have a height of at least $\frac{1}{3}$ of the original height of the feeder, so that the small amount of porosity will never penetrate into the casting. The maximum size of the shrinkage cavity in adequately heated feeder heads is thus 67 per cent, compared with 14 per cent in non-exothermic feeders. Figure 345 shows the relationships in a cylindrical feeder head with $H = 1.5 \times D$, and various wall thicknesses of exothermic sleeve.

The left side of the diagram shows the non-exothermic feeder head with an exothermic sleeve thickness of zero, and on the extreme right a feeder with a sleeve thickness of $w = 0.15 \times d$. The two central diagrams

show the average shrinkage cavity structure with smaller wall thicknesses of exothermic sleeve. These cavity shapes represent a mean value between non-exothermic and adequately heated exothermic feeder heads. Corresponding to the maximum volume of the cavity in the feeder head there also exists a mean value, which is given in the small table of Fig. 345.

Figure 346 shows the relationship between the volume of the cavity in the feeder head and the maximum volume of casting which can be fed adequately. The casting and feeder represent in the first place a physical system with a total volume of $(V_C + V_F)$. This volume shrinks by S per cent. To avoid misunderstanding, the contraction in volume of the liquid metal up to the end of solidification is termed the "shrinkage S ." The reduction in volume in the solid state is termed "contraction".

The shrinkage cavity volume V_{sc} forming in the feeder head is therefore equal to:

$$\left. \begin{aligned} V_{sc} &= (V_C + V_F) \times S/100, \text{ or } \\ V_{sc} &= (100 \times V_{sc}) - (S \times V_F) \end{aligned} \right\} \quad (157)$$

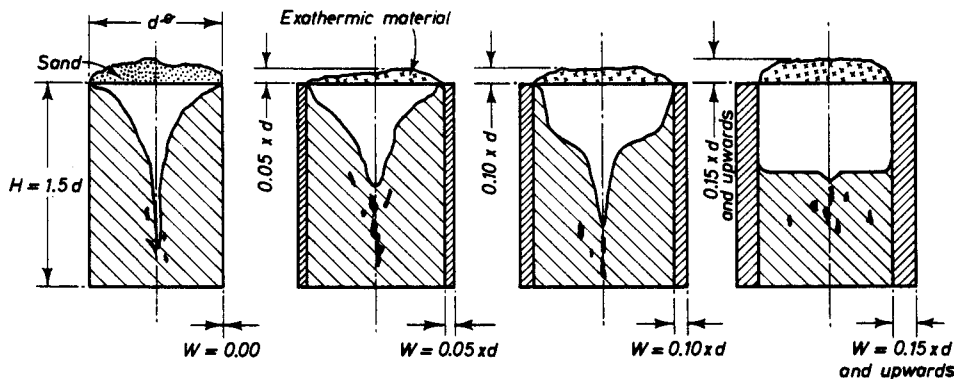


Fig. 345. Formation of the shrinkage cavity for various wall thicknesses of exothermic sleeve.

Initial volumes of all feeder heads (before feeding of metal commences) at $H = 1.5 \times d$, $V_F = 1.18 \times d^3$.

Thickness w of the sleeve	Max. vol. of shrinkage cavity $V_{sc \text{ max}}$	Vol. of residual metal V_R , at $V_{sc \text{ max}}$	Height b of a solid metal cylinder $d\phi$ of the same volume	Thickness w of the sleeve	Max. vol. of shrinkage cavity $V_{sc \text{ max}}$	Vol. of residual metal V_R , at $V_{sc \text{ max}}$	Height b of a solid metal cylinder $d\phi$ of the same volume
$0.00 \times d$	$0.14 \times V_F$	$0.86 \times V_F$	$1.27 \times d$	$0.10 \times d$	$0.50 \times V_F^*$	$0.50 \times V_F$	$0.75 \times d$
$0.05 \times d$	$0.212 \times V_F^*$	$\sim 0.79 \times V_F$	$1.15 \times d$	0.15 and upwards	$0.67 \times V_F$	$0.33 \times V_F$	$0.50 \times d$

* Mean values of t large numbers of measurements.

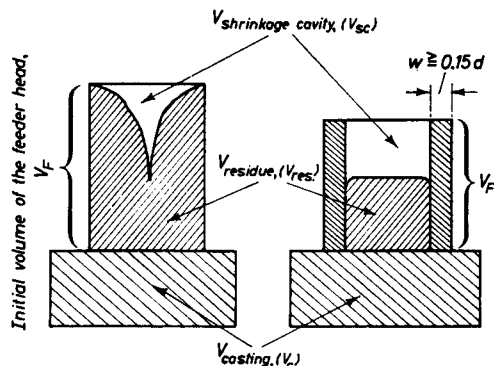


Fig. 346. Volume relationships with non-exothermic and exothermic feeder heads.

For non-exothermic and exothermic feeder heads we have:

$$V_F = V_{sc} + V_{res}.$$

Before shrinkage commences a physical casting with the total volume $(V_C + V_F)$ exists. This volume shrinks by $S\%$. The shrinkage cavity in the feeder head thus has a volume:

$$\begin{aligned} V_{sc} &= (V_C + V_F) \times S/100 \text{ or} \\ V_C &= \frac{100 \times V_{sc} - S \times V_F}{S} \end{aligned}$$

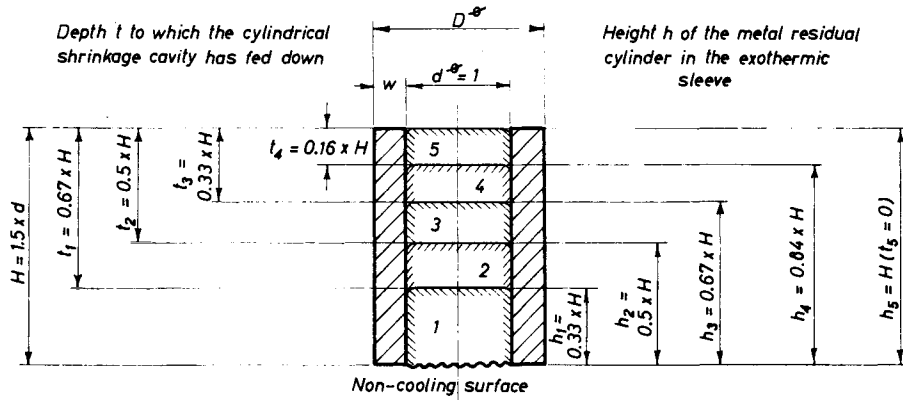


FIG 347. Investigation of various depths of withdrawal of feed metal at $d\phi = 1$ (valid for wall thicknesses $w > 0.15d$).

Case	Depth of shrinkage t	Shrinkage cavity volume V_{sc} at $d = 1$	Residual height b	Residual volume V_{res} at $a = 1$	Residual surface area A_{res}^*	Residual modulus V_{res}/A_{res}^*
1	$0.67 \times H = 1.0d$	$0.785 \times d^3$	$0.33 \times H = 0.5 \times d$	$0.395 \times d^3$	$2.355 \times d^2$	$0.1667 \times d$
2	$0.5 \times H = 0.75d$	0.59	$0.5 \times H = 0.75 \times d$	0.59	3.145	0.1875
3	$0.33 \times H = 0.5d$	0.395	$0.67 \times H = 1.0 \times d$	0.785	3.925	0.2000
4	$0.16 \times H = 0.24d$	0.1885	$0.84 \times H = 1.26 \times d$	0.99	4.745	0.2085
5	0 = 0	0	$1.0 \times H = 1.5 \times d$	1.18	5.505	0.2340

* The non-cooling base surface is not counted in when calculating the surface.

i.e. a quite specific casting volume is mathematically correlated with every shrinkage cavity. Corresponding to the numerous states of withdrawal of metal from exothermic feeders, five depths of shrinkage cavity were shown pointwise in Fig. 347, and the various suction stages denoted by steps 1–5. Table 44 calculates the maximum volume which can be fed adequately for these five cases.

It will be mentioned here that the dimensions are expressed in absolute units for all the calculations. The

internal diameter of all the feeder heads is given as 1, so that the metric system (dm for example) or the British system of measurement (ft) are equally valid mathematically.

Table 45 shows analogously the maximum adequately feedable casting volume for non-exothermic feeder heads. The various stages of metal withdrawal are indicated in this case by Roman numerals I–IV. Fig. 348 reviews these cases.

TABLE 44 (to Fig. 347). CALCULATION OF THE MAXIMUM FEEDABLE VOLUME OF CASTING FOR VARIOUS SHRINKAGES VALID FOR EXOTHERMIC FEEDER HEADS WITH DIMENSIONS:

$$d\phi = 1; H = 1.5d; V_F = 1.8d^3$$

Shrinkage S %	Case 1	Case 2	Case 3	Case 4
	$100 V_{sc} - S \times V_F$	$100 V_{sc} - S \times V_F$	$100 V_{sc} - S \times V_F$	$100 V_{sc} - S \times V_F$
	$V_c = \frac{100 \times V_{sc} - S \times V_F}{S}$	V_c	V_c	V_c

TABLE 45. CALCULATION OF THE MAXIMUM FEEDABLE VOLUME OF CASTING FOR VARIOUS SHRINKAGES. VALID FOR NON-EXOTHERMIC FEEDER HEADS WITH THE DIMENSIONS:

$$d\phi = 1; H = 1.5d\phi; V_F = 1.18d^3$$

Shrinkage S %	Case I	Case II	Case III	Case IV
	$100 V_{sc} - S \times V_F$	$100 \times V_{sc} - S \times V_F$	$100 \times V_{sc} - S \times V_F$	$100 V_{sc} - S \times V_F$
	$V_c = \frac{100 \times V_{sc} - S \times V_F}{S}$	V_c	V_c	V_c

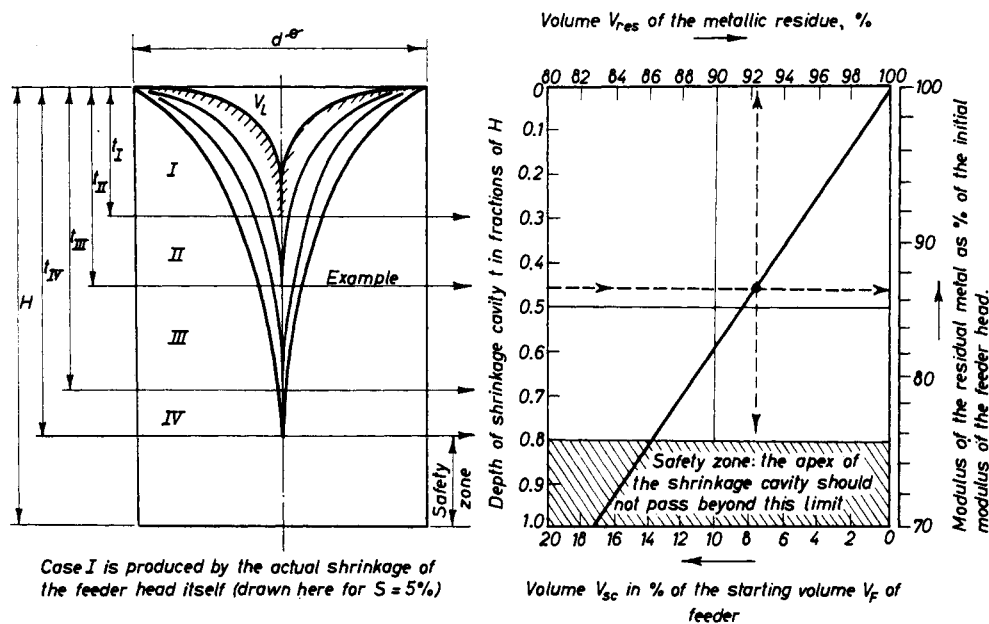


Fig. 348. Solidification geometry of non-exothermic feeder heads. The diagram is valid for any given ratios $H/d\phi$.

12.2.3. THE MODULUS CHARACTERISTICS OF NON-EXOTHERMIC AND EXOTHERMIC FEEDER HEADS. INFLUENCE OF THE SHAPE OF SHRINKAGE CAVITY AND DEPTH ON THE TIME OF SOLIDIFICATION OF THE FEEDER HEAD

We will first describe an adequately heated feeder head, as shown in Fig. 347. According to the metal to be drawn away, i.e. according to the volume of the casting to be fed, a residual metallic cylinder, varying in height, remains behind in the feeder head. The levels b are also given in Fig. 347 for cases I-V. Each of these residual bodies has a corresponding volume and a cooling surface which can readily be calculated. The feeder/casting interface, at which no cooling occurs for a long period during the solidification process, must not be included in the surface area calculation. According to the formula $M = V/A$, the corresponding residual geometrical modulus M is to be calculated for each of these residual cylinders, and this is also shown in Fig. 347.

As mentioned in connection with the testing of exothermic materials in the sphere test, compact cylinders of this type can be compared, from the point of view of their moduli, with the corresponding sphere. The geometrical modulus of the residual cylinders is thus increased by a specific factor, due to the action of the heating material. According to Fig. 340, this factor is a function of the wall thickness of the exothermic sleeve, and it is easy to see that the solidification time will be prolonged (i.e. the modulus will become greater) in proportion to the increase in wall thickness of this sleeve. The corresponding factors can be derived directly from Fig. 340. These enlargement factors are determined in Table 46 for each of these residual cylinders from I to V, and are plotted for the wall thicknesses $w = 0.15 \times d$, $0.20 \times d$, $0.25 \times d$ and $0.35 \times d$. The effective modulus

TABLE 46. CALCULATION OF THE MODULUS INCREASED BY EXOTHERMIC ACTION WITH LARGER EXOTHERMIC SLEEVE WALL THICKNESSES w

Wall thickness
Case
Geometrical modulus M of the metallic residual body.
w as % of M
Enlargement factor $f(\rho)$
Effective modulus = M_e

in each case under the action of the exothermic material is therefore equal to the geometrical modulus of the residual metal multiplied by the corresponding enlargement factor.

The feeder head should in no circumstances solidify earlier than the casting. On the other hand, it is uneconomic to allow the feeder to solidify later than the casting, because it is completely unimportant once the casting has solidified whether liquid metal is still present in the feeder head or not. The most economic solution is to arrange matters so that both feeder and casting solidify at the same time, which means that the metallic residue in the head and the actual casting must have the same solidification time and thus the same modulus. We have just determined the effective modulus of the heated residual body in Table 46. These moduli are therefore equal to the maximum permissible modulus of the casting for the case in question. In this way the casting volume governs the degree of withdrawal of metal on one hand, and the height and hence the geometrical modulus of the residual feeder head on the other hand, which is then increased by a certain amount due to the action of the exothermic material.

The relationships in non-exothermic feeder heads are basically the same, except that the residual metal in the

feeder, due to the conical shape of the shrinkage cavity (Fig. 348) is no longer represented by a simple hollow cylinder, but is a complicated body.

With an increasing shrinkage cavity in the feeder head, i.e. with a greater degree of withdrawal of metal, the metallic residue in the head becomes correspondingly less. Because of the formation of the very unfavourable cone-shaped cavity, the heat-radiating surface of the feeder is increased; this can be calculated accurately by means of the shrinkage cavity parabola mentioned above, and is also represented in Fig. 348. Here also the diminishing volume and the increasing cooling surface produce a considerable decrease in the modulus with increasing abstraction of molten metal. The diagram in Fig. 348 names the following values for non-exothermic feeder heads:

- The depth of shrinkage cavity t ;
- The volume of the residual metal as a percentage of the original volume;
- The volume of the shrinkage cavity, also as a percentage;
- The modulus of the residual metal as a percentage of the original modulus.

Here again the casting volume, which determines the degree of feeding, and governs the depth of cavity t , is related mathematically to the metallic residue in the feeder head. It is also true for non-exothermic feeder heads that these residual bodies have the same modulus as the casting at the moment when the casting solidifies.

Feeders with thin exothermic sleeves ($w = 0.05 \times d$ and $0.10 \times d$) which according to Fig. 345 occupy an intermediate position between non-exothermic and highly exothermic feeder heads, also have intermediate modulus ratios. The corresponding moduli are calculated in Table 47 in accordance with the following scheme:

TABLE 47. CALCULATION OF THE MODULUS INCREASED BY HEATING EFFECT. VALID FOR SMALL WALL THICKNESSES OF EXOTHERMIC SLEEVE, $w = 0.05d$ AND $w = 0.10d$

Initial geometrical modulus (for $d = 1$ and $H = 1.5d$)
 $M = 0.2145 \times d$
 Wall thickness w
 Case
 Geometrical modulus of the metallic residual body.
 w as % of M
 Enlargement factor $f(\epsilon)$
 Effective (\dagger) modulus = M_e

\dagger On safety grounds the calculated effective modulus in the characteristic is reduced by $\sim 5\%$ with small wall thicknesses of this type.

For cases I-IV the shape of the shrinkage cavity and the modulus of the residual metal were derived for non-exothermic feeder heads. This geometrical residual modulus is then increased by the appropriate factor, corresponding to the effect of the exothermic material. Allowance must be made for the fact that the experimental results sometimes show a wider scatter with thinner exothermic sleeves, so that the calculated modulus must be reduced by about 5 per cent to allow for errors.

12.3. The Characteristic of Exothermic Feeder Heads

IMPORTANT FOR PRACTICE

12.3.1. WHAT IS A FEEDER HEAD CHARACTERISTIC, WHAT PURPOSE DOES IT SERVE, AND HOW IS IT CALCULATED?

We have already seen that the properties of a feeder head in respect of feeding capacity and solidification time can fluctuate widely, according to the casting to which it is attached. Figure 349 shows three cases, A, B

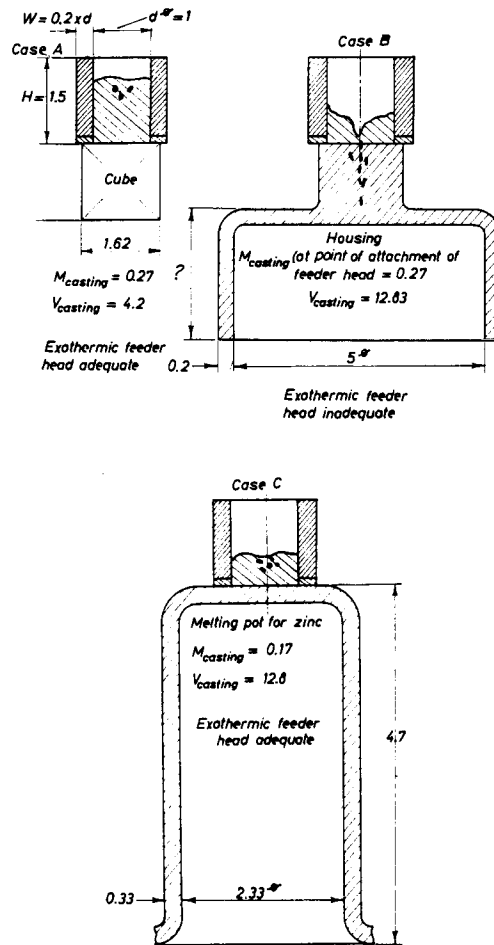


FIG. 349. The same size of exothermic feeder head was placed on each of the castings A, B and C. This was adequate for A, but not for B, although the modulus is the same in each case. The feeder head is again adequate in case C, although B and C have the same weight.

and C, out of the large number of possibilities. The same exothermic feeder head is placed on all three castings. The feeder is adequate for the massive cube (case A). Although the modulus in the housing of case B is the same as that of the cube, the feeder head is more strongly evacuated and is no longer adequate. In case C the casting is again the same weight as in case B, but now the feeder head is adequate for its purpose. Although we know that the size of the exothermic head is governed

by the volume and modulus of the casting, such cases are very confusing in practice, and it is necessary to give the foundryman a method of determining reliably the feeding capacity of an exothermic head. In view of the large number of confusing possibilities, it is not surprising that mistakes are often made, even by very experienced operators, i.e. shrinkage cavities are found in the casting, or exothermic heads are chosen which are much too large and wasteful in material, because of the existing uncertainty.

Tables 44 to 47 are represented graphically in Fig. 350. The individual cases of metal withdrawal are plotted as points in the diagram, and the relevant wall thicknesses are shown. This diagram represents the characteristic of feeder heads $d = 1$; $H = 1.5 \times d$ for various wall thicknesses from $W = 0$ (non-exothermic feeder head) to a maximum value of $W = 0.35 \times d$.

EXAMPLE

Casting modulus = 0.26, volume of casting = 9.0. It can be seen at once that an exothermic head with a wall thickness of $0.20 \times d$ is inadequate and a thickness

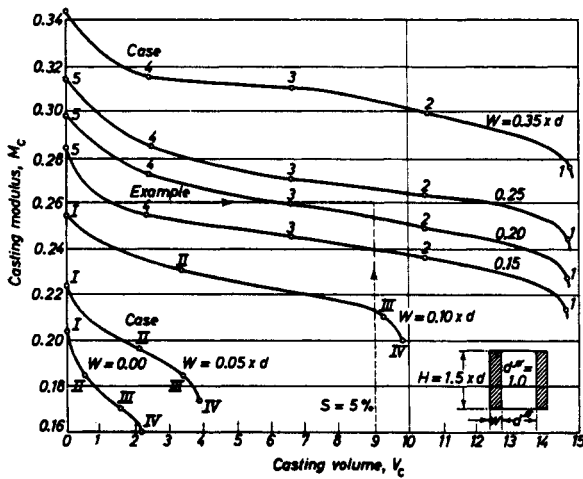


FIG. 350. Example of the plotting of characteristics of non-exothermic and exothermic feeder heads.

of $0.25 \times d$ must be selected. With the help of the characteristic, therefore, it is possible to determine at a glance the appropriate exothermic feeder head for any desired casting volume and the related modulus.

Thus the characteristic of any design of exothermic feeder head is calculated by assuming three or four cases of feeding, computing the appropriate geometrical (and later the effective) modulus due to exothermic action for each of the metallic bodies remaining in the head; the appropriate casting volumes which can be fed satisfactorily are calculated at the same time in accordance with the example shown. After some practice the labour of such a calculation becomes comparatively light, and above all it need only be done once. Once the characteristic has been plotted, the capacity of the exothermic feeder in the case of any given volume-modulus is

established once and for all, for every example occurring in practice, without additional calculation.

12.3.2. SELECTION OF THE MOST SUITABLE DIAMETER/HEIGHT RATIO.

FURTHER COMPUTATION OF THE CHARACTERISTICS FOR PRACTICAL REQUIREMENTS

The height/diameter ratio of an exothermic sleeve should as far as possible be selected so that a compact residual cylinder with $H = d$ remains after solidification. The geometrical modulus of such a massive body is comparatively large, and because of its shape is very economical. But if it is assumed that in many cases about

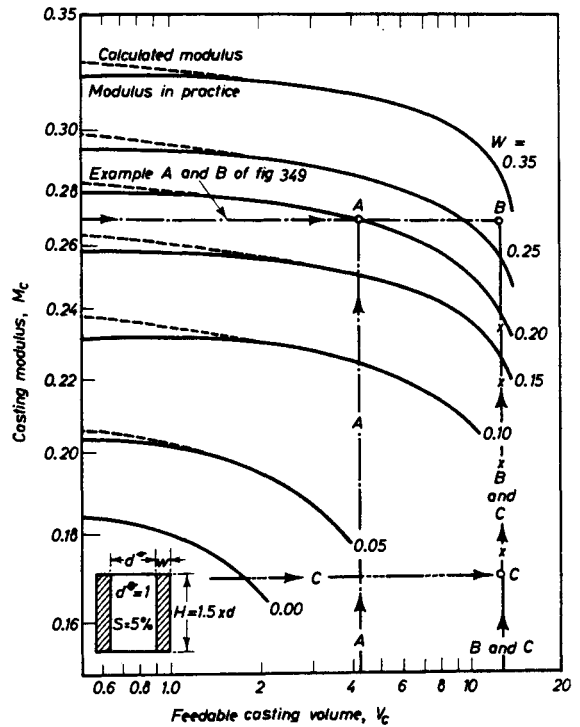


FIG. 351. Characteristic of Fig. 350, converted to logarithmic scale.

one-third of the metal is drawn out of the feeder head, then the most favourable initial height of the feeder head will be $H = 1.5 \times d$.

For this reason the examples and characteristics mentioned here will first be determined for this type of feeder head. All exothermic feeder heads, irrespective of the size of the internal diameter d , therefore represent geometrically similar bodies. The feeder characteristic from Fig. 350 is reproduced in Fig. 351 on a log-log scale. This method of representation has the following advantages:

The feeder head characteristic, once it is calculated, or the plotted curve, can be used for all geometrically similar feeder head sizes, and only requires a parallel displacement in this scale system.

The characteristics of feeder heads with $H = 1.5 \times d$ are represented in Fig. 351 for comparison purposes, for

wall thicknesses of 0-0.35. The three examples A, B, C from Fig. 349 are plotted in this diagram, and it can be understood at once why the casting is fed adequately in case A by an exothermic feeder having a wall thickness of $w = 0.2 \times d$, while in case B the casting has a shrinkage cavity, and in case C the casting is sound once again.

In most cases a sleeve thickness of a certain ratio will be decided upon. The selection of this wall thickness ratio is governed finally by economic considerations, and will be discussed in detail in Section 12.6. It will first be assumed that the exothermic head has the dimension $w = 0.2 \times d$. The characteristic of such geometrically similar feeder heads is represented in Fig. 352; instead of the casting volume, the maximum weight of

increased to about 10 per cent. In the metric system of measurement the specific weight is calculated as 7.0 instead of 7.8.

Some safety allowances are also necessary when calculating the casting modulus. It is assumed that the calculation is based on a completely full head, i.e. that the initial level of metal in the feeder is $H = 1.5 \times d$. In practice, however, the exothermic feeder head is often not filled to the top, so that it is advisable as a factor of safety to reduce the calculated modulus by 5-10 per cent, and to plot the reduced modulus in the characteristic. In Fig. 351 the calculated modulus was plotted as a broken line, while the modulus which can be applied in practice is shown as a heavy black line.

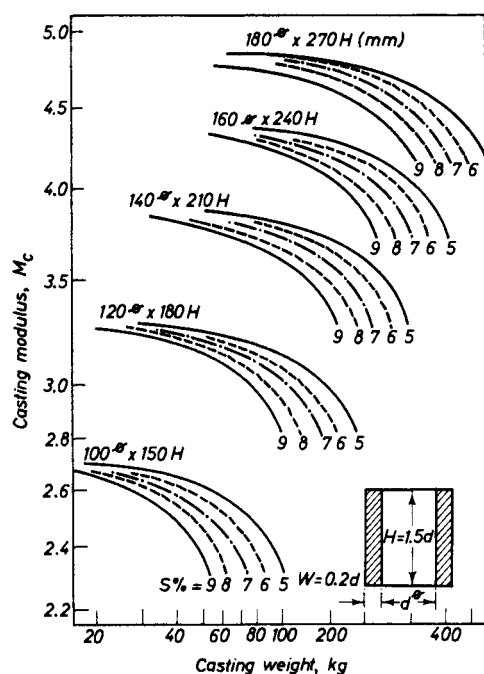


FIG. 352. Characteristic converted to operating conditions, represented in metric units.

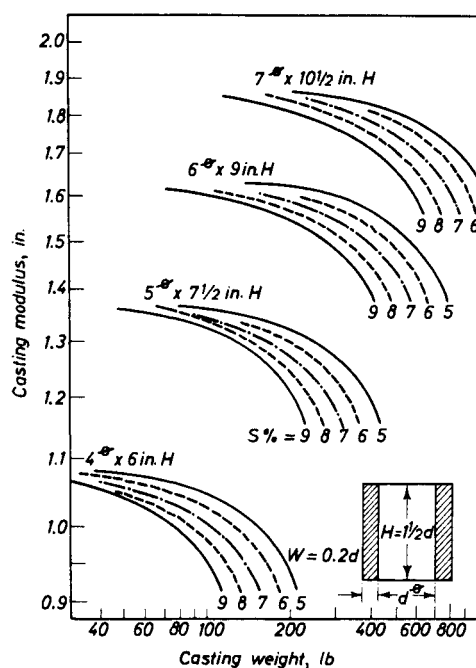


FIG. 353. Characteristic converted to operating conditions, represented in English units.

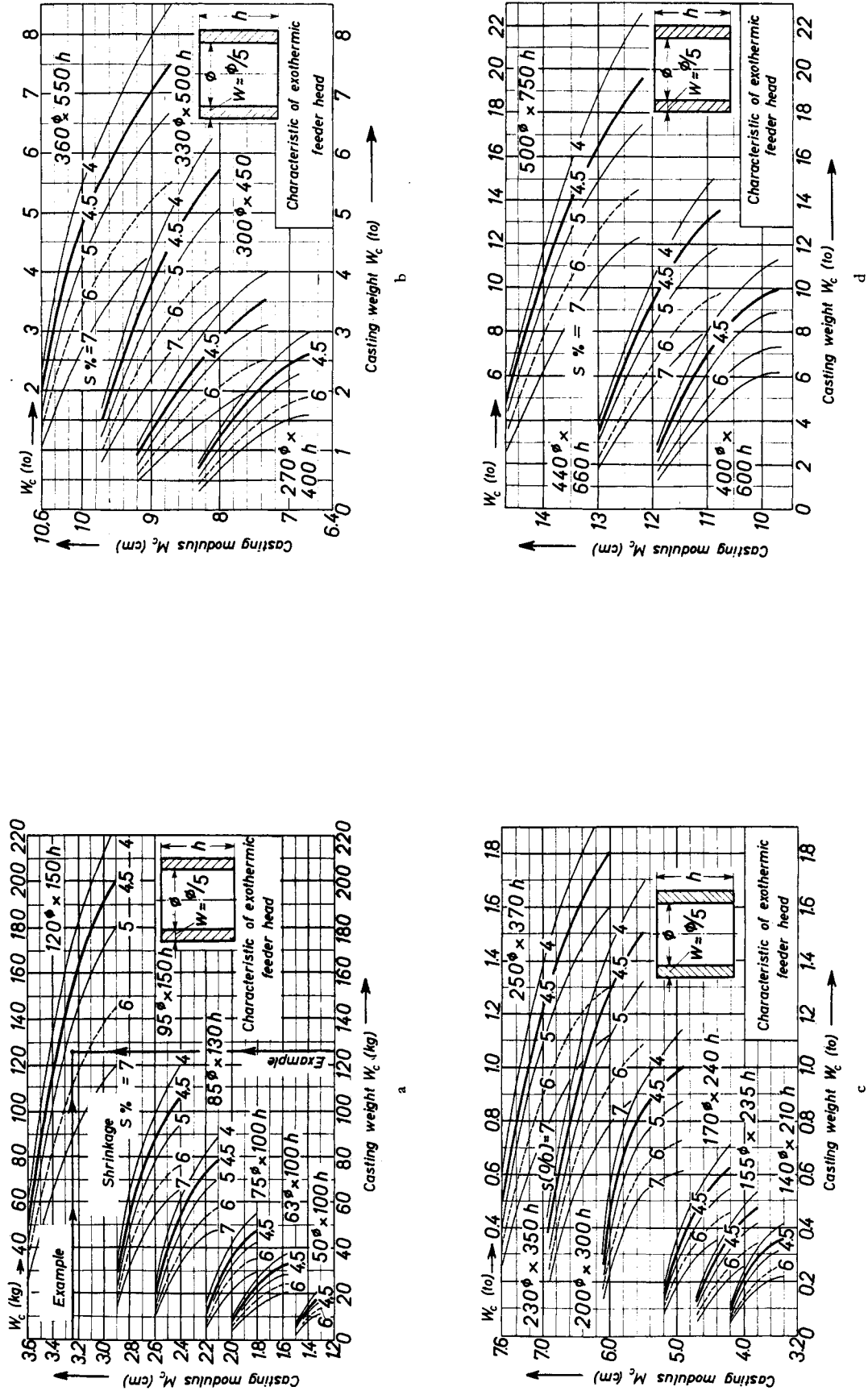
casting which can be fed satisfactorily is given in kg; cm and mm were selected as units of measurement for this characteristic. The curves of the characteristic are calculated for shrinkages of 5.6, 7.8 and 9 per cent. In this way a group of curves is obtained which, when drawn on a template (such as transparent paper), can be given a parallel displacement in every case.

The following should be noted when determining the casting weight from the volume of casting that can be fed:

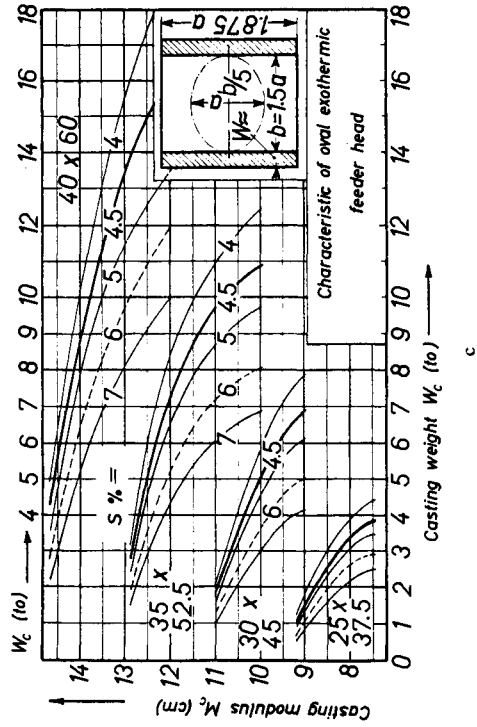
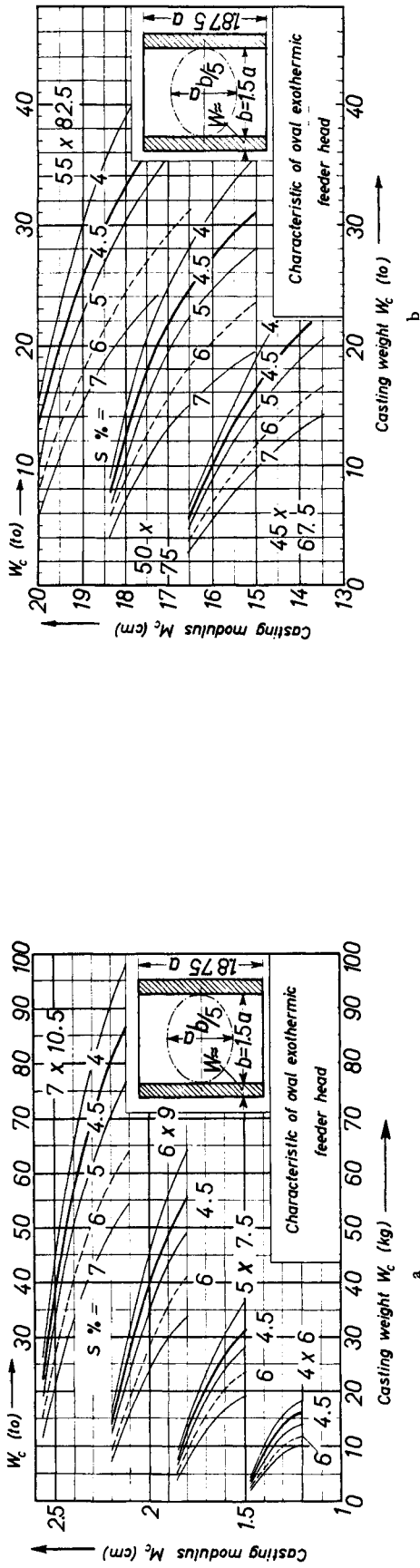
The specific weight of the cold metal need not be substituted, but the amount of contraction must be allowed for in the pattern. If we assume a linear contraction of 2 per cent then a volume increase of 6 vol. per cent is obtained. If it is also assumed that the metal is forced slightly into the mould, the volume difference will be

A similar characteristic is represented in British units in Fig. 353, the log-log scale being again used.

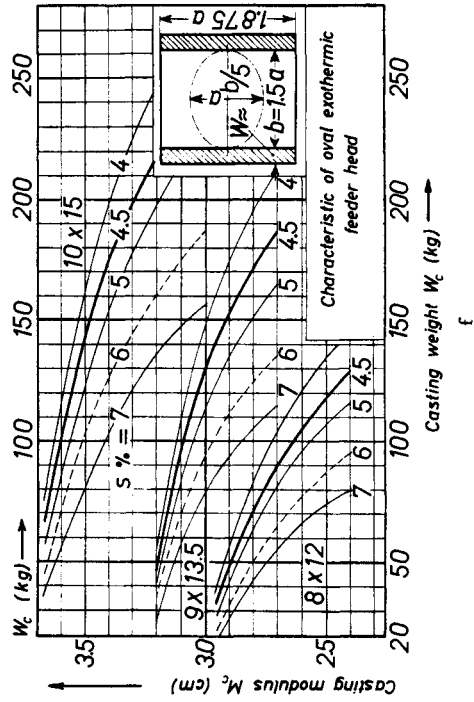
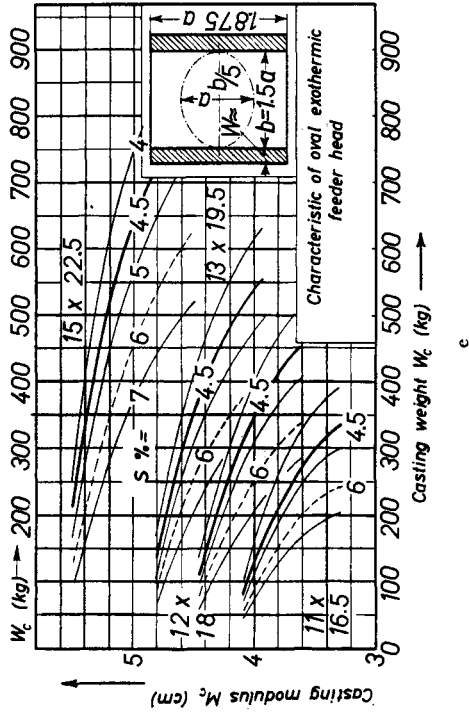
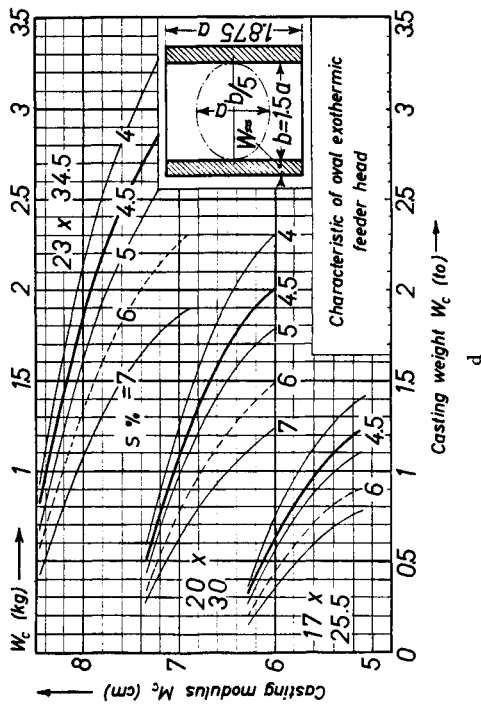
The same curve templates as in the metric system can be employed. In Figs. 354-362 inclusive characteristics are shown which were calculated for practical requirements and have been found to give excellent results over a period of several years. When the modulus calculation has been used, the author has not had a single scrapped casting due to shrinkage cavities under the exothermic heads. In the few cases where cavities did occur below the feeder it was shown that it is often necessary to set additional long or short exothermic sleeves on the casting, on technical grounds. For this reason, circular sleeves of this type are also described in Figs. 354-362, which can be used either singly or in tandem, as standardized exothermic sleeves.



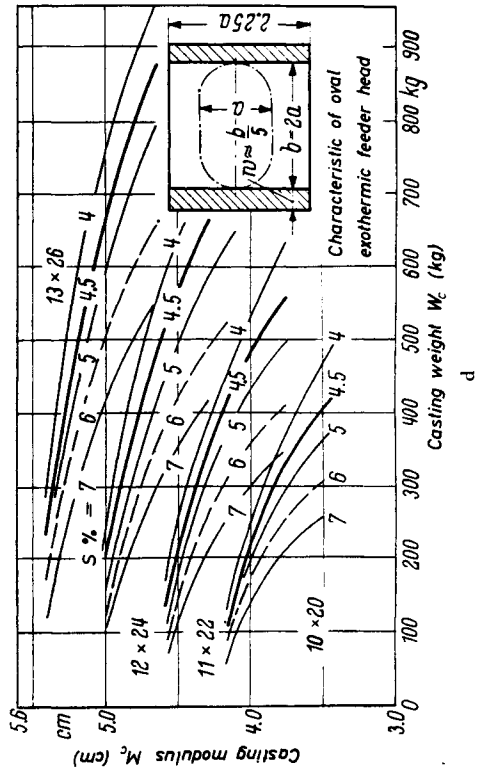
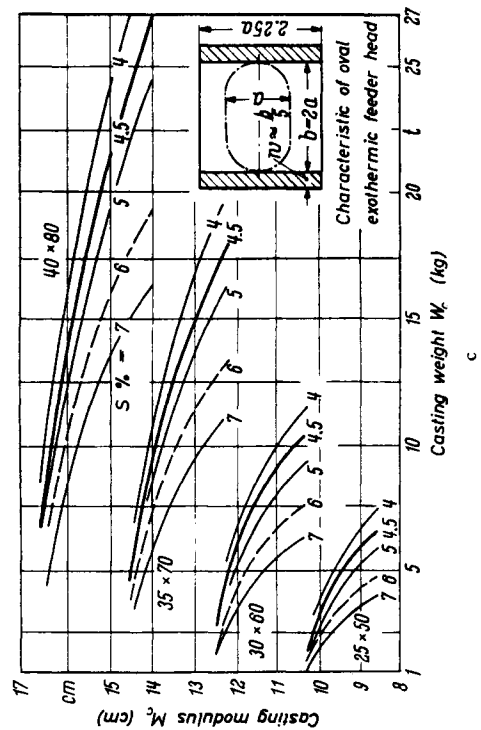
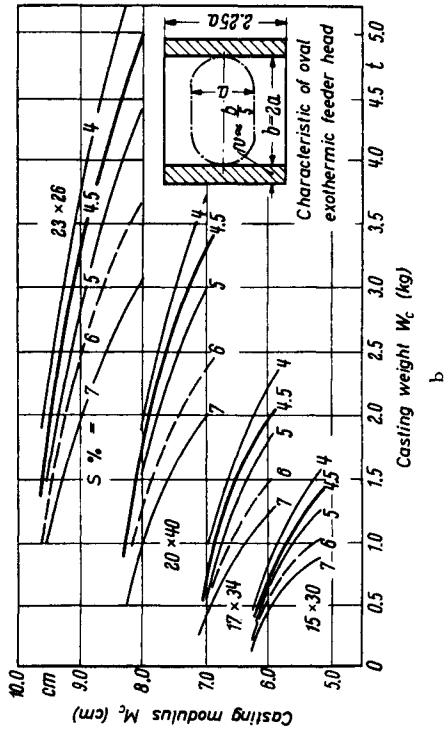
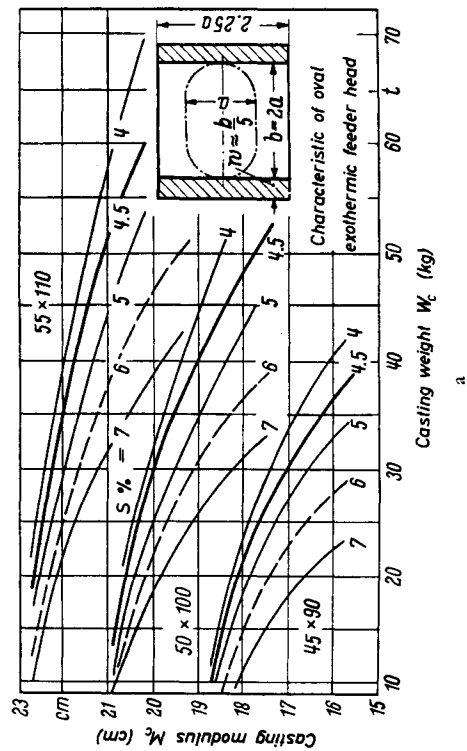
FIGS. 354a-d. Rapid determination of internally cylindrical exothermic feeder heads.



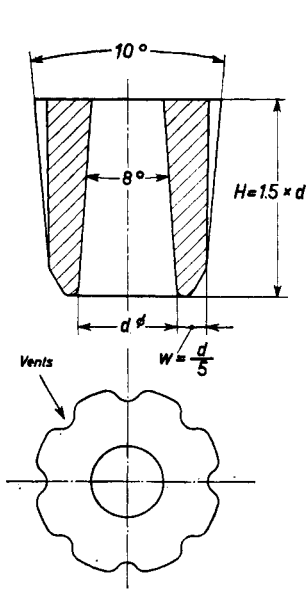
Figs. 355a-c. Rapid determination of internally oval exothermic feeder heads.



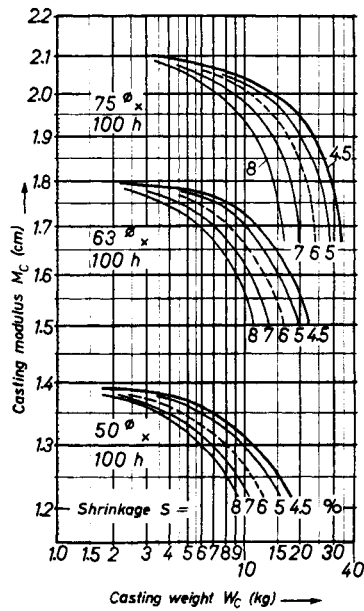
FIGS. 355.d-f. Rapid determination of internally oval exothermic feeder heads.



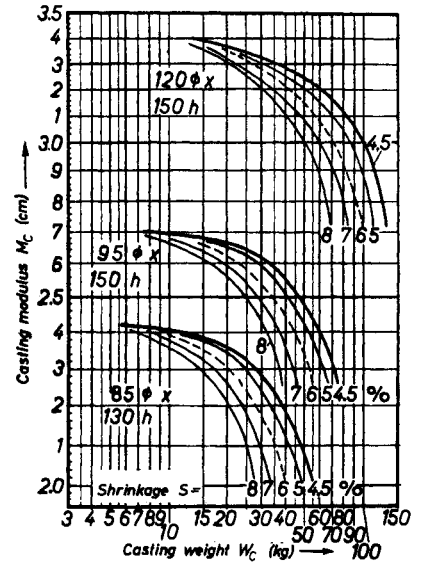
Figs. 356a-d. Rapid determination of internally oval exothermic feeder heads.



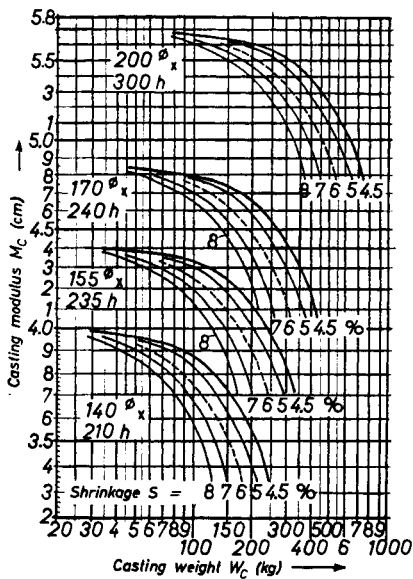
a



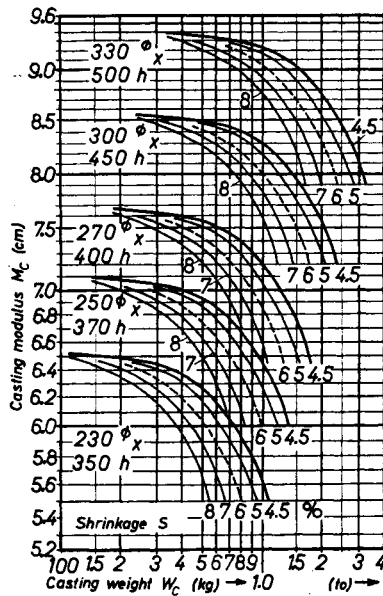
b



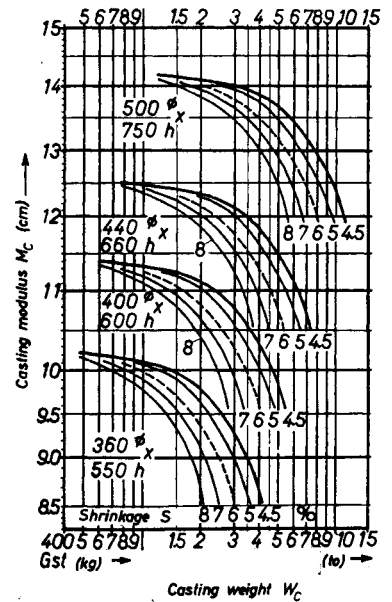
c



d

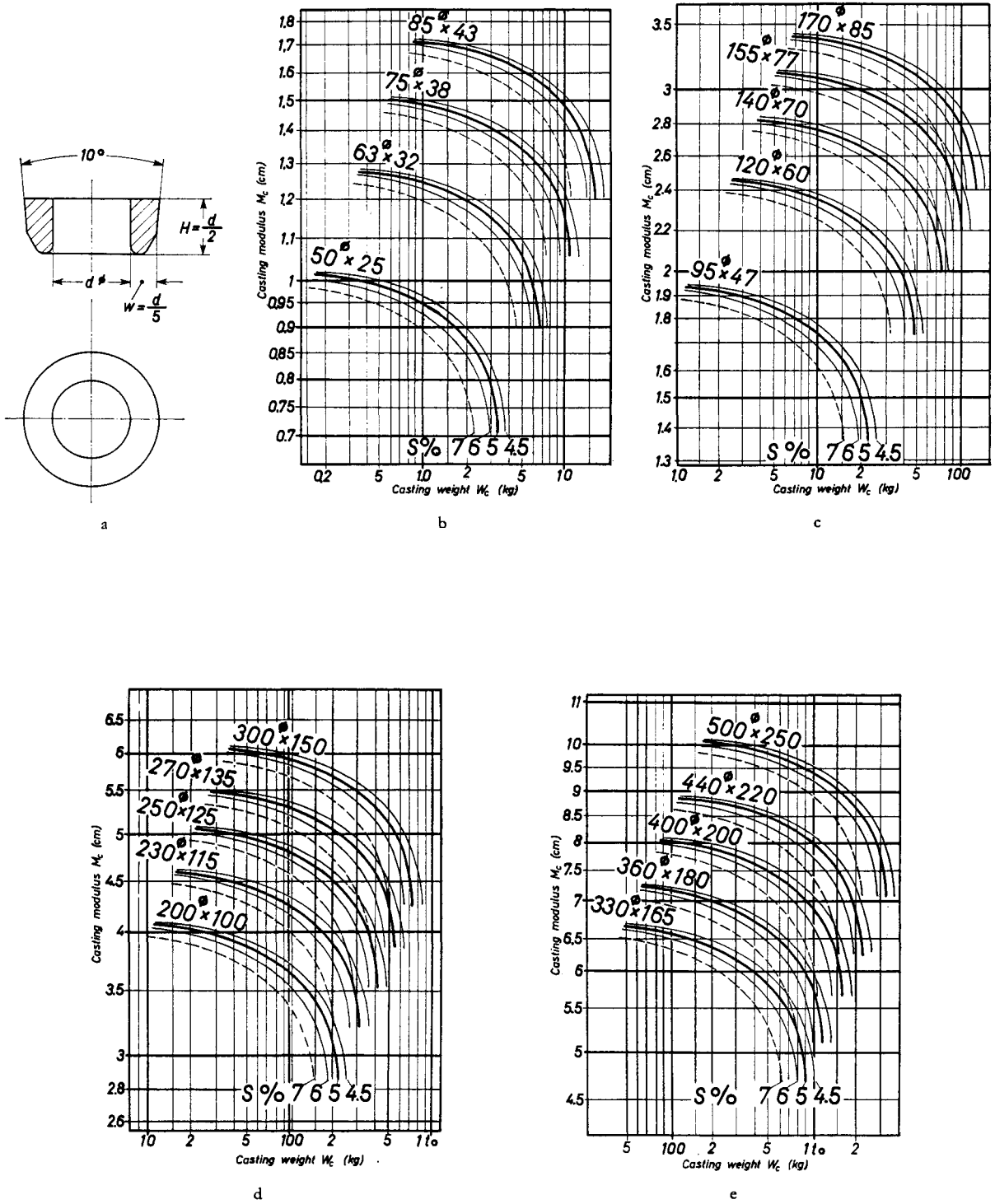


e

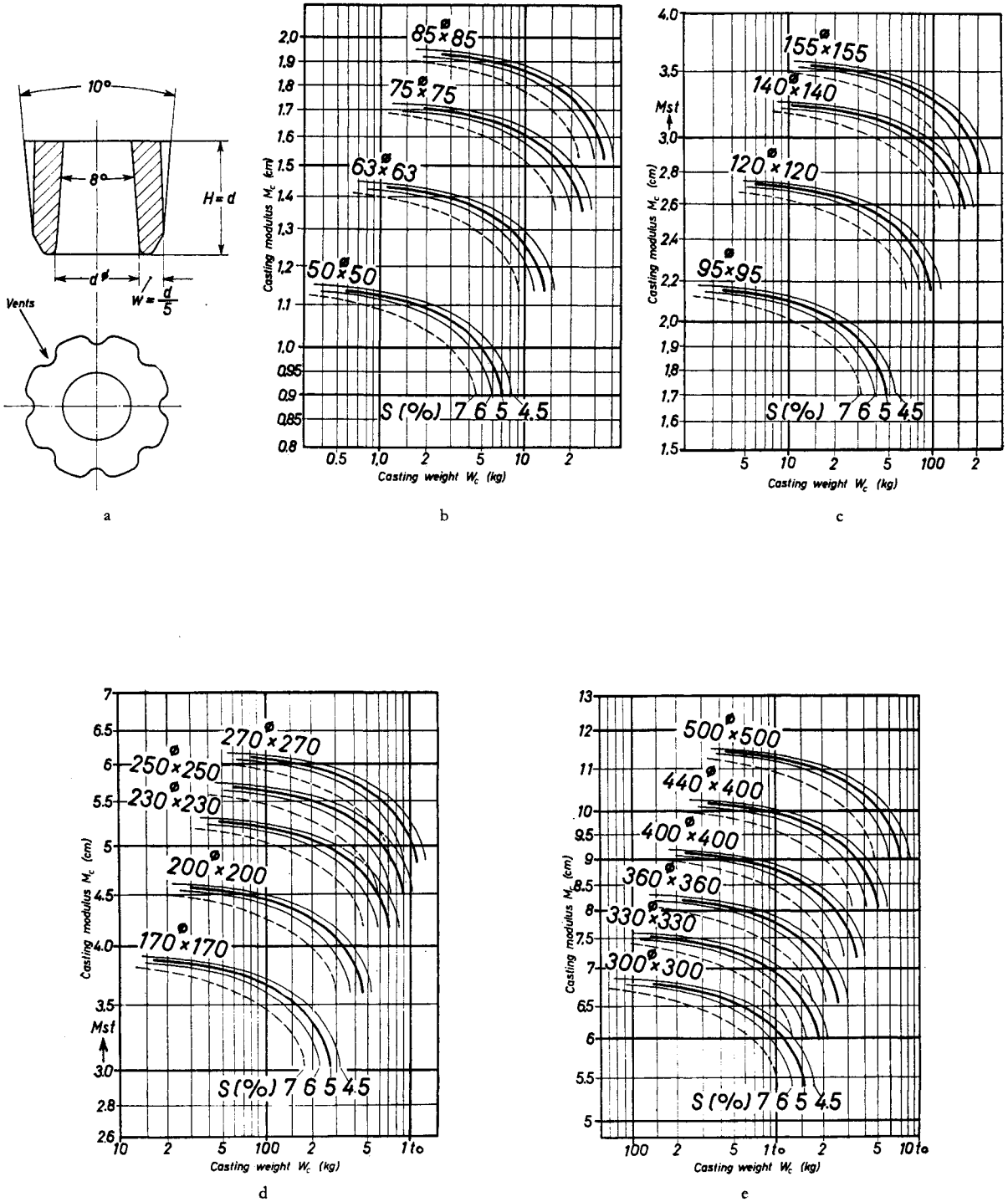


f

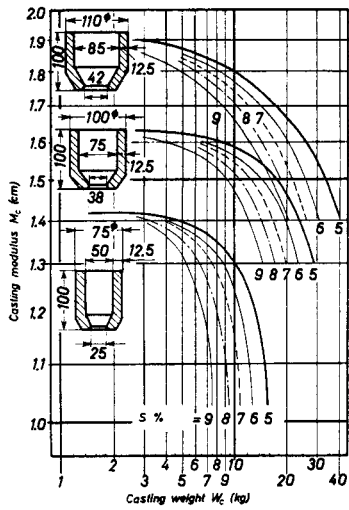
FIGS. 357a-f. Rapid determination of internally conical exothermic feeder heads. The feedable volume (or weight) of the casting is influenced by the fact that the internal volume of the feeder head is less than in the cylindrical form.



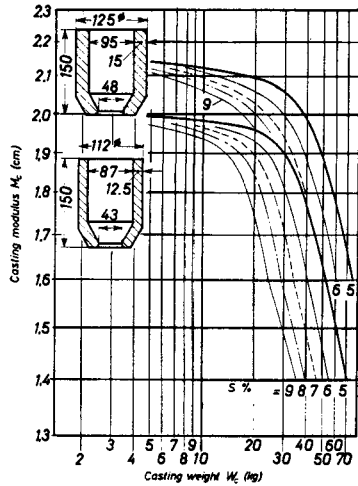
FIGS. 358a-e. Ring characteristic.



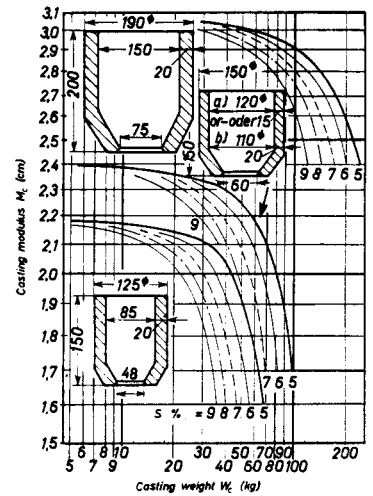
FIGS. 359a-e. Characteristic of two rings, one above the other.



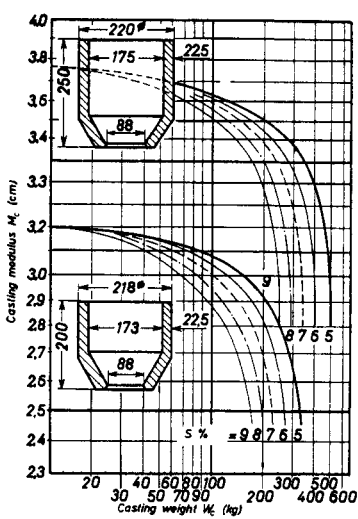
a



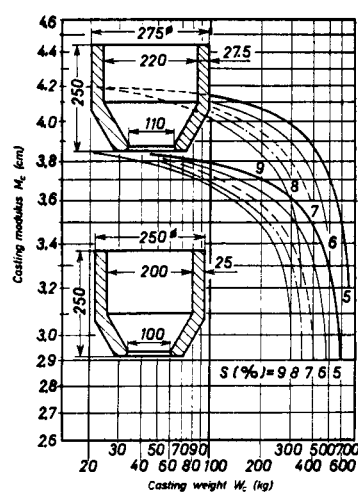
b



c

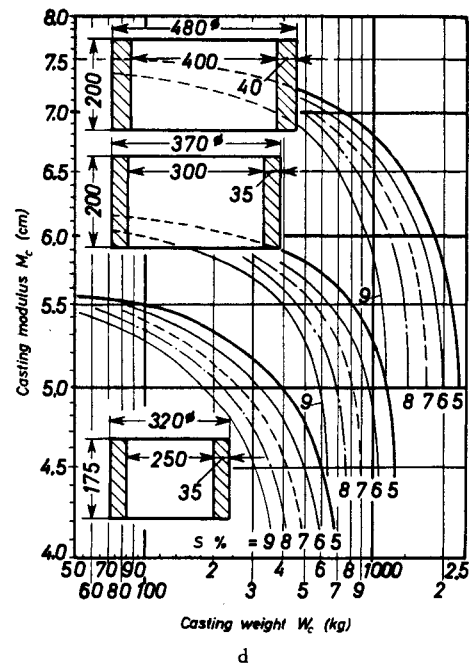
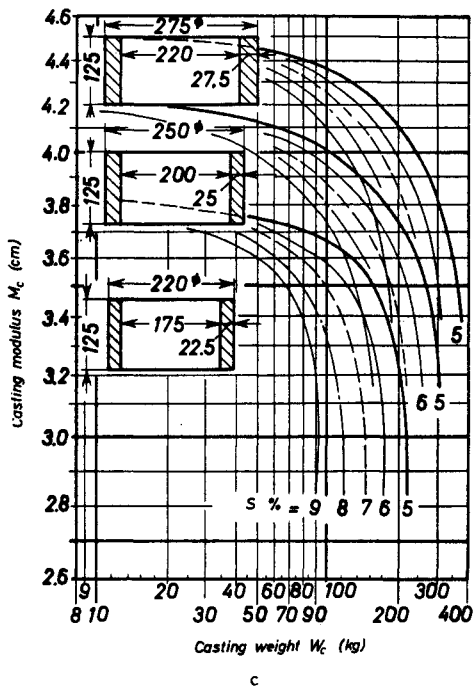
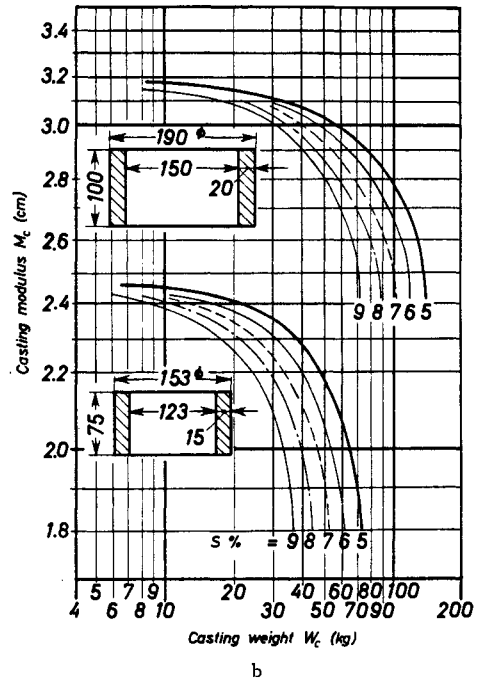
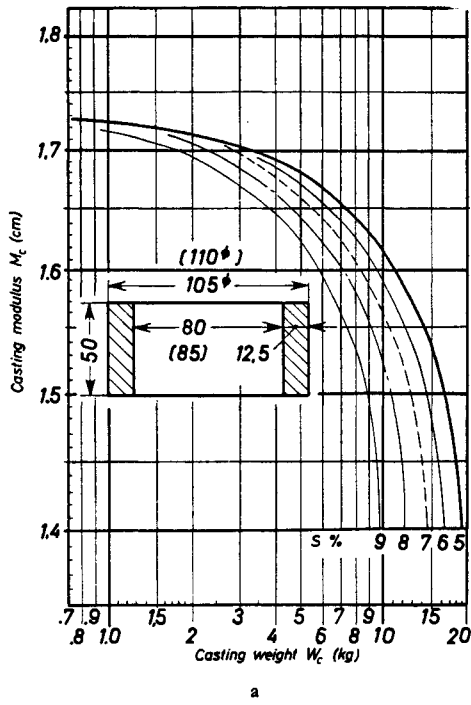


d

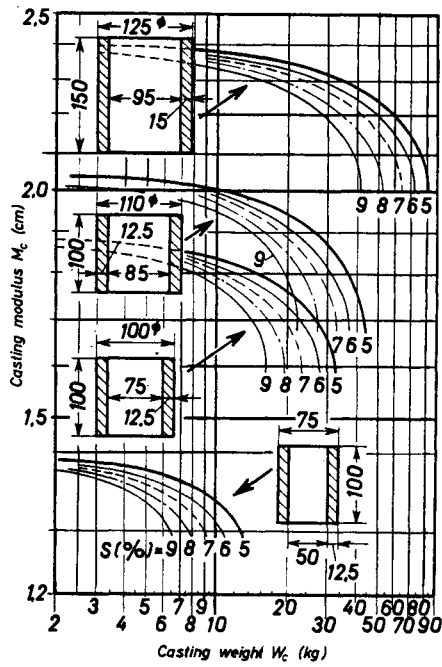


e

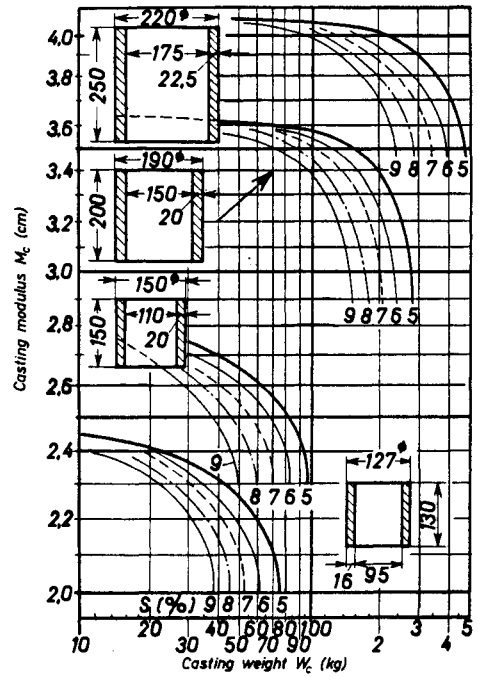
FIGS. 360a-c. Characteristic of one ring and one standard exothermic sleeve, one above the other.



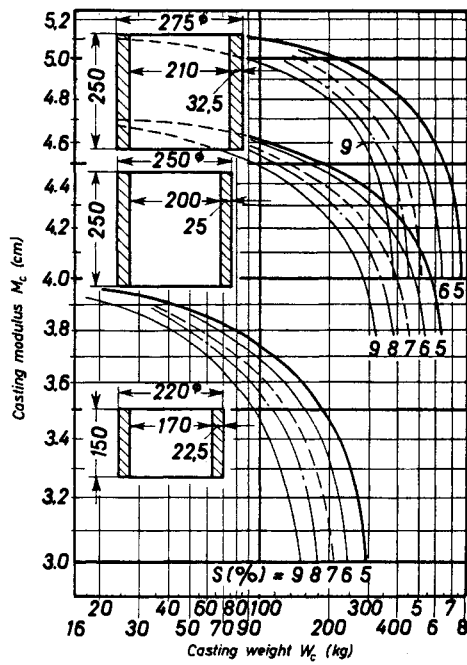
Figs. 361 a-d. Characteristic of a Foseco feeder head.



a



b



c

Figs. 362a-c. As Fig. 361, but with superimposed ring to give greater height.

12.4. On the Practice of Exothermic Feeder Head Manufacture

IMPORTANT FOR PRACTICE

12.4.1. CHEMICAL REQUIREMENTS AND HEALTH REGULATIONS FOR EXOTHERMIC MATERIALS

No chemical changes should take place in the metal as a result of using exothermic materials. A large part of this metal feeds into the casting and would impair the quality of the steel if changes in composition took place. A case is known to the author in which the steel was heavily enriched with silicon by the use of exothermic material, with the result that many of the castings showed hard, brightly polished spots after machining which were mistaken for shuts. The castings were rejected.

Exothermic materials should also give off a minimum of fumes when burning, so as to cause as little trouble as possible to the operators. In no circumstances must the fume be corrosive, or contain harmful fluorine gases. The author has known cases from his own experience where fumes of this kind have caused the foundry to be hurriedly evacuated, as though after an attack of poison gas!

12.4.2. MECHANICAL AND PHYSICAL REQUIREMENTS FOR EXOTHERMIC MATERIALS (OMITTING THE THERMAL REQUIREMENTS ALREADY DESCRIBED). ORDER OF MAGNITUDE OF THE AMOUNTS OF GAS EVOLVED

Exothermic sleeves should be strong enough to withstand the very rough treatment often given to them at the hands of the workmen. This can be achieved by consultation with the suppliers of exothermic material who will make suitable adjustments to the content of bonding material.

It is important in this connection for the prescribed water content to be maintained as accurately as possible. The resistance to abrasion of the exothermic sleeve is particularly important; defects are always produced when small sections of the sleeve become detached and fall into the mould.

Values for compressive and shear strength have been intentionally omitted, because these values, obtained in the laboratory, often do not allow satisfactory conclusions to be drawn concerning resistance to abrasion. This is best tested by rubbing with the fingers.

The gas permeability of the exothermic material is of very great importance. It is dependent partly on the size grading of the various raw materials and on the binder, and is also influenced by the water content. The author tested large numbers of test pieces on the "Georg-Fischer" (GF) sand testing apparatus; the results are reproduced in Figs. 363a and b for a certain product. It is necessary that every manufacturer of exothermic materials should give characteristic diagrams of this kind

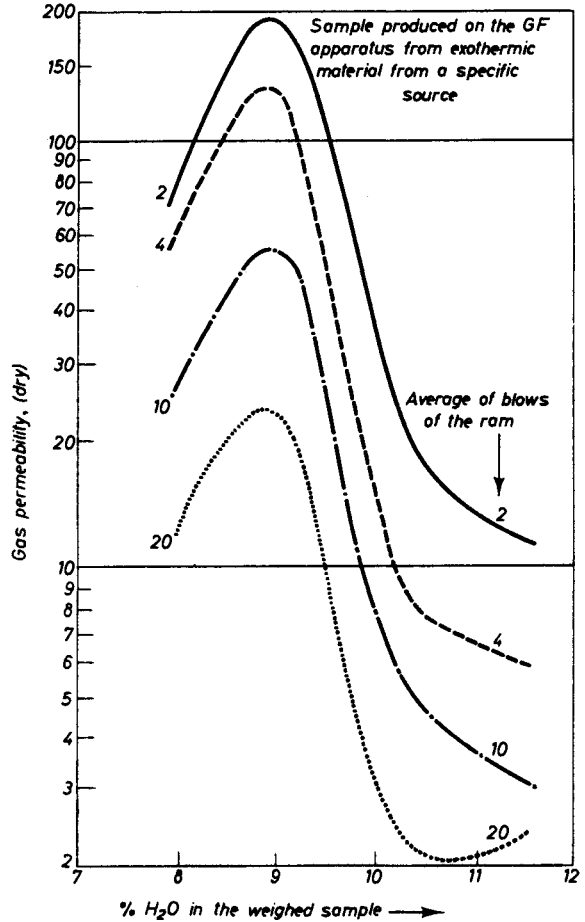


Fig. 363a. Relationship: gas permeability/initial water content.

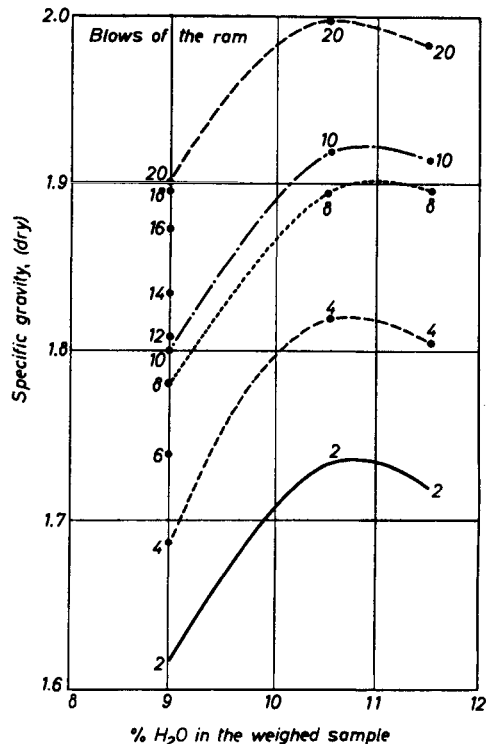


Fig. 363b. Relationship: specific gravity (g/cm³)/initial water content.

on request. We see first that the gas permeability shows a sharp maximum (at exactly 9 per cent water in this case). The permeability drops very sharply, both with more and with less water. With many other products the tolerance in water content is somewhat wider, but there is always a maximum. Suitable data are therefore required from the manufacturer.

It is also found, of course, that the gas permeability falls rapidly when the sample is compacted by repeated blows with the ram. This raises the question of how compact the actual exothermic sleeves should be made in practice. The author cut out test pieces from a production series of exothermic sleeves and determined carefully these specific gravities and gas permeabilities (the water content was known accurately). It was found that the average consolidation corresponded to 1 or 2 blows of the ram in the "GF" apparatus, and just occasionally to 3 blows of the ram. Nonetheless these exothermic sleeves were satisfactory. Thus the usual 3 or 4 blows of the ram in the sand laboratory apparatus did not correspond to the actual degree of compaction with most exothermic materials.

According to the author's experience the gas permeability of the dried test piece, with the most favourable water content, must amount to at least 180–200 units after 2 blows of the ram.

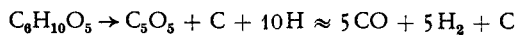
The author has also found that strict quality control is also necessary, together with a manufacturer's guarantee of the described thermal, mechanical and other physical properties.

Significant—in some cases almost incredible—improvements can be achieved with exothermic materials. However, it must not be forgotten that rejects due to fluctuations in quality are possible, leading to very high proportions of scrap or high repair costs. After such an experience the use of exothermic materials is often abandoned prematurely.

APPENDIX: CALCULATION OF THE AMOUNTS OF GAS LIBERATED

The following calculation illustrates the need for a high gas permeability.

The gases originate mainly from the binder. Let us start with 100 kg of an exothermic material containing an average of 5 wt per cent of a cellulose binder, or another binder of similar strength. The chemical formula of the cellulose is $(C_6H_{10}O_5)_x$, with unimportant deviations. At the high combustion temperature of the exothermic material ($\sim 1500^\circ\text{C}$) the binder decomposes very rapidly:



i.e. equal proportions by volume of carbon monoxide and hydrogen are evolved during combustion. The ~ 5 kg of evolved gas corresponds at 0°C to a volume of 6.95 m^3 . At the combustion temperature of $\sim 1500^\circ\text{C}$ we have, according to the well-known equation:

$$V_T = V_0(1 + \alpha \times T) \tag{158a}$$

$$V_{1500} = 6.95 \left(1 + \frac{1500}{273} \right) = 45 \text{ m}^3, \tag{158b}$$

i.e. about 45 m^3 of gas are liberated from 100 kg of exothermic material!

This value varies in individual cases according to the tube and amount of binder, but gas volumes as high as $80 \text{ m}^3/100 \text{ kg}$ have been found. This order of magnitude certainly gives food for thought!

12.4.3. THE DESIGN AND MANUFACTURE OF EXOTHERMIC SLEEVES. THE MOST SUITABLE WALL THICKNESSES OF THE SLEEVES

A minimum wall thickness of $w = d/5$ should be maintained, according to the author's experience. In many cases even thicker walls are an advantage. A set of standard feeder heads of this type is illustrated in Fig. 364. Reference should be made to Section 12.6, and

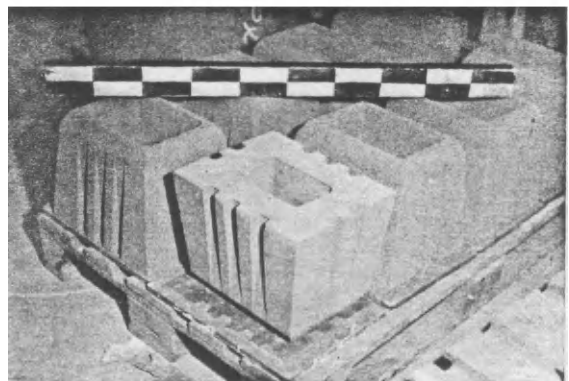
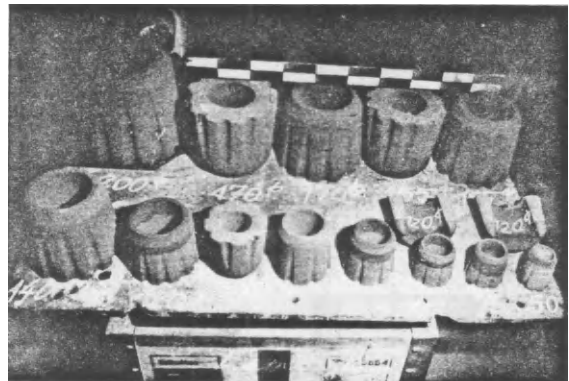


Fig. 364. Different sizes of standardized exothermic sleeves. (Courtesy Sulzer Bros.)

in particular to Fig. 396 for the determination of the optimum wall thickness. It will only be emphasized at this point that this wall thickness can vary very considerably according to the steel costs and the type of article being made.

The natural gas permeability of the exothermic material is of special importance. A great deal can be achieved by venting, etc., but allowance must always be made for badly trained and negligent personnel. Experience has shown that such additional work is often "forgotten", with the result that the metal bleeds back due to the low gas permeability.

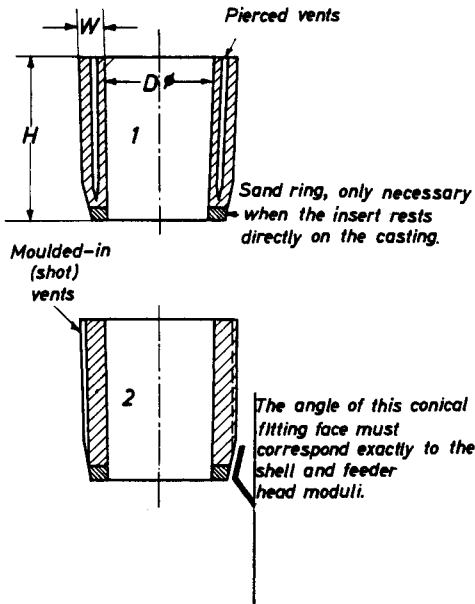


FIG. 365. Venting of exothermic sleeves.

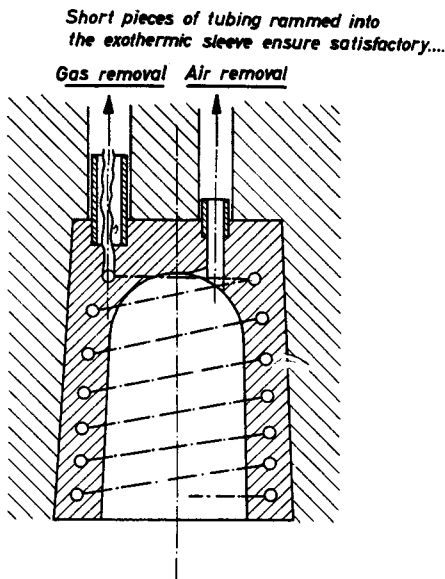


FIG. 366a. Blind exothermic feeder head with satisfactory venting using rammed-in spiral hollows or straw rope.

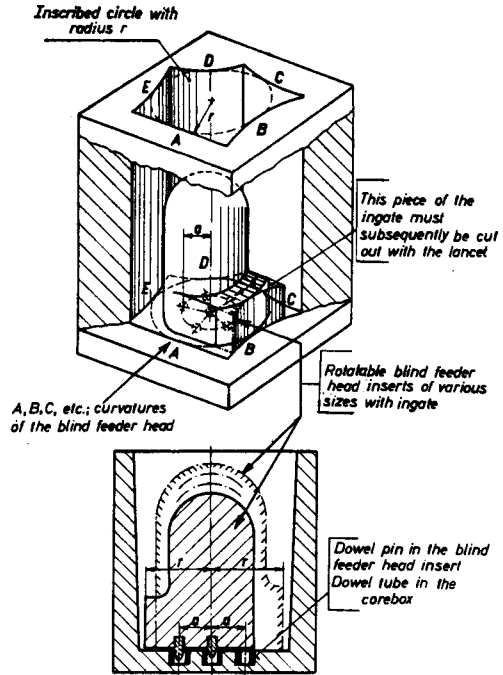


FIG. 366b. The core box shows an irregular polygon in plan.

The curvatures of the sides of the polygon correspond to the curvatures of the standard chills (Table 25). The feeder head core can thus be placed on castings of different shapes and sizes.

Up to four feeder head inserts of various sizes can be fitted into each core box. The feeder neck is attached firmly and made with the dimensions corresponding to the correct modulus.

The neck can be turned to every side of the polygon (A, B, C, etc.); the correct position is ensured by a central dowel pin and five others in the circle of radius a .

The notation for such a feeder insert is, for example, M14B, where M stands for the feeder head insert, 14 for the diameter of the feeder in cm and B the desired side of the polygon to which the feeder neck must point. In this way universally applicable feeder heads can be manufactured for a small expenditure on standardized pattern components.

Breaker or Williams cores can also be used with similar inserts. Instead of the polygon a round hole is provided with radius r . Inserts both of insulating and exothermic materials can then be made with the same core box (of Fig. 367). The inserts can be closed.

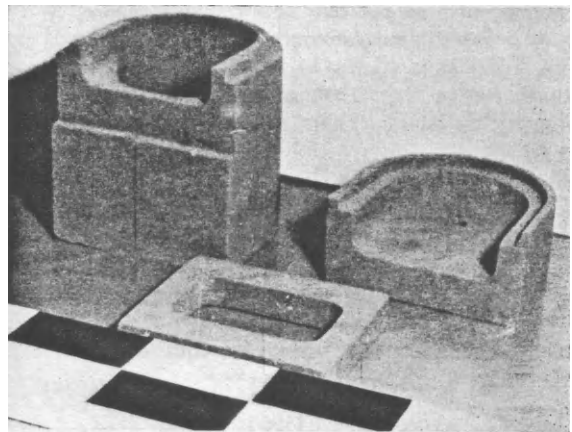


FIG. 366c. Blind feeder head moulded entirely as an exothermic core can be rammed up with the mould in inaccessible positions.

According to Fig. 365 the air vents in exothermic sleeves can be pre-pierced or moulded in as grooves. When metal flows behind or over the sleeve the vents become blocked, sometimes causing vigorous boiling and ejection of metal. Hence exothermic sleeves must possess a well-fitting conical face, which reliably prevents the metal from flowing behind it. With larger inserts the back side is filled with loose, dry sand.

With blind (covered) exothermic feeder heads and with large heads of exothermic material (Fig. 366) the air must be led away by means of carefully placed plaits, wax, string, etc., which open out to a venting channel into which no metal can penetrate. If care is not taken considerable metal ejection can take place, which can even lead to explosive disintegration of the mould.

The exothermic sleeves are manufactured either by hand or on the core-shooting machine. The core bosses

but these cause trouble by evolving ammoniacal fumes due to the action of the moisture.

Occasionally, an exothermic puncture core is used instead of one of oil sand in smaller blind feeder heads. No additional pressure effect or significant heating up can be attained in this way, but, particularly with smaller blind feeder heads and with dull metal, a further cooling of the steel at the puncture core does not occur, and the formation of a prematurely solidified skin which would hinder the action of the atmospheric pressure is also prevented. The reliability of the operation is increased considerably.

12.5. Practical Examples and Hints for the Use of Exothermic Feeder Heads

The following sequence of operations should always be followed:

1. Divide up the casting into feeding areas (see Chapter 3).
2. Determine the modulus at the point of attachment of the feeder head (see Sections 2.4 and 2.5).
3. Estimate the weight of each feeding area (the total weight of the casting, with all casting additions, such as shoulders, dirt traps, etc., must of course be known for each case).
4. Select the corresponding exothermic sleeve from Figs. 354-362.

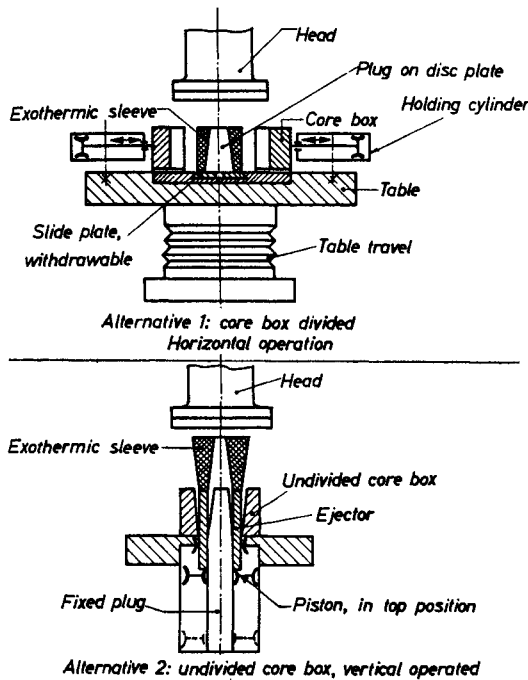


FIG. 367. Examples of the economical manufacture of exothermic sleeves on core-shooting machines with special equipment.

can either be jointed or unjointed. In the latter case it pays when producing large quantities to have a special clamping device, as shown in Fig. 367, which is constructed by the appropriate firms. Exothermic materials are dried at 110-220°C, according to the product.

Most exothermic materials are moisture-sensitive, i.e. damp sleeves cannot ignite, or at any rate ignite incompletely, leading to scrap and bleeding back. With green sand moulding, therefore, exothermic inserts should be placed in position as short a time before casting as possible. If this cannot be done, or, as frequently happens, finished moulds cannot be used quickly, then exothermic inserts with a cheap watertight plastic sheath should be fitted, or in some circumstances can be rammed in directly. Some exothermic materials are "self-drying"

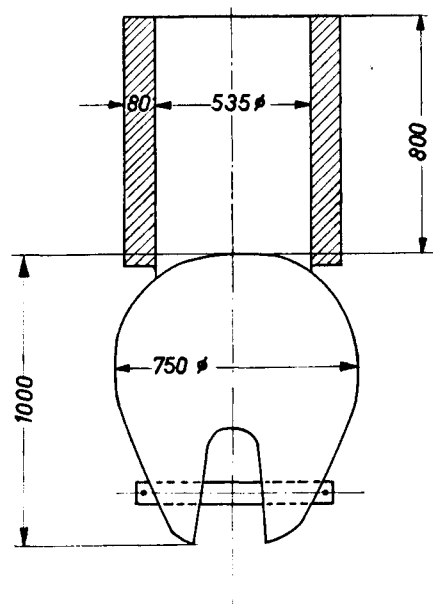


FIG. 368a. Tup.

Many examples of modulus calculations, etc., have already been worked out in this book, and it has not been thought necessary to repeat the entire calculation for the greater part of the following diagrams (Figs. 368 to 393). Most of these examples will therefore serve only to indicate the possibilities offered by the use of exothermic feeder heads.

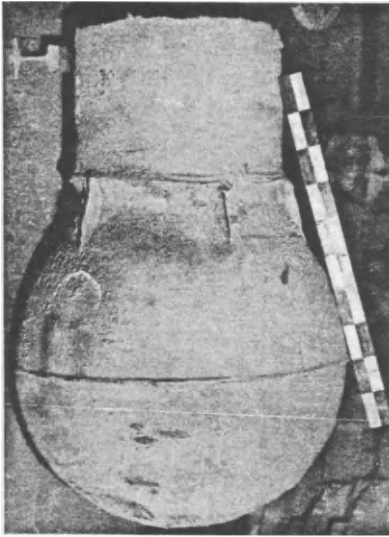


FIG. 368b. Tup for a scrap plant. Fed by means of an exothermic feeder head. No internal chills were inserted in the casting.



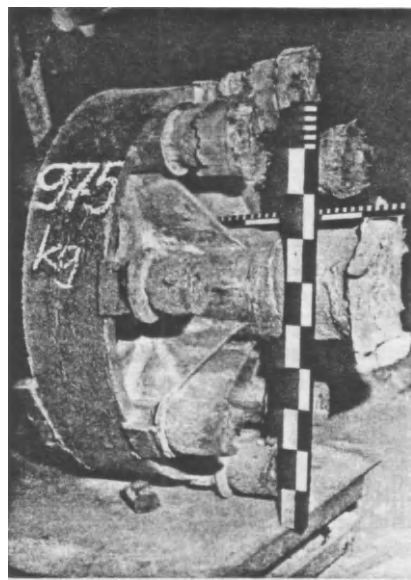
a



b



c



d

FIGS. 369a-d. Crane pulley, a and b without, c and d with, exothermic feeder heads. By using these feeder heads working time was also saved in the dressing shop, and less machining was required.

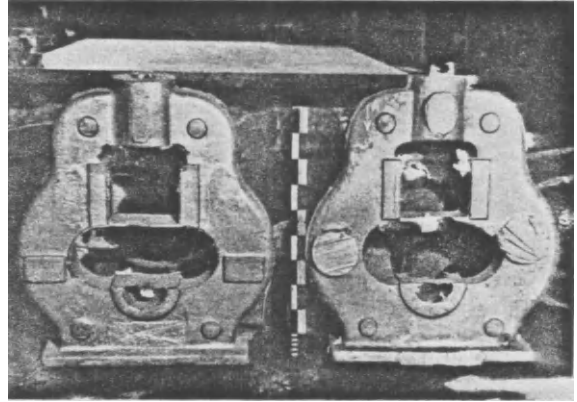
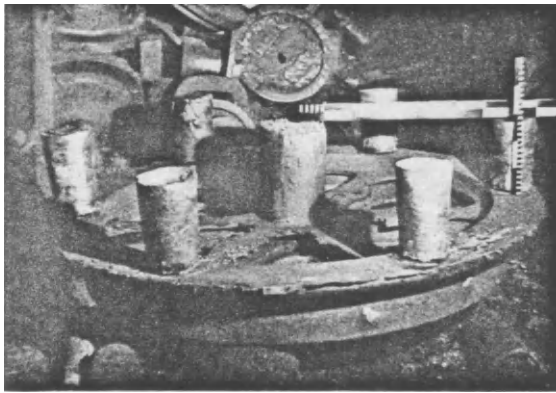
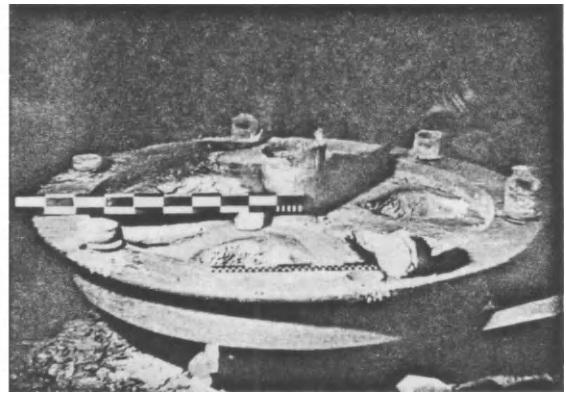


FIG. 371. Roll housing with exothermic feeder heads and intermediate chills to generate artificial end zones.

FIG. 370. Clamp leg, top poured through the exothermic feeder head. Yield 93%. The inside of the exothermic insert was faced to prevent premature ignition.



a



b

FIGS. 372a and b. Guide pulley (a) without, (b) with exothermic feeder heads and intermediate chills. Note the considerable withdrawal of metal from the exothermic feeder heads.

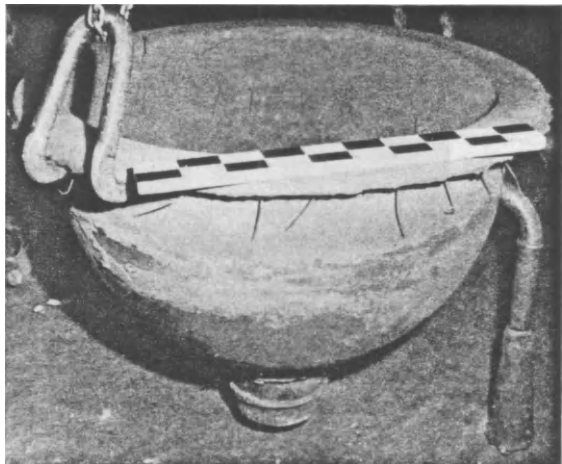


FIG. 373. Melting pot, fed by a single exothermic feeder head. Yield 91.5%.
(Courtesy Sulzer Bros.)



FIG. 374. Kneading arm made from 18-8 steel.
(Courtesy Sulzer Bros.)

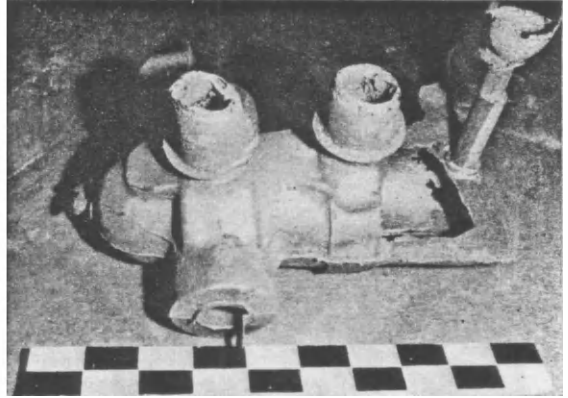


FIG. 375. Housing. Note the central exothermic feeder head with clover leaf shoulder.

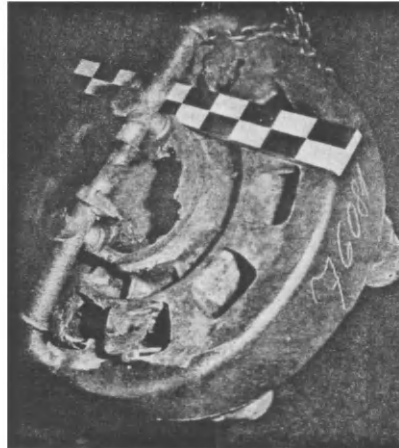
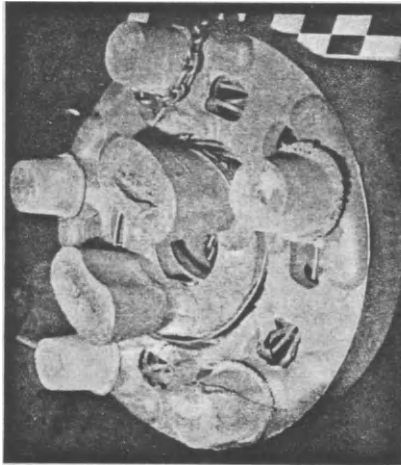
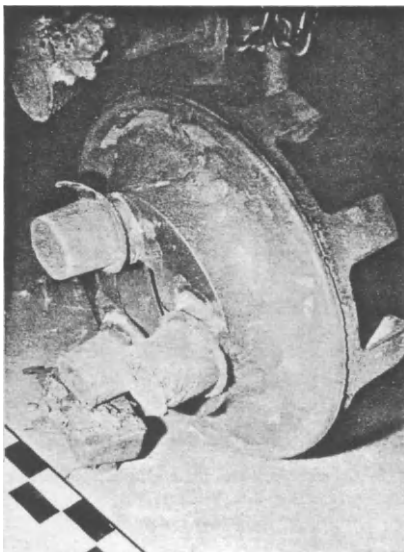
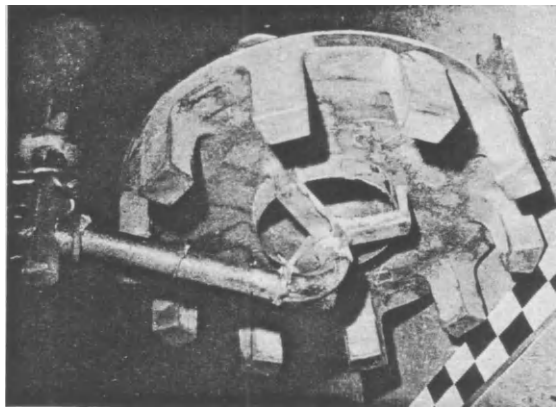


FIG. 376. Spider for an electric locomotive. Cast through runner brick, and fed both with exothermic feeder heads (via shoulders) and without. Radiographically sound.
(Courtesy Sulzer Bros.)

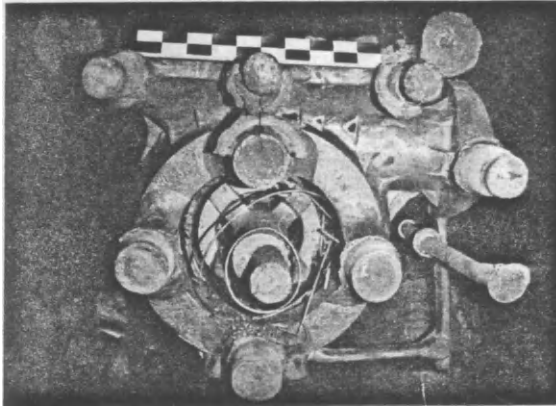


a

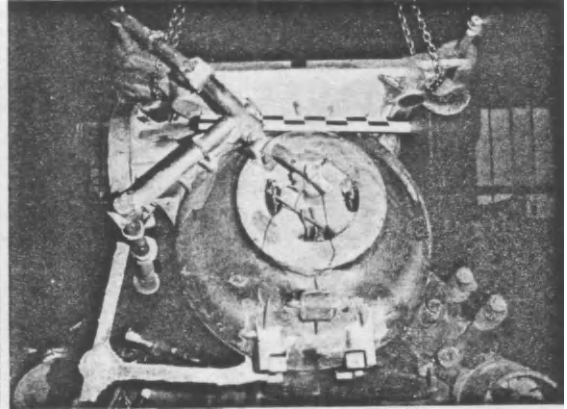


b

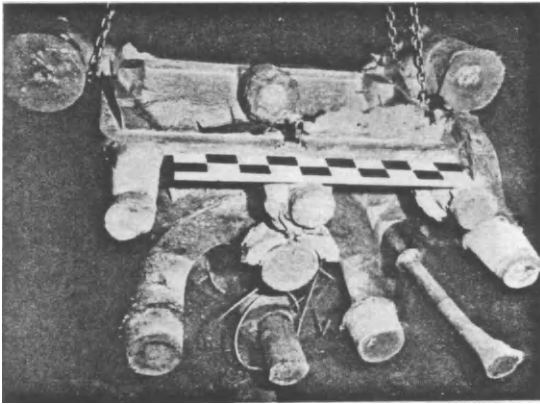
FIGS. 377a and b. Driver of an electric locomotive, radiographically sound. Teeth fed from disc dimensioned according to the correct modulus. Fed through three exothermic feeder heads Cast through runner brick.
(Courtesy Sulzer Bros.)



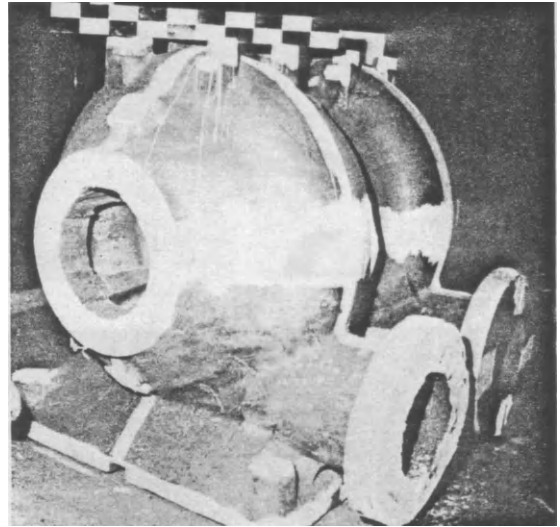
a



b

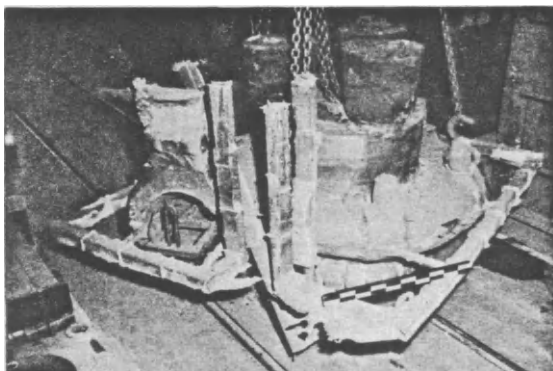


c

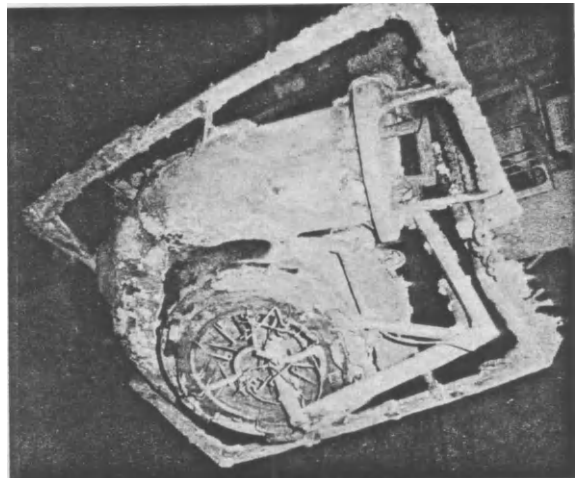


d

Figs. 378a-d. Casting technology of a pump casing.
(Courtesy Sulzer Bros.)

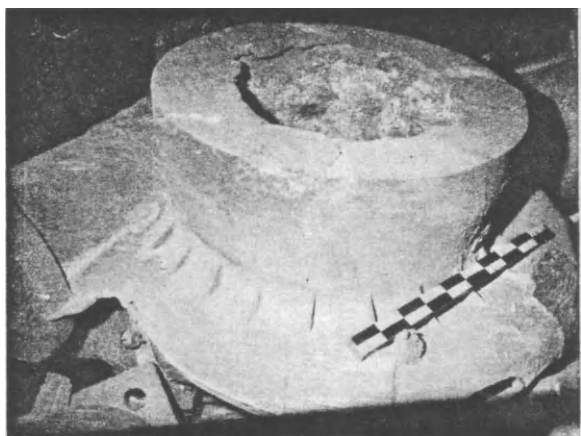


a



b

Figs. 379a-f.



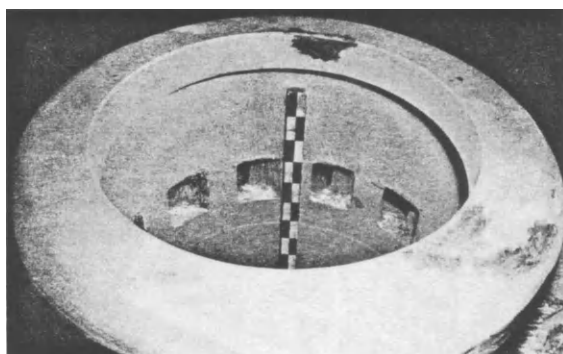
c



d



e



f

FIGS. 379a-f. Casting technology of a pump casing (reproduced by courtesy of Sulzer Bros., Winterthur).



a



b

FIG. 380a and b. Small turbine casing. (Courtesy Sulzer Bros.)

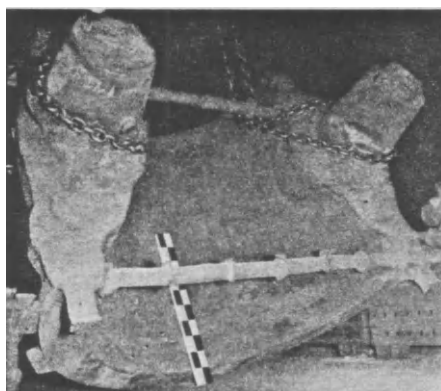
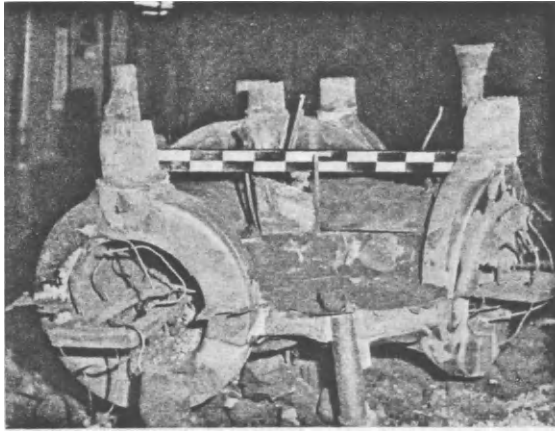
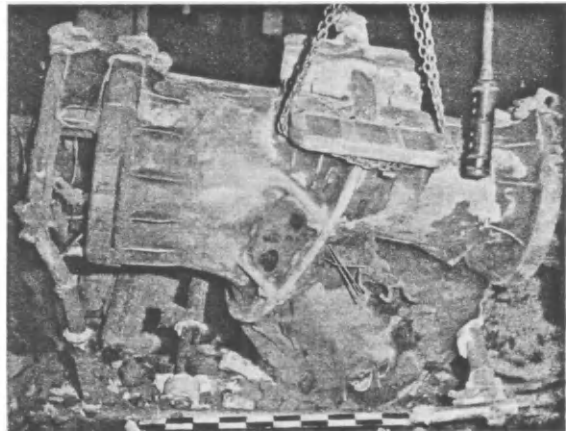


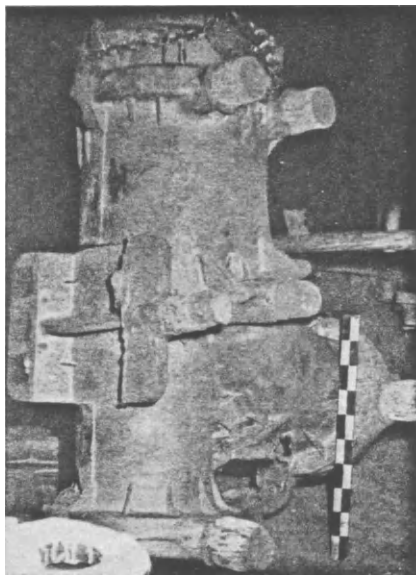
FIG. 380c. Large, thick-walled turbine casing, with exothermic feeder heads and contraction bars.



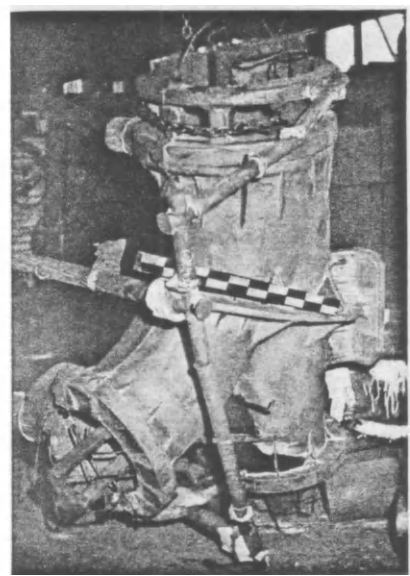
a



b

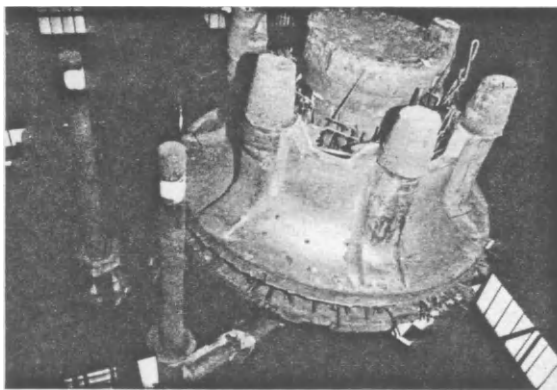


c

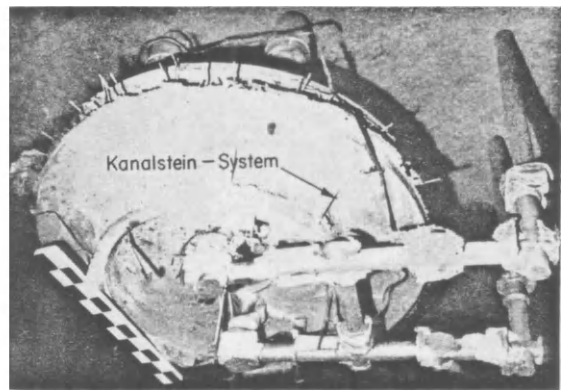


d

FIG. 381 a-d. Branch pipe.



a



b

FIG. 382 a and b. Pump impeller. (By courtesy of Sulzer Bros., Winterthur.)
Kanalstein-System = Runner brick system.

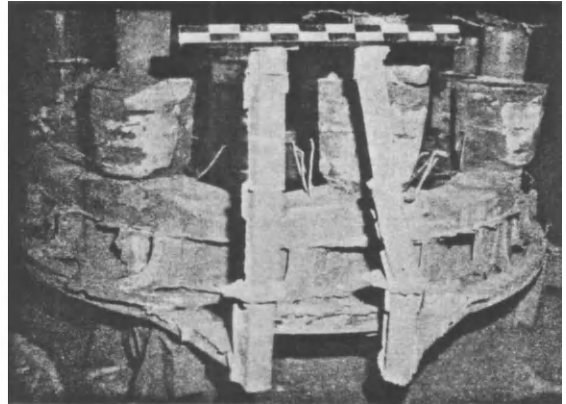
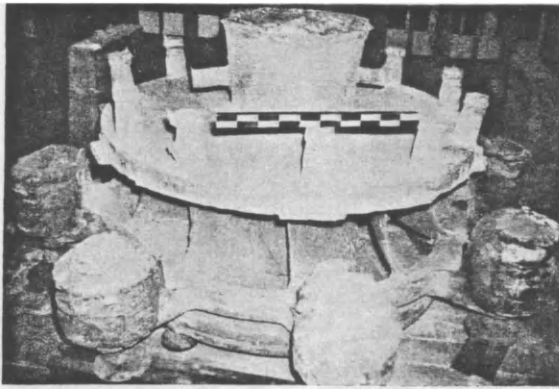
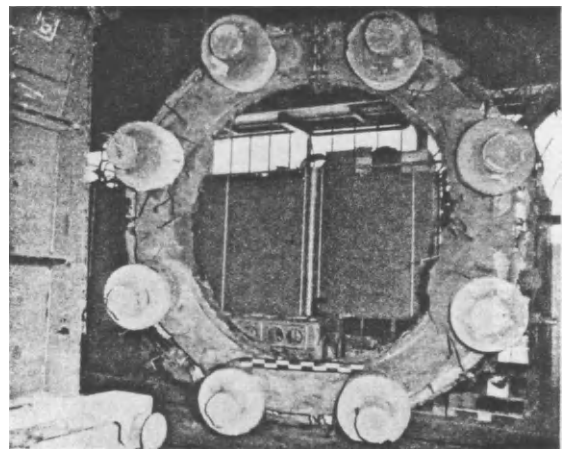


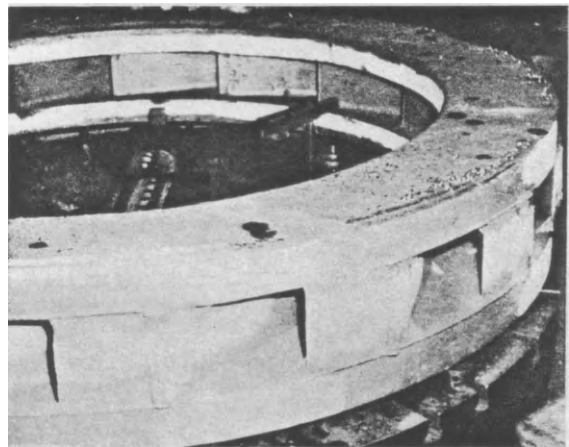
FIG. 383. Turbine wheel.

*Top: exothermic feeder bead.
Bottom: exothermic side feeder beads.*

a



b

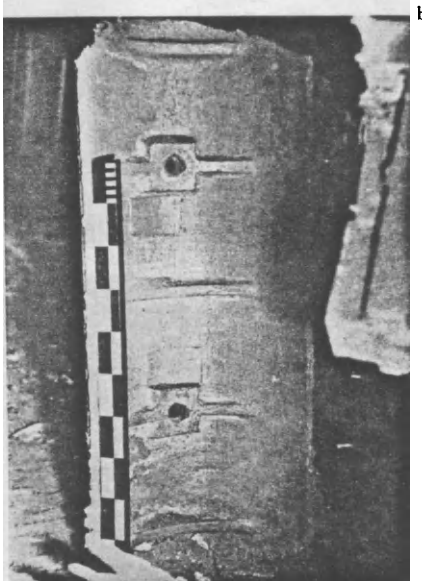
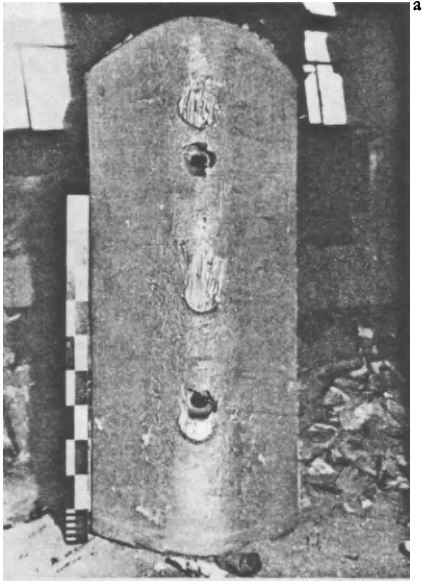


c

FIGS. 384 a-c. Ball race.



FIG. 385. Pump impeller.



FIGS. 386a and b. Cover plate with exothermic feeder heads and intermediate chills.

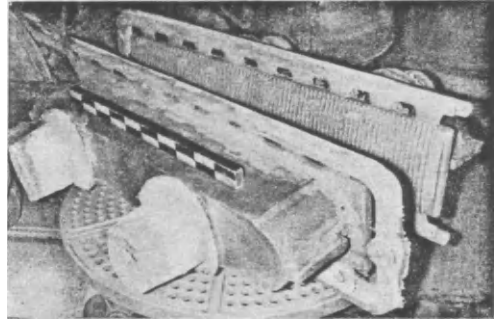


FIG. 387b. Pole cores of an electrical machine.

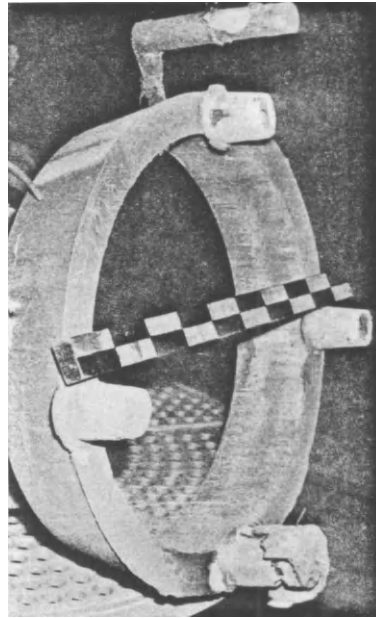


FIG. 388. Ring. Gross yield 91 %.



FIG. 387a. Bridge bearing plates.

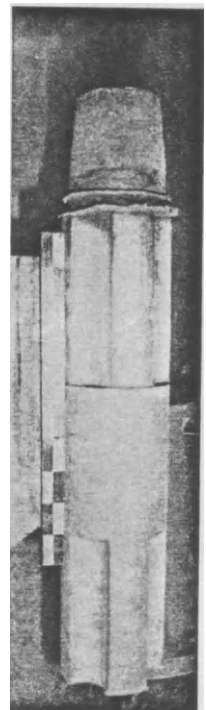
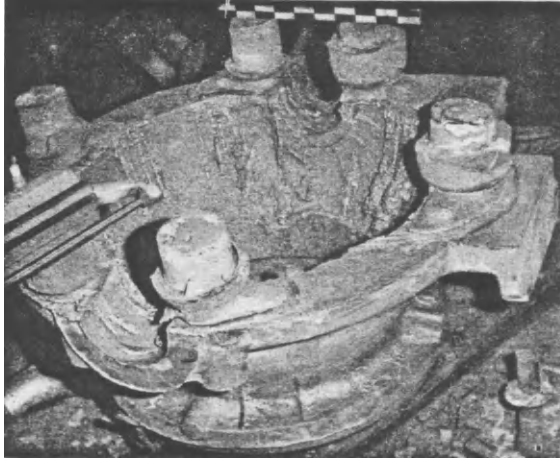
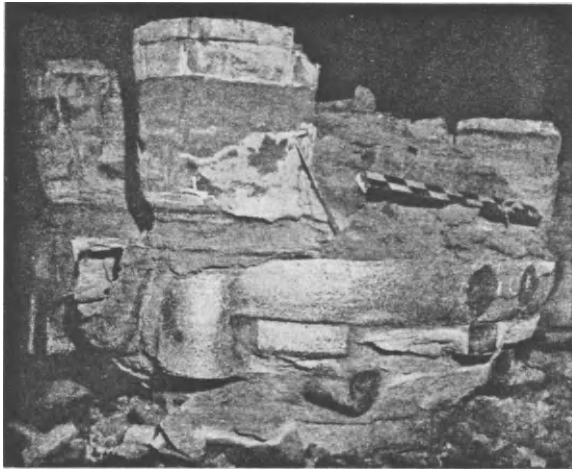
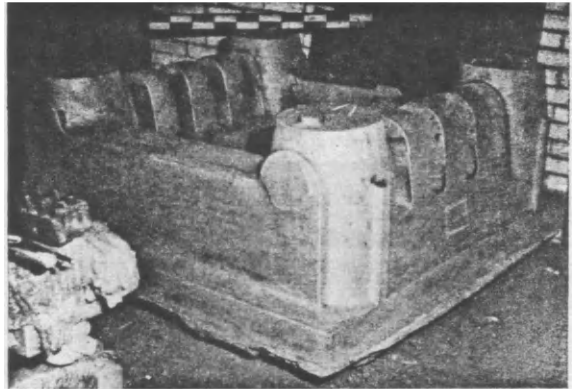
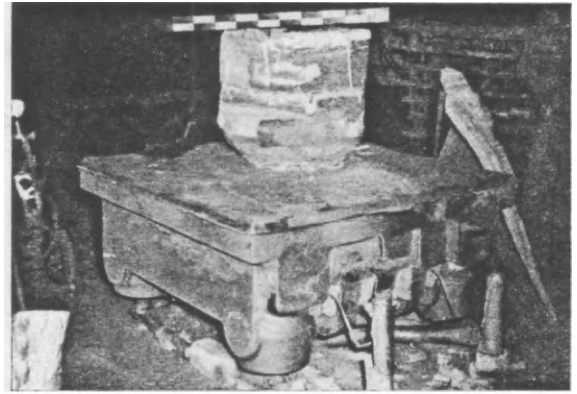


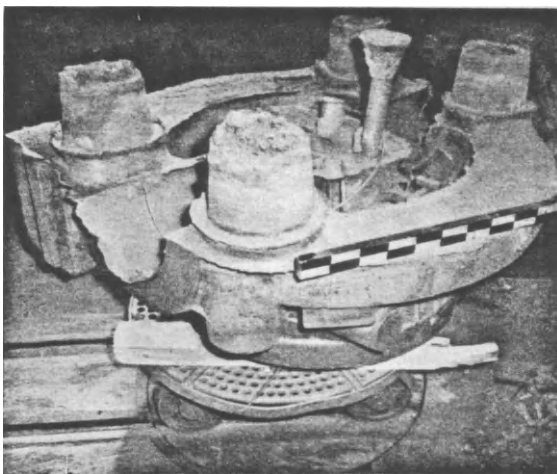
FIG. 389. Rolling mill spindle.



a



b



c

FIGS. 390a-c. Cut-off valve (ball valve) housing for a water turbine.

(Courtesy Sulzer Bros.)

Housing (a) is not identical with the housing of (b) and (c).

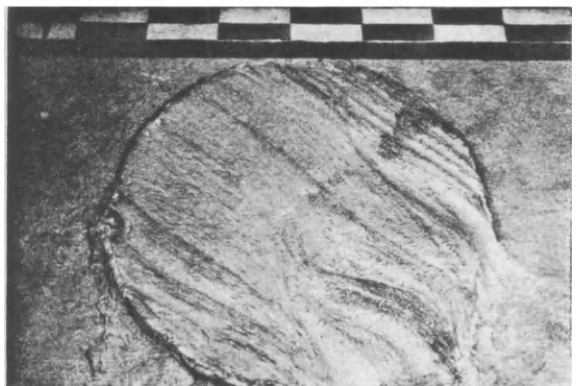


FIG. 391. Squeezer plate for a large diecasting machine. Gross yield 93%.

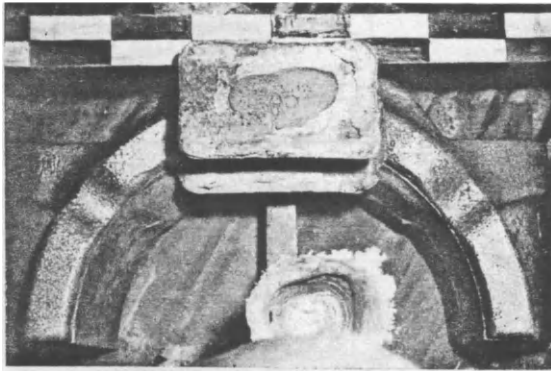
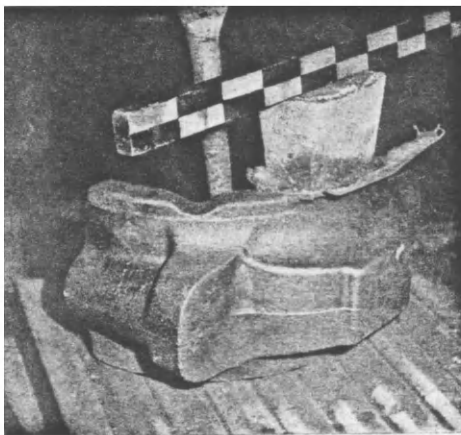
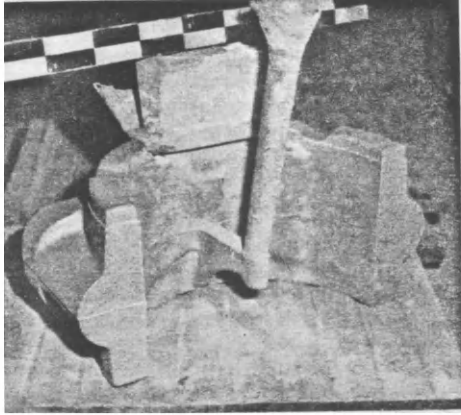


FIG. 392. Bearing cap of a marine engine.
(Courtesy Sulzer Bros.)

It will be noted that the metal in the sleeve must in all cases be covered with a highly exothermic powder, as otherwise the heat losses will be considerable. A rule to follow is that the powder must cover the metal to a depth approximately equal to the thickness of the exothermic sleeve. If this rule is broken the favourable shape of shrinkage cavity which is aimed for is not obtained, with the result that the cavity often extends into the casting.



FIG. 393. Bearing bush of a marine engine.

It is recommended that antipiping powder should be previously weighed out in small paper or plastic bags, in various weight categories. In this way all waste is avoided.

12.6. The Economics of Exothermic Feeder Heads

12.6.1. GENERAL

IMPORTANT FOR PRACTICE

If the above rule is followed conscientiously, no scrap will result from the use of exothermic feeder heads. This disposes of one important objection to the use of such feeders on economic grounds.

In calculating economic aspects an *objective* answer must be given to the following questions:

1. What is the cost of a non-exothermic, but accurately calculated feeder head?
2. What is the cost of a correctly calculated exothermic feeder head, and what is the difference?

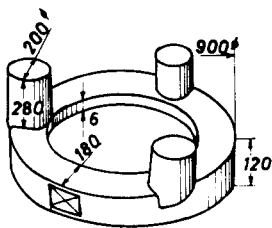


Fig. 394. Apparent and actual expenditure of exothermic materials in relation to the saving of liquid steel.

It is not permissible to compare very large, overdimensioned non-exothermic heads with very small exothermic heads (Fig. 394). This method would be self-contradictory. An objective comparison also requires the knowledge of

1. The cost of 1 kg exothermic material in its final processed condition.
2. The level of the pure melting costs per kg of steel (i.e. costs of electric current, oxidation losses, wages, etc.). In considering melting costs the capacity situation of the furnace operation must also be taken into account. Unalloyed and low-alloy steels are correspondingly cheaper than high-alloy steels.

In the first place the cost factor p must be determined for every plant, based on its special economic position. This factor is given by:

$$p = \frac{\text{costs per 1 kg exothermic material, prepared ready for use}}{\text{pure melting costs per 1 kg steel}} \quad (159)$$

The next section 12.6.2. need not necessarily be read by the practical foundryman, but section 12.6.3. is of importance to him.

12.6.2. THE FEEDER HEAD COMPARISON ;
MAKING USE OF THE CHARACTERISTIC

In order to compare the effectiveness of (1) non-exothermic, (2) exothermic feeder heads with various sleeve thicknesses w , the characteristic of the following feeder head was plotted in the log-log scale in Fig. 395a: $d_{int} = 1$, $H = 1.5$ (again given in general units, i.e. dm, ft, etc.). The wall thicknesses cover the following range:

Table to Fig. 394.

<p>a. Gear rim with an oversized, non-exothermic feeder head</p>	<p>Feeder head made too large because of incorrect estimate. Weight of circulating scrap 355 kg using 4 exothermic feeder heads 125 kg apparent saving of steel 230 kg 4 exothermic feeder heads at 4.5 kg 18 kg amount used for each 100 kg steel saved = $18/2.3 = 7.8$ kg exothermic material (point A).</p>
<p>b. Gear rim with 4 inaccurately calculated exothermic feeder heads.</p>	<p>To provide an adequate safety factor 4 exothermic feeder heads were used, with intermediate chills. Dimensions of the exothermic inserts: \varnothing internal = 160 mm \varnothing external = 210 mm Height = 180 mm weight = 4.5 kg modulus = 4 cm If the feeding requirements in the casting had been calculated accurately, 3 exothermic feeder heads with intermediate chills would have been sufficient.</p>
<p>c. Accurate calculation of gear rim with 3 exothermic feeder heads.</p>	<p>Weight of casting 265 kg i.e. $265/3 = 88$ kg per feeder head modulus of casting $M_c = 3$ cm Modulus of non-exothermic feeder head $M_F = 1.2 \cdot 3 = 3.6$ cm. From Table 19: $F \approx 200 \varnothing \times 280$ h; $W_F \approx 60$ kg. Total weight of feeder head = $3 \times 60 = 180$ kg From Fig. 354 or 359 an exothermic feeder head $120 \varnothing \times 150$ h is derived. Weight of exothermic material = 2.1 g, + 0.2 kg exothermic powder; $2.3 \text{ kg} = \sim 7$ kg for 3 feeder heads. Weight of steel core fed down in the head ~ 5 kg feeder head weight $3 \times 5 = 15$ kg Circulating scrap saved = 165 kg Exothermic material used per 100 kg steel saved = $\frac{7}{1.65} = 4.25$ kg</p>

- $w = 0$ (non-exothermic)
- $w = 0.5 \times d$
- $w = 0.1 \times d$
- $w = 0.15 \times d$
- $w = 0.2 \times d$
- $w = 0.25 \times d$
- $w = 0.35 \times d$

It will be recollected that the curves may be given a parallel displacement on the log-log scale. This parallel displacement scale was also plotted for internal diameters from $d = 0.7$ to $d = 1.8$.

Six points I to VI were taken at random and marked on the characteristic of the exothermic feeder head $d = 1$, $w = 0.15 \times d$. Point I corresponds to a casting having a modulus $M = 0.255$ dm and a volume $V = 1.6$ dm³. Point VI relates to a casting of modulus $M = 0.21$ dm and volume $V = 14$ dm³.

The points I-VI each correspond to a specific q -value. This value is discussed in section 5.6, equation (27), page 51. Massive bodies, such as cubes, have small q values ($q \leq 200$) while large, thin plates have large values ($q \leq 1000$). The shape of a casting, whether massive or platelike, can thus be described in general terms by means of the q -value.

A transparent sheet of paper is placed on this diagram and the group of curves is drawn, the result being shown in Fig. 395b. This transparent paper is given a parallel displacement. Thus we obtain in effect a graphical slide rule, the method of application and possibilities of which are illustrated by the following example:

Point IV corresponds to the values $M_{\text{casting}} = 0.245$; $V_{\text{casting}} = 7.5$; $q = 500$. According to the q -value, this represents a medium-weight casting, for example a wheel rim. Of course, this casting can be fed with different types of feeder, i.e. unheated, or heated with exothermic sleeves of different wall thicknesses. The basic problem is to decide which type of feeder is the most economical under the conditions prevailing in a given foundry.

Fig. 395a is covered with Fig. 395b (plotted on transparent paper). If we move the family of curves along the scale, each curve cuts point IV in turn, and the internal diameter is read off for each case. For example, the exothermic feeder curve for $w = 0.25d$ cuts the point IV at a position corresponding to the internal diameter $d_i \approx 0.92$. Because $H = 1.5 \times d_i$, we also know the volume of metal inside the sleeve, and also the volume and weight of exothermic material. However, the height h of the residual metal in the sleeve is also shown on Fig. 395b; in the case under consideration this is $h = 0.77 \times d_i$ (see Table 48).

In this way it is possible to compare the costs of the residual, or added, metal with those of the exothermic material, by making use of the cost factor p (equation 159) and to express the exothermic costs as a proportion of the melting costs (Tables 49a and b). The minimum values correspond to the most economic case for the example in question.

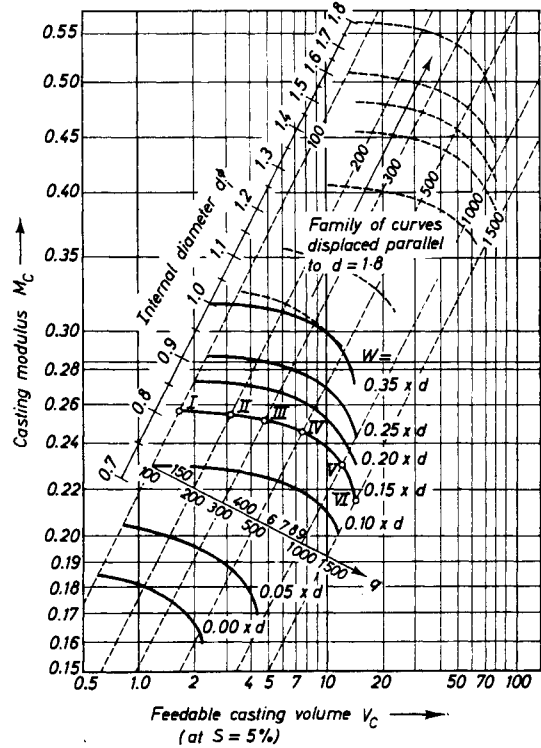


FIG. 395a. Characteristic of exothermic feeder heads $d = 1$, for different wall thicknesses.

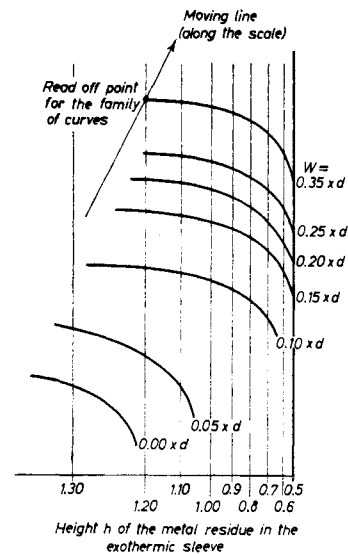


FIG. 395b. Template curve for parallel displacement.

TABLE 48. d_i internal diameter b_m height of the metal residue in the exothermic sleeve
 G_H weight of the exothermic material G_R weight of the metal cylinder residue in the exothermic sleeve

Point no.	Calculated for shrinkage $\mathcal{S} = 5\%$	The point value is obtained by the exothermic wall—thickness $w =$															
		$w = 0.00$ (unheated feeder)				$w = 0.05 \times d$				$w = 0.10 \times d$				$w = 0.15 \times d$			
		d_i^p	G_H	b_m	G_R	d_i^p	G_H	b_m	G_R	d_i^p	G_H	b_m	G_R	d_i^p	G_H	b_m	G_R
IV	500	1.49	0	1.26	25	1.30	0.7	1.21	15	1.10	0.88	1.06	7.7	1.0	1.05	93	5.5

Point no.	Calculated for shrinkage $\mathcal{S} = 5\%$	The point value is obtained by the exothermic wall—thickness $w =$											
		$w = 0.20 \times d$				$w = 0.25 \times d$				$w = 0.35 \times d$			
		d_i^p	G_H	b_m	G_R	d_i^p	G_H	b_m	G_R	d_i^p	G_H	b_m	G_R
IV	500	0.96	1.5	0.85	4.4	0.92	1.5	0.77	3.6	0.85	1.7	0.65	2.5

TABLE 49a. SUMMATION OF THE COSTS OF THE EXOTHERMIC SLEEVE (EXPRESSED AS A PROPORTION OF THE MELTING COSTS, ACCORDING TO COST FACTOR p) AND THE MELTING COSTS OF THE RESIDUAL METAL IN THE SLEEVE. THE MINIMUM VALUES (FRAMED) ARE THE MOST ECONOMICAL FOR THE GIVEN q -VALUES.

		q	1500	1000	500	300	200	100	q	1500	1000	500	300	200	100
$w = 0.15 \times d$	$P =$	G_H	1.05	1.05	1.05	1.05	1.05	1.05	$w = 0.20 \times d$	1.7	1.6	1.5	1.5	1.5	1.5
		G_R	3	3.8	5.5	6.3	7	7.7		3	3.2	4.4	5.2	5.8	6.8
	1	$G_H \times 1$	1.05	1.05	1.05	1.05	1.05	1.05	4	1.7	1.6	1.5	1.5	1.5	1.5
		Σ	4.05	4.85	6.55	7.35	8.05	8.75		4.7	4.8	5.9	6.7	7.3	8.3
	4	$G_H \times 4$	4.2	4.2	4.2	4.2	4.2	4.2	6	6.8	6.4	6.0	6.0	6.0	6.0
		Σ	7.2	8.0	9.7	10.5	11.2	11.9		9.8	9.6	10.4	11.2	11.8	12.8
	6	$G_H \times 6$	6.3	6.3	6.3	6.3	6.3	6.3	8	10.2	9.6	9.0	9.0	9.0	2.0
		Σ	9.3	10.1	11.8	12.6	13.3	14.0		13.2	12.8	13.4	14.2	14.8	15.8
	8	$G_H \times 8$	8.4	8.4	8.4	8.4	8.4	8.4	10	13.6	12.8	12.0	12.0	12.0	12.0
		Σ	11.4	12.2	13.9	14.7	15.4	16.1		16.6	16.0	16.4	17.2	17.8	18.8
10	$G_H \times 10$	10.5	10.5	10.5	10.5	10.5	10.5		17.0	16.0	15.0	15.0	15.0	15.0	
	Σ	13.5	19.3	16.0	16.8	17.5	18.2		20.0	19.2	19.4	20.2	20.8	21.8	
$w = 0.25 \times d$	$P =$	G_H	1.9	1.6	1.5	1.4	1.4	1.4	$w = 0.35 \times d$	2.8	2.5	1.7	1.6	1.5	1.5
		G_R	3	2.6	3.6	4.3	4.8	5.5		3	2.6	2.5	2.8	3.2	3.8
	1	$G_H \times 1$	1.9	1.6	1.5	1.4	1.4	1.4	4	2.8	2.5	1.7	1.6	1.5	1.5
		Σ	4.9	4.2	5.1	5.7	6.2	6.9		5.8	5.1	4.2	4.4	4.7	5.3
	4	$G_H \times 4$	7.6	6.4	6.0	5.6	5.6	5.6	6	11.2	10.0	6.8	6.4	6.0	6.0
		Σ	10.6	9.0	9.6	9.9	10.4	11.1		14.2	12.6	9.3	9.2	9.2	9.8
	6	$G_H \times 6$	11.4	9.6	9.0	8.4	8.4	8.4	8	16.8	15.0	10.2	9.6	9.0	9.0
		Σ	14.4	12.2	12.6	12.7	13.2	13.9		19.8	17.6	12.7	12.4	12.0	12.8
	8	$G_H \times 8$	15.2	12.8	12.0	11.2	11.2	11.2	10	22.4	20.0	13.6	12.8	12.0	12.0
		Σ	18.2	15.4	15.6	15.5	16.0	16.7		25.4	22.6	16.1	15.6	15.2	15.8
10	$G_H \times 10$	19.0	16.0	15.0	14.0	14.0	14.0		28.0	25.0	17.0	16.0	15.0	15.0	
	Σ	21.0	18.6	18.6	18.3	18.8	19.5		31.0	27.6	19.5	18.8	18.2	18.8	

TABLE 49b.
COSTS OF EXOTHERMIC SLEEVE PLUS COSTS OF RESIDUAL METAL IN THE FEEDER HEAD (CLASSIFIED ACCORDING TO COST FACTOR p).

☐ MINIMUM VALUES

$0.35 \times d$	$0.25 \times d$	$0.20 \times d$	$0.15 \times d$	$0.10 \times d$	$0.05 \times d$	0.00 unheated feeder head	exothermic sleeve wall thickness ω	
☐ 5.3	6.9	8.3	8.75	12.94	16.61	21	$q = 100$	cost factor $p = 1$
☐ 4.7	6.2	7.3	8.05	10.9	16.63	21	200	
☐ 4.4	5.7	6.7	7.35	10.9	16.66	21	300	
☐ 4.2	5.1	5.9	6.55	8.58	15.7	25	500	
5.1	☐ 4.2	4.8	4.85	6.85	17.81	37	1000	
5.8	4.9	4.7	☐ 4.05	5.3	19.95	45	1500	
☐ 9.8	11.1	12.8	11.9	15.75	18.43	21	$q = 100$	$p = 4$
☐ 9.2	10.4	11.8	11.2	13.6	18.52	21	200	
☐ 9.2	9.9	11.2	10.5	12.7	18.64	21	300	
☐ 9.3	9.6	10.4	9.7	11.12	17.8	25	500	
12.6	9.0	9.6	☐ 8.0	9.4	20.22	37	1000	
14.2	10.6	9.8	☐ 7.2	7.7	22.8	45	1500	
☐ 12.8	13.9	15.8	14.0	17.65	19.65	21	$q = 100$	$p = 6$
☐ 12.0	13.2	14.8	13.3	15.4	19.72	21	200	
☐ 12.4	12.7	14.2	12.6	14.5	19.95	21	300	
12.7	12.6	13.4	☐ 11.8	12.95	19.2	25	500	
17.6	12.2	12.8	☐ 10.1	11.1	21.85	37	1000	
19.8	14.4	13.2	☐ 9.3	9.3	24.7	45	1500	
☐ 15.8	16.7	18.8	16.1	19.5	20.88	21	$q = 100$	$p = 8$
☐ 15.2	16.0	17.8	15.4	17.2	21.05	21	200	
15.6	15.5	17.2	☐ 14.7	16.3	21.3	21	300	
16.1	15.6	16.4	☐ 13.9	14.75	20.6	25	500	
22.6	15.4	16.0	☐ 12.2	12.8	23.5	37	1000	
25.4	18.2	16.6	11.4	☐ 10.9	26.6	45	1500	
18.8	19.5	21.8	☐ 18.2	21.4	22.1	21	$q = 100$	$p = 10$
18.2	18.8	20.8	☐ 17.5	19.0	22.3	21	200	
18.8	18.3	20.2	☐ 16.8	18.1	22.6	21	300	
19.5	18.6	19.4	☐ 16.0	16.5	32.0	25	500	
27.6	18.6	19.2	☐ 14.3	14.5	25.1	37	1000	
31.0	21.0	20.0	13.5	☐ 12.5	28.5	45	1500	

12.6.3. THE RAPID DETERMINATION OF THE MOST ECONOMICAL SLEEVE WALL THICKNESS

IMPORTANT FOR PRACTICE

The most economic wall thickness was calculated for various cases in the previous section by making use of the characteristic of the exothermic feeder head. The results are shown in Fig. 396, which should always be consulted when introducing exothermic feeder heads.

EXAMPLE I

Cost factor $p = 3$ (i.e. the exothermic material costs about three times as much as the costs of melting 1 kg of steel. This ratio refers mainly to medium or high alloy steels). The shrinkage S is also large for these steels, in this case $S = 7.5$ per cent. This steel will be used mainly for fittings, highly-stressed gear wheels, etc. Follow the arrow *I*, and read off at $p = 3$ an economic wall thickness of $w = 0.18 \times d$.

EXAMPLE III

Unalloyed, very cheap steel (an exceptional case), with $S = 5.5$ per cent and $p = 9$. This will be used mainly for thin-walled housings (considered geometrically these are thin plates). Follow the arrow *III* and read off an economic wall thickness of $w = 0.11 \times d$.

The following surprising fact emerges: The wall thickness zero, corresponding to a non-exothermic feeder head, is never reached, so that *even with a very low-priced steel exothermic feeder heads are still an economic proposition*. This is a very important result, because Fig. 387 was drawn in accordance with a very rigorous and objective principle.

As a general rule it can be stated that:

The cheaper the exothermic material is compared with the steel melting costs, the thicker the sleeve wall should be made. Or in other words: The higher

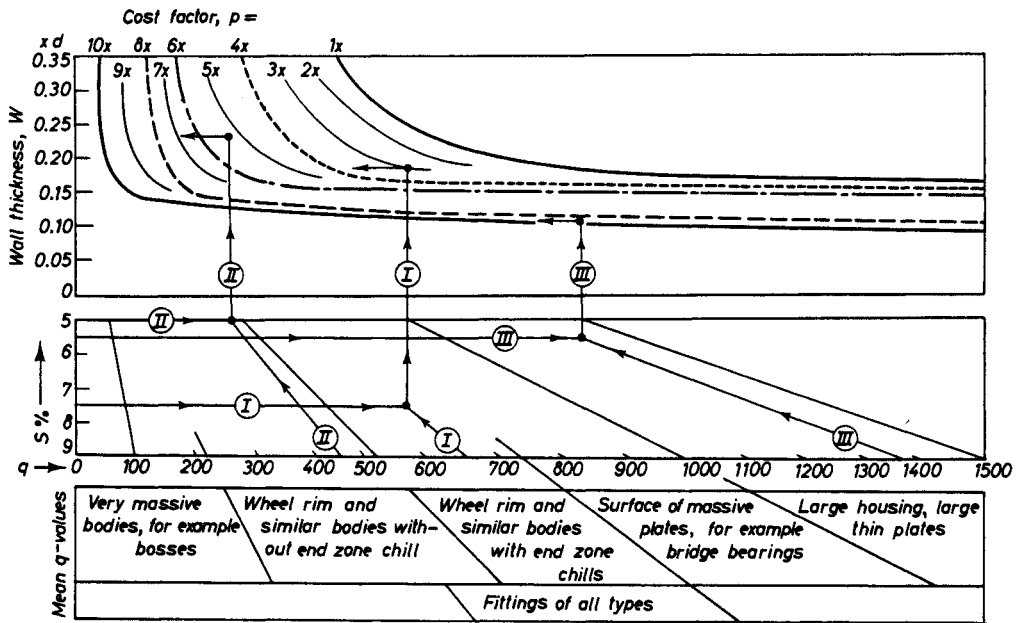


FIG. 396. Diagram for the rapid determination of the most economical thicknesses of exothermic sleeve (three examples, *I*, *II* and *III* are plotted).

EXAMPLE II

This refers to low-alloy or plain carbon steel, with a cost factor $p = 5.5$. The shrinkage in this case is only $S = 5$ per cent. Fittings or similar castings will also be cast, but these will be more massive than in Example I. Follow the arrow *II* and read off at $p = 5.5$ an economic wall thickness of $w = 0.23 \times d$. It can be recognized clearly that when the cost factor p is only slightly less (i.e. when the exothermic material is only slightly cheaper, or the steel melting costs are only a little higher) the economic wall thickness would immediately become greater, and would in fact increase considerably.

the melting costs of the steel (costs of alloying additions, high electric current costs, high wages) the thicker the insert should be.

Furthermore:

The more massive the average castings, the thicker the sleeve wall should be. Conversely the thinner and more platelike the casting, the thinner the wall.

For series production it will not always pay to make up special inserts as in Fig. 396. For the remaining castings, which usually constitute the great majority, a compromise must be reached for the sake of sleeve

standardization. As a rule wall thicknesses of $w = 0.20 \times d$ to $0.30 \times d$ are indicated for the usual steel castings: these values were also obtained on the basis of the characteristics shown in Figs. 354-362.

12.7. The Use of Exothermic Antipiping Powder

12.7.1. THE TESTING OF EXOTHERMIC ANTIPILING POWDERS. THE STRUCTURE OF THE SHRINKAGE CAVITY IN COVERED FEEDER HEADS

IMPORTANT FOR PRACTICE

Here again, as in Section 12.2.1, the cumulative action of thermal and insulating properties is decisive in determining the effectiveness of these powders. Testing by measuring the properties of individual components again does not lead to the desired result, so that an effective assessment is possible only by measuring the increase in the solidification time of a test body.

A cylinder $d = 200$, $H = 100$ mm, cast in a cored mould, is used as the test body (Fig. 397). An overflow

guarantees that the height of 100 mm will be maintained. The cylinder base is formed from an exothermic plate made from (tested) mouldable exothermic material. Hence no cooling takes place on the base surface during a long period—as in an actual casting, where the feeder head/casting interface also represents a non-cooling surface.

As a basis for comparison the steel cylinder is covered only with dry sand. Corresponding experiments showed that a depth of sand of 40-50 mm gives the best properties. If more sand is spread on the surface the solidification time again becomes (somewhat) shorter.

This test method is more accurate than testing feeder heads on actual castings. With feeder heads the amount of steel never remains constant as metal is drawn out from the head by the casting during the solidification process.

With high-grade exothermic powders the shrinkage cavity has a favourable structure, similar to that produced in exothermic feeder heads; the metal surface is approximately horizontal.

Characteristics can be plotted in the same way as with exothermic sleeves (Figs. 398-400). Table 50 fulfils the same purpose, but is less flexible for intermediate sizes.

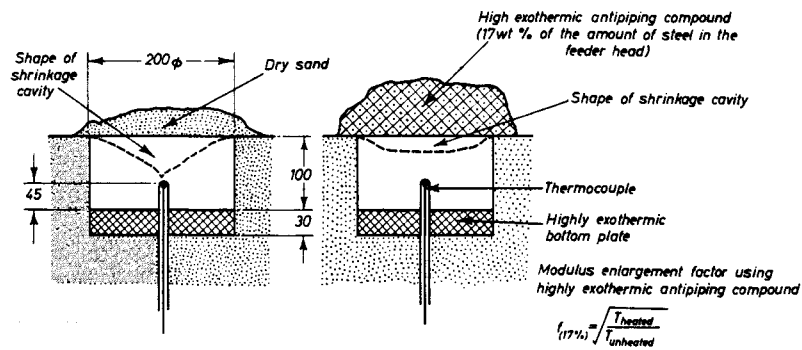
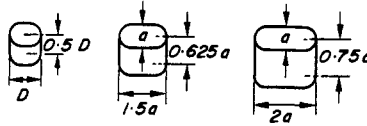


FIG. 397. Arrangement for determining the attainable increase in solidification time, using antipiping powder under industrial conditions.

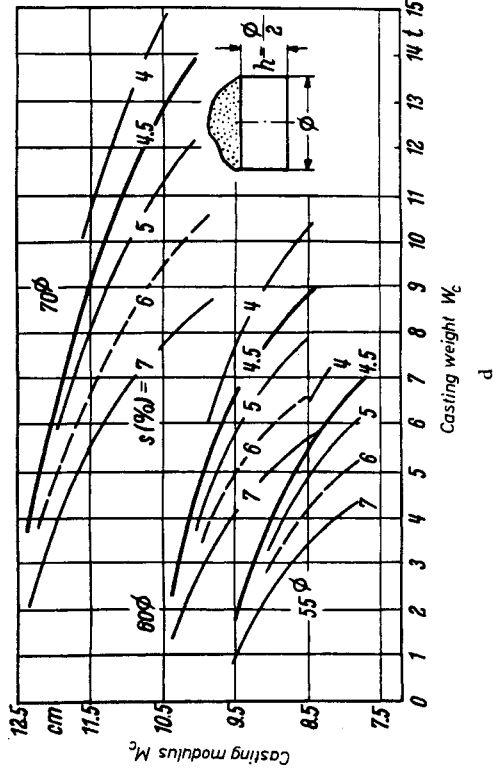
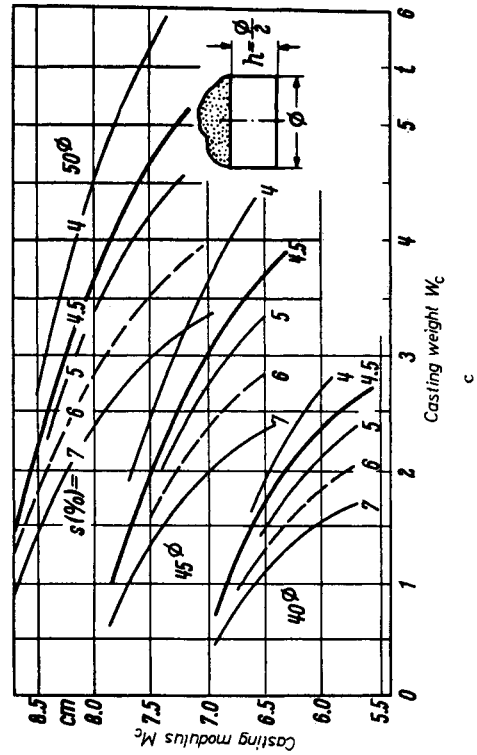
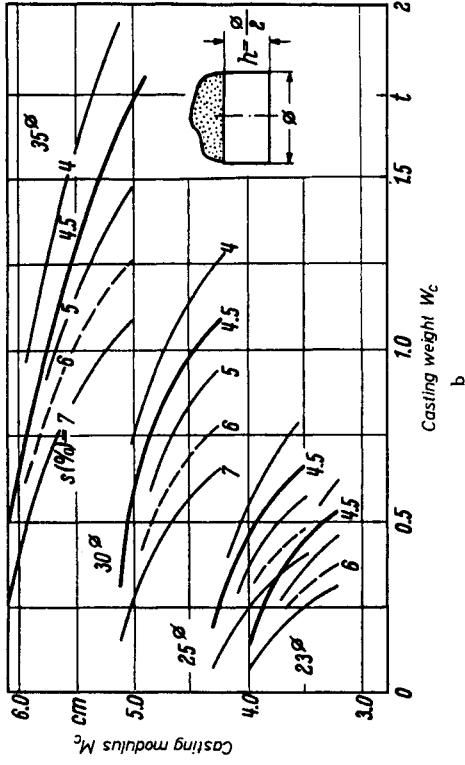
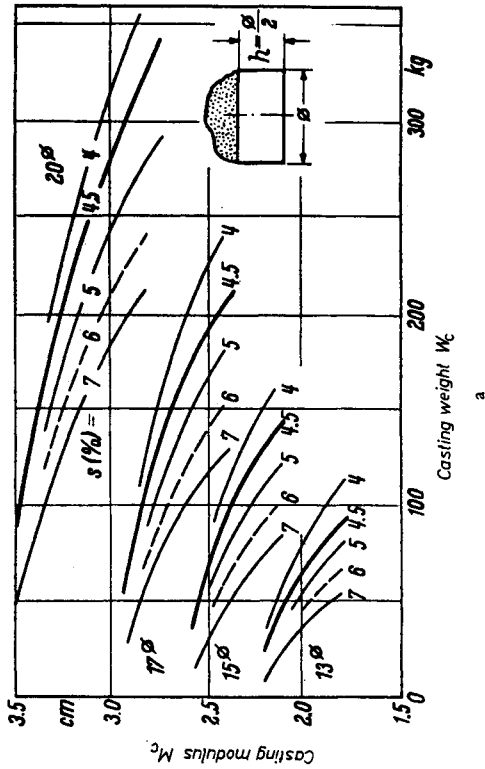
TABLE 50. EXOTHERMIC FEEDER HEAD WITH THE ADDITION OF ANTIPING POWDERS. SHRINKAGE $S = 4.5\%$ 

Feeder head					Exothermic material		Shape modulus and weight of the casting (feeding area)					
Dimensions			Volume, weight		Amount † kg	Waiting †† time min	Massive, such as cubes, massive cylinder		Bars, plates only with feeding zone		Plates with feeder head + end zone combined with casting	
$D\phi$ a cm	b cm	H cm	V Lit.	W † kg m. ton			M_c cm	G kg m. ton	M_c cm	G kg m. ton	M_c cm	G kg m. ton
13	ϕ	7	0.9	5.5	1.2	3	2.2	23	2.0	64	1.8	92
13	19.5	8	1.8	11	2.5	4	2.8	49	2.5	130	2.2	190
13	26	10	3.0	18	4.2	6	3.2	82	2.9	220	2.6	320
15	ϕ	8	1.35	8.2	1.5	5	2.6	36	2.4	100	2.1	142
15	22.5	9.5	2.8	17	3.5	9	3.2	76	2.9	200	2.6	296
15	30	11	4.7	29	5.0	12	3.6	125	3.3	350	3.0	500
17	ϕ	9	2.0	12	2.5	8	2.9	54	2.7	150	2.4	212
17	25.5	11	4.0	27	4.5	12	3.6	110	3.3	300	2.9	425
17	34	13	6.7	40	7.0	15	4.2	180	3.8	490	3.4	710
20	ϕ	10	3.2	19	3.8	12	3.5	86	3.2	230	2.8	340
20	30	12.5	6.4	38	7.0	15	4.3	174	3.9	470	3.5	680
20	40	15	11	66	12	19	4.9	300	4.5	820	4.0	1.1
23	ϕ	11	4.9	30	5.5	14	4.0	135	3.7	360	3.2	520
23	34.5	14	10	60	10	18	4.8	270	4.4	740	4.0	1.0
23	46	17	17	100	18	22	5.3	460	5.1	1.2	4.6	1.8
25	ϕ	12	6.2	37	7.0	16	4.3	167	4.0	460	3.5	660
25	37.5	15	13	78	14	20	5.3	350	4.8	1.0	4.3	1.4
25	50	19	21	130	23	24	6.1	570	5.5	1.5	5.0	2.2
30	ϕ	15	11	66	12	20	5.1	300	4.8	820	4.2	1.1
30	45	19	22	132	23	23	6.4	600	5.4	1.6	5.1	2.3
30	60	22	36	220	38	25	7.3	970	5.6	2.7	6.0	3.8
35	ϕ	17	17	100	18	25	6.1	460	5.6	1.2	4.9	1.8
35	52.5	22	35	210	37	32	7.5	950	6.8	2.6	6.1	3.7
35	70	26	58	350	61	38	8.5	1.6	7.8	4.3	7.0	6.1
40	ϕ	20	26	156	28	29	6.9	700	6.4	1.9	5.6	2.7
40	60	25	52	320	56	38	8.5	1.4	7.7	3.8	6.9	5.5
40	80	30	86	520	90	48	9.8	2.3	8.9	6.4	8.0	9.1
45	ϕ	27	37	220	39	35	7.8	1.0	7.2	2.7	6.3	3.9
45	67.5	28	75	450	80	45	9.6	2.1	8.7	5.6	7.8	8.0
45	90	33	125	750	130	55	11.1	3.4	10.0	9.3	9.0	14.3
50	ϕ	25	50	300	53	40	8.7	1.4	8.0	3.7	7.0	5.3
50	75	31	100	600	110	52	10.6	2.7	9.7	7.4	8.7	10.6
50	100	37	167	1.0	180	65	12.0	4.5	11.2	12.3	10.0	17.7
55	ϕ	27	66	400	70	45	9.5	1.8	8.7	4.9	7.7	7.0
55	82.5	34	134	800	140	58	11.6	3.6	10.6	10	9.5	14.2
55	110	41	225	1.4	250	70	13.5	6.0	12.2	16.5	11.0	23.9
60	ϕ	30	85	520	90	55	10.4	2.3	9.6	6.3	8.4	9.0
60	90	37	174	1.1	190	66	12.7	4.7	11.6	12.9	10.4	18.5
60	120	45	290	1.7	300	75	14.6	7.8	13.4	21.5	12.0	30.5
70	ϕ	35	135	0.8	140	65	12.2	3.7	11.3	10	9.8	14.3
70	105	43	275	1.7	300	75	14.8	7.5	13.5	20.5	12.2	29.0
70	140	52	460	2.8	490	85	17.0	12.5	15.6	34	14.0	48.8

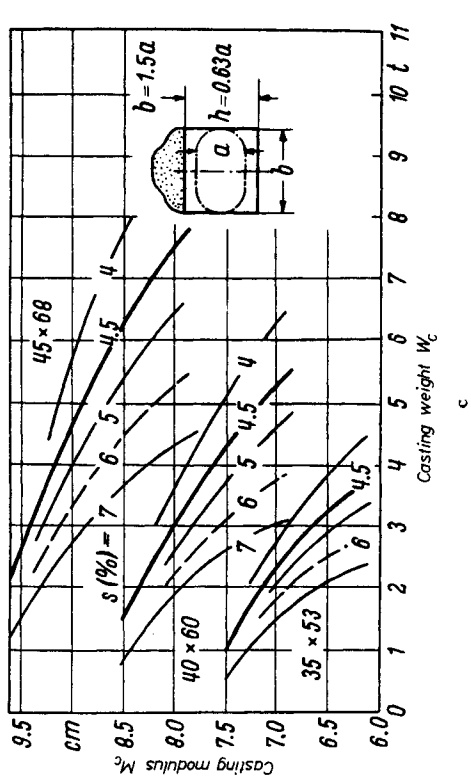
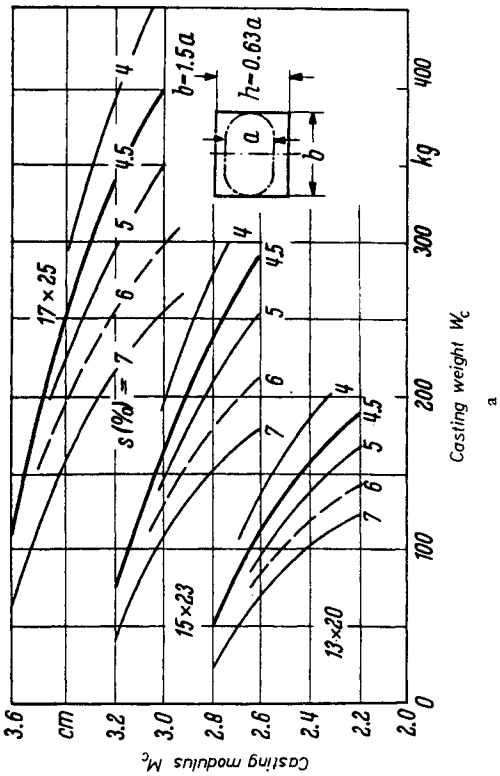
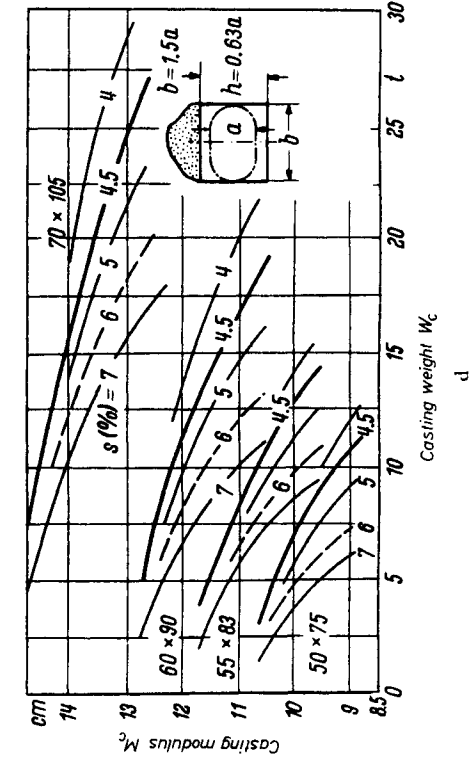
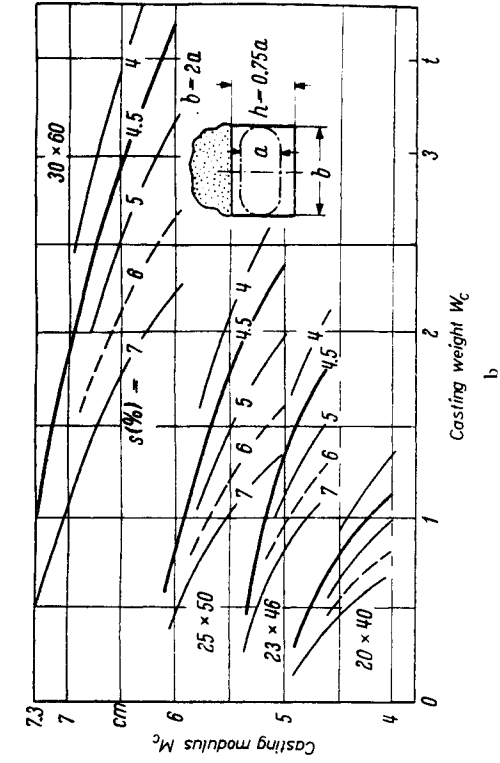
† Allowing for the shrinkage cavity, $\gamma \approx 6.0$.

‡ Mean value; can be reduced somewhat with very good exothermic materials.

†† Increase by up to about 20% for hot melts; reduce by up to the same amount with cold melts. In the case of large feeder heads the progress of solidification should be checked once more with an iron rod before adding the antipiping powder.



Figs. 398a-d. Characteristic of round exothermic feeder head using exothermic antipiping powders.



FIGS. 399a-d. Characteristic of oval exothermic feeder head using exothermic antipiping powders.

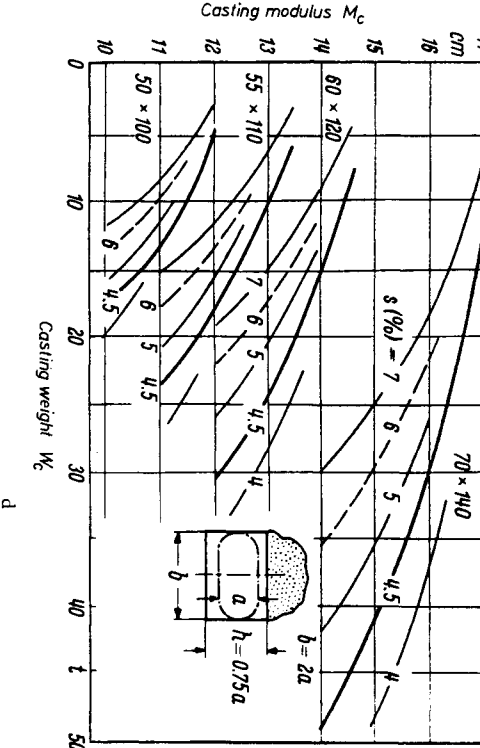
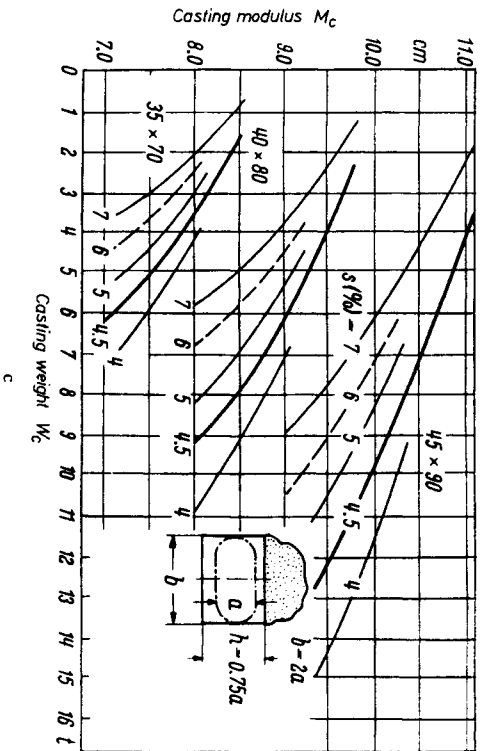
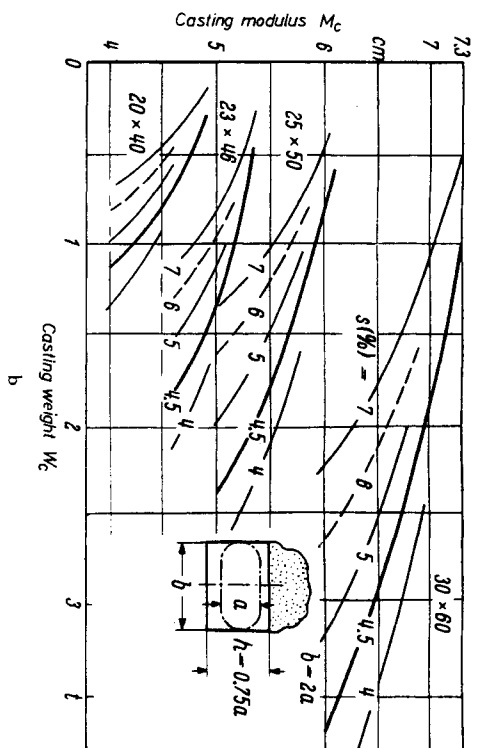
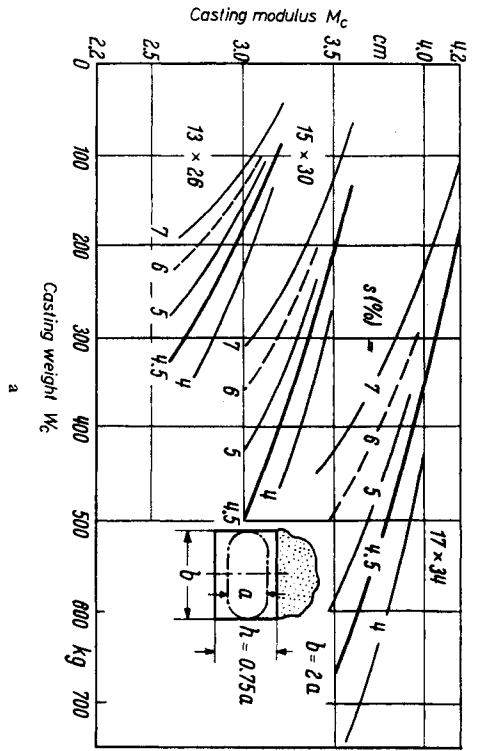


Fig. 400-a-d. Characteristic of oval exothermic feeder head using exothermic antipiping powders.

12.7.2. ON THE USE OF ANTIPIPING POWDERS. COMPARISON WITH EXOTHERMIC FEEDER HEADS

IMPORTANT FOR PRACTICE

The amounts of highly exothermic powder to be added can be derived from Fig. 401. In this diagram the values are plotted on the basis of results of the cylinder test mentioned above, and from data provided by a manufacturing firm.

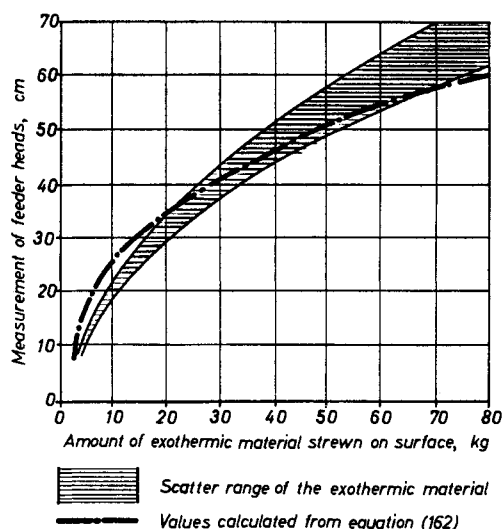


FIG. 401. Amount of loose highly exothermic anti-piping powder added as a function of the diameter of the feeder head.

The total amount of exothermic material is the same whether using exothermic sleeves or non-exothermic heads with anti-piping powder. However, the author's experience with actual operating conditions indicates that the exothermic feeder head enables much more accurate working to be achieved. Using elongated feeder head castings such as those shown in Fig. 83 (p. 31), Fig. 128 (p. 68) or Fig. 402 are often produced, and in addition expensive exothermic material is still thrown on to feeder heads which are very much too high.

It is therefore necessary to indicate the feeder head levels in the mould, for example, by marking with chalk or with nails (Fig. 403). The marking must be done in such a way that the casting ladle does not conceal the marking when suspended above the mould. Marking must of course be properly organized in the shop so that the current levels are always clearly visible, and the most suitable amount of powder, neither too much or too little, is always added to every mould, however many there are.

The methods of using anti-piping powders and exothermic sleeves are roughly equivalent in cost, provided that they are operated correctly. However, the numerous rejects obtained when anti-piping powder is used,

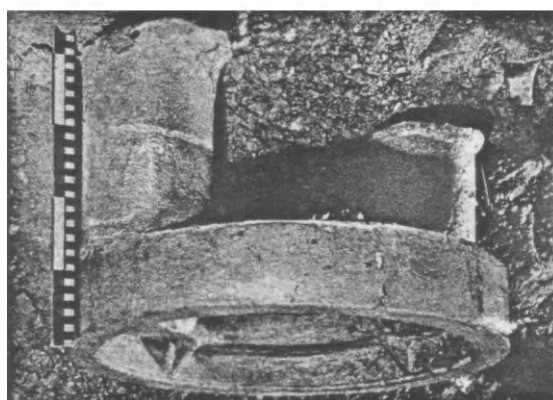


FIG. 402. Waste of steel due to the feeder head being filled too high.



FIG. 403. Remedy—easily visible marks on the feeder head.

which can only be established in actual production reduce its economic efficiency considerably; in many cases very significant losses are obtained, as far as this can be checked objectively.

For these reasons the author uses exothermic sleeves for exothermic feeder heads of up to 500 mm internal diameter, and uses antipiping powder only for larger diameters. When the powder method is used the following procedure is adopted:

1. Pour up to the mark.
2. Cover immediately with the exothermic material.
3. Top up after one to five hours, according to the modulus. This is done by carefully removing the exothermic powder from the first addition, then topping up, and finally adding the necessary amount of antipiping powder.

Obviously careful supervision such as we have described is quite possible with large individual castings, but unsuitable with long runs of small and medium castings.

Many firms recommend a waiting period before adding the powder. This waiting time leads to a desirable increase in the time of solidification of the metal in the feeder head, because the superheat of the steel is first conducted away. The hotter the steel on pouring, the longer this waiting time can be. Relevant data are given in Table 50 and Fig. 404. The most favourable time is

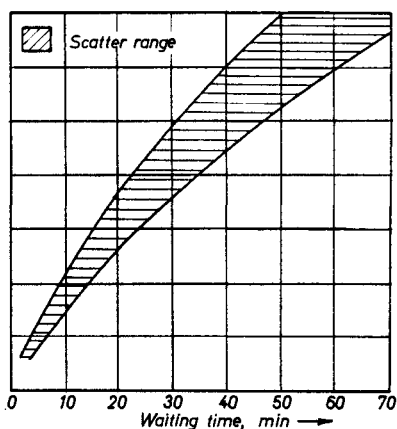


FIG. 404. Waiting times with highly-exothermic antipiping powders.

determined by means of an iron bar, with which the fluidity of the steel is tested at regular intervals. As soon as the metal shows signs of becoming viscous the powder is added.

It is recommended that the powder should be weighed beforehand into bags, and the weight marked on each bag. In this way gross errors are prevented, and waste is avoided.

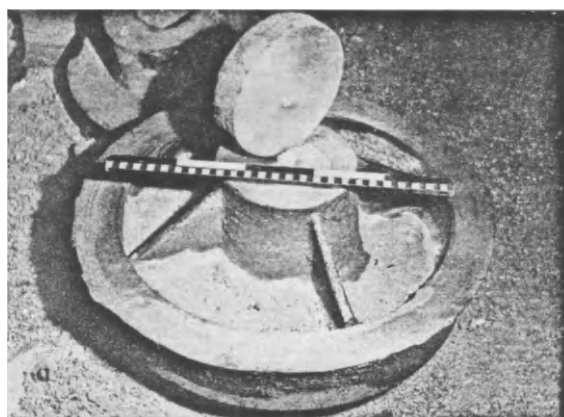
12.7.3. EXAMPLES OF THE USE OF EXOTHERMIC POWDERS

IMPORTANT FOR PRACTICE

One advantage of exothermic powder is that feeder heads supplying the same casting can be kept to the same height, as shown in Fig. 405. A similar result can be



a



b

FIGS 405 a and b. Wheel with the boss feeder head kept low by the use of exothermic antipiping powders.

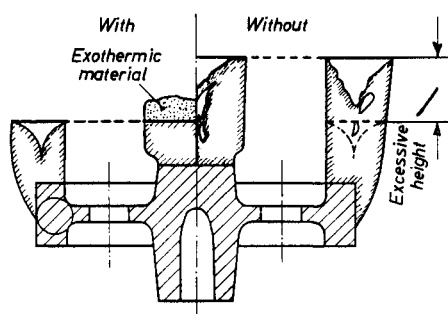


FIG. 405 c. The shape of the boss forces the use of too high a feeder head on the rim, unless exothermic material is used.

obtained, however, by using shorter, squat type exothermic rings (characteristic Fig. 358).

Figures 406-410 illustrate some further examples, some of which provide an economic comparison with non-exothermic feeder heads (Table 51).

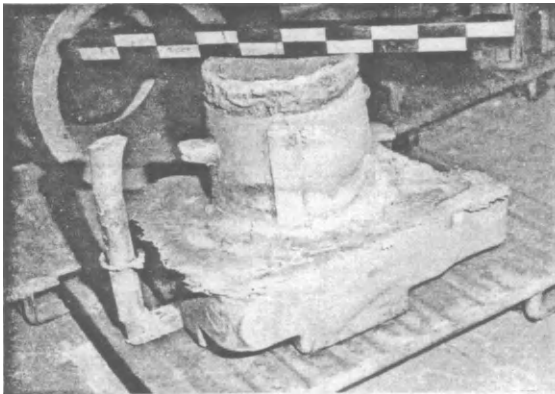


a



b

FIGS. 406a and b. Trunnion plate of a casting ladle.
a. without and b. with exothermic feeder heads.



a

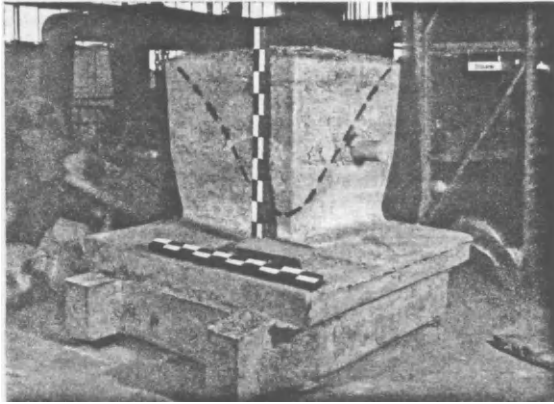


b

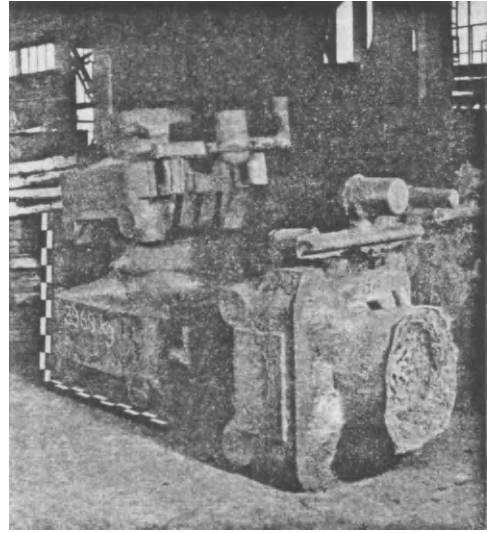


c

FIGS. 407a-c. Shield plates, with and without exothermic feeder head.



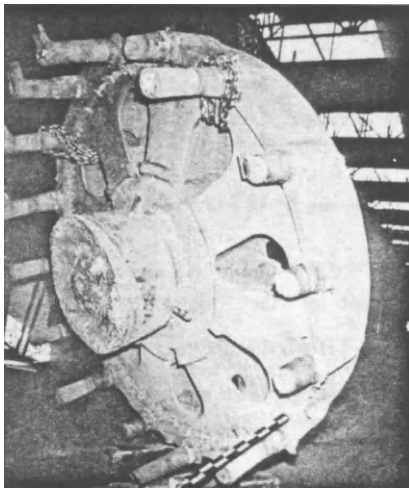
a



b

FIGS. 408a and b. Squeezer plates for diecasting machines. (a) large plate, moulded conventionally. Gross yield 43%. (b) small plates, fed with exothermic feeder heads. Gross yield 68%.

(Courtesy Sulzer Bros.)



a

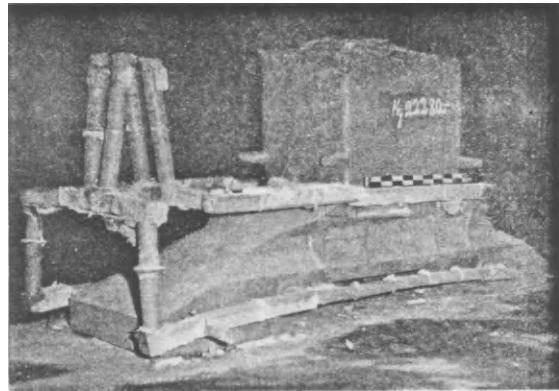
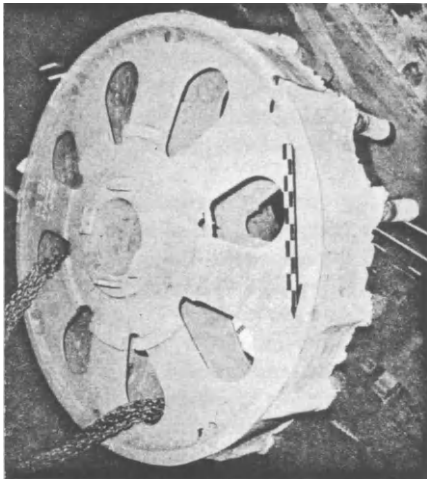


FIG. 410a.



b

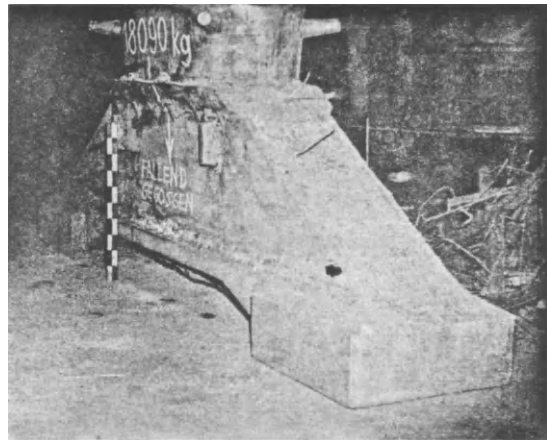


FIG. 410b.

FIGS. 409a and b. Large wheel castings. Rim fed by exothermic feeder heads. Boss feeder head treated with exothermic antipiping powder.

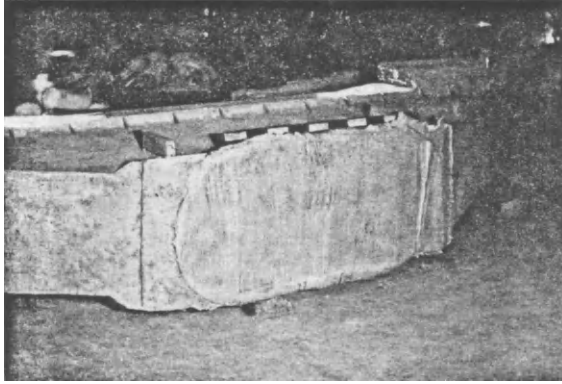


FIG. 410c.

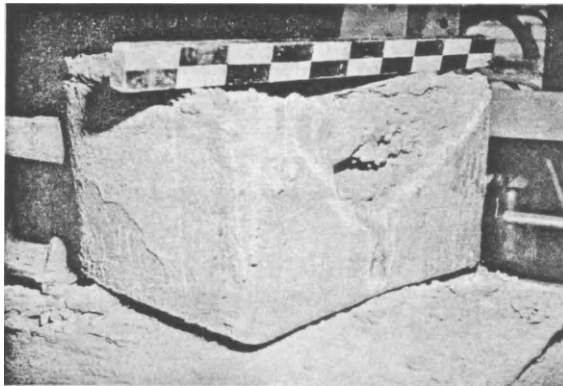


FIG. 410d.

Figs. 410a-c. Heavy bridge bearing.

(a) This bridge bearing was cast conventionally. (b) and (c) This casting was fed by an exothermic feeder head.

For economic comparison see Table 51.

(Courtesy Sulzer Bros.)

TABLE 51. ECONOMIC COMPARISON OF METHODS OF CASTING THE BRIDGE BEARING SHOWN IN FIGS. 410a AND b

Bearing according to Fig. 410a
 Conventional, modern method of casting.
 Despatched weight (weighed) kg.
 As-cast weight (weighed) kg.
 Yield of liquid steel, %.
 Antipiping powder added (weighed) kg.
 If the bearing of Fig. 410a had also been cast by the modern method.
 If the bearing of Fig. 410b had been cast by the old, conventional method.
 (50 kg, 50 kg topped up).
 (50 kg, 300 kg topped up).
 ~250 kg more powder would have been used.
 ~6720 kg steel would have been saved (at 81.6% yield).
 ~250 kg less powder would have been used.
 ~7810 kg more steel would have been used (at 57% yield).
 It is recommended that the costs for exothermic powder and the steel melting costs should be included in the above economic comparison for each concern.

12.8. Heat Theory and the Calculation of Exothermic Materials

(From the practical standpoint it is not necessary to study this section.)

12.8.1. THE VALIDITY OF CALCULATION FORMULAE PUBLISHED UP TO THE PRESENT TIME

The solidification time of a casting is prolonged by the use of exothermic materials, that is, its modulus in the unheated state (M_0) is correspondingly increased to M_V .

According to Nicolas⁽¹⁰⁾ the weight of exothermic material can be calculated as follows:

$$W_{\text{exothermic material}} = V_0 \frac{\gamma \times L}{H_u} \times \frac{M_V - M_0}{M_0} \quad (160)$$

where H_u is the useful heat of the exothermic material in cal/kg of material, γ is the specific gravity of the steel (7.8) and L is the latent heat of fusion of the steel (63 cal/kg).

The expression $M_V - M_0/M_0$ was derived in the same way as in equations 95 and 96 (p. 123). In that case the starting point was an apparently reduced volume V_r , while here we start with an apparently increased volume V_v .

The same formula, expressed in a different style, is based on arguments developed by Thierry⁽⁴⁹⁾:

$$W_{\text{ex. mat.}} = (V_v - V_0) \times \frac{\gamma \times L}{H_u} \quad (161a)$$

in which $V_v = V_0 \times \frac{M_V}{M_0}$.

The concept of the "useful" amount of heat $W \left(\frac{\text{cal}}{\text{kg ex. mat.}} \right)$ is of the greatest importance in equations (160) and (161). With many exothermic materials this figure is a nominal 2000 cal/kg. According to data published by Trommer⁽³⁸⁾ a value of 1700 cal/kg should be used to ensure success. According to Thierry⁽⁴⁹⁾, on the other hand, only 600 down to 420 cal/kg should be assumed.

The author was able to check the accuracy of these figures by means of a very large number of sphere tests (see section 12.2.1, Figs. 337 and 338) using exothermic materials from various sources, and was thus able to make a basic appraisal of the physical validity of equations 160 and 161.

Figure 411 reproduced the geometrical relationships in one of these tests, while the solidification times are worked out in the associated Table 52 in accordance with equations (160) and (161) respectively for the values $w = 1700$ cal/kg and 600 cal/kg.

According to equation (160) (Nicolas), it appears that the sphere must remain liquid 96 (!) times longer, due to the heating effect of exothermic materials, than an unheated sphere. Equation (161) (Thierry) indicates that the sphere would remain liquid 17 (!) times longer.

In the sphere test the exothermic material is applied to the same thickness ($1/5 d_{\text{int}}$) as is found in many exothermic sleeves. These results are therefore of great practical importance. Measurements by American in-

investigators⁽²⁾ and the numerous measurements made by the author (see also Fig. 339a) indicate that the solidification time of a sphere in exothermic material is actually twice, or occasionally $2\frac{1}{2}$ times the time taken for a sphere of the same size to solidify in non-exothermic material.

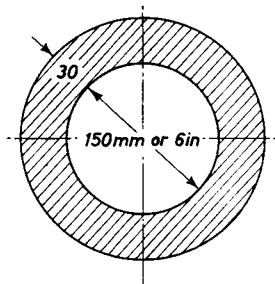


FIG. 411. Geometrical relationships in the sphere test with exothermic materials (see Figs. 337 and 338).

Geometrical modulus of the (non-exothermic) steel sphere 150 \varnothing
 $M_0 = d/6 = 2.5$ cm.

Geometrical volume of the steel sphere 150 \varnothing $V_{geom.} = 1.76$ dm³.

Effective volume of the steel sphere 150 \varnothing (reduced by 5% liquid contraction) $V_{effect.} = V_0 \approx 1.67$ dm³.

Volume of the exothermic material:

outer sphere (210 \varnothing) 9.25 dm³ \times 0.524 minus inner sphere (150 \varnothing)

3.36 dm³ \times $0.524 = 3.08$ dm³ = volume of hollow exothermic sphere.

Specific gravity of moulded exothermic material (mean value from a large number of products, but fluctuations are very small):

$\gamma_{ex. material} \approx 1.4$ kg/dm³

and weight of the above hollow sphere = $1.4 \times 3.08 \approx 4.3$ kg.

TABLE 52 (for Fig. 411). CALCULATION OF THE THEORETICAL SOLIDIFICATION TIMES OF A SPHERE CAST IN EXOTHERMIC MATERIAL, BASED ON THE DATA GIVEN BY 1. NICOLAS⁽¹⁰⁾ AND 2. THIERRY⁽⁴⁹⁾

$$1. W = \frac{V_0 \times \gamma \times L}{T} \times M_I - M_0; \quad M_0 = 2.5 \text{ cm}$$

$$M_0^3 = 6.25 \text{ cm}^3$$

$$4.3 = 1.67 \cdot \frac{7 \times 8 \times 63}{1700} \frac{M_I - 2.5}{2.5}$$

Hence the modulus increased by the action of the exothermic material is

$$M_I = 24.75 \text{ cm, and } M_I^3 = 600.19 \text{ cm}^3.$$

The solidification times vary as the square of the modulus, so that

$$\frac{t_{heated}}{t_{unheated}} = \frac{600.19}{6.25} = 96,$$

i.e. the heated sphere must remain liquid 96 times longer than the unheated one.

$$2. W = V_I - V_0 \frac{7.8 \cdot 6.3}{600}, \quad \text{whence } V_I = 6.93 \text{ dm}^3.$$

$$V_I = V_0 \frac{M_I}{M_0}; \quad M_0 = 2.5, \text{ so that}$$

$$M_I = 10.4 \text{ cm; } M_I^3 = 107 \text{ cm}^3.$$

The ratio of solidification times is thus:

$$\frac{t_{heated}}{t_{unheated}} = \frac{107}{6.25} = 17,$$

i.e. the heated sphere must remain liquid 17 times longer than the unheated one.

The difference between the theoretical and actual results is so considerable that either:

1. the amount of useful heat H_u is much less than is assumed (1700 or 600 cal/kg), i.e. the thermal efficiency of the exothermic materials is very low, and amounts at best to 2-5 per cent, or

2. the physical assumptions on which equations (160) and (161) are based are false. Both equations start off from the—apparently correct—assumption that a large proportion of the heat of the exothermic material is transferred to the liquid steel, thereby retarding its solidification.

To clear up these points the author carried out the following experiment repeatedly: a thermocouple was inserted in the exothermic sleeve, the sleeve ignited with a welding torch, and the actual combustion temperature measured. After overcoming some initial technical difficulties it was found that the combustion temperature in commercial exothermic materials was about 1400°C, in some cases rising to 1500°C, and only reaching 1600°C in a single special product of his own manufacture.

Provided that the steel is cast at a true temperature between 1520 and 1650°C, and that the heat can be transferred only from the hotter to the cooler body, this signifies that no heat, or only a very little in some rare cases, can pass from the exothermic sleeve to the steel.

This was also confirmed by the fact that an increase in temperature of the liquid steel above the casting temperature was hardly ever observed in the numerous sphere tests; the temperature increased by 3-5°C in only two cases. These results also indicate that the physical assumptions on which equations (160) and (161) are based are not correct, and that other factors must be effective in the casting of steel.

To allow for errors in application the author made the following additional experiment: an exothermic sphere was ignited with the welding torch, allowed to burn for about two minutes, and filled with steel after a waiting time of 7 minutes. No significant shortening was found in the solidification time compared with the above-mentioned value of 2-2.5.

In logical agreement with these experimental results it has been shown conclusively that heat is transferred from the exothermic material to metals having a lower melting point than steel. With grey cast iron, ductile iron and aluminium bronze the temperature increase of the metal in the experimental sphere usually amounts to about 50°C, and occasionally approaches 100°C, according to the casting temperature. An increase of up to 150°C is observed with light metals.

It should be pointed out, however, that this rise in temperature could be undesirable, and has led in practice to the development of special exothermic materials in which the combustion temperature is lower and the heat transfer is correspondingly less.

In grey cast iron the graphite is sometimes coarsened significantly by the temperature increase. In ductile iron the spheroidal graphite degenerates to a lamellar structure. In the case of aluminium bronze and light metals the metal becomes considerably enriched in gases due

to the superheating of the melt, if large amounts of gas are present. In consequence the metal near the feeder head deteriorates in quality or becomes porous if the above-mentioned special products are not used. The author does in fact use the same exothermic sleeve both for aluminium bronze and cast steel, but he ignites the sleeve for 15–25 min (according to size) before using it for the non-ferrous alloy. In spite of this the solidification time increases by a factor of about 2.5.

12.8.2. TRUE PHYSICAL CAUSES OF THE EXTENDED SOLIDIFICATION TIME

The heat balance of exothermic materials can be estimated from Fig. 412. The amount of heat actually used to heat up the exothermic material itself to $\sim 1500^{\circ}\text{C}$ can be determined fairly accurately, and amounts to about 360 cal/kg. The remaining sources of heat loss were

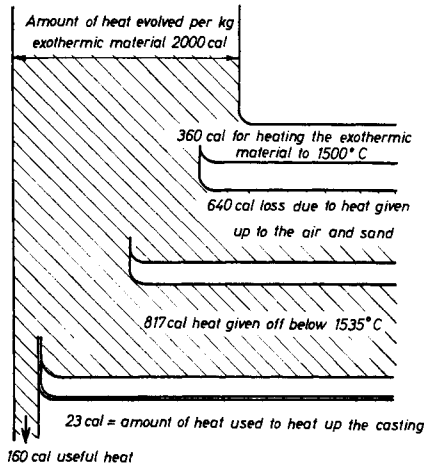


FIG. 412. Heat balance of exothermic materials (partly based on estimated values).

estimated, but are not likely to change the final result to any great extent.

Assuming that equations (160) and (161) were correct, the thermal efficiency would only be a few per cent (3–5 per cent) (due to the very small amount of heat transferred to the steel). As, however, the above equations were found to be false, the thermal efficiency must be calculated from the 360 cal/kg used in self-heating the exothermic materials to 1500°C , and is thus:

$$\eta \approx \frac{360 \times 100}{2000} \approx 18\% \quad (162)$$

The exothermic substance thus has the effect of a self-heating insulating material.

While normal insulating materials such as diatomaceous earths still withdraw heat from the steel until the steel and insulator reach the same temperature, this is not the case with exothermic materials. These heat up rapidly to (approximately) the temperature of the steel without abstracting any heat from the metal, apart from the heat of ignition (which can sometimes cause a significant drop in the steel temperature when aluminium-rich materials are used).

Because the specific heats of steel (0.2) and exothermic substances (0.24) are approximately equal, the heated sphere behaves (Fig. 411) almost as if it were an unheated steel sphere with an external diameter of 210 mm (the external diameter of the exothermic shell).

Calculations of actual exothermic sleeves in accordance with equations (160) and (161) give very thin walls. From practical strength considerations this sleeve will be made thicker, i.e. it will be dimensioned in accordance with experimental principles. The great difference between theoretical calculation and practical results is therefore not clearly discernible in practice. According to Thierry⁽⁴⁹⁾ the calculation also embodies several multiplying safety factors, which increase the geometrical modulus of the casting considerably. Due to these safety factors the results derived from equation (161) are no longer recognizable as a basis for practical operations.

CHAPTER 13

THE USE OF EXOTHERMIC PADS TO INCREASE THE THERMAL GRADIENT

13.1. Principles of the Calculation of Exothermic Pads

IMPORTANT FOR PRACTICE

13.1.1. HEAT TECHNOLOGY AND GENERAL PRINCIPLES

By placing exothermic pads on a casting (Fig. 413) the solidification time of the thinner cross-section can be prolonged, so that the thicker part can be fed sound. This method is not new and was described by Bishop⁽⁶⁰⁾. Apart from a few individual cases, however, the technique was not found to be practicable, as porosity and contraction cavities of all types tend to be produced.

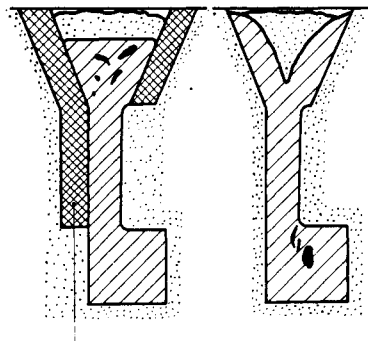


FIG. 413. Exothermic pad.

to the superheating of the melt, if large amounts of gas are present. In consequence the metal near the feeder head deteriorates in quality or becomes porous if the above-mentioned special products are not used. The author does in fact use the same exothermic sleeve both for aluminium bronze and cast steel, but he ignites the sleeve for 15–25 min (according to size) before using it for the non-ferrous alloy. In spite of this the solidification time increases by a factor of about 2.5.

12.8.2. TRUE PHYSICAL CAUSES OF THE EXTENDED SOLIDIFICATION TIME

The heat balance of exothermic materials can be estimated from Fig. 412. The amount of heat actually used to heat up the exothermic material itself to $\sim 1500^{\circ}\text{C}$ can be determined fairly accurately, and amounts to about 360 cal/kg. The remaining sources of heat loss were

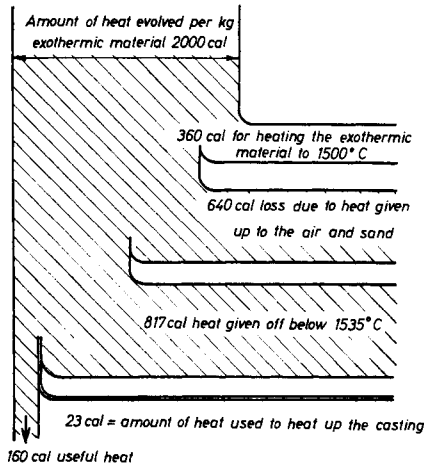


FIG. 412. Heat balance of exothermic materials (partly based on estimated values).

estimated, but are not likely to change the final result to any great extent.

Assuming that equations (160) and (161) were correct, the thermal efficiency would only be a few per cent (3–5 per cent) (due to the very small amount of heat transferred to the steel). As, however, the above equations were found to be false, the thermal efficiency must be calculated from the 360 cal/kg used in self-heating the exothermic materials to 1500°C , and is thus:

$$\eta \approx \frac{360 \times 100}{2000} \approx 18\% \quad (162)$$

The exothermic substance thus has the effect of a self-heating insulating material.

While normal insulating materials such as diatomaceous earths still withdraw heat from the steel until the steel and insulator reach the same temperature, this is not the case with exothermic materials. These heat up rapidly to (approximately) the temperature of the steel without abstracting any heat from the metal, apart from the heat of ignition (which can sometimes cause a significant drop in the steel temperature when aluminium-rich materials are used).

Because the specific heats of steel (0.2) and exothermic substances (0.24) are approximately equal, the heated sphere behaves (Fig. 411) almost as if it were an unheated steel sphere with an external diameter of 210 mm (the external diameter of the exothermic shell).

Calculations of actual exothermic sleeves in accordance with equations (160) and (161) give very thin walls. From practical strength considerations this sleeve will be made thicker, i.e. it will be dimensioned in accordance with experimental principles. The great difference between theoretical calculation and practical results is therefore not clearly discernible in practice. According to Thierry⁽⁴⁹⁾ the calculation also embodies several multiplying safety factors, which increase the geometrical modulus of the casting considerably. Due to these safety factors the results derived from equation (161) are no longer recognizable as a basis for practical operations.

CHAPTER 13

THE USE OF EXOTHERMIC PADS TO INCREASE THE THERMAL GRADIENT

13.1. Principles of the Calculation of Exothermic Pads

IMPORTANT FOR PRACTICE

13.1.1. HEAT TECHNOLOGY AND GENERAL PRINCIPLES

By placing exothermic pads on a casting (Fig. 413) the solidification time of the thinner cross-section can be prolonged, so that the thicker part can be fed sound. This method is not new and was described by Bishop⁽⁶⁰⁾. Apart from a few individual cases, however, the technique was not found to be practicable, as porosity and contraction cavities of all types tend to be produced.

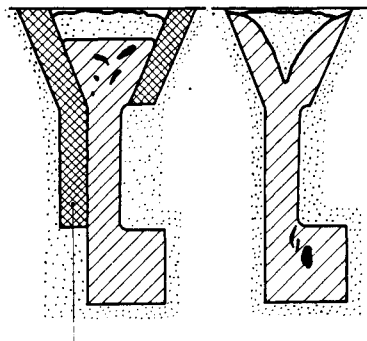


FIG. 413. Exothermic pad.

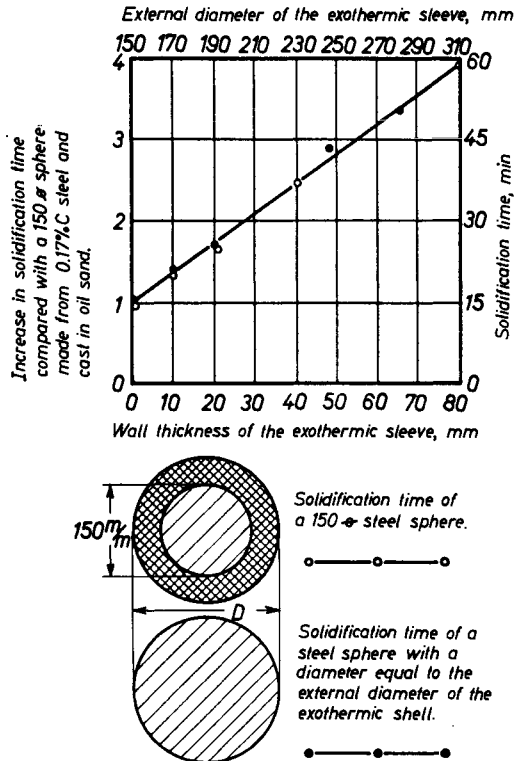


FIG. 414.

In carrying out the basic calculation for exothermic materials in general, therefore, their applicability to exothermic pads was also investigated.

Reference was made in Section 12.8.2 to the equivalent cooling of steel and exothermic materials. Figure 414 illustrates relevant experiments made by the author. The starting point was the sphere test which has already been mentioned so often (see Section 12.2). The experimental results can be formulated as follows:

The solidification time of a heated sphere d° (external diameter of the exothermic sleeve D°) is equal to the time of solidification of an unheated steel sphere with a diameter of D° cast in dry oil sand,

i.e. instead of the exothermic sleeve with a wall thickness of $w = (D^{\circ} - d^{\circ})/2$, a steel layer of equal thickness—with the same thermal effect—can be imagined, and conversely (with a certain limitation to be mentioned later).

Deviations from this result in accordance with the source of the exothermic material are possible, but are small in normal industrial production.

It was pointed out in Section 12.8.1 that the effect of exothermic materials on steel consists only of insulation, i.e. they are considered to be self-heating insulating materials.

No heat is transferred from the exothermic substance to the steel (except for an insignificantly small amount with a combustion temperature of 1600°C). However, the incandescent sleeves retard the cooling of the casting in the same sense as a very strongly preheated mould.

This physically correct method of viewing the process is extremely important for understanding the action of exothermic pads. All representations based on the transfer of heat from the exothermic material to the steel⁽¹⁶⁰⁾ are physically incorrect. The methods of calculation developed from these false assumptions (i.e. equations (160) and (161)) led to incorrect results in the practical application of exothermic pads which at first sight appeared inexplicable.

Given the thermal equivalence of exothermic materials and steel in accordance with Fig. 414, we are justified in asking where the economy lies in the use of exothermic feeder heads. These exothermic sleeves certainly represent a special case of exothermic pads, and exothermic materials cost more as a rule than the melting costs of the steel. The economy of exothermic feeder heads lies in the fact that the form of the shrinkage cavity is much more favourable than in unheated feeder heads, so that considerable steel savings are possible. This was treated in detail in Sections 12.1–12.6.

Naturally, the shape of the shrinkage cavity plays no part as far as exothermic pads are concerned, as no cavity should be formed. Consequently the steel saving is very small. Nonetheless, the pads can pay for themselves, because they replace the type of metal wedge padding described in Chapter 6, and so enable substantial savings in dressing and machining costs to be achieved.

The use of exothermic pads is not possible in all cases, because physical limits are set to this technique; but wherever they can be applied they represent a revolution in the moulding methods commonly used up to the present for cast steel.

The practice of exothermic pads has grown to maturity, as examples will show, but the field of application can still be extended considerably.

13.1.2. PRINCIPLES OF FEEDING AND METHODS OF CALCULATION FOR EXOTHERMIC PADS

According to Fig. 415 exothermic pads can be attached to a plate. No heat is conducted at the surface of contact; the only effect is to retard cooling. While the dendrites grow from both sides to the centre in an unheated plate (Fig. 415.1), solidification in a plate suitably heated on one side (Fig. 415.2) takes place only on one side, so that the crystallites also grow preferentially from one side.

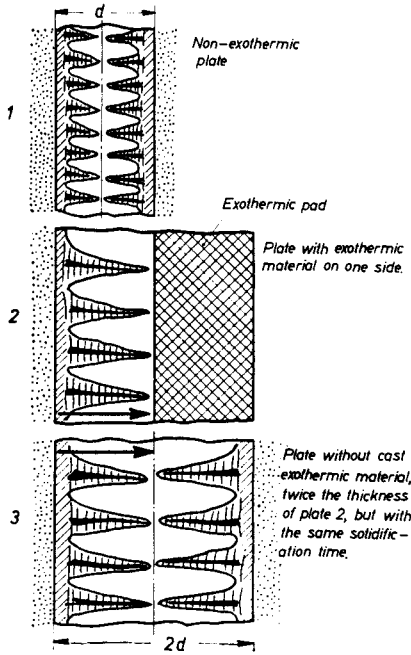


FIG. 415.

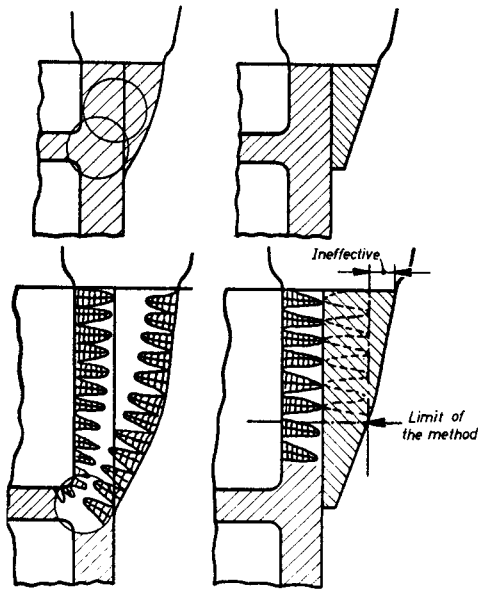


FIG. 416.

This fact has led to the development of a simple, graphical method for calculating exothermic pads. A wheel rim is to be fed in accordance with Fig. 416 (top):

1. Draw the circles for the cross-section by Heuver's method (Section 6.2), or using the curved rule shown in Fig. 167.

2. Replace the wedge-shaped steel padding so obtained by an exothermic pad of the same thickness.

The limitations of the method can also be established graphically. The wheel rim is very deep in Fig. 416 (bottom) and the steel padding is correspondingly thicker. As soon as this thickness exceeds that of the actual steel plate, exothermic pads placed on one side are no longer applicable; but even here the solidification time can be correspondingly prolonged by fitting the pads on two sides.

Such a plate, heated on one side (thickness d) thus solidifies in the same time as an unheated plate (Fig. 415.3) with twice the thickness $2d$. In both cases (2 and 3) the dendrites have the same length and rate of growth.

Here again, it can be stated that the exothermic pad solidifies in approximately the same way as if it consisted of steel (in accordance with the law formulated in Section 13.1.1 and with Fig. 414).

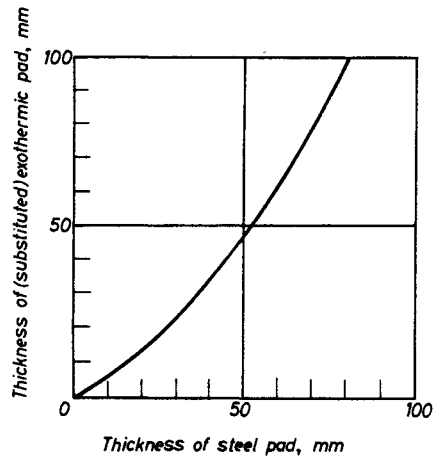


FIG. 417. Thickness relationship steel pad/exothermic pad. After Griffiths, Neu and Hall⁽⁶¹⁾.

At the same time the physical limits of the method are evident. As the pad only insulates and does not conduct heat, the solidification process in the plate (415.2) is complete in every case when the dendrites have grown to the heated (or insulated) face. This growth rate is equal to the rate of solidification of the plate. The rate is a function merely of the cooling conditions (for example of the moulding material) on the unheated side. The insulating action of the exothermic pad has reached its physical and theoretical maximum when cooling becomes hindered during the solidification period. If the pad were increased in ignorance of this fact beyond the maximum effective thickness ($\approx d$), this would bring no further increase in the solidification time (it can even have a deleterious effect, as will be shown later). Apart from slight deviations, it can therefore be stated that exothermic pads should not be thicker than the heated steel plate.

In their excellent paper on exothermic pads, Griffiths and Neu⁽⁶¹⁾ give an experimentally determined diagram for the necessary pad thicknesses (Fig. 417) which is valid for FEDEX 61.*

* Registered trade mark of Foseco International Ltd.

EXAMPLE 1

If the thickness of the wedge-shaped steel padding is 25 mm, the maximum permissible and effective thickness of the substituted pad of FEDEX 61 is 19 mm.

EXAMPLE 2

With 50 mm metal padding thickness the thickness of the exothermic pad is also 50 mm.

EXAMPLE 3

At 75 mm metal padding thickness the exothermic pad is 90 mm thick.

The diagram also defines the previously-mentioned slight deviations from the law which states that the thickness of the metal wedge padding is equal to that of the exothermic pad. It must be emphasized once more, however, to prevent misunderstandings arising from Fig. 417, that the effective limit given in Fig. 416 must be noted in all circumstances. This limit is reached when the metal wedge padding attains the thickness of the actual section of the casting.

Plates insulated on two sides can theoretically be kept fluid for any length of time, when the exothermic pads are of a suitable thickness. Unfortunately it is technically difficult or impossible in many cases to place the pads on two sides. With thin steel sections and thick exothermic pads (two or three times the thickness of the steel section), coarsening of the grain structure of the steel takes place. All these considerations, although based on conjecture, could be confirmed experimentally in accordance with Figs. 418a-b, in which the solidification times of a heated and an unheated plate were measured directly. Both plates were located on one and the same casting, so that other conditions were completely identical.

According to Fig. 415 the thickness of a plate heated on one side is apparently approximately doubled, i.e. the solidification modulus ($M_0 = d/2$) is increased to

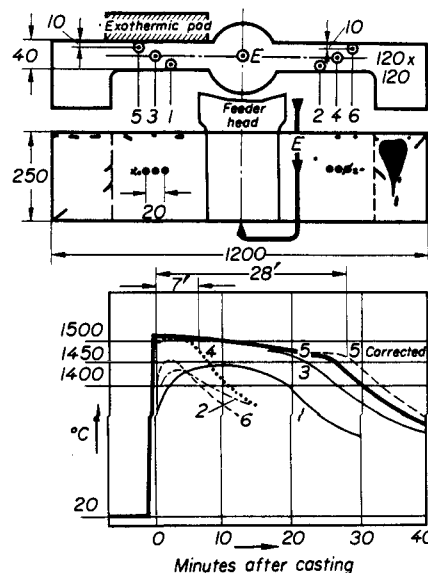
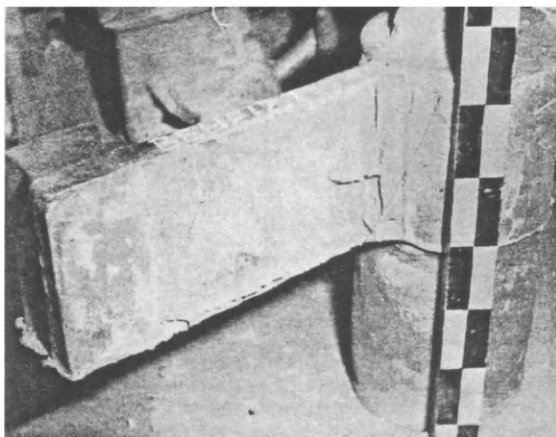
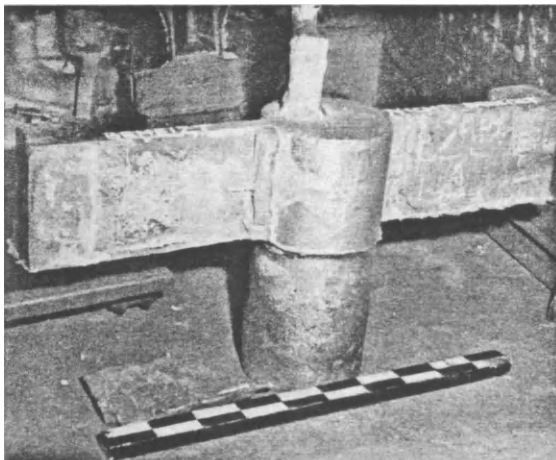
$$M_{\text{heated}} \approx \frac{2d}{2} \approx d$$

The modulus is thus about twice that of an unheated plate. The solidification time increases according to the basic equation (1) as the square of the modulus, hence:

$$\frac{T_{\text{heated}}}{T_{\text{unheated}}} = \frac{(M_{\text{heated}})^2}{(M_0)^2} = \frac{2^2}{1^2} = 4, \quad (162)$$

i.e. the solidification time becomes four times as long. This was confirmed accurately by the curves of Fig. 418b.

Based on these considerations the author⁽⁶²⁾ proposed a simple method of calculating the modulus of large, platelike exothermic pads. The contact face of the pad becomes a non-cooling surface in the modulus calculation due to the insulation, and as such is not included



The solidification time of the plate at point 5 was corrected by allowing for the fact that the thermocouple was placed 10 mm from the wall.

Figs. 418a and b. Experimental arrangement for measuring the solidification times of plates with and without exothermic pads.

in the calculation (just as the appropriate non-cooling surfaces in Section 2.5, Figs. 13 and 18, not included in the calculation, are subtracted from the geometrical surface). It remains uncertain whether the accuracy of this approximate method can be improved in the light of subsequent measurements.

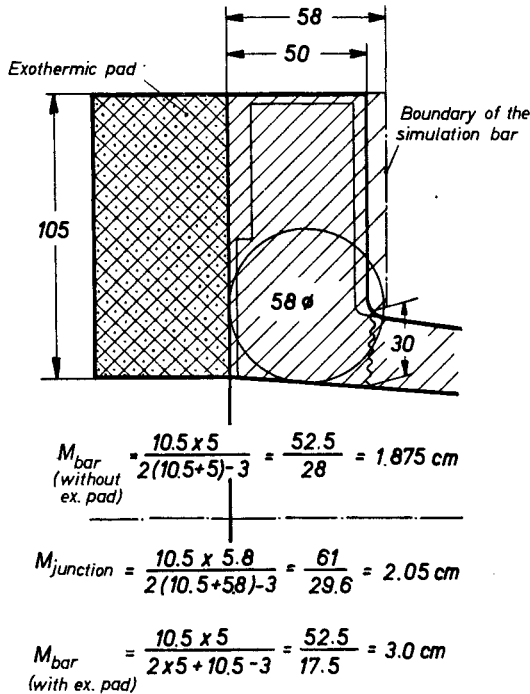


FIG. 419.

EXAMPLE

The junction of a flange (Fig. 419) is to be cast (as in Fig. 18, p. 10). The modulus of the junction is determined from the rule given there, and is 2.05 cm. The modulus of the unheated flange is only 1.875 cm. In order to feed the junction through the flange bar, this is heated on one side. Hence the heated face (of length = 105 mm) is no longer a cooling surface, and the modulus of the bar is increased from 1.875 to 3.0 cm.

It is of the utmost importance that the feeder head is calculated for this increased modulus, otherwise shrinkage cavities will be the inevitable result.

OF GREAT PRACTICAL IMPORTANCE

It is immaterial in this connection whether a heated or unheated feeder head is used. Exothermic pads and feeder heads are used together as a rule, but this is not absolutely necessary. It is only important to dimension the feeder head according to the modulus, whether heated or not.

As exothermic materials and steel behave similarly as regards cooling, a further approximation in the calculation is possible by treating the system (exothermic pad + casting) as a single unit and determining the modulus of the combined system. In two-sided heating (which in effect means heating on practically all sides)

this type of calculation is fairly accurate, but when heating is confined to one side it is valid only up to the maximum effective thickness of the exothermic pad.

13.2. Shape and Venting of Exothermic Pads. Heated Breaker Cores

IMPORTANT FOR PRACTICE

It is extremely important to maintain a high gas permeability of 150–200 units in the pad. The directions given in Section 12.4.2 must be followed scrupulously. It is particularly important to maintain the correct water content, as according to Fig. 363 the necessary high gas permeability can be attained only within close tolerance limits.

In order to dispose of the large amounts of gas which are evolved, good venting arrangements such as in the examples shown in Figs. 420 and 421 are advisable. It must not be forgotten, however, that venting of this type, due to negligence, is often done badly, or not at all,

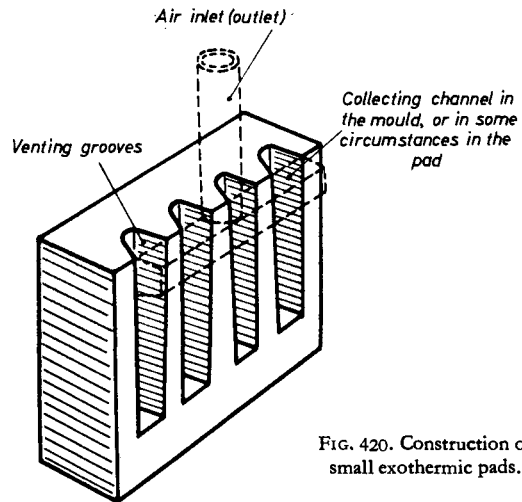


FIG. 420. Construction of small exothermic pads.

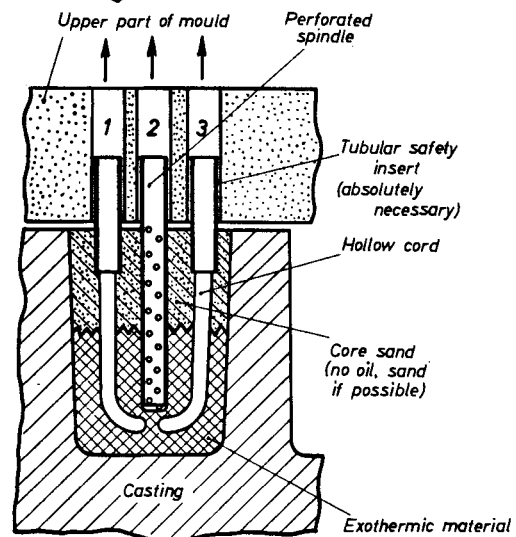


FIG. 421. Basic construction of large pads, round which steel flows on several sides. There are at least three independent venting systems, incorporating a perforated spindle. This is a precaution against accidents.

and that steel can even penetrate into the venting channels.

With large exothermic pads (Fig. 421) controlled removal of air is essential if accidents are to be prevented.

With smaller pads it is better, in the author's experience, to rely mainly on good gas permeability, removing the gas merely by venting through the pad to the sand mould behind.

Exothermic pads can be made with equal effectiveness either with a taper (Fig. 422) or as a rectangular block (Fig. 419). Tapered pads are placed on the pattern and rammed up with the moulding sand. Rectangular pads are inserted as cores in the finished mould. Both methods have their advantages and drawbacks in practice.

If a tapered pad is selected, the author has found that the pads can be combined with breaker cores, as shown in Fig. 423. On flanges, etc., breaker core gates are used in order to avoid tearing the casting when knocking-off.

The dimensions of such breaker cores are frequently made too small. This arises from the argument that the breaker core is heated and also that a very thin neck will not freeze. This view is false and leads to the formation of shrinkage cavities in the casting, for the following reason:

According to Chapter 7 on breaker cores, such a core is raised by the steel superheat to a temperature of about 1485°C, corresponding to the solidus temperature. In this way the cooling of the thin neck is retarded. Nonetheless the breaker core loses heat from its end faces, so that the neck cannot be made indefinitely thin, but must have the exact dimensions laid down in Table 25.

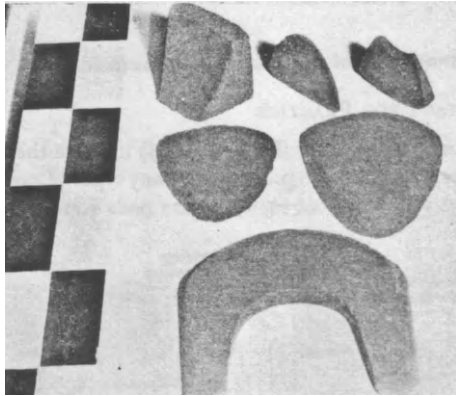


FIG. 422. Various simple standardized shapes made from FEDEX 61 for wheel castings and plate gate valves. (Produced at Sheepbridge, Chesterfield, and made available by Mr. Griffiths.)

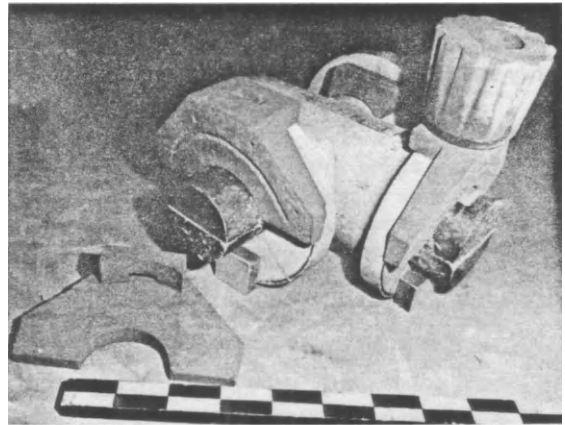
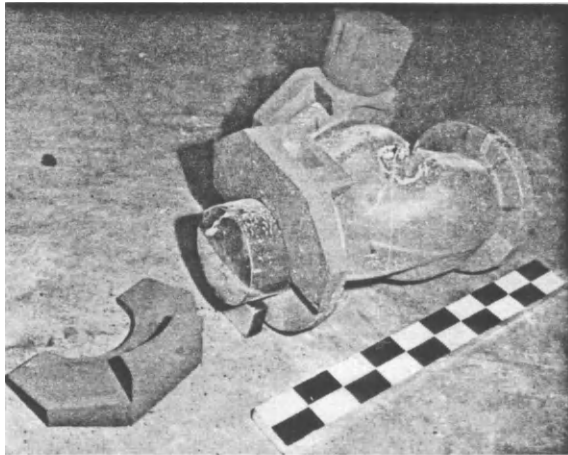


FIG. 423 b. Tapered exothermic pads, combined with breaker core, on a gate valve casing.

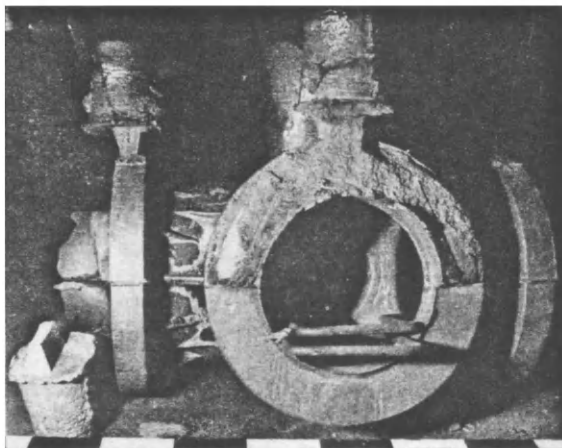
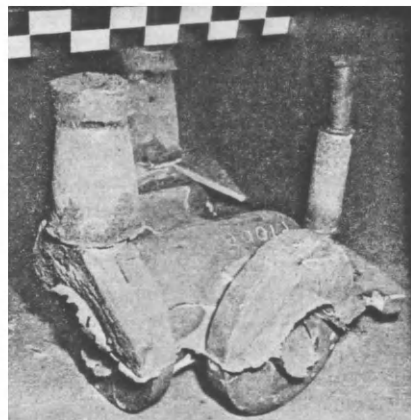


FIG. 423 a. Tapered exothermic pads, combined with breaker core, on a valve casing.



This neck represents a quasi-infinite bar, and its dimensions can also be presented as part of the bar modulus (see equations (46), (47), (48) and (49), p. 88).

A heated breaker core also has a temperature of 1400°C to 1500°C, corresponding to the combustion temperature of the exothermic materials (sect. 12.8.1), except that this temperature stems from the material itself, and not from the steel. Thus the heated breaker core becomes no hotter than the unheated one. Incandescent exothermic materials and incandescent sand or fireclay are identical in this respect. Here again there is no difference between heated and unheated breaker cores.

Exothermic breaker cores must therefore be dimensioned as accurately as unheated cores, using Table 25 or the equations mentioned above. Only one exception is permissible, namely the cores can be made up to twice the thickness of the values given in Table 25 or equation (46). Non-exothermic breaker cores only reach the desired temperature of 1485°C when they are thin and in thermal equilibrium with the steel. Exothermic breaker cores are independent of these conditions and can therefore be made thicker, which is often an advantage in practice.

The cross-section of the neck must be preserved in all circumstances, however, and must be dimensioned for the modulus of the heated casting (not approximately for the modulus of the unheated casting!).

EXAMPLE

If the flange of Fig. 419 is to incorporate a breaker core, this must be calculated for an increased modulus of 3 cm, and must therefore have an opening, according to Table 25, of ~70 mm \varnothing , or, as this is technically impossible in the present case, a rectangular cross-section, according to equation (49), with a modulus of:

$$M_{\text{neck}} = 0.59 \times M_{\text{casting}} = 0.59 \times 3.0 = 1.77 \text{ cm.}$$

Any suitable cross-section can then be selected from Fig. 7, for example 4.5 \times 16 cm or 5 \times 12 cm. Here also the physical laws must be obeyed implicitly.

The standardization of exothermic pads is an important practical simplification. Pads for wheels of all types can be dimensioned on similar lines to the standard chills of Table 26. All types of fitting flanges are similarly standardized, so that exothermic pads can also be standardized on the basis of existing standardization. This does not mean that any apparently suitable exothermic pad can be fitted to the casting. In preparing the work the physical possibility of using the pads must first be examined for each casting, on the basis of directions which have been given here. The importance of standardized exothermic cores lies solely in the fact that a separate core box does not need to be prepared for every pattern.

Many exothermic materials are hygroscopic; a test piece can take up as much as 0.5 per cent moisture. Pads made from such materials should be re-dried shortly before use, or stored in a warm oven.

The drying time and temperature play an important part in removing as high a proportion as possible of the chemically combined water. Data supplied by the manu-

facturer should be followed in this connection. Usually a drying time of 1 hr per 1 in. pad thickness must be allowed, with a drying temperature of 200–250°C.

The surface of the casting on the side where the pad is attached is rougher with most exothermic products than that resulting from a sand mould, and this cannot be greatly improved by sleeing the pads. At present only one special product is known which will give a smooth surface without sleeing.

13.3. Examples of the Use of Exothermic Pads

IMPORTANT FOR PRACTICE

Numerous examples (Figs. 424–443) indicate the possibilities offered by this process for many types of casting. Castings are illustrated in which the pads were inserted

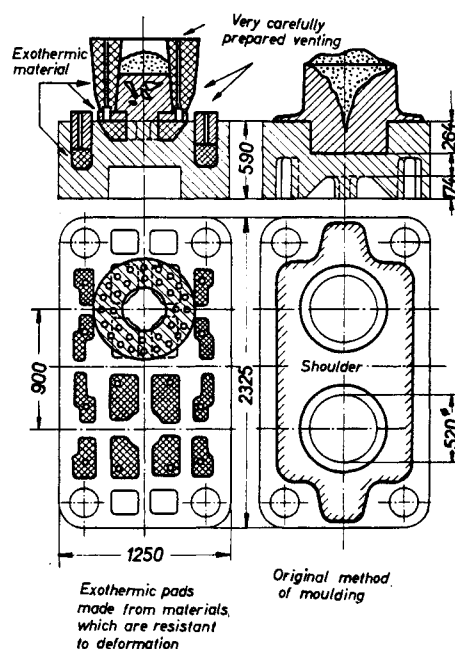


FIG. 424. Press plate, 15 m. ton finished weight.

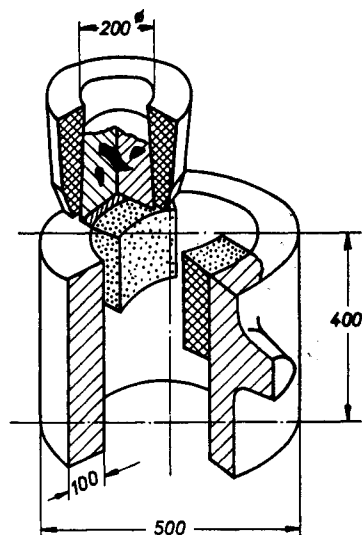
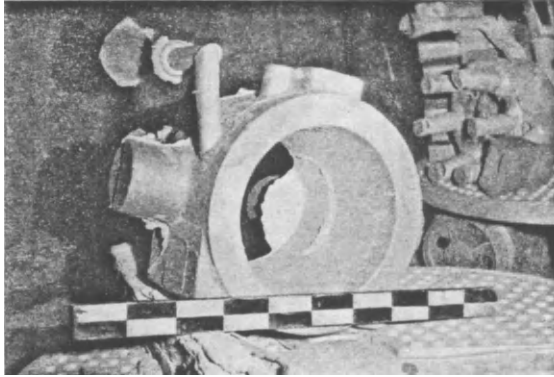
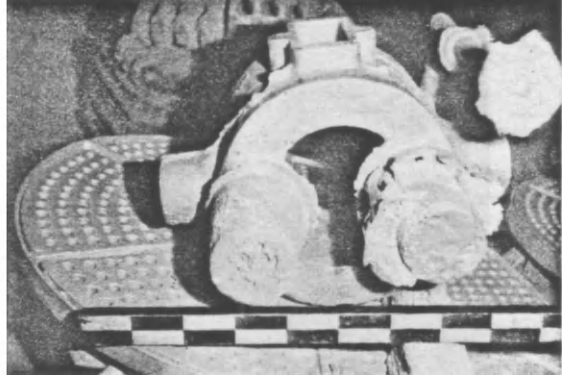


FIG. 425



a



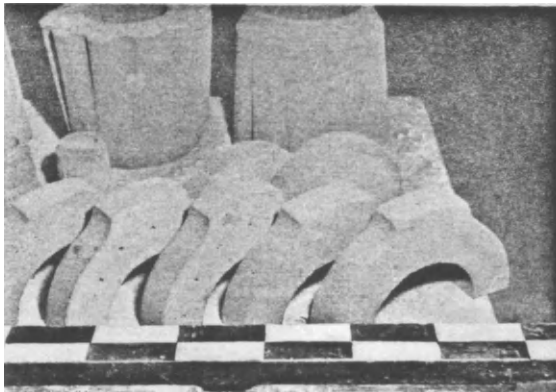
b

FIG. 425a and b. Bearing casting with exothermic pads.

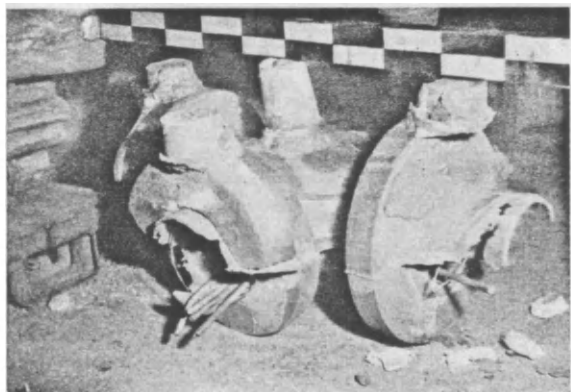
in the finished mould as a core, as well as those where the pads were rammed up with the mould.

A very interesting example is the valve housing shown in Fig. 429, where only a single exothermic head feeds the entire casting via a clover-leaf type of pad. This is of course possible only when the wall of the housing

is fairly thick, so that the basic physical principles outlined in Section 13.1.2 are still obeyed. In addition the feeding of wheel bosses of all types in accordance with Figs. 441 to 443 can be very important, as the rough machining of the opening, which has been customary up to now, is omitted.



a



b



c



d

FIG. 426a-c. Valves manufactured with rectangular section exothermic pads.

FIG. 426d. Valves manufactured with exothermic pads, ready for despatch.

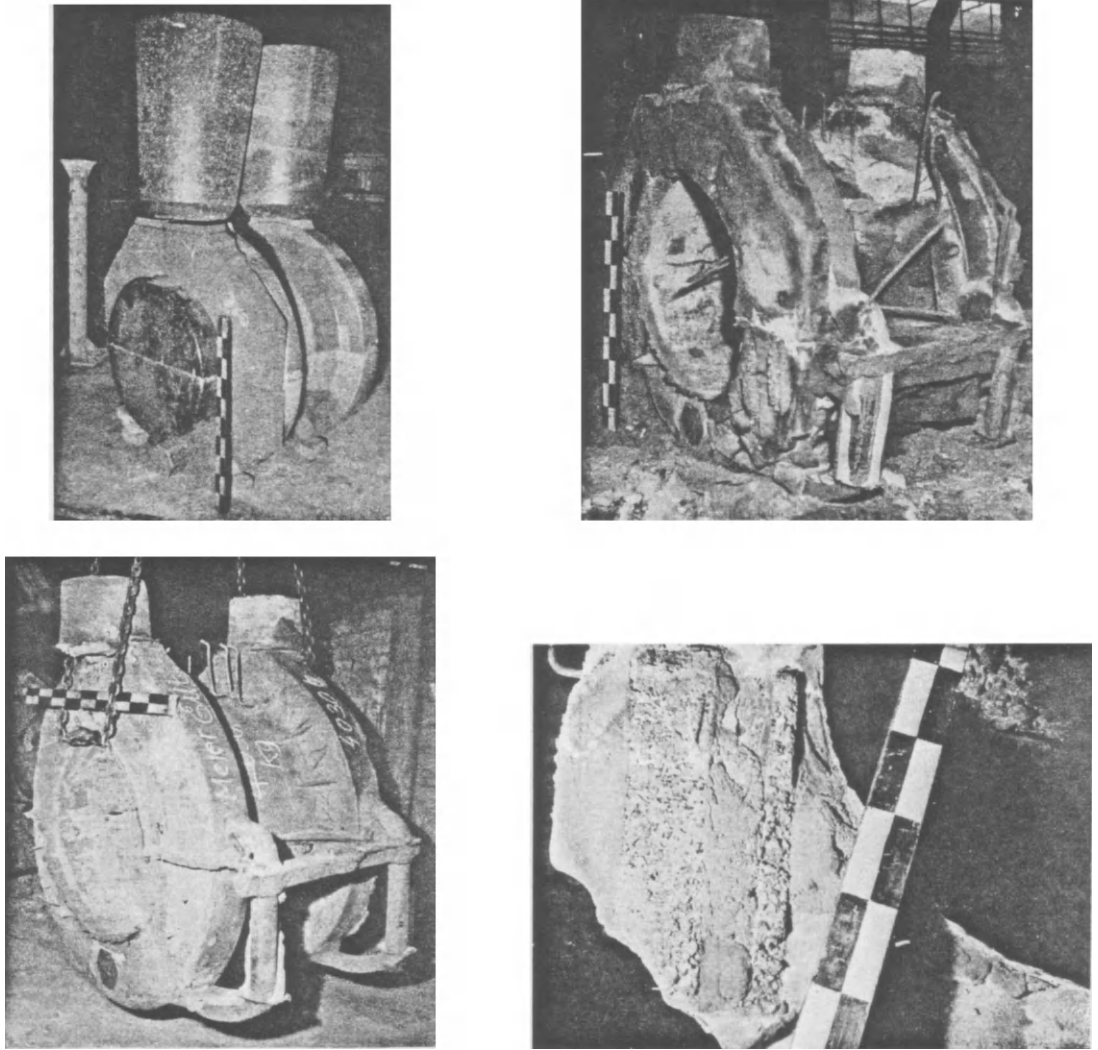
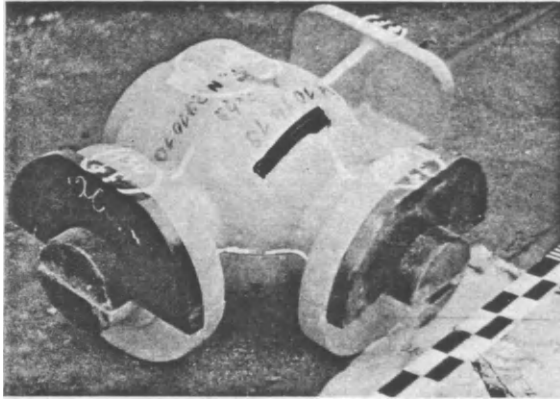


FIG. 427. Large double flange, cast with exothermic pads. The casting was certainly sound, but its surface was rough. As at 1962 this size of casting represents the extreme limit of applicability of exothermic pads.
(Courtesy Sulzer Bros.)



FIG. 428. Pattern (top) and undressed casting (bottom) of a gate valve casing, using exothermic pads.



a



b



FIG. 431. Two examples of pipe fittings using exothermic pads.

FIGS. 429a-b. (a) Pattern of a pipe fitting with an exothermic pad inserted as a core. (b) Undressed casting. The finished casting was ultrasonically sound.

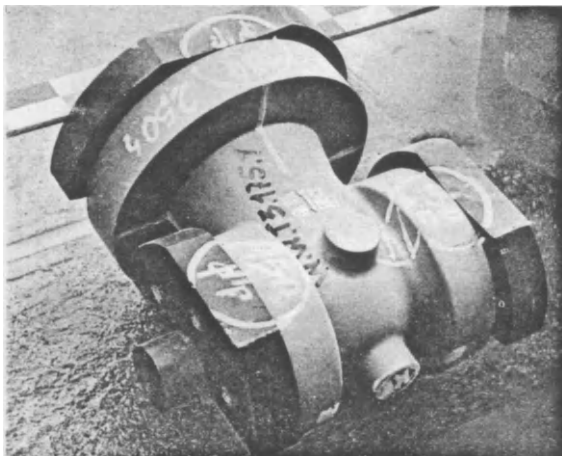


FIG. 430. Patterns of pipe fittings with exothermic pads.

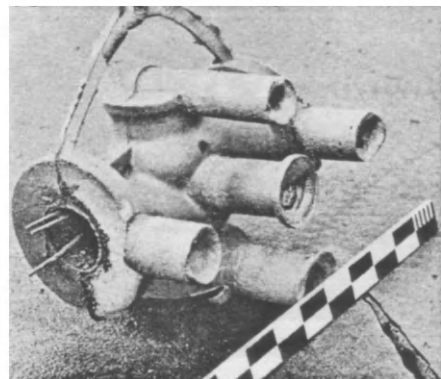
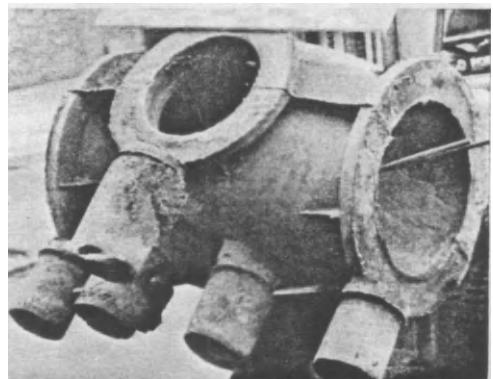


FIG. 432. Two examples of pipe fittings with exothermic pads, before final dressing.

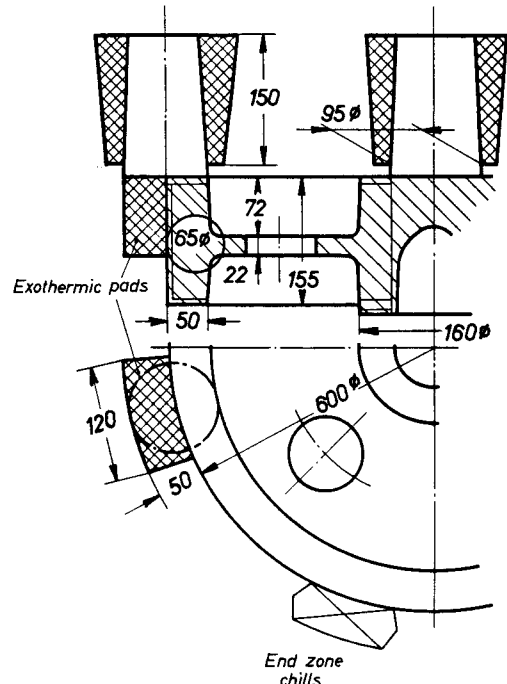
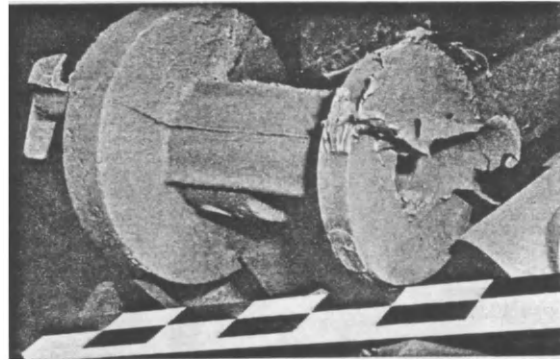


FIG. 434a. Gear wheel with 3 exothermic feeder heads and exothermic pads at the periphery and intermediate end zone chills—radiographically sound.



FIG. 433. Various fitting components with exothermic pads.

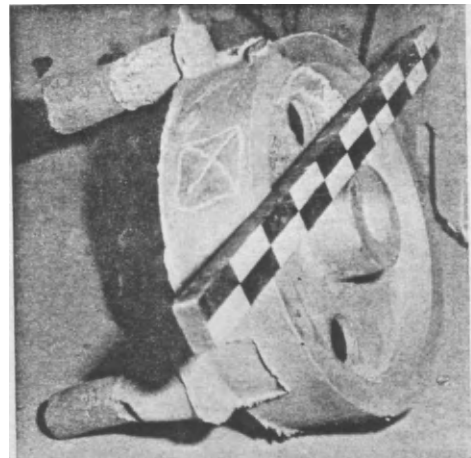


FIG. 434b. Wheel with exothermic pad.

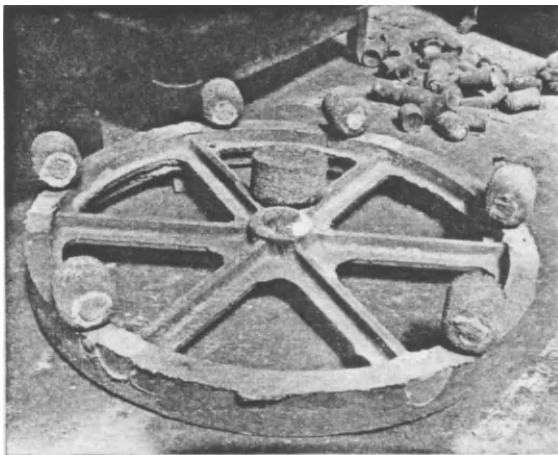
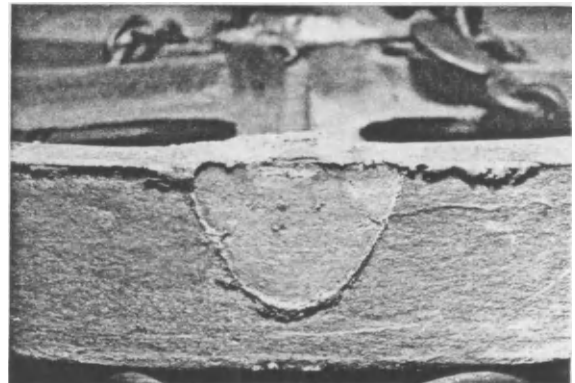
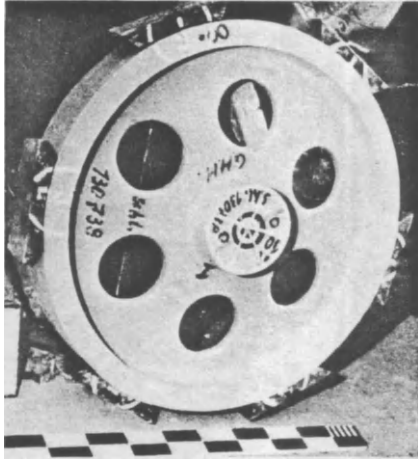


FIG. 435a. Wheel. After Griffith, Neu and Hall⁽⁶¹⁾.

FIG. 435b. According to ⁽⁶¹⁾.



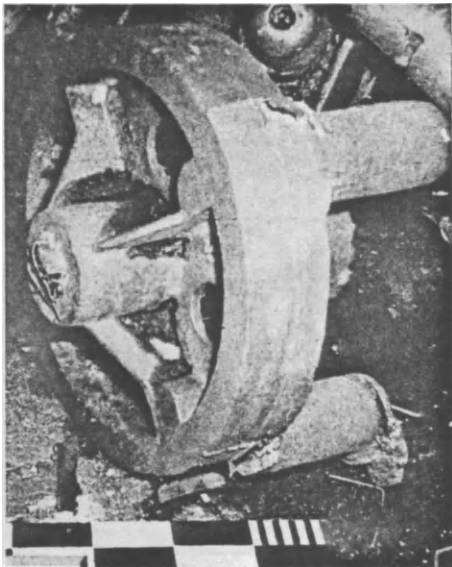


a



b

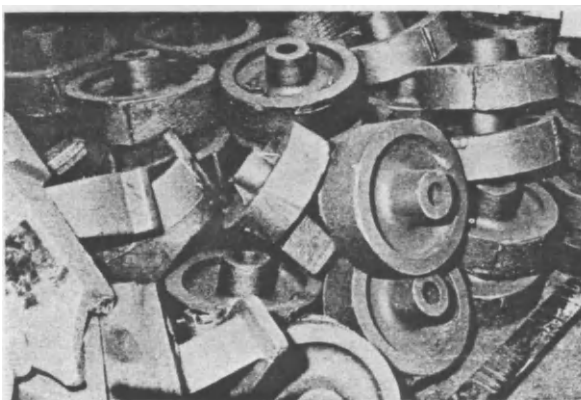
FIG. 436. Gear wheel with exothermic pads, ultrasonically sound.
(a) pattern (b) undressed casting.



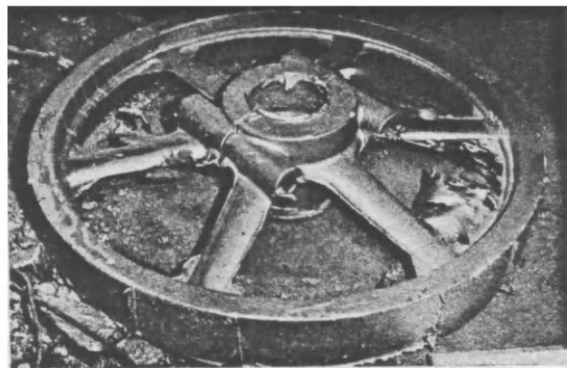
a



b

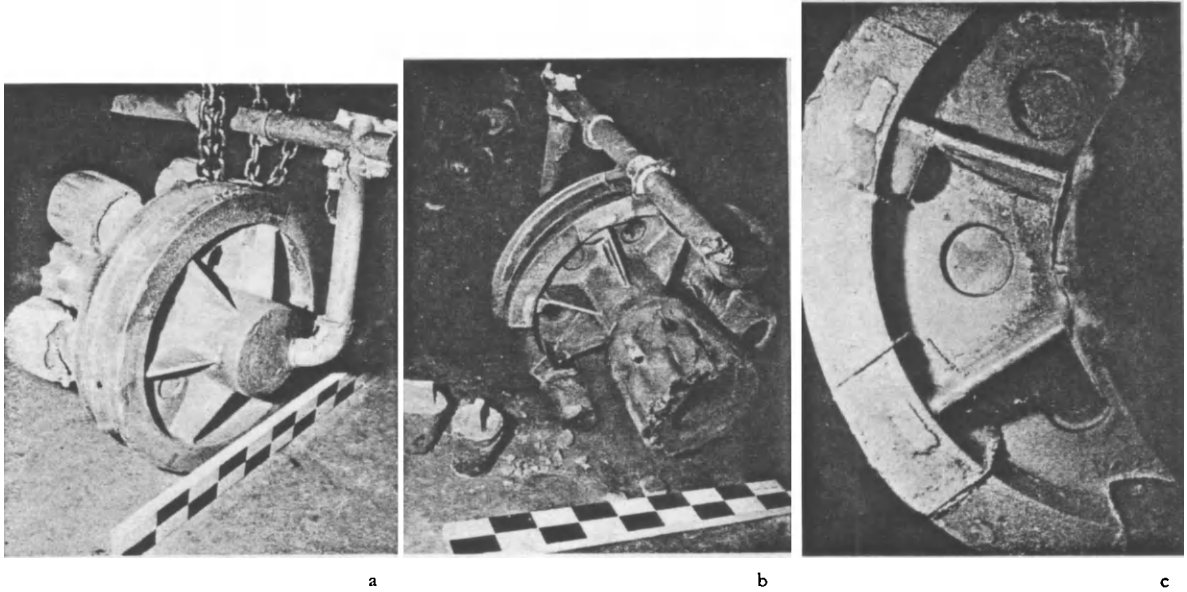


c



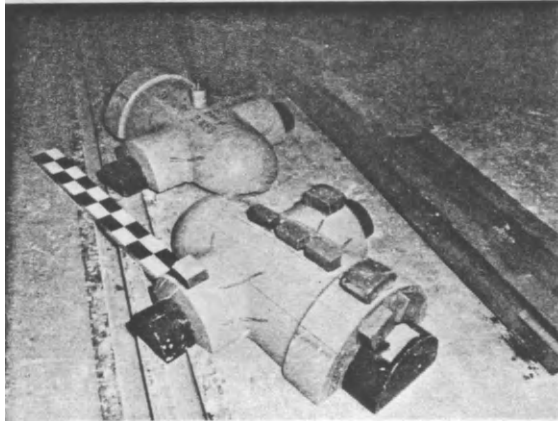
d

FIGS. 437a-d. Various wheel castings with exothermic pads.

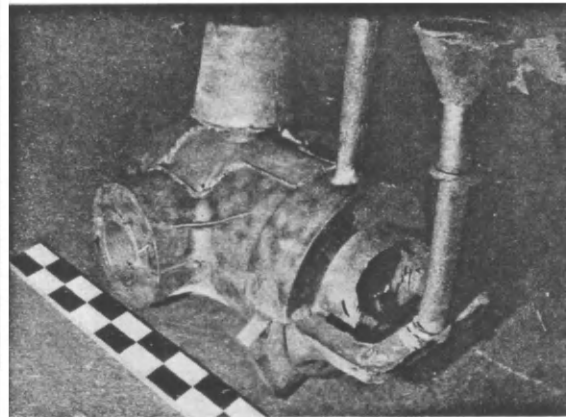


FIGS. 438a-c. Crane bogie wheel with exothermic pads, combined with breaker cores.

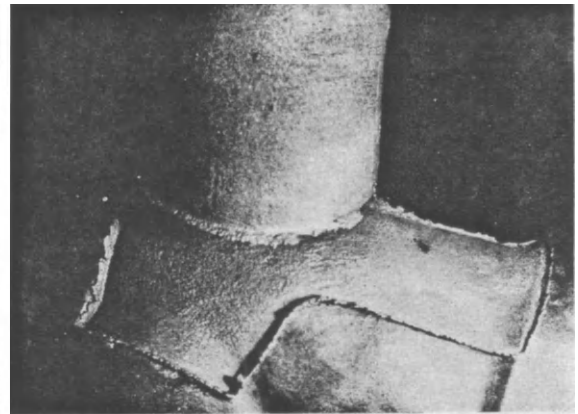
The exothermic pads were applied to the inner side in this instance. In such cases they should only have about half the thickness shown in Fig. 417 (because of the additional retention of heat in the junction). In this case (pads applied to the inner side) preliminary trials are also to be recommended. The wheels shown were radiographically sound.



(a) As-cast condition.



(b) Pattern, with attached end zone chills.



(c) and (d) Detail photographs of the feeder head neck and the exothermic pad surface.

FIGS. 439a-d. Gate valve casing, radiographically sound, fed by an exothermic feeder head by means of cross-shaped exothermic pads in the upper part.

(By courtesy of Sulzer Bros., Winterthur.)

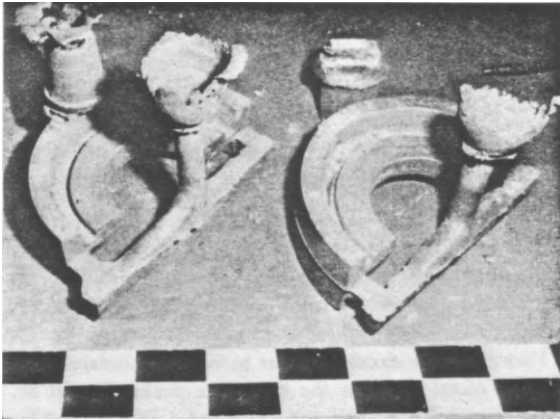


FIG. 440. Half wheel, manufactured with inside exothermic pads, similar to the example shown in Fig. 438. Here also two preliminary trials were necessary. A very large number of radiographically sound castings was manufactured by this method. (By courtesy of Sulzer Bros., Winterthur.)

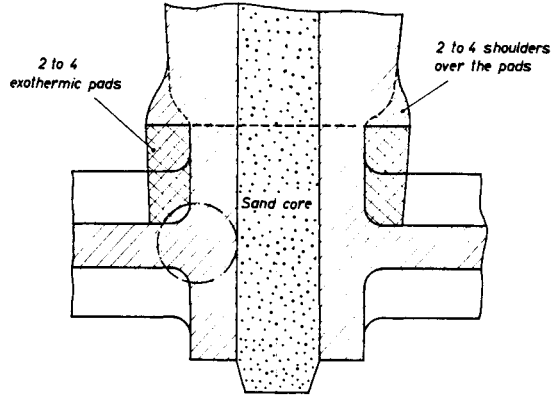
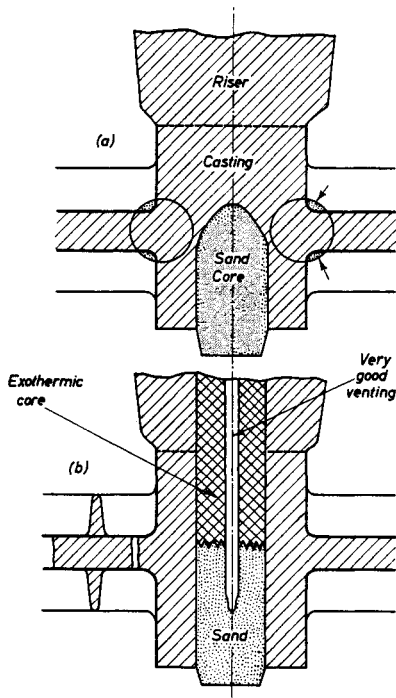


FIG. 442. Exothermic pads applied externally to bosses.

Just as in Fig. 441 the metallic wedge pad was applied to the internal, or core, side, i.e. the sand core was tapered, these metal wedges can also be placed on the outside. However, it is often impossible to remove the pads due to ribs etc., so that this method is not often operated. With exothermic pads the construction is more flexible, so that the external Hewers wedge can be replaced by such an exothermic pad. This method has proved very satisfactory and is less sensitive to defective venting than the method illustrated in Fig. 441 b.



FIGS. 441 a and b. (a) Usual construction of a boss feeder head. See also Figs. 151 and 152 (p. 16). (b) Construction using exothermic internal core.

The exothermic core and the sand core beneath it were rammed together in a core box to form a single unit. The exothermic core is carried through with the feeder head and taken high enough to ensure that no steel can penetrate into the vent. Venting must be carried out very carefully.



FIG. 443a. Use of exothermic pads on the boss of a gear wheel. The use of exothermic feeder heads is not necessary for this purpose, as the above example shows.

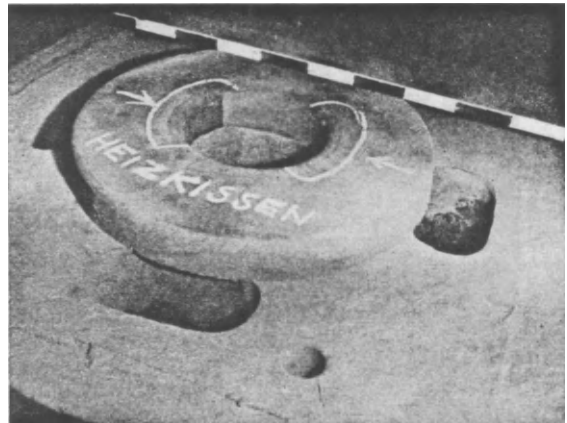


FIG. 443b. Exothermic pads in the mould. Exothermic pads

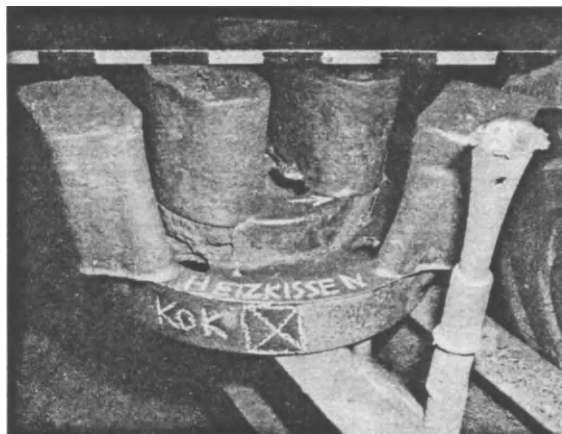


FIG. 443c. Exothermic pads in a gear wheel in the as-cast state.

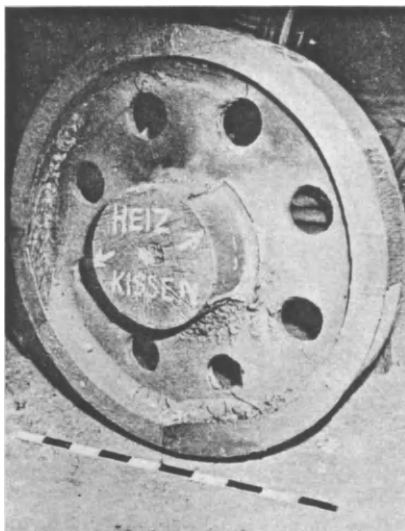


FIG. 443d. A further example of the use of exothermic pads on bosses.



FIG. 443e.

13.4. Frequently Occurring Defects with Exothermic Pads

IMPORTANT FOR PRACTICE

13.4.1. SHRINKAGE CAVITIES FORMED BECAUSE THE PADS HAVE BEEN MADE TOO THICK

Due in the first place to ignorance, a gear rim as shown in Figs. 444a-c was fitted with too thick a pad. According to the principles laid down in Section 13.1.2, no additional increase in solidification time could thereby be achieved.

However, the excessive heat insulation hindered the flow of metal between the crystallite peaks. It will be remembered that, according to Section 3.4, Fig. 58 (p. 22), the dendrites have a much coarser structure in thick walled plates than in thin plates. This also has the effect of impairing satisfactory feeding; beyond a certain thickness, in fact, centre-line segregation is inevitable.

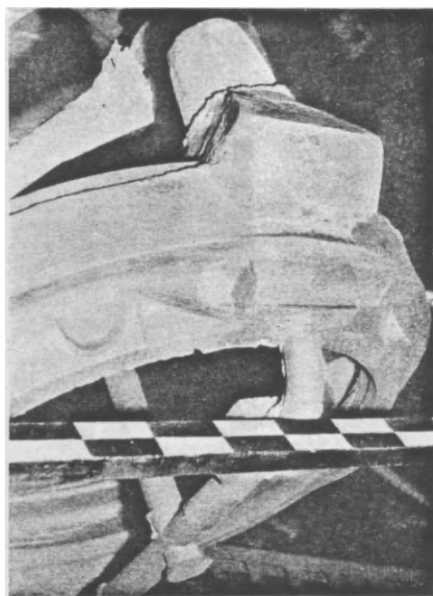
This case is produced artificially by the use of overdimensioned exothermic pads, except that the centre-line segregation is now displaced to the pad/casting interface.

When machining castings of this type porosity is uncovered which consists of a true centre-line cavity (even although this is displaced). In this case the surface of the casting usually appears rough, and small, parallel wrinkles (rather like the skin formed on heated milk) cover the surface (Fig. 444d). These parallel, fine creases can be considered to be the fronts of dendrites which are occasionally found on the inside surfaces of shrinkage cavities (cf. Fig. 39a, p. 17). *Too large an exothermic pad will therefore produce scrap.*

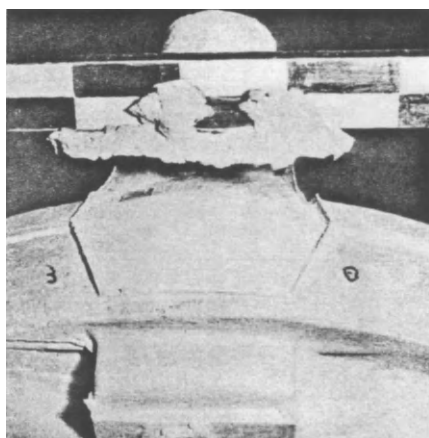
This fact is again illustrated in Fig. 444e. A massive parallelepiped-shaped exothermic pad was experimentally placed at the base of an 18 cm steel wall, the parallelepiped having of course a much longer solidification time than the usual pad. It was found from this experiment, which was repeated several times, that the thick section could be fed satisfactorily by exothermic plates, even with large castings. An undesirable side effect was the yielding of the exothermic material due to the high pressure of liquid metal. Further experiments established that this effect could be prevented by the use of convex pads; alternatively the desired contour was obtained after allowing for the yielding effect. The shrinkage cavity visible in the thin wall was found again, however. It is caused by the high resistance to flow offered by the crystallites which are heated on one side; these shorten the feeding range, i.e. the sound feeding zone, with large cross-sections of this type. This diagram shows the limits of the method at the present time (1962).

13.4.2. BLOWHOLES UNDER EXOTHERMIC PADS

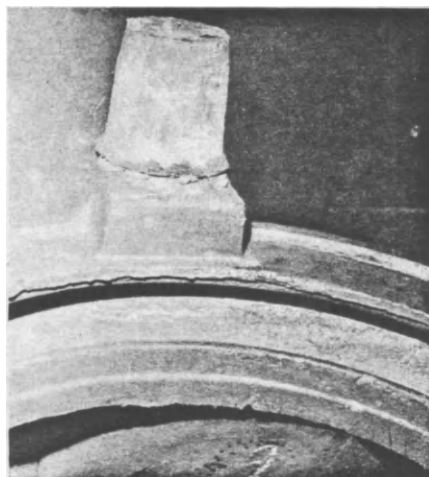
Blowholes are not observed under exothermic pads with satisfactorily melted and correctly deoxidized steels with low gas contents. (An exception to this rule is given by pads which "boil" visibly due to low gas permeability. If the pad behaves quietly during pouring, it is certain that the blowholes do not originate from the pad.)



a



b



c

FIGS. 444 a-c. Over-dimensioned exothermic pads on a gear wheel rim.



FIG. 444d. Appearance of the casting surface associated with the use of over-dimensioned pads. This shows the fronts of dendrites which have not been fed with metal (cf. Fig. 39a, p. 17).

The blame for scrap is often laid on the pad, when incorrect melting practice is actually the cause. In such cases, however, the force of the argument can be checked (provided that the pad is satisfactory) by insisting on hot metal tests as shown in Fig. 269. In general Section 8.3.2 also applies here.

When cases of this type occur, accurate works observations are necessary. In very many instances porosity of this kind is also found with other castings in which exothermic pads were not used.

The gases in the steel are often forced from the solidifying dendrites into the residual melt, where they become concentrated and form pores. This phenomenon represents the stage immediately preceding "bleeding back" ("cauliflowing") which can be caused, for example, by incomplete deoxidation or hydrogen enrichment.

The metal remains liquid longest under exothermic pads, with the result that porosity often occurs in that position, without being produced by the pad itself.

Presumably different gases can give rise to different phenomena in this way, which could explain the variety of defects which are found even with unheated castings.

Figures 445 a-c show experimental plates with exothermic pads on one side. The melts were intentionally poured insufficiently "killed", thus having an increasing oxygen content. It was found that no porosity was found initially underneath the pad; on the contrary, the pores appeared to be compressed together on the

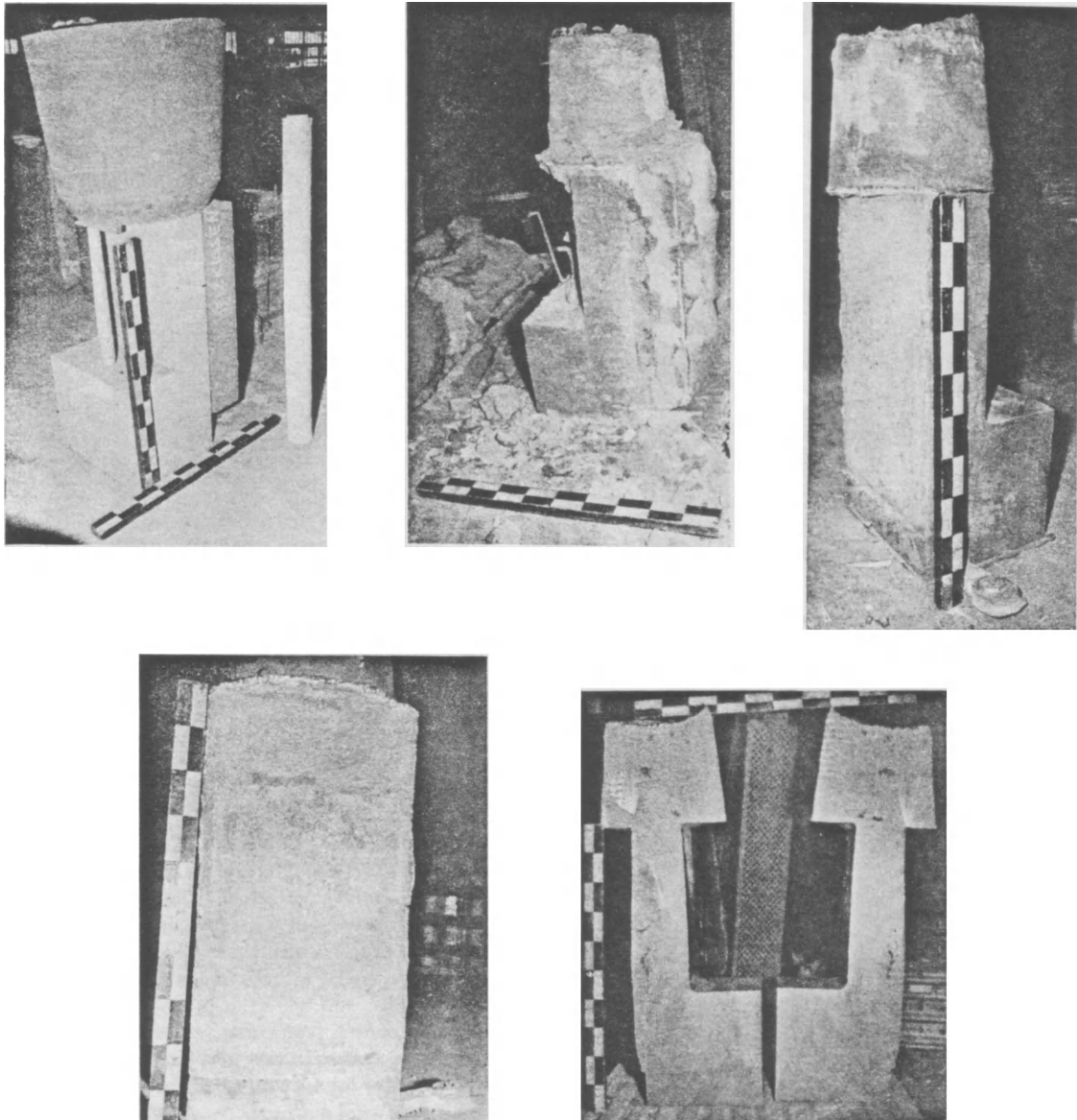


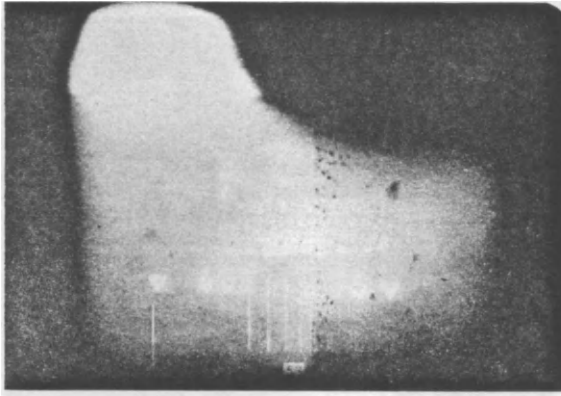
FIG. 444e. Trial cast to test the use of exothermic pads on ~18 cm thick steel walls.
(Courtesy Sulzer Bros.)

sand side. The boundary separating the pad and the sand is razor-sharp, and is delineated by an accumulation of pores on the sand side. Only when the melt deteriorates further does porosity occur under the pad, but is in every case less marked than on the sand side. Possibly the cooler sand acts as a chill in this case, so that pinhole porosity occurs as in Figs. 264–266 (pp. 118, 119). This sharply delineated limit of porosity on the sand side could often be observed on actual castings, on all the pad/sand interfaces, including the core opening (Fig. 445 d).

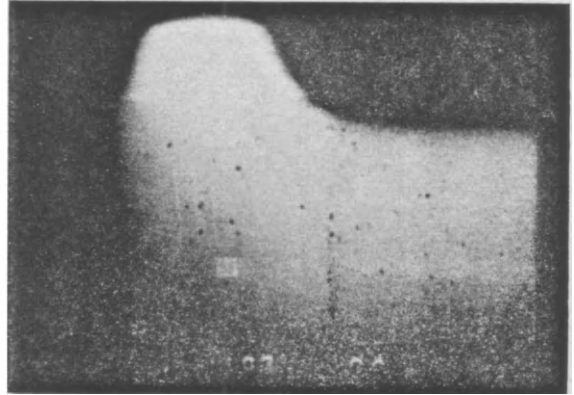
With melts with obviously very high gas contents,

which are badly deoxidized, an accumulation of pores directly under the pad can be observed (Fig. 446), where the pores are retouched with Indian ink for the sake of clarity. This accumulation of pores is the preliminary stage prior to “cauliflowing” and also occurs with other wedge pads on unheated castings, near the feeder head (Figs. 447–450).

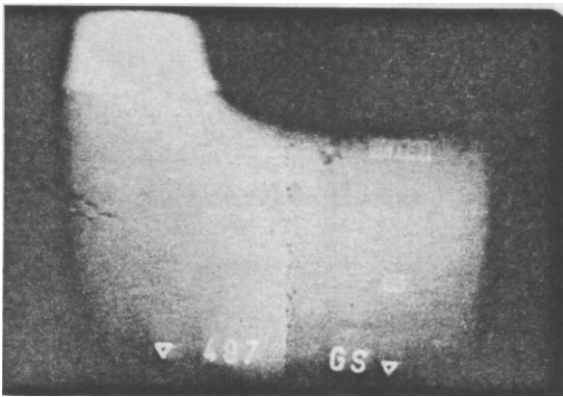
The above examples show how necessary it is to make a thorough investigation, and not to yield to the widespread tendency to ascribe defects to a fundamentally different cause.



a



c



b

FIGS. 445a-c. Radiographs of trial casts poured from badly deoxidized melts.



FIG. 445d. Pinhole porosity on the sand side of the exothermic pad/steel/sand interface.

Thin steel fins of metal which has penetrated with the interspace between the exothermic pad and the valve casing core can be seen clearly.

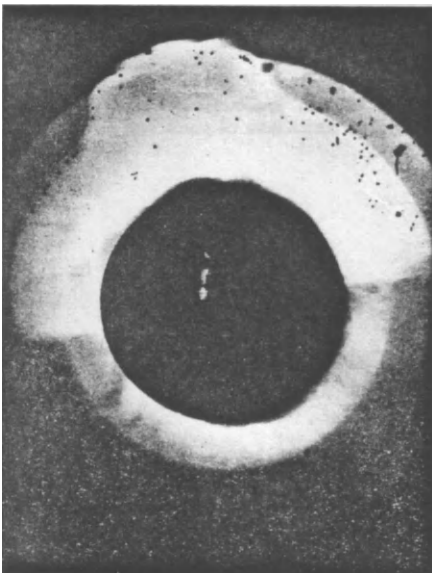


FIG. 446. Porosity underneath the surface of application of an exothermic pad.



FIG. 447. Porosity at the surfaces of application of exothermic pads. The charge of metal represents a boundary case of the so-called "cauliflowing". Note, however, the concentration of pores on the sand side of the central flange.

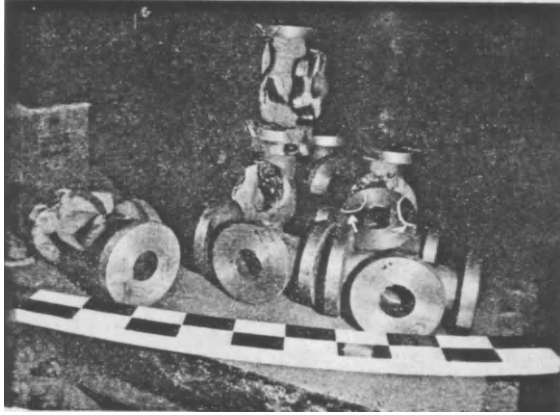


FIG. 448. The same pattern of porosity as in Fig. 447 is shown by these valve casings, which in this case were manufactured without exothermic pads, using conventional wedge pads.

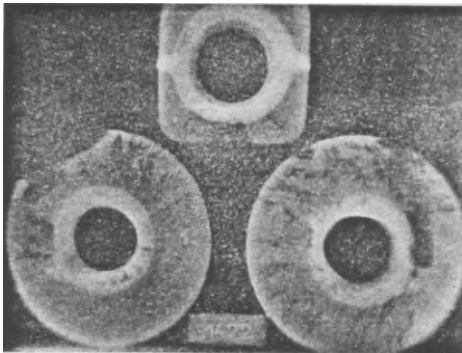
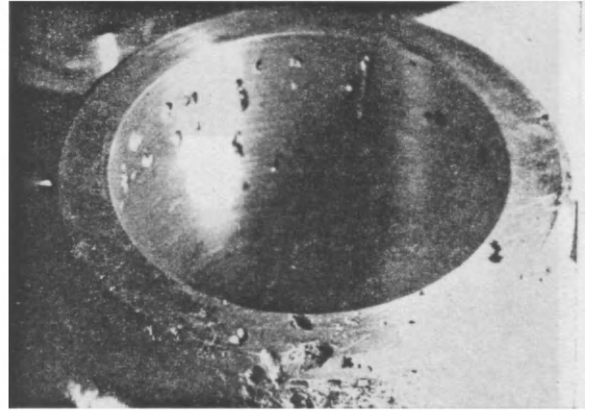


FIG. 449. Porosity in valve flanges where exothermic pads were not used.

Note particularly the flange on the left of the diagram. Here also the porosity is very pronounced under the metallic wedge pad, because the steel remained liquid longest in this position.

If an exothermic pad had been attached at this position, then the temptation to ascribe the defect to the exothermic pad would have been very great.



FIG. 450. This lever arm (made without exothermic pads) also exhibits a typical enrichment of pores near the feeder head.

CHAPTER 14

BRIEF NOTE ON THE USE OF INSULATING MATERIALS IN STEEL CASTINGS

IT IS possible in principle to insulate feeder heads for steel castings by means of materials which are not self-heating.

Up to the present time, however, (1962), no insulating materials are known which fulfil the following requirements simultaneously:

Refractoriness, with the good surface associated with this property (particularly important for insulated pads placed on the casting).

Good mouldability—most insulating materials, diatomaceous earth, for example, have poor moulding characteristics.—Cheapness.

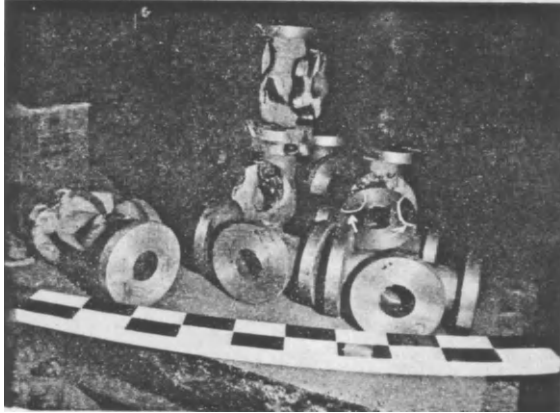


FIG. 448. The same pattern of porosity as in Fig. 447 is shown by these valve casings, which in this case were manufactured without exothermic pads, using conventional wedge pads.

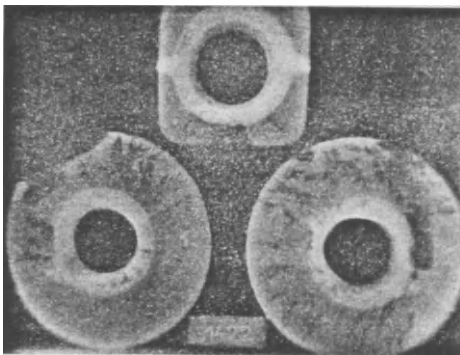
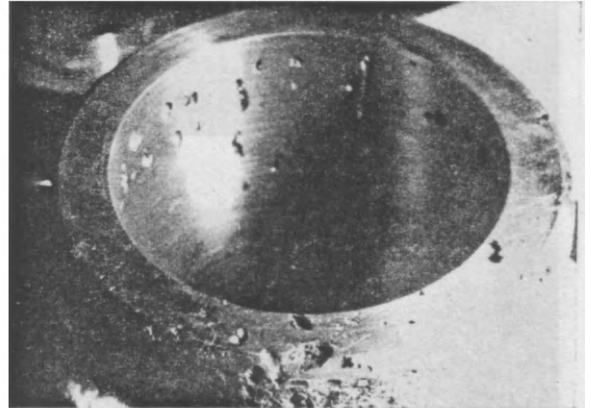


FIG. 449. Porosity in valve flanges where exothermic pads were not used.

Note particularly the flange on the left of the diagram. Here also the porosity is very pronounced under the metallic wedge pad, because the steel remained liquid longest in this position.

If an exothermic pad had been attached at this position, then the temptation to ascribe the defect to the exothermic pad would have been very great.



FIG. 450. This lever arm (made without exothermic pads) also exhibits a typical enrichment of pores near the feeder head.

CHAPTER 14

BRIEF NOTE ON THE USE OF INSULATING MATERIALS IN STEEL CASTINGS

IT IS possible in principle to insulate feeder heads for steel castings by means of materials which are not self-heating.

Up to the present time, however, (1962), no insulating materials are known which fulfil the following requirements simultaneously:

Refractoriness, with the good surface associated with this property (particularly important for insulated pads placed on the casting).

Good mouldability—most insulating materials, diatomaceous earth, for example, have poor moulding characteristics.—Cheapness.

A good insulating effect at the steel temperatures.

Strength of the insulating sleeve and pad.

While insulating materials are used successfully with metals having a lower melting point, these materials are not satisfactory in every case, for example with grey cast iron which is poured hot. Moreover, these "exotic"

insulating materials are not cheap, and do not have the same effect as exothermic substances.

Various insulating materials were described in the German edition of this book. Due to the rapid development of exothermic materials, however, trials on the application of insulating substances have been suspended, at least provisionally.

CHAPTER 15

CAVITIES IN STEEL CASTINGS WHICH ARE FREQUENTLY CONFUSED WITH TRUE SHRINKAGE CAVITIES

IMPORTANT FOR PRACTICE

IT IS understandable that nobody likes to take the blame for scrap. Very many cavities in castings originate in the unsatisfactory condition of the steel, which can (1) be high in hydrogen, (2) be badly deoxidized and (3) suffer from a combination of defects (1) and (2), or (4) be permeated by finely emulsified slag. The origin of these defects is often not known, or is falsely attributed to the moulding shop or the moulding sand.

It is not the task of this book to discuss the many existing theories concerning defects of this kind. Only a few typical illustrative examples will be given. It will be emphasized that defects arising from the quality of the steel cannot be improved by measures based on moulding technology either by a (presumably) better placing of the feeder head or by using a different moulding sand. Such false "remedial measures" only have the effect of impairing economic efficiency and obscuring the facts. This is very dangerous, because the ill effects of an unsatisfactory melting technique are not thereby eliminated and several unfavourable factors can operate at the same time.

15.1. Blowholes Which Can Be Confused with Shrinkage Cavities

IMPORTANT FOR PRACTICE

Gas porosity of this kind has already been mentioned several times in this book, namely in Sections 8.3.2 (Figs. 263-267), 11.1 (Fig. 314) and 13.4.2 (Figs. 445-450). This porosity manifests itself in many ways, and some further examples will be given here.

Very often gas porosity is confused with true shrinkage cavity phenomena for the following reasons:

1. The pores represent localized insulation in the casting, in the form of a pad resembling sponge rubber. The natural flow of heat is often seriously impaired.
2. Gas pores in the steel hinder the orderly flow of metal back from the feeder head into the casting, with the result that secondary cavities are formed (Fig. 451).

Figure 452 shows covers made from a badly deoxidized melt, a fact which was not recognized at first. The defect was explained as a "shrinkage cavity" and a larger feeder head was asked for. On more careful examination, which is always extremely important in such cases, pinholes were also found in other parts of the casting, and the casting was then X-rayed. The radiographs of several castings from the same charge showed the true cause to be gas porosity.

Figures 453 and 454 indicate clearly that gases are responsible. In Fig. 455 the origin was again in doubt, because the pores ran in bands parallel to the blades in the lower part, and were therefore considered to be junction cavities. In coming to this conclusion, however, it was now noted that with "bleeding back" in the riser, i.e. in "gassy" melts, the gases concentrate in the parts of the casting which stay liquid the longest (this has already been shown several times). These concentrations happened to coincide with the blade junction.

Figure 456, the sectioned feeder head of a wheel boss, cast with a "gassy" metal, shows similar horizontal groups of pores. Had this feeder head been cut parallel to the plane of the circle, this would have given a picture similar to that in Fig. 455.

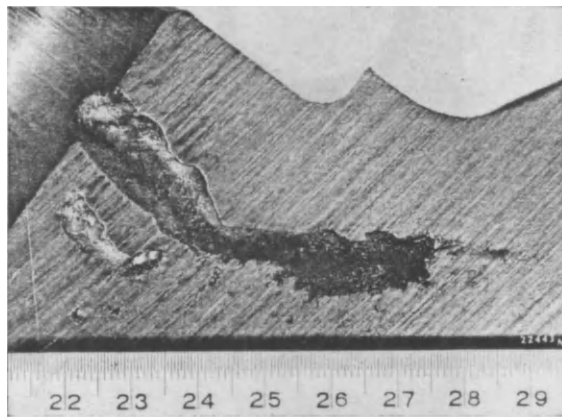


FIG. 451. Typical secondary shrinkage cavity (with rough inner wall) in the wake of primary porosity.

A good insulating effect at the steel temperatures.

Strength of the insulating sleeve and pad.

While insulating materials are used successfully with metals having a lower melting point, these materials are not satisfactory in every case, for example with grey cast iron which is poured hot. Moreover, these "exotic"

insulating materials are not cheap, and do not have the same effect as exothermic substances.

Various insulating materials were described in the German edition of this book. Due to the rapid development of exothermic materials, however, trials on the application of insulating substances have been suspended, at least provisionally.

CHAPTER 15

CAVITIES IN STEEL CASTINGS WHICH ARE FREQUENTLY CONFUSED WITH TRUE SHRINKAGE CAVITIES

IMPORTANT FOR PRACTICE

IT IS understandable that nobody likes to take the blame for scrap. Very many cavities in castings originate in the unsatisfactory condition of the steel, which can (1) be high in hydrogen, (2) be badly deoxidized and (3) suffer from a combination of defects (1) and (2), or (4) be permeated by finely emulsified slag. The origin of these defects is often not known, or is falsely attributed to the moulding shop or the moulding sand.

It is not the task of this book to discuss the many existing theories concerning defects of this kind. Only a few typical illustrative examples will be given. It will be emphasized that defects arising from the quality of the steel cannot be improved by measures based on moulding technology either by a (presumably) better placing of the feeder head or by using a different moulding sand. Such false "remedial measures" only have the effect of impairing economic efficiency and obscuring the facts. This is very dangerous, because the ill effects of an unsatisfactory melting technique are not thereby eliminated and several unfavourable factors can operate at the same time.

15.1. Blowholes Which Can Be Confused with Shrinkage Cavities

IMPORTANT FOR PRACTICE

Gas porosity of this kind has already been mentioned several times in this book, namely in Sections 8.3.2 (Figs. 263-267), 11.1 (Fig. 314) and 13.4.2 (Figs. 445-450). This porosity manifests itself in many ways, and some further examples will be given here.

Very often gas porosity is confused with true shrinkage cavity phenomena for the following reasons:

1. The pores represent localized insulation in the casting, in the form of a pad resembling sponge rubber. The natural flow of heat is often seriously impaired.
2. Gas pores in the steel hinder the orderly flow of metal back from the feeder head into the casting, with the result that secondary cavities are formed (Fig. 451).

Figure 452 shows covers made from a badly deoxidized melt, a fact which was not recognized at first. The defect was explained as a "shrinkage cavity" and a larger feeder head was asked for. On more careful examination, which is always extremely important in such cases, pinholes were also found in other parts of the casting, and the casting was then X-rayed. The radiographs of several castings from the same charge showed the true cause to be gas porosity.

Figures 453 and 454 indicate clearly that gases are responsible. In Fig. 455 the origin was again in doubt, because the pores ran in bands parallel to the blades in the lower part, and were therefore considered to be junction cavities. In coming to this conclusion, however, it was now noted that with "bleeding back" in the riser, i.e. in "gassy" melts, the gases concentrate in the parts of the casting which stay liquid the longest (this has already been shown several times). These concentrations happened to coincide with the blade junction.

Figure 456, the sectioned feeder head of a wheel boss, cast with a "gassy" metal, shows similar horizontal groups of pores. Had this feeder head been cut parallel to the plane of the circle, this would have given a picture similar to that in Fig. 455.

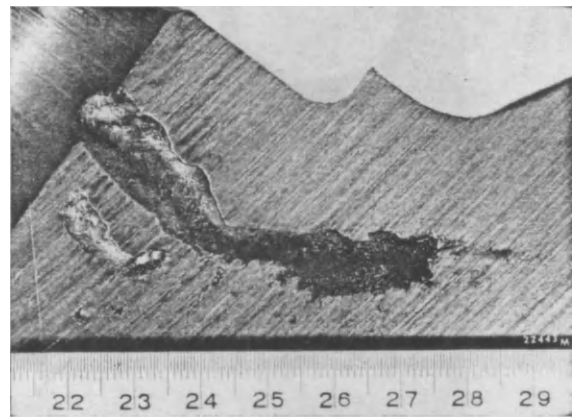


FIG. 451. Typical secondary shrinkage cavity (with rough inner wall) in the wake of primary porosity.

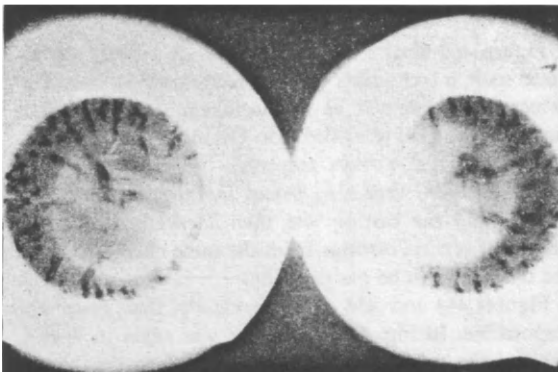
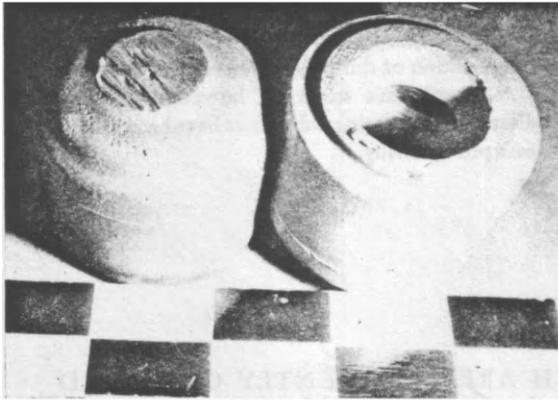


FIG. 452. Covers made from "rising" metal.

The defect was at first thought to be a shrinkage cavity (above), and it was only after radiographic examination that the true cause was shown to be porosity. On closer inspection, however, pinholes could be clearly seen on the casting.

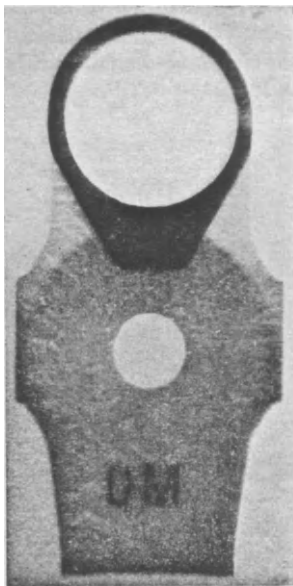


FIG. 453. Severe pinhole porosity shown in the X-ray photograph.

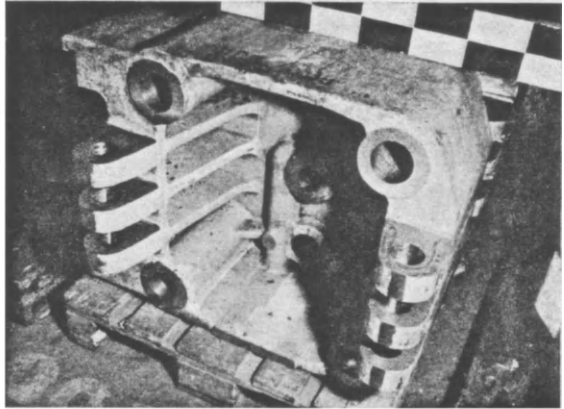
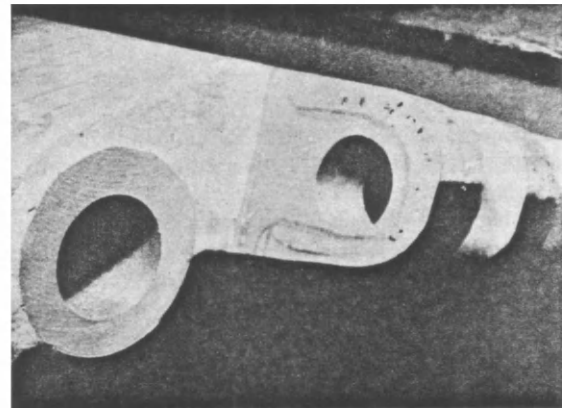


FIG. 454. Pinholes on the hinge of a squeezer press.



A typical characteristic of such defects is that they usually occur in batches. Individual castings where gas porosity is suspected should never be thrown out, but should be put on one side. In the course of a few weeks several other castings will appear; very often all of the castings will originate from the same heat. It is useful to keep a record, as often porous castings are supplied to the customer as apparently satisfactory, and it may be a year before trouble arises.

In practice, it is usual to find that not all the castings from a given unsatisfactory metal are affected. Sometimes sub-surface defects can be discovered by circulating castings through the annealing furnace and scaling off the casting surface; this being the method used to reduce the odds of a gassy casting going to a customer. This is a completely unreliable method, which can be avoided by the measures discussed earlier.

A frequent form of pinhole defect both in green and dry sand moulding is a typical scab formation, as shown in Figs. 457 and 458. This scab formation is possibly related to re-oxidation processes, in connection with the flow path of the steel in the mould^(63, 64, 65).

Pinholes of this kind appear even more often in dry sand castings; they can even give a very unpleasant appearance to test bars which are affected in this way,

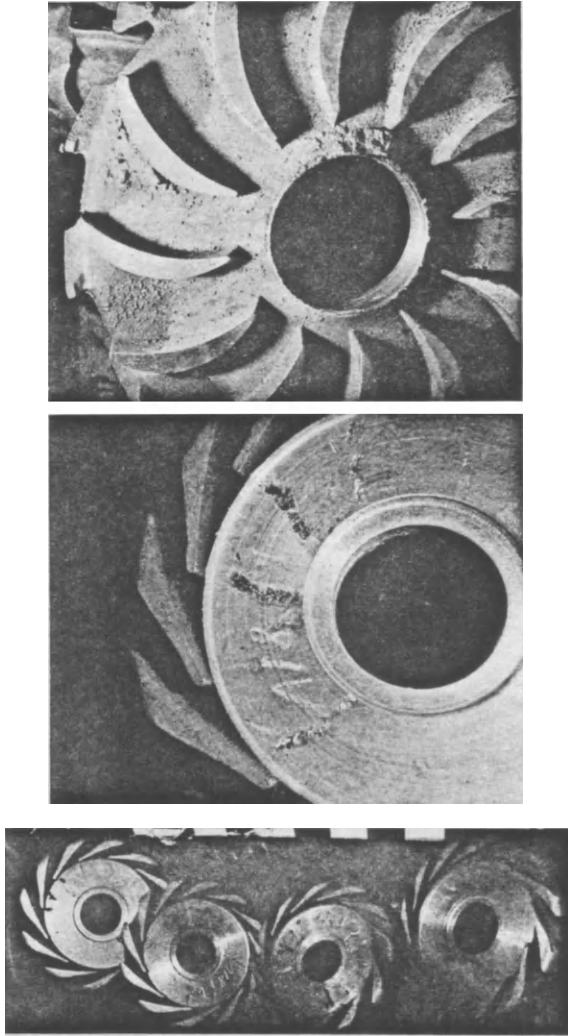


FIG. 455. Impellers of 18% Cr steel. The metal had "risen" but this had not been recognized.

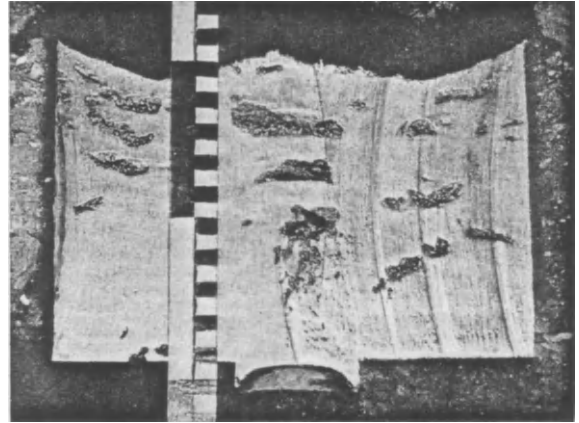
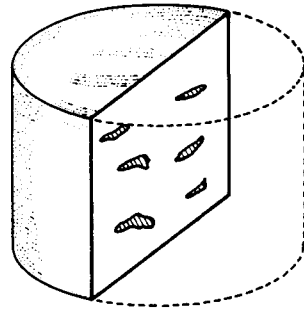


FIG. 456. Horizontal and radial groups of pores in a feeder head (this casting was made from a different heat than the wheels in Fig. 455).



although the actual casting is often sound. Alternatively pinholes in dry sand castings are usually technically unimportant because of thick walls, but they are physically present, and are important in assessing the quality of the batch (Figs. 459a-c).

Reference should be made to Section 8.3.2, Figs. 268 and 269, regarding the testing of the batch for gas content.

15.2. Slag Blowholes, Which Are Confused with Shrinkage Cavities

IMPORTANT FOR PRACTICE

This does not refer to slag which rises to the surface during pouring, or into the dirt trap shortly afterwards. The type of slag to be described separates only during solidification, whereby very finely emulsified droplets of slag are forced from the dendrites into the residual melt,

where they become concentrated (Fig. 460). Only then do the drops float and thrust against the upper wall, which has already solidified into a thick layer.

This slag porosity is often exposed only with the final cut during machining, and the castings are then irrecoverably lost.

Slag porosity is recognized by the fact that the slag can be detected on close examination. Often it occurs only as a thin skin (Fig. 461), as slag beads (Fig. 462), or as larger angular fragments (Fig. 463). Severe cases are comparatively rare (Fig. 464) but when present they give a clear indication of their presence (see also Fig. 465).

The slag itself is often not uniform, but is heterogeneous. Frequently small, silvery iron beads can be seen, which are an indication of chemical reactions in the (carbide) slag, in the course of which considerable amounts of carbon monoxide can be evolved, and lead

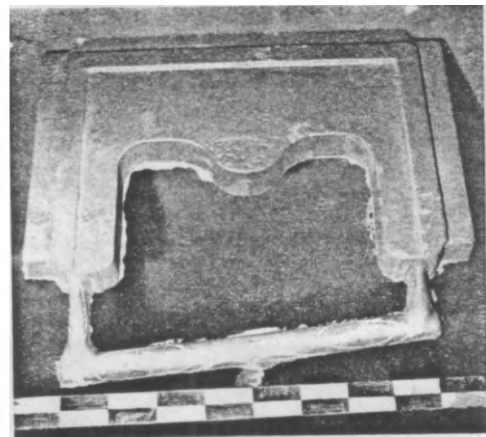
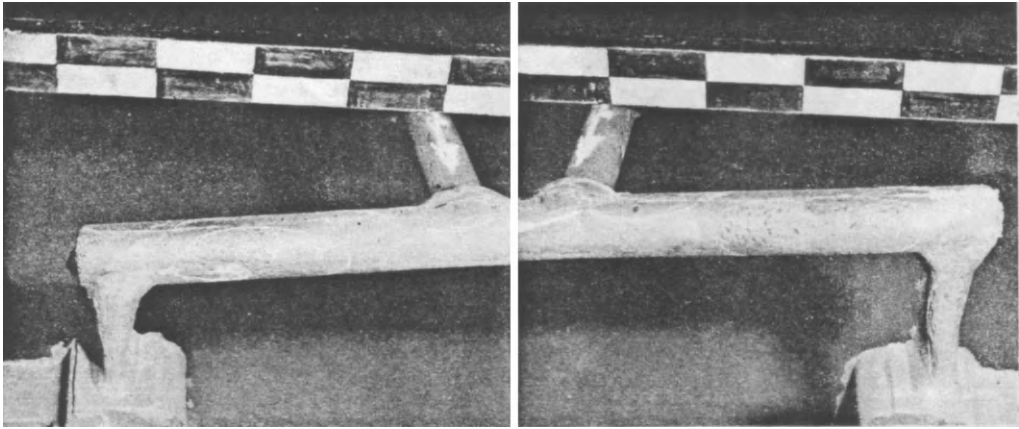


FIG. 457. Scab formation in the gating system, corresponding to the direction of flow of the steel. Scabs were also formed on the steel, as well as pinholes (not shown here).

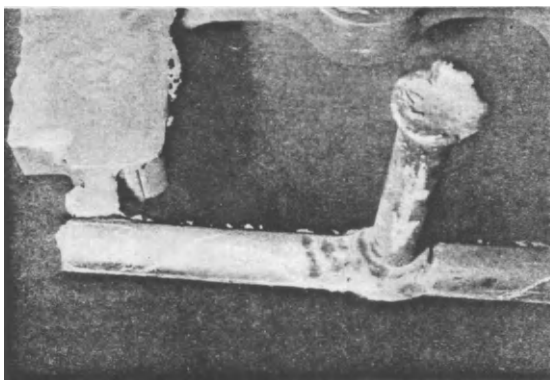
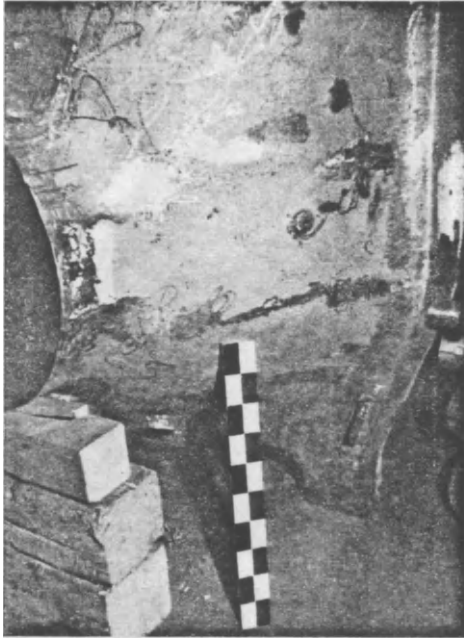


FIG. 458. Scab formation on a flat plate.

Careful preparation before dressing shows that the top layer of moulding sand which becomes plastic during casting, is curved down into the small scabs. This phenomenon has nothing to do with sand scabs. It is much more likely that vacuum processes resulting from pinhole formation cause the moulding material to be "sucked in".





a

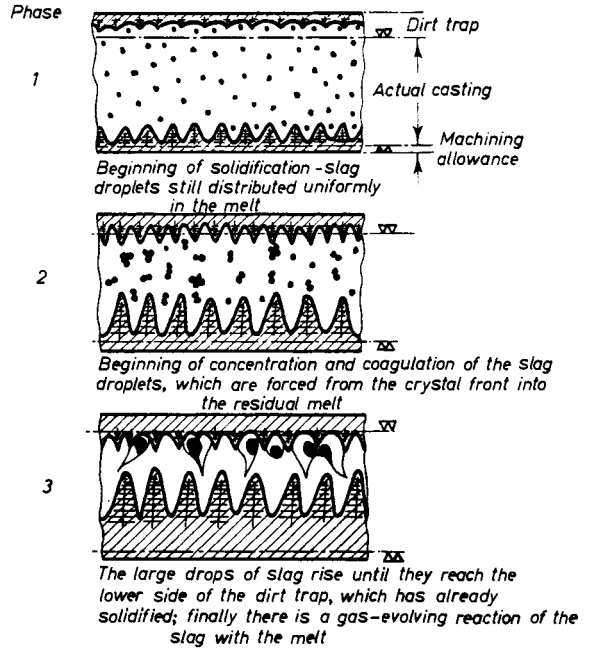
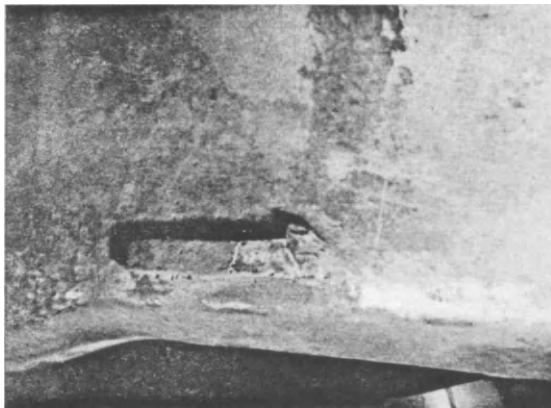


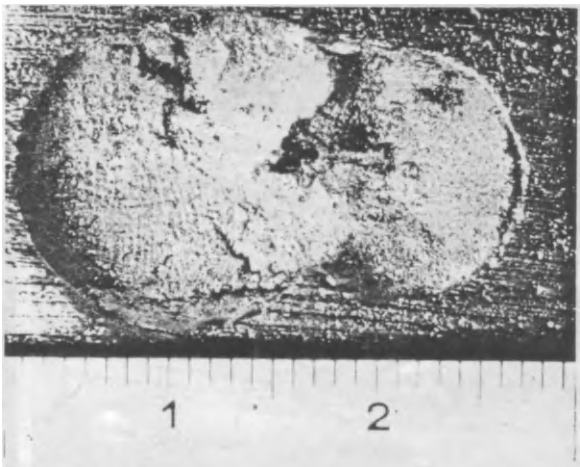
FIG. 460. Possible formation mechanism of slag blowholes.



b



c



FIGS. 459a-c. Pinholes on faces, corners and sample bars of a turbine casing, which was moulded in fireclay.

FIG. 461. Thin skin of slag in a blowhole.

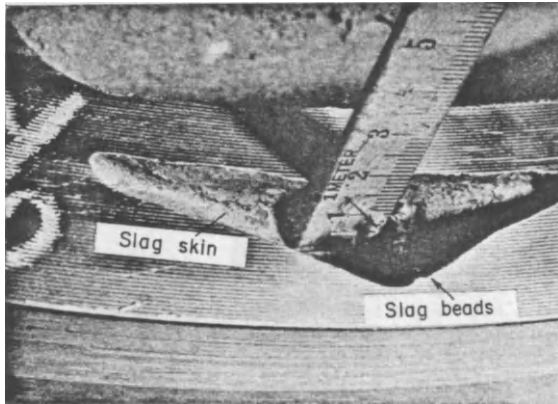
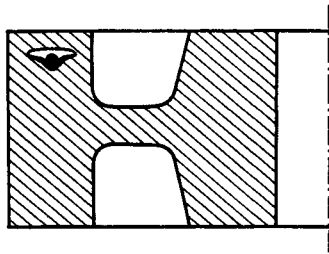


FIG. 462. Slag blowhole in a wheel casting.

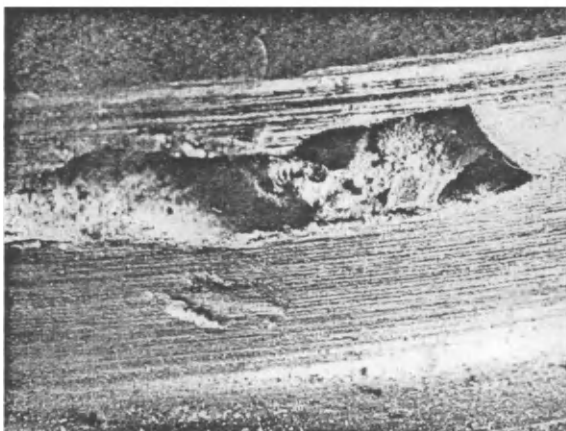
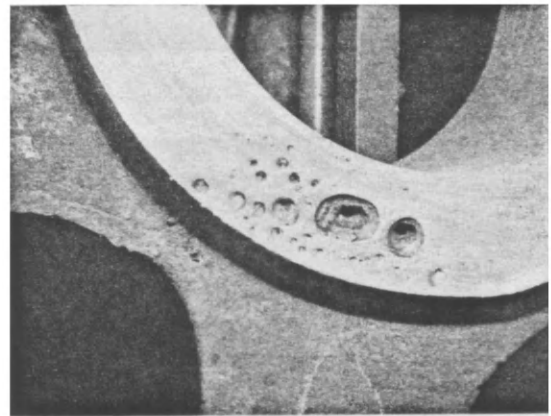


FIG. 463. Lumps of slag in a turbine wheel.

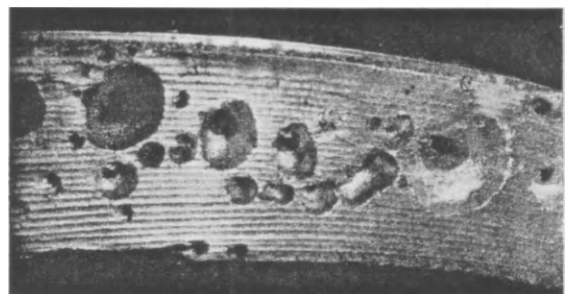
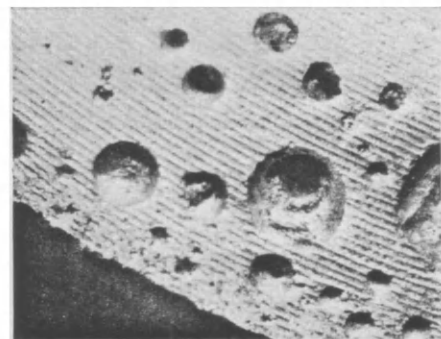


FIG. 464. Slag blowholes in a gear wheel casting.

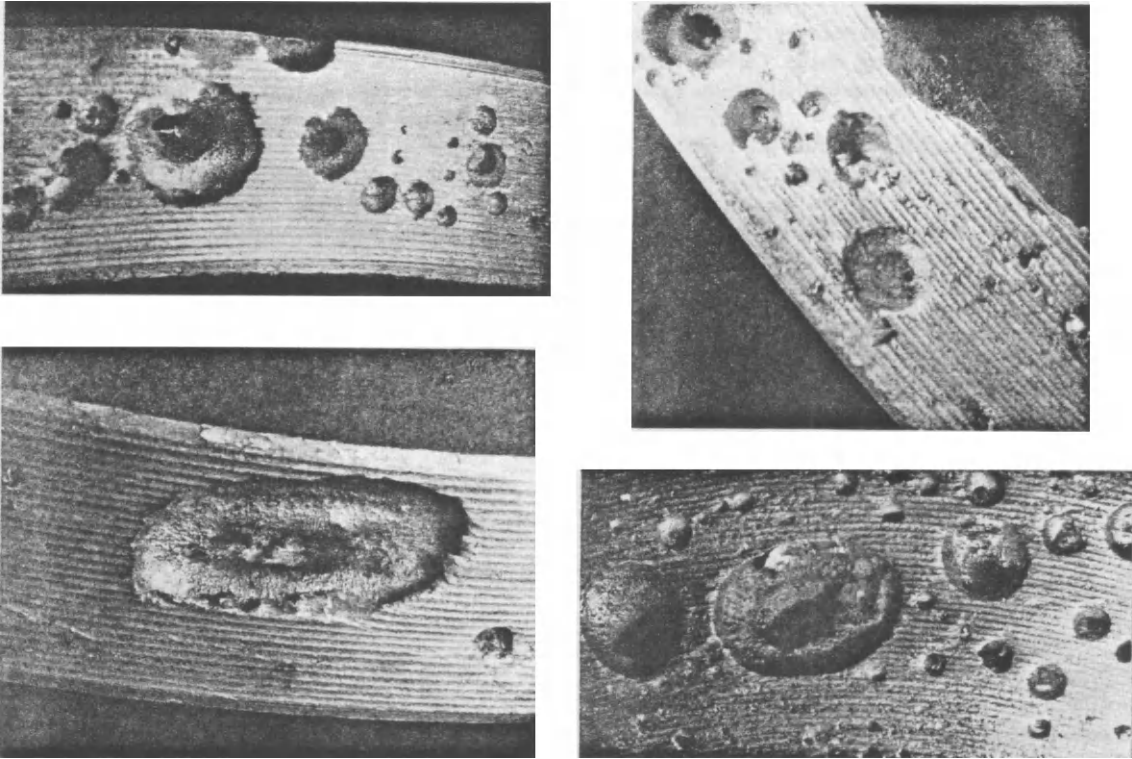


FIG. 464.



FIG. 465. X-ray photograph of typical slag blowholes in a gear wheel rim.

to the formation of the actual porosity. Also gases from the steel can separate on slag nuclei. Carbide slags, in the author's experience, are specially liable to emulsification of this kind.

It is sometimes possible to confuse this porosity with shrinkage cavities. A case is known to the author in which a foundry tried to get rid of slag porosity by increasing the size of the feeder head—unsuccessfully of course—and when the defect continued to appear, especially with large castings and heavy cross-sections

(which are particularly susceptible) was driven to despair.

In such doubtful cases, a smooth or slightly roughened surface, which in some cases can appear silvery-white, is a valuable method of distinguishing the defects from the true shrinkage cavity dendrites according to Fig. 39. Every foundry should also make use of the ASTM catalogue of defects, with its numerous radiographs. With all defects of this kind, *fundamental knowledge must be supplemented by the most accurate observation.*

CHAPTER 16

FINAL BRIEF WORD

THE emphasis to be laid on one or other of the possibilities dealt with in this book will depend on the operating conditions. For their successful application, however, the following points must be borne in mind:

1. Stepwise procedure. Do not be dazzled by initial successes. Do not overshoot the mark. The question must also be asked repeatedly: Is the steel quality satisfactory?
2. If material is rejected: Establish the causes objectively. Every defect cannot be attributed to "innovation." Occasionally, however, a feeder head can be wrongly dimensioned because of an error in calculation, which in any case would happen much more often if calculation was omitted. The "psychological" side of scientific moulding practice is as important as

its technical aspects. The works personnel, including the moulder and the labourers (we need only think of cleaning "chills", for example!) must be informed of certain basic rules. And if something does go wrong, it is no use being discouraged and reverting to "rule of thumb" methods.

3. Other countries (i.e. outside Germany) have to some extent "outflanked" us in the field of scientific moulding practice. If we wish to progress in the long term we shall have to make ourselves conversant with such advances. Whether the plant in question is in a position to take advantage of these modern developments is not only a question of ability, intelligence and practice, but above all it depends on taking determined and appropriate action.

to the formation of the actual porosity. Also gases from the steel can separate on slag nuclei. Carbide slags, in the author's experience, are specially liable to emulsification of this kind.

It is sometimes possible to confuse this porosity with shrinkage cavities. A case is known to the author in which a foundry tried to get rid of slag porosity by increasing the size of the feeder head—unsuccessfully of course—and when the defect continued to appear, especially with large castings and heavy cross-sections

(which are particularly susceptible) was driven to despair.

In such doubtful cases, a smooth or slightly roughened surface, which in some cases can appear silvery-white, is a valuable method of distinguishing the defects from the true shrinkage cavity dendrites according to Fig. 39. Every foundry should also make use of the ASTM catalogue of defects, with its numerous radiographs. With all defects of this kind, *fundamental knowledge must be supplemented by the most accurate observation.*

CHAPTER 16

FINAL BRIEF WORD

THE emphasis to be laid on one or other of the possibilities dealt with in this book will depend on the operating conditions. For their successful application, however, the following points must be borne in mind:

1. Stepwise procedure. Do not be dazzled by initial successes. Do not overshoot the mark. The question must also be asked repeatedly: Is the steel quality satisfactory?
2. If material is rejected: Establish the causes objectively. Every defect cannot be attributed to "innovation." Occasionally, however, a feeder head can be wrongly dimensioned because of an error in calculation, which in any case would happen much more often if calculation was omitted. The "psychological" side of scientific moulding practice is as important as

its technical aspects. The works personnel, including the moulder and the labourers (we need only think of cleaning "chills", for example!) must be informed of certain basic rules. And if something does go wrong, it is no use being discouraged and reverting to "rule of thumb" methods.

3. Other countries (i.e. outside Germany) have to some extent "outflanked" us in the field of scientific moulding practice. If we wish to progress in the long term we shall have to make ourselves conversant with such advances. Whether the plant in question is in a position to take advantage of these modern developments is not only a question of ability, intelligence and practice, but above all it depends on taking determined and appropriate action.

CONVERSION FACTORS

1 metre (m)	= 39.37 in. = 3.28 ft	1 dm ³	= 61.024 in ³ = 0.035 ft ³
1 decimetre (dm)	= 3.97 in.	1 cm ³	= 0.061 in ³
1 centimetre (cm)	= 0.397 in.	1 mm ³	= 6.10 × 10 ⁻⁵ in ³
1 millimetre (mm)	= 0.040 in.	1 g	= 0.035 oz
1 dm ²	= 15.500 in ² = 0.108 ft ²	1 kg	= 35.274 oz = 2.205 lb
1 cm ²	= 0.155 in ²	1 metric ton = 1000 kg	= 0.984 long tons (2240 lb)
1 mm ²	= 0.00155 in ²		= 1.102 short (net) tons (2000 lb)

SYMBOLS USED IN THIS BOOK

Some of the symbols used frequently in the text include:

V = volume

A = surface area

P = periphery

M = modulus

M_F = feeder head modulus

M_C = casting modulus

W_C = casting weight

V_{SC} = volume of shrinkage cavity

Other symbols are defined, or their meaning is clear from the context.

CONVERSION FACTORS

1 metre (m)	= 39.37 in. = 3.28 ft	1 dm ³	= 61.024 in ³ = 0.035 ft ³
1 decimetre (dm)	= 3.97 in.	1 cm ³	= 0.061 in ³
1 centimetre (cm)	= 0.397 in.	1 mm ³	= 6.10 × 10 ⁻⁵ in ³
1 millimetre (mm)	= 0.040 in.	1 g	= 0.035 oz
1 dm ²	= 15.500 in ² = 0.108 ft ²	1 kg	= 35.274 oz = 2.205 lb
1 cm ²	= 0.155 in ²	1 metric ton = 1000 kg	= 0.984 long tons (2240 lb)
1 mm ²	= 0.00155 in ²		= 1.102 short (net) tons (2000 lb)

SYMBOLS USED IN THIS BOOK

Some of the symbols used frequently in the text include:

V = volume

A = surface area

P = periphery

M = modulus

M_F = feeder head modulus

M_C = casting modulus

W_C = casting weight

V_{SC} = volume of shrinkage cavity

Other symbols are defined, or their meaning is clear from the context.

REFERENCES

1. CHVORINOV, N. *Gießerei*, **27**, 177-186, 201-208, 222-225 (1940).
2. LOCKE, C., BRIGGS, C. W., and ASHBROOK, R. L. *Amer. Foundrym. Soc., Annual Meeting Preprint* 589-594 (1954).
- 2a. CZIKEL, J., and DIEPSCHLAG, E. *Casting Technology of Semi-Finished Products*, Halle (Saale) (1954).
3. PELLINI, W. S., and BISHOP, H. F. *Foundry*, **80**, No. 2, 86 et seq. (1952).
4. CECH, R. A. *Foundry*, **81**, No. 10, 128-131, abstracted in *Gießerei*, **44**, 37-45 (1957).
5. NAMUR, R. abstracted by KOPPE, W. *Gießerei*, **45**, 469-474 (1958).
6. PEARSON, A. *Gießerei*, **46**, 41-42 (1959).
7. BENEDICKS, C., ERICSSON, N., and ERICSON, G. *Arch. Eisenhüttenwes.*, **3**, 473-486 (1929/30).
8. KOTHNY, E. *Good Casting Practice*. Berlin, 34 (1939).
9. STEIN, H., ISKE, F., and KARCHER, D. *Gießerei, techn.-wiss. Beih.*, No. 21, 1115-1124 (1958).
10. NICOLAS, P. *Fonderie*, 3715-3725 (1953).
11. CAINE, J. B. *Trans. Amer. Foundrym. Soc.*, **56**, 492-501 (1948).
12. BISHOP, H. F., and JOHNSON, H. W. *Foundry*, **84**, No. 2, 70-74; No. 3, 136-141 (1956).
13. STEIN, H. *Gießerei*, **44**, 697-700 (1957).
14. HEUVERS, A. *Stahl u. Eisen*, **49**, 1249, *Gießerei*, **30**, 201 (1943).
15. BRINSON, S. W., and DUMAS, J. A. *Trans. Amer. Foundrym. Soc.*, **50**, 657-765 (1942).
16. STEIN, H. *From the Principles and Practice of Foundry Technology*, Düsseldorf, 358-370 (1955).
17. NAMUR, R. *Gießerei, techn.-wiss. Beih.*, No. 20, 1077-1087 (1958).
18. HOLLIER, C. C. *Amer. Foundrym.* **20**, No. 4, 30-32 (1951).
19. HALL, J. A. *Foundry*, **80**, No. 3, 112-115, 257-258; No. 4, 104-107, 255-257 (1952).
20. ROTH, A. *Gießerei*, **39**, 585-587 (1952).
21. MYTKOWSKI, E. T., BISHOP, H. F., and PELLINI, W. S. *Amer. Foundrym. Soc., Annual Meeting Preprint*, 583-587 (1954).
22. JOHNSON, W. H., BISHOP, H. F., and PELLINI, W. S. *Amer. Foundrym. Soc., Annual Meeting Preprint*, 243-251 (1954).
23. KRESTSCHANOVSKI, N. S. *High-Duty Steel Castings*, Berlin (1955).
24. WLODAWER, R. *Gießerei*, **47**, 1-7 (1960).
25. HEIDE, O. *Porosity in Steel Castings*, Contribution (No. C13). Presented at the 26th International Foundry Congress in Madrid, Oct. 1959.
26. RELLERMAYER, H. *Stahl u. Eisen*, **75**, 724-727 (1955).
27. PELLINI, W. S. *Amer. Foundrym.*, **23**, No. 2, 69-76; No. 3, 59-68 (1953).
28. STEIN, H. *Gießerei*, **41**, 381-388 (1954).
29. ROTH, A. *Gießerei*, **45**, 289-295 (1958).
30. BARDENHEUER, P. *Mitt. Kais.-Wilb.-Inst. Eisenforsch.*, Düsseldorf, **11**, 273 (1929).
31. WLODAWER, R. *Gating Technology in Steel Casting Practice*, Taschenbuch d. Giesserei-Praxis, Berlin, 139-214 (1959).
32. PELLINI, W. S. *Amer. Foundrym.*, **24**, No. 5, 58-66; No. 6, 62-71 (1953).
33. BRANDT, F. A., BISHOP, H. F., and PELLINI, W. S. *Amer. Foundrym. Soc., Annual Meeting Preprint* 646-653 (1954).
34. LANZENDÖRFER, E. *Gießerei*, **19**, 181-186 (1932).
35. LANZENDÖRFER, E., and HILTERHAUS, K. *Gießerei*, **39**, 483-486 (1952).
36. TAYLOR, H. F., and ROMINSKY, E. A. *Trans. Amer. Foundrym. Soc.*, **48**, 481-517 (1940/41); abstracted by HUYISIN, B.: *Gießerei*, **44**, 407-408 (1957).
37. LANZENDÖRFER, E. *Gießerei*, **38**, 661-664 (1951).
38. TROMMER, W. *Gießerei*, **44**, 37-45 (1957).
39. BOYLE, E. D. *Amer. Foundrym.*, **19**, No. 2, 45-50 (1949).
40. REMMECKE, L. *Gießerei*, **46**, 34-37 (1959).
41. ADAMS, JR. C. M., and TAYLOR, H. F. *Trans. Amer. Foundrym. Soc.*, 686-693 (1953).
42. STEIN, H., and BOHLEN, H. *Gießereikalender*, Düsseldorf, 208-211 (1957).
43. ROLL, F. The Formation of Cavities in Castings. *Die Neue Gießerei*, 45-52 (1950).
44. BRANDT, F. A., BISHOP, H. F., and PELLINI, W. S. Solidification at Corner and Core Positions. *Amer. Foundrym. Soc.*, 451-456 (1953).
45. EPSTEIN, H. J., WALSH, J. H., and KING, T. B. *Trans. ASME*, **74**, 403-413 (1952).
46. PIPER, E., HAGEDORN, H., and BECKER, H. *Stahl u. Eisen*, **73**, 817-828 (1953).
47. SNELSON, D. H. *Brit. Foundrym.*, Oct., 486-499 (1958).
48. NAMUR, R. *Fond. Belge*, **6**, 89-122 (1956).
49. THIERRY, R. *Exothermic Feeder Heads*. Mar., Doittau Products Metallurgie, Corbeil, (S & O) France. (1953).
50. BISHOP, H. F. *Foundry*, Aug., 75-79, Sept., 116-123, Oct., 114-119 (1960).
51. GRIFFITHS, M. H., NEU, M. G. and HALL, C. *Brit. Foundrym.*, Mar., 93-102 (1962).
52. WLODAWER, R. Paper presented at the Conference of V. D. Gießereifachleute, Düsseldorf, on Oct. 5, 1961. See also *Gießerei*, Dec. 28, 765-769 (1961).
53. WLODAWER, R. *Gießerei*, Sept. 6, 605-610 (1961).
54. WLODAWER, R. *Gießerei*, Jan. 14, 1-7 (1960).
55. WLODAWER, R. *Gießerei-Praxis*, Berlin, 2-10, 25-34 (1961). Translated in *Foundry Tr. J.*, May, 571 and 605 (1962).